

DISSERTATION

ZEOLITE-AMENDED BACKFILLS FOR ENHANCED METALS CONTAINMENT VIA  
SOIL-BENTONITE VERTICAL CUTOFF WALLS

Submitted by

Catherine SooJung Hong

Department of Civil and Environmental Engineering

In partial fulfillment of the requirements

For the Degree of Doctor of Philosophy

Colorado State University

Fort Collins, Colorado

Summer 2016

Doctoral Committee:

Advisor: Charles D. Shackelford

Christopher Bareither

Mike A. Malusis

Thomas C. Sale

Mary E. Stromberger

Copyright by Catherine SooJung Hong 2016

All Rights Reserved

## ABSTRACT

### ZEOLITE-AMENDED BACKFILLS FOR ENHANCED METALS CONTAINMENT VIA SOIL-BENTONITE VERTICAL CUTOFF WALLS

Low hydraulic conductivity ( $k$ ), soil-bentonite (SB) vertical cutoff walls are commonly used to contain contaminated groundwater in geoenvironmental applications. The low  $k$  of the SB cutoff walls is attributed, in part, to the high swelling property of the bentonite component of the backfill. In addition, the high cation exchange capacity ( $CEC$ ) of the bentonite, typically on the order of 80 to 150  $\text{cmol}_c/\text{kg}$ , imparts some intrinsic attenuation capacity to the backfill for cations (*e.g.*, metals) via cation exchange. However, due to the low amounts of bentonite in typical SB cutoff walls (*i.e.*,  $< 10\%$  by dry weight), this attenuation capacity is limited in traditional SB cutoff walls. Therefore, consideration has been given to amending SB backfills with zeolites to enhance the attenuation or adsorption capacity. Zeolites are naturally occurring aluminosilicates with high  $CEC$  (180 to 400  $\text{cmol}_c/\text{kg}$ ) and a cage-like structure that allow the zeolites to perform as a molecular sieve and as adsorbents for ammonium, heavy metals, cations, and radioactive wastewater.

In this study, three types of zeolites (two types of chabazite and a clinoptilolite) were used as amendments for SB backfills to enhance the adsorption capacity with respect to two metals, *viz.*, potassium (K) and zinc (Zn). The results of measurements of the slump, consolidation behavior, and  $k$  of the unamended and zeolite-amended SB backfills with  $\leq 10\%$  zeolite (by dry weight) confirmed that the zeolite-amended SB backfills exhibited similar physical properties compared to those for the unamended SB backfill, including the low  $k$  ( $\leq$

$1.0 \times 10^{-9}$  m/s) typically required for SB vertical cutoff walls. The results of batch equilibrium adsorption tests (BEATs) indicated that the added zeolite increased the adsorption capacity of the SB backfill, but the effectiveness differed for different types of zeolite and the different metals (*i.e.*, K and Zn). The results of numerical simulations for transport of K and Zn through a hypothetical 1-m thick model cutoff wall based on the results of the BEATs indicated that the barrier containment durations increased relative to that for the unamended SB backfill by as much as 108 yr and 228 yr for backfills with 5 and 10 % zeolite amendment, respectively. Finally, the results of long-term column tests (1.05 to 3.75 yr) indicated that the retardation factor ( $R_d$ ) for K with the 5 % zeolite-amended SB backfills was 2.4 to 3.2 times greater than that for the unamended SB backfill, whereas  $R_d$  for Zn was 1.4 to 2.2 times greater than that for the unamended SB backfill. Based on the results of this study, the addition of small amounts of zeolite ( $\leq 10$  % by dry weight) to traditional SB backfills can significantly enhance the adsorption capacity of the SB backfills for metals, thereby enhancing the containment performance of vertical cutoff walls comprising zeolite-amended SB backfills. However, the magnitude of any enhanced containment is dependent on both the adsorption capacity and the adsorption behavior of the specific metal with the specific backfill, and will be dependent on both the type and amount of the added zeolite.

## ACKNOWLEDGMENTS

I would like to extend my sincere gratitude to Dr. Charles D. Shackelford for serving as my advisor and for his helpful insight, guidance, and support throughout my graduate study. I am blessed to be able to work with Dr. Shackelford who is not only a knowledgeable researcher but also an honorable individual. I would also like to thank Dr. Christopher A. Bareither, Dr. Mike A. Malusis, Dr. Thomas C. Sale and Dr. Mary E. Stromberger for serving on my committee.

I would like to thank my fellow graduate students for their support and camaraderie throughout this research, including Gretchen Bohnhoff, Kristin Sample-Lord, Jin Chul Joo, Jong Beom Kang, Amara Meier, and Shan Tong. Thanks to Joe Wilmetti for his support in mechanical aspects throughout the laboratory experiments.

Finally, I would like to thank my parents, Sung Wan Hong and Soon Ok Chang, brother Tae Joon Hong, for their experience-based advice and encouragement throughout my graduate education. I would also like to thank my 99-year-old grandmother Sung Ok Choi, aunt In Sook Hong, and the rest of my family for their prayers and support.

The U.S. National Science Foundation (NSF), Arlington, VA, under Grant CMS-0625159, provided financial support for this study, which is part of a collaborative research between Colorado State University and Bucknell University. The author thanks Central Builders Supply (Lewisburg, PA), GSA Resources (Tucson, AZ), and Wyo-Ben (Billings, MT) for providing the mortar sand, zeolites and bentonite used in this study. The opinions expressed in this document are solely those of the author and are not necessarily consistent with the policies or opinions of the sponsors.

## TABLE OF CONTENTS

ABSTRACT.....	ii
ACKNOWLEDGMENTS .....	iv
TABLE OF CONTENTS.....	v
LIST OF TABLES .....	x
LIST OF FIGURES .....	xii
CHAPTER 1. INTRODUCTION.....	1
1.1 BACKGROUND .....	1
1.2 GOALS AND OBJECTIVES .....	4
1.3 OVERVIEW OF DISSERTATION.....	6
REFERENCES.....	9
CHAPTER 2. CONSOLIDATION AND HYDRAULIC CONDUCTIVITY .....	12
2.1 INTRODUCTION .....	12
2.2 MATERIALS AND METHODS.....	14
2.2.1 Constituent Materials.....	14
2.2.2 Base Mixtures for Backfills .....	16
2.2.3 Bentonite-Water Slurry.....	16
2.2.4 Backfill Slump Testing.....	16
2.2.5 Backfill Preparation .....	17
2.2.6 Consolidation Testing.....	17
2.2.7 Flexible-Wall Hydraulic Conductivity Testing .....	18
2.3 RESULTS .....	19

2.3.1 Slump .....	19
2.3.2 Stress-Strain Behavior .....	20
2.3.3 Hydraulic Conductivity.....	20
2.3.4 Coefficients of Consolidation .....	21
2.4 DISCUSSION .....	22
2.4.1 Effect of Zeolite on Slump.....	22
2.4.2 Effect of Zeolite on Compression and Swell .....	23
2.4.3 Effect of Zeolite on Hydraulic Conductivity .....	25
2.4.4 Effect of Zeolite on Coefficient of Consolidation .....	26
2.5 SUMMARY AND CONCLUSIONS .....	27
REFERENCES.....	46
CHAPTER 3. ADSORPTIVE BEHAVIOR.....	50
3.1 INTRODUCTION .....	50
3.2 MATERIALS AND METHODS.....	53
3.2.1 Sorbents.....	53
3.2.2 Batch Equilibrium Adsorption Tests (BEATs).....	55
3.2.3 Evaluating BEAT Results .....	57
3.2.4 Cation Exchange Capacities of the Sorbents .....	60
3.3 RESULTS .....	61
3.3.1 Adsorption Results.....	61
3.3.2 Mechanisms for Metals Adsorption.....	62
3.4 DISCUSSION .....	65
3.4.1 Effect of Zeolite Content on Fitted Langmuir Model Parameters .....	65

3.4.2	Effect of Zeolite Content on Fitted Freundlich Model Parameters.....	67
3.4.3	Effect of Zeolite Content on Adsorption Capacity .....	67
3.4.4	Effect of Type of Zeolite.....	69
3.4.5	Effect of Type of Sorbate.....	70
3.5	SUMMARY AND CONCLUSIONS .....	73
	REFERENCES.....	97
CHAPTER 4. NUMERICAL MODELING .....		106
4.1	INTRODUCTION .....	106
4.2	METHODS .....	108
4.2.1	Solute Transport Model .....	108
4.2.2	Simulation Scenarios .....	113
4.3	RESULTS .....	116
4.3.1	Flux Breakthrough Curves for Potassium.....	116
4.3.2	Flux Breakthrough Curves for Zinc.....	120
4.3.3	Effect of Magnitude and Direction of Hydraulic Gradient on Flux Breakthrough Curves .....	122
4.3.4	Barrier Flux Breakthrough Times.....	124
4.4	DISCUSSION .....	126
4.4.1	Effect of Amount and Type of Zeolite.....	126
4.4.2	Influence of Magnitude and Direction of Hydraulic Gradient.....	128
4.4.3	Effect of the Source Concentration.....	131
4.5	SUMMARY AND CONCLUSIONS .....	131
	REFERENCES.....	162

CHAPTER 5. LONG-TERM COLUMN TESTING.....	166
5.1 INTRODUCTION .....	166
5.2 MATERIALS AND METHODS.....	168
5.2.1 Liquids .....	168
5.2.2 Constituent Materials for Specimens .....	170
5.2.3 Testing Apparatus .....	170
5.2.4 Specimen Preparation .....	173
5.2.5 Testing Procedure .....	176
5.2.6 Methods of Chemical Transport Analysis .....	177
5.2.7 Consideration of Other Factors Potentially Affecting Analyses.....	183
5.2.8 Testing Plan .....	185
5.3 RESULTS .....	186
5.3.1 Physical Characterization.....	186
5.3.2 Hydraulic Properties .....	188
5.3.3 Effluent Chemistry.....	191
5.3.3.1 Breakthrough Curves .....	191
5.3.3.2 Charge Balance .....	193
5.3.3.3 Electrical Conductivity and pH.....	193
5.3.4 Chemical Transport Analyses.....	195
5.3.5 Linearity of Adsorption.....	200
5.4 DISCUSSION .....	203
5.4.1 Effect of Type of Zeolite on Cl <sup>-</sup> and K <sup>+</sup> Migration.....	203
5.4.2 Effect of Type of Zeolite on Cl <sup>-</sup> and Zn <sup>2+</sup> Migration.....	205

5.4.3 Effect of Amount of Zeolite.....	206
5.4.4 Effect of Type of Metal.....	208
5.4.5 Effect of Cation Competition.....	210
5.5 SUMMARY AND CONCLUSIONS .....	213
REFERENCES.....	296
CHAPTER 6. SUMMARY AND CONCLUSIONS .....	301
6.1 SUMMARY .....	301
6.2 CONCLUSIONS.....	301
6.3 RELEVANCE OF RESEARCH .....	304
6.4 RECOMMENDATIONS FOR FUTURE RESEARCH.....	304
APPENDIX A. SUPPLEMENTARY DATA FOR CHAPTER 2.....	305
APPENDIX B. SUPPLEMENTARY DATA FOR CHAPTER 3 .....	324
APPENDIX C. ZINC SPECIATION (CHAPTER 3).....	327
APPENDIX D. CONCAVE AND NONLINEAR ADSORPTION (CHAPTER 4) .....	336
APPENDIX E. SUPPLEMENTARY DATA FOR CHAPTER 4 .....	342
APPENDIX F. SUPPLEMENTARY DATA FOR CHAPTER 5 .....	370

## LIST OF TABLES

Table 2.1	Physical and chemical properties and mineralogical compositions of constituent materials used for backfills.....	29
Table 2.2	Atterberg limits (ASTM D4318) of backfills with compositions corresponding to those for a 125-mm (5-in) slump.....	30
Table 2.3	Measured hydraulic conductivity ( $k$ ) and porosity ( $n$ ) in fixed-ring oedometer cell as a function of consolidation effective stress zeolite-amended backfills with a total bentonite content of 5.8 % by dry weight.....	31
Table 2.4	Flexible-wall hydraulic conductivity test results for replicated specimens of zeolite-amended backfills with a total bentonite content of 5.8 % by dry weight.....	32
Table 3.1	Comparison of the measured and calculated cation exchange capacities for the sorbents evaluated in this study.....	76
Table 3.2	Fitting parameter values for adsorption testing results.....	77
Table 3.3	Equivalent liquid-phase concentrations of exchangeable metals and soluble metals in the sorbents.....	78
Table 3.4	Comparison of Langmuir adsorption capacities versus maximum solid-phase concentrations based on measured <i>CEC</i> values.....	79
Table 3.5	Reported selectivity series for zeolites and bentonite.....	80
Table 3.6	Hydration ion charge density for the principle cations of this study.....	81
Table 4.1	Regressed parameter values from results of batch equilibrium adsorption tests (data from Chapter 3).....	135
Table 4.2	Values of relative nonlinearity ( $\lambda$ ) based on data from Table 4.1 for unamended and zeolite amended backfills.....	136
Table 4.3	Values of the secant distribution coefficient, $K_{d,secant}$ , based on data from Table 4.1 for unamended and zeolite-amended backfills.....	137
Table 4.4	Predicted barrier flux breakthrough times for $Cl^-$ , K, and Zn with a 1-m-thick ( $L = 1$ m) soil-bentonite vertical cutoff wall comprising unamended or zeolite-amended backfills as a function of source concentration and type of adsorption model using data from Table 4.1.....	138
Table 4.5	Predicted barrier flux breakthrough times for Zn based on different criteria ( $f = 0.05$ or $f = 0.50$ ) with 1-m-thick ( $L = 1$ m) vertical cutoff wall as a function of source	

	concentration and type of adsorption model using data from Table 4.1.....	139
Table 4.6	Increment in the predicted barrier flux breakthrough time for Cl <sup>-</sup> , K, and Zn with a 1-m-thick ( $L = 1$ m) soil-bentonite vertical cutoff wall comprising a zeolite-amended backfill relative to that comprising an unamended backfill as a function of source concentration and type of adsorption model using data from Table 4.4.....	140
Table 4.7	Predicted barrier flux breakthrough times for potassium (K) and zinc (Zn) corresponding to $J^*(L,t) = 0.015$ with a 1-m-thick ( $L = 1$ m) soil-bentonite vertical cutoff wall comprising unamended or zeolite-amended backfills as a function of type of adsorption model, source concentration, and magnitude and direction of hydraulic gradient.....	141
Table 4.8	Incremental change in barrier flux breakthrough time due to reversal in hydraulic gradient for $J^*(L,t)$ of 0.015.....	142
Table 5.1	Source chemical properties of the permeant liquids used for column testing.....	218
Table 5.2	Estimated electrical conductivity of typical groundwater.....	219
Table 5.3	Test condition summary for column testing.....	220
Table 5.4	Physical properties of the column test specimens.....	221
Table 5.5	Comparison of the chemical transport parameters corrected for the residual volume, $V_{res}$ .....	222
Table 5.6	Hydraulic properties of the column test specimens.....	223
Table 5.7	Evaluation of the measured pH of the column test effluents.....	224
Table 5.8	Chemical transport parameters of the column tested specimens of the unamended and zeolite-amended backfills.....	225
Table 5.9	Comparison of the chemical transport parameters calculated from the batch equilibrium adsorption test (BEAT) with the chemical transport parameters of the column tested specimens of the unamended and zeolite-amended backfills.....	226

## LIST OF FIGURES

Figure 2.1	Measured particle-size distributions (ASTM D422) for constituent materials used in study. Letter designations associated with curves represent classifications based on the Unified Soil Classification System (ASTM D2487) .....	33
Figure 2.2	Backfill slump versus backfill gravimetric water content: (a) unamended backfill compared with the results of Yeo (2003); (b) backfills amended with different percentages of the same zeolites (chabazite-LB); (c) backfills amended with same amount (5 %) of different types of zeolites .....	34
Figure 2.3	Stress-strain curves for confined compression of unamended and zeolite-amended backfills: (a) effect of different amounts of the same zeolite (chabazite-LB); (b) effect of same amount (5 %) of different types of zeolite. $C_c$ = compression index; $C_s$ = swell index.....	35
Figure 2.4	Hydraulic conductivity measured in fixed-ring oedometer cells as a function of consolidation effective stress for unamended and zeolite-amended backfills: (a) effect of different amounts of the same zeolite (chabazite-LB); (b) effect of same amount (5 %) of different types of zeolite.....	36
Figure 2.5	Correlation between geometric mean of hydraulic conductivity, $k$ , measured in flexible-wall cell at an average effective stress, $\sigma'$ , of 34.5 kPa (5.0 psi) versus $k$ measured in fixed-ring oedometer cell for 24 kPa (3.5 psi) and 48 kPa (7.0 psi) ....	37
Figure 2.6	Coefficients of consolidation based on Casagrande and Taylor methods for unamended and zeolite-amended backfills as a function of consolidation effective stress: (a), (c) effect of different amounts of the same zeolite (chabazite-LB); (b), (d) effect of same amount (5 %) of different types of zeolite.....	38
Figure 2.7	Backfill water content required to achieve a 125-mm (5-in) slump: (a) effect of different amounts of the same zeolite (chabazite-LB); (b) effect of the same amount (5 %) of different types of zeolite.....	39
Figure 2.8	Compression and swell indices for unamended backfill and zeolite-amended backfills amended with the same zeolite (chabazite-LB): (a) effect of amount of zeolite; (b) effect of backfill water content.....	40
Figure 2.9	Compression and swell indices for zeolite-amended backfills amended with the same amount (5 %) of different types of zeolites: (a) effect of type of zeolite; (b) effect of backfill water content .....	41
Figure 2.10	Correlation between initial void ratio and compression index zeolite-amended backfills with different amounts and/or types of zeolites .....	42
Figure 2.11	Effect of the amount of the same zeolite (chabazite-LB) on the hydraulic	

conductivity,  $k$ , of zeolite-amended backfills: (a) geometric mean of  $k$  values measured using flexible-wall cells; (b)  $k$  values measured in fixed-ring oedometer cells as a function of consolidation effective stress,  $\sigma'$ ; (c) ratio of geometric mean  $k$  values measured using flexible-wall cells; (d) ratio of  $k$  values measured in fixed-ring oedometer cells as a function of  $\sigma'$ . .....43

Figure 2.12 Effect of the same amount (5 %) of different zeolites on the hydraulic conductivity,  $k$ , of zeolite-amended backfills: (a) geometric mean of  $k$  values measured using flexible-wall cells at an average consolidation effective stress,  $\sigma'$ , of 34.5 kPa (5.0 psi); (b)  $k$  values measured in fixed-ring oedometer cells at different values of  $\sigma'$ . ....44

Figure 2.13 Effect of the amount of the same zeolite (chabazite-LB) on the coefficient of consolidation,  $c_v$ , of zeolite-amended backfills as a function of consolidation effective stress,  $\sigma'$ : (a)  $c_v$  based on Casagrande method; (b)  $c_v$  based on Taylor method; (c) ratio of  $c_v$  based on Casagrande method; (d) ratio of  $c_v$  based on Taylor method .....45

Figure 3.1 Formation of precipitation in zinc chloride solution: (a) after batch test for source concentration of 98 mM without acid addition; (b) after batch test for source concentration of 124 mM without acid addition; (c) stock solution with target concentration of 200 mM before acid addition (pH 5.27); (d) stock solution with target concentration of 200 mM after addition of 1 mL of 37 % HCl (pH 2.76) .....82

Figure 3.2 Fitted Freundlich (dashed line) and Langmuir (solid line) adsorption models for potassium (K) adsorption: (a) unamended backfill sorbent; (b) 100 % chabazite-LB; (c) 100 % chabazite-UB; (d) 100 % clinoptilolite .....83

Figure 3.3 Fitted Freundlich (dashed line) and Langmuir (solid line) adsorption models for zinc (Zn) adsorption: (a) unamended backfill sorbent; (b) 100 % chabazite-LB; (c) 100 % chabazite-UB; (d) 100 % clinoptilolite.....84

Figure 3.4 Fitted Freundlich (dashed line) and Langmuir (solid line) adsorption models for potassium (K) adsorption to zeolite-amended backfill sorbents: (a) 5 % chabazite-LB; (b) 10 % chabazite-LB; (c) 5 % chabazite-UB; (d) 10 % chabazite-UB; (e) 5 % clinoptilolite; (f) 10 % clinoptilolite .....85

Figure 3.5 Fitted Freundlich (dashed line) and Langmuir (solid line) adsorption models for zinc (Zn) adsorption to zeolite-amended backfill sorbents: (a) 5 % chabazite-LB; (b) 10 % chabazite-LB; (c) 5 % chabazite-UB; (d) 10 % chabazite-UB; (e) 5 % clinoptilolite; (f) 10 % clinoptilolite .....86

Figure 3.6 Initial salt solution pH versus the equilibrium (final) pH of the sorbate-sorbent suspension for sorbents with different percentages of zeolite amendment: (a) K with chabazite-LB; (b) Zn with chabazite-LB; (c) K with chabazite-UB; (d) Zn with chabazite-UB; (e) K with clinoptilolite; (f) Zn with clinoptilolite .....87

Figure 3.7 Ratio of the maximum adsorption capacity,  $Q_L$  (mg/kg) to the theoretical maximum

	solid-phase concentration, $C_{s,max}$ (mg/kg) for different types and amounts of zeolite: (a) $K^+$ ; (b) $Zn^{2+}$ ; (c) $ZnOH^+$ .....	88
Figure 3.8	Best-fit values of the Langmuir energy of adsorption ( $K_L$ ), maximum adsorption capacity ( $Q_L$ ), and $K_LQ_L$ for different types and amounts of zeolite: (a) $K_L$ for K; (b) $K_L$ for Zn; (c) $Q_L$ for K; (d) $Q_L$ for Zn; (e) $K_LQ_L$ for K; (f) $K_LQ_L$ for Zn .....	89
Figure 3.9	Best-fit values of the Freundlich unit adsorption capacity ( $K_f$ ) and exponent ( $N_f$ ) for different types and amounts of zeolite: (a) $K_f$ for K; (b) $K_f$ for Zn; (c) $N_f$ for K; (d) $N_f$ for Zn .....	90
Figure 3.10	Adsorption test results fitted to the Freundlich (dashed line) and Langmuir (solid line) adsorption models for different amounts of added zeolite: (a) K with chabazite-LB; (b) Zn with chabazite-LB; (c) K with chabazite-UB; (d) Zn with chabazite-UB; (e) K with clinoptilolite; (f) Zn with clinoptilolite .....	91
Figure 3.11	Comparison of the ratio of the maximum adsorption capacity ( $Q_L$ ) of the zeolite-amended backfill sorbents ( $Q_{L,amended}$ ) relative to the $Q_L$ of the unamended backfill sorbent ( $Q_{L,unamended}$ ) for different types and amounts of zeolite: (a) K including 100 % zeolite; (b) Zn including 100 % zeolite; (c) K for zeolite content $\leq 10$ %; (d) Zn for zeolite content $\leq 10$ % .....	92
Figure 3.12	Adsorption test results fitted to the Freundlich (dashed line) and Langmuir (solid line) adsorption models for different amounts and types of zeolite: (a) K with 5 % zeolite; (b) Zn with 5 % zeolite; (c) K with 10 % zeolite; (d) Zn with 10 % zeolite; (e) K with 100 % zeolite K; (f) Zn with 100 % zeolite .....	93
Figure 3.13	Comparison of the ratio of the maximum adsorption capacity ( $Q_L$ ) of the zeolite-amended backfill sorbents ( $Q_{L,amended}$ ) relative to the $Q_L$ of the unamended backfill sorbent ( $Q_{L,unamended}$ ) for different types of zeolite: (a) K with 5 % zeolite; (b) Zn with 5 % zeolite; (c) K with 10 % zeolite; (d) Zn with 10 % zeolite; (e) K with 100 % zeolite; (f) Zn with 100 % zeolite .....	94
Figure 3.14	Comparison of potassium (K) versus zinc (Zn) adsorption including fitted Freundlich (dash lines) and Langmuir (solid lines) adsorption models: (a) unamended backfill sorbent; (b) 100 % chabazite-LB; (c) 100 % chabazite-UB; (d) 100 % clinoptilolite.....	95
Figure 3.15	Comparison of potassium (K) versus zinc (Zn) adsorption including fitted Freundlich (dash lines) and Langmuir (solid lines) adsorption models for zeolite-amended backfill sorbents: (a) 5 % chabazite-LB; (b) 10 % chabazite-LB; (c) 5 % chabazite-UB; (d) 10 % chabazite-UB; (e) 5 % clinoptilolite; (f) 10 % clinoptilolite .....	96
Figure 4.1	Schematic of soil-bentonite vertical cutoff wall scenarios for model simulations: (a) plan view showing divergent groundwater flow; (b) cross-sectional view of cutoff wall illustrating boundary conditions .....	143

- Figure 4.2 Flux breakthrough curves for potassium as a function of adsorption model (Langmuir and Freundlich), zeolite content (0, 5, 10 %), and source concentration ( $C_o$ ): (a) chabazite-LB,  $C_o = 100$  mg/L; (b) chabazite-LB,  $C_o = 1,000$  mg/L; (c) chabazite-LB,  $C_o = 10,000$  mg/L; (d) chabazite-UB,  $C_o = 100$  mg/L; (e) chabazite-UB,  $C_o = 1,000$  mg/L; (f) chabazite-UB,  $C_o = 10,000$  mg/L; (g) clinoptilolite,  $C_o = 100$  mg/L; (h) clinoptilolite,  $C_o = 1,000$  mg/L; (i) clinoptilolite,  $C_o = 10,000$  mg/L...  
.....144
- Figure 4.3 Effect of adsorption behavior on potassium flux breakthrough curves for unamended backfill based on different adsorption models (Langmuir and Freundlich): (a), (c), (e) adsorption behaviors for concentration ranges of 100, 1,000, and 10,000 mg/L, respectively; (b), (d), (f) flux breakthrough curves for a source concentration ( $C_o$ ) of 100, 1,000, and 10,000 mg/L, respectively .....145
- Figure 4.4 Flux breakthrough curves for zinc as a function of adsorption model (Langmuir and Freundlich), zeolite content (0, 5, 10 %), and source concentration ( $C_o$ ): (a) chabazite-LB,  $C_o = 100$  mg/L; (b) chabazite-LB,  $C_o = 1,000$  mg/L; (c) chabazite-LB,  $C_o = 10,000$  mg/L; (d) chabazite-UB,  $C_o = 100$  mg/L; (e) chabazite-UB,  $C_o = 1,000$  mg/L; (f) chabazite-UB,  $C_o = 10,000$  mg/L; (g) clinoptilolite,  $C_o = 100$  mg/L; (h) clinoptilolite,  $C_o = 1,000$  mg/L; (i) clinoptilolite,  $C_o = 10,000$  mg/L .....146
- Figure 4.5 Effect of adsorption behavior on flux breakthrough curves for zinc based on different contents (0, 5, 10 %) of chabazite-UB and adsorption models (Langmuir and Freundlich): (a), (c), (e) adsorption behaviors over concentration ranges of 100, 1,000, and 10,000 mg/L, respectively; (b), (d), (f) flux breakthrough curves for a source concentration ( $C_o$ ) of 100, 1,000, and 10,000 mg/L, respectively .....147
- Figure 4.6 Effect of direction and magnitude of hydraulic gradient ( $i$ ) on flux breakthrough curves for unamended and zeolite-amended backfills based on the Langmuir adsorption model for a constant source concentration ( $C_o$ ) of 100 mg/L: (a) potassium (K), unamended; (b) zinc (Zn), unamended; (c) K, 5 % chabazite-LB-amended; (d) Zn, 5 % chabazite-LB-amended; (e) K, 10 % chabazite-LB-amended; (f) Zn, 10 % chabazite-LB-amended; (g) K, 5 % clinoptilolite-amended; (h) Zn, 5 % clinoptilolite-amended .....148
- Figure 4.7 Effect of direction and magnitude of hydraulic gradient ( $i$ ) on flux breakthrough curves for unamended and zeolite-amended backfills based on the Freundlich adsorption model for a constant source concentration ( $C_o$ ) of 100 mg/L: (a) potassium (K), unamended; (b) zinc (Zn), unamended; (c) K, 5 % chabazite-LB-amended; (d) Zn, 5 % chabazite-LB-amended; (e) K, 10 % chabazite-LB-amended; (f) Zn, 10 % chabazite-LB-amended; (g) K, 5 % clinoptilolite-amended; (h) Zn, 5 % clinoptilolite-amended .....149
- Figure 4.8 Effect of the zeolite content on barrier flux breakthrough times,  $T_B^*$  and  $t_B$ , based on  $f$  of 0.05 and source concentration ( $C_o$ ) of 100, 1,000, 10,000 mg/L for potassium (a, c, e) or zinc (b, d, f): (a) & (b) chabazite-LB; (c) & (d) chabazite-UB; (e) & (f) clinoptilolite .....150

- Figure 4.9 Effect of potassium (K) versus zinc (Zn) on the flux breakthrough curves for unamended and zeolite-amended backfills as a function of adsorption model (Langmuir and Freundlich), zeolite content (0, 5, 10 %), and source concentration ( $C_o$ ): (a) unamended,  $C_o = 100$  mg/L; (b) unamended,  $C_o = 1,000$  mg/L; (c) unamended,  $C_o = 10,000$  mg/L; (d) 5 % chabazite-LB,  $C_o = 100$  mg/L; (e) 5 % chabazite-LB,  $C_o = 1,000$  mg/L; (f) 5 % chabazite-LB,  $C_o = 10,000$  mg/L; (g) 10 % chabazite-LB,  $C_o = 100$  mg/L; (h) 10 % chabazite-LB,  $C_o = 1,000$  mg/L; (i) 10 % chabazite-LB,  $C_o = 10,000$  mg/L.....151
- Figure 4.10 Effect of potassium (K) versus zinc (Zn) on the flux breakthrough curves for unamended and zeolite-amended backfills as a function of adsorption model (Langmuir and Freundlich), zeolite content (0, 5, 10 %), and source concentration ( $C_o$ ): (a) unamended,  $C_o = 100$  mg/L; (b) unamended,  $C_o = 1,000$  mg/L; (c) unamended,  $C_o = 10,000$  mg/L; (d) 5 % chabazite-UB,  $C_o = 100$  mg/L; (e) 5 % chabazite-UB,  $C_o = 1,000$  mg/L; (f) 5 % chabazite-UB,  $C_o = 10,000$  mg/L; (g) 10 % chabazite-UB,  $C_o = 100$  mg/L; (h) 10 % chabazite-UB,  $C_o = 1,000$  mg/L; (i) 10 % chabazite-UB,  $C_o = 10,000$  mg/L .....152
- Figure 4.11 Effect of potassium (K) versus zinc (Zn) on the flux breakthrough curves for unamended and zeolite-amended backfills as a function of adsorption model (Langmuir and Freundlich), zeolite content (0, 5, 10 %), and source concentration ( $C_o$ ): (a) unamended,  $C_o = 100$  mg/L; (b) unamended,  $C_o = 1,000$  mg/L; (c) unamended,  $C_o = 10,000$  mg/L; (d) 5 % clinoptilolite,  $C_o = 100$  mg/L; (e) 5 % clinoptilolite,  $C_o = 1,000$  mg/L; (f) 5 % clinoptilolite,  $C_o = 10,000$  mg/L; (g) 10 % clinoptilolite,  $C_o = 100$  mg/L; (h) 10 % clinoptilolite,  $C_o = 1,000$  mg/L; (i) 10 % clinoptilolite,  $C_o = 10,000$  mg/L.....153
- Figure 4.12 Effect of the type of zeolite on the flux breakthrough curve for unamended backfill versus zeolite-amended backfill for a potassium source concentration ( $C_o$ ): (a) 5 % zeolite,  $C_o = 100$  mg/L; (b) 5 % zeolite,  $C_o = 1,000$  mg/L; (c) 5 % zeolite,  $C_o = 10,000$  mg/L; (d) 10 % zeolite,  $C_o = 100$  mg/L; (e) 10 % zeolite,  $C_o = 1,000$  mg/L; (f) 10 % zeolite,  $C_o = 10,000$  mg/L (Z-LB = chabazite-LB-amended backfill, Z-UB = chabazite-UB-amended backfill, Z-CL = clinoptilolite-amended backfill) .....154
- Figure 4.13 Effect of the type of zeolite on the flux breakthrough curve for unamended backfill versus zeolite-amended backfill for a zinc source concentration ( $C_o$ ): (a) 5 % zeolite,  $C_o = 100$  mg/L; (b) 5 % zeolite,  $C_o = 1,000$  mg/L; (c) 5 % zeolite,  $C_o = 10,000$  mg/L; (d) 10 % zeolite,  $C_o = 100$  mg/L; (e) 10 % zeolite,  $C_o = 1,000$  mg/L; (f) 10 % zeolite,  $C_o = 10,000$  mg/L (Z-LB = chabazite-LB-amended backfill, Z-UB = chabazite-UB-amended backfill, Z-CL = clinoptilolite-amended backfill).....155
- Figure 4.14 Relationship between direction and magnitude of hydraulic gradient ( $i$ ) and barrier flux breakthrough time based  $J^*(L,t)$  of 0.015 for unamended and 5 % zeolite-amended backfills: (a), (c), (e) potassium source concentration ( $C_o$ ) of 100, 1,000, and 10,000 mg/L, respectively; (b), (d), (f) zinc  $C_o$  of 100, 1,000, and 10,000 mg/L respectively. Note: dashed line = Freundlich adsorption model; solid line = Langmuir adsorption model.....156

Figure 4.15	Relative effect of zeolite amendment on the incremental change in barrier flux breakthrough time due to a reversal in hydraulic gradient, $\Delta t_{B,i,amended}/\Delta t_{B,i,unamended}$ , as a function of zeolite content: (a), (c), (e) potassium source concentration ( $C_o$ ) of 100, 1,000, and 10,000 mg/L, respectively; (b), (d), (f) zinc $C_o$ of 100, 1,000, and 10,000 mg/L respectively. Note: solid line = Langmuir adsorption model; dashed line = Freundlich adsorption model.....	157
Figure 4.16	Effect of constant potassium source concentration ( $C_o$ ) on the dimensionless barrier breakthrough times, $T_B^*$ (a, c, e) for $f = 0.05$ and flux breakthrough curves (b, d, f) for unamended and zeolite-amended backfills: (a) & (b) unamended; (c) & (d) 5 % chabazite-LB-amended; (e) & (f) 5 % chabazite-UB-amended; (g) & (h) 5 % clinoptilolite-amended.....	158
Figure 4.17	Effect of constant potassium source concentration ( $C_o$ ) on the dimensionless barrier breakthrough times, $T_B^*$ (a, c, e) for $f = 0.05$ and flux breakthrough curves (b, d, f) for unamended and zeolite-amended backfills: (a) & (b) unamended; (c) & (d) 10 % chabazite-LB-amended; (e) & (f) 10 % chabazite-UB-amended; (g) & (h) 10 % clinoptilolite-amended.....	159
Figure 4.18	Effect of constant zinc source concentration ( $C_o$ ) on the dimensionless barrier breakthrough times, $T_B^*$ (a, c, e) for $f = 0.05$ and flux breakthrough curves (b, d, f) for unamended and zeolite-amended backfills: (a) & (b) unamended; (c) & (d) 5 % chabazite-LB-amended; (e) & (f) 5 % chabazite-UB-amended; (g) & (h) 5 % clinoptilolite-amended.....	160
Figure 4.19	Effect of constant zinc source concentration ( $C_o$ ) on the dimensionless barrier breakthrough times, $T_B^*$ (a, c, e) for $f = 0.05$ and flux breakthrough curves (b, d, f) for unamended and zeolite-amended backfills: (a) & (b) unamended; (c) & (d) 10 % chabazite-LB-amended; (e) & (f) 10 % chabazite-UB-amended; (g) & (h) 10 % clinoptilolite-amended.....	161
Figure 5.1	Schematic of testing apparatus.....	227
Figure 5.2	Pictorial views of (a) Apparatus No. 1 (Model 944); (b) Apparatus No. 2 (Model 940); (c) Apparatus No. 3 (Model 940).....	228
Figure 5.3	Schematic scenario for placement of soil-bentonite (SB) vertical cutoff wall down gradient from a migrating contaminant plume.....	229
Figure 5.4	Comparison of the chemical analysis methods: (a) relative concentration ( $RC$ ); (b) cumulative mass ratio ( $CMR$ ) and the x-intercept from the $CMR$ -to- $T$ plot; (c) $T$ - $CMR$ .....	230
Figure 5.5	Pictorial view of the finished column test specimens.....	231
Figure 5.6	Temporal trends in pressure differences across columns of unamended backfills permeated with different salt solutions: (a) 35 mM KCl (Test No. 1); (b) 20 mM $ZnCl_2$ (Test No. 2).....	232

Figure 5.7	Temporal trends in pressure differences across columns of backfills amended with 5 % chabazite-UB and permeated with different salt solutions: (a) 35 mM KCl (Test No. 3); (b) 20 mM ZnCl <sub>2</sub> (Test No. 4); (c) 17.5 mM KCl plus 10 mM ZnCl <sub>2</sub> (Test No. 5).....	233
Figure 5.8	Temporal trends in pressure differences across columns of backfills amended with 5 % clinoptilolite and permeated with different salt solutions: (a) 35 mM KCl (Test No. 6); (b) 20 mM ZnCl <sub>2</sub> (Test No. 7); (c) 17.5 mM KCl plus 10 mM ZnCl <sub>2</sub> (Test No. 8).....	234
Figure 5.9	Temporal trends in pressure differences across columns of backfills amended with different amounts of chabazite-LB and permeated with a solution of 35 mM KCl: (a) 5 % chabazite-LB (Test No. 9); (b) 10 % chabazite-LB (Test No. 10).....	235
Figure 5.10	Temporal trends in hydraulic conductivity for columns of unamended backfills permeated with different salt solutions: (a) 35 mM KCl (Test No. 1); (b) 20 mM ZnCl <sub>2</sub> (Test No. 2).....	236
Figure 5.11	Temporal trends in hydraulic conductivity for columns of backfills amended with 5 % chabazite-UB and permeated with different salt solutions: (a) 35 mM KCl (Test No. 3); (b) 20 mM ZnCl <sub>2</sub> (Test No. 4); (c) 17.5 mM KCl plus 10 mM ZnCl <sub>2</sub> (Test No. 5).....	237
Figure 5.12	Temporal trends in hydraulic conductivity for columns of backfills amended with 5 % clinoptilolite and permeated with different salt solutions: (a) 35 mM KCl (Test No. 6); (b) 20 mM ZnCl <sub>2</sub> (Test No. 7); (c) 17.5 mM KCl plus 10 mM ZnCl <sub>2</sub> (Test No. 8).....	238
Figure 5.13	Temporal trends in hydraulic conductivity for columns of backfills amended with different amounts of chabazite-LB and permeated with a solution of 35 mM KCl: (a) 5 % chabazite-LB (Test No. 9); (b) 10 % chabazite-LB (Test No. 10).....	239
Figure 5.14	Comparison of the measured hydraulic conductivity based on column test, $k_{DRW}$ versus $k_{salt}$ .....	240
Figure 5.15	Temporal trends in effluent solute concentrations for columns of unamended backfills permeated with different salt solutions: (a) 35 mM KCl (Test No. 1); (b) 20 mM ZnCl <sub>2</sub> (Test No. 2).....	241
Figure 5.16	Temporal trends in effluent solute concentrations for columns of backfills amended with 5 % chabazite-UB and permeated with different salt solutions: (a) 35 mM KCl (Test No. 3); (b) 20 mM ZnCl <sub>2</sub> (Test No. 4); (c) 17.5 mM KCl plus 10 mM ZnCl <sub>2</sub> (Test No. 5).....	242
Figure 5.17	Temporal trends in effluent solute concentrations for columns of backfills amended with 5 % clinoptilolite and permeated with different salt solutions: (a) 35 mM KCl (Test No. 6); (b) 20 mM ZnCl <sub>2</sub> (Test No. 7); (c) 17.5 mM KCl plus 10 mM ZnCl <sub>2</sub> (Test No. 8).....	243

Figure 5.18	Temporal trends in effluent solute concentrations for columns of backfills amended with different amounts of chabazite-LB and permeated with a solution of 35 mM KCl: (a) 5 % chabazite-LB (Test No. 9); (b) 10 % chabazite-LB (Test No. 10)....	244
Figure 5.19	Temporal trends in effluent solute flux for columns of unamended backfills permeated with different salt solutions: (a) 35 mM KCl (Test No. 1); (b) 20 mM ZnCl <sub>2</sub> (Test No. 2).....	245
Figure 5.20	Temporal trends in effluent solute flux for columns of backfills amended with 5 % chabazite-UB and permeated with different salt solutions: (a) 35 mM KCl (Test No. 3); (b) 20 mM ZnCl <sub>2</sub> (Test No. 4); (c) 17.5 mM KCl plus 10 mM ZnCl <sub>2</sub> (Test No. 5) .....	246
Figure 5.21	Temporal trends in effluent solute flux from for columns of backfills amended with 5 % clinoptilolite and permeated with different salt solutions: (a) 35 mM KCl (Test No. 6); (b) 20 mM ZnCl <sub>2</sub> (Test No. 7); (c) 17.5 mM KCl plus 10 mM ZnCl <sub>2</sub> (Test No. 8).....	247
Figure 5.22	Temporal trends in effluent solute flux for columns of backfills amended with different amounts of chabazite-LB and permeated with a solution of 35 mM KCl: (a) 5 % chabazite-LB (Test No. 9); (b) 10 % chabazite-LB (Test No. 10).....	248
Figure 5.23	Temporal trends in effluent charge balance for columns of unamended backfills permeated with different salt solutions: (a) 35 mM KCl (Test No. 1); (b) 20 mM ZnCl <sub>2</sub> (Test No. 2). [Note: absolute values for the $\sum$ anion equivalents are shown] ....	249
Figure 5.24	Temporal trends in effluent charge balance for columns of backfills amended with 5 % chabazite-UB and permeated with different salt solutions: (a) 35 mM KCl (Test No. 3); (b) 20 mM ZnCl <sub>2</sub> (Test No. 4); (c) 17.5 mM KCl plus 10 mM ZnCl <sub>2</sub> (Test No. 5). [Note: absolute values for the $\sum$ anion equivalents are shown] .....	250
Figure 5.25	Temporal trends in effluent charge balance for columns of backfills amended with 5 % clinoptilolite and permeated with different salt solutions: (a) 35 mM KCl (Test No. 6); (b) 20 mM ZnCl <sub>2</sub> (Test No. 7); (c) 17.5 mM KCl plus 10 mM ZnCl <sub>2</sub> (Test No. 8). [Note: absolute values for the $\sum$ anion equivalents are shown] .....	251
Figure 5.26	Temporal trends in effluent charge balance for columns of backfills amended with different amounts of chabazite-LB and permeated with a solution of 35 mM KCl (Test No. 9): (a) 5 % chabazite-LB; (b) 10 % chabazite-LB (Test No. 10). [Note: absolute values for the $\sum$ anion equivalents are shown].....	252
Figure 5.27	Temporal trends in the electrical conductivity of the effluent for columns with unamended backfills permeated with different salt solutions: (a) 35 mM KCl (Test No. 1); (b) 20 mM ZnCl <sub>2</sub> (Test No. 2) .....	253
Figure 5.28	Temporal trends in the electrical conductivity of the effluent from columns of backfills amended with 5 % chabazite-UB permeated with different salt solutions: (a) 35 mM KCl (Test No. 3); (b) 20 mM ZnCl <sub>2</sub> (Test No. 4); (c) 17.5 mM KCl plus	

	10 mM ZnCl <sub>2</sub> (Test No. 5) .....	254
Figure 5.29	Temporal trends in the electrical conductivity of the effluent for columns of backfills amended with 5 % clinoptilolite permeated with different salt solutions: (a) 35 mM KCl (Test No. 6); (b) 20 mM ZnCl <sub>2</sub> (Test No. 7); (c) 17.5 mM KCl plus 10 mM ZnCl <sub>2</sub> (Test No. 8) .....	255
Figure 5.30	Temporal trends in the electrical conductivity of the effluent for columns of backfills amended with different amounts of chabazite-LB and permeated with a solution of 35 mM KCl: (a) 5 % chabazite-LB (Test No. 9); (b) 10 % chabazite-LB (Test No. 10) .....	256
Figure 5.31	Temporal trends in the pH of the effluent for columns with unamended backfills permeated with different salt solutions: (a) 35 mM KCl (Test No. 1); (b) 20 mM ZnCl <sub>2</sub> (Test No. 2) .....	257
Figure 5.32	Temporal trends in the pH of the effluent from columns of backfills amended with 5 % chabazite-UB permeated with different salt solutions: (a) 35 mM KCl (Test No. 3); (b) 20 mM ZnCl <sub>2</sub> (Test No. 4); (c) 17.5 mM KCl plus 10 mM ZnCl <sub>2</sub> (Test No. 5) .....	258
Figure 5.33	Temporal trends in the pH of the effluent for columns of backfills amended with 5 % clinoptilolite permeated with different salt solutions: (a) 35 mM KCl (Test No. 6); (b) 20 mM ZnCl <sub>2</sub> (Test No. 7); (c) 17.5 mM KCl plus 10 mM ZnCl <sub>2</sub> (Test No. 8) .....	259
Figure 5.34	Temporal trends in the pH of the effluent for columns of backfills amended with different amounts of chabazite-LB and permeated with a solution of 35 mM KCl: (a) 5 % chabazite-LB (Test No. 9); (b) 10 % chabazite-LB (Test No. 10) .....	260
Figure 5.35	Chemical transport analyses for determination of column Péclet number ( $P_L$ ) and/or retardation factor ( $R_d$ ) for unamended backfill permeated with 35 mM KCl (Test No. 1): (a) regression of relative concentration ( $RC$ ) data; (b) regression of cumulative mass ratio ( $CMR$ ) data; (c) $T_o (= R_d)$ and $T - CMR$ analyses for $R_d$ ...	261
Figure 5.36	Chemical transport analyses for determination of column Péclet number ( $P_L$ ) and/or retardation factor ( $R_d$ ) for unamended backfill permeated with 20 mM ZnCl <sub>2</sub> (Test No. 2): (a) regression of relative concentration ( $RC$ ) data; (b) regression of cumulative mass ratio ( $CMR$ ) data; (c) $T_o (= R_d)$ and $T - CMR$ analyses for $R_d$ ...	262
Figure 5.37	Chemical transport analyses for determination of column Péclet number ( $P_L$ ) and/or retardation factor ( $R_d$ ) for unamended backfill permeated with 20 mM ZnCl <sub>2</sub> (Test No. 2): (a) regression of relative concentration ( $RC$ ) data; (b) regression of cumulative mass ratio ( $CMR$ ) data; (c) $T_o (= R_d)$ and $T - CMR$ analyses for $R_d$ ...	263
Figure 5.38	Chemical transport analyses for determination of column Péclet number ( $P_L$ ) and/or retardation factor ( $R_d$ ) for backfill amended with 5 % chabazite-UB and permeated with 35 mM KCl (Test No. 3): (a) regression of relative concentration ( $RC$ ) data; (b)	

- regression of cumulative mass ratio (*CMR*) data; (c)  $T_o (= R_d)$  and  $T - CMR$  analyses for  $R_d$ .....264
- Figure 5.39 Chemical transport analyses for determination of column Péclet number ( $P_L$ ) and/or retardation factor ( $R_d$ ) for backfill amended with 5 % chabazite-UB and permeated with 20 mM  $ZnCl_2$  (Test No. 4): (a) regression of relative concentration (*RC*) data; (b) regression of cumulative mass ratio (*CMR*) data; (c)  $T_o (= R_d)$  and  $T - CMR$  analyses for  $R_d$ .....265
- Figure 5.40 Chemical transport analyses for determination of column Péclet number ( $P_L$ ) and/or retardation factor ( $R_d$ ) for backfill amended with 5 % chabazite-UB and permeated with 17.5 mM KCl plus 10 mM  $ZnCl_2$  (Test No. 5): (a) regression of relative concentration (*RC*) data; (b) regression of cumulative mass ratio (*CMR*) data; (c)  $T_o (= R_d)$  and  $T - CMR$  analyses for  $R_d$  .....266
- Figure 5.41 Chemical transport analyses for determination of column Péclet number ( $P_L$ ) and/or retardation factor ( $R_d$ ) for backfill amended with 5 % clinoptilolite and permeated with 35 mM KCl (Test No. 6): (a) regression of relative concentration (*RC*) data; (b) regression of cumulative mass ratio (*CMR*) data; (c)  $T_o (= R_d)$  and  $T - CMR$  analyses for  $R_d$ .....267
- Figure 5.42 Chemical transport analyses for determination of column Péclet number ( $P_L$ ) and/or retardation factor ( $R_d$ ) for backfill amended with 5 % clinoptilolite and permeated with 20 mM  $ZnCl_2$  (Test No. 7): (a) regression of relative concentration (*RC*) data; (b) regression of cumulative mass ratio (*CMR*) data; (c)  $T_o (= R_d)$  and  $T - CMR$  analyses for  $R_d$ .....268
- Figure 5.43 Chemical transport analyses for determination of column Péclet number ( $P_L$ ) and/or retardation factor ( $R_d$ ) for backfill amended with 5 % clinoptilolite and permeated with 17.5 mM KCl plus 10 mM  $ZnCl_2$  (Test No. 8): (a) regression of relative concentration (*RC*) data; (b) regression of cumulative mass ratio (*CMR*) data; (c)  $T_o (= R_d)$  and  $T - CMR$  analyses for  $R_d$  .....269
- Figure 5.44 Chemical transport analyses for determination of column Péclet number ( $P_L$ ) and/or retardation factor ( $R_d$ ) for backfill amended with 5 % chabazite-LB and permeated with 35 mM KCl (Test No. 9): (a) regression of relative concentration (*RC*) data; (b) regression of cumulative mass ratio (*CMR*) data; (c)  $T_o (= R_d)$  and  $T - CMR$  analyses for  $R_d$ .....270
- Figure 5.45 Chemical transport analyses for determination of column Péclet number ( $P_L$ ) and/or retardation factor ( $R_d$ ) for backfill amended with 10 % chabazite-LB and permeated with 35 mM KCl (Test No. 10): (a) regression of relative concentration (*RC*) data; (b) regression of cumulative mass ratio (*CMR*) data; (c)  $T_o (= R_d)$  and  $T - CMR$  analyses for  $R_d$ .....271
- Figure 5.46 Comparison of the retardation factor ( $R_d$ ): (a)  $R_d$  from relative concentration (*RC*) versus  $R_d$  from cumulative mass ratio (*CMR*); (b)  $R_d$  from *RC* versus  $R_d$  from steady-state *CMR*; (c)  $R_d$  from *CMR* versus  $R_d$  from steady-state *CMR*; (d)  $R_d$  from

	$(T-CMR)$ versus $T_o$ .....	272
Figure 5.47	Comparison of the Péclet Number ( $P_L$ ), and dispersion coefficient ( $D$ ) from relative concentration ( $RC$ ) and cumulative mass ratio ( $CMR$ ): (a) $P_L$ from $RC$ versus $CMR$ ; (b) $R_d$ from $RC$ versus steady-state $CMR$ ; (b) $D$ from $RC$ versus $CMR$ .....	273
Figure 5.48	The Freundlich sorption parameters as a function of (a) soil-to-solution ratio and (b) the gravimetric water content (data from Manassero <i>et al.</i> 1998) .....	274
Figure 5.49	Comparison of the retardation factor ( $R_d$ ) and distribution coefficient ( $K_d$ ) based on the column test and batch equilibrium adsorption tests (BEATs): (a) $R_{d,BEAT}$ (Langmuir model) versus $R_{d,Column}$ ; (b) $R_{d,BEAT}$ (Freundlich model) versus $R_{d,Column}$ ; (c) $K_{d,BEAT}$ (Langmuir model) versus $K_{d,Column}$ ; (d) $K_{d,BEAT}$ (Freundlich model) versus $K_{d,Column}$ .....	275
Figure 5.50	Comparison of the retardation factor ( $R_d$ ) and distribution coefficient ( $K_d$ ) based on the $CMR$ regression to the column test and batch equilibrium adsorption tests (BEATs): (a) $R_{d,BEAT}$ (Langmuir model) versus $R_{d,Column}$ ; (b) $R_{d,BEAT}$ (Freundlich model) versus $R_{d,Column}$ ; (c) $K_{d,BEAT}$ (Langmuir model) versus $K_{d,Column}$ ; (d) $K_{d,BEAT}$ (Freundlich model) versus $K_{d,Column}$ .....	276
Figure 5.51	Comparison of the retardation factor ( $R_d$ ) based on the $CMR$ regression to the column test and batch equilibrium adsorption test (BEAT): (a) $R_{d,BEAT}$ (Langmuir model) versus $R_{d,Column}$ for 35 mM KCl; (b) $R_{d,BEAT}$ (Freundlich model) versus $R_{d,Column}$ for 35 mM KCl; (c) $R_{d,BEAT}$ (Langmuir model) versus $R_{d,Column}$ for 20 mM ZnCl <sub>2</sub> ; (d) $R_{d,BEAT}$ (Freundlich model) versus $R_{d,Column}$ for 20 mM ZnCl <sub>2</sub> ; (e) $R_{d,BEAT}$ (Langmuir model) versus $R_{d,Column}$ for 17.5 mM KCl plus 10 mM ZnCl <sub>2</sub> ; (f) $R_{d,BEAT}$ (Freundlich model) versus $R_{d,Column}$ for 17.5 mM KCl plus 10 mM ZnCl <sub>2</sub> .....	277
Figure 5.52	Comparison of the retardation factor ( $K_d$ ) based on the $CMR$ regression to the column test and batch equilibrium adsorption test (BEAT): (a) $K_{d,BEAT}$ (Langmuir model) versus $K_{d,Column}$ for 35 mM KCl; (b) $K_{d,BEAT}$ (Freundlich model) versus $K_{d,Column}$ for 35 mM KCl; (c) $K_{d,BEAT}$ (Langmuir model) versus $K_{d,Column}$ for 20 mM ZnCl <sub>2</sub> ; (d) $K_{d,BEAT}$ (Freundlich model) versus $K_{d,Column}$ for 20 mM ZnCl <sub>2</sub> ; (e) $K_{d,BEAT}$ (Langmuir model) versus $K_{d,Column}$ for 17.5 mM KCl plus 10 mM ZnCl <sub>2</sub> ; (f) $K_{d,BEAT}$ (Freundlich model) versus $K_{d,Column}$ for 17.5 mM KCl plus 10 mM ZnCl <sub>2</sub> .....	278
Figure 5.53	Breakthrough curves for unamended and zeolite-amended backfills permeated with 35 mM KCl: (a) chloride (Cl <sup>-</sup> ) versus time ( $t$ ); (b) Cl <sup>-</sup> versus dimensionless time ( $T$ ); (c) potassium (K <sup>+</sup> ) versus $t$ ; (d) K <sup>+</sup> versus $T$ .....	279
Figure 5.54	Effect of type of zeolite on retardation of potassium (K <sup>+</sup> ) for columns of unamended and zeolite-amended backfills permeated with 35 mM KCl: (a) retardation factor ( $R_d$ ); (b) ratio of $R_d$ for the zeolite-amended backfill relative to $R_d$ for the unamended backfill ( $R_{d,amended}/R_{d,unamended}$ ); (c) cation exchange capacity ( $CEC$ ) of backfill and $R_d$ of K <sup>+</sup> .....	280
Figure 5.55	Effect of type of zeolite on transport parameters for columns of unamended and	

	zeolite-amended backfills permeated with 35 mM KCl: (a) Péclet number ( $P_L$ ) for chloride ( $\text{Cl}^-$ ); (b) hydrodynamic dispersion coefficient ( $D$ ) for $\text{Cl}^-$ ; (c) $P_L$ for potassium ( $\text{K}^+$ ); (d) $D$ for $\text{K}^+$ .....	281
Figure 5.56	Breakthrough curves for unamended and zeolite-amended backfills permeated with 20 mM $\text{ZnCl}_2$ : (a) chloride ( $\text{Cl}^-$ ) versus time ( $t$ ); (b) $\text{Cl}^-$ versus dimensionless time ( $T$ ); (c) zinc ( $\text{Zn}^{2+}$ ) versus $t$ ; (d) $\text{Zn}^{2+}$ versus $T$ .....	282
Figure 5.57	Effect of type of zeolite on retardation of zinc ( $\text{Zn}^{2+}$ ) for columns of unamended and zeolite-amended backfills permeated with 20 mM $\text{ZnCl}_2$ : (a) retardation factor ( $R_d$ ); (b) ratio of $R_d$ for the zeolite-amended backfill relative to $R_d$ for the unamended backfill ( $R_{d,amended}/R_{d,unamended}$ ); (c) cation exchange capacity ( $\text{CEC}$ ) of backfill and $R_d$ of $\text{Zn}^{2+}$ .....	283
Figure 5.58	Effect of type of zeolite on transport parameters for columns of unamended and zeolite-amended backfills permeated with 20 mM $\text{ZnCl}_2$ : (a) Péclet number ( $P_L$ ) for chloride ( $\text{Cl}^-$ ); (b) hydrodynamic dispersion coefficient ( $D$ ) for $\text{Cl}^-$ ; (c) $P_L$ for potassium ( $\text{K}^+$ ); (d) $D$ for $\text{K}^+$ .....	284
Figure 5.59	Breakthrough curves for backfills with 0 (unamended), 5 and 10 % chabazite-LB permeated with 35 mM KCl: (a) chloride ( $\text{Cl}^-$ ) versus time ( $t$ ); (b) $\text{Cl}^-$ versus dimensionless time ( $T$ ); (c) potassium ( $\text{K}^+$ ) versus $t$ ; (d) $\text{K}^+$ versus $T$ .....	285
Figure 5.60	Effect of amount of zeolite on retardation of potassium ( $\text{K}^+$ ) for backfills with 0 (unamended), 5 and 10 % chabazite-LB permeated with 35 mM KCl: (a) retardation factor ( $R_d$ ); (b) ratio of $R_d$ for the zeolite-amended backfill relative to $R_d$ for the unamended backfill ( $R_{d,amended}/R_{d,unamended}$ ); (c) cation exchange capacity ( $\text{CEC}$ ) of backfill and $R_d$ of $\text{K}^+$ .....	286
Figure 5.61	Effect of amount of zeolite on the Péclet number ( $P_L$ ) and hydrodynamic dispersion coefficient ( $D$ ) of chloride ( $\text{Cl}^-$ ) and potassium ( $\text{K}^+$ ) for backfills with 0 (unamended), 5 and 10 % chabazite-LB permeated with 35 mM KCl: (a) $P_L$ for $\text{Cl}^-$ ; (b) $D$ for $\text{Cl}^-$ ; (c) $P_L$ for $\text{K}^+$ ; (d) $D$ for $\text{K}^+$ .....	287
Figure 5.62	Breakthrough curves for unamended backfill permeated with 35 mM KCl or 20 mM $\text{ZnCl}_2$ : (a) chloride ( $\text{Cl}^-$ ) versus time ( $t$ ); (b) $\text{Cl}^-$ versus dimensionless time ( $T$ ); (c) potassium ( $\text{K}^+$ ) and zinc ( $\text{Zn}^{2+}$ ) versus $t$ ; (d) $\text{K}^+$ and $\text{Zn}^{2+}$ versus $T$ .....	288
Figure 5.63	Effect of type of metal on transport parameters for columns of unamended backfill permeated with 35 mM KCl or 20 mM $\text{ZnCl}_2$ : (a) Péclet number ( $P_L$ ) for chloride ( $\text{Cl}^-$ ); (b) hydrodynamic dispersion coefficient ( $D$ ) for $\text{Cl}^-$ ; (c) retardation factor ( $R_d$ ) for potassium ( $\text{K}^+$ ) and zinc ( $\text{Zn}^{2+}$ ); (d) $Q_L$ versus $K_d$ ; (e) $P_L$ for $\text{K}^+$ and $\text{Zn}^{2+}$ ; (f) $D$ for $\text{K}^+$ and $\text{Zn}^{2+}$ .....	289
Figure 5.64	Breakthrough curves for backfill amended with 5 % chabazite-UB and permeated with 35 mM KCl or 20 mM $\text{ZnCl}_2$ : (a) chloride ( $\text{Cl}^-$ ) versus time ( $t$ ); (b) $\text{Cl}^-$ versus dimensionless time ( $T$ ); (c) potassium ( $\text{K}^+$ ) and zinc ( $\text{Zn}^{2+}$ ) versus $t$ ; (d) $\text{K}^+$ and $\text{Zn}^{2+}$ versus $T$ .....	290

- Figure 5.65 Effect of type of metal on transport parameters for columns of 5 % chabazite-UB-amended backfill permeated with 35 mM KCl or 20 mM ZnCl<sub>2</sub>: (a) Péclet number ( $P_L$ ) for chloride (Cl<sup>-</sup>); (b) hydrodynamic dispersion coefficient ( $D$ ) for Cl<sup>-</sup>; (c) retardation factor ( $R_d$ ) for potassium (K<sup>+</sup>) and zinc (Zn<sup>2+</sup>); (d)  $Q_L$  versus  $K_d$ ; (e)  $P_L$  for K<sup>+</sup> and Zn<sup>2+</sup>; (f)  $D$  for K<sup>+</sup> and Zn<sup>2+</sup> .....291
- Figure 5.66 Breakthrough curves for backfill amended with 5 % clinoptilolite and permeated with 35 mM KCl or 20 mM ZnCl<sub>2</sub>: (a) chloride (Cl<sup>-</sup>) versus time ( $t$ ); (b) Cl<sup>-</sup> versus dimensionless time ( $T$ ); (c) potassium (K<sup>+</sup>) and zinc (Zn<sup>2+</sup>) versus  $t$ ; (d) K<sup>+</sup> and Zn<sup>2+</sup> versus  $T$  .....292
- Figure 5.67 Effect of type of metal on transport parameters for backfill amended with 5 % clinoptilolite and permeated with 35 mM KCl or 20 mM ZnCl<sub>2</sub>: (a) Péclet number ( $P_L$ ) for chloride (Cl<sup>-</sup>); (b) hydrodynamic dispersion coefficient ( $D$ ) for Cl<sup>-</sup>; (c) retardation factor ( $R_d$ ) for potassium (K<sup>+</sup>) and zinc (Zn<sup>2+</sup>); (d)  $K_d$  versus  $R_d$ ; (e)  $P_L$  for K<sup>+</sup> and Zn<sup>2+</sup>; (f)  $D$  for K<sup>+</sup> and Zn<sup>2+</sup> .....293
- Figure 5.68 Effect of cation competition on transport parameters for backfill amended with 5 % chabazite-UB and permeated with 17.5 mM KCl plus 10 mM ZnCl<sub>2</sub> solution: (a) retardation factor ( $R_d$ ) for potassium (K<sup>+</sup>) and zinc (Zn<sup>2+</sup>); (b)  $Q_L$  versus  $K_d$ ; (c) Péclet number ( $P_L$ ) for K<sup>+</sup> and Zn<sup>2+</sup>; (d)  $D$  for K<sup>+</sup> and Zn<sup>2+</sup> .....294
- Figure 5.69 Effect of cation competition on transport parameters for backfill amended with 5 % clinoptilolite and permeated with 17.5 mM KCl plus 10 mM ZnCl<sub>2</sub> solution: (a) retardation factor ( $R_d$ ) for potassium (K<sup>+</sup>) and zinc (Zn<sup>2+</sup>); (b)  $Q_L$  versus  $K_d$ ; (c) Péclet number ( $P_L$ ) for K<sup>+</sup> and Zn<sup>2+</sup>; (d)  $D$  for K<sup>+</sup> and Zn<sup>2+</sup> .....295

## CHAPTER 1 INTRODUCTION

### 1.1 BACKGROUND

Soil-bentonite (SB) vertical cutoff walls are used extensively as *in situ* containment barriers to prevent or control subsurface migration of contaminated groundwater (*e.g.*, USEPA 1984; Ryan 1984, 1987; Daniel and Koerner 1993; Manassero *et al.* 1995; Rumer and Mitchell 1995; Rumer and Ryan 1995; LaGrega *et al.* 2001; Mitchell *et al.* 2007; Fan *et al.* 2014; Du *et al.* 2015; Hudak 2016). These barriers are constructed by excavating a trench to a desired depth, typically using a backhoe for shallower depths and a clamshell for deeper depths, placing a bentonite slurry comprising a mixture of water with 3-5 % (dry weight) sodium bentonite into the excavated trench to maintain trench stability, mixing the trenched spoils with the bentonite slurry to achieve a desired slump of 100 to 150 mm (3.9 to 5.9 in), and backfilling the slurry filled trench with the slurry mixed trench spoils (*i.e.*, backfill), thereby displacing the slurry from the trench and forming a relatively low-permeability barrier that impedes groundwater flow (Xanthakos 1979, D'Appolonia 1980, Spooner *et al.* 1984, Ryan 1987, Millet *et al.* 1992, Evans 1994, Rumer and Ryan 1995). The width of SB vertical cutoff walls generally is the same as the width of the trenching equipment, which typically is on the order of  $1.0 \pm 0.5$  m. Depths on the order of 50 m are possible (*e.g.*, Ryan and Spaulding 2008), although shallower depths (< 30 m) are more common.

The preferred use of SB vertical cutoff walls relative to other options such as *in situ* treatment technologies results from several considerations. First, SB vertical cutoff walls typically are cheaper than treatment systems. Second, SB vertical cutoff walls cause less risk of contaminant exposure during construction. Third, SB vertical cutoff walls can be used to contain contaminated groundwater until more efficient and/or more cost effective treatment technologies

are developed (Shackelford and Jefferis 2000). For cases in which treatment of subsurface contamination contained with SB vertical cutoff walls is not feasible due to a lack of cost-effective treatment technologies, the performance period required for cutoff walls to effectively contain the contaminants often is undefined (Inyang and de Brito Galvao 2004). In these cases, a cutoff wall may be expected to perform for a long period (*e.g.*, a decade or more). For this reason, increasingly greater consideration is being given to contaminant attenuation within the SB backfill due to physical, chemical, and/or biological reactions. Although most SB vertical cutoff walls have some intrinsic capacity to attenuate specific contaminants during migration through the walls (*e.g.*, via adsorption of metals to the bentonite portion of the backfill), available evidence suggests that this intrinsic attenuation capacity is limited (Shackelford 1997, 2014). As a result, the concept of designing SB vertical cutoff walls with enhanced attenuation capacities, often referred to as "reactive barriers," has emerged over the past few decades (*e.g.*, Bierck and Chang 1994; Evans *et al.* 1997; Evans and Prince 1997; Park *et al.* 1997; Rabideau *et al.* 1999; Shackelford 1997; Malusis *et al.* 2009, 2010; Hong *et al.* 2012, 2016). In the case where the primary attenuation mechanism is adsorption, for example via cation exchange, the amended barriers are referred to more specifically as "sorbing" barriers (*e.g.*, Rabideau *et al.* 2001; Matott *et al.* 2009). Barriers with enhanced adsorption capacity can delay solute (contaminant) breakthrough for prolonged periods (*e.g.*, Malusis *et al.* 2010), and a number of different sorptive amendments have been considered for earthen containment barriers, including zeolites (Evans *et al.* 1990, Allerton *et al.* 1996, Evans *et al.* 1997).

Zeolites are naturally occurring, hydrated aluminosilicate minerals formed by alteration of glass rich volcanic rocks (tuff) with fresh or saline water (Evans *et al.* 1990; Bailey *et al.* 1999; Badillo-Almaraz *et al.* 2003; Gebremedhin-Haile *et al.* 2003; Castaldi *et al.* 2008). The zeolites

are commonly used as adsorbents for ammonium, heavy metals, cations, and radioactive wastewater treatments (Bernal and Lopez-Real 1993; Jacobs and Forstner 1999; Yuan *et al.* 1999; Erdem *et al.* 2004; Inglezakis 2005; Castaldi *et al.* 2008). The adsorption mechanism of zeolite is known to be cation-exchange, due to the relatively high CECs of zeolite, typically on the order of 180 to 400 cmol<sub>c</sub>/kg, and cage-like structure that allows zeolites to perform as molecular sieves (Evans *et al.* 1990; Colella 1996; Mumpton 1999; Bish 2006). Factors that affect the cation exchange of zeolite are concentration, size and charge of the cation, the anion associated with the cation, temperature, solvent and structural characteristics (*i.e.*, size and geometry of the pores, cavities and intramineral microchannels) or cage structure of the zeolite framework (Mondale *et al.* 1995; Gebremedhin-Haile *et al.* 2003). Compared to clay minerals, zeolites have similar surface chemistry but in nature can occur as  $\geq$  mm-size particles and are free of shrink-swell behavior (Gebremedhin-Haile *et al.* 2003). In nature, there are more than 40 different species of zeolitic minerals, with clinoptilolite, mordenite, ferrierite and erionite being found abundantly (Zamzow *et al.* 1990).

The potential use of zeolite amendments for compacted sand-bentonite mixtures or compacted clay as liners for waste containment applications has been evaluated in a limited number of studies (Evans *et al.* 1990, Kayabali 1997, Tuncan *et al.* 2003, Kaya and Durukan 2004). The results of these studies suggest that amending SB backfill with zeolites also may be useful as a means to enhance the sorption capacity of SB cutoff walls for inorganic contaminants, such as heavy metals (*e.g.*, Cd<sup>2+</sup>, Zn<sup>2+</sup>). However, few studies have evaluated zeolites as amendments to enhance the attenuation capacity of backfills for vertical cutoff walls, all of which have been limited in scope (Bradl 1997; Evans and Prince 1997; Evans *et al.* 1997). Such evaluations typically require batch adsorption tests and/or column tests with barrier specific

materials and site-specific chemical solutions to determine the viability and optimum amounts of reactive materials considered for use in the reactive barriers.

For example, the study by Bradl (1997) included experimental adsorption test results with sorbents containing 5 % of two zeolites with respect to two potential contaminants, *viz.* lead and toluene. However, no adsorption or transport modeling based on the adsorption test results was evaluated. Evans and Prince (1997) evaluated the use of different amounts of one type of zeolite with respect to the sorption of cadmium ( $\text{Cd}^{2+}$ ) over a limited concentration range where the adsorption behavior was considered linear. Also, Evans *et al.* (1997) evaluated two zeolites with respect to  $\text{Cd}^{2+}$  and zinc ( $\text{Zn}^{2+}$ ), with sorbents containing only 5 % zeolite, and the concentration ranges of the contaminants were limited to the extent that the adsorption behaviors of  $\text{Cd}^{2+}$  and  $\text{Zn}^{2+}$  were considered linear in support of analytical transport modeling.

## **1.2 GOALS AND OBJECTIVES**

Given the aforementioned background, the primary goal of this research was to evaluate the existence and persistence of enhanced attenuation capacity for zeolite-amended SB backfills compared to the unamended SB backfill. This goal was accomplished by evaluating the following hypothesis:

Because of the high cation exchange capacities offered by natural zeolites, the addition of small amounts ( $\leq 10$  % by dry weight) of zeolite to an otherwise soil-bentonite (SB) backfill will result in enhanced performance of the backfill with respect to extending the duration of containment of metals without significantly affecting the other engineering properties of the backfill such as compressibility and hydraulic conductivity.

This hypothesis was evaluated by completing the following objectives:

- (1) evaluate the applicability of zeolite-amended SB vertical cutoff walls as hydraulic barriers;
- (2) quantify the enhanced attenuation or adsorption capacity of the zeolite-amended SB backfills compared to the unamended SB backfill;
- (3) compare the delay in solute transport through a hypothetical vertical cutoff wall comprising the unamended or zeolite-amended SB backfills via numerical modeling; and
- (4) confirm the enhanced adsorption capacity of the zeolite-amended SB backfills relative to the unamended SB backfill by performing long-term column testing under flow conditions comparable to those for an actual cutoff wall.

The primary goal of this research was achieved by characterizing the physical and chemical properties of the zeolite-amended SB backfills in comparison to the unamended or traditional SB backfill. The physical characteristics of the zeolite-amended SB backfills with different types and amounts of added zeolite were evaluated in terms of slump, consolidation behavior, and hydraulic conductivity. The enhanced adsorption capacity with respect to potassium (K) and zinc (Zn) of the zeolite-amended SB backfills with different types and amounts of added zeolite was verified experimentally in terms of both batch equilibrium adsorption tests (BEATs) and column tests.

The results of this research extend the results of previous studies by including the adsorption behaviors of two metals over a wider range of concentrations and for a wider variety of zeolite-amended backfills than have previously been evaluated. In addition, the duration and unique aspects of the long-term column tests, which lasted from 1.05 to 3.75 yr, conducted in

this study have not heretofore been attempted. Although the BEAT and column test results confirmed the potential use of zeolite amendment to increase the attenuation capacity of SB backfills for enhanced metals containment, the extent of improvement was affected by the testing conditions and the selectivity of the added zeolite.

Overall, the results of this research confirmed the proposed hypothesis in that the zeolite-amended SB backfills exhibited similar engineering properties but greater adsorption capacities that would equate to longer containment durations of both K and Zn. As a result, this research advances our present understanding on the performance of the zeolite-amended SB backfills and contributes to the base of knowledge needed towards incorporating zeolite-amended SB backfills in the design of SB vertical cutoff walls for subsurface chemical containment.

### **1.3 OVERVIEW OF DISSERTATION**

This dissertation includes six chapters. Chapters 1 and 6 provide the "Introduction" and "Conclusions," respectively, for the overall study. The substantive results of the study are included in Chapters 2 through 5.

Chapter 2 on "Consolidation and Hydraulic Conductivity" presents the results of a comparison of the measured slump, consolidation behavior, and hydraulic conductivity ( $k$ ) of an unamended SB backfill and the same SB backfill amended with 5 % (by dry weight) of two different types of natural zeolite, referred to as chabazite-UB and clinoptilolite, and 0, 2, 5, and 10 % (dry weight) of a zeolite referred to as chabazite-LB. The results show that, although the slump, consolidation behavior, and  $k$  of the zeolite-amended SB backfill differed slightly relative to that for the unamended SB backfill, all of the tested zeolite-amended SB backfills satisfied the low  $k \leq 1.0 \times 10^{-9}$  m/s typically required for many geoenvironmental containment applications.

Chapter 3 on "Adsorptive Behavior" includes results of batch equilibrium adsorption tests (BEATs) using unamended and zeolite-amended SB backfills with 5 and 10 % of the aforementioned three types of zeolite as the sorbents and KCl and ZnCl<sub>2</sub> solutions with concentrations ranging from 0.1 to 1,000 mM as the sorbates. The BEAT results were regressed using the Langmuir and Freundlich adsorption models to obtain the adsorption parameters which were used subsequently as input for numerical model simulations in Chapter 4. The results show that zeolite amendment significantly increased the adsorption capacity of the SB backfill for each metal, although the increase in adsorption capacity for K was greater than that for Zn, all other factors being equal. The greater increase in adsorption capacity for K relative to Zn was attributed to the preferential selectivity of the added zeolites for K. Also, the adsorption behavior of both K and Zn was consistent with cation exchange as the dominant mechanism, provided chemical speciation (complexation) of Zn was taken into account.

Chapter 4 on "Numerical Modeling" presents the results of model simulations for a hypothetical 1-m-thick cutoff wall comprising the unamended or zeolite-amended SB backfills with 5 or 10 % of the aforementioned three types of zeolite used to contain chemical solutions of KCl or ZnCl<sub>2</sub> at constant concentrations of 100, 1,000, and 10,000 mg/L. The regressed parameters for the Langmuir and Freundlich model obtained in Chapter 3 were used as input for modeling the adsorption behavior of K and Zn during migration through the barrier. The simulation results were evaluated in terms of flux breakthrough curves and breakthrough time for K and Zn. The results show that the adsorption capacity of the backfills depleted faster as the source concentration increased, resulting in an earlier solute breakthrough. The breakthrough of K through the barrier increased with increasing zeolite content, whereas an increase in breakthrough with increasing zeolite content occurred for Zn only in the case of the highest

source concentration for  $\text{ZnCl}_2$  of 10,000 mg/L. The earlier breakthrough in Zn for the zeolite-amended backfills relative to the unamended backfill resulted directly from the anomalous adsorption behavior for Zn at the two lower source concentrations (*i.e.*, 100 and 1,000 mg/L), whereby the maximum adsorbed concentration of Zn generally was greater for the unamended backfill relative to the zeolite-amended backfills due to the overlap in regressed adsorption behaviors at the lower concentrations.

Chapter 5 on "Long-Term Column Testing " presents the results of long-term column tests for the unamended and zeolite-amended SB backfills comprising 5 % of chabazite-UB or clinoptilolite, or 5 and 10 % of chabazite-LB, permeated with solutions of KCl,  $\text{ZnCl}_2$ , or a mixture of KCl and  $\text{ZnCl}_2$ . Different methods for analyzing the effluent concentration data were evaluated with the conclusion that the cumulative mass ratio (*CMR*) analysis produced the most reliable results. The hydraulic conductivity when permeated with the salt solution increased, exhibiting some incompatibility, still all of the backfills satisfied the low hydraulic conductivity requirement for geoenvironmental containment applications (*i.e.*,  $k \leq 1.0 \times 10^{-9}$  m/s). The increase in the adsorption capacity of the metals correlated well with the measured cation exchange capacity (*CEC*) of the backfills, supporting the conclusion of Chapter 3 that the primary mechanism of adsorption for the metals was cation exchange. Comparison of the column test results with the BEAT results from Chapter 3 confirmed that the excess soluble salts and selectivity of the added zeolites interfered with the adsorption of Zn for the zeolite-amended backfills for the BEATs, such that when the interference was removed for the column tests, the adsorption of Zn correctly reflected the *CEC* for chabazite-UB and clinoptilolite.

## REFERENCES

- Allerton, D.K., Desborough, G.A., Olsen, H.W., and Chang, N.Y. (1996). "Waste containment barrier enhancement with zeolite." *Tailings and Mine Waste '96*, Balkema, Rotterdam, The Netherlands, 255-264.
- Badillo-Almaraz, V., Trocellier, P., and Dávila-Rangel, I. (2003). "Adsorption of aqueous Zn(II) species on synthetic zeolites." *Nuclear Instruments and Methods in Physics Research Section B: Beam Interactions with Materials and Atoms*, B210, 424-428.
- Bailey, S.E., Olin, T.J., Bricka, R.M., and Adrian, D.D. (1999). "A review of potentially low-cost sorbents for heavy metals." *Water Research*, 33(11), 2469-2479.
- Bernal, M.P. and Lopez-Real, J.M. (1993). "Natural zeolites and sepiolite as ammonium and ammonia adsorbent materials." *Bioresource Technology*, 43(1), 27-33.
- Bish, D.L. (2006). "Parallels and distinctions between clay minerals and zeolites." Section 13.2, *Developments in Clay Science*, Elsevier, New York, 1097-1112.
- Bradl, H.B. (1997). "Vertical barriers with increased sorption capacities." *Proceedings, 1997 International Containment Technology Conference*, NTIS (National Technical Information Service), Springfield, VA, 645-651.
- Castaldi, P., Santona, L., Enzo, S., and Melis, P. (2008). "Sorption processes and XRD analysis of a natural zeolite exchanged with  $Pb^{2+}$ ,  $Cd^{2+}$  and  $Zn^{2+}$  cations." *Journal of Hazardous Materials*, 156(1-3), 428-434.
- Colella, C. (1996). "Ion exchange equilibria in zeolite minerals." *Mineralium Deposita*, 31(6), 554-562.
- Daniels, J.L., Inyang, H.I., and Chien, C.C. (2004). "Verification of contaminant sorption by soil bentonite barrier materials using scanning electron microscopy/energy dispersive x-ray spectrometry." *Journal of Environmental Engineering*, 130(8), 910-917.
- Erdem, E., Karapinar, N., and Donat, R. (2004). "The removal of heavy metal cations by natural zeolites." *Journal of Colloid and Interface Science*, 280(2), 309-314.
- Evans, J.C. and Prince, M.J. (1997). "Additive effectiveness in mineral-enhanced slurry walls." *In Situ Remediation of the Geoenvironment*, ASCE, Reston, VA, 181-196.
- Evans, J.C., Adams, T.L., and Prince, M.J. (1997). "Metals attenuation in mineral-enhanced slurry walls." *1997 International Containment Technology Conference*, NTIS (National Technical Information Service), Springfield, VA, 679-687.
- Evans, J.C., Sambasivan, Y., and Zarlinski, S. (1990). "Attenuating materials in composite liners." *Waste Containment Systems: Construction, Regulation, and Performance*, R. Bonaparte, Ed., ASCE, NY, 246-263.

- Gebremedhin-Haile, T., Olguín, M.T., and Solache-Ríos, M. (2003). "Removal of mercury ions from mixed aqueous metal solutions by natural and modified zeolitic minerals." *Water, Air, and Soil Pollution*, 148(1), 179-200.
- Grim, R., 1968. *Clay Mineralogy*, 2nd ed., McGraw-Hill, New York.
- Inglezakis, V.J. (2005). "The concept of 'capacity' in zeolite ion-exchange systems." *Journal of Colloid and Interface Science*, 281(1), 68-79.
- Jacobs, P.H. and Forstner, U. (1999). "Concept of subaqueous capping of contaminated sediments with active barrier systems (ABS) using natural and modified zeolites." *Water Research*, 33(9), 2083-2087.
- Kaya, A. and Durukan, S. (2004). "Utilization of bentonite-embedded zeolite as clay liner." *Applied Clay Science*, 25(1-2), 83-91.
- Kayabali, K. and Mollamahmutoğlu, M. (2000). "The influence of hazardous liquid waste on the permeability of earthen liners." *Environmental Geology*, 39(3-4), 201-210.
- Kayabali, K. (1997). "Engineering aspects of a novel landfill liner material: Bentonite-amended natural zeolite." *Engineering Geology*, 46(2), 105-114.
- Ören, A.H., Kaya, A., and Kayalar, A.Ş. (2011). "Hydraulic conductivity of zeolite-bentonite mixtures in comparison with sand-bentonite mixtures." *Canadian Geotechnical Journal*, 48(9), 1343-1353.
- Malusis, M.A., Barben, E.J., and Evans, J.C. (2009). "Hydraulic conductivity and compressibility of soil-bentonite backfill amended with activated carbon." *Journal of Geotechnical and Geoenvironmental Engineering*, 135(5), 664-672.
- Malusis, M.A., Maneval, J.E., Barben, E.J., Shackelford, C.D., and Daniels, E.R. (2010). "Influence of adsorption on phenol transport through soil-bentonite vertical barriers amended with activated carbon." *Journal of Contaminant Hydrology*, 116(1-4), 58-72.
- Mitchell, J.K. and Soga, K. (2005). *Fundamentals of Soil Behavior*, 3rd ed., John Wiley & Sons, Inc., New York.
- Mondale, K.D., Carland, R.M., and Aplan, F.F. (1995). "The comparative ion exchange capacities of natural sedimentary and synthetic zeolites." *Minerals Engineering*, 8(4-5), 535-548.
- Mumpton, F.A. (1999). "La roca magica: Uses of natural zeolites in agriculture and industry." *Proceedings of the National Academy of Sciences of the United States of America*, 96(7), 3463-3470.
- Rouse, J.V. and Pyrih, R.Z. (1993). "Geochemistry." Chapter 2, *Geotechnical Practice for Waste Disposal*, Chapman and Hall, London, U.K., 15-32.

- Shackelford, C.D. (1999). "Panel discussion: Reactive nature of passive containment barriers." *14th International Conference on Soil Mechanics and Foundation Engineering*, Hamburg, Germany, 2535-2536.
- Shackelford, C.D. and Jefferis, S.A. (2000). "Geoenvironmental engineering for in situ remediation." *International Conference on Geotechnical and Geoenvironmental Engineering (GeoEng2000)*, Melbourne, Australia, Nov. 19-24, Technomic, Inc., Lancaster, PA, Vol. 1, 121-185.
- Shackelford, C.D. and Nelson, J.D. (1996). "Geoenvironmental design considerations for tailings dams." *Proceedings, International Symposium on Seismic and Environmental Aspects of Dams Design: Earth, Concrete and Tailings Dams*, Santiago, Chile, Oct. 14-18, Sociedad Chilena de Geotecnia, Vol. I., 131-187.
- Shackelford, C.D., Benson, C.H., Katsumi, T., Edil, T.B., and Lin, L. (2000). "Evaluating the hydraulic conductivity of GCLs permeated with non-standard liquids." *Geotextiles and Geomembranes*, 18(2-4), 133-161.
- Tuncan, A., Tuncan, M., Koyuncu, H., and Guney, Y. (2003). "Use of natural zeolites as a landfill liner." *Waste Management Research*, 21(1), 54-61.
- Yuan, G., Seyama, H., Soma, M., Theng, B.K.G., and Tanaka, A. (1999). "Adsorption of some heavy metals by natural zeolites: XPS and batch studies." *Environmental Science and Engineering*, Part A, 34(3), 625-648.
- Zamzow, M.J., Eichbaum, B.R., Sandgren, K.R., and Shanks, D.E. (1990). "Removal of heavy metals and other cations from wastewater using zeolites." *Separation Science and Technology*, 25(13-15), 1555-1569.

## CHAPTER 2 CONSOLIDATION AND HYDRAULIC CONDUCTIVITY

### 2.1 INTRODUCTION

Soil-bentonite (SB) vertical cutoff walls historically have been used as *in situ* barriers to control groundwater during construction (LaGrega *et al.* 2001). The typical construction process of SB slurry-trench cutoff walls involves excavating a trench into subsurface soils and simultaneously filling the trench with bentonite-water slurry to maintain the stability of the trench prior to backfilling. Trench spoils or imported materials are mixed with amendments (*e.g.*, dry bentonite) and backfilled into the trench, and mixed with the bentonite-water slurry to create a backfill with consistency to provide a low hydraulic conductivity,  $k$  (*i.e.*,  $k \leq 1.0 \times 10^{-8}$  m/s), and impede groundwater flow (Xanthakos 1979; D'Appolonia 1980; Spooner *et al.* 1984; Ryan 1987; Millet *et al.* 1992; Evans 1994; Rumer and Ryan 1995).

The application of SB cutoff walls for geoenvironmental containment to prevent or control subsurface migration of contaminated groundwater has been prevalent (USEPA 1984), and is becoming more common, as these vertical barriers are typically cheaper than treatment systems, cause less risk of contaminant exposure during construction, and can be used to contain contaminated groundwater until a more efficient and/or more cost effective treatment technology is developed (Shackelford and Jefferis 2000). For cases in which treatment of subsurface contamination contained with SB cutoff walls is not feasible due to a present lack of cost-effective treatment technologies, the performance period required for cutoff walls to effectively contain the contaminants often is undefined (Inyang and de Brito Galvao 2004). In these cases, the cutoff wall may be expected to perform for a long period (years to decades), such that contaminant diffusion may adversely impact the containment performance of the cutoff wall.

For this reason, increasingly greater consideration is being given to contaminant attenuation (*e.g.*, adsorption capacity) as an important mechanism for improving the long-term performance of SB cutoff walls used for geoenvironmental containment (*e.g.*, Shackelford 1999; Daniels *et al.* 2004; Malusis *et al.* 2009). Barriers with enhanced adsorption capacity can delay solute (contaminant) breakthrough for prolonged periods (*e.g.*, Malusis *et al.* 2010), and a number of different adsorptive amendments have been considered for earthen containment barriers, including zeolites (Evans *et al.* 1990; Allerton *et al.* 1996; Evans *et al.* 1997).

Zeolites are crystalline, microporous aluminosilicates with relatively high cation exchange capacities (CECs), typically in the order of 180 to 400 cmol<sub>c</sub>/kg (Dyer 1988; Evans *et al.* 1990; Colella 1996; Mumpton 1999; Bish 2006). As a result, zeolites commonly are used commercially as adsorbents to remove cations from wastewater (Jacobs and Forstner 1999; Yuan *et al.* 1999; Erdem *et al.* 2004; Inglezakis 2005). The potential use of zeolite amendments for compacted sand-bentonite mixtures or compacted clay as liners for waste containment applications has been evaluated in a limited number of studies (Evans *et al.* 1990, Kayabali 1997; Tuncan *et al.* 2003; Kaya and Durukan 2004). The results of these studies suggest that amending SB backfill with zeolites may be useful as a means to enhance the adsorption capacity of SB cutoff walls for inorganic contaminants, such as heavy metals (*e.g.*, Cd<sup>2+</sup>, Zn<sup>2+</sup>).

However, adding zeolite to enhance the adsorption capacity of a SB cutoff wall should not compromise the integrity of the cutoff wall in terms of traditional design properties, most notably the consolidation behavior and *k* of the backfill. For example, the backfill should provide a relatively rigid skeleton with smaller particles filling the voids to minimize settlement, seepage, and piping (D'Appolonia 1980; Ryan 1987; Evans 1994; Evans *et al.* 1995). In addition,  $k \leq 1.0 \times 10^{-9}$  m/s typically is specified for vertical barriers used in geoenvironmental containment

applications, regardless of any enhanced reactivity exhibited by the barrier material (*e.g.*, LaGrega *et al.* 2001). Based on these considerations, the objective of this study was to evaluate the influence of zeolite amendment on the consolidation behavior and hydraulic conductivity of a model SB backfill. The evaluation included an assessment of the effects of different amounts of a specific zeolite in the backfill, as well as the effects of the same amount of three different types of zeolite minerals.

## **2.2 MATERIALS AND METHODS**

### *2.2.1 Constituent Materials*

The backfills comprised clean, fine sand, powdered sodium bentonite, and one of three types of zeolite. The sand was the same as that used by Malusis *et al.* (2009) to represent construction of a slurry trench cutoff wall through a sandy aquifer. The powdered sodium bentonite is available commercially under the trade name NATURALGEL<sup>®</sup> (Wyo-Ben, Inc., Billings, MT). NATURALGEL<sup>®</sup> is commonly used in slurry trenching, diaphragm walls, and as a soil-mixture additive, and previously has been used as a constituent of model SB backfills (Yeo *et al.* 2005a,b; Malusis *et al.* 2009). The three zeolites were commercially available from GSA Resources, Inc. (Tucson, AZ) and included two types of product ZS500A chabazite, referred to as chabazite-upper bed (chabazite-UB) and chabazite-lower bed (chabazite-LB), and one type of clinoptilolite (product name ZS403H).

The particle-size distributions of the constituent materials are shown in Figure 2.1, and the physical and chemical properties and mineralogical compositions of the constituent materials are summarized in Table 2.1. In terms of particle-size distributions (Figure 2.1), all three zeolites are dominated by silt-sized particles, with distributions ranging between those of the bentonite

and the sand. In terms of physical properties (Table 2.1), the zeolites are characterized by relatively low specific gravities ( $2.35 \leq G_s \leq 2.37$ ) and measureable Atterberg limits, with the two chabazites being classified (ASTM D2487-ASTM 2008) as high plasticity clays (CH) and the clinoptilolite being classified as a low plasticity clay (CL). In terms of chemical properties (Table 2.1), the exchangeable and soluble metals of the zeolites and the bentonite are dominated by sodium ( $\text{Na}^+$ ). The pH of the two chabazites and the bentonite are essentially the same (*i.e.*, pH  $\sim 8$ ), whereas that of the clinoptilolite is more basic (pH = 9.5). Also, the two chabazites are significantly more electrolytic than the other constituent materials. In terms of mineralogy, the chabazite-LB and chabazite-UB are dominated by the mineral Na-chabazite (32-38 %) with significant amounts of the mineral clinoptilolite (8-20 %) and amorphous material (21-45 %), whereas the clinoptilolite is dominated by the mineral clinoptilolite (28-45 %) with significant amounts of amorphous material (20-30 %).

The specific surface areas for the chabazite-LB, chabazite-UB, and clinoptilolite used in this study are 521, 350, and 40  $\text{m}^2/\text{g}$ , respectively (Table 2.1). The significantly higher specific surface areas for the two chabazites relative to the clinoptilolite are in contrast to the similar particle-size distributions for all three zeolites (Figure 2.1), and are attributed to greater internal specific surface areas for the chabazites relative to that for the clinoptilolite. The higher *CECs* for the two chabazites relative to the clinoptilolite and the difference in classifications between the two chabazites relative to the clinoptilolite (see Table 2.1) also can be attributed, at least in part, to the greater specific surface areas for the two chabazites relative to that for the clinoptilolite, and the aforementioned differences in mineralogy of the zeolites as indicated in Table 2.1.

### 2.2.2 *Base Mixtures for Backfills*

The base mixtures used to prepare the backfills included an unamended sand-bentonite mixture and zeolite-amended sand-bentonite mixtures containing 2, 5, or 10 % chabazite-LB, 5 % chabazite-UB, or 5 % clinoptilolite (by dry weight). The unamended base mixture comprised air-dried sand mixed with 4 % sodium bentonite (by dry weight.) and tap water to adjust the gravimetric moisture content to 4.8 %. The zeolite-amended base mixtures then were made by mixing the required amount of a given zeolite with the unamended base mixture.

### 2.2.3 *Bentonite-Water Slurry*

Bentonite-water slurry (5 % bentonite by weight) was prepared by mixing bentonite and tap water in a Cuisinart® blender for five minutes. The measured pH and electrical conductivity, *EC*, of the tap water at 25°C were 6.6 and 1.35 mS/m, respectively. The slurry was allowed to hydrate for a minimum of 24 h prior to use. After hydration, the measured density and Marsh funnel viscosity of the slurry were 1.03 Mg/m<sup>3</sup> and 46 s, respectively, and the measured pH and *EC* of the slurry at 25°C were 8.7 and 114.0 mS/m, respectively.

### 2.2.4 *Backfill Slump Testing*

The bentonite-water slurry was mixed with each of the base mixtures in various proportions using a KitchenAid® six-quart stand mixer to determine the amount of slurry and corresponding water content required to create backfills with a slump (ASTM C143-ASTM 2005) of 125 mm (5 in), as the required slump for SB backfills is 100 to 150 mm (3.9 to 5.9 in) (Evans 1993). Three slump tests were performed for each backfill at any given water content, to evaluate the variability in the measured slump and the corresponding backfill water content,  $w_B$ .

### 2.2.5 Backfill Preparation

Bulk volumes of unamended and zeolite-amended SB backfills used for consolidation and  $k$  testing were prepared separately following the procedures described in Malusis *et al.* (2009). The masses of sand, bentonite, zeolite, and water were adjusted to maintain the zeolite content (*i.e.*, 0, 2, 5, or 10 % by dry weight) and total bentonite content (5.8 % by dry weight) of each backfill, while adjusting the water content to obtain the slump within the target range of 100 to 150 mm (3.9 to 5.9 in), based on the slump test results. This method was chosen to eliminate bentonite content as a variable in the testing program. Further details of the procedure for preparing the backfills are provided in Malusis *et al.* (2009).

### 2.2.6 Consolidation Testing

Each backfill was subjected to one-dimensional consolidation (*i.e.*, confined compression) using a fixed-ring oedometer cell and incremental loading following the procedures described by Yeo *et al.* (2005a) and Malusis *et al.* (2009). The tests were conducted in accordance with ASTM D2435 (ASTM 2004), except that the hydraulic conductivity,  $k$ , was measured at the end of each loading increment, prior to placement of the subsequent load (*e.g.*, Yeo *et al.* 2005a).

Each specimen of prepared backfill was placed in a fixed-ring oedometer, rodded to eliminate large voids, and subjected to a small seating load for a minimum of 24 h prior to initiating an incremental loading sequence. The loading began at 24 kPa (3.5 psi or 0.25 tsf) and was subsequently doubled after each loading stage, up to a maximum vertical effective stress,  $\sigma'$ , of 1,532 kPa (222 psi or 16 tsf). The specimens then were unloaded by reducing the loading incrementally by a factor of four for each stage (Yeo *et al.* 2005a; Malusis *et al.* 2009).

After deformation was complete for each stage of the loading sequence (*i.e.*, a minimum of 24 h after the loading), the specimens were permeated with tap water using the falling-head procedure until the termination criteria described in ASTM D5084 (ASTM 2004) for flexible-wall  $k$  testing were achieved, *i.e.*, (1) the results of three  $k$  values were within 25 percent of the mean, (2) the ratio of the inflow rate to the outflow rate was between 0.75 and 1.25, and (3) no distinct upward or downward trend in  $k$  was observed. The maximum hydraulic gradients ranged between 30 and 50 for all specimens, and  $k$  was calculated using the final (post-deformation) thickness of the specimens after each loading increment (Yeo *et al.* 2005a; Malusis *et al.* 2009).

### 2.2.7 Flexible-Wall Hydraulic Conductivity Testing

Flexible-wall  $k$  tests using tap water as the permeant liquid also were conducted on duplicate specimens of each backfill, in accordance with the falling headwater-rising tailwater method (Method C) described in ASTM D5084 (ASTM 2004). The experimental procedures and testing apparatus were the same as those described by Malusis *et al.* (2009), and involved the use of a custom-fabricated, rigid acrylic cylinder placed around the flexible membrane to provide lateral support for the soft backfill prior to consolidation. Briefly, test specimens were prepared by depositing the backfill within the stretched membrane in three lifts, with each lift being rodded several times to eliminate large voids before the top filter paper, porous stone, and end cap were set in place. The cell was assembled and filled, and a cell pressure of 34.5 kPa (5 psi) was applied for a minimum of 24 h.

Prior to permeation, each specimen was back-pressured under a constant  $\sigma'$  of 34.5 kPa (5 psi) by increasing the cell pressure and pore-water (back) pressure in equal increments over several hours until a  $B$  value of  $\geq 0.95$  was achieved in accordance with ASTM D5084 (ASTM

2004). To ensure that an average  $\sigma'$  of 34.5 kPa (5 psi) and a hydraulic gradient less than 30 were maintained during permeation (as required by ASTM D5084 (ASTM 2004) for  $k < 1.0 \times 10^{-9}$  m/s), the hydraulic gradient was applied by setting the cell pressure at 345 kPa (50 psi) and the headwater (bottom) pressure at 321 kPa (46.5 psi), and leaving the tailwater (top) pressure at 300 kPa (43.5 psi). Each specimen was permeated until the aforementioned termination criteria described in ASTM D5084 (ASTM 2004) were achieved. Further details on the procedures for performing the flexible-wall hydraulic conductivity tests can be found in Malusis *et al.* (2009).

## 2.3 RESULTS

### 2.3.1 Slump

The measured values of the slump,  $-\Delta H (= H_o - H_f$ , where  $H_o$  and  $H_f$  are the initial and final heights, respectively, of the specimen in the slump cone), are plotted versus  $w_B$  for all of the backfills in Figure 2.2. As indicated in Figure 2.2, an increase in  $w_B$  results in an increase in  $-\Delta H$  for a given backfill composition.

As shown in Figure 2.2a, the value of  $w_B$  corresponding to  $-\Delta H = 125$  mm (5 in) for the unamended sand-bentonite backfill tested in this study was 42.1 %, which is close to the value for  $w_B$  of 43.2 % at  $-\Delta H = 128$  mm (5 in) for the same unamended sand-bentonite backfill reported by Malusis *et al.* (2009). The results in Figure 2.2a for the unamended sand-bentonite backfill used in this study also are shown to be similar to those reported by Yeo (2003) for a backfill consisting of the same bentonite and slurry but a different sand.

As shown in Figure 2.2b, the values of  $w_B$  at  $-\Delta H = 125$  mm (5 in) for the sand-bentonite backfills amended with 2, 5, and 10 % chabazite-LB were 39.8 %, 40.1 %, and 41.3 %, respectively, whereas those for the sand-bentonite backfills amended with either 5 %

clinoptilolite or 5 % chabazite-UB shown in Figure 2.2c were 38.1 % or 43.0 %, respectively. Thus, the value of  $w_B$  required to achieve a slump of 125 mm (5 in) for the unamended sand-bentonite backfill was affected only slightly by the addition of 2 to 10 % zeolite.

Finally, the  $w_B$  value at  $-\Delta H = 125$  mm (5 in) for each backfills was greater than the measured liquid limit,  $LL$  (see Table 2.2). This relative difference is expected on the basis of the liquid consistency required of backfills to properly displace the bentonite slurry within the excavated trench during backfilling (USEPA 1984).

### 2.3.2 *Stress-Strain Behavior*

The stress-strain curves resulting from the consolidation tests are plotted in the form of void ratio,  $e$ , versus logarithm of the consolidation effective stress,  $\sigma'$ , or  $e$ -log  $\sigma'$  curves, in Figure 2.3. As expected with remolded soils, no stress history (*i.e.*, preconsolidation stress) is apparent in the results. The compression and swell indices ( $C_c$  and  $C_s$ , respectively) listed in Figure 2.3 represent the slopes of the loading and unloading portions of the  $e$ -log  $\sigma'$  curves, respectively, for each backfill.

### 2.3.3 *Hydraulic Conductivity*

The  $k$  values measured in the fixed-ring oedometer cells at the end of each loading stage of the consolidation tests are summarized in Table 2.3 and plotted as a function of  $\sigma'$  in Figure 2.4. As illustrated in Figure 2.4, the measured  $k$  of a given backfill decreased with increasing  $\sigma'$ , as expected based on the inverse relationship between  $\sigma'$  and  $e$  (Figure 2.3). The bentonite distribution within the pore space between the larger sand particles is a critical factor affecting the  $k$  of sand-bentonite mixtures (Kenney *et al.* 1992), and inadequate bentonite is a primary

reason for high  $k$  values and lack of correlation between  $k$  and  $\sigma'$  in sandy SB backfills (Yeo *et al.* 2005a). Thus, the low measured  $k$  values and the trend of decreasing  $k$  with increasing  $\sigma'$  suggest that the bentonite distribution was sufficiently uniform for each backfill.

The results of the flexible-wall  $k$  tests for all of the backfills are summarized in Table 2.4. The duplicate specimens prepared from a given backfill exhibited similar values of porosity ( $n$ ), dry unit weight ( $\gamma_d$ ), and  $k$ . Also, as shown in Figure 2.5, the values of  $k$  measured using the flexible-wall cells (Table 2.4) at an average  $\sigma'$  of 34.5 kPa (5 psi) generally were similar to those measured using the fixed-ring oedometer cells (Table 2.3) at similar values of  $\sigma'$  (*i.e.*, 24 kPa (3.5 psi) and 48 kPa (7 psi)). The notable exception in Figure 2.5 pertains to the backfill containing 2 % chabazite-LB, where the  $k$  values measured using the fixed-ring oedometer cells ranged from 38 to 74 % of the geometric mean of the duplicate  $k$  values measured using the flexible-wall cells. However, these differences in measured  $k$  are not significant.

#### 2.3.4 Coefficients of Consolidation

Coefficients of consolidation,  $c_v$ , computed by both the Casagrande (logarithm-of-time) and Taylor (square-root-of-time) methods are displayed graphically in Figure 2.6. Both the Casagrande and Taylor methods yielded  $c_v$  values that are similar in range (*i.e.*, between  $10^{-5}$  and  $10^{-7}$  m<sup>2</sup>/s) and increase with increasing  $\sigma'$ . These results and trends are consistent with those reported by Yeo *et al.* (2005a) for a sandy SB backfill and Malusis *et al.* (2009) for the same unamended SB backfill as evaluated in this study as well as the SB backfill amended with 2 to 10 % activated carbon. The increasing trend in  $c_v$  with increasing  $\sigma'$  is attributed to a greater decrease in the coefficient of volume compressibility,  $m_v$ , with increasing  $\sigma'$  relative to the decrease in  $k$  with increasing  $\sigma'$  (Yeo *et al.* 2005a; Malusis *et al.* 2009).

## 2.4 DISCUSSION

### 2.4.1 Effect of Zeolite on Slump

The effects of the zeolite content,  $X_Z$ , and type of zeolite on the backfill-slurry water content,  $w_B$ , required to achieve a slump,  $-\Delta H$ , of 125 mm (5 in) based on the results of the slump tests (Figure 2.2) are shown in Figure 2.7. For a given amount and/or type of zeolite, the possible range in  $w_B$  values based on the variability in the measured data indicated in Figure 2.7 was determined by assuming lines with the same slopes as the best-fit linear regressions shown in Figure 2.2 through each data point, and determining the resulting minimum and maximum values of  $w_B$  corresponding to  $-\Delta H = 125$  mm (5 in).

As indicated in Figure 2.7a, the values of  $w_B$  corresponding to  $-\Delta H = 125$  mm (5 in) based on the linear regressions to the slump testing results for the chabazite-LB amended backfills (Figure 2.2b) increased slightly from 39.8 to 41.3 % as  $X_Z$  increased from 2 to 10 %, respectively. However, this range in values of  $w_B$  corresponding to  $-\Delta H = 125$  mm (5 in) is within the range in variability associated with the unamended backfill (*i.e.*,  $39.5 \% \leq w_B \leq 43.7 \%$ ). Thus, amending the sand-bentonite backfill with chabazite-LB had little effect on the resulting  $w_B$  corresponding to a  $-\Delta H$  of 125 mm (5 in).

As shown in Figure 2.7b, for the backfills amended with the same amount (5 %) of different types of zeolites, the values of  $w_B$  corresponding to a  $-\Delta H$  of 125 mm (5 in) fell in the order: clinoptilolite ( $w_B = 38.1 \%$ ) < chabazite-LB ( $w_B = 40.1 \%$ ) < chabazite-UB ( $w_B = 43.0 \%$ ). Both of these values of  $w_B$  for the two backfills containing 5 % chabazite are within the range in variability of  $w_B$  associated with the unamended backfill (*i.e.*,  $39.5 \% \leq w_B \leq 43.7 \%$ ), whereas the value of  $w_B$  for the 5 % clinoptilolite was slightly lower than this range. Therefore, amending the sand-bentonite backfill with 5 % of either chabazite also had little effect on the resulting  $w_B$

corresponding to a  $-\Delta H$  of 125 mm (5 in). These results are in contrast to those reported by Malusis *et al.* (2009) for the same base sand and bentonite, but a different amendment, *i.e.*, activated carbon (AC) instead of zeolite, in that the  $w_B$  required to achieve a slump of 125 mm (5 in) increased significantly with an increase in the amount of AC. The differences in the results are undoubtedly related to the different characteristics of the two different amendment materials.

For example, the AC used by Malusis *et al.* (2009) is inherently hydrophobic, whereas the zeolites used in this study are inherently hydrophilic. Thus, similar to bentonites, the zeolites would tend to attract water, whereas the AC would tend to repel water. Also, although the particle sizes of the AC used by Malusis *et al.* (2009) were coarser than those of the zeolites used in this study, the specific surface areas of the granular AC (1166 m<sup>2</sup>/g) and the powdered AC (1140 m<sup>2</sup>/g) as reported by Malusis *et al.* (2010) were significantly greater than those of the zeolites used in this study (see Table 2.1), due to the dominance ( $\geq 80$  %) of an internal (intra-particle) surface areas associated with the two ACs (Malusis *et al.* 2010). This difference in surface area suggests that the AC, despite being hydrophobic, would have more intra-particle capacity available for storing water. Regardless of the actual mechanisms causing the different results, the primary conclusion is that different amendments to an otherwise identical backfill can result in significantly different behaviors.

#### 2.4.2 Effect of Zeolite on Compression and Swell

Values of the compression index,  $C_c$ , and the swell index,  $C_s$ , for the backfills amended with different amounts of chabazite-LB are plotted in Figure 2.8a as a function of  $X_Z$ . The values of  $C_c$  for the zeolite-amended SB backfills increased slightly from 0.20 to 0.23 as  $X_Z$  increased from 2 to 10 %, respectively, although all of these values of  $C_c$  were slightly lower than the

value of  $C_c$  ( $= 0.24$ ) for the unamended SB backfill (*i.e.*,  $X_Z = 0$ ). In contrast, the values of  $C_s$  steadily decreased from 0.016 to 0.008 as  $X_Z$  increased from 0 to 10 %, respectively.

As indicated in Figure 2.8b, the trend in  $C_c$  is consistent with the water content of the backfill,  $w_B$ , *i.e.*, the compressibility of the mixture tended to increase with increase in  $w_B$ . In contrast, the swelling behavior of the chabazite-LB-amended SB backfills tended to decrease with increasing  $w_B$ , except for the unamended SB backfill at the highest value for  $w_B$  of 42.1 %, which correlated with the overall highest value for  $C_s$  of 0.016. The correlation between  $C_c$  and  $w_B$  is consistent with a weakening of the backfill with increasing  $w_B$ , whereas the reason for the lack of correlation between  $C_s$  and  $w_B$  is not entirely clear, especially since all backfills contained the same amount (*i.e.*, 5.8 %) of high-swelling bentonite. Nonetheless, the results indicate that  $C_c$  correlated better with  $w_B$  than  $X_Z$ , whereas  $C_s$  correlated better with  $X_Z$  than  $w_B$ .

The effect of amending the SB backfill with the same amount (5 %) of the three different types of zeolite is illustrated Figure 2.9a. The differences in the values of  $C_c$  and  $C_s$  for different types of zeolite amendment are relatively minor, with the only apparent trends being that  $C_c$  decreased in the order chabazite-LB > chabazite-UB > clinoptilolite, whereas  $C_s$  increased in the order chabazite-LB < chabazite-UB < clinoptilolite. As indicated in Figure 2.9b, no apparent trend existed between  $C_c$  or  $C_s$  and  $w_B$  based on type of zeolites, likely due to the relative similarity among the values for  $C_c$  and  $C_s$ .

Overall, the value of  $C_c$  tends to increase with increasing initial void ratio,  $e_o$ , independent of the amount or type of zeolite amendment, as shown in Figure 2.10. This relationship between  $C_c$  and  $e_o$  is common for natural soils (*e.g.*, see Rendon-Herrero 1980), and illustrates further that the compression behavior of the backfills was affected more by the initial void ratio than by the amount or type of zeolite in the amended backfill.

### 2.4.3 Effect of Zeolite on Hydraulic Conductivity

The measured values of hydraulic conductivity,  $k$ , for the backfills amended with different amounts of chabazite-LB are plotted in Figure 2.11 as a function of  $X_Z$ , with the results based on the flexible-wall tests shown in Figure 2.11a, and the results based on the fixed-ring oedometer tests at three values of  $\sigma'$  shown in Figure 2.11b. The values of  $\sigma'$  for which  $k$  values are reported in Figure 2.11b represent the minimum, maximum, and geometric mean of the range of  $\sigma'$  applied in the consolidation tests.

Regardless of method of measurement or value of  $\sigma'$ , the trends in the measured  $k$  values in terms of  $X_Z$  are identical, *i.e.* the value of  $k$  decreases in the order:  $k$  at  $X_Z = 2\% > k$  at  $X_Z = 0\% > k$  at  $X_Z = 10\% > k$  at  $X_Z = 5\%$ . However, as shown in Figure 2.11c, the geometric means of the  $k$  values measured using flexible-wall cells varied only by a factor of about two over the entire range in  $X_Z$  evaluated in the study, whereas the  $k$  values measured using the fixed-ring oedometer cells varied only by a factor of about 1.4 over the same range in  $X_Z$ , as shown in Figure 2.11d. Thus, amending the backfill with 2 to 10% of chabazite-LB had little effect on  $k$ , regardless of method of measurement or magnitude of effective stress.

The effect of amending the backfill with the same amount (5%) of the three different types of zeolite on the measured  $k$  values is illustrated Figure 2.12, with the results based on the flexible-wall tests shown in Figure 2.12a and the results based on the fixed-ring oedometer tests shown in Figure 2.12b. Regardless of the method of measurement or the value of  $\sigma'$ , the values of  $k$  always were in the order:  $k$  for chabazite-UB  $>$   $k$  for chabazite-LB  $>$   $k$  for clinoptilolite. However, regardless of method of measurement or magnitude of effective stress,  $k$  varied by a factor of  $\leq 3.2$  in all cases, indicating that amending the backfill with the same amount of the three different types of zeolite had little effect on  $k$ .

The relative insensitivity in  $k$  to amount or type of zeolite in the backfills can be attributed to the dominance of the bentonite component of the backfills in governing the hydraulic behavior of the backfills. Although the zeolites used in this study were predominately silt-sized particles (Figure 2.1), the zeolites do not exhibit the same swelling behavior as the bentonite and, therefore, do not contribute to reducing the  $k$  based on swelling in the same manner as the bentonite component. Thus, because the bentonite content in all of the backfills was held constant at 5.8 %, the  $k$  of the backfills also was relatively constant (*i.e.*, all other factors being the same).

#### 2.4.4 Effect of Zeolite on Coefficient of Consolidation

The values of the coefficient of consolidation,  $c_v$ , based on Casagrande and Taylor methods for the SB backfills amended with different amounts of chabazite-LB are plotted as a function of  $X_Z$  in Figure 2.13a and Figure 2.13b, respectively. The variability in the  $c_v$  values as a function of  $X_Z$  obtained by the Taylor method is noticeably greater than that obtained by the Casagrande method. However, as shown in Figure 2.13c, the  $c_v$  values for the zeolite-amended SB backfills based on the Casagrande method vary at most by a factor of three relative to that for the unamended SB backfill. In terms of the Taylor method of analysis, the upper limit in the range of the  $c_v$  values for the zeolite-amended SB backfills relative to that for the unamended SB backfill is only about a factor of two (Figure 2.13d), whereas the lower limit in the range of the  $c_v$  values for the zeolite-amended SB backfills relative to that for the unamended SB backfill is significantly greater by a factor of about 20. Nonetheless, amending the SB backfill with 2 to 10 % of chabazite-LB had little effect on the resulting values of  $c_v$  regardless of the magnitude of effective stress, especially when considering the  $c_v$  values based on the Casagrande method of

analysis. Again, this relative insensitivity in  $c_v$  to the amount or type of zeolite in the backfill implies that the  $c_v$  value is dominated by the hydraulic conductivity of the backfill which, as previously noted, is also relatively insensitive to the amount or type of zeolite in the backfill, *i.e.*, due to the constant content of bentonite in the backfills.

## 2.5 SUMMARY AND CONCLUSIONS

The objective of this study was to evaluate three types of zeolites, *viz.*, chabazite-LB, chabazite-UB, and clinoptilolite, as amendments to a typical SB backfill on the consolidation behavior and hydraulic conductivity,  $k$ , of the backfill. The purpose of the zeolite amendment is to enhance the adsorption capacity of the backfill for inorganic contaminants (*e.g.*,  $\text{Cd}^{2+}$ ,  $\text{Zn}^{2+}$ ) and, thereby, improve the long-term sustainability in the containment function of the backfill used in a vertical cutoff wall. The backfills consisted of clean sand mixed with dry bentonite, zeolite ( $\leq 10\%$  by dry weight), and bentonite-water slurry to achieve a slump of 100 to 150 mm (3.9 to 5.9 in) with a total bentonite content of 5.8% (by dry weight). The zeolite amendment was 2, 5, 10% chabazite-LB, 5% chabazite-UB, or 5% clinoptilolite.

The consolidation test results indicated that adding zeolite had little impact on either the consolidation behavior or the  $k$  of the SB backfill, regardless of the amount or type of zeolite. For example, the compression index,  $C_c$ , for the unamended SB backfill (*i.e.*, 0% zeolite) was 0.24, whereas values of  $C_c$  for the zeolite-amended SB backfills were in the range  $0.19 \leq C_c \leq 0.23$ . Similarly, the  $k$  for the unamended SB backfill based on flexible-wall tests was  $2.4 \times 10^{-10}$  m/s, whereas values of  $k$  for zeolite-amended SB backfills were in the range  $1.2 \times 10^{-10} \leq k \leq 3.9 \times 10^{-10}$  m/s. Finally, values of the coefficient of consolidation,  $c_v$ , for the chabazite-LB-amended SB backfills based on the Casagrande method of analysis varied at most by a factor of

three relative to that for the unamended SB backfill. Variability in  $c_v$  based on the Taylor method of analysis was somewhat greater. Similarly, the same amount (5 %) of the three different zeolites had little or marginal impact of the values of  $C_c$ ,  $k$ , and  $c_v$  relative to those for the unamended SB backfill. Overall, the results of the study suggest that, presuming that adding zeolite will enhance the adsorption capacity, zeolite amendment to typical SB backfills will not likely to have significant effect on the consolidation behavior or  $k$  of the backfill, provided that the amount of added zeolite is small ( $\leq 10$  %).

Table 2.1. Physical and chemical properties and mineralogical compositions of constituent materials used for backfills.

Property	Standard	Constituent Material				
		Mortar Sand	Bentonite	Type of Zeolite		
				Chabazite-LB	Chabazite-UB	Clinoptilolite
Specific Gravity, $G_s$	ASTM D854	2.69	2.67	2.35	2.35	2.37
Liquid Limit, $LL$ (%)	ASTM D4318	NA	511	75.2	71.4	48.9
Plastic Limit, $PL$ (%)	ASTM D4318	NA	54	29.2	13.1	31.0
Plasticity Index, $PI$ (%)	ASTM D4318	NA	457	46.0	58.3	17.9
Classification	ASTM D2487	SP	CH	CH	CH	CL
Specific Surface ( $m^2/g$ )	a	NA	NA	521	350	40
Principal Minerals (%):	b	NA				
Montmorillonite			69			
Cristobalite			14			
Quartz			12	0-1	0-1	2-7
Plagioclase Feldspar (Albite)			2	2		4
Calcite			3			5-7
Herschelite (Na-Chabazite)				33-38	32-35	0
Heulandite (Clinoptilolite)				8-16	12-20	28-45
Analcime				19	25	
Albite				0-2	0-3	0-12
Mixed-Layered Illite/Smectite				0-5	0-3	2-10
Chlorite						1-9
Microcline						0-4
Erionite				0-4	0-4	0-3
Kaolinite				0-1	0-1	0-4
Illite/Mica				0-1	0-1	1
K-Feldspar (Microcline)						5
Gypsum						2
Amorphous				25-45	21-40	20-30
Cation Exchange Capacity, $CEC$ ( $cmol_c/kg$ )	c	NA	83.4	259	240	182
Exchangeable Metals ( $cmol_c/kg$ ):	c	NA				
$Ca^{2+}$			4.9	30.9	19.9	20.6
$Mg^{2+}$			8.8	14.5	21.6	0.3
$Na^+$			73.4	194	188	114
$K^+$			<u>1.1</u>	<u>7.1</u>	<u>6.8</u>	<u>37.6</u>
Sum			88.2	246.5	236.3	172.5
Soluble Metals ( $mg/kg$ ):	c	NA				
$Ca^{2+}$			46.1	231	175	33.2
$Mg^{2+}$			15.3	199	144	530
$Na^+$			2042	3797	3707	1506
$K^+$			58.4	71.8	76.6	143
Soil pH	ASTM D4972	6.8	8.1	8.0	8.2	9.5
Electrical Conductivity, $EC$ ( $mS/m$ ) @ 25 °C	c	6.5	200	1450	1570	150

<sup>a</sup> From GSA Resources, Inc., Tucson, AZ; <sup>b</sup> Based on X-ray diffraction (XRD) analysis performed for bentonite (2007) and zeolite (2012, 2016) by Mineralogy Inc., Tulsa, OK; <sup>c</sup> Soil, Water, and Plant Testing Laboratory, Colorado State University.

Table 2.2. Atterberg limits (ASTM D4318-ASTM 2008) of backfills with compositions corresponding to those for a 125-mm (5-in) slump.

Amount and Type of Zeolite Amendment	Atterberg Limits		
	Liquid Limit, <i>LL</i> (%)	Plastic Limit, <i>PL</i> (%)	Plasticity Index, <i>PI</i> (%)
0 % (Unamended)	31.2	10.5	20.7
2 % Chabazite-LB	31.3	7.3	24.0
5 % Chabazite-LB	30.0	6.7	23.3
10 % Chabazite-LB	34.1	19.0	15.1
5 % Chabazite-UB	32.1	20.1	12.0
5 % Clinoptilolite	30.7	4.8	25.9

Table 2.3. Measured hydraulic conductivity ( $k$ ) and porosity ( $n$ ) in fixed-ring oedometer cell as a function of consolidation effective stress zeolite-amended backfills with a total bentonite content of 5.8 % by dry weight.

Effective stress, $\sigma'$ [kPa (psi)]	Amount and Type of Zeolite Amendment											
	0 % (Unamended)		2 % Chabazite-LB		5 % Chabazite-LB		10 % Chabazite-LB		5 % Chabazite-UB		5 % Clinoptilolite	
	$k$ (m/s)	$n$	$k$ (m/s)	$n$	$k$ (m/s)	$n$	$k$ (m/s)	$n$	$k$ (m/s)	$n$	$k$ (m/s)	$n$
24 (3.5)	$2.6 \times 10^{-10}$	0.532	$2.9 \times 10^{-10}$	0.513	$2.1 \times 10^{-10}$	0.516	$2.3 \times 10^{-10}$	0.519	$2.7 \times 10^{-10}$	0.503	$1.2 \times 10^{-10}$	0.496
48 (7)	$2.2 \times 10^{-10}$	0.520	$2.8 \times 10^{-10}$	0.499	$1.7 \times 10^{-10}$	0.499	$1.9 \times 10^{-10}$	0.503	$2.5 \times 10^{-10}$	0.488	$1.0 \times 10^{-10}$	0.481
96 (14)	$2.0 \times 10^{-10}$	0.498	$2.5 \times 10^{-10}$	0.483	$1.4 \times 10^{-10}$	0.483	$1.6 \times 10^{-10}$	0.484	$2.3 \times 10^{-10}$	0.471	$8.8 \times 10^{-11}$	0.467
192 (28)	$1.6 \times 10^{-10}$	0.480	$2.2 \times 10^{-10}$	0.466	$1.2 \times 10^{-10}$	0.463	$1.3 \times 10^{-10}$	0.465	$2.0 \times 10^{-10}$	0.453	$6.9 \times 10^{-11}$	0.449
383 (56)	$1.5 \times 10^{-10}$	0.459	$2.2 \times 10^{-10}$	0.448	$1.0 \times 10^{-10}$	0.443	$1.1 \times 10^{-10}$	0.445	$1.7 \times 10^{-10}$	0.436	$6.2 \times 10^{-11}$	0.430
766 (111)	$1.2 \times 10^{-10}$	0.440	$1.5 \times 10^{-10}$	0.428	$8.4 \times 10^{-11}$	0.421	$1.0 \times 10^{-10}$	0.422	$1.5 \times 10^{-10}$	0.413	$5.1 \times 10^{-11}$	0.412
1532 (222)	$1.1 \times 10^{-10}$	0.415	$1.5 \times 10^{-10}$	0.408	$7.8 \times 10^{-11}$	0.397	$9.4 \times 10^{-11}$	0.398	$1.3 \times 10^{-10}$	0.392	$4.1 \times 10^{-11}$	0.392

Table 2.4. Flexible-wall hydraulic conductivity test results for replicated specimens of zeolite-amended backfills with a total bentonite content of 5.8 % by dry weight.

Amount and Type of Zeolite Amendment	Porosity, $n$	Dry Unit Weight, $\gamma_d$ [kN/m <sup>3</sup> (lb/ft <sup>3</sup> )]	Hydraulic Conductivity, $k$ (m/s)		
			Measured Value	Arithmetic Mean	Geometric Mean
0 % (Unamended)	0.469	13.8 (87.6)	$4.3 \times 10^{-10}$	$2.8 \times 10^{-10}$	$2.4 \times 10^{-10}$
	0.482	14.0 (89.3)	$1.3 \times 10^{-10}$		
2 % Chabazite-LB	0.403	13.7 (86.9)	$4.3 \times 10^{-10}$	$3.9 \times 10^{-10}$	$3.9 \times 10^{-10}$
	0.462	14.0 (89.0)	$3.5 \times 10^{-10}$		
5 % Chabazite-LB	0.467	13.7 (87.2)	$2.7 \times 10^{-10}$	$2.0 \times 10^{-10}$	$1.9 \times 10^{-10}$
	0.477	14.3 (90.8)	$1.4 \times 10^{-10}$		
10 % Chabazite-LB	0.455	13.9 (88.7)	$1.9 \times 10^{-10}$	$2.0 \times 10^{-10}$	$2.0 \times 10^{-10}$
	0.441	14.4 (91.9)	$2.2 \times 10^{-10}$		
5 % Chabazite-UB	0.362	14.6 (92.7)	$2.1 \times 10^{-10}$	$2.5 \times 10^{-10}$	$2.4 \times 10^{-10}$
	0.533	13.1 (83.6)	$2.8 \times 10^{-10}$		
5 % Clinoptilolite	0.443	14.0 (89.2)	$1.4 \times 10^{-10}$	$1.2 \times 10^{-10}$	$1.2 \times 10^{-10}$
	0.442	15.2 (96.8)	$9.5 \times 10^{-11}$		

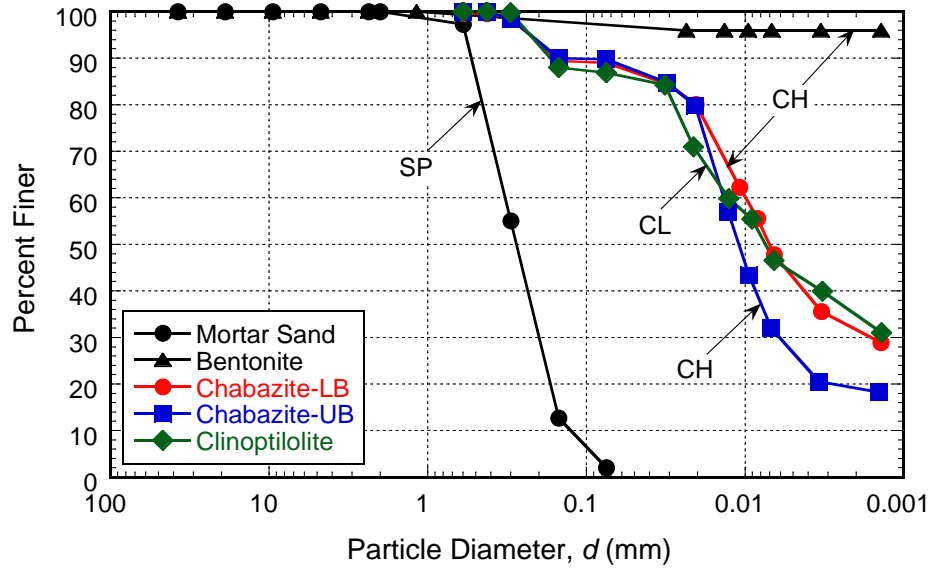


Figure 2.1. Measured particle-size distributions (ASTM D422-ASTM 2007) for constituent materials used in study. Letter designations associated with curves represent classifications based on the Unified Soil Classification System (ASTM D2487-ASTM 2008).

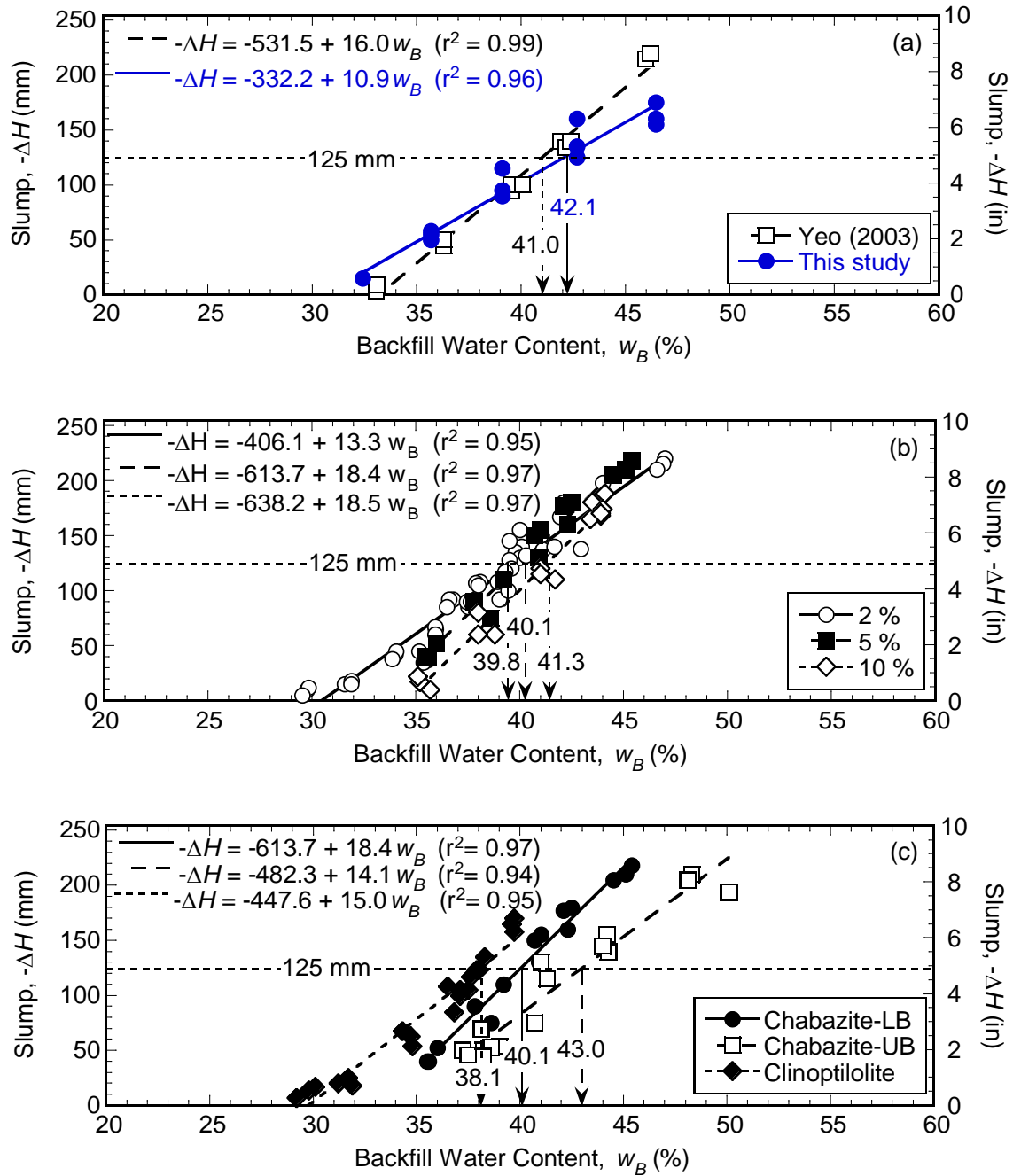


Figure 2.2. Backfill slump versus backfill gravimetric water content: (a) unamended backfill compared with the results of Yeo (2003); (b) backfills amended with different percentages of the same zeolites (chabazite-LB); (c) backfills amended with same amount (5 %) of different types of zeolites.

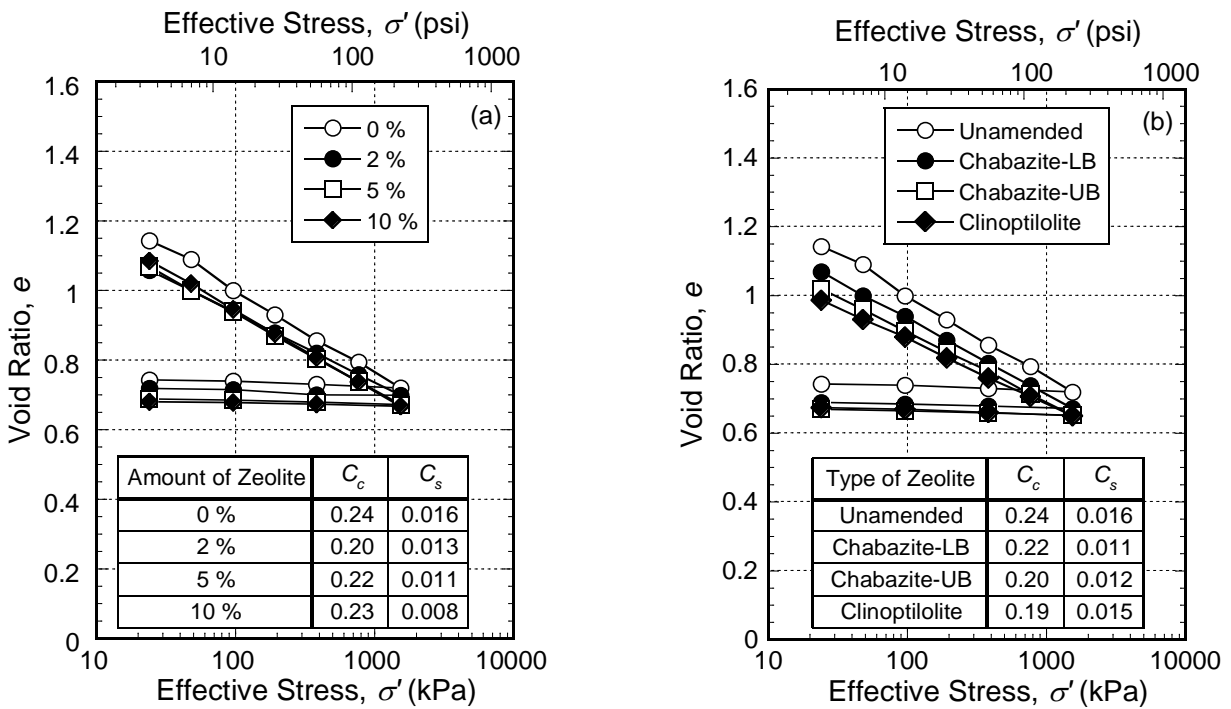


Figure 2.3. Stress-strain curves for confined compression of unamended and zeolite-amended backfills: (a) effect of different amounts of the same zeolite (chabazite-LB); (b) effect of same amount (5 %) of different types of zeolite.  $C_c$  = compression index;  $C_s$  = swell index.

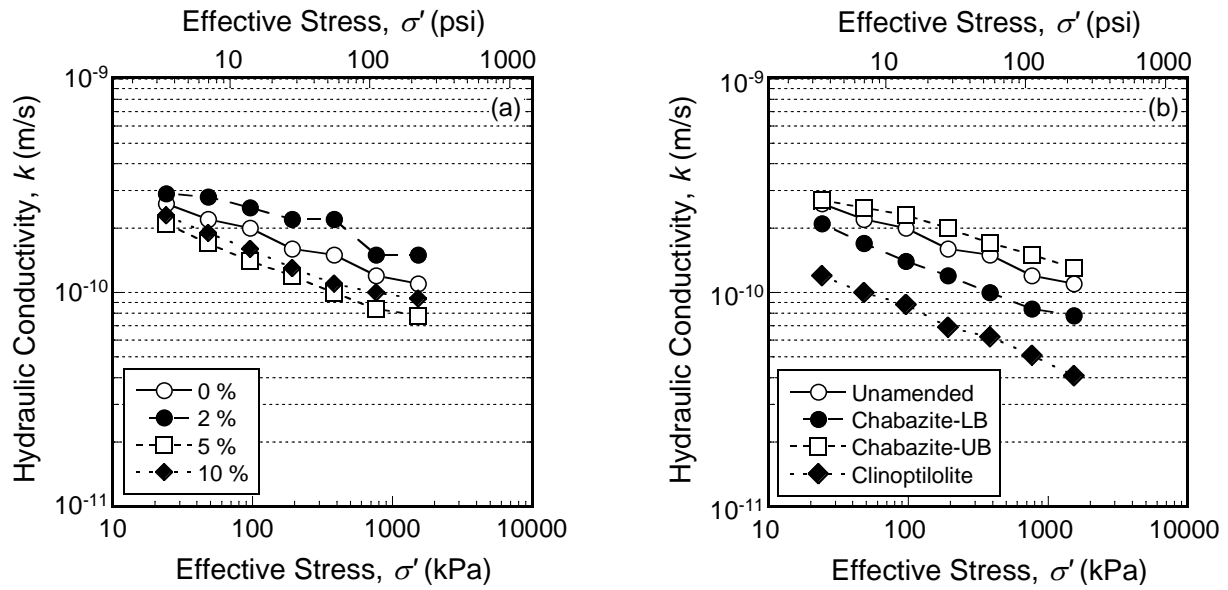


Figure 2.4. Hydraulic conductivity measured in fixed-ring oedometer cells as a function of consolidation effective stress for unamended and zeolite-amended backfills: (a) effect of different amounts of the same zeolite (chabazite-LB); (b) effect of same amount (5 %) of different types of zeolite.

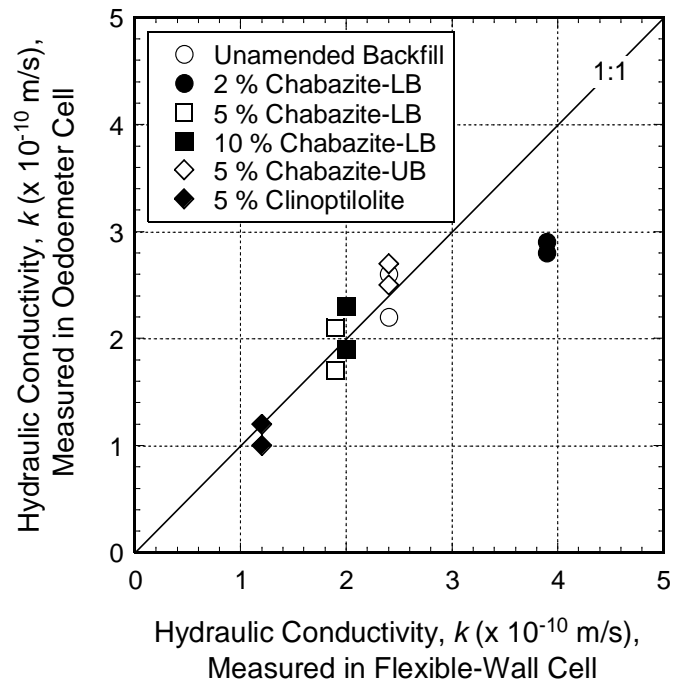


Figure 2.5. Correlation between geometric mean of hydraulic conductivity,  $k$ , measured in flexible-wall cell at an average effective stress,  $\sigma'_v$ , of 34.5 kPa (5.0 psi) versus  $k$  measured in fixed-ring oedometer cell for 24 kPa (3.5 psi) and 48 kPa (7.0 psi).

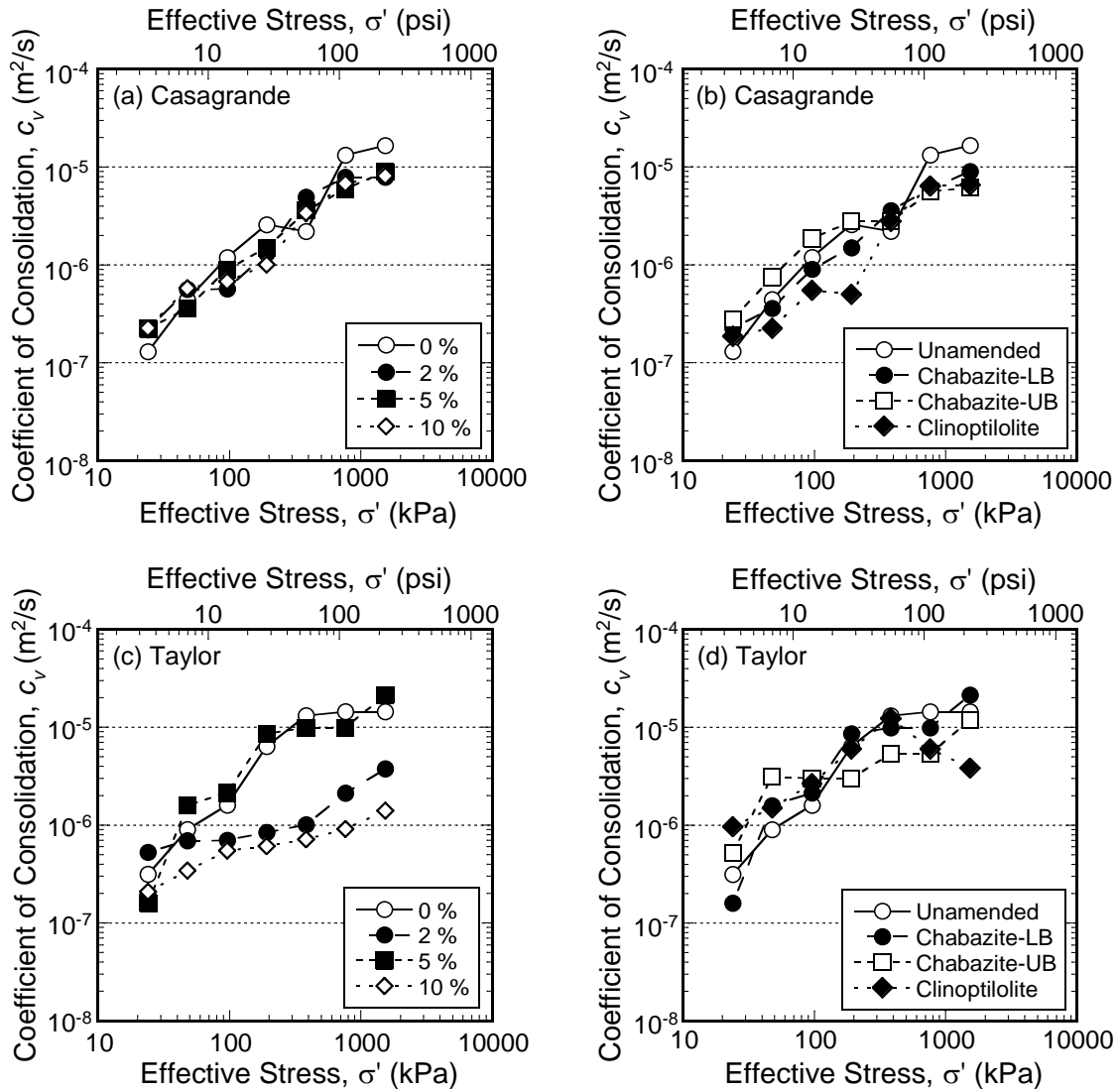


Figure 2.6. Coefficients of consolidation based on Casagrade and Taylor methods for unamended and zeolite-amended backfills as a function of consolidation effective stress: (a), (c) effect of different amounts of the same zeolite (chabazite-LB); (b), (d) effect of same amount (5 %) of different types of zeolite.

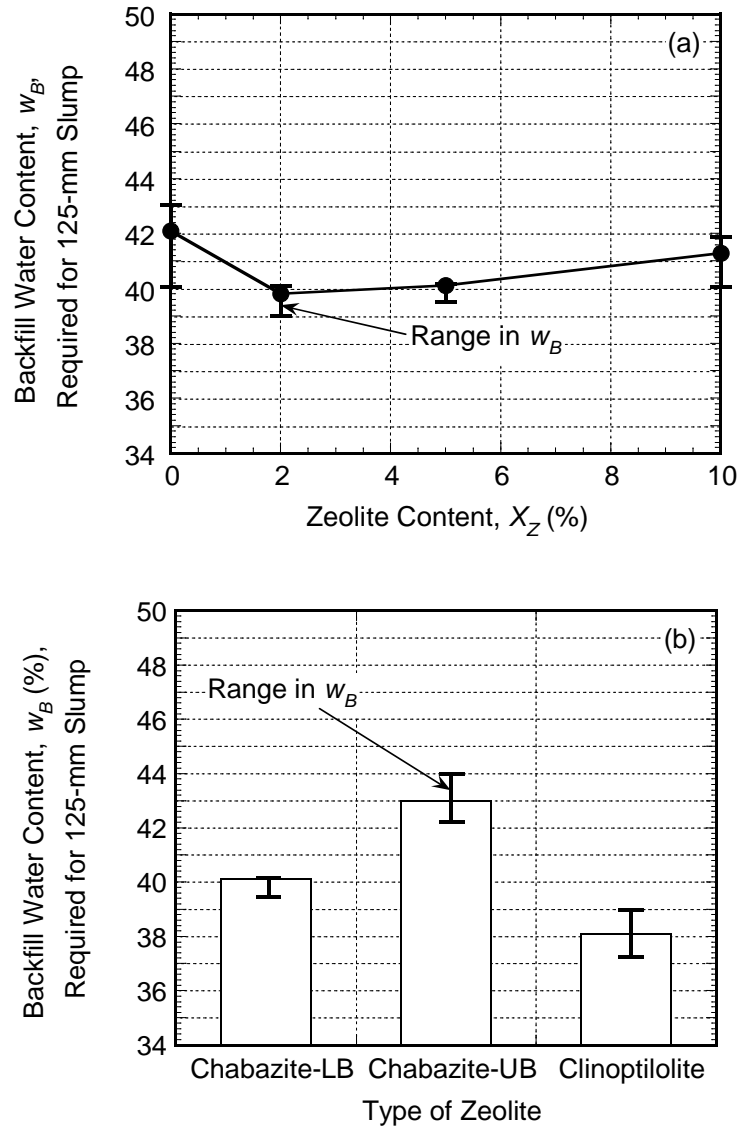


Figure 2.7. Backfill water content required to achieve a 125-mm (5-in) slump: (a) effect of different amounts of the same zeolite (chabazite-LB); (b) effect of the same amount (5 %) of different types of zeolite.

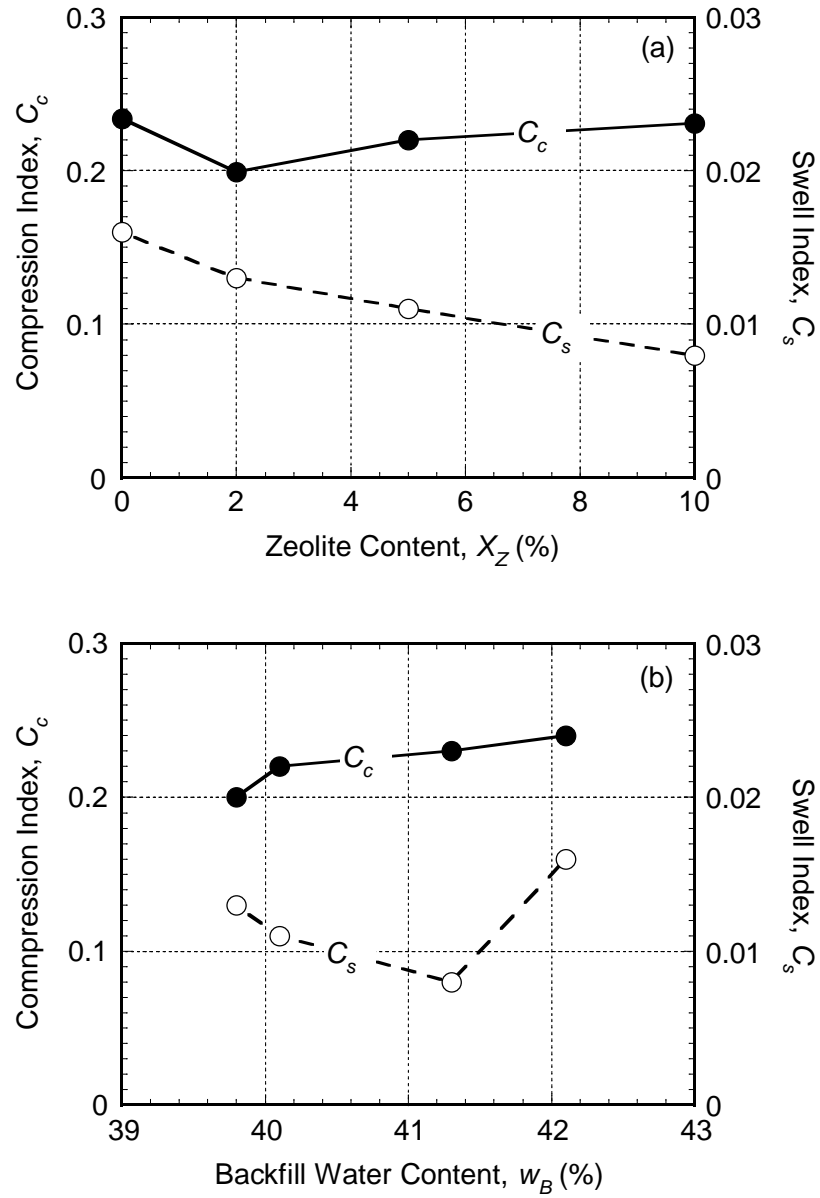


Figure 2.8. Compression and swell indices for unamended backfill and zeolite-amended backfills amended with the same zeolite (chabazite-LB): (a) effect of amount of zeolite; (b) effect of backfill water content.

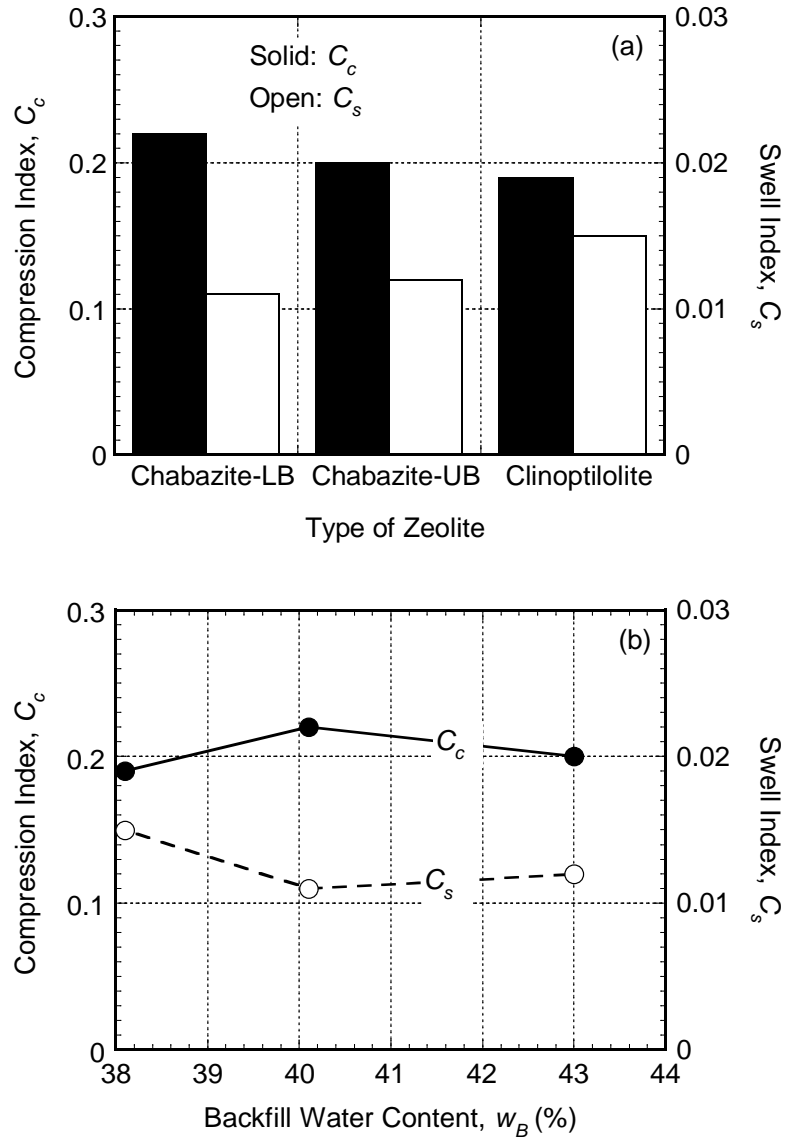


Figure 2.9. Compression and swell indices for zeolite-amended backfills amended with the same amount (5 %) of different types of zeolites: (a) effect of type of zeolite; (b) effect of backfill water content.

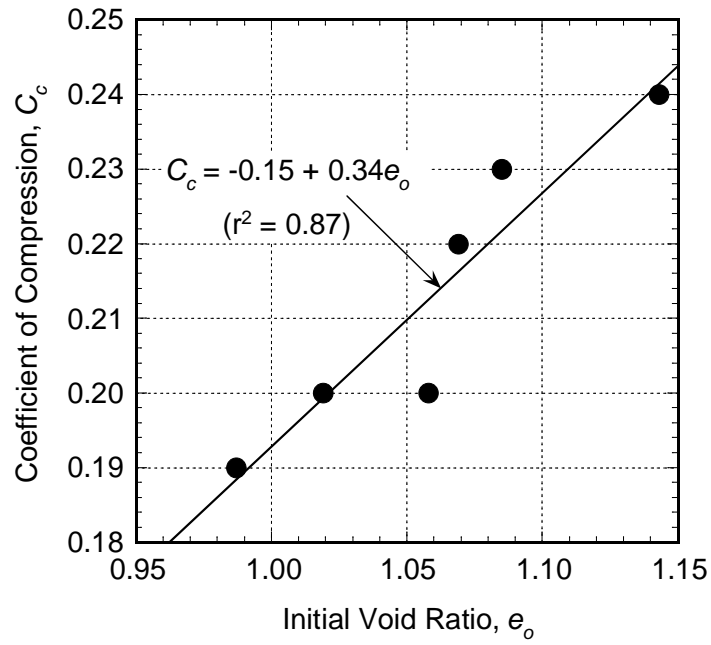


Figure 2.10. Correlation between initial void ratio and compression index zeolite-amended backfills with different amounts and/or types of zeolites.

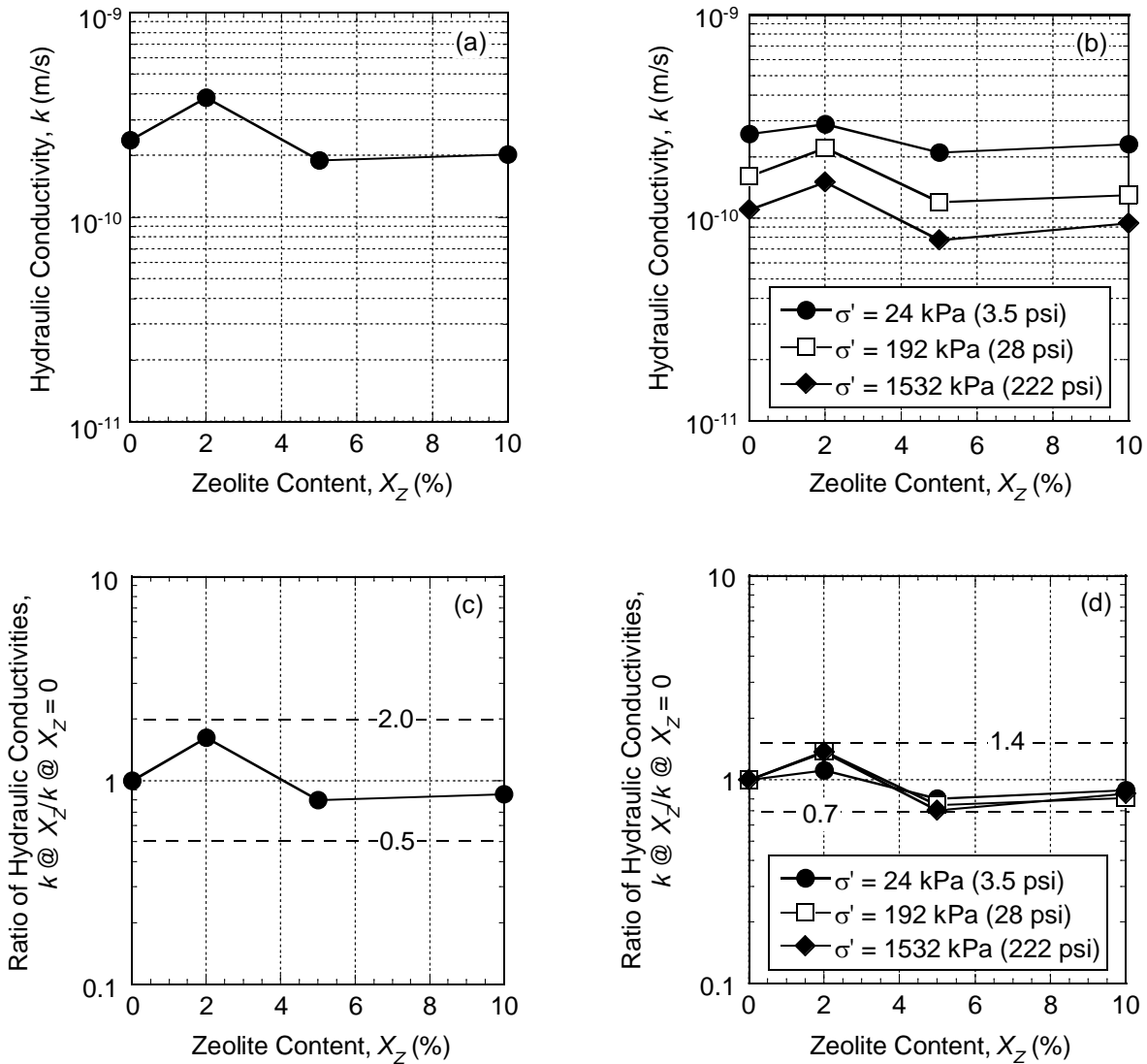


Figure 2.11. Effect of the amount of the same zeolite (chabazite-LB) on the hydraulic conductivity,  $k$ , of zeolite-amended backfills: (a) geometric mean of  $k$  values measured using flexible-wall cells; (b)  $k$  values measured in fixed-ring oedometer cells as a function of consolidation effective stress,  $\sigma'$ ; (c) ratio of geometric mean  $k$  values measured using flexible-wall cells; (d) ratio of  $k$  values measured in fixed-ring oedometer cells as a function of  $\sigma'$ .

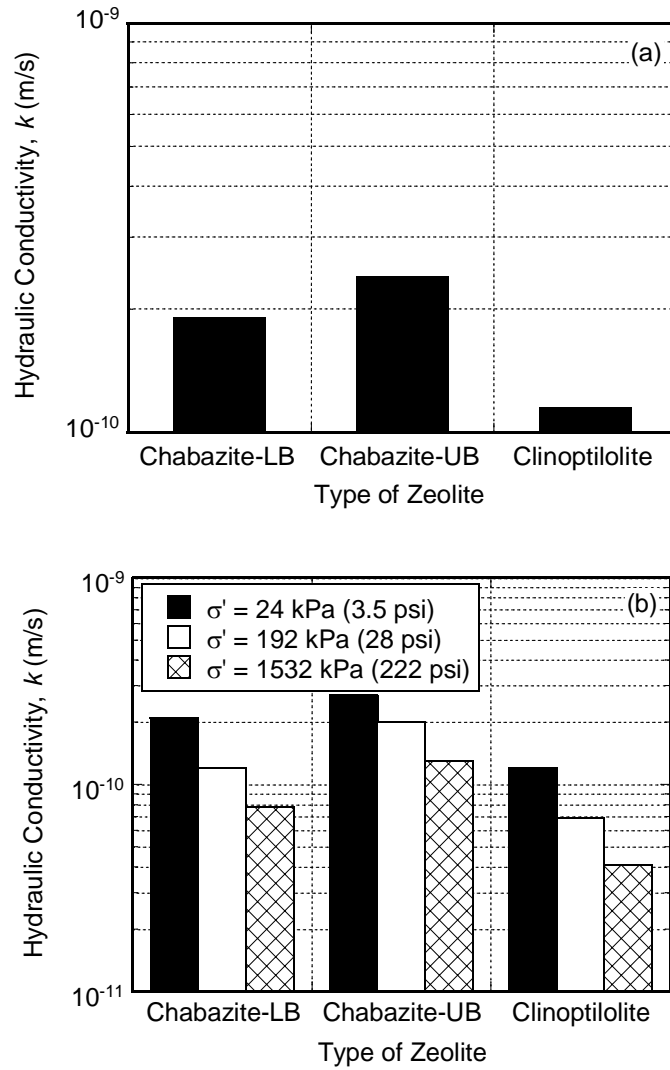


Figure 2.12. Effect of the same amount (5 %) of different zeolites on the hydraulic conductivity,  $k$ , of zeolite-amended backfills: (a) geometric mean of  $k$  values measured using flexible-wall cells at an average consolidation effective stress,  $\sigma'_v$ , of 34.5 kPa (5.0 psi); (b)  $k$  values measured in fixed-ring oedometer cells at different values of  $\sigma'_v$ .

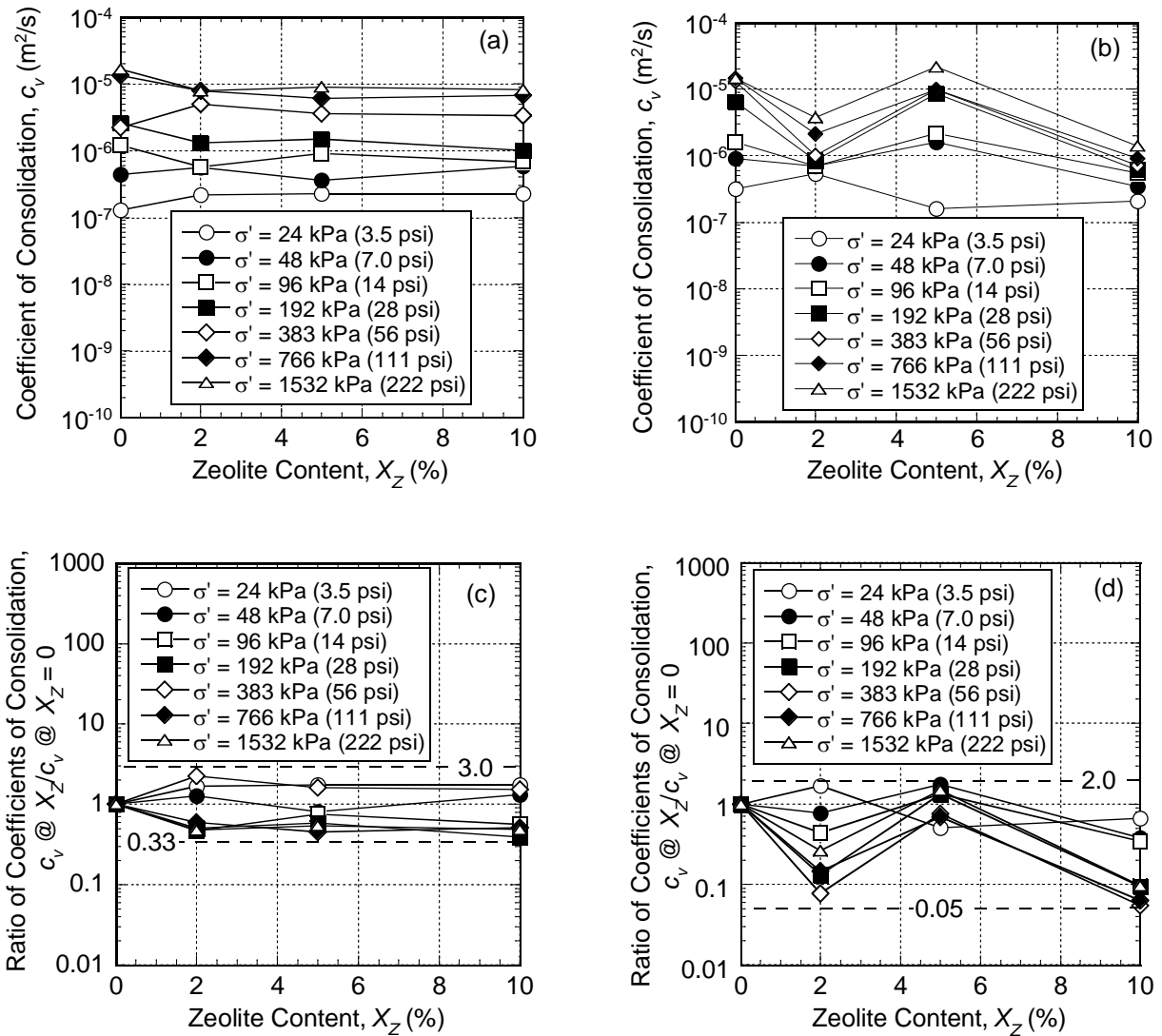


Figure 2.13. Effect of the amount of the same zeolite (chabazite-LB) on the coefficient of consolidation,  $c_v$ , of zeolite-amended backfills as a function of consolidation effective stress,  $\sigma'$ : (a)  $c_v$  based on Casagrande method; (b)  $c_v$  based on Taylor method; (c) ratio of  $c_v$  based on Casagrande method; (d) ratio of  $c_v$  based on Taylor method.

## REFERENCES

- Allerton, D.K., Desborough, G.A., Olsen, H.W., and Chang, N.Y. (1996). "Waste containment barrier enhancement with zeolite." *Tailings and Mine Waste '96*, Balkema, Rotterdam, The Netherlands, 255-264.
- ASTM (2004). "Standard test methods for one-dimensional consolidation properties of soils using incremental loading." *ASTM D2435-03*, ASTM International, West Conshohocken, PA.
- ASTM (2004). "Standard test methods for measurement of hydraulic conductivity of saturated porous materials using a flexible wall permeameter." *ASTM D5084-03*, ASTM International, West Conshohocken, PA.
- ASTM (2005). "Standard test method for slump of hydraulic cement concrete." *ASTM C143-05a*, ASTM International, West Conshohocken, PA.
- ASTM (2006). "Standard test methods for specific gravity of soil solids by water pycnometer." *ASTM D854-05*, ASTM International, West Conshohocken, PA.
- ASTM (2007). "Standard test method for particle-size analysis of soils." *ASTM D422-63*, ASTM International, West Conshohocken, PA.
- ASTM (2008). "Standard practice for classification of soils for engineering purposes (Unified Soil Classification System)." *ASTM D2487-06*, ASTM International, West Conshohocken, PA.
- ASTM (2008). "Standard test methods for liquid limit, plastic limit, and plasticity index of soils." *ASTM D4318-05*, ASTM International, West Conshohocken, PA.
- Bish, D.L. (2006). "Parallels and distinctions between clay minerals and zeolites." Section 13.2, *Developments in Clay Science*, Elsevier, New York, 1097-1112.
- Colella, C. (1996). "Ion exchange equilibria in zeolite minerals." *Mineralium Deposita*, 31(6), 554-562.
- D'Appolonia, D.J. (1980). "Soil-bentonite slurry trench cutoffs." *Journal of the Soil Mechanics and Foundations Division*, 106(4), 399-417.
- Daniels, J.L., Inyang, H.I., and Chien, C.C. (2004). "Verification of contaminant sorption by soil bentonite barrier materials using scanning electron microscopy/energy dispersive X-ray spectrometry." *Journal of Environmental Engineering*, 130(8), 910-917.
- Dyer, A. (1988). *An Introduction to Zeolite Molecular Sieves*, John Wiley & Sons, Inc. Chichester, U.K.
- Erdem, E., Karapinar, N., and Donat, R. (2004). "The removal of heavy metal cations by natural

- zeolites." *Journal of Colloid and Interface Science*, 280(2), 309-314.
- Evans, J.C. (1993). *Geotechnical Practice for Waste Disposal*, D.E. Daniel, Ed., Chapman and Hall, London.
- Evans, J.C. (1994). "Hydraulic conductivity of vertical cutoff walls." *Hydraulic Conductivity and Waste Contaminant Transport in Soil*, D.E. Daniel and S.J. Trautwein, Eds., ASTM STP 1142, West Conshohocken, PA, 79-93.
- Evans, J.C., Adams, T.L., and Prince, M.J. (1997). "Metals attenuation in mineral-enhanced slurry walls." *1997 International Containment Technology Conference*, St. Petersburg, FL, NTIS (National Technical Information Service), Springfield, VA, 679-687.
- Evans, J.C., Costa, M.J., and Cooley, B. (1995). "The state-of-stress in soil-bentonite slurry trench cutoff walls." *Geoenvironment 2000*, Y.B. Acar and D.E. Daniel, Eds., ASCE, Reston, VA, 1173-1191.
- Evans, J.C., Sambasivan, Y., and Zarlinski, S. (1990). "Attenuating materials in composite liners." *Waste Containment Systems: Construction, Regulation, and Performance*, R. Bonaparte, Ed., ASCE, New York, 246-263.
- Inglezakis, V.J. (2005). "The concept of 'capacity' in zeolite ion-exchange systems." *Journal of Colloid and Interface Science*, 281(1), 68-79.
- Inyang, H.I. and de Brito Galvao, T.C. (2004). "The application of innovative materials in waste containment barriers." *Journal of Environmental Engineering*, 130(8), 834-835.
- Jacobs, P.H. and Forstner, U. (1999). "Concept of subaqueous capping of contaminated sediments with active barrier systems (ABS) using natural and modified zeolites." *Water Research*, 33(9), 2083-2087.
- Kaya, A. and Durukan, S. (2004). "Utilization of bentonite-embedded zeolite as clay liner." *Applied Clay Science*, 25(1-2), 83-91.
- Kayabali, K. (1997). "Engineering aspects of a novel landfill liner material: bentonite-amended natural zeolite." *Engineering Geology*, 46(2), 105-114.
- Kenney, T.C., Van Veen, W.A., Swallow, M.A., and Sungaila, M.A. (1992). "Hydraulic conductivity of compacted bentonite-sand mixtures." *Canadian Geotechnical Journal*, 29(3), 364-374.
- LaGrega, M.L., Buckingham, P.L., and Evans, J.C. (2001). *Hazardous Waste Management*, 2nd ed., McGraw-Hill Book Company, New York.
- Malusis, M.A., Barben, E.J., and Evans, J.C. (2009). "Hydraulic conductivity and compressibility of soil-bentonite backfill amended with activated carbon." *Journal of Geotechnical and Geoenvironmental Engineering*, 135(5), 664-672.

- Malusis, M.A., Maneval, J.E., Barben, E.J., Shackelford, C.D., and Daniels, E.R. (2010). "Influence of adsorption on phenol transport through soil-bentonite vertical barriers amended with activated carbon." *Journal of Contaminant Hydrology*, 116(1-4), 58-72.
- Millet, R.A., Perez, J.Y., and Davidson, R.R. (1992). "USA practice slurry wall specifications 10 years later." *Slurry Walls: Design, Construction and Quality Control*, D.B. Paul, R.R. Davidson, and N.J. Cavalli, Eds., ASTM STP 1129, West Conshohoken, PA, 42-67.
- Mumpton, F.A. (1999). "La roca magica: Uses of natural zeolites in agriculture and industry." *Proceedings of the National Academy of Sciences of the United States of America*, 96(7), 3463-3470.
- Rendon-Herrero, O. (1980). "Universal compression index equation." *Journal of the Geotechnical Engineering Division*, 106(11), 1179-1200.
- Rumer, R.R. and Ryan, M.E. (1995). *Barrier Containment Technologies for Environmental Remediation Applications*, John Wiley & Sons, Inc., New York.
- Ryan, C.R. (1987). "Vertical barriers in soil for pollution containment." *Geotechnical Practice for Waste Disposal '87*, R.D. Woods, Ed., ASCE, Reston, VA, 182-204.
- Shackelford, C.D. (1999). "Reactive nature of passive containment barriers." D. 6.1, Proceedings, *14th International Conference on Soil Mechanics and Foundation Engineering*, Hamburg, Germany, Sept. 6-12, 1997, Balkema, Rotterdam, Vol. 4, 2535-2536.
- Shackelford, C.D. and Jefferis, S.A. (2000). "Geoenvironmental engineering for in situ remediation." *Proceedings, International Conference on Geotechnical and Geoenvironmental Engineering (GeoEng2000)*, Melbourne, Australia, Nov. 19-24, Technomic, Inc., Lancaster, PA, Vol. 1, 121-185.
- Shackelford, C.D. and Redmond, P.L. (1995). "Solute breakthrough curves for processed kaolin at low flow rates." *Journal of Geotechnical Engineering*, 121(1), 17-32.
- Spooner, P.A., Wetzel, R.S., Spooner, C.E., Furman, C.A., Tokarski, E.F., and Hunt, G.E. (1984). "Slurry trench construction for pollution migration control." *EPA-540/2-84-001*, U.S. EPA, Cincinnati, OH.
- Tuncan, A., Tuncan, M., Koyuncu, H., and Guney, Y. (2003). "Use of natural zeolites as a landfill liner." *Waste Management Research*, 21(1), 54-61.
- USEPA (1984). "Slurry Trench Construction for Pollution Migration Control". *EPA-540/2-84-001*, United States Environmental Protection Agency, Office of Emergency and Remedial Response, Washington, DC.
- Xanthakos, P.P. (1979). *Slurry Walls*, McGraw-Hill Book Co., New York.
- Yeo, S.-S. (2003). *Hydraulic Conductivity, Consolidation, and Membrane Behavior of Model Backfill-Slurry Mixtures for Vertical Cutoff Walls*, M.S. Thesis, Department of Civil

Engineering, Colorado State University, Fort Collins, CO.

- Yeo, S.-S., Shackelford, C.D., and Evans, J.C. (2005a). "Consolidation and hydraulic conductivity of nine model soil-bentonite backfills." *Journal of Geotechnical and Geoenvironmental Engineering*, 131(10), 1189-1198.
- Yeo, S.-S., Shackelford, C.D., and Evans, J.C. (2005b). "Membrane behavior of model soil-bentonite backfills." *Journal of Geotechnical and Geoenvironmental Engineering*, 131(4), 418-429.
- Yuan, G., Seyama, H., Soma, M., Theng, B.K.G., and Tanaka, A. (1999). "Adsorption of some heavy metals by natural zeolites: XPS and batch studies." *Journal of Environmental Science and Health. Part A, Environmental Science and Engineering, Part A*, 34(3), 625-648.

## CHAPTER 3 ADSORPTIVE BEHAVIOR

### 3.1 INTRODUCTION

Attenuation refers to the reduction in the rate and/or magnitude of contaminant migration due to physical, chemical, and/or biological reactions (*e.g.*, Shackelford and Nelson 1996). Geochemical attenuation specifically refers to attenuation resulting from geochemical interactions between natural geological materials and chemical constituents in the pore water (Rouse and Pyrih 1993). Some possible geochemical attenuation mechanisms include cation and anion exchange with clays, adsorption of cations and anions on hydrous metal oxides (*e.g.*, iron and manganese oxides), adsorption within or onto organic matter or organic carbon, precipitation and/or co-precipitation of metals from solution (Rouse and Pyrih 1993; Shackelford 1999; Shackelford and Jefferis 2000).

Most low-permeability soil barriers used for chemical containment (*e.g.*, compacted clay liners, soil-bentonite vertical cutoff walls) have some intrinsic attenuation capacity (*e.g.*, Rouse and Pyrih 1993; Thornton *et al.* 1993; Shackelford 1999; Bello and Osinubi 2011). However, the concept of designing chemical containment barriers with enhanced attenuation capacities, often referred to as reactive barriers, has received considerable attention (*e.g.*, Evans *et al.* 1990, 1997; Mott and Weber 1992; Bierck and Chang 1994; Lo *et al.* 1994, 1997; Smith and Jaffe 1994; Gray 1995; Park *et al.* 1996, 1997; Evans and Prince 1997; Kayabali 1997; Jacobs and Forstner 1999; Rabideau *et al.* 1999; Shackelford 1999; Kayabali and Mollamahmutoglu 2000; Gullick and Weber 2001; Lo 2001, 2003; Lo and Yang 2001a,b; Voudrias 2002; Tuncan *et al.* 2003; Inyang and de Brito Galvao 2004; Kaya and Durukan 2004; Yang and Lo 2004; Bartelt-Hunt *et al.* 2005, 2006; Malusis *et al.* 2009, 2010; Ören *et al.* 2011; Hong *et al.* 2012). The design of such reactive barriers requires knowledge not only of the physical properties (*e.g.*,

hydraulic conductivity) but also the chemical properties (*i.e.*, attenuation mechanisms) of the barrier materials that will affect the migration rate of the contaminants in the pore water (Cherry *et al.* 1984). Thus, an understanding of the potential attenuation mechanisms for the principal chemical species of interest is required.

Thornton *et al.* (1993) identified the principal attenuation mechanisms for many of the inorganic chemical solutions of concern as ion exchange, precipitation, dilution, and neutralization. However, the two primary attenuation mechanisms with respect to heavy metal migration are ion exchange and/or precipitation, both of which have been referred to as adsorption mechanisms (Reardon 1981). For example, cation exchange can be enhanced in a barrier by using additive materials that increase the overall cation exchange capacity (*CEC*) of the barrier, whereas precipitation can be enhanced by adding materials such as lime (CaO) that will increase the pH of the pore water.

The potential use of zeolites with relatively high *CEC* on the order of 180 to 400 cmol<sub>c</sub>/kg (180 to 400 meq/100 g) as a barrier amendment for the purpose of increasing the adsorption capacity of a containment barrier (*e.g.*, compacted clay liner, vertical cutoff wall) has been evaluated in several studies (Evans *et al.* 1990; Colella 1996; Evans *et al.* 1997; Allerton *et al.* 1996; Bradl 1997; Evans and Prince 1997; Kayabali 1997; Jacobs and Forstner 1999; Mumpton 1999; Kayabali and Mollamahmutoğlu 2000; Tuncan *et al.* 2003; Kaya and Durukan 2004; Bish 2006; Ören *et al.* 2011; Hong *et al.* 2012; Obiri-Nyarko *et al.* 2014). Such evaluations typically require batch equilibrium adsorption tests (BEATs) and/or column tests with barrier specific materials and site-specific chemical solutions to determine the viability and optimum amounts of reactive materials being considered for use in the reactive barriers.

However, only a limited number of the aforementioned studies have focused specifically on the enhanced attenuation of backfills for vertical cutoff walls (*e.g.*, Mott and Weber 1992; Bierck and Chang 1994; Bradl 1997; Evans *et al.* 1997; Evans and Prince 1997; Park *et al.* 1997; Rabideau *et al.* 1999; Malusis *et al.* 2009, 2010; Hong *et al.* 2012), and a fewer number of these studies, all of which have been limited in scope, have evaluated the potential use of zeolites as adsorption amendments (Bradl 1997; Evans *et al.* 1997; Evans and Prince 1997; Hong *et al.* 2012). For example, the study by Bradl (1997) included experimental adsorption test results for each of two zeolites in terms of two potential contaminants, *viz.* lead (Pb) and toluene. However, Bradl (1997) evaluated only 5 % zeolite content, and no adsorption modeling based on the adsorption test results was conducted. The study by Evans *et al.* (1997) also included evaluations of two zeolites with respect to two metals, *viz.*, cadmium (Cd) and zinc (Zn). However, this study evaluated only 5 % zeolite content, and the concentration ranges of the contaminants were limited to the extent that the adsorption behaviors of both Cd and Zn were considered to be linear, allowing for the use of analytical transport modeling. Finally, the study by Evans and Prince (1997) evaluated the adsorption behavior of Cd to backfills amended with 2, 4, 6, and 8 % contents (by dry weight) of only one type of zeolite (Ca-chabazite), with all concentration ranges being limited such that only linear adsorption behavior was observed.

The study in Chapter 2 focused on evaluating the consolidation and hydraulic conductivity behaviors of five zeolite-amended backfills, three of which contained one type of zeolite (chabazite-LB) at three different contents (2, 5, and 10 %), with the other two backfills containing 5 % of two different types of zeolites (chabazite-UB and clinoptilolite). The behaviors of these five backfills were compared versus those for an unamended backfill containing the same bentonite content of 5.8 % (by dry weight). The results indicated that the addition of zeolite

had little impact on either the consolidation behavior or the hydraulic conductivity,  $k$ , of the backfill, regardless of the amount or type of the zeolite. Furthermore, based on permeation with tap water, values of  $k$  for zeolite-amended specimens were in the range  $1.2 \times 10^{-10} \leq k \leq 3.9 \times 10^{-10}$  m/s, indicating that the zeolite-amended backfills would be suitable for use as low-permeability containment barriers in the absence of any significant incompatibility with the containment liquids.

Given the aforementioned considerations, the purpose of the present study was to evaluate a subset of the same backfills previously evaluated in Chapter 2 in terms of the ability of these backfills to provide an enhanced adsorption capacity for two metals, potassium (K) and zinc (Zn). This evaluation was facilitated by conducting BEATs using mixtures of the solid backfill constituents (*i.e.*, sand, bentonite, and zeolite) as the sorbents and salt solutions containing a wide range of KCl or ZnCl<sub>2</sub> concentrations as the sorbates. The resulting adsorptive behaviors of K and Zn with respect to the backfill sorbents were evaluated using two nonlinear adsorption models, *i.e.*, the Freundlich and the Langmuir models. Overall, the results of this study extend the results of previous studies by including the adsorption behaviors of two metals over a wider range of concentrations and for a wider variety of zeolite-amended backfills than have previously been evaluated.

## **3.2 MATERIALS AND METHODS**

### *3.2.1 Sorbents*

The sorbents evaluated in this study were prepared to represent a subset of the backfills evaluated in Chapter 2. These backfill sorbents consisted of fine sand, sodium bentonite, and 0, 5, or 10 % of one of three types of zeolite, including two types of chabazite referred to as

chabazite-lower bed (chabazite-LB) and chabazite-upper bed (chabazite-UB), and a clinoptilolite (Chapter 2). These zeolites represent two of the major categories of naturally occurring zeolites, chabazite and clinoptilolite, commonly used in a wide variety of commercial and industrial applications (Evans *et al.* 1990). The sand was clean, fine mortar sand, and the bentonite was a powdered sodium bentonite (Malusis *et al.* 2009; Hong *et al.* 2012). The backfill sorbents were prepared by mixing dry masses of the fine sand, sodium bentonite (5.8 %), and the specified amounts of a zeolite (0, 5, or 10 %). The pure (100 %) zeolites also were evaluated as sorbents to provide an upper limit in comparing the adsorption capacity for each type of backfill. However, the high  $k$  associated with zeolites likely precludes the sole use of zeolites as backfills for low-permeability cutoff walls. In fact, zeolites have been used as the reactive media in high-permeability reactive walls for *in situ* treatment of radionuclide contaminated groundwater (Rabideau *et al.* 2005).

All three zeolites are dominated by silt-sized particles, with distributions ranging between those of the bentonite and sand (Chapter 2). The physical properties of the zeolites are characterized by relatively low specific gravities ( $2.35 \leq G_s \leq 2.37$ ) and measureable Atterberg limits, with chabazite-LB and chabazite-UB being classified as high plasticity clays (CH) and clinoptilolite being classified as a low plasticity clay (CL) (ASTM D2487-ASTM 2006).

In terms of the chemical properties, the exchangeable and soluble metals of the zeolites and the bentonite are dominated by sodium (Na). Values of  $CEC$  for the chabazite-LB, chabazite-UB and clinoptilolite based on the product literature are 259, 240, and 182  $\text{cmol}_c/\text{kg}$ , respectively. The pH values of chabazite-LB and chabazite-UB and the bentonite are essentially the same (*i.e.*,  $\text{pH} \sim 8$ ), whereas that of the clinoptilolite is more basic ( $\text{pH} = 9.5$ ). Further details on properties of the constituent materials are provided in Chapter 2.

### 3.2.2 Batch Equilibrium Adsorption Tests (BEATs)

Stock solutions (1 M) of the two metals, K and Zn, were prepared by mixing the appropriate amount of either KCl (certified A.C.S.; Fisher Scientific, Fair Lawn, NJ) or ZnCl<sub>2</sub> (A.C.S. grade, Analytical Reagent; Mallinckrodt Chemical Works, St. Louis, MO) with deionized water (DIW). These two metals were selected to contrast any differences between the adsorption behaviors of metals that typically are expected to exist primarily in a monovalent (K<sup>+</sup>) versus divalent (Zn<sup>2+</sup>) form, as well as to evaluate the behavior of a toxic, heavy metal (Zn) that is relevant to actual contamination problems. The chemical solutions used for the BEATs then were prepared by serial dilution of the stock solutions to provide target salt concentrations of 0.1, 0.5, 1, 5, 10, 20, 30, 40, 50, 100, 150, 250, 500, and 1,000 mM, with the higher concentrations representing an attempt to exhaust the adsorption capacity of the sorbents.

In preparing the ZnCl<sub>2</sub> solutions, the formation of what appeared to be a white precipitate was observed. For example, as shown in Figure 3.1a, the source solution (first tube on the left) was murky, and a thin layer of white precipitate appeared above the layer of the tested backfill sorbent (adjacent tubes). As shown in Figure 3.1b, a thick layer of white precipitate formed in both the source solution and the solution that was mixed with the backfill sorbent. This white precipitate was likely in the form of zinc oxychloride, such as zinc chloride hydroxide monohydrate, tetrabasic zinc chloride, basic zinc chloride, and zinc hydroxychloride (O'Neil *et al.* 2006). As a result, 37 % hydrogen chloride (HCl) was added to the ZnCl<sub>2</sub> solutions in 100- $\mu$ L increments until precipitation was no longer observed (compare Figures 3.1c and 3.1d). As the addition of HCl for the stock solution was prepared separately for the BEATs conducted using lower target concentrations (*i.e.*, 0.1 – 50 mM) versus those using higher target concentrations (*i.e.*, 100 – 1,000 mM), the resulting values of pH for the chemical solutions were different. Also,

the values of pH for the  $\text{ZnCl}_2$  solutions ( $0.9 \leq \text{pH} \leq 5.5$ ) were lower than those for the KCl solutions ( $3.9 \leq \text{pH} \leq 7.7$ ), as precipitation was not observed in the KCl solutions.

The procedure for the BEATs followed the guidelines described in Roy *et al.* (1992). Three sorbent cases were evaluated: (1) the base case corresponding to the unamended backfill (0 % zeolite); (2) the case of a zeolite-amended backfill with either 5 % or 10 % of one of the three zeolites; and (3) the pure (100 %) zeolite case. As per Chapter 2, the unamended and zeolite-amended backfill sorbents all contained 5.8 % bentonite by dry mass, to eliminate the bentonite content as a variable.

A soil-to-solution ratio of 1-to-4 (1:4) by mass was used, consisting of 10 g of sorbent (by dry weight) in 40 mL of chemical solution (*i.e.*, assuming a liquid density of 1 g/mL). Roy *et al.* (1992) evaluated the effects of a wide range of soil-to-solution ratios, and recommended against using ratios lower than 1:4 (*e.g.*, 1:2) due to limitations in mixing. The samples were duplicated and agitated in a rotating, end-over-end tumbler at 30 rpm for 48 h in a constant temperature room (22°C). Kaya and Ören (2005) found that a 48-h mixing period was sufficient to achieve steady-state (equilibrium) adsorption of zinc to bentonite, whereas Iskander *et al.* (2011) reported a mixing period of only 2 h for adsorption of zinc and manganese to natural zeolite and bentonite. After the 48-h mixing period, the samples were centrifuged (IEC Centra CL2, Thermo Fisher Scientific, Waltham, MA) at 3,000 rpm to separate the soil and solution. The concentration of K or Zn in the resulting supernatant was measured using inductively coupled plasma-atomic emission spectrometry, or ICP-AES (IRIS<sup>®</sup> Advantage/1000 ICAP Spectrometer, Thermo Jarrel Ash Co., Franklin, MA), and the measured concentration was used to determine the solid-phase (adsorbed) concentration of the sorbate,  $C_s$ , in accordance with the following equation:

$$C_s = \frac{C_o - C}{m_s} V \quad (3.1)$$

where  $C_s$  is the solid-phase (adsorbed) concentration defined as the mass of the sorbate (K or Zn) per unit mass of sorbent (mg/kg),  $m_s$  is the mass of sorbent (oven-dried basis) added to the reaction container (*i.e.*, 10 g),  $C_o$  is the initial aqueous-phase concentration before exposure to the sorbent (mg/L),  $C$  is the aqueous-phase concentration at equilibrium after exposure to the sorbent (mg/L), and  $V$  is the volume of the salt solution added to the reaction container (*i.e.*, 40 mL).

### 3.2.3 Evaluating BEAT Results

Although there are a wide variety of adsorption models (*e.g.*, Kinniburgh 1986; Limousin *et al.* 2007), the Langmuir and Freundlich models are probably the two most commonly applied models for describing nonlinear adsorption of contaminants through porous media (*e.g.*, Domenico and Schwartz 1990; Fetter 1993; Shackelford 1993). In particular, the Langmuir model has been used extensively to describe the adsorption of heavy metals (Cd, Cu, Pb, Zn) by soils and zeolites (Harter 1979; Travis and Etnier 1981; Kinniburgh 1986; Roy *et al.* 1992; Bernal and Lopez-Real 1993; Mellah and Chegrouche 1997; Gullick and Weber 2001; Sheta *et al.* 2003; Erdem *et al.* 2004; Kaya and Ören 2005; Prasad *et al.* 2008; Motsi *et al.* 2009; Iskander *et al.* 2011; Musso *et al.* 2014). Accordingly, the results of the BEATs were regressed using both the Langmuir and Freundlich nonlinear adsorption models.

The Langmuir model originally was developed to describe the adsorption of gases on flat surfaces (Roy *et al.* 1992), based on the assumption that adsorption occurs at identical sites with each site retaining one molecule of the solute that is energetically and sterically independent of

the amount of adsorption (Harmsen 1979; Weber *et al.* 1992; Limousin *et al.* 2007; Yadla *et al.* 2012; Musso *et al.* 2014). The Langmuir model can be expressed as follows (*e.g.*, Kinniburgh 1986; Shackelford 1993; Limousin *et al.* 2007; Malusis *et al.* 2009, 2010):

$$C_s = \frac{Q_L K_L C}{1 + K_L C} \quad (3.2)$$

where  $K_L$  is the Langmuir constant, representing the affinity or binding strength (*i.e.*, energy of adsorption) of the solute (Kinniburgh 1986; Roy *et al.* 1992; Weber *et al.* 1992; Fetter 1993; Jacobs and Forstner 1999; Limousin *et al.* 2007; Malusis *et al.* 2010; Musso *et al.* 2014), and  $Q_L$  is the maximum adsorbed concentration (*i.e.*, adsorption capacity) of the sorbent for the sorbate (Davidson *et al.* 1976; Domenico and Schwartz 1990; Roy *et al.* 1992; Weber *et al.* 1992; Fetter 1993; Jacobs and Forstner 1999; Gullick and Weber 2001; Limousin *et al.* 2007; Malusis *et al.* 2010; Yadla *et al.* 2012; Musso *et al.* 2014). As the equilibrium concentration,  $C$ , approaches zero, the slope of the Langmuir isotherm model becomes linear (Kinniburgh 1986; Limousin *et al.* 2007), as follows:

$$\lim_{C \rightarrow 0} \frac{dC_s}{dC} = \lim_{C \rightarrow 0} \frac{Q_L K_L}{(1 + K_L C)^2} = Q_L K_L = K_d \quad (3.3)$$

where  $K_d$  is the distribution coefficient associated with linear adsorption behavior, *i.e.*,  $C_s = K_d C$  (*e.g.*, Freeze and Cherry 1979). Also, in the limit as the equilibrium concentration increases,  $C_s$  approaches the limiting value,  $Q_L$ , as follows (Davidson *et al.* 1976; Travis and Etnier 1981; Melnyk 1985; Fetter 1986; Jacobs and Forstner 1999; Limousin *et al.* 2007):

$$\lim_{C \rightarrow \infty} C_s = \lim_{C \rightarrow \infty} \left( \frac{Q_L K_L C}{1 + K_L C} \right) = \lim_{C \rightarrow \infty} \left( \frac{Q_L K_L}{\frac{1}{C} + K_L} \right) = Q_L = C_{s, \max} \quad (3.4)$$

where  $C_{s, \max}$  represents the maximum solid-phase concentration.

The Freundlich model has been used extensively to describe the adsorption of solutes by soils (Davidson *et al.* 1976; Travis and Etnier 1981; Kinniburgh 1986; Weber *et al.* 1992; Khan *et al.* 1995; Mellah and Chegrouche 1997; Gullick and Weber 2001; Sheta *et al.* 2003; Erdem *et al.* 2004; Cabrera *et al.* 2005; Kaya and Ören 2005; Prasad *et al.* 2008; Motsi *et al.* 2009; Iskander *et al.* 2011; Musso *et al.* 2014). The Freundlich model is an empirical power function that can be represented as follows (*e.g.*, Kinniburgh 1986; Fetter 1993; Shackelford 1993; Limousin *et al.* 2007; Malusis *et al.* 2010):

$$C_s = K_f C^{N_f} \quad (3.5)$$

where  $K_f$  is the unit adsorption capacity parameter (Suffet and McGuire 1980; Weber *et al.* 1992; Gullick and Weber 2001; Malusis *et al.* 2010; Musso *et al.* 2014), also referred to as the adsorption equilibrium constant (Yadla *et al.* 2012), and  $N_f$  has been referred to as the Freundlich exponent (Weber *et al.* 1992; Malusis *et al.* 2010), the adsorption intensity constant (Yadla *et al.* 2012; Musso *et al.* 2014), or the dimensionless site energy heterogeneity (or linearity) factor (Gullick and Weber 2001). The parameter  $N_f$  has been considered to be a measure of both the relative magnitude and diversity of adsorption energies for concave, nonlinear ( $N_f < 1$ ) adsorption (Weber *et al.* 1992; Malusis *et al.* 2010), and an indicator of the intensity of adsorption or how the capacity of the sorbent varies with the equilibrium solute concentration

(Suffet and McGuire 1980). For  $N_f = 1$ , the Freundlich model is the same as the linear model such that  $K_f = K_d$  (Domenico and Schwartz 1990; Jacobs and Forstner 1999).

### 3.2.4 Cation Exchange Capacities of the Sorbents

The *CEC* of a given sorbent theoretically represents the upper limit or maximum adsorption capacity of the sorbent for cations when the primary mechanism for adsorption is cation exchange. Therefore, the *CEC* is a useful parameter for comparing the results of BEATs in that the maximum adsorption capacity of a given sorbent for a given sorbate should be limited by the *CEC* of the sorbent, *i.e.*, if the dominant mechanism for adsorption is cation exchange.

The *CEC* for each sorbent evaluated in this study was measured in accordance with ASTM D7503 (ASTM 2010), and the results are shown in Table 3.1. The measured *CEC* values for the chabazite-LB, chabazite-UB, and clinoptilolite of 232, 250, and 180  $\text{cmol}_c/\text{kg}$  were similar to the aforementioned product literature values 259, 240, and 182  $\text{cmol}_c/\text{kg}$ , respectively. Also shown in Table 3.1 are the calculated values of *CEC* based on the assumption of a linear relationship between the measured value of *CEC* of the pure (100 %) bentonite of 83.4  $\text{cmol}_c/\text{kg}$  as reported in Chapter 2 and the measured values of the pure (100 %) zeolites (see Table 3.1). For example, the *CEC* of the unamended backfill sorbent was calculated by multiplying the content of bentonite with the *CEC* of bentonite (*i.e.*,  $0.058 \times 83.4 \text{ cmol}_c/\text{kg} = 4.84 \text{ cmol}_c/\text{kg}$ ). The results indicate a close agreement between measured and calculated *CEC* values for the backfill, which implies that the bentonite and zeolite constituents did not interfere with each other to any significant extent in terms of cation exchange.

### 3.3 RESULTS

#### 3.3.1 Adsorption Results

The results from the BEATs for each sorbent are shown in Figures 3.2 – 3.5. The best-fit values of the Langmuir and Freundlich parameters were obtained by unweighted, least-square regression of the isotherms as recommended by Kinniburgh (1986). The resulting regressed parameters for the Langmuir and Freundlich models and the associated values for the coefficient of determination ( $r^2$ ) are summarized in Table 3.2.

For all of the sorbents except the unamended backfill sorbent, both adsorption models fit the experimental data reasonably well, based on the regressed values for the coefficient of determination,  $r^2 \geq 0.836$ . However, the adsorption models fit the data for the unamended backfill sorbent somewhat poorer ( $0.518 \leq r^2 \leq 0.666$  for K and  $0.721 \leq r^2 \leq 0.934$  for Zn), which is consistent with other studies involving adsorption of metals to bentonite (Skyrman 1997; Banat *et al.* 2000; Kaya and Ören 2005; Lake and Rowe 2005; Malusis *et al.* 2010). Since the measured CEC of the unamended backfill sorbent was relatively low (*i.e.*, 4.65 cmol<sub>c</sub>/kg) due to the low bentonite content (5.8 %), the full adsorption capacity likely was depleted at relatively low concentrations. Also, the upper limits for measurement of the metals concentrations by the ICP were 3.8 mM (150 mg/L) for K and 1.5 mM (100 mg/L) for Zn. As a result, some of the samples for chemical analysis of the higher concentrations had to be diluted by a factor as high as 625, such that small differences in the measured concentrations of the diluted source ( $C_o$ ) and equilibrium solution ( $C$ ) likely resulted in significantly greater differences (or scatter) in the calculated values of solid-phase (adsorbed) concentration,  $C_s$ .

### 3.3.2 Mechanisms for Metals Adsorption

As noted by Reardon (1981), adsorption of metals can result from several mechanisms, including ion exchange, precipitation, and/or co-precipitation. Although the primary mechanism for adsorption of the two metals evaluated in this study was expected to be cation exchange, precipitation and/or co-precipitation also could have been active mechanisms.

One way to estimate the likelihood of cation exchange as the dominant mechanism for adsorption is to compare the regressed value for the maximum adsorption capacity from the Langmuir model,  $Q_L$ , with the maximum solid-phase concentration based on the measured  $CEC$ ,  $C_{s,max}$ . Accordingly, the measured values of  $CEC$  (Table 3.1) for the backfill sorbents and pure zeolites were converted to values of  $C_{s,max}$  for both metals, as follows:

$$C_{s,max} \left[ \frac{\text{mg-cation}}{\text{kg-soil}} \right] = CEC \left[ \frac{\text{cmol}_c}{\text{kg-soil}} \right] \times \sum_{i=1}^n \left( \frac{f_i \times MW_i \left[ \frac{\text{g}}{\text{mol}} \right]}{z_i \left[ \frac{\text{mol}_c}{\text{mol}} \right]} \right) \times \left( \frac{\text{mol}_c}{100 \text{ cmol}_c} \times \frac{1000 \text{ mg}}{\text{g}} \right) \quad (3.6)$$

where  $MW_i$  is the molecular weight of the sorbate,  $z_i$  is the valence (charge) of the cation,  $f_i$  is the fractional composition of the existing chemical species  $i$  in aqueous solution, and  $n$  is the number of chemical species contributing to  $C_{s,max}$ . In general, considering all possible chemical species (complexes) in solution, the  $\sum f_i = 1$  at any given pH. However, since  $C_{s,max}$  as given by Eq. 3.6 is based only on cation exchange, only cationic species (complexes) should be included in the calculation, such that  $0 \leq \sum f_i \leq 1$ .

In the case of Zn, the results of Reichle *et al.* (1975) and Powell *et al.* (2013) indicate that various hydroxide complexes of Zn exist, depending on the pH of the chemical solution, as follows:  $Zn^{2+}$  for  $pH < 10$ ,  $Zn(OH)^+$  for  $6 \leq pH \leq 11$ ,  $Zn(OH)_2$  for  $7 \leq pH \leq 13$ ,  $Zn(OH)_3^-$  for  $9 \leq$

pH, and  $\text{Zn(OH)}_4^{2-}$  for  $11 \leq \text{pH}$  (see Appendix C). For example, at  $\text{pH} = 8$ ,  $f_1$  for  $\text{Zn}^{2+}$  is 0.383,  $f_2$  for  $\text{Zn(OH)}^+$  is 0.559,  $f_3$  for  $\text{Zn(OH)}_2$  is 0.058, and  $f_4$  and  $f_5$  for  $\text{Zn(OH)}_3^-$  and  $\text{Zn(OH)}_4^{2-}$ , respectively, are less than  $10^{-4}$ . However, since only  $\text{Zn}^{2+}$  and  $\text{Zn(OH)}^+$  contribute to cation exchange, the  $\sum f_i$  is equal to 0.942. Thus, the fractional composition of each Zn hydroxide complex present during the BEATs would have been a function of the pH.

In reality, the pH varied during each BEAT. For example, as shown in Figure 3.6, the final pH after equilibrium generally was greater than the initial pH of the salt solutions for each BEAT, presumably due, in part, to the natural buffering capacity of the constituent materials for each sorbent (*e.g.*, Yong and Phadungchewit 1993). In the case of the BEATs performed with  $\text{ZnCl}_2$  solutions, the initial values of pH of the  $\text{ZnCl}_2$  solutions were  $0.9 \leq \text{pH} \leq 5.5$ , whereas the final values of pH after equilibration were  $4.4 \leq \text{pH} \leq 9.3$ . Thus, for the higher equilibrium values of pH (*e.g.*,  $6 \leq \text{pH} \leq 9.3$ ), zinc likely existed in the form of both  $\text{Zn}^{2+}$  and  $\text{Zn(OH)}^+$ . However, the actual system of chemical species was more complex than that portrayed by this analysis, due to the existence of other salts in solution that would have been present (*e.g.*, Table 3.3). Thus, the actual initial conditions and conditions during testing were variable.

The situation for K adsorption is simpler than that for Zn adsorption because the dominant chemical species for K over a wide range of pH is monovalent  $\text{K}^+$  (O'Neil *et al.* 2006). Thus,  $C_{s,max}$  can be based only on  $\text{K}^+$  (*i.e.*,  $MW = 39.0983$  g/mol,  $n = i = 1$ ,  $z = +1$ ,  $\sum f_i = 1$ ).

As a result of the aforementioned considerations, only the limiting values of  $C_{s,max}$  for adsorption of either  $\text{Zn}^{2+}$  (*i.e.*,  $MW = 65.38$  g/mol,  $z = +2$ ,  $f_1 = 1$ ) or  $\text{Zn(OH)}^+$  (*i.e.*,  $MW = 82.40$  g/mol,  $z = +1$ ,  $f_2 = 1$ ) were determined, to provide an indication of the possible range in  $C_{s,max}$  due only to hydroxide complexation of  $\text{Zn}^{2+}$ . The resulting values for  $C_{s,max}$  for  $\text{Zn}^{2+}$  ( $C_{s,max,\text{Zn}^{2+}}$ ) and  $\text{Zn(OH)}^+$  ( $C_{s,max,\text{ZnOH}^+}$ ), as well as the values for  $\text{K}^+$  ( $C_{s,max,\text{K}^+}$ ), are shown in Figures 3.2

through 3.5, and the respective values of  $Q_L/C_{s,max}$  for each chemical species are summarized in Table 3.4 and shown as a function of zeolite content in Figure 3.7. Most of the  $Q_L/C_{s,max,K^+}$  values were less than unity, indicating that the actual adsorption capacities for  $K^+$  were lower than those based on the measured *CEC* values. As a result, the primary mechanism for adsorption of K was likely cation exchange of  $K^+$ . In contrast, all of the values of  $Q_L/C_{s,max,Zn^{2+}}$  with the backfill sorbents were greater than unity, whereas all of the values of  $Q_L/C_{s,max,ZnOH^+}$  with the backfill sorbents were less than unity. Thus, cation exchange could have been the dominant adsorption mechanism for Zn, provided chemical complexation of Zn is considered.

Another possible reason for values of  $Q_L/C_{s,max,Zn^{2+}} > 1$  for the unamended and zeolite-amended backfill sorbents is precipitation. In this regard, there are conflicting results as to the pH at which precipitation of Zn will occur. For example, Semmens and Seyfarth (1978) indicated that Zn may precipitate as  $Zn(OH)_{2(s)}$  or  $ZnO_{(s)}$  from a 1 mM  $Zn(NO_3)_2 \cdot 6H_2O$  solution at  $6.98 \leq pH \leq 7.63$ . Ouki and Kavannagh (1997, 1999) found that, for solutions containing 10 mg/L of Pb, Cd, Cu, Zn, Cr, Ni, or Co, precipitation would not occur until  $pH \geq 11.7$ , which was sufficiently high such that precipitation was negligible and the predominant mechanism for metal removal by two zeolites (chabazite and clinoptilolite) was attributed to ion exchange. However, Ören and Kaya (2006) stated that 2.5 to 20 mg/L of  $Zn^{2+}$  in solution may form complexes with  $OH^-$  in the form of  $Zn(OH)_2$ ,  $Zn(OH)_3^-$ , and  $Zn(OH)_4^{2-}$  at  $pH > 6$ , such that these zinc hydroxyl species may precipitate onto the zeolite. Thus, based on the final (equilibrium) range in pH for the BEATs involving zinc as the sorbate, *i.e.*,  $4.4 \leq pH \leq 9.3$ , zinc hydroxyl species in the form of  $Zn(OH)_2$  and/or  $Zn(OH)_3^-$  may have precipitated onto the sorbents. Also, Brümmer *et al.* (1983) showed that, as the concentration of  $Zn^{2+}$  increases, the pH at which  $Zn^{2+}$  precipitates decreases, such that precipitation may occur at lower pH for higher concentrations of  $Zn^{2+}$ .

Precipitation of Zn via sulfate-reducing or metal-reducing bacteria under neutral or anaerobic conditions also was unlikely since sulfate was not included in the added salt solutions or backfill sorbents (Crawford and Crawford 1996; Stapleton and Singh 2002; Singh *et al.* 2009). Also, although some of the measured pH of the backfill and solution mixtures were in a range that is optimum for biosorption for Zn (*i.e.*,  $4 \leq \text{pH} \leq 5$ ), reduced bioavailability was expected due to the high CEC of the bentonite and zeolite of the backfills (Stapleton and Singh 2002; Singh *et al.* 2009).

### 3.4 DISCUSSION

#### 3.4.1 Effect of Zeolite Content on Fitted Langmuir Model Parameters

The best-fit values of the Langmuir constants  $K_L$  and  $Q_L$ , and the values for the product of these two parameters,  $K_L Q_L$ , are summarized in Table 3.2 and plotted versus the zeolite content in Figure 3.8. All of the  $Q_L$  (maximum adsorption capacity) for the zeolite-amended backfill sorbents ( $Q_{L,amended}$ ) for both K and Zn were greater than the respective  $Q_L$  for the unamended backfill sorbent ( $Q_{L,unamended}$ ), indicating an increase in the adsorption capacity for the backfill sorbents amended with zeolite. However, there is no consistent trend in  $K_L$  (energy of adsorption) for K with increasing zeolite content among the three types of zeolites. For example,  $K_L$  increased from 0 to 10 % and then decreased from 10 to 100 % for chabazite-LB, increased from 0 to 5 % and decreased from 5 to 100 % for chabazite-UB, and decreased from 0 to 5 % and then increased from 5 to 100 % for clinoptilolite. The only consistent result for K is that  $K_L$  for all three pure zeolites were less than the  $K_L$  for the unamended backfill sorbent.

For Zn,  $K_L$  for the zeolite-amended backfill sorbents and pure zeolites were less than the  $K_L$  for the unamended backfill sorbent, with a slight increase in  $K_L$  as the zeolite content

increased from 5 to 100 %. Since greater values of  $K_L$  generally indicate more favorable adsorption such that the increase in  $C_s$  is greater for the same increase in  $C$  (Foo and Hameed 2010; Hamidpour *et al.* 2011), this observation is contradictory relative to the trends in the values of  $Q_L$ , which increased as the zeolite content increased. However, the Langmuir model assumes an identical site which is energetically and sterically independent of the amount of adsorption (Harmsen 1979; Weber *et al.* 1992; Limousin *et al.* 2007; Yadla *et al.* 2012; Musso *et al.* 2014). As a result,  $K_L$  is affected by the concentration and valence (*i.e.*, ionic strength) of the cations in the solution, whereas  $Q_L$  is an innate property of the sorbent that is not affected by the energy of adsorption. Thus, an increase in the concentrations of soluble metals inherent in the zeolites, especially  $\text{Na}^+$  (Table 3.3), due to the increase in the zeolite component of the sorbent likely would have caused increased competition with the various chemical species of Zn for the available exchange sites (*e.g.*, Reynolds *et al.* 1982), resulting in lower values of  $K_L$  for Zn with increasing zeolite content. This same effect apparently was not as dominant in the case of K adsorption, presumably due to more favorable exchange of K relative to competing metals (*e.g.*, Table 3.5).

Finally, values of  $K_L Q_L$  ( $\approx K_d$  at low concentrations) for the zeolite-amended backfill sorbents were greater than those of the unamended backfill sorbent for K, whereas the opposite conclusion is apparent in the case of Zn. Thus, at low concentrations where the BEAT results are approximately linear, the zeolite-amended backfill sorbents would likely be more effective in adsorbing K, whereas the unamended backfill sorbent would be more effective than the zeolite-amended backfill sorbent in adsorbing Zn.

### 3.4.2 Effect of Zeolite Content on Fitted Freundlich Model Parameters

The best-fit values of  $K_f$  (Freundlich unit adsorption capacity) and  $N_f$  (Freundlich exponent) are summarized in Table 3.2 and plotted versus the zeolite content in Figure 3.9. All of the  $N_f$  were less than unity, indicating concave (favorable), nonlinear adsorption. The  $K_f$  for K adsorption to the zeolite-amended backfill sorbents were greater than the  $K_f$  for the unamended backfill sorbent. In contrast, the  $K_f$  for Zn adsorption to the zeolite-amended backfill sorbents were lower than the  $K_f$  for the unamended backfill sorbent.

As shown in Figures 3.2 – 3.5, extrapolations of the Freundlich model beyond the range of measured concentrations for each sorbent resulted in an overestimation of the sorbent adsorption capacities, because a limiting (maximum) adsorption capacity is not inherent in the Freundlich model (Davidson *et al.* 1976; Travis and Etnier 1981; Melnyk 1985; Kinniburgh 1986; Roy *et al.* 1992; Fetter 1993; Johnson 1994; Limousin *et al.* 2007; Matott *et al.* 2009, 2015). For this reason, the Freundlich model should be fit only to the range of measured data that corresponds to the applicable concentrations of interest (Davidson *et al.* 1976; Travis and Etnier 1981; Melnyk 1985; Kinniburgh 1986; Roy *et al.* 1992; Fetter 1993; Limousin *et al.* 2007; Matott *et al.* 2009, 2015).

### 3.4.3 Effect of Zeolite Content on Adsorption Capacity

The effect of zeolite content (*i.e.*, 0, 5, 10 %) on the adsorption behaviors for K and Zn with each type of zeolite is shown in Figure 3.10. For K, an increase in the adsorption capacity resulting from a 10 % zeolite amendment relative to a 5 % zeolite amendment is clearly apparent in the case of the two chabazites (Figures 3.10a,c), whereas for the clinoptilolite, the 10 % amendment provides only a marginal increase in adsorption capacity relative to the 5 %

amendment (Figure 3.10e). In contrast, for Zn, the effect of increased zeolite content (5 % to 10 %) on the adsorption capacity is marginal for all three zeolites (Figures 3.10b,d,f), although the increase in adsorption capacity is more apparent for clinoptilolite (Figure 3.10f). Thus, the benefit in terms of an increase in the adsorption capacity resulting from an increase in the amount of zeolite amendment is a function of both the type of zeolite and the specific metal. The extent of increase in adsorption capacity for the unamended versus 5 % zeolite-amended backfill was greater than that for the 5 % zeolite-amended versus 10 % zeolite-amended backfill, probably due to the increase in zeolite content resulted in limited access to the surface area of the added zeolite and increased excess soluble cations associated with the added zeolite interfered with the added solute for adsorption which will be discuss later.

The effect of the zeolite amendment can be evaluated in terms of the ratio  $Q_{L,amended}/Q_{L,unamended}$ . The resulting  $Q_{L,amended}/Q_{L,unamended}$  are plotted as a function of zeolite content in Figure 3.11 and summarized in Table 3.4. All of the values of  $Q_{L,amended}/Q_{L,unamended}$  for the zeolite-amended backfill sorbents were greater than unity, indicating that the maximum adsorption capacity increased by adding zeolite. For K, the values of  $Q_{L,amended}/Q_{L,unamended}$  for the backfill sorbents with 5 % zeolite ranged from 6.2 to 7.3, whereas those with 10 % zeolite ranged from 7.5 to 13.5. For Zn, the values of  $Q_{L,amended}/Q_{L,unamended}$  for the backfill sorbents with 5 % zeolite ranged from 2.8 to 3.4 with 5 % added zeolite, whereas those with 10 % zeolite ranged from 3.1 to 3.7. Thus, the increase in the adsorption capacity by increasing the amount of zeolite amendment is a function of both the type of zeolite and metal.

#### 3.4.4 Effect of Type of Zeolite

The adsorption behaviors of each type of zeolite are compared directly in Figure 3.12. For the zeolite-amended backfill sorbents, a distinction in results based on type of zeolite is apparent only for the case of 10 % added zeolite with respect to K adsorption (Figure 3.12c). In this case, K adsorption appears to be in the order chabazite-LB > chabazite-UB > clinoptilolite. Otherwise, there was little difference in the effect of type of zeolite on the adsorption of K or Zn for the zeolite-amended backfill sorbents (*i.e.*, chabazite-LB  $\approx$  chabazite-UB  $\approx$  clinoptilolite). For the case of the pure (100 %) zeolites, adsorption for K was in the relative order chabazite-LB  $\approx$  chabazite-UB > clinoptilolite (Figure 3.12e), which is consistent with the measured *CECs* (Table 3.1), whereas adsorption for Zn was in the relative order clinoptilolite > chabazite-LB  $\approx$  chabazite-UB. These results are consistent with those previously noted.

Values of  $Q_{L,amended}/Q_{L,unamended}$  are shown as a function of the type of zeolite for each backfill in Figure 3.13. Values of  $Q_{L,amended}/Q_{L,unamended}$  for adsorption of K to backfill sorbents with 5 % zeolite were in the order clinoptilolite > chabazite-UB > chabazite-LB, whereas those for backfill sorbents with 10 % zeolite were in the order chabazite-UB > chabazite-LB > clinoptilolite (Figure 3.13a,c). Thus, clinoptilolite was more effective for backfill sorbents with 5 % zeolite, whereas chabazite was more effective for backfill sorbents with 10 % zeolite.

Values of  $Q_{L,amended}/Q_{L,unamended}$  for adsorption of Zn to the backfill sorbents with 5 % zeolite were in the relative order chabazite-UB > clinoptilolite > chabazite-LB, whereas those for backfill sorbents with 10 % zeolite were in the relative order clinoptilolite > chabazite-UB > chabazite-LB (Figure 3.13b,d). These results are approximately opposite to those for K, in that clinoptilolite was more effective than chabazite for the backfill sorbents with 10 % zeolite, while chabazite-UB was more effective than clinoptilolite for the backfill sorbents with 5 % zeolite.

The measured *CEC* is in the relative order chabazite-UB  $\geq$  chabazite-LB  $>$  clinoptilolite (Table 3.1), which agrees with the values of  $Q_{L,amended}/Q_{L,unamended}$  for the 10 % zeolite amendment regarding K, but not for the other results. The explanation for this lack of agreement between the relative values of *CEC* for the zeolites and the corresponding  $Q_{L,amended}/Q_{L,unamended}$  may be due the selectivity of zeolite, which is discussed in the following section.

### 3.4.5 Effect of Type of Sorbate

The adsorptive behaviors for K and Zn are compared directly in Figure 3.14 for the unamended backfill sorbent and the pure zeolite sorbents, and in Figure 3.15 for the zeolite-amended backfill sorbents. For the unamended backfill sorbent, about three times more Zn was adsorbed than K. For the pure zeolites, the amount of K adsorbed was greater than that for Zn for the two chabazites, but less than that for Zn for the clinoptilolite. For the zeolite-amended backfill sorbents, the difference between the amounts of K and Zn adsorbed,  $\Delta Q_L (= Q_{L,Zn} - Q_{L,K})$ , tended to decrease with increasing zeolite content for the chabazite-LB, whereas for clinoptilolite,  $\Delta Q_L$  tended to increase with increasing zeolite content. For the zeolite-amended backfill sorbent with chabazite-UB, the  $Q_{L,Zn}/Q_{L,K}$  was 1.9 for 5 % zeolite, whereas the  $Q_{L,Zn}/Q_{L,K}$  was 0.96 for 10 % zeolite.

For a given backfill sorbent, the values of the  $Q_L$  for Zn were greater than those for K (Table 3.2, Figure 3.8c,d). Thus, regardless of the mechanism(s) for adsorption, the adsorption capacities for the backfill sorbents in terms of mass for the Zn were greater than those for K. However, the relative increase in adsorption capacity ( $Q_{L,amended}/Q_{L,unamended}$ ) resulting from zeolite amendment was greater for K relative to Zn. This relative difference is even more clear based on the results shown in Figure 3.11 for the pure (100 %) zeolite sorbents, where the

$Q_{L,amended}/Q_{L,unamended}$  ranged from 43 to 82 for K, versus only from 7.1 to 14 for Zn (Table 3.4, Figure 3.11a,b).

Considering the pure zeolites, all three zeolites were less effective in adsorbing Zn relative to K (compare Figures 13e and f). Also, even though the CECs for the two chabazites were greater than the CEC for the clinoptilolite, adsorption of Zn by the two chabazites was less than that by the clinoptilolite (Figure 3.13f). These differences in adsorption behavior relative to Zn for the two basic types of zeolites (*i.e.*, chabazite versus clinoptilolite) may be due, in part, to factors affecting the relative sorptive affinities for the two metals.

For example, consider the selectivity (replaceability) series summarized in Table 3.5. Based on these selectivity series, the preferential adsorption sequence for chabazite is  $K^+ > Pb^{2+} > Zn^{2+}$  and  $K^+ > Na^+ > Ca^{2+}$ , whereas that for clinoptilolite is  $K^+ > Na^+ > Ca^{2+} > Zn^{2+}$ . Therefore, for both chabazite and clinoptilolite, the selectivity series for the principal cations of interest in this study is expected to be in the order  $K^+ > Zn^{2+}$  and  $K^+ > Na^+ > Ca^{2+}$ . Of course, these series do not recognize the potential role of chemical speciation, *e.g.*, the existence of both  $Zn^{2+}$  and  $ZnOH^+$ . This overall preference for  $K^+$  adsorption is in accordance with the greater charge density of  $K^+$  relative to  $Zn^{2+}$  (*e.g.*, Ouki and Kavannah 1997; Sherry 2003; Wingenfelder *et al.* 2005). For example, based on the charge densities shown in Table 3.6, the expected cation selectivity for zeolites is in the relative order  $K^+ > Na^+ > Zn^{2+}$ .

Also, because Zn is not preferentially adsorbed relative to other cations, the adsorption of Zn should have been affected by the soluble metals associated with the sorbents (*e.g.*,  $Na^+$ ) to a greater extent than  $K^+$ , which has been reported in other studies (Zamzow *et al.* 1990; Ouki and Kavannah 1997; Yuan *et al.* 1999; Cabrera *et al.* 2005; Wingenfelder *et al.* 2005; Motsi *et al.* 2009). Since the soluble metals associated with the constituent materials of the sorbents were

redissolved into the solution upon mixing with the KCl or ZnCl<sub>2</sub> solutions, the soluble metals represent competition for the exchange sites of the sorbents with the dissolved K or Zn.

For example, Reynolds *et al.* (1982) found that the adsorption parameters for cesium and strontium based on batch testing were lower than those back-calculated from column testing. They attributed this difference to ion competition with redissolved soluble salts in the case of the batch tests, which was not the case for the column tests because the liquid flow through the columns had flushed the redissolved soluble salts from the columns, reducing cation competition for available adsorptive sites.

As a result of this consideration, the concentrations of soluble metals in the added solution for each sorbent were calculated (Table 3.3). These calculated soluble metal concentrations were based on the soluble metal concentrations associated with each constituent material (*i.e.*, bentonite and zeolite) as reported in Chapter 2 and the amounts of each material comprising the sorbent based on the soil-to-solution ratio of 1:4 (*i.e.*, 10 g sorbent + 40 mL solution), assuming all of the soluble metals of the sorbents dissolved in the added 40 mL of solution. As shown in Table 3.3, the dominant soluble metal for each backfill was Na<sup>+</sup>, and for a given amount of zeolite amendment, the soluble Na<sup>+</sup> concentrations associated with the two chabazites were significantly greater than that associated with the clinoptilolite. Therefore, based on the aforementioned selectivity series, whereby K<sup>+</sup> adsorption is preferred relative to Na<sup>+</sup> adsorption, which in turn is preferred relative to Zn<sup>2+</sup> adsorption, preferential adsorption of K<sup>+</sup> relative to the Zn species in the case of the two chabazites may have been due, in part, to greater concentration of dissolved Na<sup>+</sup> in the BEATs involving the chabazites relative to the clinoptilolites. However, as Reynolds *et al.* (1982) noted, this conclusion does not necessarily mean that an actual cutoff wall constructed with a chabazite-amended backfill would be less

effective compared to that with clinoptilolite-amended backfill, because the soluble metals will be removed from the backfills via groundwater flow, resulting in less cation competition upon introduction of the contaminant metals into the backfill.

### 3.5 SUMMARY AND CONCLUSIONS

The potential use of three zeolites, *i.e.*, two chabazites (chabazite-LB and chabazite-UB) and a clinoptilolite, as amendments for backfill to enhance the adsorption capacity with respect to two metals, potassium (K) and zinc (Zn), was evaluated by conducting batch equilibrium adsorption tests (BEATs). The sorbents included an unamended backfill comprising a fine sand mixed with 5.8 % bentonite, and zeolite-amended backfills comprising the unamended backfill sorbent with either 5 or 10 % of one of three zeolites. The pure (100 %) zeolites also were evaluated as sorbents to provide an indication of the limiting case. The results of the BEATs were evaluated using the Freundlich and Langmuir nonlinear adsorption models.

All of the values for the Freundlich exponent,  $N_f$ , were less than unity, indicating concave (favorable), nonlinear adsorption over the range in salt concentrations (either KCl or ZnCl<sub>2</sub>) evaluated in this study. Also, a comparison of the results of the BEATs with the maximum adsorbed (solid-phase) concentration ( $C_{s,max}$ ) of the backfill sorbents based on the measured cation exchange capacity (CEC) for each backfill sorbent revealed that the adsorption behavior of the two metals was consistent with cation exchange as the dominant mechanism, provided chemical speciation (complexation) of Zn was taken into consideration. The possibility of precipitation of Zn also was considered. However, based on the relatively low values of pH for the BEATs, the available evidence from the literature suggested that precipitation likely was not a significant adsorption mechanism in this study.

Values for the Langmuir maximum adsorption capacity,  $Q_L$ , for both K and Zn were greater for the zeolite-amended backfill sorbents than for the unamended backfill sorbent, indicating an increase in the adsorption capacity for the backfill sorbents amended with zeolite. The incremental increase in  $Q_L$  for K resulting from increasing the zeolite content from 5 % to 10 % was readily apparent for the two chabazites, but only marginal for the clinoptilolite. In contrast, the incremental increase in  $Q_L$  for Zn resulting from increasing the zeolite content from 5 % to 10 % was marginal for all three zeolites.

Also, although the  $Q_L$  for the backfill sorbents were greater for Zn relative to K, the relative increase in adsorption capacity represented by  $Q_{L,amended}/Q_{L,unamended}$  resulting from zeolite amendment was greater for K relative to Zn. For example, depending on the specific zeolite, the addition of only 5 % zeolite increased  $Q_{L,amended}/Q_{L,unamended}$  by a factor ranging from 6.2 to 7.3 times for K and from 2.8 to 3.4 times for Zn, whereas 10 % zeolite amendment increased  $Q_{L,amended}/Q_{L,unamended}$  by a factor ranging from 7.5 to 13.5 for K and 3.1 to 3.7 for Zn. Thus, the benefit in terms of an increase in the adsorption capacity resulting from an increase in the amount of zeolite amendment is a function of both the type of zeolite and the specific metal.

Except for the case of 10 % added zeolite with respect to K adsorption, there was little difference in the effect of type of zeolite on the adsorption of either K or Zn for the zeolite-amended backfill sorbents (*i.e.*, chabazite-LB  $\approx$  chabazite-UB  $\approx$  clinoptilolite). The  $Q_L$  for each type of zeolite was within the range of about 50 to 100 percent of the measured *CEC* for K. However, adsorption of Zn by the two chabazites was less than that by the clinoptilolite even though the *CECs* for the two chabazites were greater than the *CEC* for the clinoptilolite. These differences in the adsorption behavior between K and Zn were attributed to the greater selectivity (adsorptive affinity) of K relative to that of Zn, and competition for available exchange sites

between Zn and other soluble metals, primarily  $\text{Na}^+$ , associated with the bentonite and zeolite of the backfill sorbents.

The results of this study indicate that the containment function of vertical cutoff walls with respect to metals can be significantly enhanced by amending the backfill with as little as 5 or 10 % of a high *CEC* zeolite. However, the enhanced adsorption capacity will be a function of both the metal and the type and amount of zeolite, such that material-specific adsorption studies will be required for practical applications. Also, given the well-recognized limitations in extending the results of BEATs to field applications, such as unrepresentative soil-to-solution ratios in the BEATs relative to the field and the existence of static (no flow) conditions in the BEATs, prudence dictates that additional evaluation may be warranted before full-scale implementation is undertaken. Such evaluation may include laboratory column testing, contaminant transport modeling, and/or pilot-scale demonstration.

Table 3.1. Comparison of the measured and calculated cation exchange capacities for the sorbents evaluated in this study.

Sorbent Amendment Characteristics		Cation Exchange Capacity, $CEC$ ( $\text{cmol}_c/\text{kg}$ )		
Type of Zeolite	Amount of Zeolite (%)	Measured <sup>a</sup>	Calculated <sup>b</sup>	Measured/Calculated
NA <sup>c</sup>	0	4.65	4.84	0.96
Chabazite-LB	5	17.4	16.4	1.06
Chabazite-LB	10	25.2	28.0	0.90
Chabazite-LB	100	232	-	-
Chabazite-UB	5	16.0	17.3	0.92
Chabazite-UB	10	26.2	29.8	0.88
Chabazite-UB	100	250	-	-
Clinoptilolite	5	14.5	13.8	1.05
Clinoptilolite	10	27.3	22.8	1.20
Clinoptilolite	100	180	-	-

<sup>a</sup> ASTM D7503 (ASTM 2010).

<sup>b</sup> Calculated  $CEC = 5.8\%/100\% \times CEC_{\text{bentonite}} + (0, 5, \text{ or } 10\%)/100\% \times CEC_{\text{zeolite}}$ , where the measured  $CEC$  of the bentonite =  $83.4\text{cmol}_c/\text{kg}$  based on Chapter 2.

<sup>c</sup> NA = Not applicable (*i.e.*, unamended backfill sorbent).

Table 3.2. Fitting parameter values for adsorption testing results.

Sorbent Amendment Characteristics		Metal	Final (Equilibrium) pH	Adsorption Model Fitting Parameters <sup>a</sup>						
Type of Zeolite	Amount of Zeolite (%)			Langmuir Model				Freundlich Model		
				$K_L$ (L/mg)	$Q_L$ (mg/kg)	$K_L Q_L$ (L/kg)	$r^2$	$K_f$ (L/kg)	$N_f$	$r^2$
NA <sup>b</sup>	0	K	6.9 – 8.0	0.00301	813	2.4	0.666	250	0.13	0.518
Chabazite-LB	5	K	7.7 – 8.0	0.00379	5,080	19.3	0.954	638	0.24	0.912
Chabazite-LB	10	K	7.5 – 7.9	0.00464	8,230	38.2	0.960	934	0.25	0.919
Chabazite-LB	100	K	7.3 – 7.9	0.000977	66,800	65.3	0.977	1090	0.44	0.928
Chabazite-UB	5	K	7.7 – 8.2	0.00305	5,460	16.7	0.946	608	0.25	0.923
Chabazite-UB	10	K	6.8 – 8.1	0.00202	11,000	22.2	0.952	635	0.32	0.972
Chabazite-UB	100	K	7.5 – 8.3	0.00122	61,200	74.7	0.964	1490	0.39	0.859
Clinoptilolite	5	K	7.4 – 8.1	0.000813	5,930	4.8	0.915	221	0.35	0.929
Clinoptilolite	10	K	7.9 – 8.2	0.00223	6,120	13.6	0.881	477	0.29	0.931
Clinoptilolite	100	K	8.1 – 9.0	0.00219	35,200	77.1	0.958	1420	0.35	0.883
NA <sup>b</sup>	0	Zn	5.3 – 6.8	0.00379	3,110	11.8	0.721	473	0.21	0.934
Chabazite-LB	5	Zn	4.8 – 5.6	0.000468	8,680	4.1	0.872	300	0.34	0.942
Chabazite-LB	10	Zn	4.8 – 5.9	0.000561	9,740	5.5	0.859	370	0.34	0.930
Chabazite-LB	100	Zn	4.7 – 7.9	0.000594	22,200	13.2	0.968	553	0.39	0.988
Chabazite-UB	5	Zn	4.7 – 5.5	0.000271	10,500	2.8	0.937	107	0.46	0.965
Chabazite-UB	10	Zn	4.9 – 5.9	0.000374	10,600	4.0	0.955	170	0.42	0.953
Chabazite-UB	100	Zn	4.4 – 8.1	0.000424	26,300	11.2	0.965	391	0.44	0.969
Clinoptilolite	5	Zn	5.1 – 5.7	0.000251	9,380	2.4	0.861	97.1	0.45	0.836
Clinoptilolite	10	Zn	5.1 – 5.8	0.000317	11,400	3.6	0.958	146	0.44	0.933
Clinoptilolite	100	Zn	4.7 – 9.3	0.000613	43,300	26.5	0.929	1290	0.36	0.968

<sup>a</sup>  $K_L$  = Langmuir constant,  $Q_L$  = maximum adsorbed concentration for the solute of interest (Eq. 3.2);  $K_f$  = Freundlich unit adsorption capacity,  $N_f$  = Freundlich exponent (Eq. 3.3);  $r^2$  = coefficient of determination.

<sup>b</sup> NA = Not applicable (*i.e.*, unamended backfill sorbent).

Table 3.3. Equivalent liquid-phase concentrations of exchangeable metals and soluble metals in the sorbents.

Sorbent Amendment Characteristics		Equivalent Liquid-Phase Soluble Metals Concentrations (mg/L) <sup>a</sup>				
Type of Zeolite	Amount of Zeolite (%)	Ca <sup>2+</sup>	Mg <sup>2+</sup>	Na <sup>+</sup>	K <sup>+</sup>	Sum
NA <sup>b</sup>	0	0.35	0.11	29.6	0.85	30.9
Chabazite-LB	5	3.00	1.72	115	1.58	121
Chabazite-LB	10	5.66	3.33	201	2.32	212
Chabazite-LB	100	212	129	6,850	58.7	7,250
Chabazite-UB	5	1.78	1.88	141	2.02	147
Chabazite-UB	10	3.20	3.66	253	3.20	263
Chabazite-UB	100	114	142	8,920	93.8	9,270
Clinoptilolite	5	1.03	1.99	42.1	5.69	50.8
Clinoptilolite	10	1.70	3.87	54.6	10.5	70.7
Clinoptilolite	100	54.1	151	1,000	387	1,590

<sup>a</sup> Calculated based on the measured exchangeable and soluble metals of the constituent materials as reported in Chapter 2 and the added amount of the constituent materials in each sorbents, and then converted to the expected concentration for the BEATs test (*i.e.*, 10 g sorbent + 40 mL solution).

<sup>b</sup> NA = Not applicable (*i.e.*, unamended backfill sorbent).

Table 3.4. Comparison of Langmuir adsorption capacities versus maximum solid-phase concentrations based on measured *CEC* values.

Sorbent Amendment Characteristics		Metal	Langmuir Adsorption Capacity, $Q_L$ (mg/kg)	Theoretical Maximum Solid-Phase Concentration, $C_{s,max}$ (mg/kg)			Adsorption Capacity Ratios			
Type of Zeolite	Amount of Zeolite (%)			$K^+$	$Zn^{2+}$	$ZnOH^+$	$Q_L/C_{s,max}$			$Q_{L,amended}/Q_{L,unamended}$
							$K^+$	$Zn^{2+}$	$ZnOH^+$	
NA <sup>a</sup>	0	K	813	1818	-	-	0.45	-	-	1.0
Chabazite-LB	5	K	5,080	6803	-	-	0.75	-	-	6.2
Chabazite-LB	10	K	8,230	9853	-	-	0.84	-	-	10
Chabazite-LB	100	K	66,800	90747	-	-	0.74	-	-	82
Chabazite-UB	5	K	5,460	6256	-	-	0.87	-	-	6.7
Chabazite-UB	10	K	11,000	10244	-	-	1.07	-	-	14
Chabazite-UB	100	K	61,200	97589	-	-	0.63	-	-	75
Clinoptilolite	5	K	5,930	5669	-	-	1.05	-	-	7.3
Clinoptilolite	10	K	6,120	10674	-	-	0.57	-	-	7.5
Clinoptilolite	100	K	35,200	70377	-	-	0.50	-	-	43
NA <sup>a</sup>	0	Zn	3,110	-	1520	3831	-	2.1	0.81	1.0
Chabazite-LB	5	Zn	8,680	-	5689	14334	-	1.51	0.60	2.8
Chabazite-LB	10	Zn	9,740	-	8239	20760	-	1.2	0.47	3.1
Chabazite-LB	100	Zn	22,200	-	75885	191122	-	0.29	0.12	7.1
Chabazite-UB	5	Zn	10,500	-	5231	13181	-	2.0	0.80	3.4
Chabazite-UB	10	Zn	10,600	-	8566	21584	-	1.2	0.49	3.4
Chabazite-UB	100	Zn	26,300	-	81607	205950	-	0.32	0.13	8.5
Clinoptilolite	5	Zn	9,380	-	4741	11945	-	2.0	0.79	3.0
Clinoptilolite	10	Zn	11,400	-	8926	22490	-	1.3	0.51	3.7
Clinoptilolite	100	Zn	43,300	-	58851	148284	-	0.74	0.29	14

<sup>a</sup> NA = Not applicable (*i.e.*, unamended backfill sorbent)

Table 3.5. Reported selectivity series for zeolites and bentonite.

Type Zeolite	Reference	Selectivity Series
Chabazite	Barrer <i>et al.</i> (1969)	$Tl^+ > K^+ > Ag^+ > Rb^+ > NH_4^+ > Pb^{2+} > Na^+ = Ba^{2+} > Sr^{2+} > Ca^{2+} > Li^+$
	Kesraoui-Ouki <i>et al.</i> (1994)	$Tl^+ > Cs^+ > K^+ > Ag^+ > Rb^+ > NH_4^+ > Pb^{2+} > Na^+ = Ba^{2+} > Sr^{2+} > Ca^{2+} > Li^+$
	Ouki and Kavannagh (1997)	$Pb^{2+} > Cd^{2+} > Zn^{2+} > Co^{2+} > Cu^{2+} > Ni^{2+} > Cr^{3+}$
	Torracca <i>et al.</i> (1998)	$NH_4^+ > K^+ > Pb^{2+} > Na^+$
	Ibrahim <i>et al.</i> (2002)	$Ni^{2+} > Cr^{3+} > Cu^{2+} > Fe^{2+} > Zn^{2+}$
	Manufacturer Product Info	$Tl^+ > Cs^+ > K^+ > Ag^+ > Rb^+ > NH_4^+ > Pb^{2+} > Na^+ = Ba^{2+} > Sr^{2+} > Ca^{2+} > Li^+$
Clinoptilolite	Blanchard <i>et al.</i> (1984)	$Pb^{2+} > NH_4^+ > Cu^{2+}, Cd^{2+} > Zn^{2+}, Co^{2+} > Ni^{2+} > Hg^{2+}$
	Cabrera <i>et al.</i> (2005)	$Cu^{2+} \gg Zn^{2+} > Ni^{2+}$
	Colella (1996)	$K^+ > NH_4^+ > Na^+ > Ca^{2+} > Mg^{2+}$
	Czárán <i>et al.</i> (1986)	$K^+ > NH_4^+ > Ag^+ \geq Pb^{2+} > Na^+ > Ca^{2+} > Li^+$
	Faghihian <i>et al.</i> (1999)	$Pb^{2+} > Cd^{2+} > Ba^{2+} > Sr^{2+} > Cs^+ > Ni^{2+}$
	Kesraoui-Ouki <i>et al.</i> (1994)	$Cs^+ > K^+ > Sr^{2+} = Ba^{2+} > Ca^{2+} \gg Na^+ > Li^+; Pb^{2+} > Ag^+ > Cd^{2+} \approx Zn^{2+} > Cu^{2+} > Na^+$
	Motsi <i>et al.</i> (2009)	$Fe^{2+} > Zn^{2+} > Cu^{2+} > Mn^{2+}$
	Mumpton (1999)	$Cs^+ > Rb^+ > K^+ > NH_4^+ > Ba^{2+} > Sr^{2+} > Na^+ > Ca^{2+} > Fe > Al > Mg^{2+} > Li^+$
	Ouki and Kavannagh (1997)	$Pb > Cu > Cd > Zn > Cr > Co > Ni$
	Yuan <i>et al.</i> (1999)	$Pb^{2+} > Cu^{2+} > Zn^{2+} > Cd^{2+}$
	Zamzow <i>et al.</i> (1990)	$Pb^{2+} > Cd^{2+} > Cs^+ > Cu^{2+} > Cr^{3+} > Zn^{2+} > Ni^{2+} > Hg^{2+}$
	Manufacturer Product Info	$Pb^{2+} > K^+ > NH_4^+ > Ca^{2+} > Cd^{2+} > Cu^{2+} > Co^{2+} > Zn^{2+} > Ni^{2+}$
Bentonite	Gast (1969)	$Cs^+ > Rb^+ > K^+ > Na^+ > Li^+$
	Kubilay <i>et al.</i> (2007)	$Zn^{2+} > Cu^{2+} > Co^{2+}$
	Álvarez-Ayuso and García-Sánchez (2003)	$Cr^{2+} > Cu^{2+} > Cd^{2+} > Ni^{2+} > Zn^{2+}$
	Bohn <i>et al.</i> (2002)	$Th^{4+} > H(Al^{3+}) \approx La^{3+} > Ba^{2+} \approx Sr^{2+} > Ca^{2+} > Mg^{2+} \approx Cs^+ > Rb^+ > K^+ \approx NH_4^+ > Na^+ \approx Li^+$

Table 3.6. Hydration ion charge density for the principle cations of this study.

Ion	Hydrated Ionic Radius, $r_h$ (Å) <sup>a</sup>	Hydrated Charge Density, $\rho_c$ (eq/Å <sup>3</sup> ) <sup>b</sup>
Ca <sup>2+</sup>	4.12	0.0068
K <sup>+</sup>	3.31	0.0066
Mg <sup>2+</sup>	4.28	0.0061
Na <sup>+</sup>	3.58	0.0052
Zn <sup>2+</sup>	4.30	0.0006

<sup>a</sup> From: Volkov *et al.* (1997).

$$^b \rho_c = \frac{|z|}{\frac{4}{3}\pi r_h^3}$$

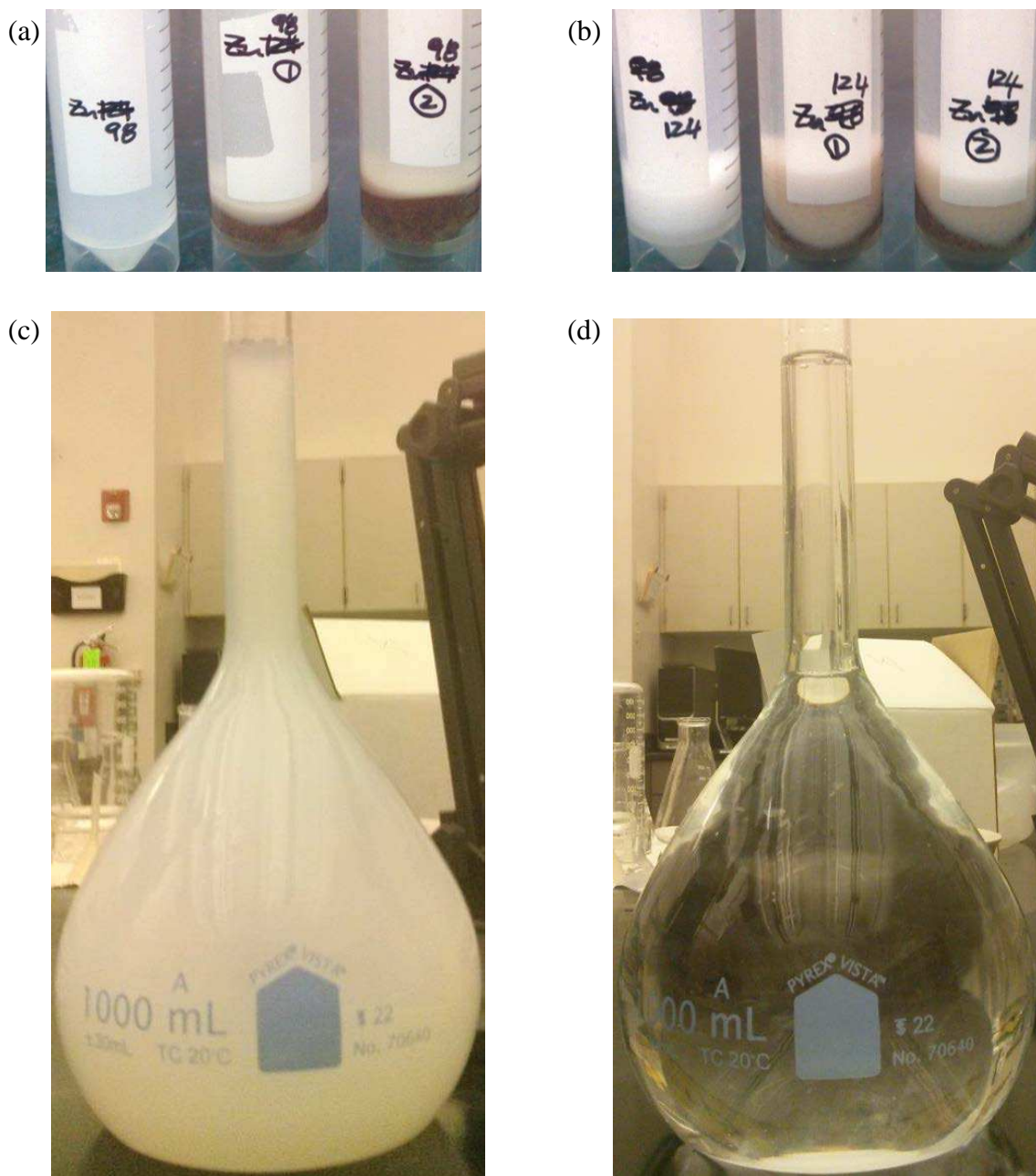


Figure 3.1. Formation of precipitation in zinc chloride solution: (a) after batch test for source concentration of 98 mM without acid addition; (b) after batch test for source concentration of 124 mM without acid addition; (c) stock solution with target concentration of 200 mM before acid addition (pH 5.27); (d) stock solution with target concentration of 200 mM after addition of 1 mL of 37 % HCl (pH 2.76).

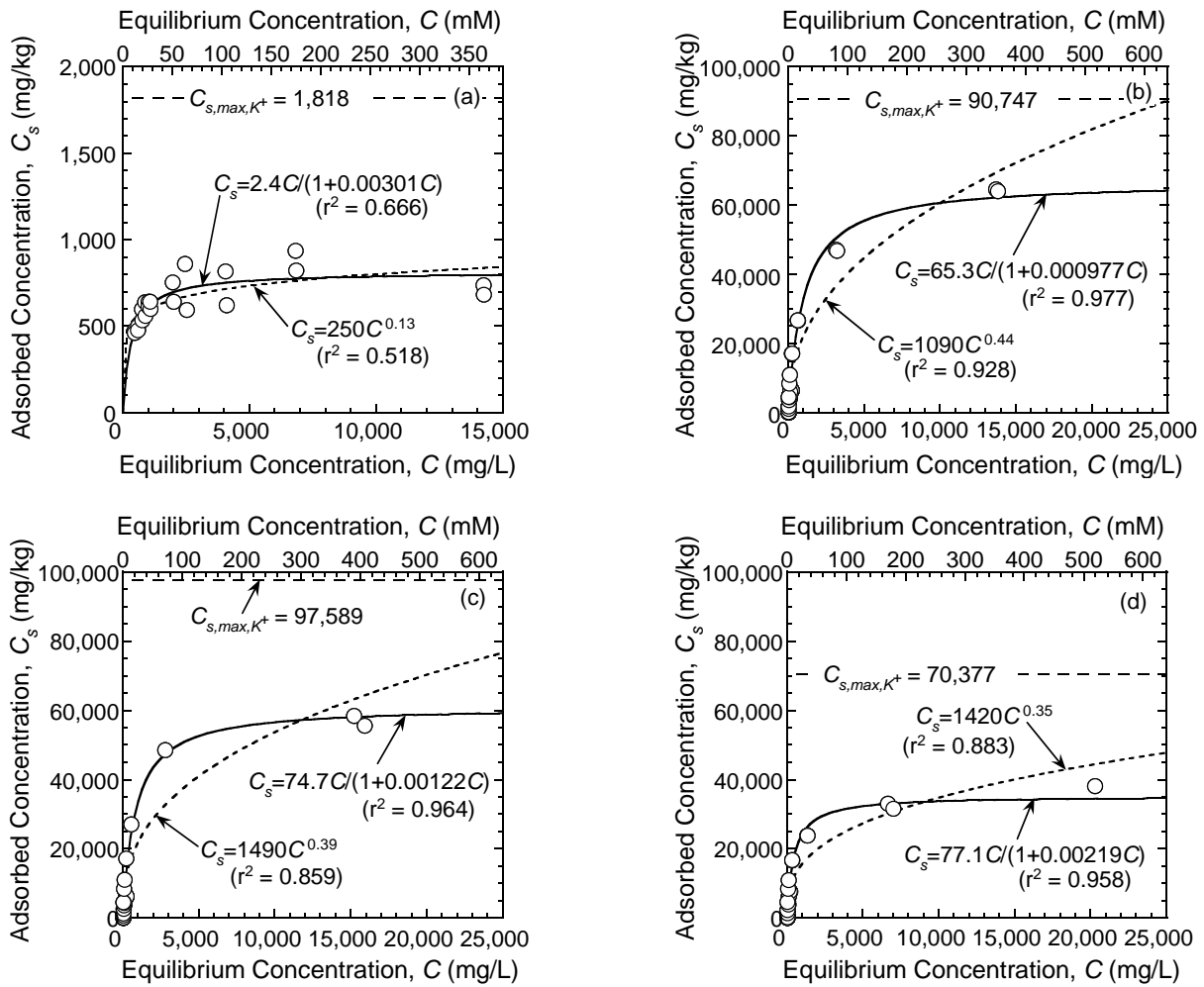


Figure 3.2. Fitted Freundlich (dashed line) and Langmuir (solid line) adsorption models for potassium (K) adsorption: (a) unamended backfill sorbent; (b) 100 % chabazite-LB; (c) 100 % chabazite-UB; (d) 100 % clinoptilolite.

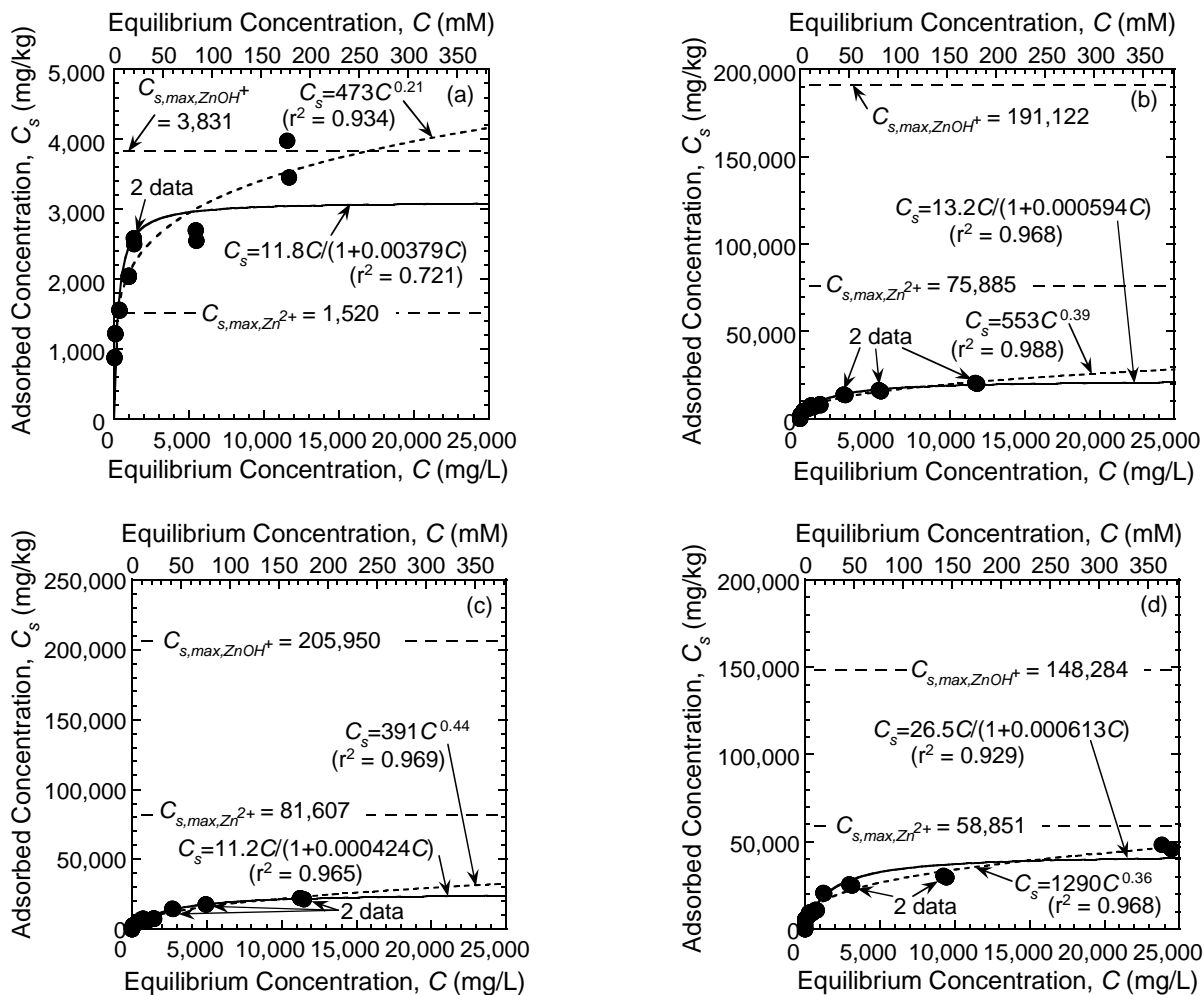


Figure 3.3. Fitted Freundlich (dashed line) and Langmuir (solid line) adsorption models for zinc (Zn) adsorption: (a) unamended backfill sorbent; (b) 100 % chabazite-LB; (c) 100 % chabazite-UB; (d) 100 % clinoptilolite.

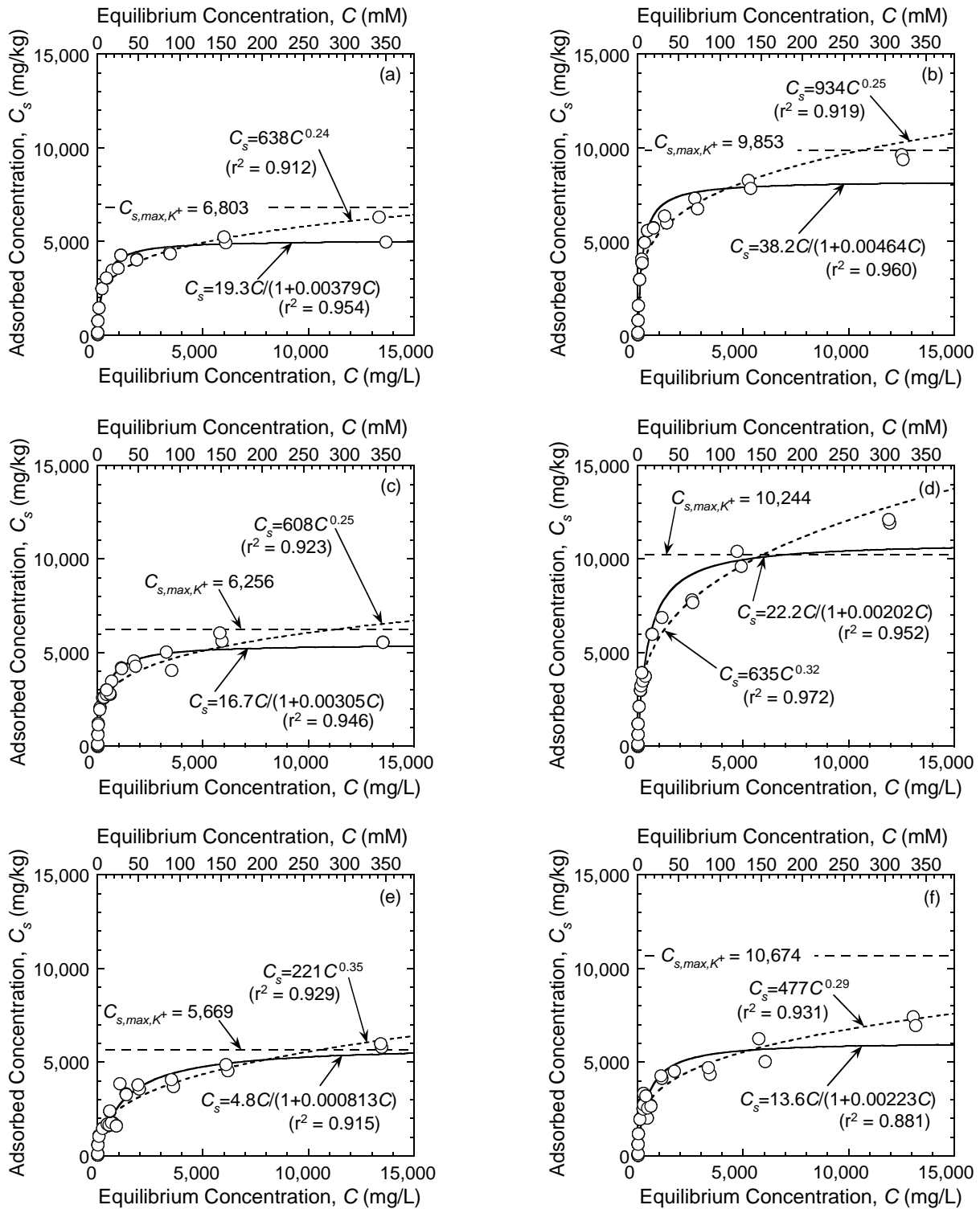


Figure 3.4. Fitted Freundlich (dashed line) and Langmuir (solid line) adsorption models for potassium (K) adsorption to zeolite-amended backfill sorbents: (a) 5 % chabazite-LB; (b) 10 % chabazite-LB; (c) 5 % chabazite-UB; (d) 10 % chabazite-UB; (e) 5 % clinoptilolite; (f) 10 % clinoptilolite.

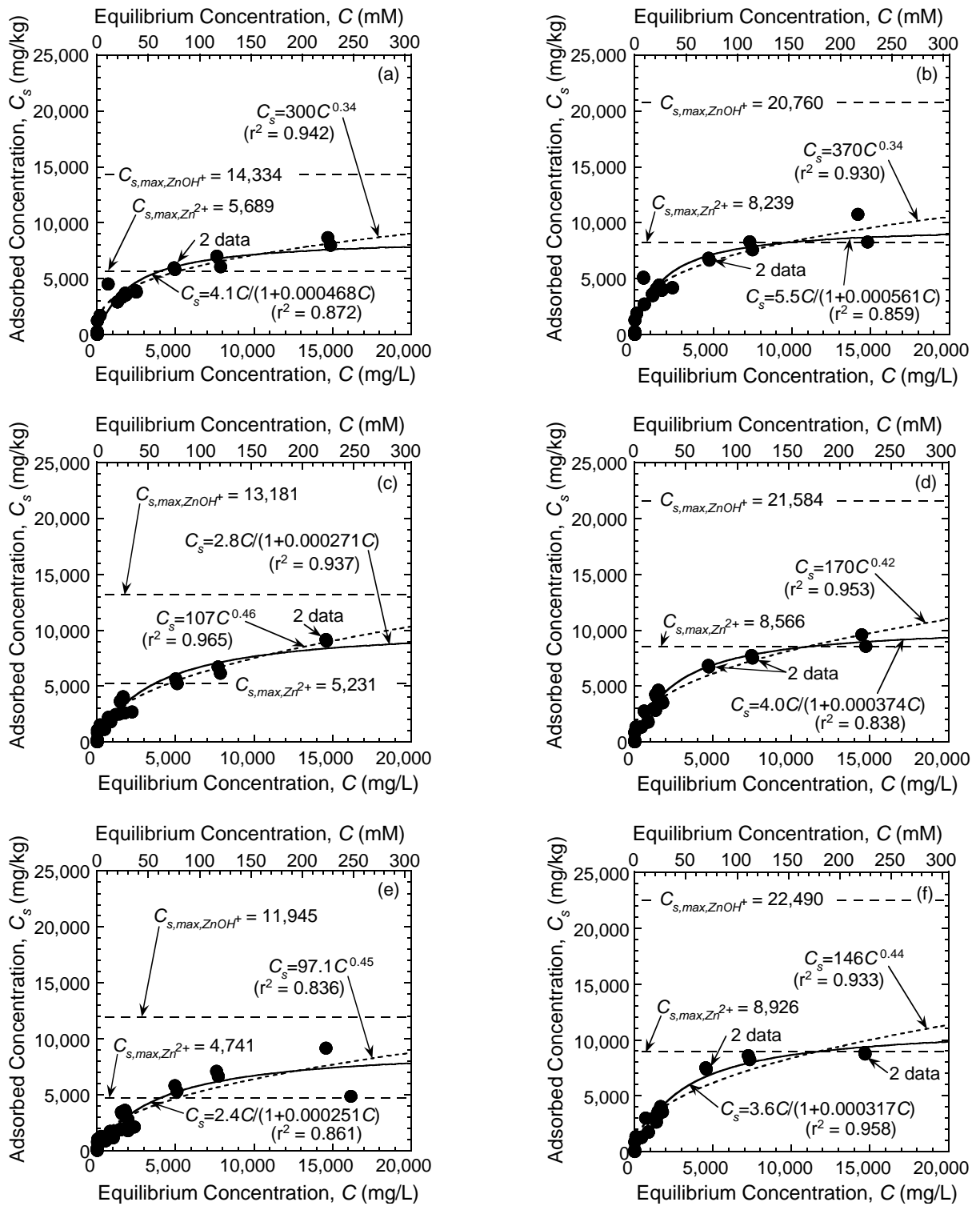


Figure 3.5. Fitted Freundlich (dashed line) and Langmuir (solid line) adsorption models for zinc (Zn) adsorption to zeolite-amended backfill sorbents: (a) 5 % chabazite-LB; (b) 10 % chabazite-LB; (c) 5 % chabazite-UB; (d) 10 % chabazite-UB; (e) 5 % clinoptilolite; (f) 10 % clinoptilolite.

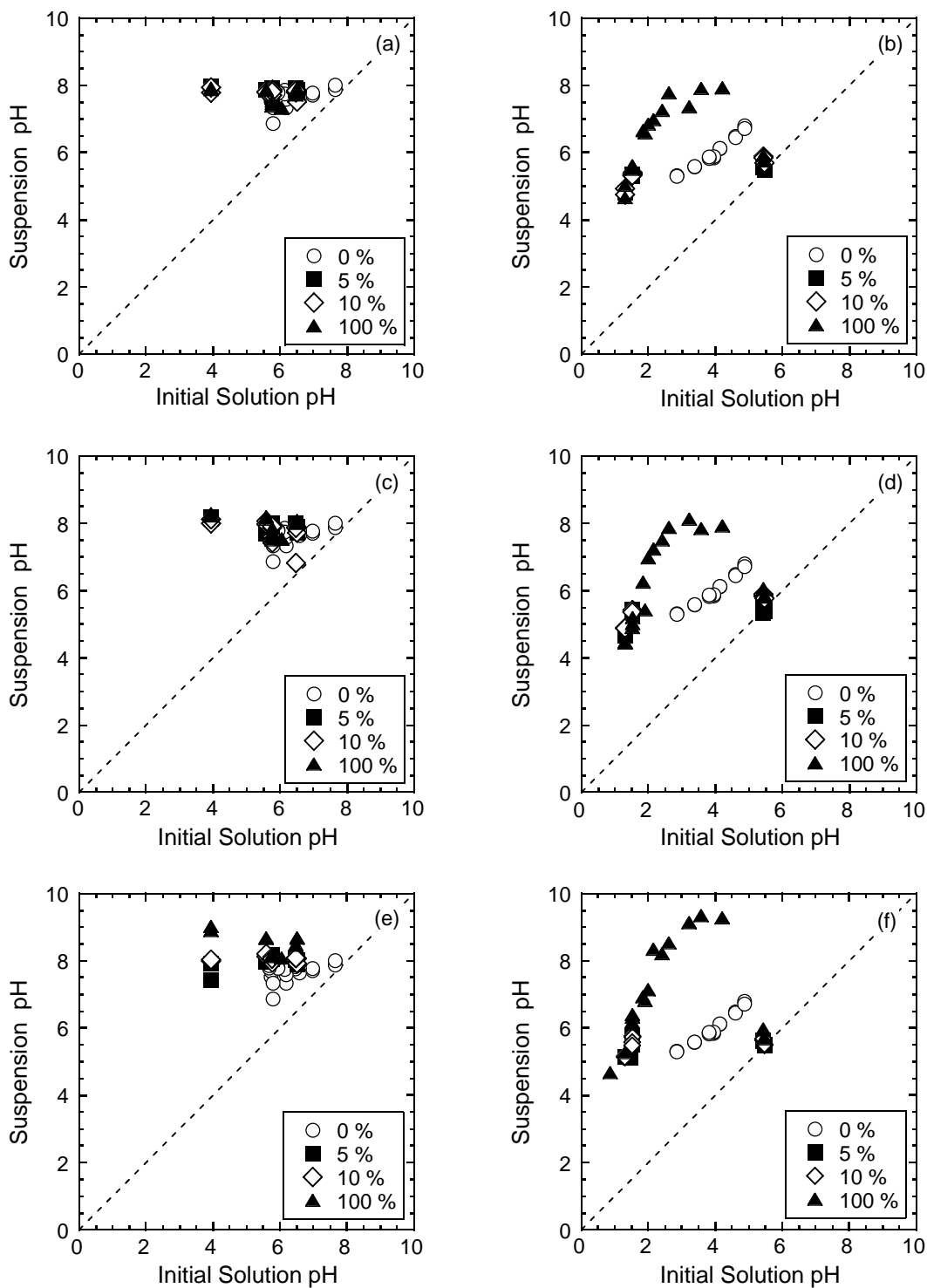


Figure 3.6. Initial salt solution pH versus the equilibrium (final) pH of the sorbate-sorbent suspension for sorbents with different percentages of zeolite amendment: (a) K with chabazite-LB; (b) Zn with chabazite-LB; (c) K with chabazite-UB; (d) Zn with chabazite-UB; (e) K with clinoptilolite; (f) Zn with clinoptilolite.

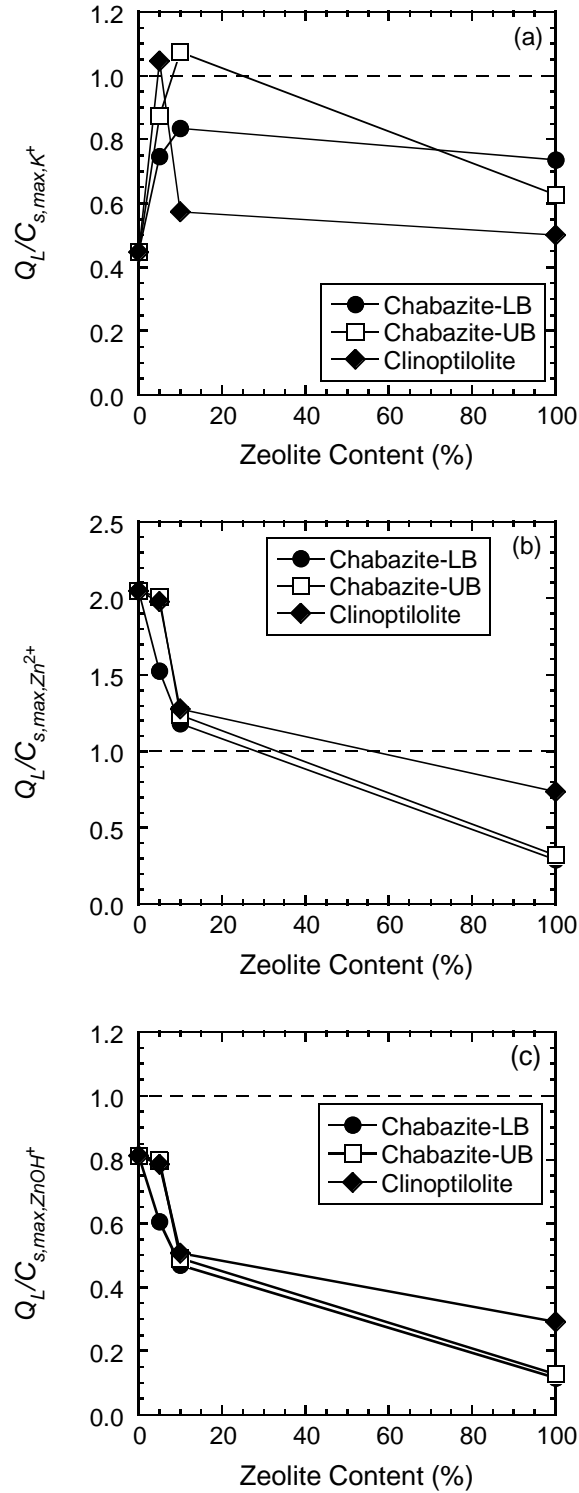


Figure 3.7. Ratio of the maximum adsorption capacity,  $Q_L$  (mg/kg) to the theoretical maximum solid-phase concentration,  $C_{s,max}$  (mg/kg) for different types and amounts of zeolite: (a)  $K^+$ ; (b)  $Zn^{2+}$ ; (c)  $ZnOH^+$ .

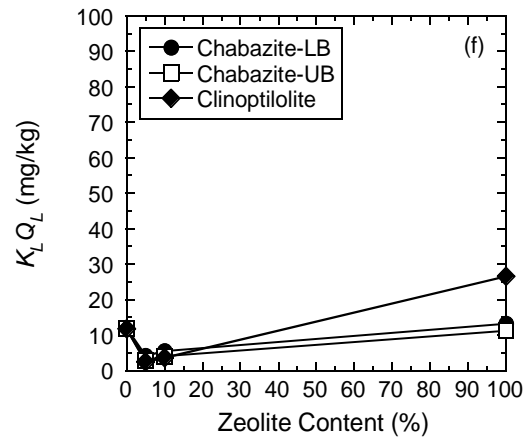
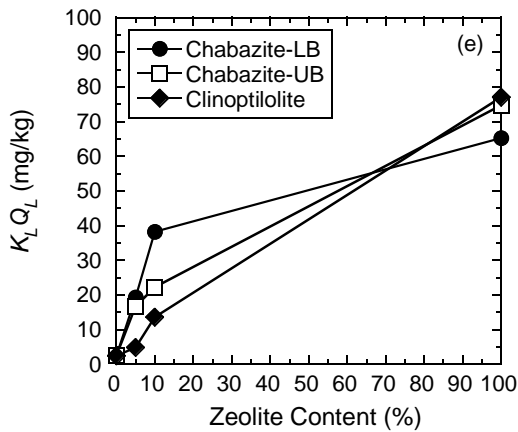
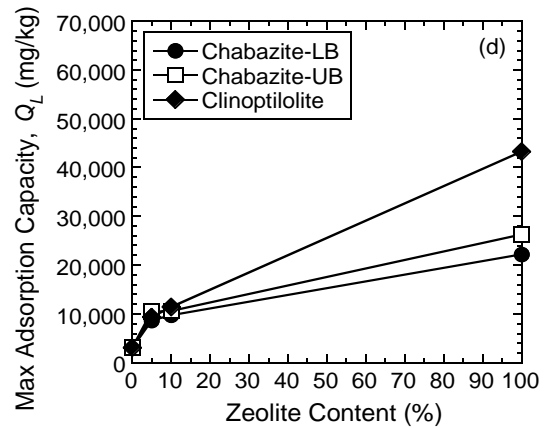
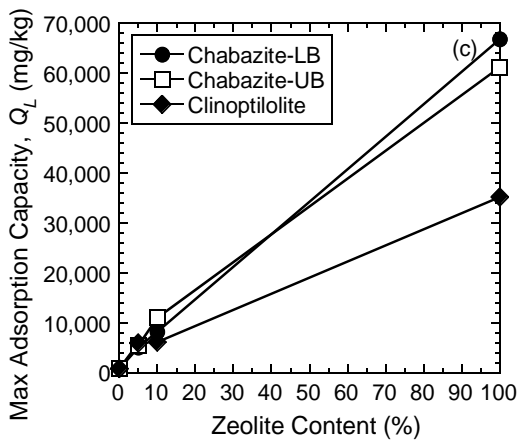
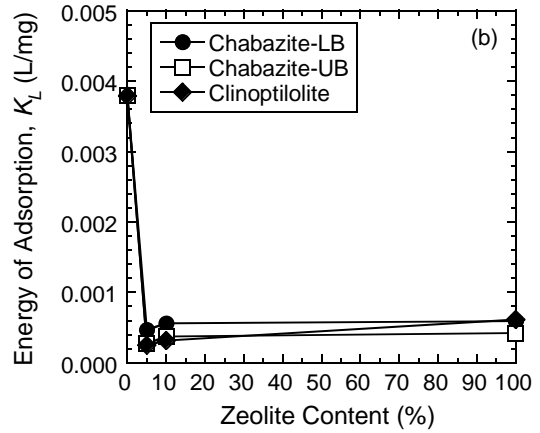
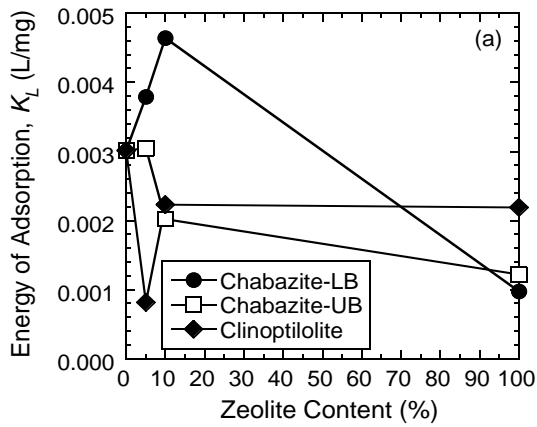


Figure 3.8. Best-fit values of the Langmuir energy of adsorption ( $K_L$ ), maximum adsorption capacity ( $Q_L$ ), and  $K_L Q_L$  for different types and amounts of zeolite: (a)  $K_L$  for K; (b)  $K_L$  for Zn; (c)  $Q_L$  for K; (d)  $Q_L$  for Zn; (e)  $K_L Q_L$  for K; (f)  $K_L Q_L$  for Zn.

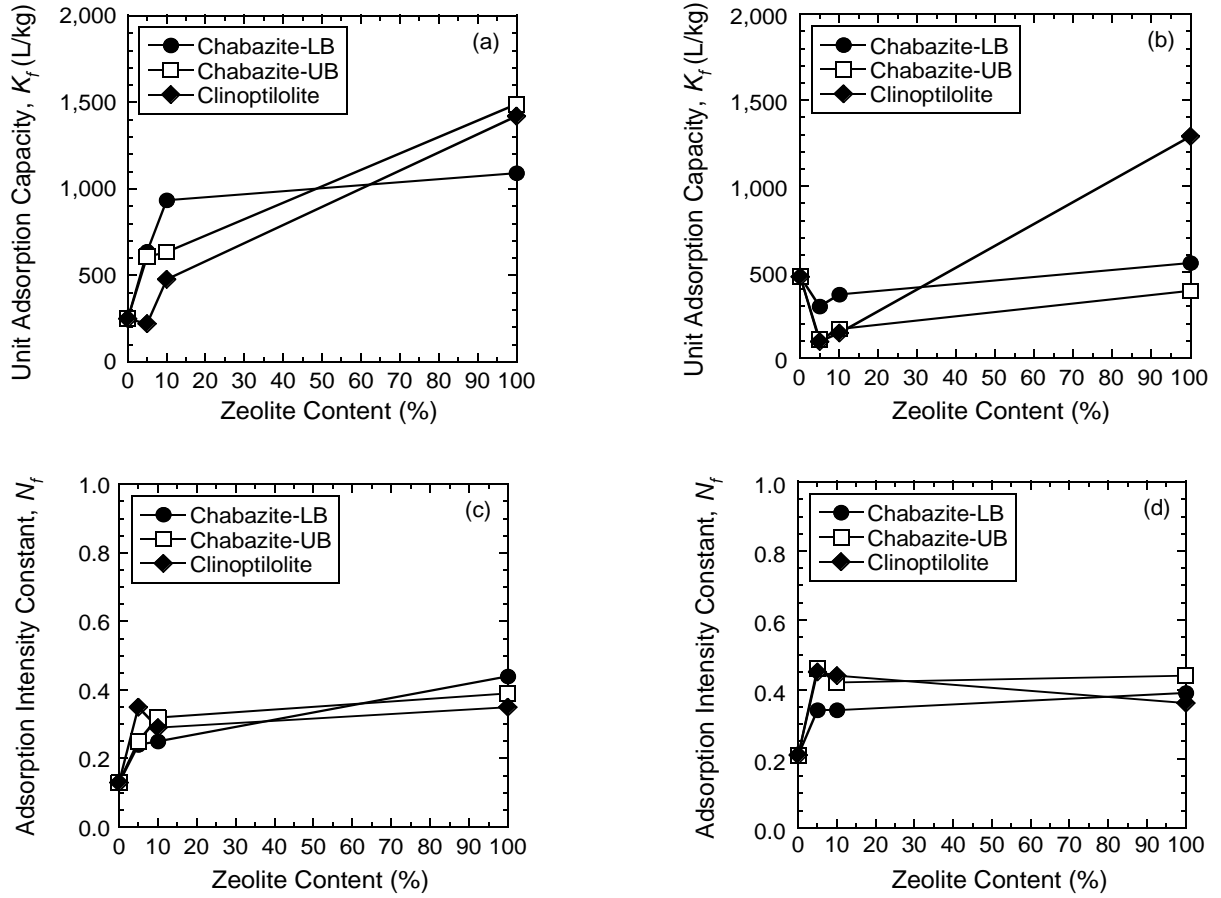


Figure 3.9. Best-fit values of the Freundlich unit adsorption capacity ( $K_f$ ) and exponent ( $N_f$ ) for different types and amounts of zeolite: (a)  $K_f$  for K; (b)  $K_f$  for Zn; (c)  $N_f$  for K; (d)  $N_f$  for Zn.

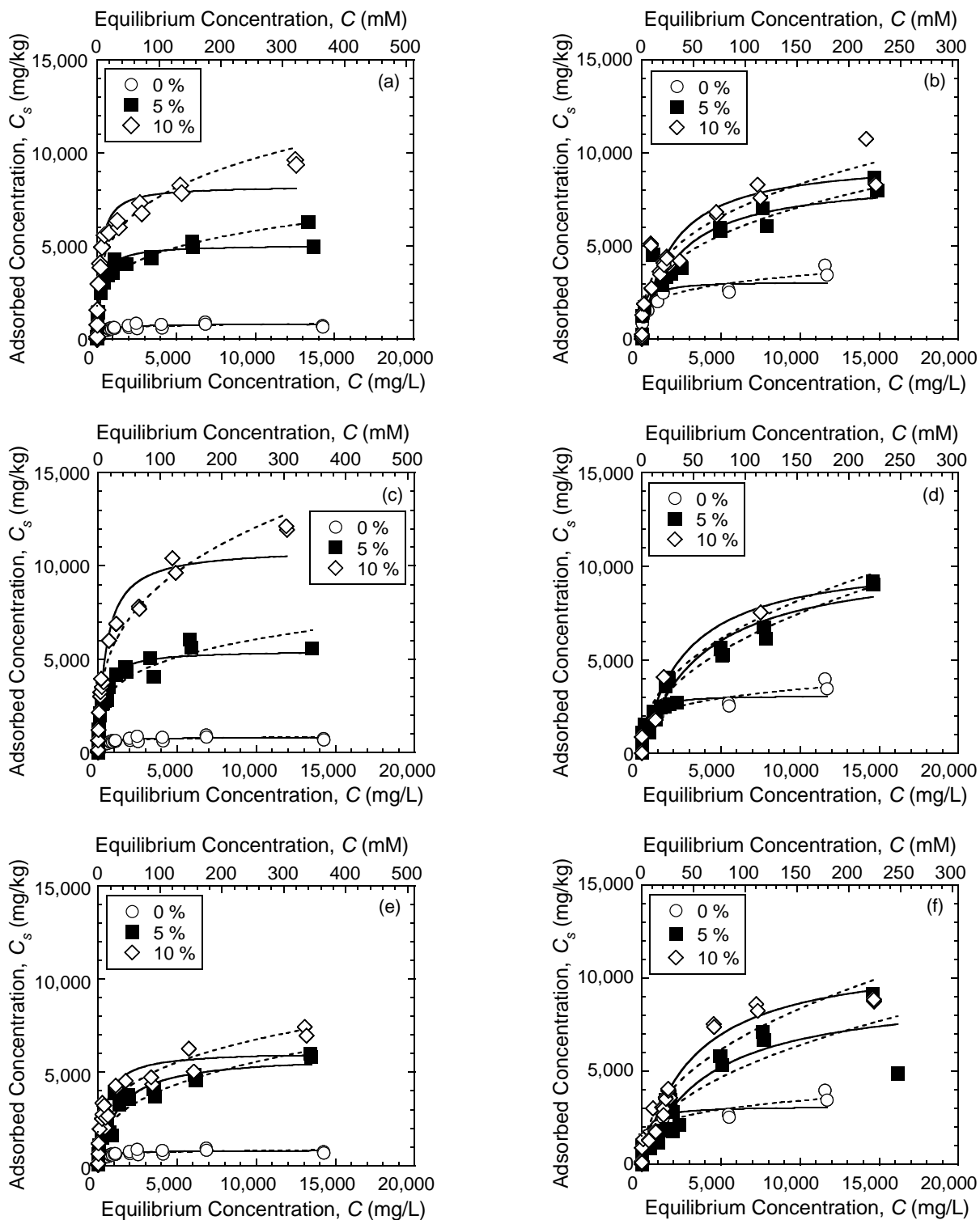


Figure 3.10. Adsorption test results fitted to the Freundlich (dashed line) and Langmuir (solid line) adsorption models for different amounts of added zeolite: (a) K with chabazite-LB; (b) Zn with chabazite-LB; (c) K with chabazite-UB; (d) Zn with chabazite-UB; (e) K with clinoptilolite; (f) Zn with clinoptilolite.

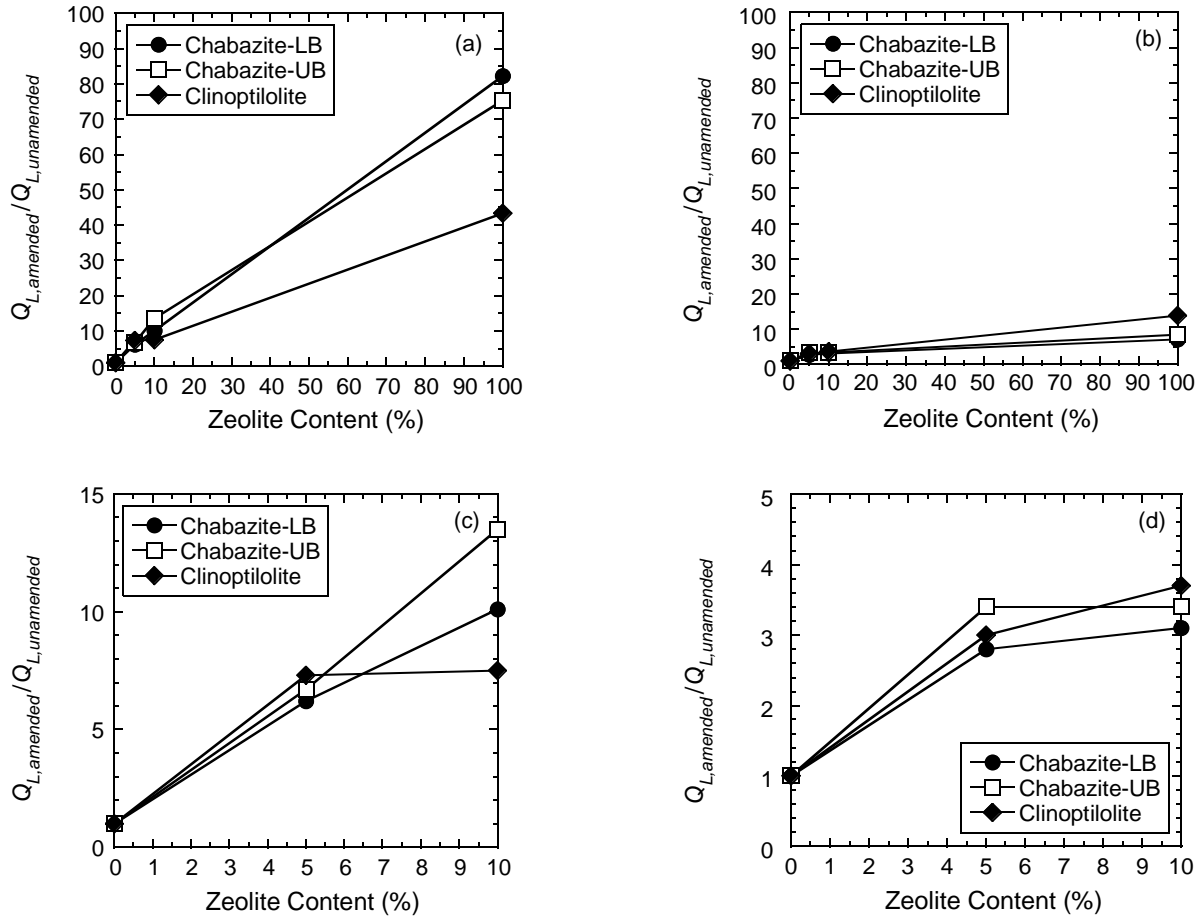


Figure 3.11. Comparison of the ratio of the maximum adsorption capacity ( $Q_L$ ) of the zeolite-amended backfill sorbents ( $Q_{L,amended}$ ) relative to the  $Q_L$  of the unamended backfill sorbent ( $Q_{L,unamended}$ ) for different types and amounts of zeolite: (a) K including 100 % zeolite; (b) Zn including 100 % zeolite; (c) K for zeolite content  $\leq 10$  %; (d) Zn for zeolite content  $\leq 10$  %.

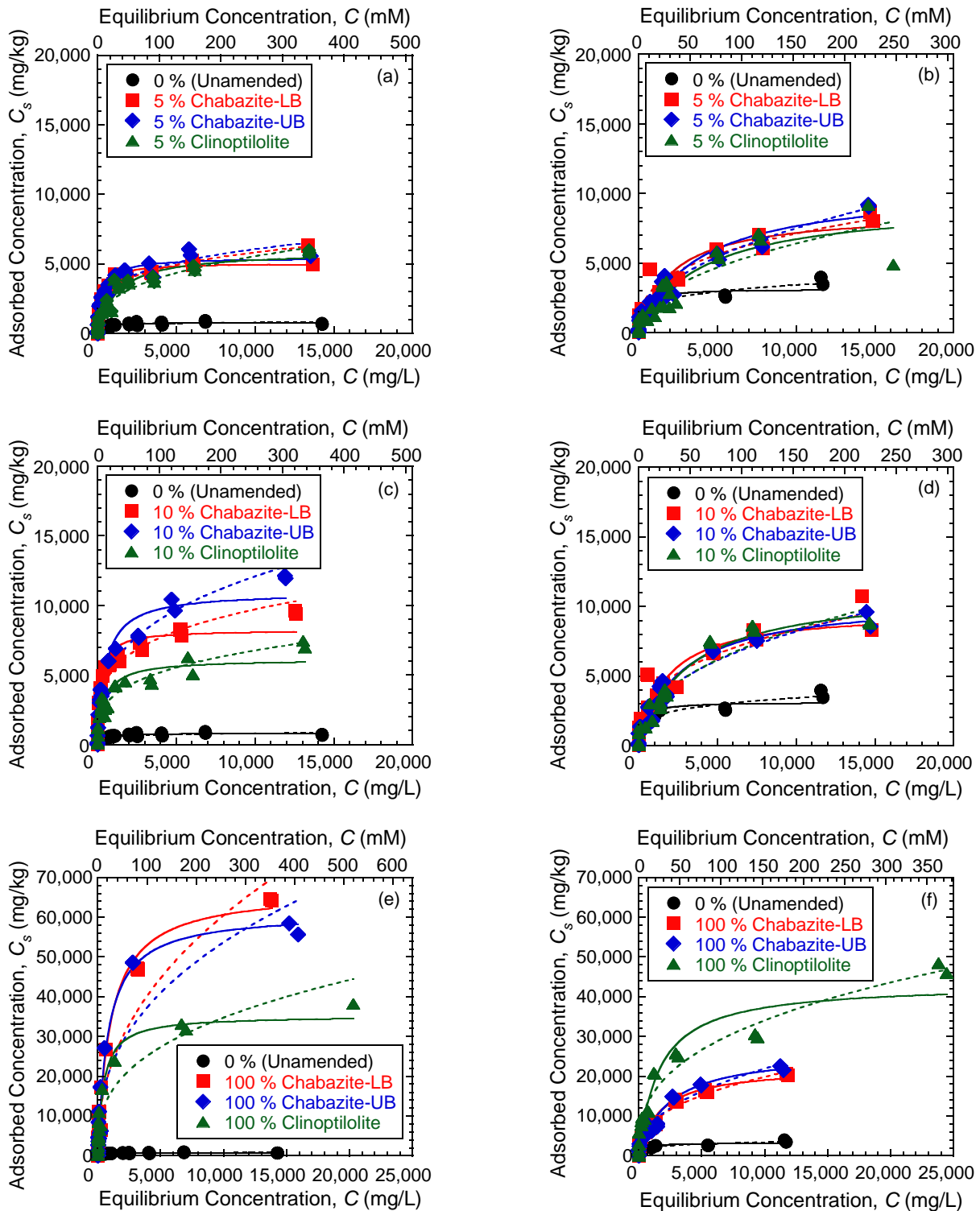


Figure 3.12. Adsorption test results fitted to the Freundlich (dashed line) and Langmuir (solid line) adsorption models for different amounts and types of zeolite: (a) K with 5 % zeolite; (b) Zn with 5 % zeolite; (c) K with 10 % zeolite; (d) Zn with 10 % zeolite; (e) K with 100 % zeolite K; (f) Zn with 100 % zeolite.

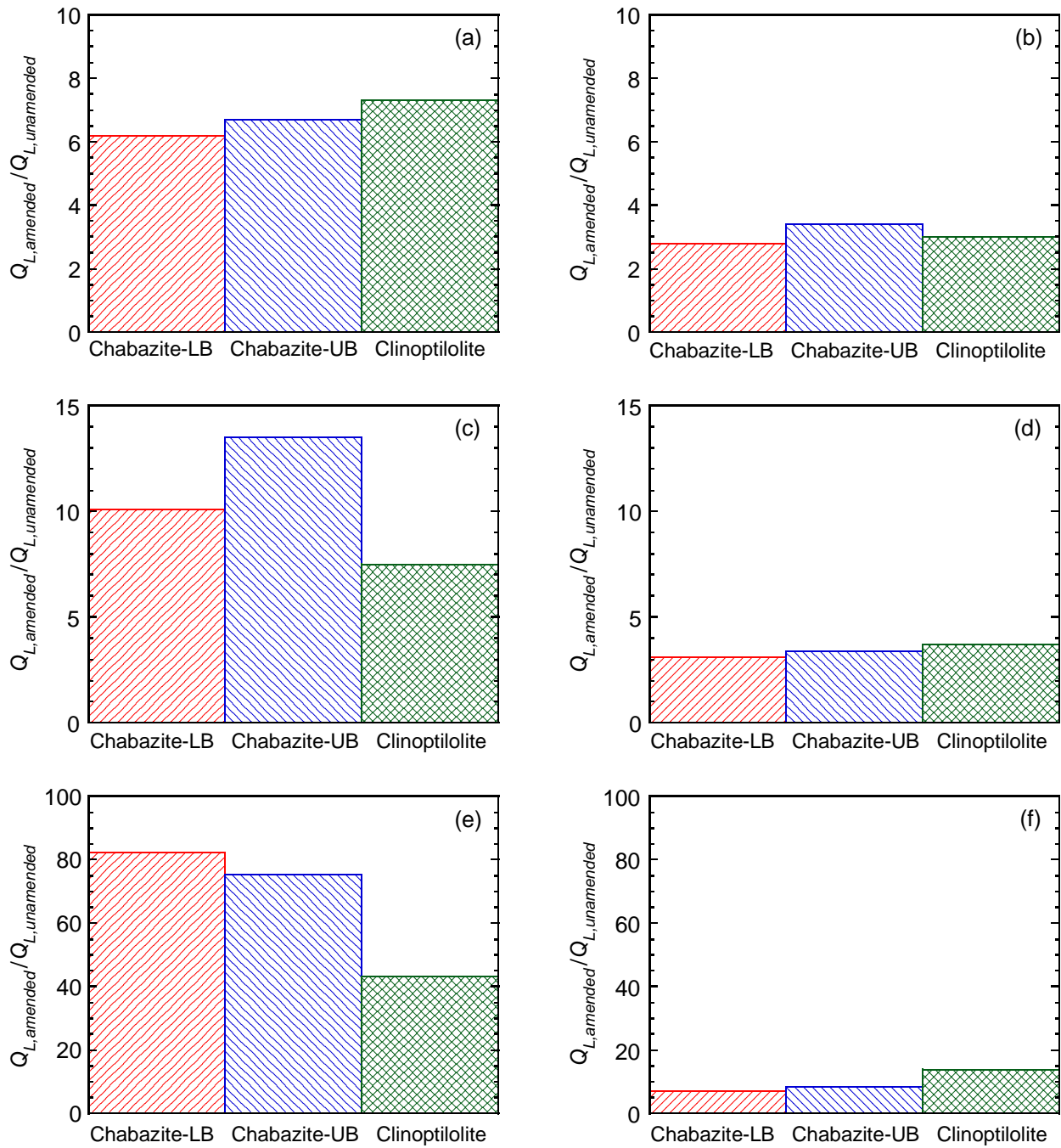


Figure 3.13. Comparison of the ratio of the maximum adsorption capacity ( $Q_L$ ) of the zeolite-amended backfill sorbents ( $Q_{L,amended}$ ) relative to the  $Q_L$  of the unamended backfill sorbent ( $Q_{L,unamended}$ ) for different types of zeolite: (a) K with 5 % zeolite; (b) Zn with 5 % zeolite; (c) K with 10 % zeolite; (d) Zn with 10 % zeolite; (e) K with 100 % zeolite; (f) Zn with 100 % zeolite.

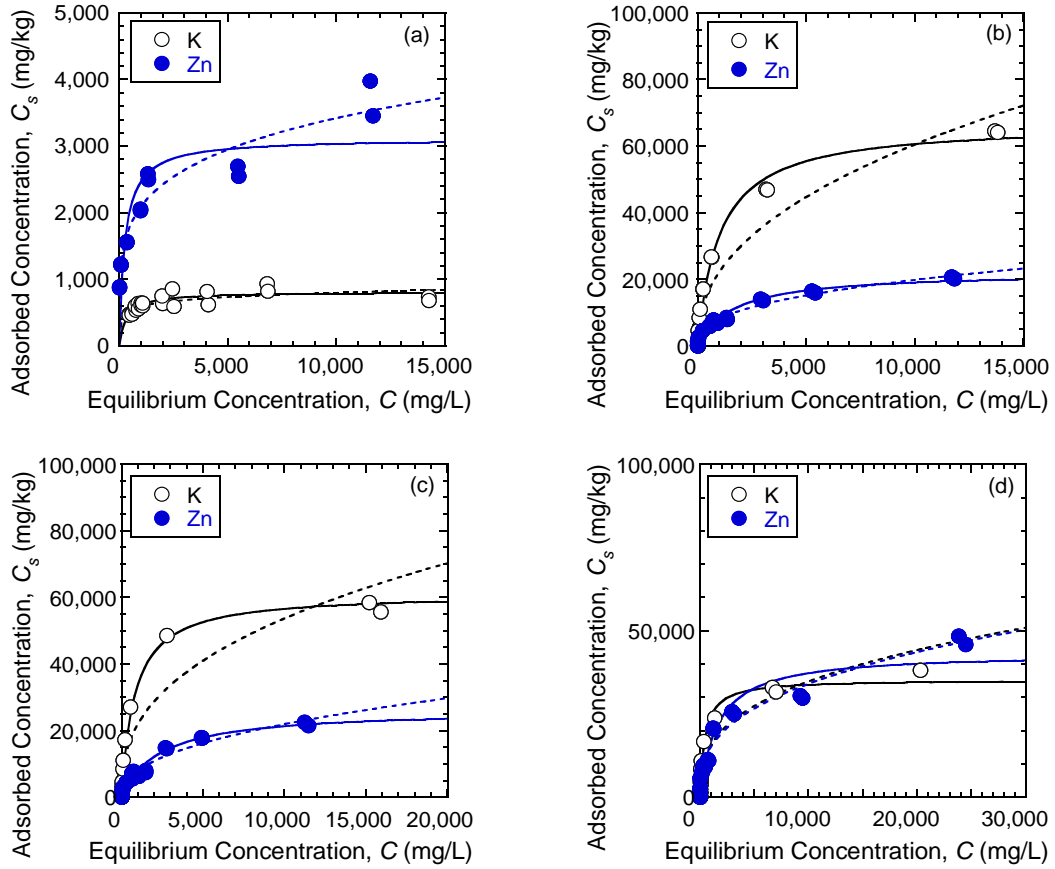


Figure 3.14. Comparison of potassium (K) versus zinc (Zn) adsorption including fitted Freundlich (dash lines) and Langmuir (solid lines) adsorption models: (a) unamended backfill sorbent; (b) 100 % chabazite-LB; (c) 100 % chabazite-UB; (d) 100 % clinoptilolite.

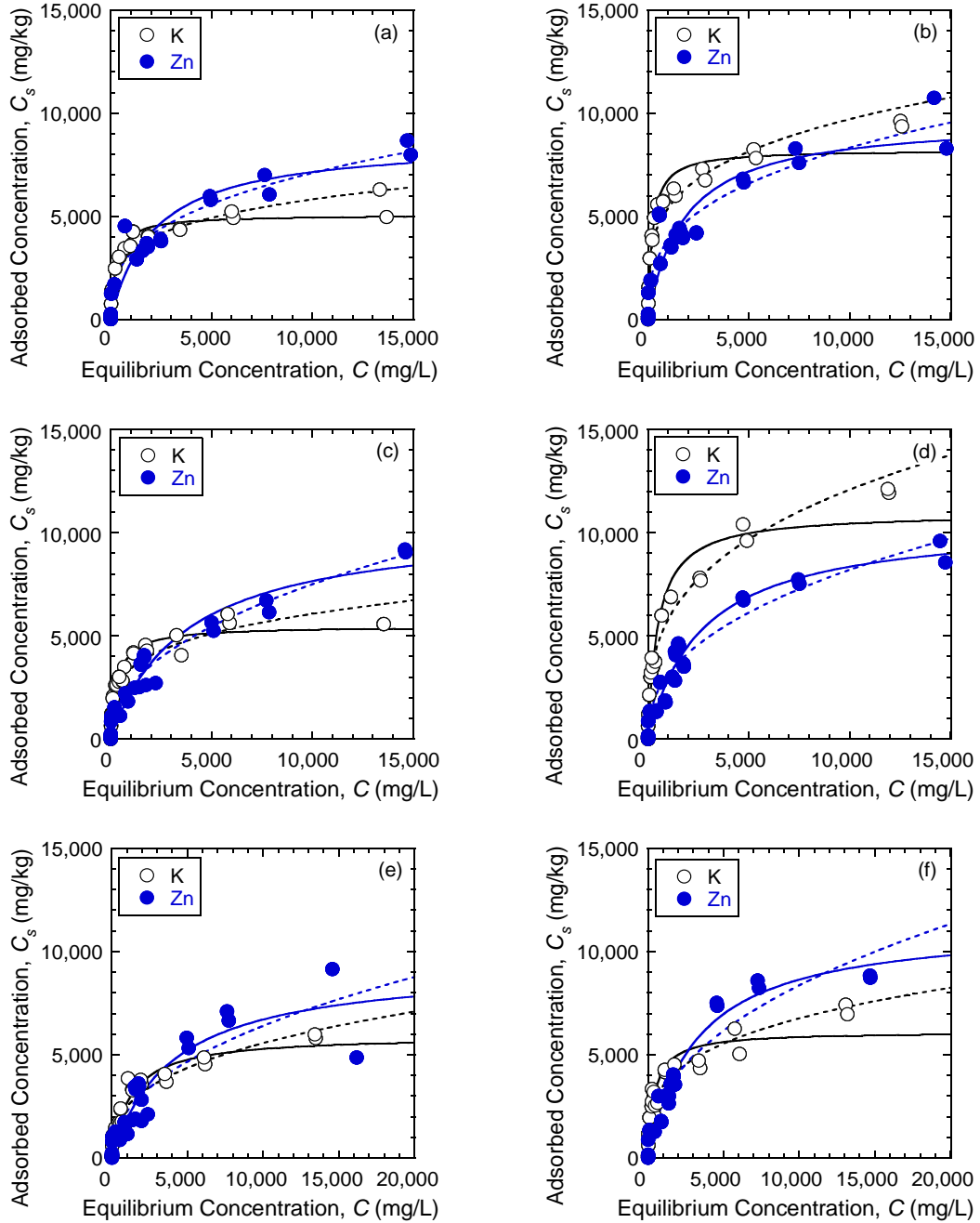


Figure 3.15. Comparison of potassium (K) versus zinc (Zn) adsorption including fitted Freundlich (dash lines) and Langmuir (solid lines) adsorption models for zeolite-amended backfill sorbents: (a) 5 % chabazite-LB; (b) 10 % chabazite-LB; (c) 5 % chabazite-UB; (d) 10 % chabazite-UB; (e) 5 % clinoptilolite; (f) 10 % clinoptilolite.

## REFERENCES

- Allerton, D.K., Desborough, G.A., Olsen, H.W., and Chang, N.Y. (1996). "Waste containment barrier enhancement with zeolite." *Tailings and Mine Waste '96*, Balkema, Rotterdam, The Netherlands, 255-264.
- Álvarez-Ayuso, E. and García-Sánchez, A. (2003). "Removal of heavy metals from waste waters by natural and Na-exchanged bentonites." *Clays and Clay Minerals*, 51(5), 475-480.
- ASTM (2006). "Standard practice for classification of soils for engineering purposes (Unified Soil Classification System)." *ASTM D2487-06*, West Conshohocken, PA.
- ASTM (2010). "Standard test method for measuring the exchange complex and cation exchange capacity of inorganic fine-grained soils." *ASTM D7503-10*, West Conshohocken, PA.
- Banat, F.A., Al-Bashir, B., Al-Asheh, S., and Hayajneh, O. (2000). "Adsorption of phenol by bentonite." *Environmental Pollution*, 107(3), 391-398.
- Barrer, R.M., Davies, J.A., and Rees, L.V.C. (1969). "Thermodynamics and thermochemistry of cation exchange in chabazite." *Journal of Inorganic and Nuclear Chemistry*, 31(1), 219-232.
- Bartelt-Hunt, S.L., Culver, T.B., Smith, J.A., Matott, L.S., and Rabideau, A.J. (2006). "Optimal design of a compacted soil liner containing sorptive amendments." *Journal of Environmental Engineering*, 132(7), 769-776.
- Bartelt-Hunt, S.L., Smith, J.A., Burns, S.E., and Rabideau, A.J. (2005). "Evaluation of granular activated carbon, shale, and two organoclays for use as sportive amendments in clay landfill liners." *Journal of Geotechnical and Geoenvironmental Engineering*, 131(7), 848-856.
- Bello, A.A. and Osinubi, K.J. (2011). "Attenuative capacity of compacted abandoned dumpsite soils." *Electronic Journal of Geotechnical Engineering*, 16(A), 71-91.
- Bernal, M.P. and Lopez-Real, J.M. (1993). "Natural zeolites and sepiolite as ammonium and ammonia adsorbent materials." *Bioresource Technology*, 43(1), 27-33.
- Bierck, B.R. and Chang, W.-C. (1994). "Contaminant transport through soil-bentonite slurry walls: Attenuation by activated carbon." *Proceedings of the Specialty Conference on Innovative Solutions for Contaminated Site Management*, Water Environment Federation, Alexandria, VA, 461-472.
- Bish, D.L. (2006). "Parallels and distinctions between clay minerals and zeolites." Section 13.2, *Developments in Clay Science*, Elsevier, New York, 1097-1112.
- Blanchard, G., Maunaye, M., and Martin, G. (1984). "Removal of heavy metals from waters by

- means of natural zeolites." *Water Research*, 18(12), 1501-1507.
- Bohn, H.L., Myer, R.A., and O'Connor, G.A. (2002). *Soil Chemistry*, John Wiley & Sons, New York.
- Bradl, H.B. (1997). "Vertical barriers with increased sorption capacities." *Proceedings, 1997 International Containment Technology Conference*, NTIS (National Technical Information Service), Springfield, VA, 645-651.
- Brümmer, G., Tiller, K.G., Herms, U., and Clayton, P.M. (1983). "Adsorption-desorption and/or precipitation-dissolution processes of zinc in soils." *Geoderma*, 31(4), 337-354.
- Cabrera, C., Gabaldón, C., and Marzal, P. (2005). "Sorption characteristics of heavy metal ions by a natural zeolite." *Journal of Chemical Technology and Biotechnology*, 80(4), 477-481.
- Cherry, J.A., Gillham, R.W., and Barker, J.F. (1984). "Contaminants in groundwater: Chemical processes." Chapter 3, *Groundwater Contamination*, National Academies Press, Washington, DC, 46-64.
- Colella, C. (1996). "Ion exchange equilibria in zeolite minerals." *Mineralium Deposita*, 31(6), 554-562.
- Crawford, R.L. and Crawford, D.L. (1996). *Bioremediation: Principles and applications*, Cambridge University Press, Cambridge.
- Czárán, E., Domokos, E., Mészároskiss, Á., and Papp, J. (1986). "Ion-exchange properties of a Hungarian sedimentary mordenite." *Acta Chimica Hungarica-Models in Chemistry*, 121(3), 243-253.
- Davidson, J.M., Ou, L.-T., and Rao, P.S.C. (1976). "Behavior of high pesticide concentrations in soil water systems." *EPA-600/9-76-015*, U.S. Environmental Protection Agency, Cincinnati, OH.
- Domenico, P. and Schwartz, F. (1990). *Physical and Chemical Hydrogeology*, Wiley, New York.
- Erdem, E., Karapinar, N., and Donat, R. (2004). "The removal of heavy metal cations by natural zeolites." *Journal of Colloid and Interface Science*, 280(2), 309-314.
- Evans, J.C., Adams, T.L., and Prince, M.J. (1997). "Metals attenuation in mineral-enhanced slurry walls." *Proceedings, 1997 International Containment Technology Conference*, NTIS (National Technical Information Service), Springfield, VA, 679-687.
- Evans, J.C. and Prince, M.J. (1997). "Additive effectiveness in mineral-enhanced slurry walls." *In Situ Remediation of the Geoenvironment*, J.C. Evans, Ed., ASCE, Reston, VA, 181-196.
- Evans, J.C., Sambasivan, Y., and Zarlinski, S. (1990). "Attenuating materials in composite liners." *Waste Containment Systems: Construction, Regulation, and Performance*, R.

- Bonaparte, Ed., ASCE, New York, 246-263.
- Faghihian, H., Ghannadi Marageh, M., and Kazemian, H. (1999). "The use of clinoptilolite and its sodium form for removal of radioactive cesium, and strontium from nuclear wastewater and  $Pb^{2+}$ ,  $Ni^{2+}$ ,  $Cd^{2+}$ ,  $Ba^{2+}$  from municipal wastewater." *Applied Radiation and Isotopes*, 50(4), 655-660.
- Fetter, C. (1993). *Contaminant Hydrology*, Macmillan Publishing Co., New York.
- Foo, K.Y. and Hameed, B.H. (2010). "Insights into the modeling of adsorption isotherm systems." *Chemical Engineering Journal*, 156(1), 2-10.
- Freeze, R. and Cherry, J. (1979). *Groundwater*, Prentice-Hall, Englewood, NJ.
- Gast, R.G. (1969). "Standard free energies of exchange for alkali metal cations on Wyoming bentonite." *Soil Science Society of America Journal*, 33(1), 37-41.
- Gray, D.H. (1995). "Containment strategies for landfill wastes." *Geoenvironment 2000*, Y.B. Acar and D.E. Daniel, Eds., ASCE, Reston, VA, 484-498.
- Gullick, R.W. and Weber, W.J., Jr. (2001). "Evaluation of shale and organoclays as sorbent additives for low-permeability soil containment barriers." *Environmental Science and Technology*, 35(7), 1523-1530.
- Hamidpour, M., Kalbasi, M., Afyuni, M., Shariatmadari, H., and Furrer, G. (2011). "Sorption of lead on Iranian bentonite and zeolite: Kinetics and isotherms." *Environmental Earth Sciences*, 62(3), 559-568.
- Harmesen, K. (1979). "Theories of cation adsorption by soil constituents: Discrete-site models." Chapter 4, *Soil Chemistry, Part B., Physico-Chemical Models*, G.H. Bolt, Ed., Elsevier, NY, 77-139.
- Harter, R.D. (1979). "Adsorption of copper and lead by Ap and B2 horizons of several northeastern United States soils." *Soil Science Society of America Journal*, 43(4), 679-683.
- Hong, C.S., Shackelford, C.D., and Malusis, M.A. (2012). "Consolidation and hydraulic conductivity of zeolite-amended soil-bentonite backfills." *Journal of Geotechnical and Geoenvironmental Engineering*, 138(1), 15-25.
- Ibrahim, K., Ed-Deen, N., and Khoury, H. (2002). "Use of natural chabazite–phillipsite tuff in wastewater treatment from electroplating factories in Jordan." *Environmental Geology*, 41(5), 547-551.
- Inyang, H.I. and de Brito Galvao, T.C. (2004). "The application of innovative materials in waste containment barriers." *Journal of Environmental Engineering*, 130(8), 834-835.
- Iskander, A.L., Khalid, E.M., and Sheta, A.S. (2011). "Zinc and manganese sorption behavior by

- natural zeolite and bentonite." *Annals of Agricultural Sciences*, 56(1), 43-48.
- Jacobs, P.H. and Forstner, U. (1999). "Concept of subaqueous capping of contaminated sediments with active barrier systems (ABS) using natural and modified zeolites." *Water Research*, 33(9), 2083-2087.
- Johnson, R.O. (1994). "Nonlinear adsorption of uranyl: Analytical modeling of linear migration." *Ground Water*, 32(2), 293-304.
- Kaya, A. and Durukan, S. (2004). "Utilization of bentonite-embedded zeolite as clay liner." *Applied Clay Science*, 25(1-2), 83-91.
- Kaya, A. and Ören, A.H. (2005). "Adsorption of zinc from aqueous solutions to bentonite." *Journal of Hazardous Materials*, 125(1-3), 183-189.
- Kayabali, K. (1997). "Engineering aspects of a novel landfill liner material: Bentonite-amended natural zeolite." *Engineering Geology*, 46(2), 105-114.
- Kayabali, K. and Mollamahmutoğlu, M. (2000). "The influence of hazardous liquid waste on the permeability of earthen liners." *Environmental Geology*, 39(3-4), 201-210.
- Kesraoui-Ouki, S., Cheeseman, C.R., and Perry, R. (1994). "Natural zeolite utilisation in pollution control: A review of applications to metals' effluents." *Journal of Chemical Technology and Biotechnology*, 59(2), 121-126.
- Khan, S.A., Riaz ur, R., and Khan, M.A. (1995). "Adsorption of chromium (III), chromium (VI) and silver (I) on bentonite." *Waste Management*, 15(4), 271-282.
- Kinniburgh, D.G. (1986). "General purpose adsorption isotherms." *Environmental Science and Technology*, 20(9), 895-904.
- Kubilay, Ş., Gürkan, R., Savran, A., and Şahan, T. (2007). "Removal of Cu(II), Zn(II) and Co(II) ions from aqueous solutions by adsorption onto natural bentonite." *Adsorption*, 13(1), 41-51.
- Lake, C.B. and Rowe, R.K. (2005). "A comparative assessment of volatile organic compound (VOC) sorption to various types of potential GCL bentonites." *Geotextiles and Geomembranes*, 23(4), 323-347.
- Limousin, G., Gaudet, J.P., Charlet, L., Sznknect, S., Barthès, V., and Krimissa, M. (2007). "Sorption isotherms: A review on physical bases, modeling and measurement." *Applied Geochemistry*, 22(2), 249-275.
- Lo, I.M.-C. (2001). "Organoclay with soil-bentonite admixture as waste containment barriers." *Journal of Environmental Engineering*, 127(8), 756-759.
- Lo, I.M.-C. (2003). "Innovative waste containment barriers for subsurface pollution control." *Practice Periodical of Hazardous, Toxic, and Radioactive Waste Management*, 7(1), 37-

45.

- Lo, I.M.-C. and Yang, X. (2001b). "Use of organoclay as secondary containment for gasoline storage tanks." *Journal of Environmental Engineering*, 127(2), 154-161.
- Lo, I.M.-C., Liljestrand, H.M., and Daniel, D.E. (1994). "Waste-soil interactions and adsorption parameters for pollutant transport through montmorillonite and modified montmorillonite clay liner materials." *Hydraulic Conductivity and Waste Contaminant Transport in Soil*, D.E. Daniel and S.J. Trautwein, Eds., STP 1142, ASTM, West Conshohoken, PA, 422-438.
- Lo, I.M.-C., Mak, R.K.M., and Lee, S.C.H. (1997). "Modified clays for waste containment and pollutant attenuation." *Journal of Environmental Engineering*, 123(1), 25-32.
- Lo, I.M.-C. and Yang, X. (2001a). "Laboratory investigation of the migration of hydrocarbons in organobentonite." *Environmental Science and Technology*, 35(3), 620-625.
- Malusis, M.A., Barben, E.J., and Evans, J.C. (2009). "Hydraulic conductivity and compressibility of soil-bentonite backfill amended with activated carbon." *Journal of Geotechnical and Geoenvironmental Engineering*, 135(5), 664-672.
- Malusis, M.A., Maneval, J.E., Barben, E.J., Shackelford, C.D., and Daniels, E.R. (2010). "Influence of adsorption on phenol transport through soil-bentonite vertical barriers amended with activated carbon." *Journal of Contaminant Hydrology*, 116(1-4), 58-72.
- Matott, L.S., Bandilla, K., and Rabideau, A.J. (2009). "Incorporating nonlinear isotherms into robust multilayer sorptive barrier design." *Advances in Water Resources*, 32(11), 1641-1651.
- Matott, L.S., Jiang, Z., Rabideau, A.J., and Allen-King, R.M. (2015). "Isotherm ranking and selection using thirteen literature datasets involving hydrophobic organic compounds." *Journal of Contaminant Hydrology*, 177-178(0), 93-106.
- Mellah, A. and Chegrouche, S. (1997). "The removal of zinc from aqueous solutions by natural bentonite." *Water Research*, 31(3), 621-629.
- Melnyk, T.W. (1985). "Effects of sorption behaviour on contaminant migration." *Atomic Energy of Canada*, Whiteshell Nuclear Research Establishment, Pinawa, MB, Canada.
- Motsi, T., Rowson, N.A., and Simmons, M.J.H. (2009). "Adsorption of heavy metals from acid mine drainage by natural zeolite." *International Journal of Mineral Processing*, 92(1-2), 42-48.
- Mott, H.V. and Weber, W.J., Jr. (1992). "Sorption of low molecular weight organic contaminants by fly ash: Considerations for the enhancement of cutoff barrier performance." *Environmental Science and Technology*, 26, 1234-1242.
- Mumpton, F.A. (1999). "La roca magica: Uses of natural zeolites in agriculture and industry."

- Proceedings of the National Academy of Sciences of the United States of America*, 96(7), 3463-3470.
- Musso, T.B., Parolo, M.E., Pettinari, G., and Francisca, F.M. (2014). "Cu(II) and Zn(II) adsorption capacity of three different clay liner materials." *Journal of Environmental Management*, 146(0), 50-58.
- Obiri-Nyarko, F., Grajales-Mesa, S.J., and Malina, G. (2014). "An overview of permeable reactive barriers for in situ sustainable groundwater remediation." *Chemosphere*, 111(0), 243-259.
- O'Neil, M.J., Heckelman P.E., Koch C.B., Roman K.J., editors. (2006) *The Merck Index: An Encyclopaedia of Chemicals, Drugs, and Biologicals*, 14th ed., Merck & Co. Inc., New York.
- Ören, A.H. and Kaya, A. (2006). "Factors affecting adsorption characteristics of  $Zn^{2+}$  on two natural zeolites." *Journal of Hazardous Materials*, 131(1-3), 59-65.
- Ören, A.H., Kaya, A., and Kayalar, A.Ş. (2011). "Hydraulic conductivity of zeolite-bentonite mixtures in comparison with sand-bentonite mixtures." *Canadian Geotechnical Journal*, 48(9), 1343-1353.
- Ouki, S.K. and Kavannagh, M. (1997). "Performance of natural zeolites for the treatment of mixed metal-contaminated effluents." *Waste Management and Research*, 15(4), 383-394.
- Ouki, S.K. and Kavannagh, M. (1999). "Treatment of metals-contaminated wastewaters by use of natural zeolites." *Water Science and Technology*, 39(10), 115-122.
- Park, J.K., Kim, J.Y., and Edil, T.B. (1996). "Mitigation of organic compound movement in landfills by shredded tires." *Water Environment Research*, 68(1), 4-10.
- Park, J.K., Kim, J.Y., Madsen, C.D., and Edil, T.B. (1997). "Retardation of volatile organic compound movement by a soil-bentonite slurry cutoff wall amended with ground tires." *Water Environment Research*, 69(5), 1022-1031.
- Powell, K.J., Brown, P.L., Byrne, R.H., Gajda, T., Hefter, G., Leuz, A.-K., Sjöberg, S., and Wanner, H. (2013). "Chemical speciation of environmentally significant metals with inorganic ligands. Part 5: The  $Zn^{2+} + OH^{-}$ ,  $Cl^{-}$ ,  $CO_3^{2-}$ ,  $SO_4^{2-}$ , and  $PO_4^{3-}$  systems (IUPAC Technical Report)." *Pure and Applied Chemistry*, 85(12), 2249-2311.
- Prasad, M., Xu, H.-y., and Saxena, S. (2008). "Multi-component sorption of Pb(II), Cu(II) and Zn(II) onto low-cost mineral adsorbent." *Journal of Hazardous Materials*, 154(1-3), 221-229.
- Rabideau, A.J., Shen, P., and Khandelwal, A. (1999). "Feasibility of amending slurry walls with zero-valent iron." *Journal of Geotechnical and Geoenvironmental Engineering*, 125(4), 330-333.

- Rabideau, A.J., Van Benschoten, J., Patel, A., and Bandilla, K. (2005). "Performance assessment of a zeolite treatment wall for removing Sr-90 from groundwater." *Journal of Contaminant Hydrology*, 79(1-2), 1-24.
- Reardon, E.J. (1981). "Kd's — Can they be used to describe reversible ion sorption reactions in contaminant migration?" *Ground Water*, 19(3), 279-286.
- Reichle, R.A., McCurdy, K.G., and Hepler, L.G. (1975). "Zinc hydroxide: Solubility product and hydroxy-complex stability constants from 12.5–75 °C." *Canadian Journal of Chemistry*, 53(24), 3841-3845.
- Reynolds, W.D., Gillham, R.W., and Cherry, J.A. (1982). "Evaluation of distribution coefficients for the prediction of strontium and cesium migration in a uniform sand." *Canadian Geotechnical Journal*, 19(1), 92-103.
- Rouse, J.V. and Pyrih, R.Z. (1993). "Geochemistry." Chapter 2, *Geotechnical Practice for Waste Disposal*, Chapman and Hall, London, 15-32.
- Roy, W.R., Krapac, I.G., Chou, S.F.J., and Griffin, R.A. (1992). "Batch-type procedures for estimating soil adsorption of chemicals." *EPA Technical Resource Document*, EPA/530-SW-87-006-F, U.S. Environmental Protection Agency, Washington, DC.
- Semmens, M. and Seyfarth, M. (1978). "The selectivity of clinoptilolite for certain heavy metals." *Natural Zeolites: Occurrence, Properties, Use*, Pergamon Press, Oxford, 517-526.
- Shackelford, C.D. (1993). "Contaminant transport." *Geotechnical Practice for Waste Disposal*, D.E. Daniel, Ed., Chapman and Hall, London, 33-65.
- Shackelford, C.D. (1999). "Reactive nature of passive containment barriers." *14th International Conference on Soil Mechanics and Foundation Engineering*, Hamburg, Germany, Sept. 6-12, 1997, Balkema, Rotterdam, Vol. 4, 2535-2536.
- Shackelford, C.D. and Jefferis, S.A. (2000). "Geoenvironmental engineering for in situ remediation." *Proceedings, International Conference on Geotechnical and Geoenvironmental Engineering (GeoEng2000)*, Melbourne, Australia, Nov. 19-24, Technomic Publ., Lancaster, PA, Vol. 1, 121-185.
- Shackelford, C.D. and Nelson, J.D. (1996). "Geoenvironmental design considerations for tailings dams." *Proceedings, International Symposium on Seismic and Environmental Aspects of Dams Design: Earth, Concrete and Tailings Dams*, Santiago, Chile, Oct. 14-18, Sociedad Chilena de Geotecnia, Vol. I. 131-187.
- Sherry, H.S. (2003). "Ion exchange." *Handbook of Zeolite Science and Technology*, Marcel Dekker, New York, 1007-1061.
- Sheta, A.S., Falatah, A.M., Al-Sewailem, M.S., Khaled, E.M., and Sallam, A.S.H. (2003). "Sorptions characteristics of zinc and iron by natural zeolite and bentonite." *Microporous*

- and Mesoporous Materials*, 61(1-3), 127-136.
- Singh, A., Kuhad, R.C., and Ward, O.P. (2009). *Advances in Applied Bioremediation*, Springer Science & Business Media, Berlin, Germany.
- Skyrman, M.L. (1997). *Adsorption of Zinc, Lead, and Cadmium with Kaolinite and Bentonite using Batch-Equilibrium Methods*, M.S. Thesis, Department of Civil Engineering, Colorado State University, Fort Collins, CO.
- Smith, J.A. and Jaffe, P.R. (1994). "Benzene transport through landfill liners containing organophilic bentonite." *Journal of Environmental Engineering*, 120(6), 1559-1577.
- Stapleton Jr, R. and Singh, V. (2002). *Biotransformations: Bioremediation Technology for Health and Environmental Protection*, Elsevier, Amsterdam, The Netherlands.
- Suffet, I.H. and McGuire, M.J. (1980). *Activated carbon adsorption of organics from the aqueous phase, v. 1*, Ann Arbor Science Publishers, Ann Arbor, MI.
- Thornton, S.F., Lerner, D.N., Bright, M.I., and Tellam, J.H. (1993). "The role of attenuation in landfill liners." *Proceedings, Fourth International Landfill Symposium*, Sardinia, Italy, Oct. 11-15, 1993, CISA, Environmental Engineering Sanitary Centre, Cagliari, Italy, 407-416.
- Torracca, E., Galli, P., Pansini, M., and Colella, C. (1998). "Cation exchange reactions of a sedimentary chabazite." *Microporous and Mesoporous Materials*, 20(1-3), 119-127.
- Travis, C.C. and Etnier, E.L. (1981). "A survey of sorption relationships for reactive solutes in soil." *Journal of Environmental Quality*, 10(1), 8-17.
- Tuncan, A., Tuncan, M., Koyuncu, H., and Guney, Y. (2003). "Use of natural zeolites as a landfill liner." *Waste Management Research*, 21(1), 54-61.
- Volkov, A., Paula, S., and Deamer, D. (1997). "Two mechanisms of permeation of small neutral molecules and hydrated ions across phospholipid bilayers." *Bioelectrochemistry and Bioenergetics*, 42(2), 153-160.
- Voudrias, E.A. (2002). "The concept of a sorption chemical barrier for improving effectiveness of landfill liners." *Waste Management and Research*, 20(3), 251-258.
- Weber, W.J., McGinley, P.M., and Katz, L.E. (1992). "A distributed reactivity model for sorption by soils and sediments. 1: Conceptual basis and equilibrium assessments." *Environmental Science and Technology*, 26(10), 1955-1962.
- Wingenfelder, U., Hansen, C., Furrer, G., and Schulin, R. (2005). "Removal of heavy metals from mine waters by natural zeolites." *Environmental Science and Technology*, 39(12), 4606-4613.
- Yadla, S.V., Sridevi, V., and Lakshmi, M.C. (2012). "A review on adsorption of heavy metals

- from aqueous solution." *Journal of Chemical, Biological and Physical Sciences*, 2(3), 1585-1593.
- Yang, X. and Lo, I.M.-C. (2004). "Flow of gasoline through composite liners." *Journal of Environmental Engineering*, 130(8), 886-890.
- Yong, R. N. and Phadungchewit, Y. (1993). "pH influence on selectivity and retention of heavy metals in some clay soils." *Canadian Geotechnical Journal*, 30(5), 821-833.
- Yuan, G., Seyama, H., Soma, M., Theng, B.K.G., and Tanaka, A. (1999). "Adsorption of some heavy metals by natural zeolites: XPS and batch studies." *Journal of Environmental Science and Health, Part A*, 34(3), 625-648.
- Zamzow, M.J., Eichbaum, B.R., Sandgren, K.R., and Shanks, D.E. (1990). "Removal of heavy metals and other cations from wastewater using zeolites." *Separation Science and Technology*, 25(13-15), 1555-1569.

## CHAPTER 4 NUMERICAL MODELING

### 4.1 INTRODUCTION

Soil-bentonite (SB) vertical cutoff walls are used extensively as *in situ* containment barriers to prevent or control subsurface migration of contaminated groundwater (*e.g.*, USEPA 1984; Ryan 1984, 1987; Daniel and Koerner 1993; Rumer and Mitchell 1995; Rumer and Ryan 1995; LaGrega *et al.* 2001; Mitchell *et al.* 2007; Hudak 2016). These barriers are constructed by excavating a trench to a desired depth, typically using a backhoe for shallower depths and a clamshell for deeper depths, placing a bentonite slurry comprising a mixture of water with 3 to 5 % (by dry weight) sodium bentonite into the excavated trench to maintain trench stability, mixing the trenched spoils with the bentonite slurry to achieve a desired slump of 100 to 150 mm (3.9 to 5.9 in), and backfilling the slurry filled trench with the slurry mixed trench spoils (*i.e.*, backfill), thereby displacing the slurry from the trench and forming a relatively low-permeability barrier to subsurface contaminant migration. The width of SB vertical cutoff walls generally is the same as the width of the trenching equipment, which typically is on the order of  $1.0 \pm 0.5$  m. Depths on the order of 50 m are possible (*e.g.*, Ryan and Spaulding 2008), although shallower depths ( $< 30$  m) are more common.

Although most SB vertical cutoff walls have some intrinsic capacity to attenuate specific contaminants during migration through the walls (*e.g.*, via adsorption of metals to the bentonite portion of the backfill), available evidence suggests that this intrinsic attenuation capacity is limited (Shackelford 1999, 2014). As a result, the concept of designing SB vertical cutoff walls with enhanced attenuation capacities, often referred to as "reactive barriers," has emerged over the past few decades (*e.g.*, Bierck and Chang 1994; Evans *et al.* 1997; Evans and Prince 1997; Park *et al.* 1997; Rabideau *et al.* 1999; Shackelford 1999; Malusis *et al.* 2009, 2010; Hong *et al.*

2012, 2016). In the case where the primary attenuation mechanism is adsorption via cation exchange or other adsorption mechanisms (*e.g.*, hydrophobic partitioning), the amended barriers are referred to more specifically as "sorbing" barriers (*e.g.*, Rabideau *et al.* 2001; Matott *et al.* 2009).

For example, the potential use of zeolites with relatively high values of cation exchange capacity, *CEC*, on the order of 180 to 400  $\text{cmol}_c/\text{kg}$  (180 to 400  $\text{meq}/100 \text{ g}$ ) as a backfill amendment for the purpose of increasing the adsorption capacity of SB vertical cutoff wall for targeted metals has been evaluated in several studies (Evans *et al.* 1990; Colella 1996; Evans *et al.* 1997; Evans and Prince 1997; Mumpton 1999; Bish 2006; Hong *et al.* 2012, 2016; Fan *et al.*, 2014; Du *et al.* 2015). Such evaluations typically have included laboratory characterization of the consolidation, hydraulic, and/or adsorptive behaviors of SB backfill mixtures, in some cases with limited evaluation of the potential for improved performance based on analytical contaminant transport modeling that assumes linear adsorption behavior (Evans *et al.* 1997; Evans and Prince 1997).

Given the aforementioned considerations, the purpose of the present study was to evaluate the potential for improved performance in terms of the containment of two metals, *viz.*, potassium (K) and zinc (Zn), via a hypothetical, 1-m-thick SB vertical cutoff wall comprising the zeolite-amended backfills previously characterized in terms of consolidation and hydraulic behavior (Chapter 2) and adsorptive behavior (Chapter 3). The backfills comprised a fine sand, 5.8 % (by dry weight) sodium bentonite, and 0, 5, or 10 % (by dry weight) of one of three types of zeolite, including two types of chabazite referred to as chabazite-lower bed (chabazite-LB) and chabazite-upper bed (chabazite-UB), and a clinoptilolite (Chapter 3). The evaluation was based on numerical simulations of solute transport using a previously developed solute transport

model that included nonlinear, equilibrium adsorptive behavior (Malusis *et al.* 2010). The adsorptive behavior of each metal was included by using the results of the BEATs reported in Chapter 3 as input parameters for the model simulations. Conditions typical of those expected for actual SB vertical cutoff walls (*e.g.*, initial and boundary conditions, thickness and hydraulic conductivity of the cutoff wall, etc.) were assumed for the simulations, so that the results could be considered representative. Comparison of the simulation results based on the zeolite-amended SB backfills versus those for the unamended SB backfill provided a relative indication of the potential benefit for enhanced metals containment offered by the zeolite-amended SB backfills.

## 4.2 METHODS

### 4.2.1 Solute Transport Model

The solute transport model used in this study was originally developed by Malusis *et al.* (2010) for evaluating phenol migration through SB cutoff walls amended with activated carbon. In brief, the model is based on solving the governing mass-balance equation for one-dimensional solute transport due to advection (hydraulically driven solute transport) and diffusion (chemically driven solute transport), assuming steady-state seepage with equilibrium adsorption, as follows (Shackelford 1993):

$$R_d \frac{\partial C}{\partial t} = D^* \frac{\partial^2 C}{\partial x^2} - v_s \frac{\partial C}{\partial x} \quad (4.1)$$

where  $R_d$  is the retardation factor that accounts for instantaneous, equilibrium adsorption of the migrating solute,  $C$  is the solute concentration within the pore water of the soil,  $t$  is time,  $D^*$  is the effective diffusion coefficient defined as per Shackelford and Daniel (1991),  $x$  is the distance

of transport, and  $v_s$  is the seepage velocity equal to  $ki/n$ , where  $i$  is the hydraulic gradient, and  $n$  is the porosity of the porous medium. Mechanical (hydraulic) dispersion of the solute was assumed to be negligible because of the short distance of transport (*i.e.*, 1 m) and the low seepage velocity resulting from the product of the low  $k$  (*i.e.*,  $\leq 1.0 \times 10^{-9}$  m/s) and low  $i$  (*i.e.*,  $-1 \leq i \leq 1$ ) commonly associated with SB vertical cutoff walls (Sleep *et al.* 2006; Shackelford 2014). Finally, Eq. 4.1 implicitly assumes that the porous medium does not exhibit semipermeable membrane behavior, which has been shown to be practically negligible for typical SB vertical cutoff walls (Yeo *et al.* 2005; Henning *et al.* 2006; Evans *et al.* 2008). This assumption of negligible membrane behavior also has been shown to result in somewhat conservative (high) estimates of solute mass flux through clay barriers (Malusis and Shackelford 2004).

For the general case of nonlinear, equilibrium adsorption,  $R_d$  can be expressed as follows (Shackelford 1993):

$$R_d = 1 + \frac{\rho_d}{n} K_p \quad (4.2)$$

where  $\rho_d$  is the dry density of the soil, and  $K_p$  is the partition coefficient defined as follows:

$$K_p = \frac{\partial C_s}{\partial C} \quad (4.3)$$

where  $C_s$  is the solid-phase (adsorbed) concentration of the solute. For a nonreactive (non adsorbing) solute,  $C_s = 0$  such that  $K_p = 0$  and  $R_d = 1$  (Shackelford 1993).

The relationship between  $C_s$  and  $C$  is given by several functions or adsorption models (e.g., Kinniburgh 1986), but two of the more commonly used functional relationships are the Langmuir and the Freundlich adsorption models defined as follows (Shackelford 1993; Hong *et al.* 2016):

$$C_s = \frac{K_L Q_L C}{1 + K_L C} \quad (4.4)$$

and

$$C_s = K_f C^{N_f} \quad (4.5)$$

where  $K_L$  and  $Q_L$  are the Langmuir adsorption model parameters representing the binding strength of the adsorption sites for the solute and the maximum adsorbed concentration of the solute, respectively (Malusis *et al.* 2009; Hong *et al.* 2016), and  $K_f$  and  $N_f$  are the Freundlich adsorption parameters referred to as the unit adsorption capacity and the relative magnitude and diversity of adsorption energies, respectively (Weber *et al.* 1992; Hong *et al.* 2016). Values of  $N_f$  less than unity ( $N_f < 1$ ) represent the case of concave (favorable), nonlinear adsorption, which is the common situation for adsorptive media (sorbents) with finite adsorption capacities such as clays (Shackelford 1993; Hong *et al.* 2016). The combination of Equations 4.2 – 4.5 results in the following general expressions for  $R_d$  based on the Langmuir and Freundlich adsorption models (Shackelford 1993):

$$R_d = 1 + \frac{\rho_d}{n} \frac{K_L Q_L}{(1 + K_L C)^2} \quad (4.6)$$

$$R_d = 1 + \frac{\rho_d}{n} K_f N_f C^{N_f - 1} \quad (4.7)$$

The solutions for solute transport with nonlinear adsorption were obtained by substituting Eq. 4.6 or Eq. 4.7 into Eq. 4.1, and numerically solving the resulting expression subject to the following initial and boundary conditions (*e.g.*, Malusis *et al.* 2010):

$$C(0 \leq x \leq L, t = 0) = C_s(0 \leq x \leq L, t = 0) = 0 \quad (4.8a)$$

$$C(x = 0, t > 0) = C_o \quad (4.8b)$$

$$C(x = L, t > 0) = 0 \quad (4.8c)$$

The initial condition (Eq. 4.8a) corresponds to an initially uncontaminated barrier of thickness  $L$ . The upper or entry boundary condition (Eq. 4.8b) assumes a constant source concentration,  $C_o$ , whereas the lower or exit boundary condition (Eq. 4.8c) represents a perfectly flushing boundary, whereby the temporal contaminant concentration at the exit end of the barrier,  $C(L, t)$ , is maintained as zero due, for example, to the divergence of the local groundwater flow exterior to the boundary being extensively more rapid than the rate of contaminant migration through the barrier (*e.g.*, see Figure 4.1a). Rabideau and Khandelwal (1998) showed that these boundary conditions are the most appropriate or conservative boundary conditions for evaluating solute transport through vertical cutoff walls. The numerical solutions representing the solute transport model were developed using the *MATLAB* (Mathworks, Inc., Natick, MA) partial differential equation solver as described in more detail by Malusis *et al.* (2010).

Because the lower boundary condition does not allow for an exit concentration greater than zero, presenting the results of the model simulations in the form of traditional concentration breakthrough curves (CBCs) is not possible (*e.g.*, see Shackelford 1994, 1995a,b). Thus, the simulation results were expressed in terms of dimensionless flux breakthrough curves, FBCs, representing the temporal trend in the relative flux,  $RF$ , defined as follows (Rabideau and Khandelwal 1998; Rubin and Rabideau 2000; Malusis and Shackelford 2004; Malusis *et al.* 2010):

$$RF = \frac{J(L, t)}{J_{ss}(L)} \quad (4.9)$$

where  $J(L,t)$  is the temporal solute mass flux emanating from the barrier, and  $J_{ss}(L)$  is the value of  $J(L,t)$  at steady state, or

$$J_{ss}(L) = \frac{P_L}{1 - \exp(-P_L)} J_{d,ss} \quad (4.10)$$

where  $P_L (= v_s L / D^* = kiL / nD^*)$  is the barrier Péclet Number, and  $J_{d,ss} (= nD^* C_o / L)$  is the steady-state mass flux based on purely diffusive transport (Shackelford 1993; Rabideau and Khandelwal 1998; Malusis *et al.* 2010). The FBCs are made fully dimensionless by defining the elapsed time in terms of the dimensionless diffusive time factor,  $T^* (= D^* t / L^2)$  (Shackelford 1993; Rabideau and Khandelwal 1998; Malusis *et al.* 2010; Shackelford 2014). Since  $J(L,t) \leq J_{ss}(L)$ ,  $RF$  is in the range  $0 \leq RF \leq 1$ , such that the resulting FBCs show a similar trend as the more traditional CBCs representing the temporal trend in  $C(L,t)/C_o$  (Shackelford 1995a,b).

#### 4.2.2 Simulation Scenarios

As illustrated in Figure 4.1b, three different containment scenarios were considered on the basis of the magnitude and direction of the hydraulic gradient across the barrier,  $i$ , defined as  $-\Delta h/L$ , where  $-\Delta h$  is the head loss across the barrier (Malusis *et al.* 2010), *viz.*: (1) solute transport with advection occurring in the same direction as diffusion (*i.e.*, co-advection) for a hydraulic gradient of unity (*i.e.*,  $-\Delta h = 1$  m,  $i = 1$ ); (2) purely diffusive solute transport (*i.e.*,  $-\Delta h = 0$  m,  $i = 0$ ); and (3) solute transport with advection occurring opposite to the direction of diffusion (*i.e.*, counter-advection) for a hydraulic gradient of negative unity (*i.e.*,  $-\Delta h = -1$  m,  $i = -1$ ). All three scenarios are commonly considered with respect to modeling solute transport across SB vertical cutoff walls, and the latter two scenarios, in particular, are relevant for vertical barrier systems in which the groundwater level on the source (contaminated) side of the barrier is lowered by pumping to eliminate the hydraulic gradient or to create an inward (reverse) gradient that reduces the outward contaminant mass flux (Shackelford 1988, 1989; Manassero and Shackelford 1994; Devlin and Parker 1996; Neville and Andrews 2006; Sleep *et al.* 2006; Mitchell *et al.* 2007; Malusis *et al.* 2010; Shackelford 2014).

The value for  $k$  was assumed to be  $1.0 \times 10^{-9}$  m/s in all cases, consistent with the design requirement of  $k \leq 1.0 \times 10^{-9}$  m/s for SB vertical cutoff walls applied for geoenvironmental containment (Malusis *et al.* 2010), as well as with the results of laboratory tests indicating that the values of  $k$  for the backfills considered in this study based on permeation with tap water were less than  $1.0 \times 10^{-9}$  m/s (Chapter 2). Because the actual measured  $k$  values for the backfills based on permeation with tap water were lower than  $1.0 \times 10^{-9}$  m/s, the use of  $k = 1.0 \times 10^{-9}$  m/s in the simulations represents some allowance for incompatibility in  $k$  (*i.e.*, an increase in  $k$ ) resulting from adverse interactions between the contaminants and the backfill during migration through

the cutoff wall (*e.g.*, Ryan 1987). Also, values for  $n$  and  $\rho_d$  of 0.5 and 1.40 Mg/m<sup>3</sup>, respectively, were assumed based on the results of Chapter 2.

Simulations were performed assuming either potassium chloride (KCl) or zinc chloride (ZnCl<sub>2</sub>) as the sources of the solutes of interest. Potassium chloride readily dissociates into chloride (Cl<sup>-</sup>) and monovalent potassium (K<sup>+</sup>), whereas ZnCl<sub>2</sub> readily dissociates into Cl<sup>-</sup> and divalent zinc (Zn<sup>2+</sup>), although chemical complexation can result in other forms of Zn depending on pH, such as zinc hydroxide (Zn(OH)<sup>+</sup>) (Chapter 3). A comparison of the results for K versus those for Zn will provide for an assessment of the effect of adsorption for a primarily monovalent metal (K<sup>+</sup>) relative to that for a primarily divalent metal (Zn<sup>2+</sup>). Both Cl<sup>-</sup> and Zn are considered by the U.S. Environmental Protection Agency as secondary drinking water contaminants with recommended limiting (maximum) concentrations of 250 and 5 mg/L, respectively (Code of Federal Regulations 2015). The Cl<sup>-</sup> typically is considered a nonadsorbing tracer ( $R_d = 1$ ) in that Cl<sup>-</sup> should not readily adsorb to the predominantly negatively charged surfaces of the bentonite and zeolite particles. Finally, to cover a broad range of source concentrations, simulations were conducted assuming  $C_o$  of 100, 1,000, and 10,000 mg/L.

The input parameters required to describe the effect of adsorption of the two metals (K and Zn) with respect to each of the adsorption models (*i.e.*, Eq. 4.4 and Eq. 4.5) based on the measured adsorption data reported in Chapter 3 are summarized in Table 4.1. Initially, an attempt was made to regress the adsorption data consistent with the range of concentrations corresponding to the  $C_o$  values assumed for the simulations (*i.e.*,  $C \leq C_o$ ) as recommended by Matott *et al.* (2009). However, issues related to insufficient data for the case of the lowest  $C_o$  (*i.e.*,  $C \leq 100$  mg/L) with the unamended backfill for K and the 5 % chabazite-LB-amended backfills for Zn precluded following this approach for these cases. As a result, the input

parameters summarized in Table 4.1 correspond to those resulting from regression of all the adsorption data regardless of the  $C_o$  used for the simulation in order to provide a consistent basis for all model simulations.

Values for  $D^*$  were calculated in accordance with the relationship,  $D^* = \tau_a D_o$ , where  $\tau_a$  is the apparent tortuosity factor and  $D_o$  is the diffusion coefficient for the solute in aqueous solution (Shackelford and Daniel 1991). A value for  $\tau_a$  of 0.35 was assumed for the backfills based on the study by Malusis *et al.* (2010), and the value of  $D_o$  used for KCl was the limiting free-solution (aqueous) diffusion coefficient for KCl at 25°C of  $1.993 \times 10^{-9}$  m<sup>2</sup>/s (Shackelford and Daniel 1991). For ZnCl<sub>2</sub>, the value for  $D_o$  was determined in accordance with the Nernst-Hartley expression as follows (*e.g.*, Robinson and Stokes 2002; Kontturi *et al.* 2008):

$$D_o = \frac{D_{o1}D_{o2}(v_1 + v_2)}{v_1D_{o2} + v_2D_{o1}} \quad (4.11)$$

where  $D_{o1}$  and  $D_{o2}$  are the limiting self-diffusion coefficients of the individual solutes resulting from complete dissociation of the salt, and  $v_1$  and  $v_2$  are the stoichiometric coefficients for the respective individual solutes. For example, for complete dissociation of ZnCl<sub>2</sub> (*i.e.*,  $\text{ZnCl}_2 \rightarrow 2\text{Cl}^- + \text{Zn}^{2+}$ ), if solute 1 is designated as Cl<sup>-</sup> and solute 2 is designated as Zn<sup>2+</sup>, then  $v_1 = 2$  and  $v_2 = 1$ . Given  $D_o = 2.03 \times 10^{-9}$  m<sup>2</sup>/s and  $D_o = 7.02 \times 10^{-10}$  m<sup>2</sup>/s for Cl<sup>-</sup> and Zn<sup>2+</sup>, respectively, at 25°C (Shackelford and Daniel 1991), the  $D_o$  for ZnCl<sub>2</sub> based on Eq. 4.11 is  $1.25 \times 10^{-9}$  m<sup>2</sup>/s. Thus, the  $D^*$  used in the simulations for K was  $6.98 \times 10^{-10}$  m<sup>2</sup>/s based on the assumption that K exists primarily as K<sup>+</sup>, whereas the value of  $D^*$  used in the simulations for Zn was  $4.36 \times 10^{-10}$  m<sup>2</sup>/s based on the assumption that Zn exists primarily as Zn<sup>2+</sup>. As previously noted, a fraction of Zn

may exist in the form of complexed species, such as  $\text{Zn}(\text{OH})^+$ , but this fraction was expected to be small based on the results of Chapter 3, such that the effect of such complexation on the diffusion of Zn was assumed to be minor. Thus, based on these values for  $D^*$  and aforementioned values for  $k$  ( $= 1.0 \times 10^{-9}$  m/s),  $L$  ( $= 1$  m), and  $n$  ( $= 0.5$ ), the values of  $P_L$  used in the simulations ranged from 1.43 (co-advection,  $i = 1$ ) to  $-1.43$  (counter-advection,  $i = -1$ ) for K and 2.29 (co-advection,  $i = 1$ ) to  $-2.29$  (counter-advection,  $i = -1$ ) for Zn. Since the focus of this study was on comparison of the effect of the zeolite-amended backfills relative to the unamended backfill on the migration behavior of K and Zn through the cutoff wall, simulations involving the migration of the nonreactive tracer  $\text{Cl}^-$  were not included in the evaluation.

## 4.3 RESULTS

### 4.3.1 Flux Breakthrough Curves for Potassium

The FBCs for K based on co-advection (*i.e.*,  $i = 1$ ,  $P_L = 1.43$ ) for each source concentration,  $C_o$  ( $= 100, 1,000, 10,000$  mg/L), type of zeolite (chabazite-LB, chabazite-UB, clinoptilolite), zeolite content (0, 5, 10 %), and adsorption model (Freundlich and Langmuir) are shown in Figure 4.2. For all cases, increasing the amount of zeolite amendment delayed or retarded breakthrough of K in the order 10 % > 5 % > 0 %, as expected based on the relative magnitudes of  $Q_{L,amended}/Q_{L,unamended}$  shown in Table 4.1, representing the maximum adsorbed concentration of the metal based on the Langmuir model regression for the zeolite-amended backfill relative to that for the unamended backfill (Chapter 3). That is, the greater the adsorption capacity of the backfill, the higher the value of  $Q_{L,amended}/Q_{L,unamended}$  and the longer the time required for the contaminant to migrate through the barrier.

For a given backfill, the shapes of the FBCs based on the Langmuir adsorption model generally were more dispersive than those based on the Freundlich model at low  $C_o$ , but became similar with increasing  $C_o$ . The reason for the difference in the shapes of the FBCs is related to the nonlinearity in the adsorption behavior of the solute and the role of dispersion via diffusion in solute migration, as described subsequently.

The Langmuir and Freundlich adsorption behaviors for the two metals considered in this study were nonlinear and concave (Chapter 3). By definition, the slope of a nonlinear, concave adsorption isotherm as given by the partition coefficient ( $K_p$ ) decreases as the concentration increases (*e.g.*, Shackelford 1993). Therefore, since  $R_d$  is directly proportional to  $K_p$  (Eq. 4.2), a given chemical species at a lower concentration is retarded to a greater extent than the same chemical species at a higher concentration. In contrast, linear adsorption results in a constant value of  $R_d$  that is independent of the solute concentration, such that the chemical species is retarded to the same extent regardless of the concentration. Also, the process of dispersion via diffusion tends to spread out the distribution of the chemical species during migration, such that lower concentrations of the chemical species are displaced ahead of the advective front, whereas higher concentrations of the same chemical species lag behind the advective front.

Based on these considerations, the concentration at the front of a migrating plume of a contaminant with nonlinear, concave (favorable) adsorptive behavior is relatively low due to dispersion, resulting in relatively high retardation, whereas the center of the plume with higher contaminant concentration migrates with relatively low retardation. Therefore, the center of the plume migrates faster to catch up with the more retarded front, resulting in a steeping of the contaminant front that is referred to as the "self-sharpening" or "front-sharpening" effect (Melnik 1985; Shackelford 1993). Thus, greater (concave) nonlinearity in the adsorptive

behavior of the chemical species results in a greater tendency for self-sharpening front of the FBC.

In order to evaluate quantitatively the extent or degree of nonlinearity, the relative nonlinearity ( $\lambda$ ) of the adsorptive behavior was calculated following the procedure described by Emancipator and Kroll (1993). Based on this approach, the greater the value of  $\lambda$  ( $0 \leq \lambda \leq 0.5$ ), the greater the nonlinearity of the adsorptive behavior, with a value for  $\lambda$  of zero ( $\lambda = 0$ ) corresponding to linear adsorptive behavior corresponding where the constant  $K_p$  is expressed as the distribution coefficient,  $K_d$  (e.g., Freeze and Cherry 1979). The resulting values of  $\lambda$  for both adsorption models and metals are summarized in Table 4.2.

As shown in Table 4.2, for each backfill, the values of  $\lambda$  based on the regressed Freundlich adsorption model were the same for all values  $C_o$ , because the value of  $\lambda$  is a function of only  $N_f$  (Appendix D). In contrast, the value of  $\lambda$  based on the Langmuir adsorption model is a function of  $K_L$ ,  $Q_L$ , and  $C_o$  (Appendix D), such that different values of  $\lambda$  are obtained for different  $C_o$ . For example, the values of  $\lambda$  for the regressed Langmuir adsorption model were closer to zero at the lowest  $C_o$  (i.e., the adsorptive behavior was closer to linear) and increased as  $C_o$  increased, reflecting a greater degree of nonlinear adsorptive behavior with increasing  $C_o$ .

In an attempt to explain the aforementioned differences in the FBCs based on the Langmuir and Freundlich adsorption models for different  $C_o$ , consider the results shown in Figure 4.3, where the results of the adsorption model regressions to the measured adsorption data for the unamended backfill with K based on Chapter 3 are shown for the range of concentrations less than or equal to the source concentrations used in the model simulations (i.e.,  $C \leq C_o$ ). The secant-based distribution coefficients,  $K_{d,secant}$ , representing linear adsorption behavior ( $\lambda = 0$ ) over the range in concentrations up to the  $C_o$  used in each simulation (i.e.,  $K_{d,secant} = C_{s,o}/C_o$ ,

where  $C_{s,o} = C_s @ C = C_o$ ) also are shown in Figures 4.3a,c,e and the values of  $K_{d,secant}$  are summarized in Table 4.3. Note that, as the adsorption data were nonlinear and concave, the values for  $K_{d,secant}$  shown in Table 4.3 decrease with increasing  $C_o$ , all other factors being the same. For  $C_o = 100$  mg/L, the values of  $C_{s,o}$  (*i.e.*, the  $C_s$  at  $C = 100$  mg/L in Figure 4.3a) based on the regressed Langmuir and Freundlich models differed significantly. Also, the regressed Langmuir model was almost linear ( $\lambda = 0.05$ ), such that the  $K_p$  were close to  $K_{d,secant}$ , whereas the regressed Freundlich model was clearly nonlinear ( $\lambda = 0.43$ ). As shown in Figure 4.3b, breakthrough for the model simulations for  $C_o = 100$  mg/L based on the Freundlich model was delayed relative to that based on the Langmuir model due to the greater adsorption capacity associated with  $C \leq C_o$  ( $= 100$  mg/L), and the shape of the FBC for the Freundlich based simulations was self-sharpening (steeper) due to the greater nonlinearity (higher  $\lambda$ ) associated with the Freundlich model to the measured adsorption data (*e.g.*, see Shackelford 1993).

In Figure 4.3c, the values of  $C_s$  at  $C = 1,000$  mg/L based on the regressed Langmuir and Freundlich models were almost the same, but the regressed Langmuir model was closer to linear ( $\lambda = 0.24$ ) relative to the regressed Freundlich model ( $\lambda = 0.43$ ). Therefore, as shown in Figure 4.3d for the model simulations with  $C_o$  of 1,000 mg/L, the difference in breakthrough based on the Freundlich versus Langmuir models was less than that for the case where  $C_o$  was 100 mg/L (Figure 4.3b), although the FBC based on the Langmuir model was still more dispersive than that based on the Freundlich model.

Finally, in Figure 4.3e, both the values of  $C_s$  at  $C = 10,000$  mg/L and the nonlinearity in the Freundlich and Langmuir models (*i.e.*,  $\lambda = 0.43$  vs.  $\lambda = 0.47$ ) were similar. As a result, both the temporal location and the shape of the FBCs based on both adsorption models for the case where  $C_o$  was 10,000 mg/L also were similar (Figure 4.3f).

#### 4.3.2 Flux Breakthrough Curves for Zinc

The FBCs for Zn based on co-advection (*i.e.*,  $i = 1$ ,  $P_L = 2.29$ ) for each  $C_o$  ( $= 100, 1,000, 10,000$  mg/L), type of zeolite (chabazite-LB, chabazite-UB, clinoptilolite), zeolite content (0, 5, 10 %), and adsorption model (Freundlich and Langmuir) are shown in Figure 4.4. In terms of the relative shapes and barrier breakthrough times of the FBCs based on the Langmuir and Freundlich adsorption models, the same general observations pertaining to the case of K also pertain to the case of Zn. However, there is one significant difference in the results associated with the relatively low  $C_o$  values of 100 and 1,000 mg/L, where breakthrough for the zeolite-amended backfills clearly occurred earlier than the breakthrough for the unamended backfill. The reason for this counterintuitive result is the difference in the adsorptive behaviors based on the regressed adsorption models at the lower concentrations.

For example, consider the adsorption model regressions and simulation results shown in Figure 4.5 for the backfills amended with chabazite-UB. For  $C \leq 100$  mg/L, the relative trend in the values of  $C_{s,o}$  at  $C = C_o = 100$  mg/L shown in Figure 4.5a was in the same order as that for the FBCs with  $C_o$  of 100 mg/L shown in Figure 4.5b, *i.e.*, increasing  $C_{s,o}$  resulted in increasing retardation of the FBC. Also, the Langmuir model regressions were almost linear, whereas the Freundlich model regressions were clearly nonlinear. Therefore, the shape of the FBCs based on the Langmuir model were more disperse, whereas the FBCs based on the Freundlich model were steeper due to the greater nonlinearity associated with the regressed Freundlich model (Figures 4.5a,b).

For  $C \leq 1,000$  mg/L (Figure 4.5c), the regressed adsorption models intersected each other over the concentration range of interest, and the Langmuir model regressions for the 5 % and 10 % zeolite-amended backfills were still close to linear (see  $\lambda$  values in Table 4.2), whereas all the

other Langmuir and Freundlich model regressions were nonlinear. For example, the most dispersive and earliest breakthrough occurred for the 5 % zeolite-amended backfill based on the Langmuir adsorption model regression (Figure 4.5d), which also correlated with close to linear adsorptive behavior ( $\lambda = 0.044$ ) and the overall lowest adsorption capacity for the majority of equilibrium concentrations (Figure 4.5c). In contrast, the latest breakthrough occurred for the 10 % zeolite-amended backfill based on the Freundlich adsorption model regression (Figure 4.5d), with the overall highest adsorption capacity (*i.e.*, highest  $C_{s,o}$ ) and the greatest relative nonlinearity ( $\lambda = 0.224$ ). Therefore, for  $C_o$  of 1,000 mg/L, the counterintuitive breakthrough behavior associated with the 5 and 10 % zeolite-amended backfills is directly related to the relatively low adsorption capacities and linearity associated with the Langmuir adsorption model behavior for these two backfills based on the measured BEAT data (Chapter 3).

Finally, for  $C \leq 10,000$  mg/L, the values of  $C_{s,o}$  at  $C = C_o = 10,000$  mg/L were in the relative order of 0 %  $\ll$  5 %  $<$  10 %, although the adsorption model regressions intersected each other at  $C \approx 1,500$  mg/L (Figure 4.5e). Similarly, the retardation in the FBCs for  $C_o$  of 10,000 mg/L (Figure 4.5f) was generally in the order of 0 %  $\ll$  5 %  $<$  10 %, as expected.

Therefore, the results for the lower values of  $C_o$  of 100 and 1,000 mg/L that indicated earlier breakthrough of Zn for the zeolite-amended backfills relative to that for the unamended backfill can be attributed to the combined effect of the lower  $C_{s,o}$  and the  $\lambda$  of the regressed adsorption models. Although both regressed adsorption models clearly indicated that the values of  $C_{s,o}$  for both K and Zn increased with increasing amount of a zeolite in the backfill based on the full range of experimental concentrations, values of  $C_{s,o}$  for Zn based on the Langmuir adsorption model regressions for the backfills amended with 5 and 10 % zeolite generally were lower than that that for the unamended backfill over the lower range in concentrations. This

behavior was previously indicated in Chapter 3, where values of  $K_L Q_L$  for Zn at low concentrations, which are approximately equivalent to values of  $K_d$ , were lower for the zeolite-amended backfills than for the unamended backfill (see Table 4.1). This anomalous adsorptive behavior was attributed to the greater scatter in the measured adsorbed concentrations of Zn for the unamended backfill, which likely affected the accuracy of the adsorption model regressions, and the greater extent of competition between re-dissolved soluble salts versus Zn for available adsorption sites that occurred at the lower equilibrium concentrations (Chapter 3). The overall conclusion from this evaluation is that, although the values of  $Q_{L,amended}/Q_{L,unamended}$  for Zn were greater than unity for all zeolite-amended backfills (Table 4.1), the zeolite-amended backfills were less effective than the unamended backfill in delaying the breakthrough of Zn at lower  $C_o$ , due to overlap in the regressed adsorption models resulting from the scatter in the measured adsorption data for the unamended backfill, such that the adsorption of Zn to the unamended backfills was greater than that to the zeolite-amended backfills at the lower concentrations.

#### 4.3.3 Effect of Magnitude and Direction of Hydraulic Gradient on Flux Breakthrough Curves

The effect of a different magnitude and direction of the hydraulic gradient,  $i$  ( $= 1, 0, -1$ ) on the FBCs for K and Zn, the lowest  $C_o$  of 100 mg/L, and backfills amended with 5 % zeolite is illustrated in Figures 4.6 and 4.7 based on the Langmuir and Freundlich adsorption models, respectively. The results in Figures 4.6 and 4.7 are presented in the form of  $T^*$  versus  $J(L,t)$  normalized with respect to the steady-state mass flux based on purely diffusive transport,  $J_{d,ss}$ , or  $J^*(L,t)$ , as follows:

$$J^*(L,t) = \frac{J(L,t)}{J_{d,ss}} = \frac{J(L,t) \cdot L}{nD^*C_o} \quad (4.12)$$

Normalizing  $J(L,t)$  with respect to  $J_{d,ss}$  instead of  $J_{ss}(L)$  as per Eq. 4.10 was preferred, because the magnitude of  $J_{d,ss}$  is independent of  $i$ , whereas the magnitude of  $J_{ss}(L)$  is a function of  $i$  (*i.e.*,  $P_L = kiL/nD^*$ ). Also, normalizing  $J(L,t)$  with respect to  $J_{d,ss}$  results in different limiting or steady-state values of  $J^*(L,t)$ ,  $J_{ss}^*$ , which are a function of only  $P_L$ , as follows (Rubin and Rabideau 2000; Malusis *et al.* 2010):

$$J_{ss}^* = \frac{P_L}{1 - \exp(-P_L)} \quad (4.13)$$

Note that, for the case where  $i = 0$ , the value for  $J_{ss}^*$  defaults to 1.0, *i.e.*,  $J_{ss}(L) = J_{d,ss}$  (Rubin and Rabideau 2000; Malusis *et al.* 2010). Also, as  $P_L$  is not a function of zeolite amendment,  $J_{ss}^*$  is independent of the type of backfill. However, the type of backfill does affect the magnitude of  $t_B$  (Figures 4.6 and 4.7).

As shown in Figures 4.6 and 4.7, reversing the applied hydraulic gradient from 1 to -1 results in a lower steady-state mass flux,  $J_{ss}^*$ , and later breakthrough of the FBC, as expected. In terms of the simulation results for co-advection ( $i = 1$ ), the lower  $D^*$  for Zn ( $4.36 \times 10^{-10}$  m<sup>2</sup>/s) relative to that for K ( $6.98 \times 10^{-10}$  m<sup>2</sup>/s) resulted in a greater  $P_L$  for Zn (2.29) relative to that for K (1.43). Thus, the contribution of advection relative to diffusion for Zn was greater than that for K, resulting in a greater value of  $J_{ss}^*$  for Zn relative to that for K. In terms of the simulation results for counter-advection ( $i = -1$ ), where inwardly directed advection works against outwardly directed diffusion to reduce the contaminant mass flux through the barrier, the lower  $D^*$  for Zn relative to that for K resulted in a lower (more negative)  $P_L$  for Zn (-2.29) relative to that for K (-1.43), which resulted in lower outwardly directed diffusion and a lower  $J_{ss}^*$  for Zn relative to

that for K. In addition, the FBCs based on the Freundlich model tend to be steeper (more self-sharpening) than those based on the Langmuir model due to the greater nonlinearity associated with the Freundlich model and the greater influence of dispersion via diffusion for the FBCs based on the Langmuir model.

#### 4.3.4 Barrier Flux Breakthrough Times

The dimensionless barrier flux breakthrough time,  $T_B^*$  is defined as the dimensionless time,  $T^*$ , corresponding to when the exit flux,  $J(L,t)$ , is a specified fraction,  $f$ , of the steady state exit flux,  $J_{ss}(L)$ , as follows (*e.g.*, Malusis *et al.* 2010):

$$T_B^* = T^* [J(L,t) / J_{ss}(L) = f] \quad (4.14)$$

Malusis *et al.* (2010) determined  $T_B^*$  for an  $f$  of 0.05 as a reasonable estimate of the earliest breakthrough flux of the contaminant. However, other  $f$  can be assumed, and given the aforementioned differences noted for the FBCs, different  $f$  may result in different conclusions pertaining to chemical breakthrough.

Values of the dimensional barrier breakthrough time,  $t_B$ , corresponding to  $T_B^*$  (Eq. 4.14) based on  $f = 0.05$  for co-advection (*i.e.*,  $i = 1$ ,  $P_L = 1.43$  for K,  $P_L = 2.29$  for Zn) are summarized in Table 4.4 for each  $C_o$  ( $= 100, 1,000, 10,000$  mg/L), type of zeolite (chabazite-LB, chabazite-UB, clinoptilolite), added amount of zeolite (0, 5, 10 %), and adsorption model (Freundlich and Langmuir). The  $t_B$  corresponding to the nonadsorbing tracer represented by chloride (Cl<sup>-</sup>) is also included in Table 4.4. The  $t_B$  for both metals were all greater than that for the tracer, indicating that the unamended backfill had some inherent attenuation capacity (*e.g.*, Shackelford 1999).

For K,  $t_B$  in all cases increased as the zeolite content increased. For example, for  $C_o$  of 1,000 mg/L, the simulation results based on the Freundlich adsorption model indicated a  $t_B$  of 25.0 yr for the unamended backfill, whereas  $t_B$  for the 5 % zeolite-amended backfill was 108 yr with chabazite-LB, 110 yr with chabazite-UB, and 71.7 yr with clinoptilolite, and  $t_B$  for the 10 % zeolite-amended backfill was 165 yr with chabazite-LB, 165 yr with chabazite-UB, and 108 yr with clinoptilolite.

Similar observations can be made with respect to the  $t_B$  for Zn (Table 4.4). However, unlike the simulations of K, the  $t_B$  based on the FBCs assuming  $C_o = 100$  and 1,000 mg/L indicate that, for a significant number of the simulations, the unamended backfill was more effective in retarding the migration of Zn than the zeolite-amended backfills. As previously noted, the earlier breakthrough of the zeolite-amended backfill compared to the unamended backfill can be attributed to the difference in the regressed adsorption behavior for the unamended backfill relative to that for the zeolite-amended backfills at the lower concentrations.

In an attempt to isolate the effect of increasing nonlinearity on adsorption (*i.e.*, increasing  $\lambda$ ) from the contrasting effect of dispersion, consideration was given to values of  $T_B^*$  and  $t_B$  at an  $f$  of 0.50, where the effect of dispersion should be relatively less, and the results are summarized in Table 4.5. The results in Table 4.5 show that changing  $f$  from 0.05 to 0.50 resulted in a slight reduction in the number of simulation cases where breakthrough occurred earlier for the zeolite-amended backfills relative to the unamended backfill (*i.e.*, from 20 to 16 simulation cases), indicating that one reason for the earlier breakthrough associated with the zeolite-amended backfills relative to the unamended backfill was the effect of dispersion. However, the results in Table 4.5 also indicate that there were still numerous simulation cases where breakthrough occurred earlier for the zeolite-amended backfills relative to the unamended backfills for the

simulations based on the lower source concentrations (*i.e.*,  $C_o = 100$  and  $1,000$  mg/L). In these cases, earlier breakthrough for the zeolite-amended backfills can be attributed to the lower values of  $C_{s,o}$  at the lower concentration ranges.

## 4.4 DISCUSSION

### 4.4.1 Effect of Amount and Type of Zeolite

The effect of the amount and type of zeolite amendment on  $T_B^*$  and  $t_B$  are shown in Figure 4.8 as a function of  $C_o$  and the adsorption model used in the simulations. In terms of K (Figures 4.8a,c,e), the values of  $T_B^*$  and  $t_B$  increased with increasing zeolite content, regardless of the type of zeolite. These results are consistent with the  $Q_{L,amended}/Q_{L,unamended}$  shown in Table 4.1, which ranged from 6.2 to 13.5 for K indicating an increasing adsorption capacity for K with increasing zeolite content. For a given  $C_o$ , the  $T_B^*$  and  $t_B$  based on the Freundlich model were greater than those based on the Langmuir model due to the greater effect of dispersion on the FBCs based on the Langmuir model as previously noted. However, the differences in  $T_B^*$  and  $t_B$  based on the two adsorption models decreased with increasing  $C_o$ , because the difference in the FBCs based on the two models diminishes with increasing  $C_o$  (*e.g.*, see Figure 4.3). Finally,  $T_B^*$  and  $t_B$  were lower for higher  $C_o$ , because increasing  $C_o$  resulted in decreasing the time required to fill the available adsorption sites with K. In terms of type of zeolite, the  $T_B^*$  and  $t_B$  for the two chabazite-amended backfills (Figures 4.8a,b) were somewhat greater than those for the clinoptilolite-amended backfills, all other factors being equal. This result is consistent with the generally higher *CEC* values for the two chabazite-amended backfills relative to the clinoptilolite-amended backfills (Chapter 3), resulting in greater adsorption capacities as reflected by the higher  $Q_{L,amended}/Q_{L,unamended}$  (Table 4.1) for the chabazite-amended backfills.

The results in terms of Zn (Figures 4.8b,d,f) are similar to those in terms of K, except that  $T_B^*$  and  $t_B$  for the zeolite-amended backfills tended to be lower than those for the unamended backfill for the two lower  $C_o$  of 100 and 1,000 mg/L. Thus, the zeolite-amended backfills were less effective than the unamended backfill in delaying the breakthrough of Zn at lower  $C_o$ . As previously noted (Figure 4.5), this counterintuitive result occurred due to overlap in the regressed adsorption models at low concentrations resulting from the scatter in the measured adsorption data for the unamended backfill, such that the adsorption of Zn to the unamended backfills was greater than that to the zeolite-amended backfills. Thus, the relative breakthrough for Zn was a function of not only the relative adsorption capacities of the backfills but also the relative Zn adsorption of the backfills over the range of concentrations considered for the simulations.

The improvement in containment performance achieved by adding zeolite can be assessed on the basis of the incremental increase in the values of  $t_B$  for the zeolite-amended backfills ( $t_{B,amended}$ ) relative to those for the unamended backfill ( $t_{B,unamended}$ ), or  $\Delta t_B (= t_{B,amended} - t_{B,unamended})$  (Table 4.6). For K,  $\Delta t_B$  ranged from 11.3 yr for a backfill amended with 5 % clinoptilolite based on  $C_o$  of 10,000 mg/L and the Langmuir adsorption model (Table 4.6, Figure 4.8e) to 759 yr for a backfill amended with 10 % chabazite-LB based on  $C_o$  of 100 mg/L and the Freundlich adsorption model (Table 4.6, Figure 4.8a). Also, based on the simulation cases for Zn that indicated improvement in containment,  $\Delta t_B$  ranged from only 0.70 yr for a backfill amended with 5 % clinoptilolite based on  $C_o$  of 10,000 mg/L and the Langmuir adsorption model (Table 4.6, Figure 4.8f) to 138 yr for a backfill amended with 10 % chabazite-LB based on  $C_o$  of 100 mg/L and the Freundlich adsorption model (Table 4.6, Figure 4.8b).

The FBCs of the unamended and zeolite-amended backfills with 5 and 10 % for the two different types of metals, viz., K versus Zn, and  $i = 1$  are compared in Figures 4.9 – 4.11. All the

results shown in these figures indicate that the first arrival was in the order of  $K < Zn$  for the unamended backfill, and  $Zn < K$  for the zeolite-amended backfills. The reason the zeolite-amended backfills appeared less effective for Zn than K is due to the reduced adsorption of Zn resulting from two effects, *i.e.*, competition for adsorption sites resulting from re-dissolved soluble metals associated with the sorbents used in the BEATs, and the possible speciation of a fraction of Zn in the form of  $Zn(OH)^+$  versus  $Zn^{2+}$ , as discussed in detail in Chapter 3.

The effect of the type of zeolite on the FBCs for  $i = 1$  is shown in Figure 4.12 for K and Figure 4.13 for Zn as a function of the type of zeolite. For K, the zeolite-amended backfills were more effective than the unamended backfill in delaying the breakthrough, with the relative order in the values of  $T_B^*$  generally being chabazite-LB-amended backfill  $\geq$  chabazite-UB-amended backfill  $>$  clinoptilolite-amended backfill  $>$  unamended backfill (Table 4.4, Figure 4.12). However, for Zn, the zeolite-amended backfills were less effective than the unamended backfill in delaying the breakthrough of Zn at lower  $C_o$ . The relative order in the values of  $T_B^*$  among the zeolite-amended backfills were chabazite-LB-amended backfill  $>$  chabazite-UB-amended backfill  $\geq$  clinoptilolite-amended backfill (Table 4.4, Figure 4.13). This relative order in  $T_B^*$  of the zeolite-amended backfills for K and Zn generally corresponds directly with the relative order in the cation exchange capacity (*CEC*) of the three zeolites (Chapter 2).

#### 4.4.2 Influence of Magnitude and Direction of Hydraulic Gradient

The effect of the magnitude and direction of the hydraulic gradient ( $i = 1, 0, -1$ ) on the  $t_B$  for unamended and 5 % zeolite-amended backfills is shown in Figure 4.14 as a function of the backfill type, metal (K or Zn),  $C_o$  (100, 1,000, 10,000 mg/L), and adsorption model (Freundlich or Langmuir), and the values of  $t_B$  are summarized in Table 4.7. Note that the  $t_B$  in Table 4.7 and

Figure 4.14 are based on a  $J^*(L,t)$  of 0.015 in accordance with Malusis *et al.* (2010), as different values of  $i$  result in different  $P_L$  and  $J_{ss}(L)$  (Eqs. 4.9 and 4.10).

For each backfill,  $t_B$  increased as  $i$  decreased, as expected (Figure 4.14). Also, for a given  $i$  and a given backfill,  $t_B$  based on the Freundlich adsorption model was always greater than  $t_B$  based on the Langmuir adsorption model, due to the relative effects of adsorption nonlinearity and solute dispersion on the FBCs (Figure 4.3).

For a given  $i$ ,  $t_B$  for K migration through the zeolite-amended backfills were all greater than  $t_B$  for the unamended backfill, as expected. However, for Zn migration, the relative difference in  $t_B$  was only evident for the simulations based on Freundlich adsorption model for  $C_o = 1,000$  mg/L and the backfill amended with chabazite-LB (Figure 4.14d) and for  $C_o = 10,000$  mg/L with all three zeolite-amended backfills (Figure 4.14f), due to the aforementioned issues related to the difference in adsorption behavior between the unamended and zeolite-amended backfills at lower concentrations (Chapter 3).

Incremental changes in flux breakthrough time based on the reversal in the direction of the hydraulic gradient,  $\Delta t_{B,i}$ , defined as the difference between  $t_B$  based on a hydraulic gradient of  $-1$ ,  $t_{B,i=-1}$ , versus that based on a hydraulic gradient of  $1$ ,  $t_{B,i=1}$  (*i.e.*,  $\Delta t_{B,i} = t_{B,i=-1} - t_{B,i=1}$ ), are summarized in Table 4.8. All  $\Delta t_{B,i}$  were greater than zero, indicating that changing the direction of advection from co-advection to counter-advection resulted in an increase in flux breakthrough time regardless of metal, adsorption model,  $C_o$ , or zeolite type and content. Values of  $\Delta t_{B,i}$  ranged from 1.8 yr for K with the unamended backfill (based on  $C_o = 10,000$  mg/L and the Langmuir adsorption model) to 1,113 yr for Zn with the unamended backfill (based on  $C_o = 100$  mg/L and the Freundlich adsorption model). Finally, all other factors being constant,  $\Delta t_{B,i}$  for K based on the zeolite-amended backfills were greater than  $\Delta t_{B,i}$  based on the unamended

backfills in all cases, whereas  $\Delta t_{B,i}$  for Zn based on the zeolite-amended backfills were lower than  $\Delta t_{B,i}$  based on the unamended backfills in the majority of cases. Thus, zeolite amendment enhanced the effect of reversing the gradient on the containment duration for K, whereas zeolite amendment generally diminished the effect of reversing the gradient on the containment duration for Zn. This difference can be due to the lower adsorption capacity for lower  $C_o$  of Zn for the zeolite-amended backfills relative to the unamended backfill.

The effect of zeolite amendment on flux breakthrough time is further elucidated by considering the results in Figure 4.15, which show the ratio of  $\Delta t_{B,i}$  for zeolite-amended backfill,  $\Delta t_{B,i,amended}$ , relative to that for unamended backfill,  $\Delta t_{B,i,unamended}$  (*i.e.*,  $\Delta t_{B,i,amended}/\Delta t_{B,i,unamended}$ ) as a function of zeolite content. In Figures 4.15a,c,e,  $\Delta t_{B,i,amended}/\Delta t_{B,i,unamended}$  for K increased with increasing zeolite content in all cases, indicating that zeolite amendment enhanced the containment of K associated with a reversal in the hydraulic gradient. The most significant increases in  $\Delta t_{B,i,amended}/\Delta t_{B,i,unamended}$  resulted from the simulations based on the Langmuir adsorption model for backfills amended with 10 % zeolite. Values of  $\Delta t_{B,i,amended}/\Delta t_{B,i,unamended}$  generally were in the order chabazite-LB  $\geq$  chabazite-UB  $>$  clinoptilolite, which is the same order as the adsorption capacities for the zeolite-amended backfills in Table 4.1. However, as shown in Figures 4.15b,d,f, with few exceptions, zeolite amendment diminished containment of Zn associated with a reversal in the hydraulic gradient (*i.e.*  $\Delta t_{B,i,amended}/\Delta t_{B,i,unamended} < 1$ ). As previously described, this counterintuitive behavior is due to the reduced adsorption capacities of the zeolite-amended backfills for Zn relative to that for the unamended backfill over the lower range in concentrations based on regression of the laboratory adsorption data.

#### 4.4.3 Effect of the Source Concentration

The effect of  $C_o$  ( $= 100, 1,000, 10,000$  mg/L) on the  $T_B^*$  for  $f = 0.05$  and the FBCs for  $i = 1$  is shown in Figures 4.16 – 4.17 for K and Figures 4.18 – 4.19 for Zn. For all cases,  $T_B^*$  decreased as  $C_o$  increased, because higher source concentrations result in quicker exhaustion of the finite adsorption capacity and earlier breakthrough.

Also, all of the  $T_B^*$  and the shapes of the FBCs based on the Langmuir versus Freundlich adsorption models differed significantly for the two lower  $C_o$  of 100 and 1,000 mg/L, but were similar for the highest  $C_o$  of 10,000 mg/L. As previously noted (see Figure 4.3), the difference in the shapes of the FBCs based on the type of adsorption model is related to the difference in  $C_{s,o}$  for a given range of concentrations, and/or the difference in the relative nonlinearity of the regressed adsorption model (*i.e.*,  $\lambda$ ). As the difference in the  $T_B^*$  based on the Langmuir versus Freundlich adsorption models differ significantly for the lower  $C_o$ , caution is required when applying the BEAT results to simulate the solute transport. This difference is due to applying the Langmuir and Freundlich parameters fitted to the BEAT results for  $C \geq 10,000$  mg/L to simulate the solute transport for a lower  $C_o$  of 100 or 1,000 mg/L. Therefore, ideally, using the BEAT results with the  $C$  closer to the  $C_o$  of interest will exhibit results where the  $T_B^*$  based on the Langmuir versus Freundlich adsorption models agree better than when using the Langmuir and Freundlich parameters fitted to the BEAT results for  $C \geq 10,000$  mg/L.

## 4.5 SUMMARY AND CONCLUSIONS

The long-term performance of a hypothetical 1-m-thick soil-bentonite vertical cutoff wall comprising a sand-bentonite backfill amended with 0, 5, or 10 % (dry weight) of one of three types of high-cation exchange capacity (CEC) zeolites, *viz.*, chabazite-LB, chabazite-UB, or

clinoptilolite, with respect to the migration of two metals, K and Zn, was evaluated via numerical simulations. The simulations were conducted using a previously developed solute transport model that included nonlinear, equilibrium adsorptive behavior, and the adsorptive behavior of each metal with respect to each backfill was based on the results of a previous study involving laboratory batch equilibrium adsorption tests (BEATs) with the metals and the backfills.

The results of the numerical evaluation indicated that the improvement in the containment of a metal as reflected by an increase in the barrier flux breakthrough time,  $t_B$ , generally increased with decreasing source concentration ( $C_o$ ) of the metal, because a higher  $C_o$  exhausted the adsorption capacity of the backfill for the metal more quickly, resulting in a lower  $t_B$ . Also, model simulations with the Freundlich adsorption model versus the Langmuir adsorption model resulted in higher values of  $t_B$  (all other factors being equal), because the greater nonlinearity (concavity) associated with the Freundlich model tended to offset the effect of dispersion on the flux breakthrough curves, resulting in more self-sharpening (steeper) flux breakthrough curves. Finally, as expected, a greater zeolite content (*i.e.*, 10 % versus 5 %) and/or use of the higher *CEC* chabazites versus the lower *CEC* clinoptilolite also resulted in higher  $t_B$  (all other factors being equal), due to an increase in the adsorption capacity of the zeolite-amended backfills for a given metal.

The improvement in containment duration, *i.e.*,  $\Delta t_B$ , generally was greater for K versus Zn, even though K was expected to exist primarily as a monovalent cation ( $K^+$ ) whereas Zn was expected to exist primarily as a divalent cation ( $Zn^{2+}$ ). Also, for the model simulations with Zn, several of the results indicated that the zeolite-amended backfills actually performed worse than the unamended backfills (*i.e.*,  $\Delta t_B < 0$ ) at the lower values for  $C_o$  of 100 and 1,000 mg/L. These counterintuitive results were a direct reflection of the results of the BEATs with Zn used as input

for the model simulations, which indicated preferential adsorption of K relative to Zn due to chemical complexation of a fraction of the Zn (*e.g.*, Zn(OH)<sup>+</sup> vs. Zn<sup>2+</sup>) and greater competition for available exchange sites between Zn and other soluble metals, primarily Na<sup>+</sup>, associated with the bentonite and zeolite in the backfills. Thus, the model simulations were highly dependent on the results of the BEATs and influenced by the limitations associated with these results.

Given the aforementioned results, improvement in containment of K due to zeolite amendment,  $\Delta t_B$ , ranged from 11.3 yr for a backfill amended with 5 % clinoptilolite (based on  $C_o = 10,000$  mg/L and the Langmuir adsorption model) to 759 yr for a backfill amended with 10 % chabazite-LB (based on  $C_o = 100$  mg/L and the Freundlich adsorption model). Based on the model simulations for Zn that indicated improvement in containment,  $\Delta t_B$  ranged from only 0.70 yr for a backfill amended with 5 % clinoptilolite based on  $C_o = 10,000$  mg/L and the Langmuir adsorption model to 138 yr for a backfill amended with 10 % chabazite-LB based on  $C_o = 100$  mg/L and the Freundlich adsorption model.

The simulation results pertaining to the scenarios where the direction of advection was reversed via a change in the hydraulic gradient,  $i$ , from outward ( $i = 1$ ) to inward ( $i = -1$ ) indicated that inward seepage enhanced containment of both K and Zn by delaying the mass flux breakthrough and reducing the steady-state mass flux of the metals, as expected. In addition, the effect of delayed mass flux breakthrough for K was enhanced with the zeolite-amended backfills relative to the unamended backfill, whereas the opposite was generally the case for Zn. This difference in behavior was attributed directly to the results of the BEATs upon which the model simulations were based, whereby K was preferentially adsorbed relative to Zn, and the adsorption capacity for Zn with the unamended backfill was greater than that for the zeolite-amended backfills at lower solute concentrations.

Overall, the results of this study indicate that containment of metals may be enhanced on the order of a century or more with zeolite-amended SB cutoff walls. However, the magnitude of any enhanced containment is highly dependent on both the adsorption capacity and the adsorption behavior of the specific metal with the specific backfill.

Table 4.1. Regressed parameter values from results of batch equilibrium adsorption tests (data from Chapter 3).

Backfill		Metal	Adsorption Model Regressed Parameters <sup>a</sup>							$\frac{Q_{L,amended}}{Q_{L,unamended}}$
Type of Zeolite	Amount of Zeolite (%)		Langmuir Model				Freundlich Model			
			$K_L$ (L/mg)	$Q_L$ (mg/kg)	$K_L Q_L$ (L/kg)	$r^2$	$K_f$ (L/kg)	$N_f$	$r^2$	
NA <sup>b</sup>	0	K	0.00301	813	2.4	0.666	250	0.13	0.518	1.0
Chabazite-LB	5	K	0.00379	5,080	19.3	0.954	638	0.24	0.912	6.2
Chabazite-LB	10	K	0.00464	8,230	38.2	0.960	934	0.25	0.919	10.1
Chabazite-UB	5	K	0.00305	5,460	16.7	0.946	608	0.25	0.923	6.7
Chabazite-UB	10	K	0.00202	11,000	22.2	0.952	635	0.32	0.972	13.5
Clinoptilolite	5	K	0.000813	5,930	4.8	0.915	221	0.35	0.929	7.3
Clinoptilolite	10	K	0.00223	6,120	13.6	0.881	477	0.29	0.931	7.5
NA <sup>b</sup>	0	Zn	0.00379	3,110	11.8	0.721	473	0.21	0.934	1.0
Chabazite-LB	5	Zn	0.000468	8,680	4.1	0.872	300	0.34	0.942	2.8
Chabazite-LB	10	Zn	0.000561	9,740	5.5	0.859	370	0.34	0.930	3.1
Chabazite-UB	5	Zn	0.000271	10,500	2.8	0.937	107	0.46	0.965	3.4
Chabazite-UB	10	Zn	0.000374	10,600	4.0	0.955	170	0.42	0.953	3.4
Clinoptilolite	5	Zn	0.000251	9,380	2.4	0.861	97.1	0.45	0.836	3.0
Clinoptilolite	10	Zn	0.000317	11,400	3.6	0.958	146	0.44	0.933	3.7

<sup>a</sup>  $K_L$  = Langmuir constant,  $Q_L$  = Langmuir maximum adsorbed concentration for the solute (Eq. 4.4);  $K_f$  = Freundlich unit adsorption capacity,  $N_f$  = Freundlich exponent (Eq. 4.5);  $r^2$  = coefficient of determination.

<sup>b</sup> NA = Not applicable (*i.e.*, unamended backfill)

Table 4.2. Values of relative nonlinearity ( $\lambda$ ) based on data from Table 4.1 for unamended and zeolite amended backfills.

Metal	Type of Adsorption Model	Source Concentration, $C_o$ (mg/L) ( $C \leq C_o$ )	Relative Nonlinearity, $\lambda^a$						
			Unamended	Chabazite-LB		Chabazite-UB		Clinoptilolite	
				5 %	10 %	5 %	10 %	5 %	10 %
K	Langmuir	100	0.048	0.058	0.069	0.048	0.034	0.014	0.037
		1,000	0.240	0.267	0.290	0.241	0.195	0.107	0.206
		10,000	0.468	0.483	0.494	0.469	0.439	0.353	0.446
	Freundlich	100, 1,000, 10,000	0.434	0.341	0.333	0.333	0.285	0.266	0.305
Zn	Langmuir	100	0.058	0.008	0.010	0.005	0.007	0.005	0.006
		1,000	0.267	0.070	0.081	0.044	0.058	0.041	0.050
		10,000	0.483	0.291	0.312	0.228	0.265	0.219	0.246
	Freundlich	100, 1,000, 10,000	0.364	0.272	0.272	0.203	0.224	0.208	0.213

<sup>a</sup> 0 (linear)  $\leq \lambda \leq 0.5$  (Emancipator and Kroll 1993).

Table 4.3. Values of the secant distribution coefficient,  $K_{d,secant}$ , based on data from Table 4.1 for unamended and zeolite-amended backfills.

Metal	Type of Adsorption Model	Source Concentration, $C_o$ (mg/L) ( $C \leq C_o$ )	Secant Distribution Coefficient, $K_{d,secant}$						
			Unamended	Chabazite-LB		Chabazite-UB		Clinoptilolite	
				5 %	10 %	5 %	10 %	5 %	10 %
K	Langmuir	100	1.9	14	26	13	18	4.5	11
		1,000	0.61	4.0	6.8	4.1	7.4	2.7	4.2
		10,000	0.08	0.49	0.81	0.53	1.1	0.53	0.59
	Freundlich	100	4.6	19	30	19	28	11	18
		1,000	0.61	3.4	5.3	3.4	5.8	2.5	3.5
		10,000	0.08	0.58	0.93	0.61	1.2	0.56	0.69
Zn	Langmuir	100	8.6	3.9	5.2	2.8	3.8	2.3	3.5
		1,000	2.5	2.8	3.5	2.2	2.9	1.9	2.7
		10,000	0.30	0.72	0.83	0.77	0.84	0.67	0.87
	Freundlich	100	12	14	18	8.9	11.8	7.7	11
		1,000	2.0	3.1	3.9	2.6	3.1	2.2	3.1
		10,000	0.33	0.69	0.85	0.74	0.81	0.61	0.84

Table 4.4. Predicted barrier flux breakthrough times for Cl<sup>-</sup>, K, and Zn with a 1-m-thick ( $L = 1$  m) soil-bentonite vertical cutoff wall comprising unamended or zeolite-amended backfills as a function of source concentration and type of adsorption model using data from Table 4.1.

Chemical	Type of Adsorption Model	Source Concentration, $C_o$ (mg/L)	Barrier Flux Breakthrough Time, $t_B$ (yr) [ $T_B^*$ ] <sup>a</sup>						
			Unamended	Chabazite-LB		Chabazite-UB		Clinoptilolite	
				5 %	10 %	5 %	10 %	5 %	10 %
Cl <sup>-</sup>	NA	100, 1000, 10,000	2.41 [0.05]	2.41 [0.05]	2.41 [0.05]	2.41 [0.05]	2.41 [0.05]	2.41 [0.05]	2.41 [0.05]
K	Langmuir	100	18.6 [0.41]	127 [2.80]	247 [5.43]	112 [2.46]	150 [3.29]	35.0 [0.77]	93.6 [2.06]
		1,000	13.6 [0.30]	83.6 [1.84]	177 [3.29]	77.3 [1.70]	116 [2.54]	31.8 [0.70]	70.0 [1.54]
		10,000	6.4 [0.14]	23.2 [0.51]	35.5 [0.78]	23.6 [0.52]	38.6 [0.85]	17.7 [0.39]	23.6 [0.52]
	Freundlich	100	155 [3.40]	600 [13.2]	914 [20.1]	591 [13.0]	777 [17.1]	300 [6.59]	536 [11.8]
		1,000	25.0 [0.55]	108 [2.38]	165 [3.63]	110 [2.42]	165 [3.63]	71.4 [1.57]	108 [2.38]
		10,000	6.4 [0.14]	22.3 [0.49]	33.2 [0.73]	23.6 [0.52]	38.2 [0.84]	19.1 [0.42]	24.1 [0.53]
Zn	Langmuir	100	122 [1.67]	48.0 [0.66]	61.8 [0.85]	34.9 [0.48]	46.6 [0.64]	29.1 [0.40]	42.9 [0.59]
		1,000	77.1 [1.06]	44.4 [0.61]	56.8 [0.78]	32.7 [0.45]	44.4 [0.61]	28.4 [0.39]	40.7 [0.56]
		10,000	21.1 [0.29]	27.6 [0.38]	32.7 [0.45]	24.7 [0.34]	29.1 [0.40]	21.8 [0.30]	28.3 [0.39]
	Freundlich	100	546 [7.50]	554 [7.62]	684 [9.40]	286 [3.93]	402 [5.52]	255 [3.51]	365 [5.01]
		1,000	95.3 [1.31]	126 [1.73]	155 [2.13]	86.6 [1.19]	111 [1.52]	76.4 [1.05]	106 [1.45]
		10,000	21.1 [0.29]	32.0 [0.44]	38.6 [0.53]	29.1 [0.40]	33.5 [0.46]	24.7 [0.34]	33.5 [0.46]

<sup>a</sup> Dimensionless barrier flux breakthrough time,  $T_B^* (= D^* t/L^2)$  for an exit mass flux,  $J^*(L,t)$ , equal to 5 % of the steady state exit mass flux ( $f = 0.05$ );  $D^* = 7.11 \times 10^{-10}$  m<sup>2</sup>/s for Cl<sup>-</sup>,  $D^* = 6.98 \times 10^{-10}$  m<sup>2</sup>/s for K,  $D^* = 4.36 \times 10^{-10}$  m<sup>2</sup>/s for Zn.

Table 4.5. Predicted barrier flux breakthrough times for Zn based on different criteria ( $f = 0.05$  or  $f = 0.50$ ) with 1-m-thick ( $L = 1$  m) vertical cutoff wall as a function of source concentration and type of adsorption model using data from Table 4.1.

$f$	Type of Adsorption Model	Source Concentration, $C_o$ (mg/L)	Barrier Flux Breakthrough Time, $t_B$ (yr) [ $T_B^*$ ] <sup>a</sup>						
			Unamended	Chabazite-LB		Chabazite-UB		Clinoptilolite	
				5 %	10 %	5 %	10 %	5 %	10 %
0.05	Langmuir	100	122 [1.67]	48.0 [0.66]	61.8 [0.85]	34.9 [0.48]	46.6 [0.64]	29.1 [0.40]	42.9 [0.59]
		1,000	77.1 [1.06]	44.4 [0.61]	56.8 [0.78]	32.7 [0.45]	44.4 [0.61]	28.4 [0.39]	40.7 [0.56]
		10,000	21.1 [0.29]	27.6 [0.38]	32.7 [0.45]	24.7 [0.34]	29.1 [0.40]	21.8 [0.30]	28.3 [0.39]
	Freundlich	100	546 [7.50]	554 [7.62]	684 [9.40]	286 [3.93]	402 [5.52]	255 [3.51]	365 [5.01]
		1,000	95.3 [1.31]	126 [1.73]	155 [2.13]	86.6 [1.19]	111 [1.52]	76.4 [1.05]	106 [1.45]
		10,000	21.1 [0.29]	32.0 [0.44]	38.6 [0.53]	29.1 [0.40]	33.5 [0.46]	24.7 [0.34]	33.5 [0.46]
0.50	Langmuir	100	268 [3.69]	116 [1.59]	150 [2.06]	83.7 [1.15]	112 [1.54]	71.3 [0.98]	103 [1.42]
		1,000	114 [1.57]	96.8 [1.33]	122 [1.67]	76.4 [1.05]	96.8 [1.33]	64.8 [0.89]	91.0 [1.25]
		10,000	24.0 [0.33]	40.7 [0.56]	46.6 [0.64]	41.5 [0.57]	45.1 [0.62]	37.1 [0.51]	45.8 [0.63]
	Freundlich	100	554 [7.62]	592 [8.13]	728 [10.0]	342 [4.70]	457 [6.28]	301 [4.13]	429 [5.89]
		1,000	99.0 [1.36]	136 [1.87]	165 [2.27]	106 [1.45]	127 [1.75]	91.0 [1.25]	126 [1.73]
		10,000	23.3 [0.32]	36.4 [0.50]	44.4 [0.61]	37.1 [0.51]	40.7 [0.56]	32.0 [0.44]	41.5 [0.57]

<sup>a</sup> Dimensionless barrier flux breakthrough time,  $T_B^* (= D^* t/L^2)$  for an exit mass flux,  $J^*(L,t)$ , equal to 5 % ( $f = 0.05$ ) or 50 % ( $f = 0.50$ ) of the steady state exit mass flux;  $D^* = 7.11 \times 10^{-10}$  m<sup>2</sup>/s for Cl<sup>-</sup>,  $D^* = 6.98 \times 10^{-10}$  m<sup>2</sup>/s for K,  $D^* = 4.36 \times 10^{-10}$  m<sup>2</sup>/s for Zn.

Table 4.6. Increment in the predicted barrier flux breakthrough time for Cl<sup>-</sup>, K, and Zn with a 1-m-thick ( $L = 1$  m) soil-bentonite vertical cutoff wall comprising a zeolite-amended backfill relative to that comprising an unamended backfill as a function of source concentration and type of adsorption model using data from Table 4.4.

Chemical	Type of Adsorption Model	Source Concentration, $C_o$ (mg/L)	Barrier Flux Breakthrough Time, $t_B$ (yr) [ $T_B^*$ ] <sup>a</sup> , for Unamended Backfill	Increment in Barrier Flux Breakthrough Time, $\Delta t_B$ (yr) [ $\Delta T_B^*$ ] <sup>b</sup> for Zeolite Amended Backfills					
				Chabazite-LB		Chabazite-UB		Clinoptilolite	
				5 %	10 %	5 %	10 %	5 %	10 %
Cl <sup>-</sup>	NA	100, 1,000, 10,000	2.41 [0.05]	2.41 [0.05]	2.41 [0.05]	2.41 [0.05]	2.41 [0.05]	2.41 [0.05]	2.41 [0.05]
K	Langmuir	100	18.6 [0.41]	108 [2.39]	228 [5.02]	93.4 [2.05]	131 [2.88]	16.4 [0.36]	75.0 [1.65]
		1,000	13.6 [0.30]	70.0 [1.54]	163 [2.99]	63.7 [1.40]	102 [2.24]	18.2 [0.40]	56.4 [1.24]
		10,000	6.4 [0.14]	16.8 [0.37]	29.1 [0.64]	17.2 [0.38]	32.2 [0.71]	11.3 [0.25]	17.2 [0.38]
	Freundlich	100	155 [3.40]	445 [9.80]	759 [16.7]	436 [9.60]	622 [13.7]	145 [3.19]	381 [8.40]
		1,000	25.0 [0.55]	83.0 [1.83]	140 [3.08]	85.0 [1.87]	140 [3.08]	46.4 [1.02]	83.0 [1.83]
		10,000	6.4 [0.14]	15.9 [0.35]	26.8 [0.59]	17.2 [0.38]	31.8 [0.70]	12.7 [0.28]	17.7 [0.39]
Zn	Langmuir	100	122 [1.67]	-74.0 [-1.01]	-60.2 [0.82]	-87.1 [-1.19]	-75.4 [-1.03]	-92.9 [-1.27]	-79.1 [-1.08]
		1,000	77.1 [1.06]	-32.7 [-0.45]	-20.3 [-0.28]	-44.4 [-0.61]	-32.7 [-0.45]	-48.7 [-0.67]	-36.4 [-0.50]
		10,000	21.1 [0.29]	6.50 [0.09]	11.6 [0.16]	3.60 [0.05]	8.00 [0.11]	0.70 [0.01]	7.20 [0.10]
	Freundlich	100	546 [7.50]	8.00 [0.12]	138 [1.90]	-260 [-3.57]	-144 [-1.98]	-291 [-3.99]	-181 [-2.49]
		1,000	95.3 [1.31]	30.7 [0.42]	59.7 [0.82]	-8.70 [-0.12]	15.7 [0.21]	-18.9 [-0.26]	10.7 [0.14]
		10,000	21.1 [0.29]	10.9 [0.15]	17.5 [0.24]	8.00 [0.11]	12.4 [0.17]	3.60 [0.05]	12.4 [0.17]

<sup>a</sup> Dimensionless barrier flux breakthrough time,  $T_B^* (= D^* t/L^2)$  for an exit mass flux,  $J^*(L,t)$ , equal to 5 % of the steady state exit mass flux ( $f = 0.05$ );  $D^* = 7.11 \times 10^{-10}$  m<sup>2</sup>/s for Cl<sup>-</sup>,  $D^* = 6.98 \times 10^{-10}$  m<sup>2</sup>/s for K,  $D^* = 4.36 \times 10^{-10}$  m<sup>2</sup>/s for Zn.

<sup>b</sup>  $\Delta t_B$  (yr) =  $t_{B,amended}$  (yr) -  $t_{B,unamended}$  (yr);  $\Delta T_B^* = T_{B,amended}^* - T_{B,unamended}^*$ .

Table 4.7. Predicted barrier flux breakthrough times for potassium (K) and zinc (Zn) corresponding to  $J^*(L,t) = 0.015$  with a 1-m-thick ( $L = 1$  m) soil-bentonite vertical cutoff wall comprising unamended or zeolite-amended backfills as a function of type of adsorption model, source concentration, and magnitude and direction of hydraulic gradient.

Metal	Type of Adsorption Model	Source Concentration, $C_o$ (mg/L)	Hydraulic Gradient, $i^a$	Barrier Flux Breakthrough Time, $t_B$ (yr) <sup>b</sup>						
				Unamended	Chabazite-LB		Chabazite-UB		Clinoptilolite	
					5 %	10 %	5 %	10 %	5 %	10 %
K	Langmuir	100	1	13	91	177	77	105	25	64
			0	15	100	196	91	118	28	73
			-1	17	118	227	105	136	32	86
		1,000	1	11	64	123	59	86	23	55
			0	12	77	141	68	100	26	59
			-1	14	91	168	82	118	31	73
		10,000	1	5.5	21	34	22	35	15	21
			0	6.4	28	45	28	44	17	27
			-1	7.3	36	59	35	55	21	33
	Freundlich	100	1	155	600	914	591	777	300	536
			0	214	814	1218	800	1023	386	705
			-1	323	1164	1736	1141	1386	518	973
		1,000	1	25	109	164	109	164	73	109
			0	33	146	218	146	218	91	141
			-1	50	205	314	205	296	118	196
		10,000	1	6.4	22	33	23	38	19	24
			0	7.7	29	43	30	50	24	31
			-1	10	40	59	41	64	31	41
Zn	Langmuir	100	1	87	31	42	23	31	20	28
			0	102	38	52	28	38	23	34
			-1	131	50	67	36	50	31	44
		1,000	1	61	31	39	23	30	19	28
			0	73	37	48	27	36	23	34
			-1	102	48	62	35	47	30	44
		10,000	1	20	22	27	19	23	16	22
			0	28	27	34	23	28	21	26
			-1	42	36	44	30	36	28	34
	Freundlich	100	1	546	553	684	284	400	255	364
			0	888	815	1004	393	560	349	509
			-1	1659	1346	1688	582	873	517	764
		1,000	1	95	124	153	87	109	73	102
			0	153	182	226	116	153	102	146
			-1	284	298	371	175	233	153	218
		10,000	1	21	32	39	28	33	25	33
			0	31	44	55	38	44	33	44
			-1	51	71	87	55	67	47	66

<sup>a</sup> For K,  $P_L = \pm 1.43$  for  $i = \pm 1$ ; For Zn,  $P_L = \pm 2.29$  for  $i = \pm 1$ ; For both K and Zn,  $P_L = 0$  for  $i = 0$ .

<sup>b</sup> Barrier flux breakthrough time,  $t_B$ , corresponding to exit flux,  $J^* = 0.015$ .

Table 4.8. Incremental change in barrier flux breakthrough time due to reversal in hydraulic gradient for  $J^*(L,t)$  of 0.015.

Metal	Type of Adsorption Model	Source Concentration, $C_o$ (mg/L)	Incremental Change in Barrier Flux Breakthrough Time due to Hydraulic Gradient Reversal, $\Delta t_{B,i}$ (yr) <sup>a</sup>						
			Unamended	Chabazite-LB		Chabazite-UB		Clinoptilolite	
				5 %	10 %	5 %	10 %	5 %	10 %
K	Langmuir	100	4	27	50	28	31	7	22
		1,000	3	27	45	23	32	8	18
		10,000	1.8	15	25	13	20	6	12
	Freundlich	100	168	564	822	550	609	218	437
		1,000	25	96	150	96	132	45	87
		10,000	3.6	18	26	18	26	12	17
Zn	Langmuir	100	44	19	25	13	19	11	16
		1,000	41	17	23	12	17	11	16
		10,000	22	14	17	11	13	12	12
	Freundlich	100	1113	793	1004	298	473	262	400
		1,000	189	174	218	88	124	80	116
		10,000	30	39	48	27	34	22	33

$$^a \Delta t_{B,i} \text{ (yr)} = t_{B,i=-1} \text{ (yr)} - t_{B,i=1} \text{ (yr)}$$

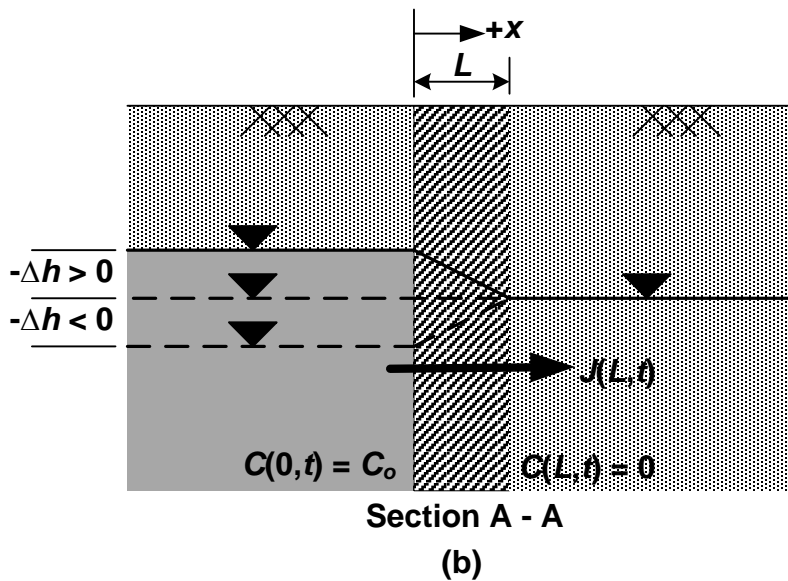
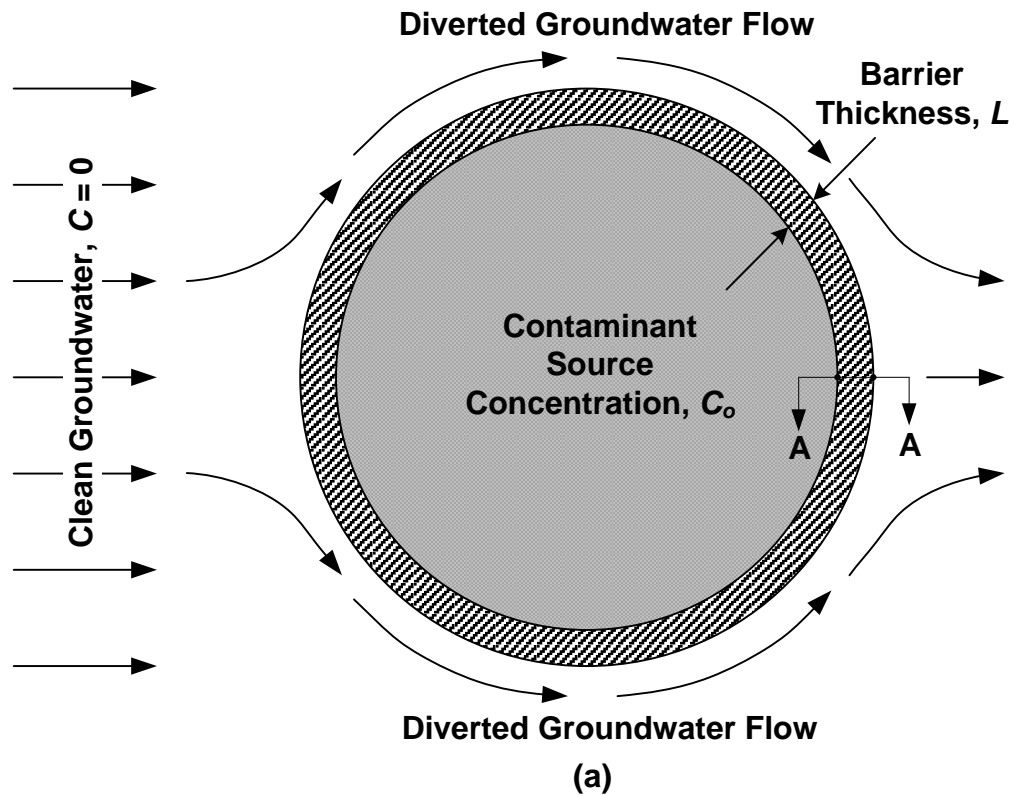


Figure 4.1. Schematic of soil-bentonite vertical cutoff wall scenarios for model simulations: (a) plan view showing divergent groundwater flow; (b) cross-sectional view of cutoff wall illustrating boundary conditions.

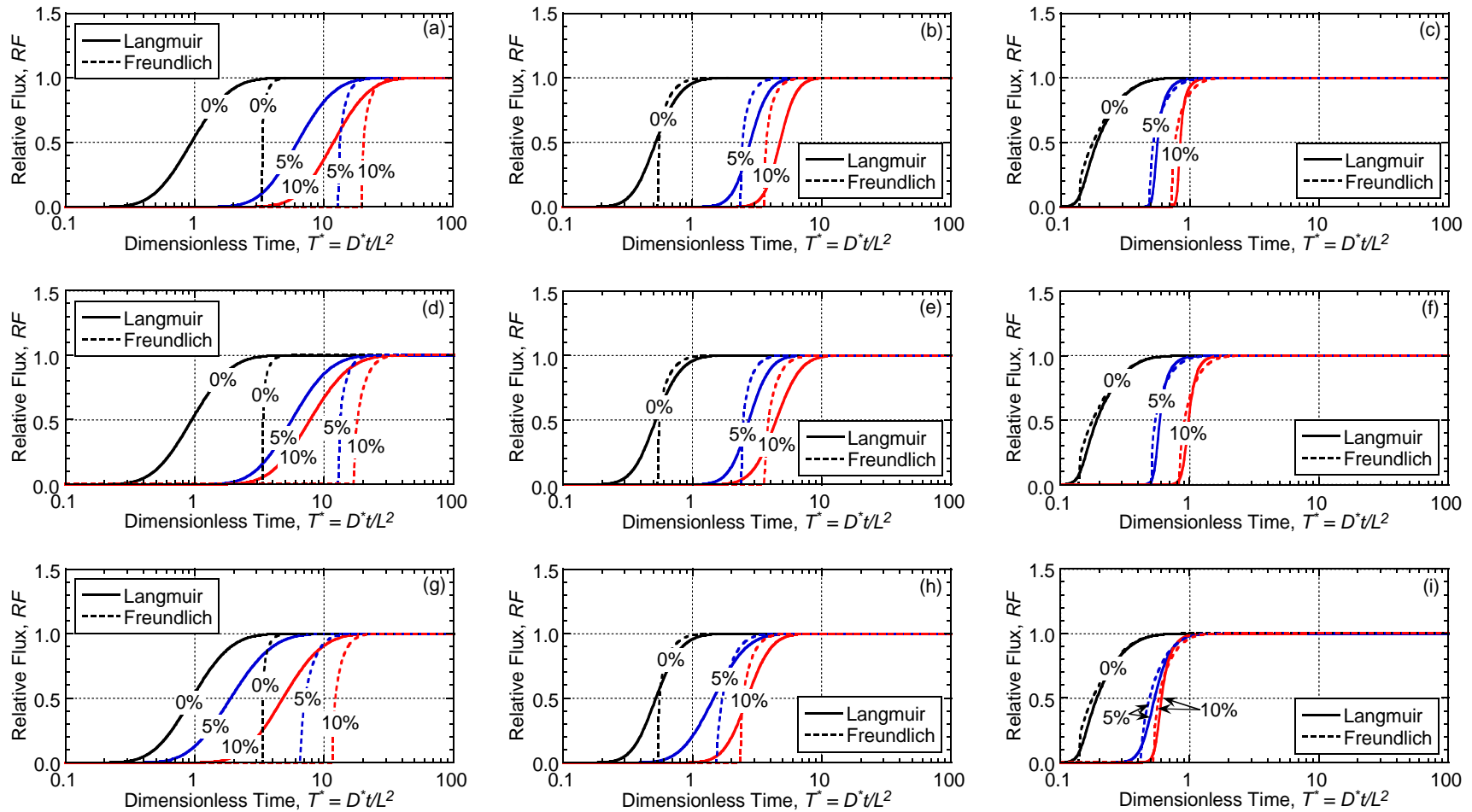


Figure 4.2. Flux breakthrough curves for potassium as a function of adsorption model (Langmuir and Freundlich), zeolite content (0, 5, 10 %), and source concentration ( $C_o$ ): (a) chabazite-LB,  $C_o = 100$  mg/L; (b) chabazite-LB,  $C_o = 1,000$  mg/L; (c) chabazite-LB,  $C_o = 10,000$  mg/L; (d) chabazite-UB,  $C_o = 100$  mg/L; (e) chabazite-UB,  $C_o = 1,000$  mg/L; (f) chabazite-UB,  $C_o = 10,000$  mg/L; (g) clinoptilolite,  $C_o = 100$  mg/L; (h) clinoptilolite,  $C_o = 1,000$  mg/L; (i) clinoptilolite,  $C_o = 10,000$  mg/L.

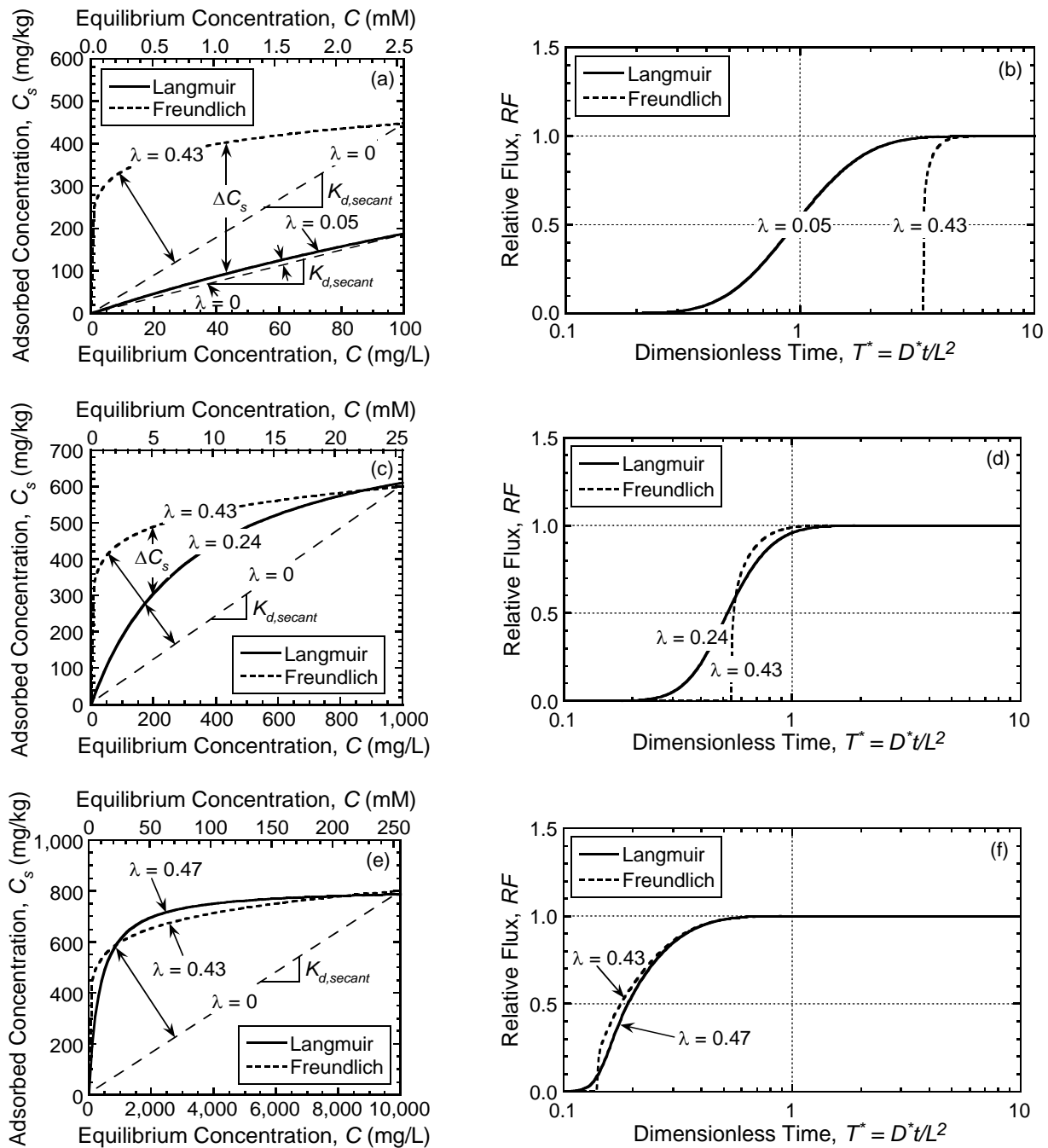


Figure 4.3. Effect of adsorption behavior on potassium flux breakthrough curves for unamended backfill based on different adsorption models (Langmuir and Freundlich): (a), (c), (e) adsorption behaviors for concentration ranges of 100, 1,000, and 10,000 mg/L, respectively; (b), (d), (f) flux breakthrough curves for a source concentration ( $C_o$ ) of 100, 1,000, and 10,000 mg/L, respectively.

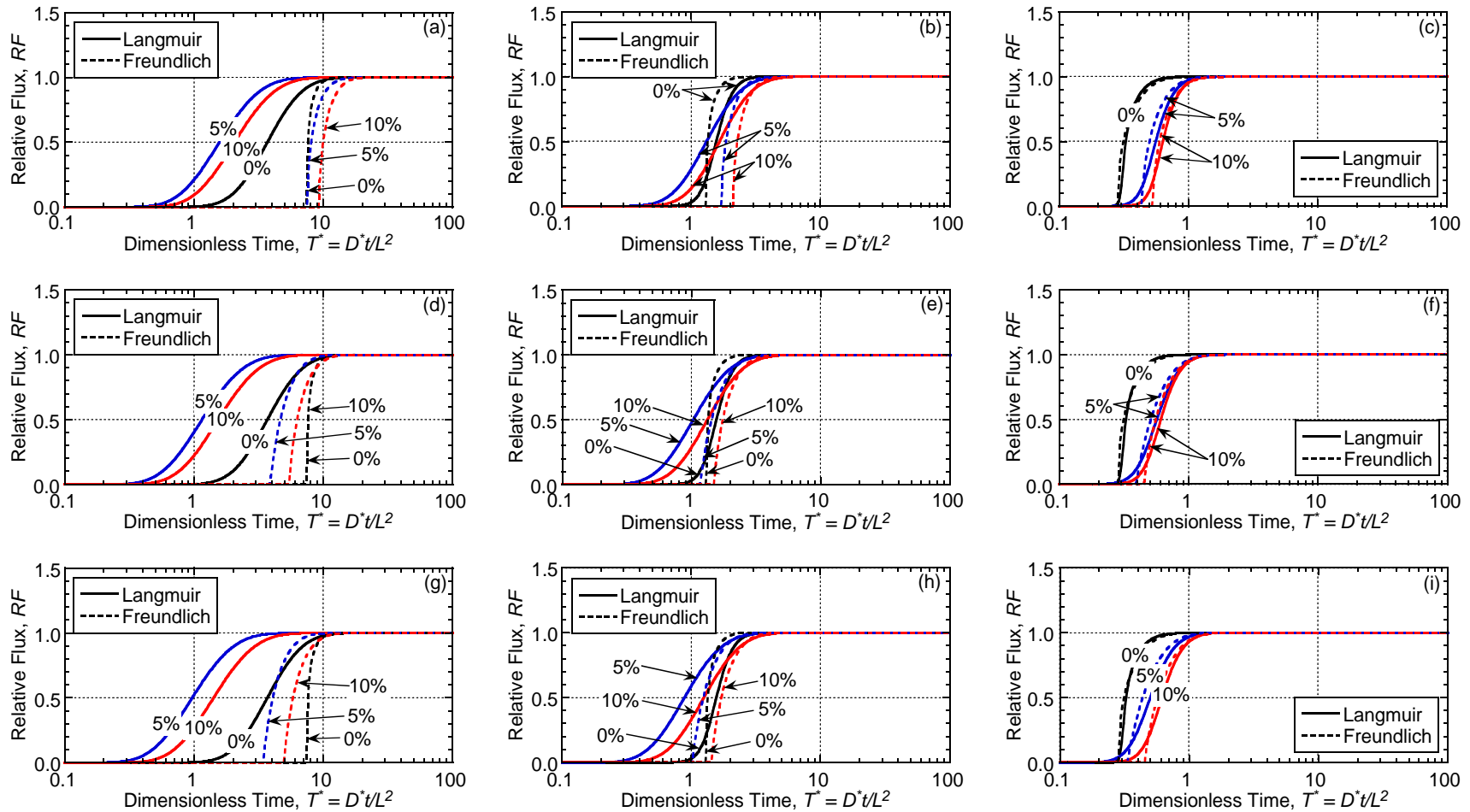


Figure 4.4. Flux breakthrough curves for zinc as a function of adsorption model (Langmuir and Freundlich), zeolite content (0, 5, 10 %), and source concentration ( $C_o$ ): (a) chabazite-LB,  $C_o = 100$  mg/L; (b) chabazite-LB,  $C_o = 1,000$  mg/L; (c) chabazite-LB,  $C_o = 10,000$  mg/L; (d) chabazite-UB,  $C_o = 100$  mg/L; (e) chabazite-UB,  $C_o = 1,000$  mg/L; (f) chabazite-UB,  $C_o = 10,000$  mg/L; (g) clinoptilolite,  $C_o = 100$  mg/L; (h) clinoptilolite,  $C_o = 1,000$  mg/L; (i) clinoptilolite,  $C_o = 10,000$  mg/L.

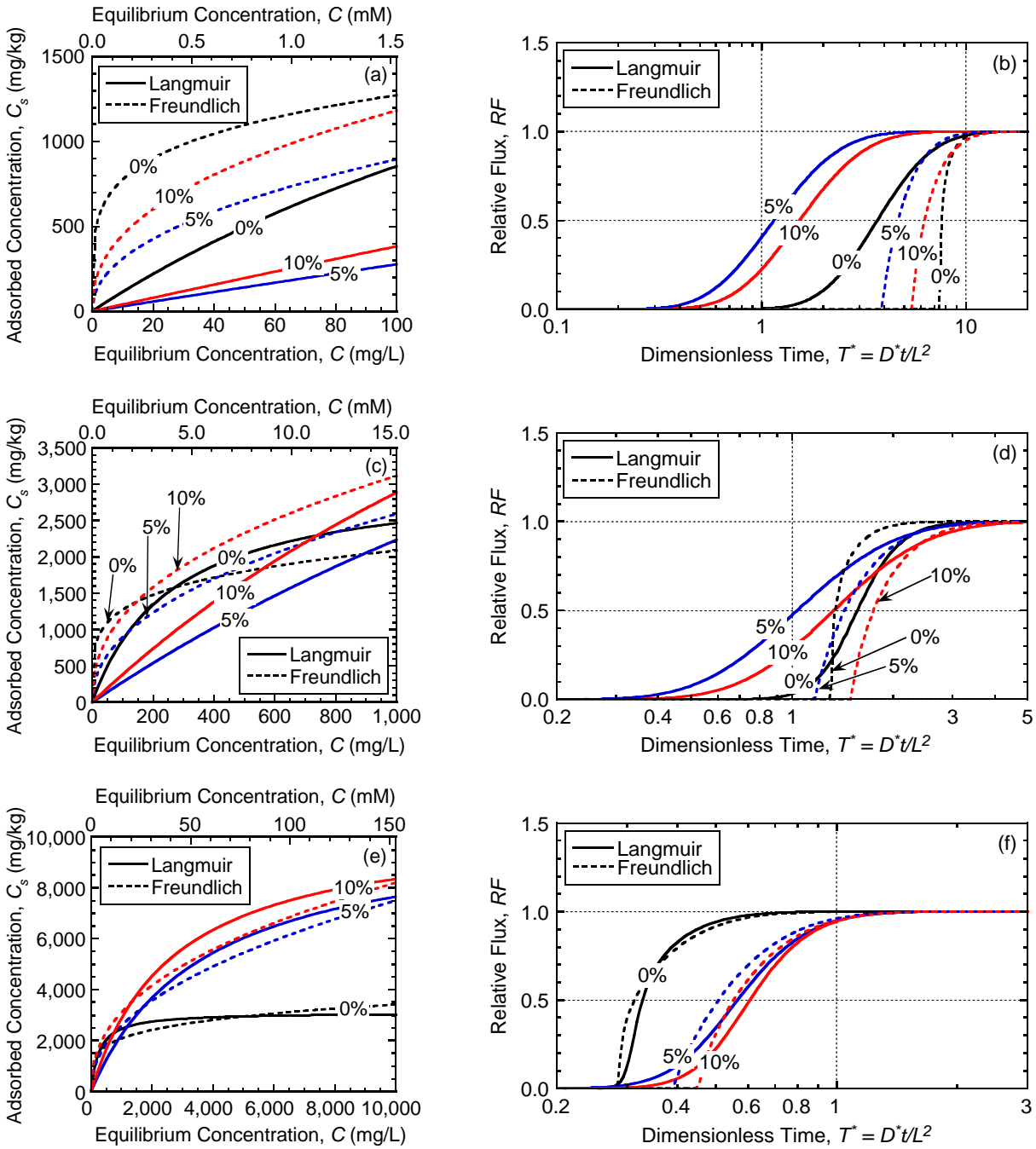


Figure 4.5. Effect of adsorption behavior on flux breakthrough curves for zinc based on different contents (0, 5, 10 %) of chabazite-UB and adsorption models (Langmuir and Freundlich): (a), (c), (e) adsorption behaviors over concentration ranges of 100, 1,000, and 10,000 mg/L, respectively; (b), (d), (f) flux breakthrough curves for a source concentration ( $C_o$ ) of 100, 1,000, and 10,000 mg/L, respectively.

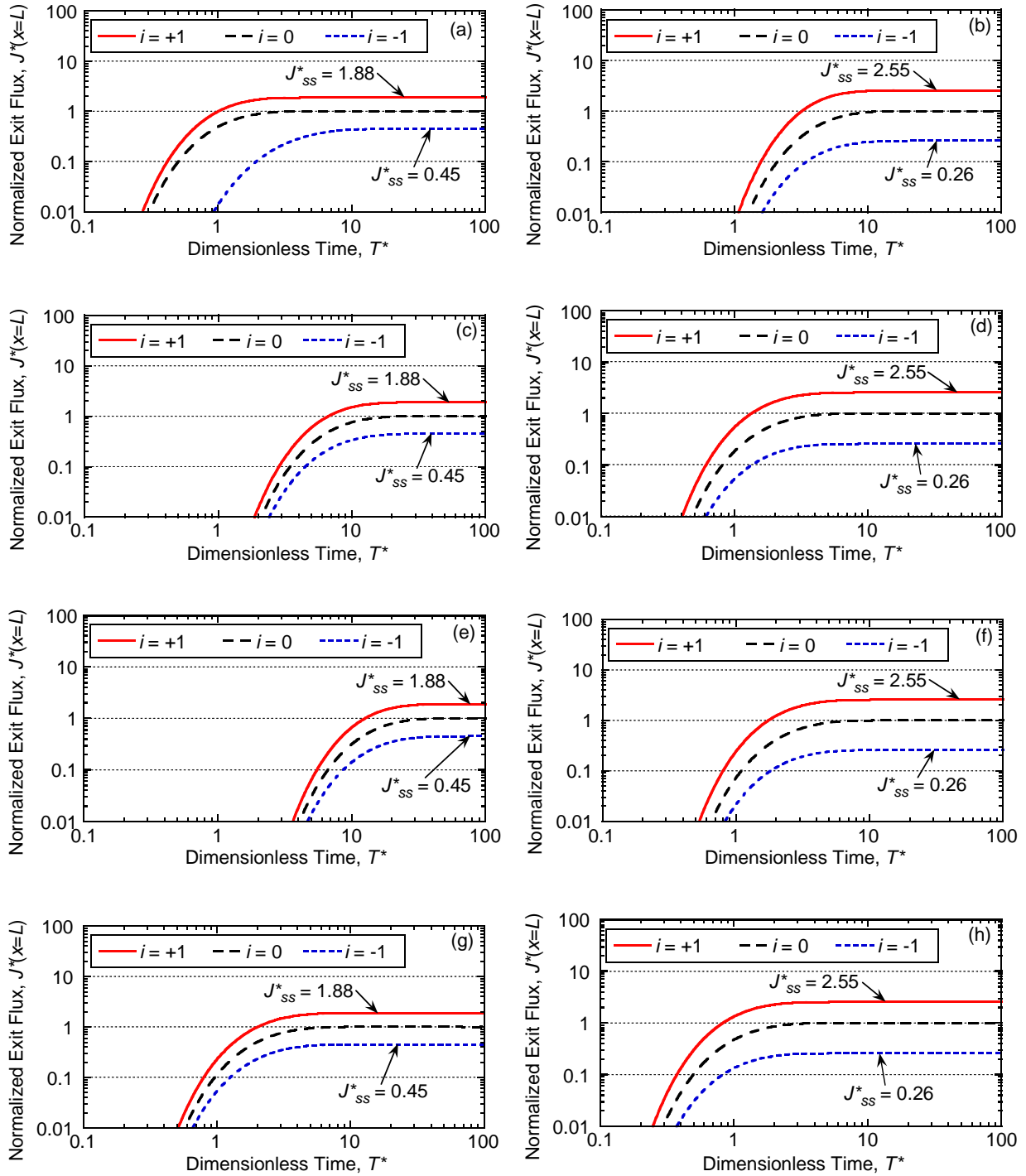


Figure 4.6. Effect of direction and magnitude of hydraulic gradient ( $i$ ) on flux breakthrough curves for unamended and zeolite-amended backfills based on the Langmuir adsorption model for a constant source concentration ( $C_o$ ) of 100 mg/L: (a) potassium (K), unamended; (b) zinc (Zn), unamended; (c) K, 5 % chabazite-LB-amended; (d) Zn, 5 % chabazite-LB-amended; (e) K, 10 % chabazite-LB-amended; (f) Zn, 10 % chabazite-LB-amended; (g) K, 5 % clinoptilolite-amended; (h) Zn, 5 % clinoptilolite-amended.

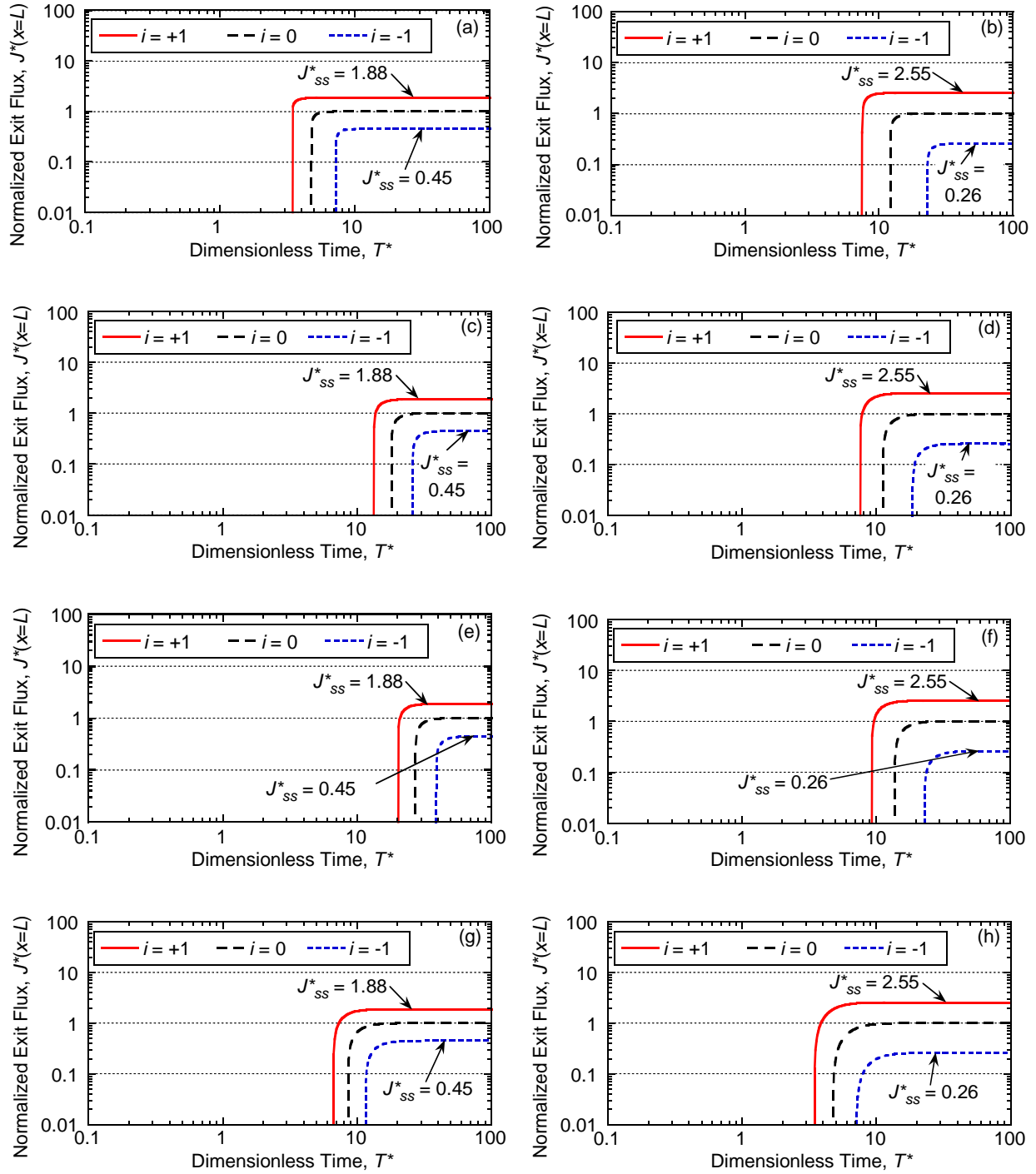


Figure 4.7. Effect of direction and magnitude of hydraulic gradient ( $i$ ) on flux breakthrough curves for unamended and zeolite-amended backfills based on the Freundlich adsorption model for a constant source concentration ( $C_o$ ) of 100 mg/L: (a) potassium (K), unamended; (b) zinc (Zn), unamended; (c) K, 5 % chabazite-LB-amended; (d) Zn, 5 % chabazite-LB-amended; (e) K, 10 % chabazite-LB-amended; (f) Zn, 10 % chabazite-LB-amended; (g) K, 5 % clinoptilolite-amended; (h) Zn, 5 % clinoptilolite-amended.

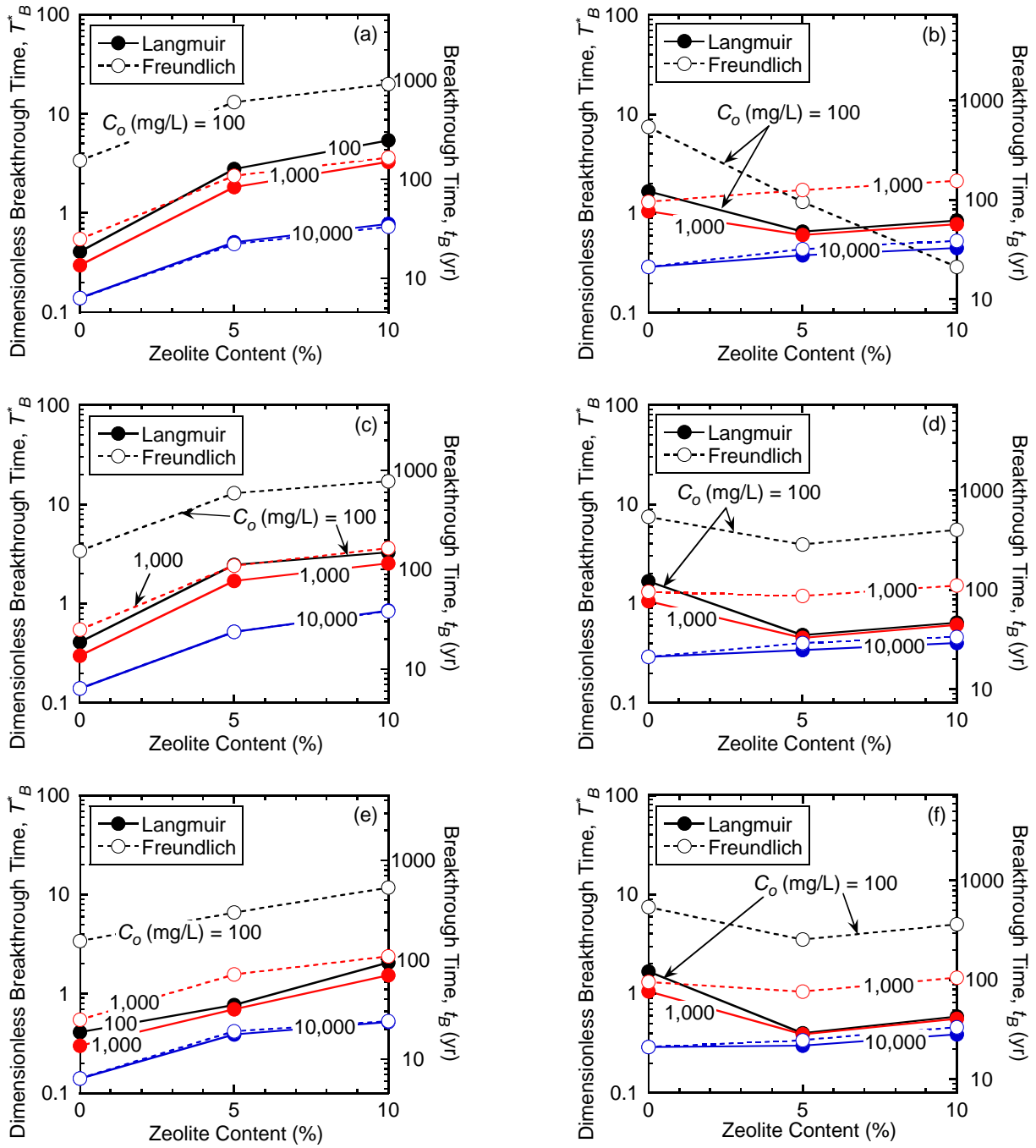


Figure 4.8. Effect of the zeolite content on barrier flux breakthrough times,  $T_B^*$  and  $t_B$ , based on  $f$  of 0.05 and source concentration ( $C_o$ ) of 100, 1,000, 10,000 mg/L for potassium (a, c, e) or zinc (b, d, f): (a) & (b) chabazite-LB; (c) & (d) chabazite-UB; (e) & (f) clinoptilolite.

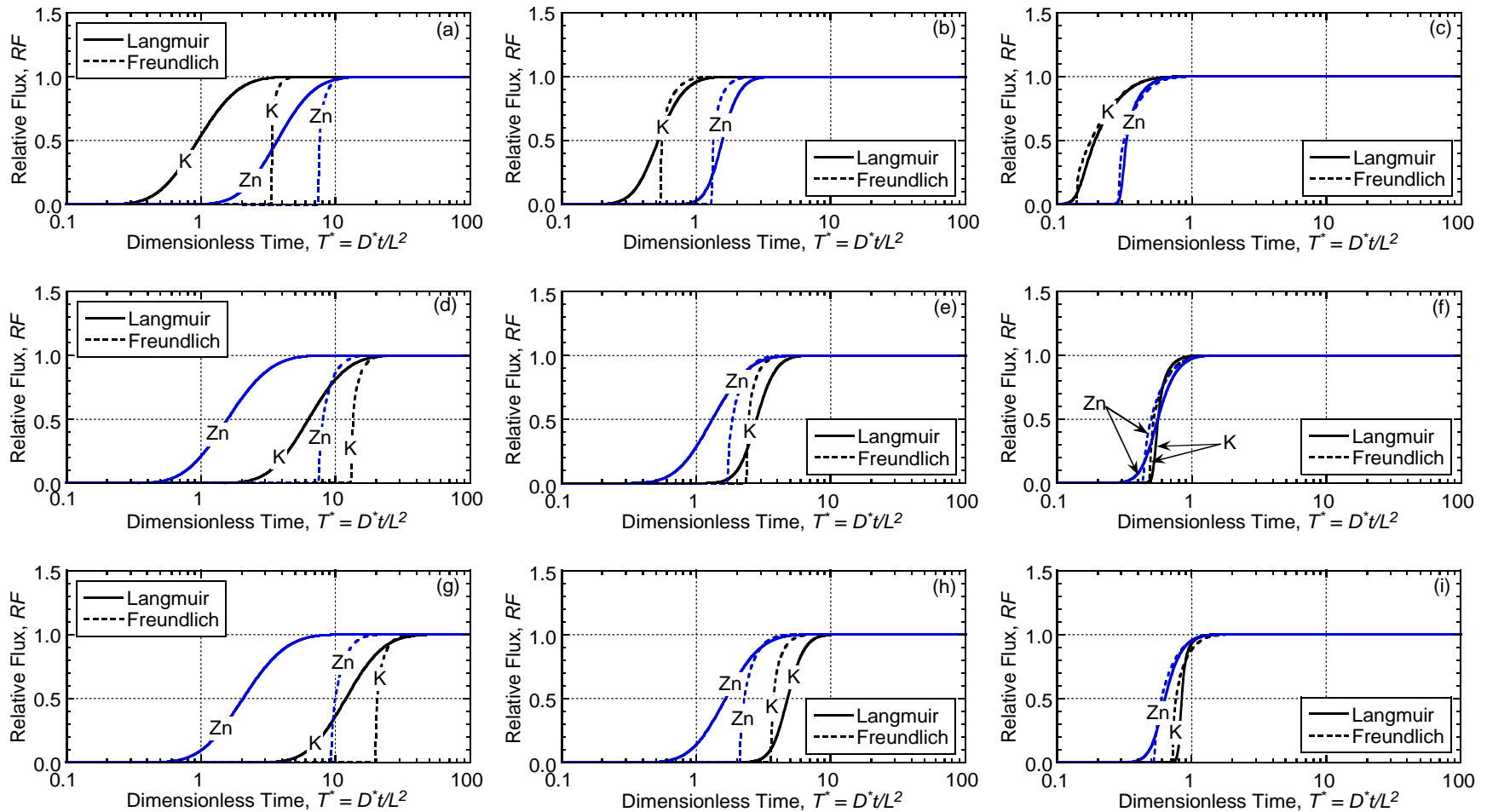


Figure 4.9. Effect of potassium (K) versus zinc (Zn) on the flux breakthrough curves for unamended and zeolite-amended backfills as a function of adsorption model (Langmuir and Freundlich), zeolite content (0, 5, 10 %), and source concentration ( $C_o$ ): (a) unamended,  $C_o = 100$  mg/L; (b) unamended,  $C_o = 1,000$  mg/L; (c) unamended,  $C_o = 10,000$  mg/L; (d) 5 % chabazite-LB,  $C_o = 100$  mg/L; (e) 5 % chabazite-LB,  $C_o = 1,000$  mg/L; (f) 5 % chabazite-LB,  $C_o = 10,000$  mg/L; (g) 10 % chabazite-LB,  $C_o = 100$  mg/L; (h) 10 % chabazite-LB,  $C_o = 1,000$  mg/L; (i) 10 % chabazite-LB,  $C_o = 10,000$  mg/L.

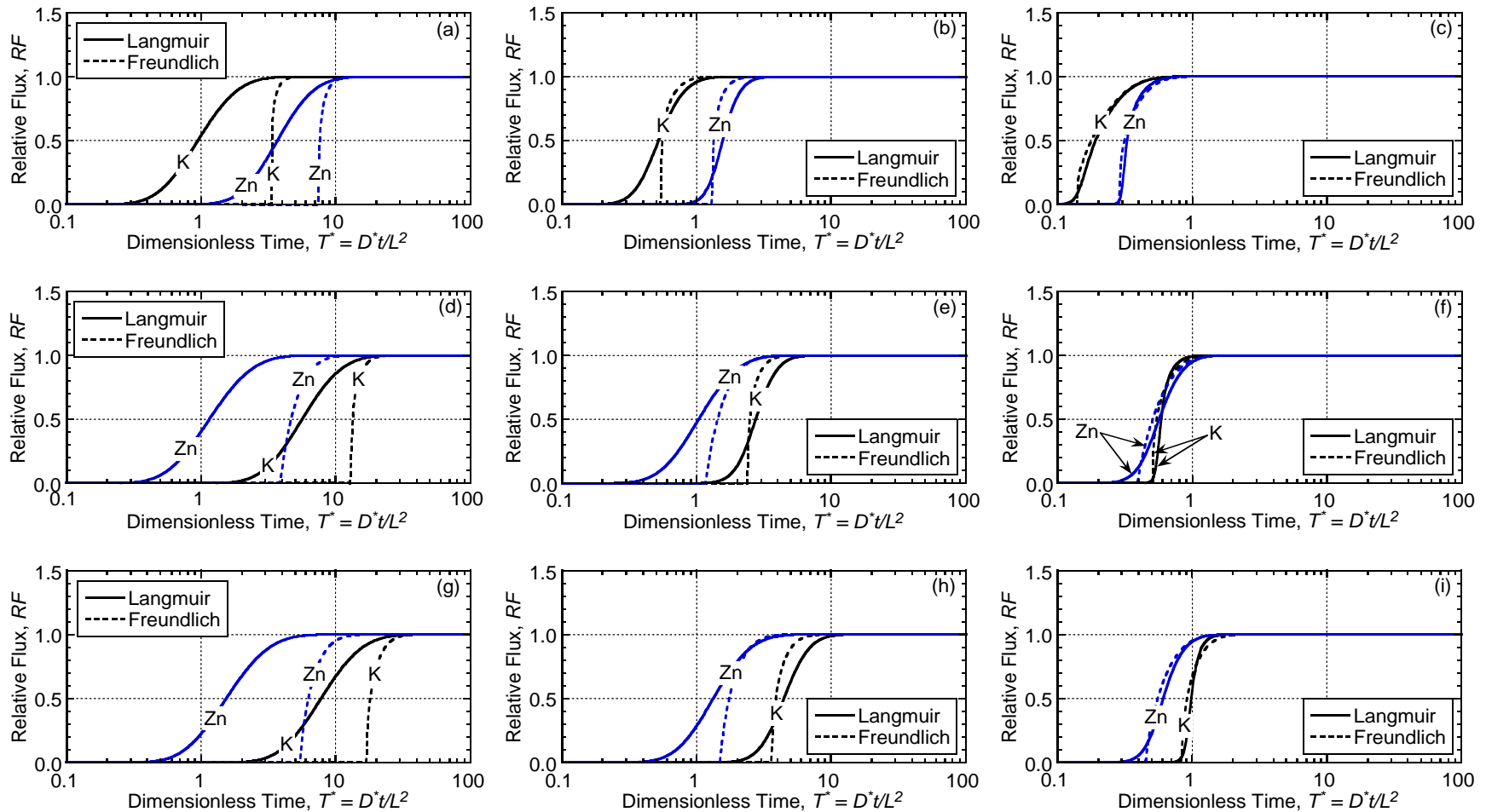


Figure 4.10. Effect of potassium (K) versus zinc (Zn) on the flux breakthrough curves for unamended and zeolite-amended backfills as a function of adsorption model (Langmuir and Freundlich), zeolite content (0, 5, 10 %), and source concentration ( $C_o$ ): (a) unamended,  $C_o = 100$  mg/L; (b) unamended,  $C_o = 1,000$  mg/L; (c) unamended,  $C_o = 10,000$  mg/L; (d) 5 % chabazite-UB,  $C_o = 100$  mg/L; (e) 5 % chabazite-UB,  $C_o = 1,000$  mg/L; (f) 5 % chabazite-UB,  $C_o = 10,000$  mg/L; (g) 10 % chabazite-UB,  $C_o = 100$  mg/L; (h) 10 % chabazite-UB,  $C_o = 1,000$  mg/L; (i) 10 % chabazite-UB,  $C_o = 10,000$  mg/L.

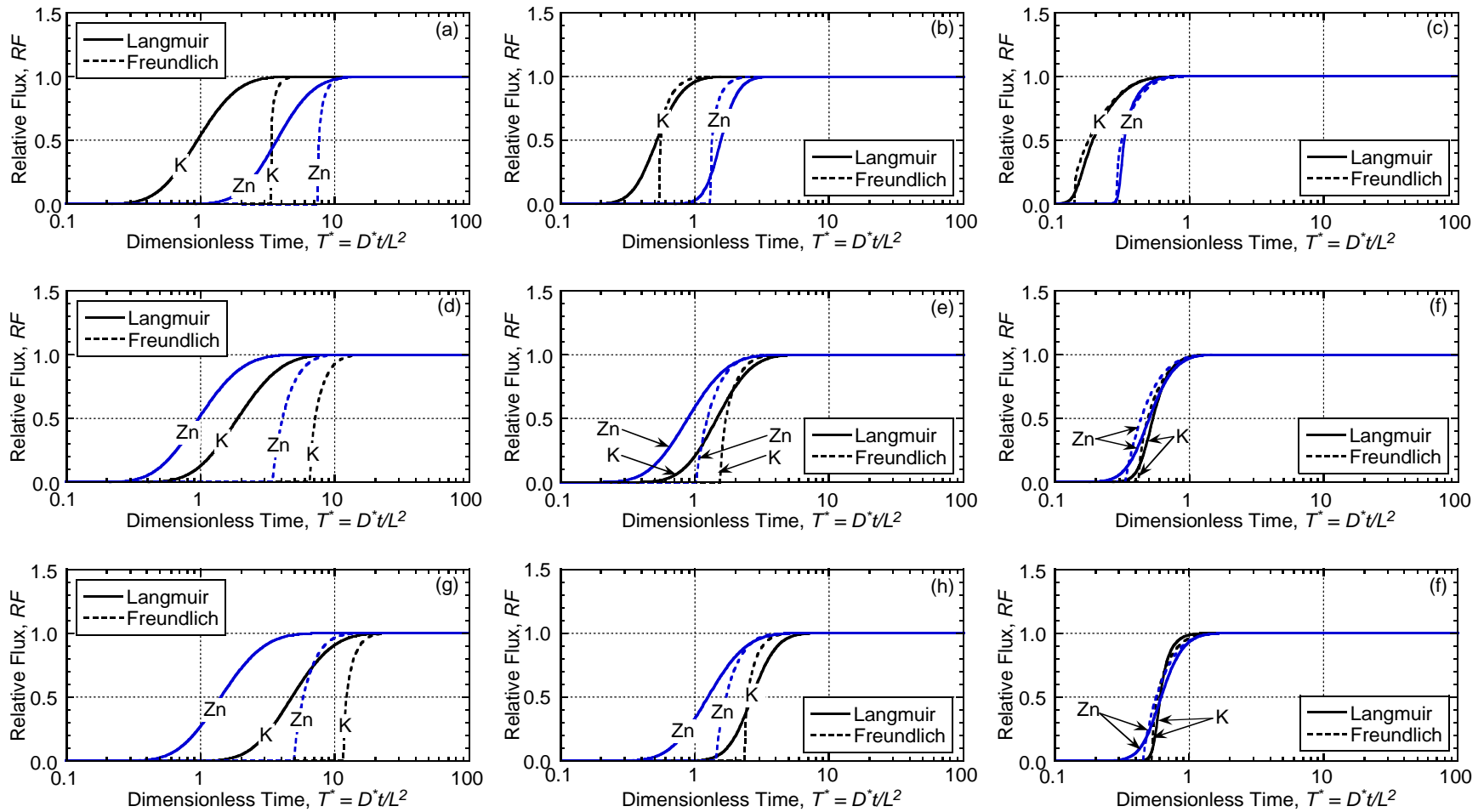


Figure 4.11. Effect of potassium (K) versus zinc (Zn) on the flux breakthrough curves for unamended and zeolite-amended backfills as a function of adsorption model (Langmuir and Freundlich), zeolite content (0, 5, 10 %), and source concentration ( $C_o$ ): (a) unamended,  $C_o = 100$  mg/L; (b) unamended,  $C_o = 1,000$  mg/L; (c) unamended,  $C_o = 10,000$  mg/L; (d) 5 % clinoptilolite,  $C_o = 100$  mg/L; (e) 5 % clinoptilolite,  $C_o = 1,000$  mg/L; (f) 5 % clinoptilolite,  $C_o = 10,000$  mg/L; (g) 10 % clinoptilolite,  $C_o = 100$  mg/L; (h) 10 % clinoptilolite,  $C_o = 1,000$  mg/L; (i) 10 % clinoptilolite,  $C_o = 10,000$  mg/L.

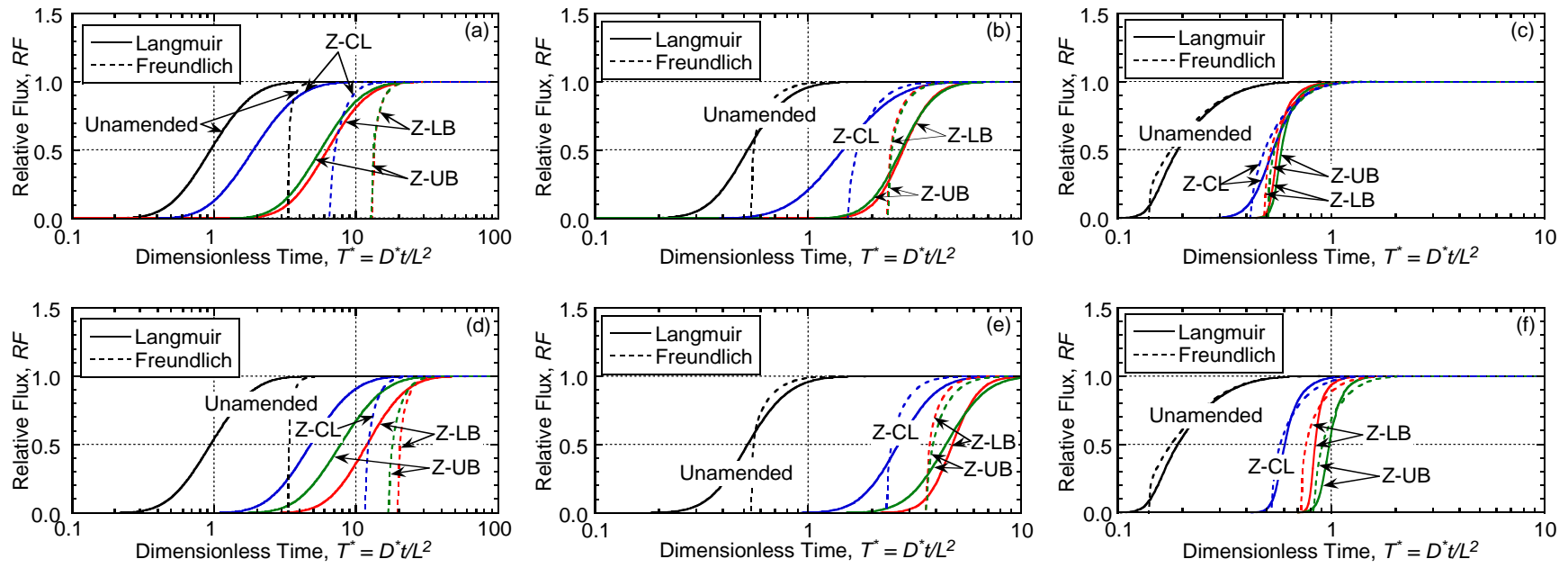


Figure 4.12. Effect of the type of zeolite on the flux breakthrough curve for unamended backfill versus zeolite-amended backfill for a potassium source concentration ( $C_o$ ): (a) 5 % zeolite,  $C_o = 100$  mg/L; (b) 5 % zeolite,  $C_o = 1,000$  mg/L; (c) 5 % zeolite,  $C_o = 10,000$  mg/L; (d) 10 % zeolite,  $C_o = 100$  mg/L; (e) 10 % zeolite,  $C_o = 1,000$  mg/L; (f) 10 % zeolite,  $C_o = 10,000$  mg/L (Z-LB = chabazite-LB-amended backfill, Z-UB = chabazite-UB-amended backfill, Z-CL = clinoptilolite-amended backfill).

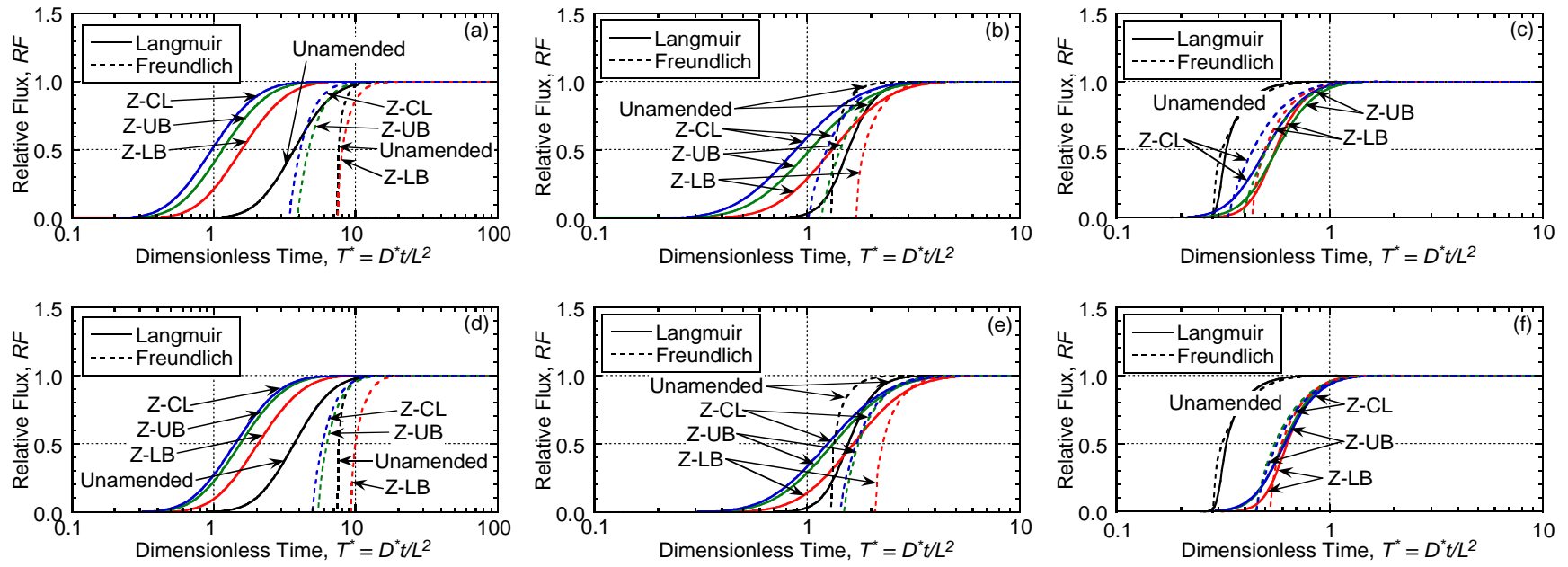


Figure 4.13. Effect of the type of zeolite on the flux breakthrough curve for unamended backfill versus zeolite-amended backfill for a zinc source concentration ( $C_o$ ): (a) 5 % zeolite,  $C_o = 100$  mg/L; (b) 5 % zeolite,  $C_o = 1,000$  mg/L; (c) 5 % zeolite,  $C_o = 10,000$  mg/L; (d) 10 % zeolite,  $C_o = 100$  mg/L; (e) 10 % zeolite,  $C_o = 1,000$  mg/L; (f) 10 % zeolite,  $C_o = 10,000$  mg/L (Z-LB = chabazite-LB-amended backfill, Z-UB = chabazite-UB-amended backfill, Z-CL = clinoptilolite-amended backfill).

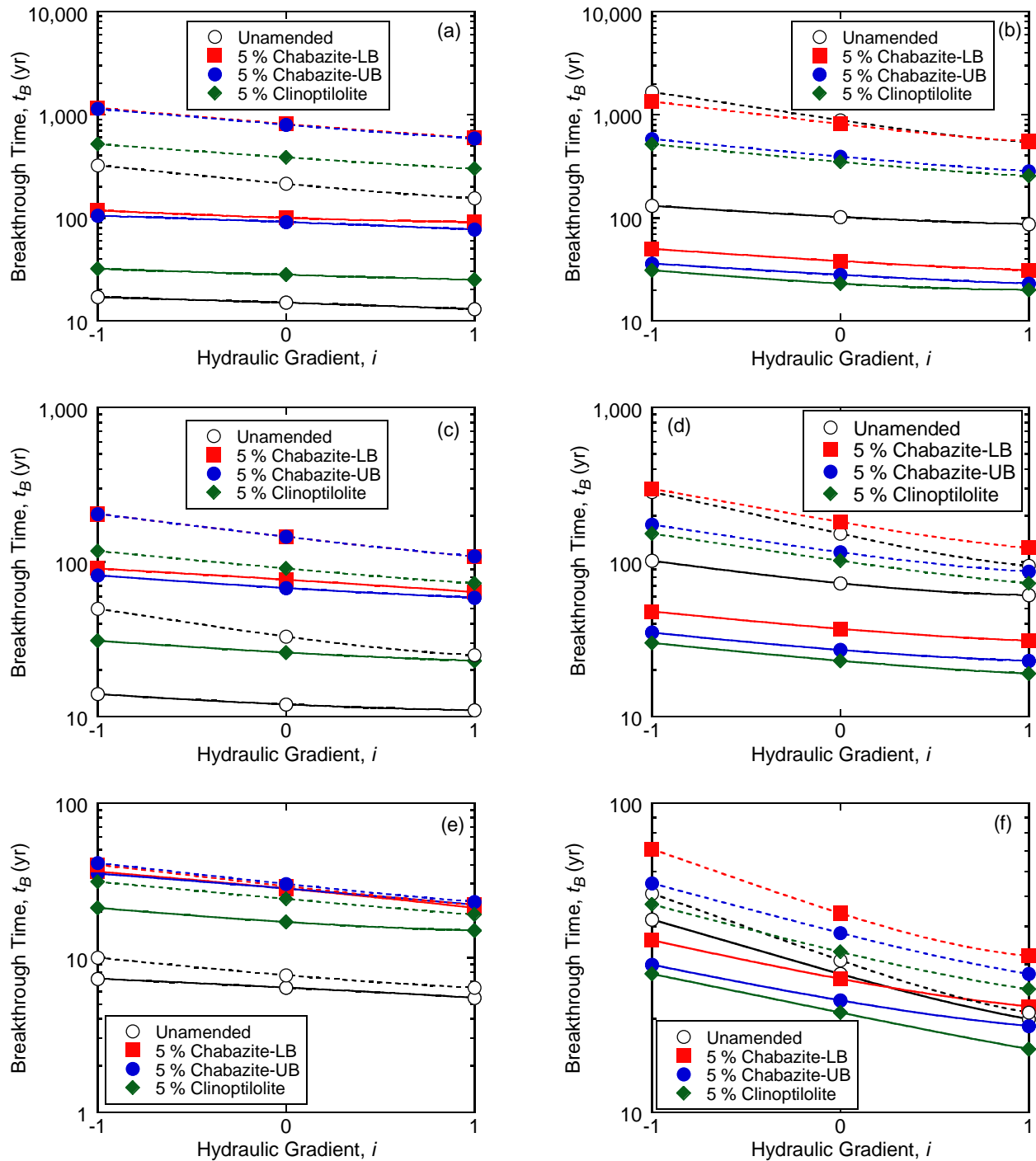


Figure 4.14. Relationship between direction and magnitude of hydraulic gradient ( $i$ ) and barrier flux breakthrough time based  $J^*(L,t)$  of 0.015 for unamended and 5 % zeolite-amended backfills: (a), (c), (e) potassium source concentration ( $C_o$ ) of 100, 1,000, and 10,000 mg/L, respectively; (b), (d), (f) zinc  $C_o$  of 100, 1,000, and 10,000 mg/L respectively. Note: dashed line = Freundlich adsorption model; solid line = Langmuir adsorption model.

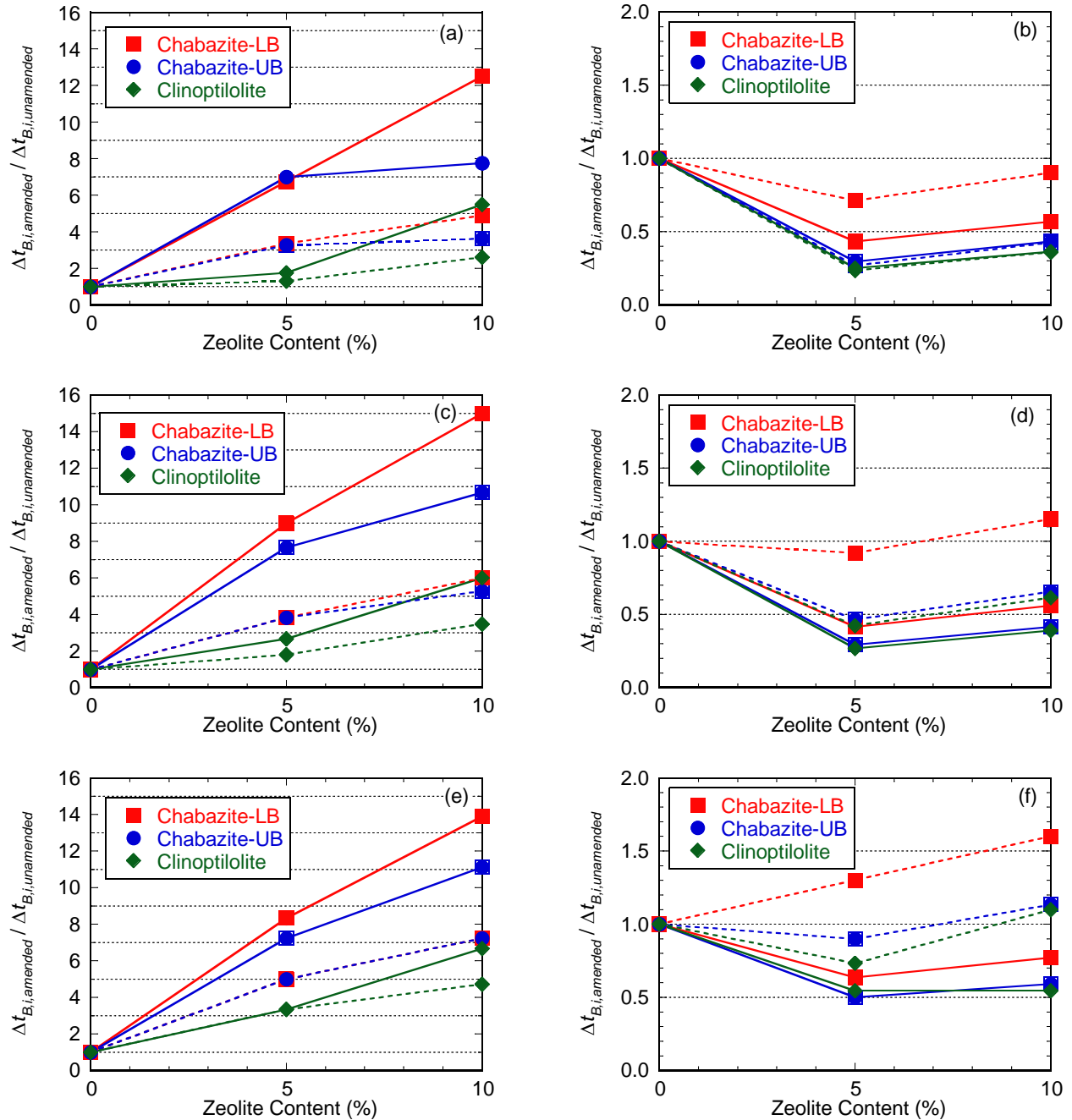


Figure 4.15. Relative effect of zeolite amendment on the incremental change in barrier flux breakthrough time due to a reversal in hydraulic gradient,  $\Delta t_{B,i,amended} / \Delta t_{B,i,unamended}$ , as a function of zeolite content: (a), (c), (e) potassium source concentration ( $C_o$ ) of 100, 1,000, and 10,000 mg/L, respectively; (b), (d), (f) zinc  $C_o$  of 100, 1,000, and 10,000 mg/L respectively. Note: solid line = Langmuir adsorption model; dashed line = Freundlich adsorption model.

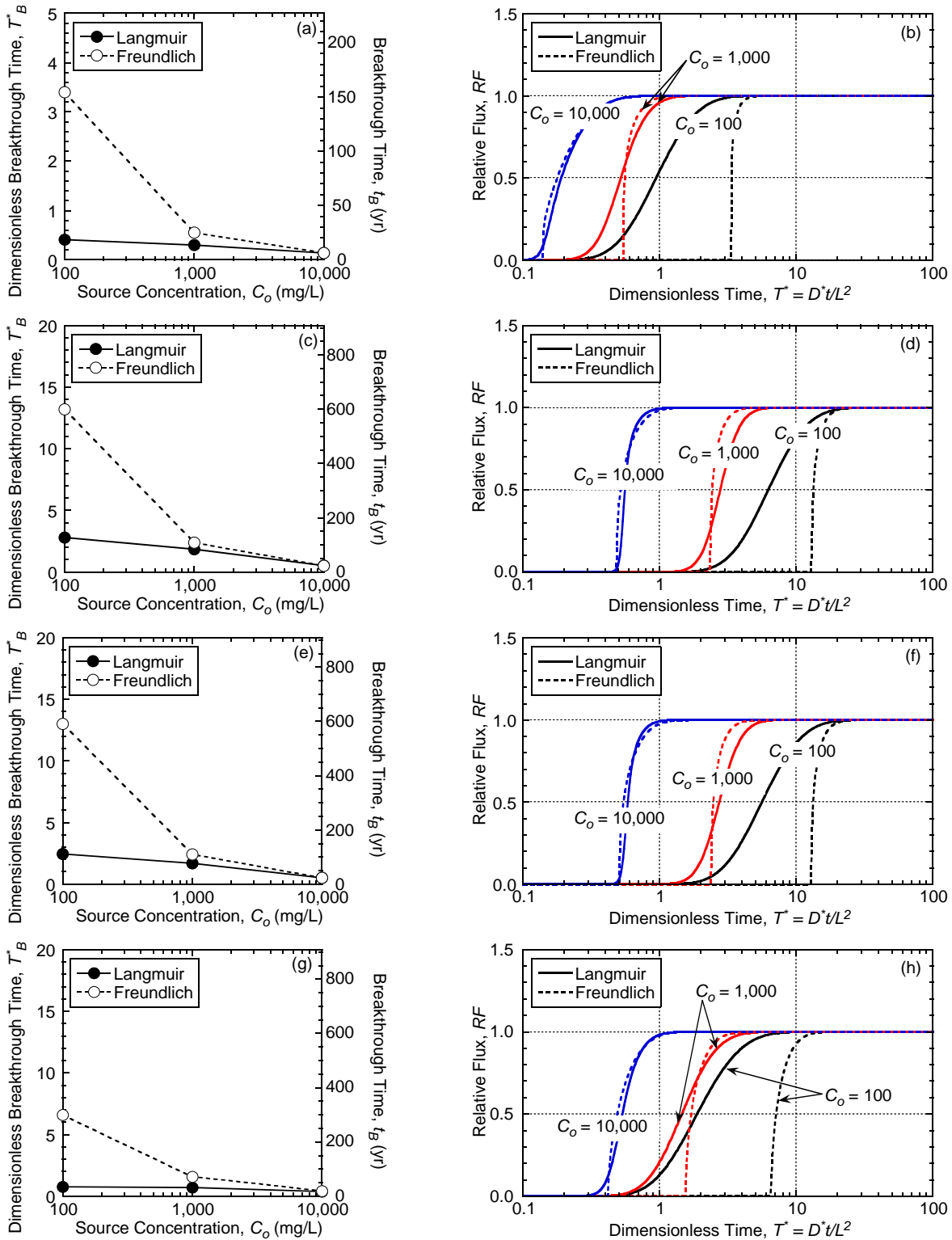


Figure 4.16. Effect of constant potassium source concentration ( $C_o$ ) on the dimensionless barrier breakthrough times,  $T_B^*$  (a, c, e) for  $f = 0.05$  and flux breakthrough curves (b, d, f) for unamended and zeolite-amended backfills: (a) & (b) unamended; (c) & (d) 5 % chabazite-LB-amended; (e) & (f) 5 % chabazite-UB-amended; (g) & (h) 5 % clinoptilolite-amended.

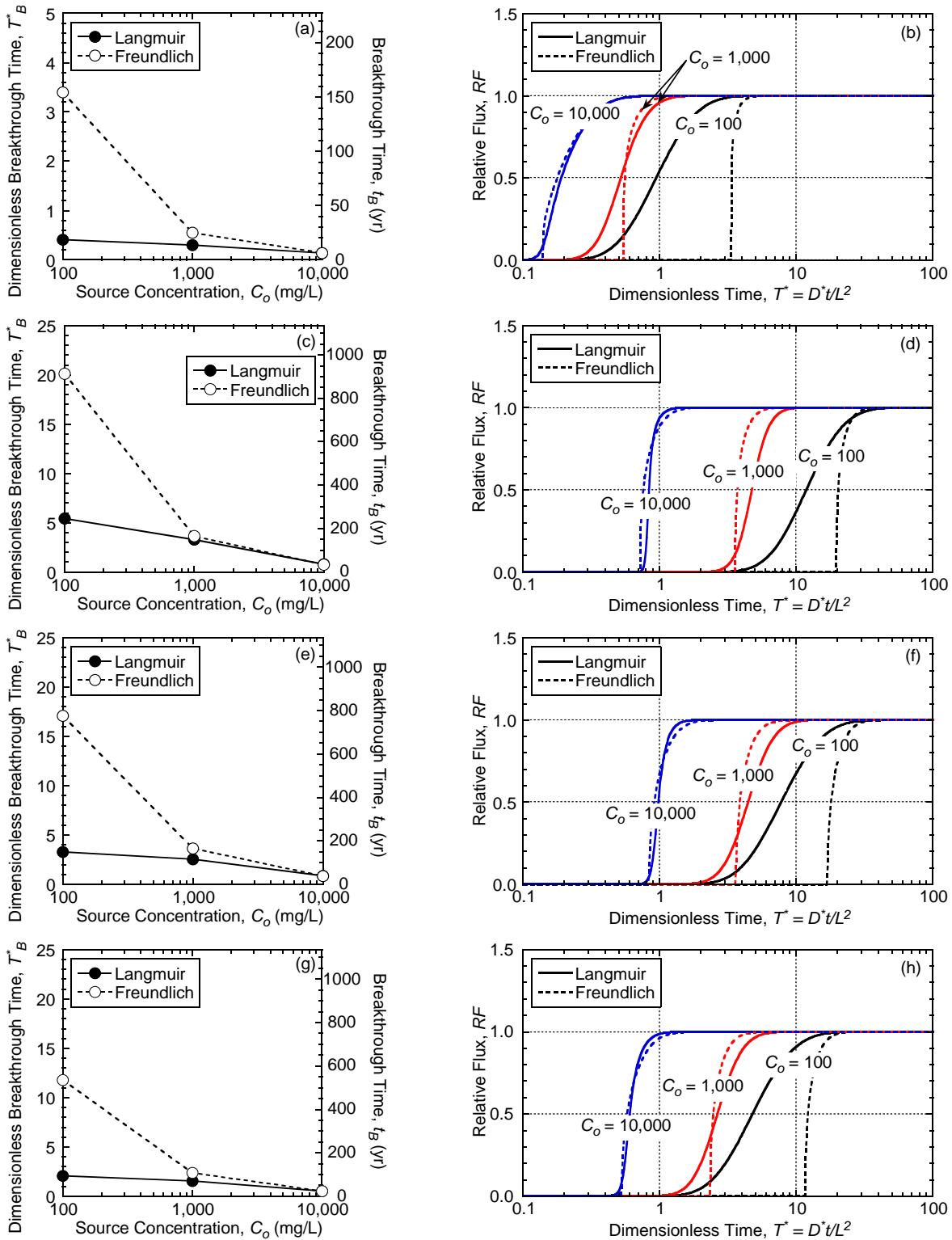


Figure 4.17. Effect of constant potassium source concentration ( $C_o$ ) on the dimensionless barrier breakthrough times,  $T_B^*$  (a, c, e) for  $f = 0.05$  and flux breakthrough curves (b, d, f) for unamended and zeolite-amended backfills: (a) & (b) unamended; (c) & (d) 10 % chabazite-LB-amended; (e) & (f) 10 % chabazite-UB-amended; (g) & (h) 10 % clinoptilolite-amended.

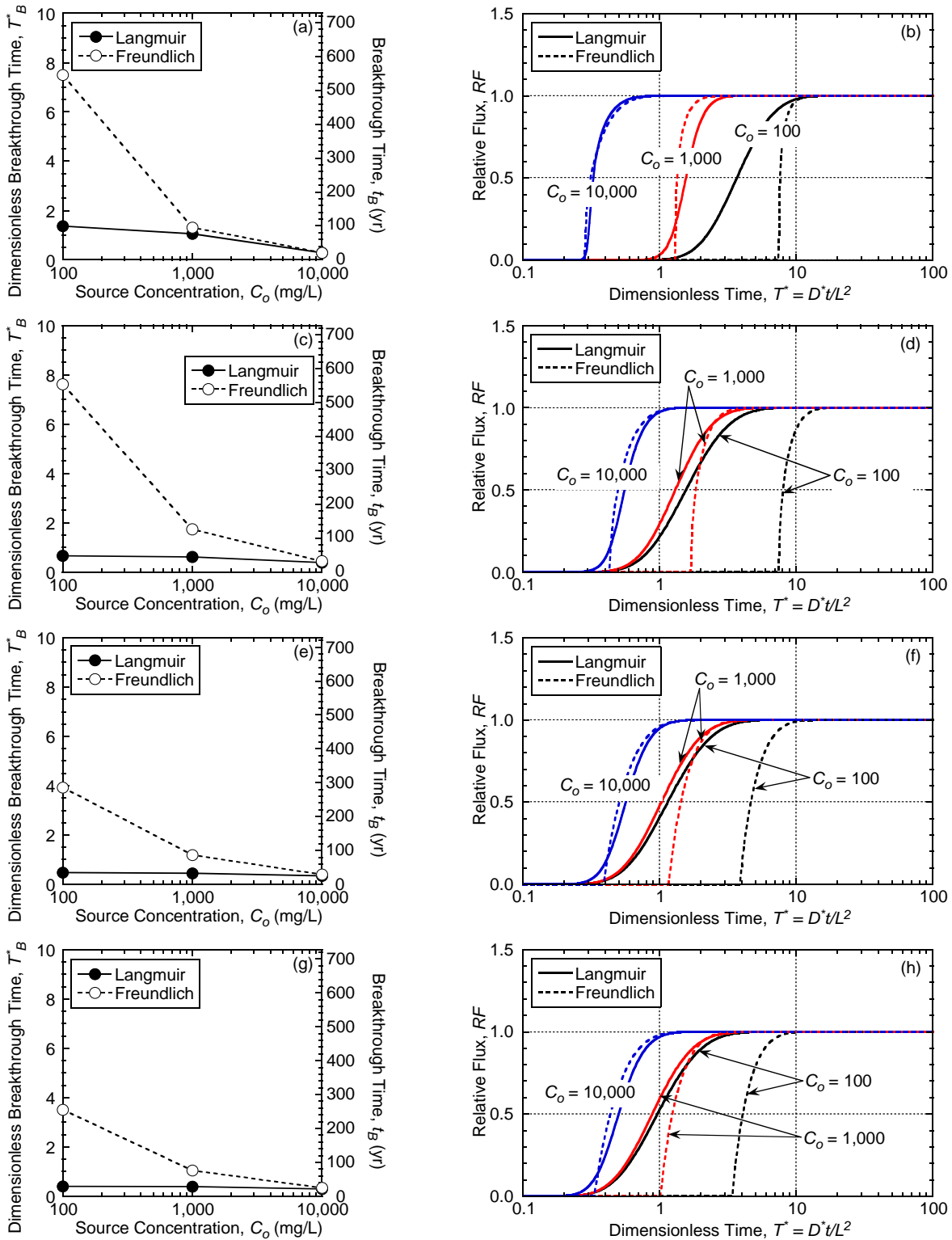


Figure 4.18. Effect of constant zinc source concentration ( $C_o$ ) on the dimensionless barrier breakthrough times,  $T_B^*$  (a, c, e) for  $f = 0.05$  and flux breakthrough curves (b, d, f) for unamended and zeolite-amended backfills: (a) & (b) unamended; (c) & (d) 5 % chabazite-LB-amended; (e) & (f) 5 % chabazite-UB-amended; (g) & (h) 5 % clinoptilolite-amended.

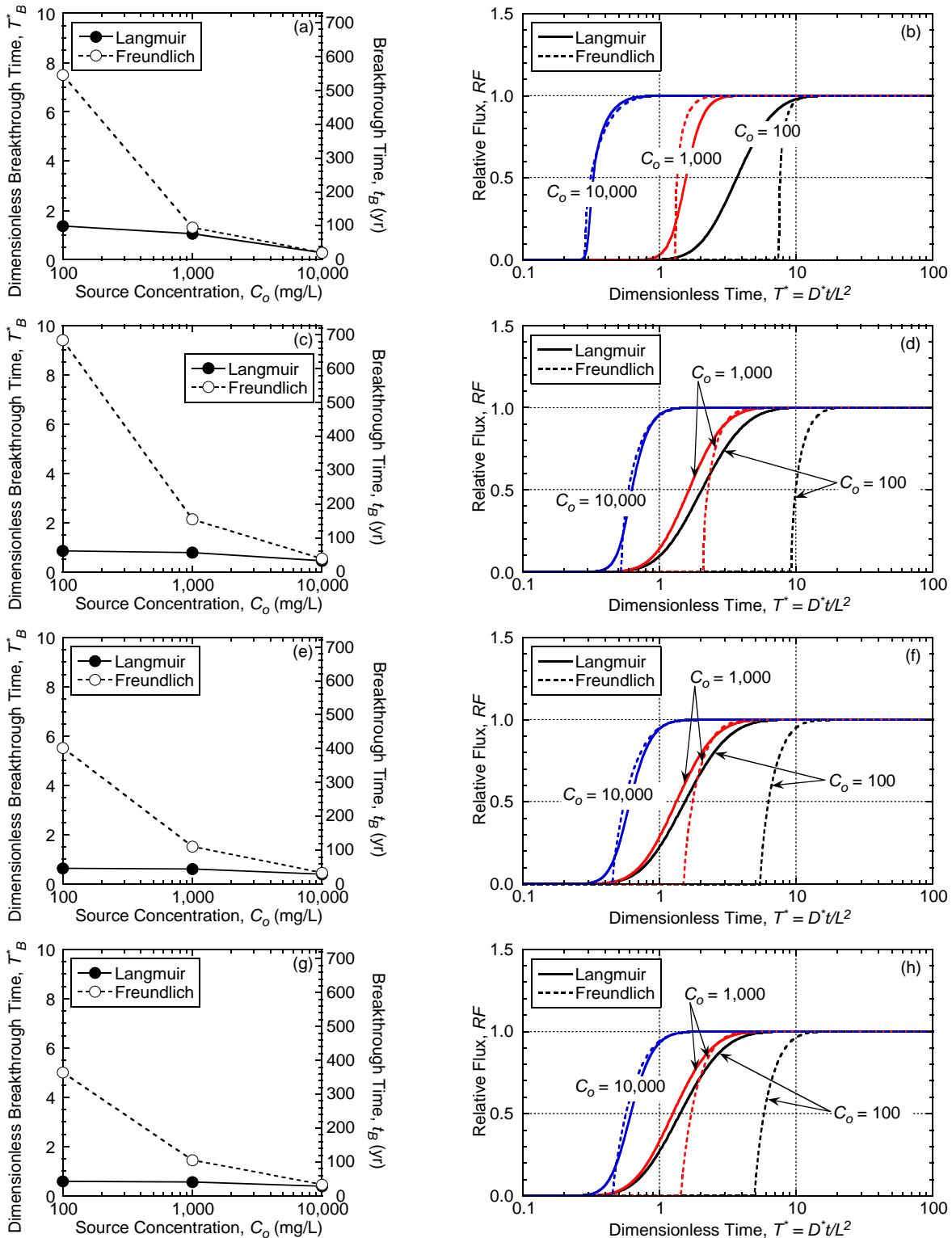


Figure 4.19. Effect of constant zinc source concentration ( $C_o$ ) on the dimensionless barrier breakthrough times,  $T_B^*$  (a, c, e) for  $f = 0.05$  and flux breakthrough curves (b, d, f) for unamended and zeolite-amended backfills: (a) & (b) unamended; (c) & (d) 10 % chabazite-LB-amended; (e) & (f) 10 % chabazite-UB-amended; (g) & (h) 10 % clinoptilolite-amended.

## REFERENCES

- Bierck, B.R. and Chang, W.-C. (1994). "Contaminant transport through soil-bentonite slurry walls: Attenuation by activated carbon." *Proceedings of the Specialty Conference on Innovative Solutions for Contaminated Site Management*, Water Environment Federation, Alexandria, VA, 461-472.
- Bish, D.L. (2006). "Parallels and distinctions between clay minerals and zeolites." Section 13.2, *Developments in Clay Science*, Elsevier, New York, 1097-1112.
- Code of Federal Regulations (2015). "National secondary drinking water regulations." *Code of Federal Regulations*, Title 40, Chapter 1, Subchapter D, Part 143.3, US Government Publishing Office, Washington, DC.
- Colella, C. (1996). "Ion exchange equilibria in zeolite minerals." *Mineralium Deposita*, 31(6), 554-562.
- Daniel, D.E. and Koerner, R.M. (1993). *Quality Assurance and Quality Control for Waste Containment Facilities*, EPA/600/R-93/182, U. S. Environmental Protection Agency, Cincinnati, OH.
- Devlin, J.F. and Parker, B.L. (1996). "Optimum hydraulic conductivity to limit contaminant flux through cutoff walls." *Ground Water*, 34(4), 719-726.
- Emancipator, K. and Kroll, M.H. (1993). "A quantitative measure of nonlinearity." *Clinical Chemistry*, 39(5), 766-772.
- Evans, J.C., Adams, T.L., and Prince, M.J. (1997). "Metals attenuation in mineral-enhanced slurry walls." *Proceedings, 1997 International Containment Technology Conference*, NTIS (National Technical Information Service), Springfield, VA, 679-687.
- Evans, J.C. and Prince, M.J. (1997). "Additive effectiveness in mineral-enhanced slurry walls." *In Situ Remediation of the Geoenvironment*, J.C. Evans, Ed., ASCE, Reston, VA, 181-196.
- Evans, J.C., Shackelford, C.D., Yeo, S.-S., and Henning, J. (2008). "Membrane behavior of soil-bentonite slurry-trench cutoff walls." *Soil and Sediment Contamination – An International Journal*, 17(4), 316-322.
- Freeze, R.A. and Cherry, J.A. (1979). *Groundwater*, Prentice-Hall, Englewood, NJ.
- Henning, J., Evans, J.C., and Shackelford, C.D. (2006). "Membrane behavior of two backfills from field-constructed soil-bentonite cutoff walls." *Journal of Geotechnical and Geoenvironmental Engineering*, 132(10), 243-249.
- Hong, C.S., Shackelford, C.D., and Malusis, M.A. (2012). "Consolidation and hydraulic conductivity of zeolite amended soil-bentonite backfills." *Journal of Geotechnical and*

- Geoenvironmental Engineering*, 138(1), 15-25.
- Hong, C.S., Shackelford, C.D., and Malusis, M.A. (2016). "Adsorptive behavior of zeolite-amended backfills for enhanced metals contained." *Journal of Geotechnical and Geoenvironmental Engineering*, 142(7), 04016021.
- Hudak, P.F. (2016). "Evaluation of non-pumped wells with slurry cutoff walls for containing and removing contaminated groundwater." *Environmental Earth Sciences*, 75(1), Art. No. 67, 1-5.
- Kinniburgh, D.G. (1986). "General purpose adsorption isotherms." *Environmental Science and Technology*, 20(9), 895-904.
- Kontturi, K., Murtomäki, L., and Manzanares, J.A. (2008). *Ionic Transport Processes in Electrochemistry and Membrane Science*, Oxford University Press, New York.
- LaGrega, M.L., Buckingham, P.L., and Evans, J.C. (2001). *Hazardous Waste Management*, McGraw-Hill, New York.
- Malusis, M.A., Barben, E.J., and Evans, J.C. (2009). "Hydraulic conductivity and compressibility of soil-bentonite backfill amended with activated carbon." *Journal of Geotechnical and Geoenvironmental Engineering*, 135(5), 664-672.
- Malusis, M.A., Maneval, J.E., Barben, E.J., Shackelford, C.D., and Daniels, E.R. (2010). "Influence of adsorption on phenol transport through soil-bentonite vertical barriers amended with activated carbon." *Journal of Contaminant Hydrology*, 116(1-4), 58-72.
- Malusis, M.A. and Shackelford, C.D. (2004). "Predicting solute flux through a clay membrane barrier." *Journal of Geotechnical and Geoenvironmental Engineering*, 130(5), 477-487.
- Manassero, M. and Shackelford, C.D. (1994). "The role of diffusion in contaminant transport through soil barriers." *Rivista Italiana di Geotecnica*, 28(1), 5-31.
- Melnyk, T.W. (1985). "Effects of sorption behaviour on contaminant migration." *Atomic Energy of Canada*, Pinawa, MB, Canada.
- Mitchell, J.K., Alvarez-Cohen, L., Atekwana, E.S., Burns, S.E., Gilbert, R.B., Kavazanjian, E., Jr., O'Riordan, W.H., Rowe, R.K., Shackelford, C.D., Sharma, H.D., and Yesiller, N. (2007). *Assessment of the Performance of Engineered Waste Containment Barriers*, National Academies Press, Washington, DC.
- Mumpton, F.A. (1999). "La roca magica: Uses of natural zeolites in agriculture and industry." *Proceedings of the National Academy of Sciences of the United States of America*, 96(7), 3463-3470.
- Neville, C.J. and Andrews, C.B. (2006). "Containment criterion for contaminant isolation by cutoff walls." *Ground Water*, 44(5), 682-686.
- Park, J.K., Kim, J.Y., Madsen, C.D., and Edil, T.B. (1997). "Retardation of volatile organic

- compound movement by a soil-bentonite slurry cutoff wall amended with ground tires." *Water Environment Research*, 69(5), 1022-1031.
- Rabideau, A. and Khandelwal, A. (1998). "Boundary conditions for modeling transport in vertical barriers." *Journal of Environmental Engineering*, 124(11), 135-1139.
- Rabideau, A., Shen, P., and Khandelwal, A. (1999). "Feasibility of amending slurry walls with zero-valent iron." *Journal of Geotechnical and Geoenvironmental Engineering*, 125(4), 330-333.
- Robinson, R.A. and Stokes, R.H. (2002). *Electrolyte Solutions*, Dover Publications, New York.
- Rumer, R.R. and Mitchell, J.K. (1995). *Assessment of Barrier Containment Technologies: A Comprehensive Treatment for Environmental Remediation Applications*, National Technical Information Service, Springfield, VA.
- Rumer, R.R. and Ryan, M.E. (1995). *Barrier Containment Technologies for Environmental Remediation Applications*, John Wiley and Sons, Inc., New York.
- Rubin, H. and Rabideau, A.J. (2000). "Approximate evaluation of contaminant transport through vertical barriers." *Journal of Contaminant Hydrology*, 40(4), 311-333.
- Ryan, C.R. (1984). "Slurry cutoff walls: Applications in the control of hazardous wastes." *Hydraulic Barriers in Soil and Rock*, STP 874, A.I. Johnson, R.K. Frobel, N.J. Cavalli, and C.B. Pettersson, Eds., ASTM, West Conshohoken, PA, 9-23.
- Ryan, C.R. (1987). "Vertical barriers in soil for pollution containment." *Geotechnical Practice for Waste Disposal*, '87, R.D. Woods, Ed., ASCE, Reston, VA, 182-204.
- Ryan, C.R. and Spaulding, C.A. (2008). "Strength and permeability of a deep soil bentonite slurry wall." *The Challenge of Sustainability in the Geo-Environment Proceedings of the Geo-Congress 2008*, ASCE, Reston, VA, 644-651.
- Shackelford, C.D. (1988). "Diffusion as a transport process in fine-grained barrier materials." *Geotechnical News*, 6(2), 24-27.
- Shackelford, C.D. (1989). "Diffusion of contaminants through waste containment barriers." *Geotechnical engineering 1989*, Transportation Research Record No. 1219, National Academy Press, Washington, DC, 169-182.
- Shackelford, C.D. (1993). "Contaminant Transport." *Geotechnical Practice for Waste Disposal*, D.E. Daniel, Ed., Chapman and Hall, London, 33-65.
- Shackelford, C.D. (1994). "Critical concepts for column testing." *Journal of Geotechnical Engineering*, 120(10), 1804-1828.
- Shackelford, C.D. (1995a). "Cumulative mass approach for column testing." *Journal of Geotechnical Engineering*, 121(10), 696-703.

- Shackelford, C.D. (1995b). "Analytical models for cumulative mass column testing." *Geoenvironment 2000*, Geotechnical Special Publication 46, Y.B. Acar and D.E. Daniel, Eds., ASCE, Reston, VA, 355-372.
- Shackelford, C.D. (1999). "Reactive nature of passive containment barriers." *14th International Conference on Soil Mechanics and Foundation Engineering*, Hamburg, Germany, Sept. 6-12, 1997, Balkema, Rotterdam, Vol. 4, 2535-2536.
- Shackelford, C.D. (2014). "The ISSMGE Kerry Rowe Lecture: The role of diffusion in environmental geotechnics." *Canadian Geotechnical Journal*, 51(11), 1219-1242.
- Shackelford, C.D. and Daniel, D.E. (1991). "Diffusion in saturated soil. I: Background." *Journal of Geotechnical Engineering*, 117(3), 467-484.
- Sleep, B.E., Shackelford, C.D., and Parker, J.C. (2006). "Modeling of fluid transport through barriers." *Barrier Systems for Environmental Contaminant Containment and Treatment*, C.C. Chien, H.I. Inyang, and L.G. Everett, Eds., CRC Press Taylor and Francis Group, LLC, Boca Raton, FL, 71-141.
- U.S. Environmental Protection Agency (USEPA) (1984). "Slurry trench construction for pollution migration control." *EPA 540*, Office of Emergency and Remedial Response, Office of Research and Development, Washington, DC.
- Weber, W.J., McGinley, P.M., and Katz, L.E. (1992). "A distributed reactivity model for sorption by soils and sediments. 1. Conceptual basis and equilibrium assessments." *Environmental Science and Technology*, 26(10), 1955-1962.
- Yeo, S.-S., Shackelford, C.D., and Evans, J.C. (2005). "Membrane behavior of model soil-bentonite backfills." *Journal of Geotechnical and Geoenvironmental Engineering*, 131(4), 418-429.

## CHAPTER 5 LONG-TERM COLUMN TESTING

### 5.1 INTRODUCTION

Soil-bentonite (SB) vertical cutoff walls are used extensively to prevent or control subsurface migration of contaminated groundwater (*e.g.*, USEPA 1984; Ryan 1984, 1987; Daniel and Koerner 1993; Manassero *et al.* 1995; Rumer and Mitchell 1995; Rumer and Ryan 1995; LaGrega *et al.* 2001; Mitchell *et al.* 2007; Fan *et al.* 2014; Du *et al.* 2015; Hudak 2016). Relative to *in situ* treatment systems, SB vertical cutoff walls typically are less costly and reduce the risk of contaminant exposure during construction (Shackelford and Jefferis 2000). Also, in the absence of an effective and/or efficient treatment technology, SB vertical cutoff walls offer the ability to contain contaminated groundwater until more efficient and/or more cost effective treatment technologies are developed (Shackelford and Jefferis 2000).

Since containment may be required for prolonged periods (years to decades), consideration has been given to enhancing the attenuation capacity of backfills for SB vertical cutoff walls for targeted contaminants to provide more sustainable containment (*e.g.*, Mott and Weber 1992; Bierck and Chang 1994; Bradl 1997; Evans *et al.* 1997; Evans and Prince 1997; Park *et al.* 1997; Rabideau *et al.* 1999; Malusis *et al.* 2009, 2010; Hong *et al.* 2012, 2016). This enhancement typically is achieved by amending the SB backfill with low amounts (typically  $\leq 15$  % by dry weight) of a reactive or sorbing material, depending on the contaminant. For example, amendments that have been considered include fly ash to enhance the sorption of low molecular weight organic contaminants (Mott and Weber 1992), activated carbon to enhance the sorption of hydrophobic organic compounds (Bierck and Chang 1994, Malusis *et al.* 2009, 2010), ground tires to enhance the retardation of volatile organic compounds (Park *et al.* 1997), zero valent iron (ZVI) to enhance the degradation of trichloroethylene (Rabideau *et al.* 1999), and zeolites to

enhance the sorption of metals (Bradl 1997; Evans *et al.* 1997; Evans and Prince 1997; Hong *et al.* 2012, 2016; Du *et al.* 2015).

With few exceptions (*e.g.*, Park *et al.* 1997), most of the studies conducted to evaluate the effectiveness of the amendment materials have been based on the results of batch experiments, whereby the unamended and amended backfills are mixed for a specified period (typically 24 or 48 h) with solutions of targeted contaminants to determine the extent of enhanced sorption or degradation. Although the results of these tests provide proof of concept, the extension of the results to practical applications is limited by the conditions inherent in the testing, such as static (no flow) conditions and soil-to-solution ratios that are similar to those of soil suspensions. For these reasons, column studies whereby the backfill is permeated with the chemical solution typically are considered to be more representative of practical applications (Reynolds *et al.* 1982; Colombani *et al.* 2015). However, because of the added complexity of column studies and the potentially longer test durations, few column studies to evaluate the effectiveness of backfill amendments have been conducted.

This study represents an extension of previous studies (Chapters 2 and 3) focused on the potential use of zeolites with high cation exchange capacities (*CECs*) as amendments to an SB backfill for the purpose of enhancing the sorption of potassium (K) and zinc (Zn). The backfills comprised fine sand with 5.8 % (dry weight) sodium bentonite and 0, 5, or 10 % (dry weight) of one of three types of zeolites. The results of Chapter 2 indicated that the addition of zeolite had little impact on either the consolidation behavior or the hydraulic conductivity,  $k$ , of the backfill, and that values of  $k$  for all zeolite-amended specimens measured in flexible-wall permeameters were in the range  $1.2 \times 10^{-10} \leq k \leq 3.9 \times 10^{-10}$  m/s based on permeation with tap water. Thus, the zeolite-amended backfills were considered suitable for use as low-permeability containment

barriers in the absence of any significant incompatibility with the containment liquids. The results of Chapter 3 based on batch equilibrium adsorption tests (BEATs) indicated that the SB backfill amended with 5 or 10 % zeolite significantly increased the adsorption capacity for K by a factor as high as 7.3 or 13.5, respectively, and for Zn by a factor as high as 3.4 or 3.7, respectively. Also, the adsorption behaviors of both K and Zn were shown to be consistent with cation exchange as the dominant sorption mechanism. However, the results of Chapter 3 are limited by the static (no-flow) condition of the BEATs and the soil-to-solution (soil:solution) ratio of 1-to-4 (1:4) by mass, consisting of 10 g of backfill (dry weight) in 40 mL of chemical solution.

In this study, long-term column tests were conducted on specimens of the same unamended and zeolite-amended SB backfills as evaluated in Chapter 3, but at soil:solution ratios and under advective (hydraulic) flow conditions that were more representative of those for practical applications. The permeant liquids included solutions of KCl, ZnCl<sub>2</sub>, and a mixture of KCl and ZnCl<sub>2</sub> to further evaluate the ability of the zeolite-amended backfills to enhance the retardation and, therefore, containment of K and Zn. Ten column tests lasting from 1.05 to 3.75 yr were conducted. Each column test specimen was evaluated for both physical properties (*e.g.*, dry density and porosity) and *k*, and the effluent chemistry was monitored and analyzed for chemical transport parameters of the major solutes, including chloride (Cl<sup>-</sup>), K, and Zn.

## **5.2 MATERIALS AND METHODS**

### *5.2.1 Liquids*

The liquids used in this study included de-ionized water (DIW), and three salt solutions with target concentrations of 35 mM KCl, 20 mM ZnCl<sub>2</sub>, and a mixture of 17.5 mM KCl and 10

mM ZnCl<sub>2</sub>. The measured pH and electrical conductivity, *EC*, of these liquids are summarized in Table 5.1. The mean and standard deviations of the actual measured concentrations for the salt solutions are given in Table F.1. The DIW was used as a permeant liquid and the solvent for the salt solutions, which also were used as permeant liquids. Solutions of KCl and ZnCl<sub>2</sub> were used to allow for comparison of the results in this study with those reported in Chapter 3. As noted in Chapter 3, these two metals often are encountered in contaminated groundwaters (Sparks 2003). Also, use of these two metals allows for comparison of the migration behaviors of a principally monovalent metal (K<sup>+</sup>) versus a principally divalent metal (Zn<sup>2+</sup>). The mixture of KCl and ZnCl<sub>2</sub> was used to evaluate the effect of competition between K and Zn for available sorption sites associated with the bentonite and zeolite components of the backfills. The concentrations of the single salt solutions (*i.e.*, 35 mM KCl and 20 mM ZnCl<sub>2</sub>) were chosen to be sufficiently low so as to be within the linear range of batch equilibrium adsorption data based on the results in Chapter 3, yet sufficiently high to overcome the soluble metals of the backfills (Table 3.3). The target concentrations of the mixed salt solution (*i.e.*, 17.5 mM KCl plus 10 mM ZnCl<sub>2</sub>) were chosen to have similar Cl<sup>-</sup> concentration as for the single salt solutions while maintaining the relative concentration differences between the K and Zn based on the single salt solutions (*i.e.*, 35 mM KCl and 20 mM ZnCl<sub>2</sub> vs. 17.5 mM KCl plus 10 mM ZnCl<sub>2</sub>).

The chemical solutions were prepared by mixing the appropriate amount of either KCl (certified A.C.S.; Fisher Scientific, Fair Lawn, NJ) or ZnCl<sub>2</sub> (A.C.S. grade, Analytical Reagent; Mallinckrodt Chemical Works, St. Louis, MO) with DIW. For the ZnCl<sub>2</sub> solution, a small amount of 37 % hydrochloric acid (HCl) was added to remove visible precipitation in the form of zinc oxychloride as described in Chapter 3. The resulting pH of 1.83 for the 20 mM ZnCl<sub>2</sub> was less than the limiting value of 2 where dissolution of soil particles may occur (Shackelford 1994).

However, this low-pH solution was expected to be buffered by the backfill specimen, and the solution can be considered as representative of acid mine drainage.

### 5.2.2 *Constituent Materials for Specimens*

The backfills for the column tests were prepared to represent a subset of the backfills evaluated in Chapters 2 and 3. These backfills comprised fine mortar sand, 5.8 % (by dry weight) of a powdered sodium bentonite, and 0, 5, or 10 % (by dry weight) of one of three types of zeolite (Malusis *et al.* 2009; Hong *et al.* 2012, 2016). The zeolites were two types of chabazite referred to as chabazite-lower bed (chabazite-LB) and chabazite-upper bed (chabazite-UB), and a clinoptilolite. Although the zeolites are dominated by silt-sized particles with relatively low specific gravities ( $2.35 \leq G_s \leq 2.37$ ), the two chabazites classified (ASTM D2487-ASTM 2006) as high plasticity clays (CH) whereas the clinoptilolite classified as a low plasticity clay (CL). The exchangeable and soluble metals of the zeolites and the bentonite are dominated by sodium (Na). The pH of the two chabazites and the bentonite was  $\sim 8$ , whereas the pH of the clinoptilolite was 9.5 (Table 2.1). The measured *CEC* of the chabazite-LB, chabazite-UB and clinoptilolite were 232, 250, and 180  $\text{cmol}_c/\text{kg}$ , respectively (Table 3.1). Further details on the physical and chemical properties and mineralogy of the constituent materials are provided in Chapter 2 (Table 2.1).

### 5.2.3 *Testing Apparatus*

The testing apparatus used for the column tests comprised a flow-pump system similar to that described by Redmond and Shackelford (1994) connected to a flexible-wall permeameter containing the test specimen (see Figures 5.1 and 5.2 for the schematic and photos of the flow

pump apparatus, respectively). Flow-pump systems maintain a constant volumetric flow rate, offering two primary advantages relative to the more traditional constant-head or falling-head methods of permeating specimens (Shackelford and Redmond 1995). First, at steady-state conditions (no volume change), the constant flow rate correlates with a constant seepage velocity, which allows analytical models describing solute transport through porous media to be used to analyze for the transport properties of the solutes. Second, the volumetric flow rate is not affected by changes in  $k$  that can result from adverse permeant liquid-soil interactions.

Two types of flow pumps referred to as Models 940 and 944 (Harvard Apparatus, Holliston, MA) were used. Both flow pumps comprised two stainless-steel syringes (actuators) on separate tracks, where each syringe was connected to one test specimen. For the "on" setting, the pistons inside each syringe forced liquids (*i.e.*, DIW or salt solution) through the test specimen from bottom to top at a constant displacement rate,  $r_p$ , and the effluent was collected separately (Figures 5.1 and 5.2). The two flow pump models differed only in terms of the ability to control  $r_p$ , with Model 940 consisting of 12 incremental values of  $r_p$  ranging from a low of 1.04 – 1.07 mm/h to a high of 5.20 – 5.35 m/h, and Model 944 allowing for a variable control ranging from 0 to 100 % of each incremental  $r_p$  value for Model 940. The slight variation in  $r_p$  from 1.04 to 1.07 mm/h is likely due to mechanical issues, as the displacement of the plunger for the two syringes attached to the flow pump was not exactly the same, and occasionally the bearings would get loose or the plunger forcing flow through the specimen would get stuck. Eight of the 10 column tests (Test Nos. 1 – 8) in this study were conducted using Model 940, whereas two of the 10 column tests (Test Nos. 9 and 10) were performed using Model 944.

Each flow pump was operated in a reciprocating manner as follows. First, the plunger (piston) used to force liquid from the syringe (actuator) was displaced in one direction forcing

permeant liquid through the column specimen while fresh permeant liquid was simultaneously refilling the syringe space behind the plunger. Then, at the end the displacement, the direction of displacement was reversed virtually instantaneously such that the plunger forced the permeant liquid within the previously refilled side of the syringe through the column specimen while the opposite side of the plunger was refilled with fresh permeant liquid (Figure 5.1). This approach allowed for essentially continuous permeation of the specimen throughout the test durations.

Flexible-wall permeameters were desired to minimize the possibility of side-wall leakage (short circuiting) during column testing, as such side-wall leakage has been known to occur with rigid-wall cells (Daniel *et al.* 1985; Daniel 1994; Bohnhoff *et al.* 2014). As described by Malusis *et al.* (2009) and in Chapter 2, a custom-fabricated, rigid acrylic cylinder was placed around the flexible membrane within the permeameter to provide lateral support for the soft backfill specimens prior to consolidation (see Figure A.2 for further details).

For the constant-flow method of permeation,  $k$  is calculated in accordance with Darcy's law as follows (*e.g.*, Redmond and Shackelford 1994; Shackelford and Redmond 1995; ASTM D5084-ASTM 2004):

$$k = \frac{q}{iA} = \frac{q}{(-\Delta u / \rho_w g L) A} = -\frac{q}{\Delta u} \cdot \frac{\rho_w g L}{A} \quad (5.1)$$

where  $q$  is the volumetric flow rate through the specimen,  $i$  is the hydraulic gradient,  $A$  is the total cross-sectional area of the specimen perpendicular to the direction of flow,  $-\Delta u (> 0)$  is the induced pressure difference across the specimen,  $\rho_w$  is the mass density of water (*i.e.*, 1.0 Mg/m<sup>3</sup>),  $g$  is acceleration due to gravity (*i.e.*, 9.81 m/s<sup>2</sup>), and  $L$  is the length of the specimen. Use of Eq. 5.1 implicitly assumes that the difference in elevation head across the specimen is

negligible relative to the difference in pressure head, which was the case in this study. Also, the density of the permeant liquid is assumed equal to the density of water, which typically is acceptable for dilute aqueous chemical solutions used in this study.

At steady-state flow through the specimen,  $q$  is equal to the volumetric flow rate through the syringe of the flow pump,  $q_p$ , as follows:

$$q = q_p = r_p A_p \quad (5.2)$$

where  $A_p$  is the constant, cross-sectional area of the plunger perpendicular to the direction of displacement. Thus, the magnitude of  $k$  in Eq. 5.1 is directly proportional to  $r_p$ . Accordingly,  $k$  was determined by measuring  $-\Delta u$  either with a differential pressure transducer (Validyne Engineering Corp., Model DP15, Northridge, CA) as shown in Figure 5.1 or two gauge transducers (model No. PX181-100G5V, Omega Engineering Inc., Stamford, CT) located on the inflow and outflow lines connected to the specimen (not shown in Figure 5.1). The transducers were connected to a data acquisition system comprising a circuit board (SCB-68, National Instruments, Austin, TX) and a data acquisition device (National Instruments, Austin, TX), and recording of  $-\Delta u$  was facilitated using the LabVIEW software (National Instruments, Austin, TX).

#### 5.2.4 Specimen Preparation

The unamended and zeolite-amended backfills were prepared by combining the masses of sand, bentonite, and zeolite to maintain a constant total bentonite content (5.8 % by dry weight) with the specified zeolite content (*i.e.*, 0, 5, or 10 % by dry weight) for each backfill,

while adjusting the gravimetric water content ( $w$ ) to obtain the slump within the target range of 100 to 150 mm (3.9 to 5.9 in) based on the slump test results reported in Chapter 2. The backfill specimens for column testing were prepared using the same procedures as described by Malusis *et al.* (2009) and in Chapter 2 for flexible-wall hydraulic conductivity testing. In brief, the backfill was deposited within the stretched membrane supported by the rigid acrylic cylinder in three lifts, with each lift rodded several times to minimize large voids before the top filter paper, porous stone, and end cap were set in place. The permeameter was assembled and filled with the confining water, and a confining stress (cell pressure),  $\sigma_c$ , of 34.5 kPa (5 psi) was applied for a minimum of 24 h. Each specimen then was back-pressured under a constant effective confining stress,  $\sigma'$ , of 34.5 kPa (5 psi) by increasing  $\sigma_c$  and the pore-water (back) pressure,  $u_b$ , in equal increments over several hours to achieve  $B$  value of  $\geq 0.95$  in accordance with ASTM D5084 (ASTM 2004).

Prior to permeation, the initial effective stress in the specimen,  $\sigma'_i$ , is equal to the difference between  $\sigma_c$  and  $u_b$  at the end of the back-pressure saturation stage (*i.e.*,  $\sigma'_i = \sigma_c - u_b$ ). However, once permeation begins, the pore-water pressure on the influent side of the specimen increases due to the hydraulic resistance of the specimen, and eventually attains a steady-state value,  $-\Delta u_{ss}$  ( $> 0$ ), based on the steady-state flow rate,  $q$ . As a result, the effective stress at the inflow side of the specimen decreases during permeation to a final effective stress,  $\sigma'_f$ , represented by the difference between  $\sigma'_i$  and  $-\Delta u_{ss}$  (*i.e.*,  $\sigma'_f = \sigma'_i - (-\Delta u_{ss})$ ). However, in order to keep the flexible-membrane intact with the specimen,  $\sigma'_f$  cannot be zero such that the limiting magnitude of  $-\Delta u_{ss}$  is  $\sigma'_i$  (*i.e.*,  $-\Delta u_{ss} < \sigma'_i$ ). Thus, the maximum value of  $-\Delta u_{ss}$  is limited by  $\sigma'_i$ , or the minimum value of  $\sigma'_i$  is limited by  $-\Delta u_{ss}$ . As indicated by Eqs. 5.1 and 5.2, the magnitude of  $-\Delta u$  and, therefore,  $-\Delta u_{ss}$ , is inversely proportional to  $k$  and directly proportional to  $r_p$  (or  $q_p$ ).

Thus, the magnitude of  $-\Delta u_{ss}$  and, therefore,  $\sigma'_f$  can be minimized by minimizing  $r_p$  (or  $q_p$ ) and/or maximizing  $k$ . Unfortunately, the magnitude of  $r_p$  (or  $q_p$ ) is limited by the flow pump equipment, and the magnitude of  $k$  is based on the hydraulic characteristics of the specimen.

The maximum  $-\Delta u_{ss}$  for the tests conducted in this study was estimated using Eq. 5.1 based on the results of flexible-wall  $k$  tests reported in Chapter 2, and the possible values of  $r_p$  for the flow pumps used for column testing. Therefore to estimate the maximum  $-\Delta u_{ss}$  during permeation, the lowest possible  $r_p$  based on the column tests using flow pump Model 940 and the lowest measured  $k$  of  $1.2 \times 10^{-10}$  m/s from the results in Chapter 2 corresponding to  $\sigma'$  of 34.5 kPa (5 psi) was used. This lowest value of  $k$  together with the lowest  $r_p$  for flow pump Model 940 of 1.04 – 1.07 mm/h, which corresponded to a  $q_p$  ( $= q$ ) of 7.86 – 8.05 mL/d, resulted in an estimated maximum value for  $-\Delta u_{ss}$  of 136 kPa (19.7 psi). Since this value of  $-\Delta u_{ss}$  was greater than the  $\sigma'_i$  of 34.5 kPa (5 psi) following backpressure saturation, membrane separation (blowout) during permeation was anticipated. Therefore, in order to prevent membrane separation (*i.e.*,  $\sigma'_f \leq 0$ ) during permeation, the  $\sigma'_i$  was increased from 34.5 kPa (5 psi) to 138 kPa (20 psi) prior to permeation. Although this  $\sigma'_i$  of 138 kPa (20 psi) is significantly higher than the effective stresses typically encountered in practical field scenarios (*e.g.*, Evans *et al.* 1995; Filz 1996; Li *et al.* 2015), the higher  $\sigma'_i$  of 138 kPa (20 psi) was necessitated due to the limitations in the flow pump equipment used in the study and the expected hydraulic behavior of the backfills. As will be shown subsequently (section 5.3.2), the actual magnitudes of  $-\Delta u_{ss}$  for Test Nos. 1 – 8 ranged from 26 kPa (3.7 psi) to 125 kPa (18.1 psi). Thus, the estimated maximum  $-\Delta u_{ss}$  of 136 kPa (19.7 psi) prior to the start of column testing proved to be reasonable for these column tests. However, for Test Nos. 9 and 10, initial permeation with DIW using  $\sigma'_i$  of 138 kPa (20 psi) resulted in  $-\Delta u_{ss}$  close to 138 kPa (20 psi), indicating that the  $k$  of the specimens were likely to

be lower than the  $k$  of  $1.2 \times 10^{-10}$  m/s that was used to estimate the maximum  $-\Delta u_{ss}$ , leading to the possibility of the membrane separation for these two column tests. As a result, these two specimens were connected to the Model 944 flow pump which allowed  $r_p$  to be reduced to 25 % of that used for the other column tests (*i.e.*,  $0.25 \times (1.04 - 1.07)$  mm/h = 0.26 – 0.27 mm/h). Although this slower displacement rate significantly prolonged the durations of these two column tests, the resulting  $-\Delta u_{ss}$  were maintained less than 138 kPa (20 psi), *i.e.*, 41 kPa (5.9 psi) and 130 kPa (18.8 psi), such that membrane separation was prevented without the need to further increase  $\sigma'_i$  for these two column specimens.

#### 5.2.5 Testing Procedure

Based on the assumption that the cutoff wall would be installed downgradient of the contaminant plume (Figure 5.3), the initial flow through the cutoff wall likely would be relatively clean groundwater. Therefore, after consolidation, the column specimens initially were permeated with DIW to establish a baseline  $k$  for the specimen with respect to DIW ( $k_{DIW}$ ) and to simulate the effect of fresh groundwater in advance of the contaminant plume flushing soluble salts from the placed backfill prior to the arrival of the plume. Although the use of DIW was expected to result in the lowest possible  $k$  (Shackelford *et al.* 2000; Lee and Shackelford 2005), DIW was preferred to reduce the influence of the background solute concentrations on the subsequent chemical analysis of the effluent (Redmond and Shackelford 1994; Shackelford and Redmond 1995). Permeation with DIW was continued until the effluent  $EC$  was within the range of  $EC$  estimated for typical groundwater (see Table 5.2), after which the specimens were permeated with the desired salt solution (*i.e.*, 35 mM KCl, 20 mM ZnCl<sub>2</sub>, or 17.5 mM KCl plus 10 mM ZnCl<sub>2</sub>) continuously until termination of the test. The  $k$  of each specimen based on

permeation with the salt solution ( $k_{sol}$ ) was then measured. The incremental volumes of effluent,  $\Delta V_e$ , were collected sequentially and continuously throughout the duration of permeation such that all of the effluent was collected. The concentrations of various chemical species within each  $\Delta V_e$  were measured using ion chromatography or IC (Dionex® 4000i IC Module, Dionex Co., Sunnyvale, CA) for the anions (*e.g.*, Cl<sup>-</sup>), and inductively coupled plasma-atomic emission spectrometry, or ICP-AES (IRIS® Advantage/1000 ICAP Spectrometer, Thermo Jarrel Ash Co., Franklin, MA) for the metals (*e.g.*, Na, Ca, K, Zn). Thus, the measured concentrations represented average concentrations of chemical species within each  $\Delta V_e$  (Shackelford 1994a, 1995a,b).

#### 5.2.6 *Methods of Chemical Transport Analysis*

The measured effluent concentrations were regressed using two methods of analysis in order to determine the relevant transport parameters associated with the migration of Cl<sup>-</sup>, K, and Zn through the backfill specimens. These two methods included the traditional, concentration-based breakthrough curve (BTC) analysis (*e.g.*, Shackelford 1994a), and the cumulative mass analysis proposed by Shackelford (1995a,b). Both of these methods are based on the same analytical solution to the advection-dispersion-reaction equation (ADRE) for one-dimensional solute transport through saturated porous media. Therefore, analyses by both methods theoretically should provide the same results. However, the cumulative mass analysis has several advantages relative to the more traditional, concentration-based analysis, particularly for column tests that are conducted at low flow rates, such as in this study (Shackelford 1995a,b).

First, the cumulative mass analysis can distinguish explicitly between early breakthrough of a nonadsorbing (nonreactive) solute or tracer (*e.g.*, Cl<sup>-</sup>) resulting from diffusion-dominated

transport versus the existence of an effective porosity ( $n_e$ ) that is lower than the total porosity ( $n$ ) (*i.e.*,  $n_e < n$ ) (*e.g.*, see Shackelford 1993). The effective porosity represents the interconnected void volume relative to the total volume of the specimen, such that only a fraction of the pore space is available for solute mass transport. The existence of  $n_e < n$  can occur, for example, in densely compacted clays due to dead-end pores and/or the attraction of fluid molecules to the surfaces of the clay particles (Shackelford 1993; Shackelford and Moore 2013). Second, the value of the retardation factor,  $R_d$ , for reactive (adsorbing) solutes (*i.e.*,  $R_d > 1$ ) determined via the cumulative mass analysis is based on the correct, mass-based definition corresponding to the relative holdup, or the area above the traditional BTC as illustrated in Figure 5.4a (*e.g.*, see Shackelford 1994a, 1995a,b). Third,  $n_e$  and  $R_d$  can be determined directly from plots of the test results. Finally, the influence of the increment of  $\Delta V_e$  on the analysis is removed from consideration, since all data are plotted at the cumulative elapsed time (Shackelford 1994a).

For the traditional BTC analysis, the relative concentrations (*RCs*) representing the effluent concentrations,  $C(L,t)$ , normalized with respect to the source concentration,  $C_o$ , were regressed using the following analytical solution to the ADRE:

$$RC = \frac{C(L,t)}{C_o} = \frac{1}{2} \left[ \operatorname{erfc}(\xi_1) + \exp(\xi_2) \operatorname{erfc}(\xi_3) \right] \quad (5.3)$$

where *erfc* is the complementary error function, and  $\xi_1$ ,  $\xi_2$ ,  $\xi_3$  are dimensionless arguments defined as follows (Shackelford 1994a, 1995a,b):

$$\xi_1 = \frac{R_d L - v_s t}{2\sqrt{R_d D t}} = \frac{R_d - T}{2\sqrt{R_d T / P_L}} \quad (5.4a)$$

$$\xi_2 = \frac{v_s L}{D} = P_L \quad (5.4b)$$

$$\xi_3 = \frac{R_d L + v_s t}{2\sqrt{R_d D t}} = \frac{R_d + T}{2\sqrt{R_d T / P_L}} \quad (5.4c)$$

where  $R_d$  is based on instantaneous, linear, and reversible sorption,  $v_s$  is the seepage (average linear) velocity,  $t$  is elapsed time,  $D$  is the hydrodynamic dispersion coefficient,  $T (= v_s t / L)$  is the dimensionless time, and  $P_L (= v_s L / D)$  is the dimensionless column Péclet number. The seepage velocity is related to the volumetric flow rate as follows:

$$v_s = \frac{q}{An_e} = \frac{v}{n_e} \quad (5.5)$$

where  $v (= ki)$  is the Darcy velocity, liquid flux or specific discharge (Freeze and Cherry 1979). However, due to the small amount of clay and soft consistency of the slumped backfill specimens evaluated in this study, all of the pore space in the specimens was assumed to be conductive such that  $n_e = n$  was considered reasonable in this study.

In classical advection-dispersion theory,  $D$  represents dispersion (spreading) of the migrating solute front due to diffusion and mechanical dispersion such that  $D = D^* + D_m$ , where  $D^*$  is the effective diffusion coefficient and  $D_m$  is the mechanical dispersion coefficient (e.g., Bear 1972; Shackelford 1993). The effective diffusion coefficient is defined by Shackelford and Daniel (1991) as the product of the apparent tortuosity factor of the porous medium,  $\tau_a$ , and the aqueous or free-solution diffusion coefficient of the solute,  $D_o$  (i.e.,  $D^* = \tau_a D_o$ ), whereas  $D_m$  is defined as the product of the longitudinal dispersion coefficient,  $\alpha$ , which is assumed to be a

characteristic property of the porous medium, and  $v_s$  (*i.e.*,  $D_m = \alpha v_s$ ). Thus,  $D_m$  is a function of  $v_s$ , whereas  $D^*$  is independent of  $v_s$ . As a result,  $D_m$  increases as  $v_s$  increases, such that mechanical dispersion plays an increasingly greater role in contributing to  $D$ , while the contribution of diffusion to dispersion diminishes (*i.e.*, as  $v_s \uparrow$ ,  $D/D_m \rightarrow 1$  and  $D^*/D \rightarrow 0$ ). In contrast, as  $v_s$  approaches zero, diffusion becomes more dominant relative to mechanical dispersion (*i.e.*, as  $v_s \rightarrow 0$ ,  $D_m/D \rightarrow 0$  and  $D^*/D \rightarrow 1$ ).

The column Péclet number,  $P_L$ , represents the relative effect of advection via  $v_s$  to dispersion via  $D$  (Shackelford 1994a). At relatively high  $P_L$  (*e.g.*,  $\geq 50$ ), advection dominates the transport process, whereas dispersion via diffusion becomes increasingly more significant for  $P_L \leq 20$  and dominant for  $P_L \leq 5$  (Shackelford 1994a).

Application of Eq. 5.3 is based on the assumptions that  $C_o$  and  $v_s$  are constant. Both of these assumptions were reasonably achieved for the column tests conducted in this study by frequently replenishing the permeant (source) solution and by using a flow-pump system to maintain a constant flow rate. For constant  $v_s$ ,  $T$  is equivalent to pore volumes of flow ( $PVF$ ).

Based on continuity, Eq. 5.3 represents a continuous distribution of an infinite number of instantaneous concentrations. However, in this study, the measured effluent concentrations represented average concentrations equivalent to the incremental solute mass,  $\Delta m$ , within  $\Delta V_e$  (*i.e.*,  $C = \Delta m / \Delta V_e$ ) collected over a finite (incremental) sampling interval,  $\Delta T$  ( $= T_{final} - T_{initial}$ ). Shackelford (1994a) showed that reasonably accurate values of  $R_d$  and  $P_L$  could be determined by regressing Eq. 5.3 versus the measured average concentrations provided the concentrations were plotted versus the elapsed time ( $T$ ) corresponding to the middle of  $\Delta T$  (*i.e.*,  $T_m = (T_{final} + T_{initial})/2$ ), and  $\Delta T$  is  $\leq 0.25$ . However, since  $\Delta T$  was  $\leq 0.33$  for the column tests conducted in this study, some error in the regressed values of  $R_d$  and  $P_L$  was expected. Based on the results

reported by Shackelford (1994a), this error in  $R_d$  and  $P_L$  was expected to be  $\leq 1\%$  and  $\leq 6\%$ , respectively. Thus, for the traditional BTC method of transport analysis, the measured effluent concentrations were plotted versus the  $T$  corresponding to  $T_m$ .

For the cumulative mass analysis, the measured effluent concentrations were converted to values of the cumulative mass ratio,  $CMR$ , representing the accumulated solute mass normalized with respect to the equilibrium solute mass within the pore water of the specimen at steady-state transport (Shackelford 1995a,b), or :

$$CMR = \frac{\sum_{i=1}^j \Delta m_i}{V_p C_o} \quad (5.6)$$

where  $V_p$  is the pore (void) volume of the column specimen, and  $j$  is the number of effluent samples upon which the value of  $CMR$  is based. The resulting values of  $CMR$  were plotted versus the elapsed pore volumes of flow corresponding to the end of the sampling interval (*i.e.*,  $T = T_{final}$ ), and then regressed using the following solution to the ADRE (Shackelford 1995a,b):

$$CMR = \frac{R_d}{2P_L} \left[ (\xi_4 - \xi_2) \operatorname{erfc}(\xi_1) + (\xi_4 + \xi_2) \exp(\xi_2) \operatorname{erfc}(\xi_3) \right] \quad (5.7)$$

where  $\xi_4 = TP_L/R_d$ . As shown schematically in Figure 5.4b, the trend in  $CMR$  versus  $T$  is initially nonlinear corresponding to a transient transport stage, followed by steady-state transport corresponding to complete solute breakthrough and indicated by a straight-line relationship between  $CMR$  and  $T (= T_{final})$  with a 1:1 slope (Shackelford 1995a,b). The extension of this

straight-line relationship to the  $T$ -axis, designated as  $T_o$ , represents the retardation factor, *i.e.*,  $R_d = T_o$  (Figure 5.4b).

Finally, Shackelford (1995a,b) also showed that, as solute transport approaches steady-state, the value of  $T - CMR$  plotted as a function of  $T (= T_{final})$  asymptotically approaches the value of  $R_d$ . As a result,  $R_d$  can be determined without regression simply by determining the steady-state value of  $T - CMR$ , or  $(T - CMR)_{ss}$ , as illustrated schematically in Figure 5.4c. The  $R_d$  based on both  $T_o$  and  $(T - CMR)_{ss}$  are theoretically the same, and represent the true, mass-balanced  $R_d$  corresponding to the relative holdup representing the area above the BTC at steady-state (Figure 5.4a), which is independent of the value of  $P_L$ .

The values of  $D$  (via  $P_L$ ) and  $R_d$  for the  $RC$  and  $CMR$  analyses were obtained by regressing the measured data using the analytical model expressed in Eqs. 5.3 and 5.6, respectively. These regressions were performed using the curve fitting functions within KaleidaGraph<sup>®</sup> (Version 4.03, Synergy Software, 2457 Perkiomen Ave. Reading, PA 19606) and MatLab<sup>™</sup> (R2013a, MathWorks, Inc., 3 Apple Hill Drive Natick, MA 01760), and the solver function within Microsoft<sup>®</sup> Excel<sup>®</sup> (2010, Microsoft, 7595 Technology Way, Denver, CO 80237). The  $D$  and  $R_d$  results obtained from Excel<sup>®</sup> occasionally did not match those from KaleidaGraph<sup>®</sup> and MatLab<sup>™</sup>, which were always identical. Therefore, all of the results presented hereafter were obtained using KaleidaGraph<sup>®</sup>. The values of  $R_d$  obtained from the linear (steady-state) portions of the plots of  $CMR$  versus  $T$  (*i.e.*,  $R_d = T_o$ ) and  $T - CMR$  versus  $T$  (*i.e.*,  $R_d = (T - CMR)_{ss}$ ) were based on simple linear regressions of the measured data requiring  $r^2 \geq 0.9995$ . The  $T_o$  was calculated from the linear fit of the  $CMR$  versus  $T$  plot with  $r^2 \geq 0.9995$ , and the  $(T - CMR)_{ss}$  was the average of the  $T - CMR$  for each  $\Delta T$  within this linear portion of the data. Finally, based on the BTC data, the time required to reach  $RC = 0.5$ ,  $t_{0.5}$ , and the

corresponding dimensionless time,  $T_{0.5}$ , were calculated by interpolating between the nearest neighboring  $RC$  data.

### 5.2.7 *Consideration of Other Factors Potentially Affecting Analyses*

Since the influent source solution and the column specimen are separated by tubing and a porous stone, the influent side of the soil column is not in direct contact with the permeant liquid. Therefore, when the permeant liquid is switched from DIW to a chemical solution, the influent solution can mix with the remnant DIW in the tubing and porous stone and become diluted. Rabideau and Khandelwal (1998) noted that the length of the mixing zone can affect the spatial distribution of the solute concentration within the porous medium, whereas there is virtually no effect on the effluent concentration. Since only the effluent concentration data were evaluated in this study, this mixing zone effect was considered as not applicable.

Another consideration was whether the porous stones should be analyzed as layers adjacent to the column specimen with different seepage velocities. However, the porosity of the porous stones were 0.426, which was similar to the final porosities,  $n_f$  of the tested soil columns ranging from 0.420 to 0.449 (Table 5.4). Therefore, for the constant flow rates applied in this study, the seepage velocities for the backfill specimens and the porous stones were practically the same. Also, since the porous stones have no attenuation capacity, accounting for the volume of solution (influent or effluent) contained in the pores of the porous stone as described subsequently was considered sufficient.

The effect of the residual volume of the effluent within the column test system on the chemical transport analysis was evaluated by Mazzieri *et al.* (2015). When bladder accumulators are used to provide the source solution and to collect the column effluent, a portion of the

effluent remains in the bladder, such that the collected effluent concentration is mixed with the remnant effluent from the previous sampling. Mazzieri *et al.* (2015) compared the results of column tests where the effluent concentrations were corrected for the residual volume,  $V_{res}$ , defined as the sum of the void volume of the porous stone, the volumes of the connecting tubes, and the volume of the effluent remaining in the bladder accumulator ( $V_{res} = V_{stone} + V_{tube} + V_{bladder}$ ), versus those where  $V_{res} = 0$ . The difference between the corrected (*i.e.*,  $V_{res} \neq 0$ ) and uncorrected (*i.e.*,  $V_{res} = 0$ ) results increased with the relative magnitude of  $V_{res}$  to  $V_p$ ; *i.e.*, as  $V_{res}/V_p$  increased, the error in the uncorrected values of  $D$  and  $R_d$  increased.

However, bladder accumulators were not used for the column tests in this study, such that  $V_{res} \approx \frac{1}{10} V_p$ . As a result, any effect of  $V_{res}$  was assumed to be minor. Nonetheless, in order to confirm whether this assumption was correct, analyses of two column tests with different flow rates (*i.e.*,  $q = 7.86$  mL/d and  $2.06$  mL/d) were performed. The resulting corrected and uncorrected values of  $R_d$  and  $P_L$  for  $V_{res}$  are compared in Table 5.5. For  $\text{Cl}^-$ , the  $R_{d,corrected}/R_{d,uncorrected}$  based on the *CMR* analysis was 97.0 % for  $q = 7.86$  mL/d and 99.0 % for  $q = 2.06$  mL/d, whereas the  $P_{L,corrected}/P_{L,uncorrected}$  based on the *CMR* analysis was 46.6 % for  $q = 7.86$  mL/d and 68.2 % for  $q = 2.06$  mL/d. For  $\text{K}^+$ , the  $R_{d,corrected}/R_{d,uncorrected}$  based on the *CMR* analysis was 97.8 % for  $q = 7.86$  mL/d and 99.2 % for  $q = 2.06$  mL/d, whereas the  $P_{L,corrected}/P_{L,uncorrected}$  based on the *CMR* analysis was 95.0 % for  $q = 7.86$  mL/d and 98.2 % for  $q = 2.06$  mL/d. Thus, the overall difference in the uncorrected and corrected  $R_d$  for  $V_{res}$  was considered to be acceptable, whereas the error in  $P_L$  for  $\text{Cl}^-$  associated with  $V_{res}$  was more significant. Also, the ratio of  $P_L$  based on the *RC* analysis relative to that based on the *CMR* analysis,  $P_{L,RC}/P_{L,CMR}$ , for  $\text{Cl}^-$  was 65.6 % for  $q = 7.86$  mL/d and 185.6 % for  $q = 2.06$  mL/d for the uncorrected data, whereas  $P_{L,RC}/P_{L,CMR}$  was 112.7 % for  $q = 7.86$  mL/d and 158.5 % for  $q =$

2.06 mL/d for the corrected data. For  $K^+$ , the  $P_{L,RC}/P_{L,CMR}$  was 114.5 % for  $q = 7.86$  mL/d and 85.1 % for  $q = 2.06$  mL/d for the uncorrected data, whereas  $P_{L,RC}/P_{L,CMR}$  was 114.3 % for  $q = 7.86$  mL/d and 85.3 % for  $q = 2.06$  mL/d for the corrected data. Thus, the  $P_L$  based on the *RC* and *CMR* analyses agreed better (*i.e.*,  $P_{L,RC}/P_{L,CMR}$  was closer to 100 %) when corrected for  $V_{res}$ . Therefore, the elapsed times for each column test were corrected by subtracting the increment in time required for displacement of  $V_{res}$  (*i.e.*,  $\Delta T = V_{res}/q$ ) from the actual elapsed times corresponding to the effluent sampling. The corrected increment in times ( $\Delta t$ ,  $\Delta T$ ) required for displacement of  $V_{res}$  are listed in Table F.2.

The final factor considered to potentially affect the regressed transport analysis results was the assumption inherent in the analytical solutions for chemical transport analysis (Eqs. 5.3 and 5.6) that sorption was linear, reversible, and instantaneous, such that  $R_d$  could be considered as a constant value. As previously noted, the  $C_o$  for the chemical solutions used in conducting the column tests were chosen to be relatively low in an attempt to comply with this assumption. To evaluate this compliance, the regressed values of  $R_d$  from the column test results were compared with secant values of  $R_d$  (*i.e.*,  $R_{d,secant}$ ) based on previously reported BEAT results (Chapter 3), and presented in section 5.3.5.

### 5.2.8 Testing Plan

The variables that were considered in developing the column testing plan included the type of zeolite (chabazite-LB, chabazite-UB, and clinoptilolite), the zeolite content (0, 5, 10 %), and the composition of the salt solutions used as the permeant liquids (*i.e.*, 35 mM KCl, 20 mM  $ZnCl_2$ , or 17.5 mM KCl plus 10 mM  $ZnCl_2$ ). The resulting testing conditions are summarized in Table 5.3. The effect of type of zeolite (unamended, backfills amended with 5 % chabazite-UB

or 5 % clinoptilolite) is evaluated by comparing the results for Test Nos. 1, 3, and 6 (35 mM KCl), and Test Nos. 2, 4, and 7 (20 mM ZnCl<sub>2</sub>). The effect of the zeolite content (0, 5, and 10 %) is evaluated by comparing the results for Test Nos. 1, 9, and 10 (unamended, backfills amended with 5 or 10 % chabazite-LB). The effect of type of metal (K and Zn) is evaluated by comparing the results for Test Nos. 1 and 2 (unamended backfill), Test Nos. 3 and 4 (backfills amended with 5 % chabazite-UB), and Test Nos. 6 and 7 (backfills amended with 5 % clinoptilolite). Finally, the effect of competing metal (*i.e.*, 35 mM KCl and 20 mM ZnCl<sub>2</sub> vs. 17.5 mM KCl plus 10 mM ZnCl<sub>2</sub>) in the permeant liquid is evaluated by comparing the results for Test Nos. 3 – 5 (backfills amended with 5 % chabazite-UB) and Test Nos. 6 – 8 (backfills amended with 5 % clinoptilolite), with the  $R_{d,secant}$  based on the BEAT results (Chapter 3).

## 5.3 RESULTS

### 5.3.1 Physical Characterization

Upon completion of the column tests, the columns were disassembled and the test specimens were measured for physical properties. As shown in Figure 5.5, the final shapes of the specimens were somewhat similar to that of an hourglass. This shape suggests that the flow through the specimens was not entirely one-dimensional, although the deviation from one-dimensional flow likely was minimal.

As a result of the shape of the specimens, the diameter was estimated as the mean of three measurements using a caliper of the diameter ( $d$ ) at the top, middle, and bottom of the specimen, whereas the height ( $h$ ) was estimated as the mean of four measurements. The mean and standard deviations of these measurements as well as the resulting calculated total volume of each column specimen,  $V_T$ , are given in Table F.3.

The initial and final physical properties of the specimens are summarized in Table 5.4. The variation in the initial water content,  $w_i$ , of the backfill specimens reflects the water content required to achieve the target slump of 100 to 150 mm (3.9 to 5.9 in) for each type backfill (*e.g.*, Chapter 2). The initial porosity ( $n_i$ ) refers to the porosity that resulted upon setting up the specimens within the permeameters, *i.e.*, based on the inner volume of the rigid acrylic cylinder, and the measured mass,  $w_i$ , and specific gravity ( $G_s$ ) of the backfill. The final porosity ( $n_f$ ) was calculated based on the measurements of the test specimen after the test was completed and the column was disassembled (Table F.3). The volume of voids,  $V_v$ , was calculated by subtracting the volume of solids,  $V_s$ , from  $V_T$ , or  $V_v = V_T - V_s$ , where  $V_s$  was calculated based on the measured dry mass of the column specimen,  $m_s$ , and the specific gravity,  $G_s$ , of the backfill (*i.e.*,  $m_s = \rho_w G_s V_s$ , where  $\rho_w$  is the density of water). The  $G_s$  of the backfills were calculated based on the added amounts and  $G_s$  of the constituent materials (see Table 2.1 for the  $G_s$  of sand, bentonite and zeolite) of each backfill (see Table F.3 for values of  $G_s$  of the backfills).

Since permeation via the flow pump results in a buildup of pore-water pressure at the influent end (bottom) of the specimen, and a concomitant decrease in  $\sigma'$ , the decrease in  $n$  from  $n_i$  to  $n_f$  indicated in Table 5.4 can be attributed primarily to consolidation of the specimen, as  $\sigma'_i$  was increased from 34.5 kPa (5 psi) to 138 kPa (20 psi) after back pressure saturation and prior to permeation (Figure 5.5). As a result, the values of  $n_f$  reported in Table 5.4 were considered to be more representative of the porosities of the specimens during the permeation stage of the column tests, such that the results presented hereafter in this study were based on the values of  $n_f$ , *i.e.*, assuming all of the voids were filled and contributed to liquid flow through the specimen.

The measured values of the final degree of saturation,  $S_f$ , for all of the specimens except those for Test Nos. 5, 7, and 10 satisfied the criterion in ASTM D5084 (ASTM 2004) for

flexible-wall  $k$  testing of saturated specimens that  $95 \leq S_f \leq 105$  %. The value for  $S_f$  of 93.5 % for Test No. 7 and 94.8 % for Test No. 10 is attributed more to the difficulty associated with the measurement than a reflection that the specimen was not saturated. In the case of the specimen for Test No. 5, which was stopped due to leakage in the testing system, the test specimen fell apart when disassembled (Figure 5.5), resulting in an unlikely measured value for  $S_f$  of 62.7 %.

Finally, the test durations noted in Table 5.4 indicate that the column tests for the unamended backfills (Test Nos. 1 and 2) lasted 1.05 and 1.37 yr, respectively, whereas those for the zeolite-amended backfills lasted from 1.47 yr (Test No. 7) to 3.75 yr (Test Nos. 9 and 10). The significantly longer test durations for Test Nos. 9 and 10 are attributed to the significantly lower flow rates imposed for these two column tests as previously discussed in section 5.2.4 (see Table 5.3).

### 5.3.2 Hydraulic Properties

The hydraulic properties of the column test specimens are summarized in Table 5.6. The  $q$  and  $v$  for Test Nos. 1 to 8 of 7.86 to 8.05 mL/d and  $2.75 \times 10^{-8}$  m/s to  $3.02 \times 10^{-8}$  m/s, respectively, were approximately four times higher than those for Test Nos. 9 and 10 of 2.06 mL/d and  $0.72 \times 10^{-8}$  m/s, respectively, due to the different  $r_p$  used in the tests. Since the actual  $r_p$  varied slightly from 1.04 to 1.07 mm/h (section 5.2.3),  $q$  was calculated based on the actual  $\sum(\Delta V_e)$  and  $\sum(\Delta t)$  for each flow pump (*i.e.*,  $q = \sum(\Delta V_e)/\sum(\Delta t)$ ). This variation in  $q$  was considered minor in that the differences were less than 2.4 %.

The steady-state hydraulic gradient,  $i_{ss}$ , was higher than maximum  $i$  of 30 for materials with  $k$  less than  $1.0 \times 10^{-9}$  m/s required by ASTM D5084 (ASTM 2004), as application of an excessively high  $i$  leads to high seepage forces that result in consolidation of the specimens

during permeation and measurement of unconservative (low) measured  $k$ . However, since the lowest possible  $r_p$  of 1.04 to 1.07 mm/h was used for column Test Nos. 1 to 8, lower hydraulic gradients were not possible for these tests. Even if limiting  $i$  to 30 had been possible, the resulting test durations would have been considerably longer, all other factors being equal. For example, based on the steady-state values of  $i$ , or  $i_{ss}$ , reported in Table 5.6, an  $i$  of 30 would have resulted in column test durations lasting from 2.11 to 15.3 yr, *i.e.*, instead of the actual durations ranging from 1.05 to 3.75 yr (Table 5.4).

The temporal trends in measured  $-\Delta u$  ( $> 0$ ) across the specimens are shown in Figures 5.6 – 5.9. Since the effluent and influent reservoirs were subjected to a back pressure of 207 kPa (30 psi), reversal of the direction of the plunger to maintain continuous permeation of the specimens was reflected by repeated, virtually instantaneous decreases and subsequent increases in  $-\Delta u$  back to the magnitude that had been established prior to reversal of the plunger direction.

Due to the extensive test durations, some anomalous behavior in  $-\Delta u$  occurred during some of the tests as a result of a variety of issues, including slight variations in the pressure supply system used to provide the back pressure and issues related to the flow pump and/or computers for data acquisition. In particular, for Test Nos. 4 and 7, the  $-\Delta u$  decreased periodically during the earlier stages of the test, as if the plunger forcing flow through the specimen had become stuck (see Figures 5.7b and 5.8b). As a result, the plunger displacement cycle for these tests was changed from 5 d to 4 d to avoid extending the plunger through the region where the plunger appeared to get stuck, which rectified the issue.

In spite of the aforementioned anomalies, the overall measured  $-\Delta u_{ss}$  were similar for the two unamended backfills when permeated with different liquids (*i.e.*, DIW versus 35 mM KCl or 20 mM ZnCl<sub>2</sub>) (Figure 5.6). However, for the zeolite-amended backfills,  $-\Delta u_{ss}$  was lower when

permeated with the salt solution (*i.e.*, 35 mM KCl, 20 mM ZnCl<sub>2</sub>, 17.5 mM KCl plus 10 mM ZnCl<sub>2</sub>) than when permeated with DIW, except for the backfill amended with 5 % clinoptilolite when permeated with 35 mM KCl. Since  $-\Delta u$  is inversely proportional to  $k$  (Eq. 5.1), a decrease in  $-\Delta u$  correlates with an increase in  $k$ , all other factors being equal. Thus, the slight increases in  $-\Delta u$  during permeation with the salt solutions relative to permeation with DIW likely represent a small measure of incompatibility between the test specimens and salt solutions.

The temporal trends in  $k$  based on the measured values of  $-\Delta u$  (Eq. 5.1) are shown in Figures 5.10 – 5.13. The resulting steady-state values of  $k$  based on  $-\Delta u_{ss}$  are shown in Table 5.6. For comparison, the measured  $k$  reported in Chapter 2 based on permeation with tap water of specimens either within an oedometer cell at  $\sigma' = 192$  kPa (27.8 psi) or within a flexible-wall cell at  $\sigma' = 34.5$  kPa (5 psi) are shown as the shaded areas in Figures 5.10 – 5.13. The values of  $k$  measured from the column tests agree well with the previously measured values of  $k$  (Chapter 2) except in the cases for the backfill amended with 5 % chabazite-UB permeated with the mixed salt solution, and for all cases for the backfill amended with 5 % clinoptilolite, where the values of  $k$  were less than one order of magnitude higher than the previously measured values of  $k$ . However, in all cases, the measured values of  $k$  satisfied the typical requirement of  $\leq 1.0 \times 10^{-9}$  m/s for hydraulic barriers for contaminant containment.

The values of  $k_{sol}/k_{DIW}$  are shown in Figure 5.14 and summarized in Table 5.6. The resulting  $k_{sol}/k_{DIW}$  were less than unity (*i.e.*,  $k_{sol}/k_{DIW} < 1$ ) for both unamended backfill specimens (Test Nos. 1 and 2), and for the backfill amended with 5 % clinoptilolite and permeated with 35 mM KCl (Test No. 6), indicating no incompatibility between the permeant liquids and the backfill specimens. In all other tests, a small measure of incompatibility was observed (*i.e.*,  $1.06 \leq k_{sol}/k_{DIW} \leq 1.94$ ). However, the extent of this incompatibility was relatively minor in that all

observed for 40 % (= 2/5) of tests for columns permeated with 35 mM KCl, 67 % (= 2/3) of tests for columns permeated with 20 mM ZnCl<sub>2</sub>, and 100 % (= 2/2) of tests for columns permeated with 17.5 mM KCl plus 10 mM ZnCl<sub>2</sub> (Figure 5.14). The relative compatibility between the permeant liquids and test specimens can be attributed to the relatively dilute salt solutions used as permeant liquids and the relatively high  $\sigma'$  of 138 kPa (20 psi) of the test specimens prior to permeation (*e.g.*, Fernandez and Quigley 1991; Shackelford 1994b).

### 5.3.3 Effluent Chemistry

#### 5.3.3.1 Breakthrough Curves

The temporal trends in the measured solute concentrations of the primary chemical species within the effluent of the column tests are shown in Figures 5.15 – 5.18. For all backfills, breakthrough of Cl<sup>-</sup> occurred relatively quickly, whereas the breakthrough of the metals of interest, *i.e.*, K<sup>+</sup> and/or Zn<sup>2+</sup>, was delayed, as expected on the basis of adsorption of these two metals (Chapter 3). Once steady-state transport of Cl<sup>-</sup> had been established, further measurement of Cl<sup>-</sup> in the effluent was deemed unnecessary. Except for Test Nos. 9 and 10 (Figure 5.18), measurement of K<sup>+</sup> and/or Zn<sup>2+</sup> concentrations was continued until steady-state transport of these metals had been achieved. The significantly lower flow rates imposed in Test Nos. 9 and 10 (see Table 5.3, section 5.2.3) resulted in extensive delay in the breakthrough of K<sup>+</sup> and exceedingly long test durations of 1370 d (3.75 yr). As a result, the tests were continued until the measured K<sup>+</sup> concentrations were at least 50 % of the source concentration of K<sup>+</sup> (*i.e.*,  $\geq 17.5$  mM K<sup>+</sup>).

For the unamended backfill (Figure 5.15), Cl<sup>-</sup> breakthrough occurred first, followed by elution of primarily Ca<sup>2+</sup>, and then breakthrough of either K<sup>+</sup> (Figure 5.15a) or Zn<sup>2+</sup> (Figure 5.15b). The dominant elution of Ca<sup>2+</sup> relative to Na<sup>+</sup> for the unamended backfill was unexpected

5.15b). The dominant elution of  $\text{Ca}^{2+}$  relative to  $\text{Na}^+$  for the unamended backfill was unexpected on the basis that the predominant soluble and exchangeable metal associated with the bentonite component of the unamended backfill was  $\text{Na}^+$ . However, since the unamended backfill contained only 5.8 % bentonite, the mass of bentonite in the backfill was low, such that permeation with DIW prior to the start of the column testing stage apparently was sufficient to leach most of the soluble  $\text{Na}^+$  associated with the unamended backfill. The subsequent elution of  $\text{Ca}^{2+}$  after the start of the column testing stage of the tests can be attributed to  $\text{K}^+$  or  $\text{Zn}^{2+}$  exchange for  $\text{Ca}^{2+}$  initially held electrostatically to the bentonite particles comprising the unamended backfill. This  $\text{Ca}^{2+}$  elution is expected to satisfy a portion of the charge balance with  $\text{Cl}^-$  in accordance with the electroneutrality requirement, thereby affecting the mobility of  $\text{K}^+$  or  $\text{Zn}^{2+}$ .

For all of the column tests conducted with the zeolite-amended backfills (Figures 5.16 – 5.18),  $\text{Na}^+$  was eluted first, followed by breakthrough of  $\text{Cl}^-$  and then elution of  $\text{Ca}^{2+}$  and/or breakthrough of  $\text{K}^+$  and/or  $\text{Zn}^{2+}$ . This difference in behavior can be attributed to the additional soluble  $\text{Na}^+$  within the zeolite-amended backfill due to the presence of the zeolite, such that permeation with DIW prior to the start of column testing was not sufficient to reduce the eluted  $\text{Na}^+$  to insignificant concentrations. As in the case of the column tests with the unamended backfill, the elution of residual soluble and exchangeable  $\text{Na}^+$  and  $\text{Ca}^{2+}$  affects the mobility of  $\text{K}^+$  and/or  $\text{Zn}^{2+}$  based on the electroneutrality constraint.

The temporal trends in the measured effluent solute fluxes ( $= C\Delta V_e/A_f\Delta t$ ) of the major chemical species appearing in the effluent are shown in Figures 5.19 – 5.22. The limiting values corresponding to the purely advective solute flux at steady state,  $J_A$  ( $= vC_o = nv_sC_o$ ) for the chemical species in the influent, *i.e.*,  $\text{Cl}^-$ ,  $\text{K}^+$  and/or  $\text{Zn}^{2+}$ , also are shown in Figures 5.19 – 5.22

and in Table F.1. In general, the trends in the solute mass fluxes mimic those previously presented in terms of effluent solute concentrations in Figures 5.15 – 5.18.

### 5.3.3.2 Charge Balance

The charge balance of the effluent for each column test was assessed by comparing the absolute value of the summation of anion equivalents relative to the summation of cation equivalents (*i.e.*,  $|\sum \text{anions}| = \sum \text{cations}$ ), and the results are shown in Figures 5.23 – 5.26. In general, the closure on the charge balance was excellent. A trace amount ( $< 20$  ppm) of nitrate ( $\text{NO}_3^-$ ) and phosphate ( $\text{PO}_4^{3-}$ ) appeared after each calibration stage of the instrument and, therefore, nitrate ( $\text{NO}_3^-$ ) and phosphate ( $\text{PO}_4^{3-}$ ) were excluded from the charge balance calculation. The disagreement in the charge balance for the initial stages of the test may be attributed, in part, to elution of nitrate ( $\text{NO}_3^-$ ) and phosphate ( $\text{PO}_4^{3-}$ ) during the early stages of the test, and the possibility of other ionic chemical species that may have been present but were not measured.

### 5.3.3.3 Electrical Conductivity and pH

The temporal trends in the measured *EC* of the column effluent for each column test are shown in Figures 5.27 – 5.30, whereas those for pH are shown in Figures 5.31 – 5.34. The final values of *EC* corresponding to the end of the initial DIW permeation stage ( $EC_{DIW,f}$ ) and at the end of the column testing stage ( $EC_{sol,f}$ ) for each column test are summarized in Table 5.6, whereas the final values of pH corresponding to the end of both the initial DIW permeation stage ( $\text{pH}_{DIW,f}$ ) and at the end of the column testing stage ( $\text{pH}_{sol,f}$ ) for each column test are summarized in Table 5.7. All of the  $EC_{DIW,f}$  values were within the estimated range of *EC* for typical

groundwater (Table 5.2) as previously noted. Complete breakthrough in  $EC$  during permeation with the salt solutions, or  $EC_{sol,f}/EC_{sol,o} = 1$ , was practically achieved for all of the column tests involving permeation with either 35 mM KCl or the mixed salt solution (17.5 mM KCl plus 10 mM  $ZnCl_2$ ). In contrast, none of the tests involving permeation with 20 mM  $ZnCl_2$  achieved complete breakthrough in electrical conductivity, or  $EC_{sol,f}/EC_{sol,o} < 1$ , with  $EC_{sol,f}/EC_{sol,o}$  values of either 0.63 (Test No. 2) or 0.62 (Test Nos. 4 and 7), despite complete effluent breakthrough of both  $Cl^-$  and  $Zn^{2+}$  in these tests (see Figures 5.19b, 5.20b, and 5.21b). The  $EC_{sol,f}/EC_{sol,o} < 1$  for column tests involving permeation with 20 mM  $ZnCl_2$  was primarily due to the initially low pH of the 20 mM  $ZnCl_2$  (pH = 1.83, Table 5.1), as HCl was added to prevent the formation of precipitates in the  $ZnCl_2$  solution (Chapter 3). As shown by Shackelford *et al.* (1999), high concentrations of protons ( $H^+$ ) or hydroxides ( $OH^-$ ) corresponding to low pH or high pH, respectively, contribute significantly to the  $EC$  of a chemical solution. As shown in Figures 5.31b, 5.32b, and 5.33b and Table 5.7, the natural buffering capacity of the backfills (see Chapter 3) presumably buffered the pH of the 20 mM  $ZnCl_2$  solution, such that pH equilibrium (*i.e.*,  $pH_{sol,f}/pH_{sol,o} = 1$ ) was never achieved, resulting in  $pH_{sol,f}$  always being greater and more neutral than  $pH_{sol,o}$  (*i.e.*,  $1.53 \leq pH_{sol,f}/pH_{sol,o} \leq 2.04$ ). As a result, the contribution of  $H^+$  to the  $EC$  of the effluent was reduced throughout the column testing stage. Although the effluent pH for the column tests involving permeation with either 35 mM KCl or the mixed salt solution also were buffered relative to the respective influent pH, *i.e.*,  $pH_{sol,f}/pH_{sol,o} > 1$  (Table 5.7), this effect was minimized in these column tests (Test Nos. 1, 3, 5, 6, 8, 9 and 10) because of the more neutral pH of the source solutions (see Table 5.1), such that the contribution of  $H^+$  to the source  $EC$  was less significant.

In terms of the temporal trends in pH (Figures 5.31 – 5.34), despite a few periods for some column tests where pH data were either missing or the trends in the pH data appeared to be anomalous (*e.g.*, Figures 5.31a, 5.32c, 5.33a), the overall trends in the pH data were generally consistent, such that the final pH of the effluent when permeated with chemical solutions were higher than the source pH of the chemical solutions (or  $\text{pH}_{\text{sol},f} > \text{pH}_{\text{sol},o}$ ). For Test Nos. 2, 4, and 7 involving permeation with the low-pH 20 mM  $\text{ZnCl}_2$  solution (*i.e.*,  $\text{pH}_{\text{sol},o} = 1.83$ ), the final effluent pH were all greater than 2 (*i.e.*,  $2.80 \leq \text{pH}_{\text{sol},o} \leq 3.74$ ), such that dissolution of the minerals comprising the backfill constituents likely was not prevalent (Shackelford 1994b). Such dissolution could result in significant increases in  $k$ , which also were not observed for these tests (see section 5.3.2 and Table 5.6). Also, for these same tests, the relatively low  $\text{pH}_{\text{sol},f}$  suggest that the hydroxide complexes of Zn (*e.g.*,  $\text{ZnOH}^+$ ) were minimal such that Zn likely existed primarily as  $\text{Zn}^{2+}$  (Chapter 3).

#### 5.3.4 Chemical Transport Analyses

The results of the analyses of the column effluent data to determine the values of  $R_d$  and  $P_L$  for all 10 column tests are illustrated in Figures 5.35 – 5.45. These analyses included regressions of the  $RC$  and  $CMR$  data shown in the (a) and (b) plots of each figure, respectively, values of  $R_d$  from the  $T_o$  and  $T - CMR$  analyses shown in the (c) plot of each figure, and values of  $T_{0.5}$  illustrated in the (a) plot of each figure. For the  $T_o$  analysis, only the data that were considered to represent steady-state transport are shown. The results shown in Figure 5.37 represent re-analysis of the results shown in Figure 5.36 for Test No. 2 to correct for porosity as explained subsequently. Finally,  $R_d$  from the aforementioned analyses are compared in Figure 5.46,  $P_L$  from the  $RC$  and  $CMR$  regressions and the resulting values of  $D$  calculated from  $P_L$  are

compared in Figure 5.47, and all the results together with the values of  $t_{0.5}$  are summarized in Table 5.8.

For Test No. 2, the  $R_d$  for  $\text{Cl}^-$  was greater than unity (see Table 5.8), ranging from 1.13 ( $RC$  regression) to 1.18 ( $T_o$  analysis), indicating sorption of  $\text{Cl}^-$ . These results suggested that the  $n_f$  used to determine  $T$  and  $v_s$  was incorrect for this test because (a) this was the only column test that resulted in  $R_d$  values substantially different than unity for  $\text{Cl}^-$  and (b) there is no known mechanism for  $\text{Cl}^-$  sorption to the constituent materials comprising the unamended backfill (*i.e.*, sand and bentonite). An error in  $n_f$  could have resulted from an error in the measured final (wet) weight of the column specimen, which would have affected the calculation for  $w_f$  and  $n_f$ . Since an overestimation in  $R_d$  for  $\text{Cl}^-$  also resulted in an overestimation in  $R_d$  for  $\text{Zn}^{2+}$ ,  $n_f$  was corrected using the  $R_d$  of 1.15 from the  $CMR$  regression and the  $T - CMR$  analysis, as this value was considered the most reliable. This correction was made by multiplying the uncorrected  $n_f$  of 0.424 by 1.15, resulting in a corrected  $n_f$  of 0.488 (*i.e.*,  $1.15 \times 0.424 = 0.488$ ). The values for  $T$  and  $v_s$  then were corrected based on the  $n_f$  of 0.488 and the resulting corrected data were reanalyzed. The original (uncorrected) results are shown in Figure 5.36, whereas the corrected results based on  $n_f$  of 0.488 are shown in Figure 5.37, and both sets of results are summarized in Table 5.8. The resulting  $CMR$  regression and  $T - CMR$  analysis of the corrected data provide an  $R_d$  for  $\text{Cl}^-$  of unity, as expected. Therefore, the subsequent discussion for Test No. 2 will consider only the results based on the corrected  $n_f$  of 0.488 in Figure 5.37.

Given the aforementioned considerations, several conclusions can be drawn from the results shown in Figures 5.35 – 5.45 and summarized in Table 5.8. First, in all cases,  $r^2$  from the  $CMR$  regression was higher than  $r^2$  from the  $RC$  regression, reflecting better model fits to the measured  $CMR$  data. This difference in  $r^2$  resulted because (a) analysis of the  $RC$  data plotted at

the middle of the sampling interval represents an approximation (Shackelford 1994a), and (b) the cumulative nature of the *CMR* data results in less scatter in the data (Shackelford 1995b).

Second,  $R_d$  from the *RC* regression was  $\leq R_d$  from the *CMR* regression ( $R_{d,RC} \leq R_{d,CMR}$ ) for the majority of analyses for  $\text{Cl}^-$ ,  $\text{K}^+$  and  $\text{Zn}^{2+}$  (16/22 = 73 %), although the differences between  $R_d$  generally were minor ( $\leq 0.212$  for  $\text{Cl}^-$ ,  $\leq 0.300$  for  $\text{K}^+$ , and  $\leq 0.790$  for  $\text{Zn}^{2+}$ ). The cases with greater differences can be attributed to not establishing steady-state transport ( $\text{Zn}^{2+}$  for Test No. 4), or diffusion significant transport  $\text{Cl}^-$  of  $P_L \leq 4.51$  for the zeolite-amended backfills permeated with the mixture of 17.5 mM  $\text{KCl}$  plus 10 mM  $\text{ZnCl}_2$  (Test Nos. 5 and 8). The  $R_d$  from *RC* regressions slightly greater ( $\leq 0.080$  for  $\text{Cl}^-$  and  $\leq 0.800$  for  $\text{K}^+$ ) than  $R_d$  from *CMR* regressions ( $R_{d,RC} \geq R_{d,CMR}$ ) for six analyses ( $\text{Cl}^-$  for Test Nos. 3, 4, 6, and  $\text{K}^+$  for Test Nos. 6, 9, 10) can be attributed, in part, to the error in the *RC* regressions resulting from plotting the measured values of *RC* at the middle of the sampling interval,  $\Delta T$ , and the use of  $\Delta T$  ranging from 0.25 (Test No. 4, when the plunger displacement cycle was changed from 5 d to 4 d, section 5.3.4) to 0.33 (Test Nos. 3, 5, 6, 8, 9, 10) that were greater than the maximum  $\Delta T$  of 0.25 recommended by Shackelford (1994a).

Third,  $R_d$  from the *CMR* regression generally was identical to two significant figures with  $R_d$  from the *T – CMR* analysis, which reflects establishment of steady-state transport conditions for the majority of the tests. For the limited cases where this observation is not valid, the column tests were either terminated prior to the establishment of steady-state transport ( $\text{K}^+$  for Test Nos. 6, 10,  $\text{Zn}^{2+}$  for Test No. 4) or subjected to diffusion significant transport ( $P_L \leq 4.51$  for  $\text{Cl}^-$  for Test Nos. 5, 8, 9, 10).

Fourth, for the vast majority of the analyses,  $R_d$  from the  $T_o$  analysis (*i.e.*,  $R_d = T_o = R_{d,T_o}$ ) were  $\leq R_d$  from the *T – CMR* analysis ( $R_d = (T - \text{CMR})_{ss} = R_{d,T - \text{CMR}}$ ). Lower  $R_{d,T_o}$  than  $R_{d,T - \text{CMR}}$

likely reflects inadvertent inclusion of some transient stage effluent data, *i.e.*, based on the criterion for establishing the steady state data of  $r^2 \geq 0.9995$  for the linear fit to the *CMR* data. In the few cases where  $R_{d,T_0} > R_{d,T-CMR}$  (Cl<sup>-</sup> for Test Nos. 9 and 10), the lowest flow rate was imposed (see Table 5.3, section 5.2.3), such that the effluent was collected only every 20 d, allowing only three samples to be analyzed every 60 d. As a consequence, the resulting deviation in measured concentration (see Table F.1) may have been affected by the limited number of *CMR* data in the linear portion for the  $T_0$  and  $T - CMR$  analyses.

Fifth, for all analyses of Cl<sup>-</sup>, the values of  $T_{0.5}$  were less than unity ( $T_{0.5} < 1$ ). Values of  $T_{0.5}$  less than unity for nonadsorbing solutes (tracers) such as Cl<sup>-</sup> have been attributed to two effects, *i.e.*, effective porosity and diffusion-dominated transport (Shackelford 1993). However, as previously noted, the *CMR* method distinguishes between these two effects, such that  $R_d$  for tracers based on the value of  $T - CMR$  at steady state (*i.e.*,  $R_d = (T - CMR)_{ss}$ ) represents the effective porosity ratio,  $n_e/n$ , separate from any effect due to diffusion (Shackelford 1995b). Since  $R_d (= (T - CMR)_{ss})$  was unity for all tests,  $n_e$  was the same as the final, total porosity,  $n_f$ , that was used to determine the values of  $T$  (Shackelford 1995b). Thus, values of  $T_{0.5}$  for Cl<sup>-</sup> less than unity likely reflect diffusion-dominated transport (Shackelford 1994a). This observation is supported by the regressed values of  $P_L (\leq 9.26)$  for Cl<sup>-</sup>. As noted by Shackelford (1994a), diffusion becomes significant for  $P_L \leq 20$ , and becomes dominant for  $P_L \leq 5$ . The majority of the values of  $D$  ( $16/20 = 80\%$ ) for Cl<sup>-</sup> were lower than  $D_o$  for KCl ( $= 1.99 \times 10^{-9} \text{ m}^2/\text{s}$ ) and ZnCl<sub>2</sub> ( $= 1.25 \times 10^{-9} \text{ m}^2/\text{s}$ ) (Chapter 4), suggesting negligible mechanical dispersion. The four cases where  $D$  for Cl<sup>-</sup> were greater than  $D_o$  (*RC* and *CMR* regressions for Test No. 4, *CMR* regression for Test Nos. 5 and 8), suggest that some mechanical dispersion may have contributed to the transport of Cl<sup>-</sup> (*i.e.*,  $D_m \neq 0$ ).

Sixth, all  $T_{0.5}$  for  $K^+$  and  $Zn^{2+}$  were lower than  $R_d$  from the *RC* regression and the various *CMR* methods of analysis (*i.e.*, *CMR* regression,  $T_o$ ,  $T - CMR$ ). As in the case of  $Cl^-$ , the regressed values of  $P_L$  for  $K^+$  or  $Zn^{2+}$  were  $< 20$  for the majority of the *RC* and *CMR* analyses ( $16/24 = 67\%$ ) and  $< 5$  for some of these analyses ( $5/24 = 21\%$ ). Thus, in these analyses, diffusion was a significant, if not dominant, transport process for  $K^+$  and  $Zn^{2+}$ . Regressed values of  $P_L$  for  $K^+$  and/or  $Zn^{2+} > 20$  were obtained for Test Nos. 5 and 8 (except for the *CMR* regression for  $K^+$  for Test No. 8) and for the *CMR* regression for Test No. 9. However, since  $D$  is inversely proportional to  $P_L$ , the back-calculated values of  $D$  in these cases were all  $\leq 2.10 \times 10^{-10}$   $m^2/s$ . These values of  $D$  less than  $D_o$  for  $KCl$  of  $1.99 \times 10^{-9}$   $m^2/s$  and  $ZnCl_2$  of  $1.25 \times 10^{-9}$   $m^2/s$  suggest that diffusion was the dominant transport process in these cases (Shackelford 1994a). Similarly, all of the  $D$  for  $K^+$  from *RC* and *CMR* regressions of effluent data for columns permeated with 35 mM  $KCl$  (Test Nos. 1, 3, 6, 9, 10) were lower than  $D_o$  for  $KCl$  of  $1.99 \times 10^{-9}$   $m^2/s$ , whereas the majority of the  $D$  ( $4/6 = 67\%$ ) for  $Zn^{2+}$  from *RC* and *CMR* regressions of effluent data from columns permeated with 20 mM  $ZnCl_2$  (Test Nos. 2, 4, 7) were lower than  $D_o$  for  $ZnCl_2$  of  $1.25 \times 10^{-9}$   $m^2/s$ . Thus, diffusion likely was the dominant transport process for  $K^+$  and  $Zn^{2+}$  in these tests (*i.e.*,  $D_m = 0$ ).

In summary, the results from the *CMR* regression are considered the most reliable for the following reasons. First, the column tests were performed in accordance with the cumulative mass approach, such that all of the effluent was collected and analyzed for all of the solute mass exiting the column specimens. The values of  $r^2$  for the *CMR* regressions were consistently higher than those for the *RC* regressions, because (a) the *CMR* data were correctly plotted at the end of the sampling interval, and (b) the cumulative nature of the *CMR* data reduces the scatter in the data relative to that for the *RC* data (Shackelford 1995b). Second, most of the  $R_d$  from the  $T -$

*CMR* analysis generally provided essentially the same  $R_d$  as the *CMR* regression, which support the accuracy of the *CMR* regression. The few analyses where the  $R_d$  from the  $T - CMR$  analysis, which are based on the establishment of steady-state transport, were different than those based on the *CMR* regression can be attributed to not fully establishing steady-state transport conditions in these tests. Finally, the results from the  $T_o$  and  $T_{0.5}$  analyses were considered less reliable due to the apparent inclusion of some transient transport data, and the inability to separate the effects of diffusion versus retardation, respectively. Based on the aforementioned considerations, the transport parameters ( $R_d$ ,  $P_L$  and  $D$ ) based on the *CMR* regression are used for comparison hereafter, as these results were considered to be the most accurate.

### 5.3.5 Linearity of Adsorption

The primary assumption made in the aforementioned analyses was that the values of  $R_d$  for the adsorbing solutes ( $K^+$  and  $Zn^{2+}$ ) determined from the column test data reflected linear adsorption. According to the experimental data of adsorption with different soil-to-solution (soil:solution) ratios reviewed by Roy *et al.* (1992), for lower soil:solution ratios, *i.e.*, greater amount of sorbent relative to the amount of solution, most of the solute will be adsorbed. Manassero *et al.* (1998) also analyzed BEAT results based on the Freundlich adsorption model and soil:solution ratios ranging from 1:4 to 1:0.75 and extrapolated to 1:0.333. They showed that the Freundlich exponent,  $N_f$  (Eq. 3.5), was approximately 0.8 (*i.e.*, the adsorption behavior approached linearity) for soil:solution ratios of 1:0.286 to 1:0.333 (Figure 5.48a). For the column tests conducted in this study, the soil:solution ratios based on  $w_f$  (*i.e.*,  $w_f^{-1}$ ) ranged from 1:0.30 (3.33:1) to 1:0.27 (3.70:1). Thus, the high soil:solution ratios ( $w_f^{-1}$ ) for the column tests of this study tend to support the assumption of linear adsorption behavior.

In order to further evaluate this assumption of linear adsorption, values of the distribution coefficient,  $K_d$ , were back-calculated from the various  $R_d$  derived from different analyses of the column test results assuming linear adsorption (*i.e.*,  $K_d = n_f (R_d - 1)/\rho_{d,f}$ , where  $n_f$  and  $\rho_{d,f}$  were the final, measured values for each column test). Also,  $K_d$  from the BEAT data previously reported in Chapter 3 and the resulting  $R_d$  (*i.e.*,  $R_d = 1 + \rho_{d,f}K_d/n_f$ ) were calculated. The  $R_d$  and  $K_d$  based on the column test and BEAT data are summarized in Table 5.9. The secant  $K_d$  for a maximum equilibrium concentration corresponding to the source concentration,  $C_o$ , for  $K^+$  or  $Zn^{2+}$ , can be determined based on the Langmuir (Eq. 3.2) and Freundlich (Eq. 3.5) adsorption model equations as follows (Freeze and Cherry 1979; Shackelford 1993; Hong *et al.* 2016):

$$K_d = \frac{C_{s,o}}{C_o} = \frac{Q_L K_L}{1 + K_L C_o} \quad (5.8)$$

$$K_d = \frac{C_{s,o}}{C_o} = K_f C_o^{N_f - 1} \quad (5.9)$$

where  $C_{s,o}$  is the adsorbed concentration corresponding to the equilibrium concentration of  $C_o$ ,  $K_L$  and  $Q_L$  are the regressed values for the Langmuir adsorption model (Table 3.2), and  $K_f$  and  $N_f$  are the regressed values for the Freundlich adsorption model (Table 3.2).

The values of  $R_d$  and  $K_d$  from the column tests are compared with those from the BEAT results based on method of analysis (*i.e.*,  $RC$  and  $CMR$  regression,  $T_o$ ,  $T - CMR$ ) in Figure 5.49, type of solute ( $K^+$  and  $Zn^{2+}$ ) in Figure 5.50, and type of solution (*i.e.*, 35 mM  $KCl$ , 20 mM  $ZnCl_2$ , 17.5 mM  $KCl$  plus 10 mM  $ZnCl_2$ ) in Figures 5.51 and 5.52. The  $R_d$  based on the column tests ( $RC$  and  $CMR$  regression) relative to that based on the BEAT results (Langmuir and Freundlich model),  $R_{d,Column}/R_{d,BEAT}$ , was in the range  $0.75 < R_{d,Column}/R_{d,BEAT} < 1.5$  for  $K^+$  (Figures 5.50a,b),

and  $1.0 < R_{d,Column}/R_{d,BEAT} < 2.0$  for  $Zn^{2+}$  (Figures 5.50c,d). For  $K^+$ ,  $R_{d,Column}/R_{d,BEAT} \geq 1.0$  for 57 % (8/14) of the column tests involving KCl (*i.e.*, 35 mM KCl and 17.5 mM KCl plus 10 mM  $ZnCl_2$ ) (Test Nos. 1, 3, 5, 6, 8, 9, 10), whereas for  $Zn^{2+}$ ,  $R_{d,Column} \geq R_{d,BEAT}$  for 100 % (10/10) of the column tests regarding  $ZnCl_2$  (*i.e.*, 20 mM  $ZnCl_2$  and 17.5 mM KCl plus 10 mM  $ZnCl_2$ ) (Test Nos. 2, 4, 5, 7, 8). Thus, in the majority of cases (18/24 = 75%), the  $R_{d,BEAT}$  underestimated the  $R_{d,Column}$ . One possible reason for  $R_{d,Column} \geq R_{d,BEAT}$  is the flushing of excess soluble cations from the pore water of the backfill specimens due to permeation of the backfill specimens with DIW prior to permeating with the salt solution, which reduced the relative competition between the soluble cations and the migrating  $K^+$  and/or  $Zn^{2+}$  for the available exchange sites on the backfill constituent materials (bentonite and zeolite). For example, Reynolds *et al.* (1982) showed that  $K_d$  based on BEATs were lower than  $K_d$  based on column tests due to removal of competing metals during permeation with water to establish steady-state flow prior to the start of the column tests. However, for the column tests involving permeation with the mixed salt solution (Test Nos. 5 and 8),  $R_{d,Column} < R_{d,BEAT}$  for  $K^+$ , whereas  $R_{d,Column} > R_{d,BEAT}$  for  $Zn^{2+}$ , such that the adsorption of  $K^+$  was affected by the existence of  $Zn^{2+}$ , which is discussed in section 5.4.5.

Finally, predicted breakthrough curves (BTCs) were compared with the measured BTCs, where the predicted BTCs were generated using the  $R_d$  obtained from the BEAT results ( $R_{d,BEAT}$ ) (Table 5.9) and the regressed  $P_L$  from the column tests (Table 5.8), so as to focus the comparison on the effect of adsorption relative to the effect of diffusion and/or dispersion. The results of these comparisons are shown in Figures F.1 – F.10. The poor fit for Test No. 4 (Figure F.4) is likely due to the uncharacteristic dispersion associated with  $Zn^{2+}$  migration for this column test ( $D \geq 23.7 \times 10^{-10} \text{ m}^2/\text{s}$ ). An  $R_d$  based on the predicted BTC,  $R_{d,predicted}$ , that is less than the actual, measured  $R_d$ ,  $R_{d,measured}$ , or  $R_{d,predicted} < R_{d,measured}$ , indicates that the predicted behavior is

conservative. The use of  $R_d$  based on the BEATs resulted in similar or conservative transport behavior in 64 % (= 9/14) of the column tests for  $K^+$  (*i.e.*, 35 mM KCl and 17.5 mM KCl plus 10 mM  $ZnCl_2$ ) (Test Nos. 1, 3, 5, 6, 8, 9, 10), and in 90 % (= 9/10) of the column tests for  $Zn^{2+}$  (*i.e.*, 20 mM  $ZnCl_2$  and 17.5 mM KCl plus 10 mM  $ZnCl_2$ ) (Test Nos. 2, 4, 5, 7, 8). As  $R_{d,predicted}$  was calculated based on the nonlinear (concave) adsorption models (Freundlich and Langmuir),  $R_{d,predicted} \leq R_{d,measured}$  for 75 % (= 18/24) of the column test analyses supports the assumption of linear adsorption behavior.

## 5.4 DISCUSSION

### 5.4.1 Effect of Type of Zeolite on Cl<sup>-</sup> and K<sup>+</sup> Migration

The effect of type of zeolite amendment on the migration of Cl<sup>-</sup> and K<sup>+</sup> through the unamended backfill (Test No. 1) and backfills amended with 5 % chabazite-UB (Test No. 3) or 5 % clinoptilolite (Test No. 6) is illustrated in Figure 5.53. The closeness in the superimposed breakthrough curves for Cl<sup>-</sup> (Figures 5.53a,b) suggests excellent reproducibility of the tests.

The migration of K<sup>+</sup> (Figures 5.53c,d) through the backfills amended with 5 % chabazite-UB or 5 % clinoptilolite was retarded to a greater extent relative to the unamended backfill. The  $R_d$  for K<sup>+</sup> was 13.0 for the backfill amended with 5 % chabazite-UB, 9.77 for the backfill amended with 5 % clinoptilolite, and 4.01 for the unamended backfill, such that the  $R_d$  for the zeolite-amended backfill relative to  $R_d$  for the unamended backfill, or  $R_{d,amended}/R_{d,unamended}$ , for K<sup>+</sup> was 3.2 for the backfill amended with 5 % chabazite-UB and 2.4 for the backfill amended with 5 % clinoptilolite (Figures 5.54a,b; Table 5.8). These differences in  $R_d$  correlate reasonably well with the *CEC* of the backfills (Figure 5.54c), supporting the previous conclusion that the primary mechanism for K<sup>+</sup> sorption to the backfills was cation exchange (Chapter 3).

The  $P_L$  and  $D$  for the three backfills are compared in Figures 5.55a,c and 5.55b,d, respectively. The  $P_L$  of 3.92 and 2.70 for  $\text{Cl}^-$  for the backfills amended with 5 % chabazite-UB or 5 % clinoptilolite were lower than the  $P_L$  of 6.56 for  $\text{Cl}^-$  for the unamended backfill (Figure 5.55a, Table 5.8). Since  $D$  is inversely proportional to  $P_L$ , dispersion associated with  $\text{Cl}^-$  migration through the backfills amended with 5 % chabazite-UB or 5 % clinoptilolite was greater than that for the unamended backfill (Figure 5.55b). The exact reasons for the differences in  $P_L$  and  $D$  for  $\text{Cl}^-$  are unknown. However, one possibility is that the addition of the zeolite amendment made the migration pathways at the pore scale more tortuous, since mechanical dispersion at the microscopic or pore scale has been attributed to variations in the pore sizes and pore interconnectivity (*e.g.*, Shackelford 1993). Since the zeolites are primarily fine-grained particles (Chapter 2), replacement of 5 % sand with an equal amount of either zeolite likely resulted in a slight variation in the pore structures of the backfills amended with 5 % chabazite-UB or 5 % clinoptilolite relative to the unamended backfill, which could have increased  $D$  of the backfills amended with 5 % chabazite-UB or 5 % clinoptilolite relative to that for the unamended backfill. However, the overall differences in  $P_L$  and  $D$  for  $\text{Cl}^-$  are less than a factor of 10.

The  $P_L$  for  $\text{K}^+$  for the backfill amended with 5 % chabazite-UB was 11.2, which is 2.5 times that of 4.47 for the unamended backfill, whereas the  $P_L$  of 4.28 for the backfill amended with 5 % clinoptilolite was almost identical to that for the unamended backfill (Figure 5.55c, Table 5.8). The reason the dispersion associated with  $\text{K}^+$  migration through the backfills amended with 5 % chabazite-UB is not greater than that associated with  $\text{K}^+$  migration through the unamended backfill is unknown.

The  $D$  for  $\text{Cl}^-$  relative to the  $D$  for  $\text{K}^+$  ( $D_{\text{Cl}^-}/D_{\text{K}^+}$ ) was 0.68 for the unamended backfill, 2.9 for the backfill amended with 5 % chabazite-UB, and 1.6 for the backfill amended with 5 %

clinoptilolite. Thus,  $\text{Cl}^-$  dispersion was greater than  $\text{K}^+$  dispersion in the backfills amended with 5 % chabazite-UB or 5 % clinoptilolite, whereas the opposite was true for the unamended backfill. These differences can be attributed, in part, to the more tortuous pore network and greater sorption capacity of the zeolite-amended backfills relative to the unamended backfill.

#### 5.4.2 Effect of Type of Zeolite on $\text{Cl}^-$ and $\text{Zn}^{2+}$ Migration

The effect of type of zeolite amendment on the migration of  $\text{Cl}^-$  and  $\text{Zn}^{2+}$  through the unamended backfill (Test No. 2) and the backfills amended with 5 % chabazite-UB (Test No. 4) or 5 % clinoptilolite (Test No. 7) is illustrated in Figure 5.56. As in the case for the tests conducted with  $\text{KCl}$ , the similarity in the superimposed breakthrough curves for  $\text{Cl}^-$  for columns permeated with  $\text{ZnCl}_2$  (Figure 5.56a,b) suggests excellent reproducibility of the test specimens.

The migration of  $\text{Zn}^{2+}$  (Figure 5.56c,d) through the backfills amended with 5 % chabazite-UB or 5 % clinoptilolite was retarded to a significantly greater extent relative to the unamended backfill. The  $R_d$  for  $\text{Zn}^{2+}$  was 15.0 for the backfill amended with 5 % chabazite-UB, 9.67 for the backfill amended with 5 % clinoptilolite, and 6.88 for the unamended backfill, such that  $R_{d,\text{amended}}/R_{d,\text{unamended}}$  for  $\text{Zn}^{2+}$  was 2.2 for the backfill amended with 5 % chabazite-UB and 1.4 for the backfill amended with 5 % clinoptilolite (Figures 5.57a,b; Table 5.8). These differences in  $R_d$  correlate reasonably well with the  $\text{CEC}$  of the backfills (Figure 5.57c), again supporting the previous conclusion that the primary mechanism for  $\text{Zn}^{2+}$  sorption to the backfills was cation exchange (Chapter 3).

The  $P_L$  and  $D$  for the three backfills are compared in Figures 5.58a,c and 5.58b,d, respectively. The  $P_L$  of 2.09 and 4.29 for  $\text{Cl}^-$  for the backfills amended with 5 % chabazite-UB and 5 % clinoptilolite, respectively, were lower than the  $P_L$  of 8.37 for  $\text{Cl}^-$  for the unamended

backfill (Figure 5.58a, Table 5.8). Thus, similar to the column tests involving 35 mM KCl (Figure 5.55b), the dispersion associated with Cl<sup>-</sup> migration through the zeolite-amended backfills was greater than that through the unamended backfill (Figure 5.58b). As previously mentioned, the differences in  $P_L$  and  $D$  for Cl<sup>-</sup> may be due to the addition of the fine-grained zeolites. However, the overall differences in  $P_L$  and  $D$  for Cl<sup>-</sup> for the unamended and zeolite-amended backfills were less than a factor of 10.

The  $P_L$  for Zn<sup>2+</sup> for the backfill amended with 5 % chabazite-UB was 1.54, which is 0.16 times that of 9.93 for the unamended backfill, whereas the  $P_L$  of 10.9 for the backfill amended with 5 % clinoptilolite was almost identical to that for the unamended backfill (Figure 5.58c, Table 5.8). The uncharacteristically low  $P_L$  for the backfill amended with 5 % chabazite-UB (Test No. 4) is related to the significant dispersion ( $D \geq 23.7 \times 10^{-10} \text{ m}^2/\text{s}$ ) associated with the Zn<sup>2+</sup> migration through this backfill evident in Figure 5.39a.

The  $D$  for Cl<sup>-</sup> relative to that for Zn<sup>2+</sup> ( $D_{\text{Cl}^-}/D_{\text{Zn}^{2+}}$ ) was 1.2 for the unamended backfill versus 0.74 and 2.5 for the backfills amended with 5 % chabazite-UB and 5 % clinoptilolite, respectively. The atypically low  $D_{\text{Cl}^-}/D_{\text{Zn}^{2+}}$  for the backfill amended with 5 % chabazite-UB (Test No. 4) is directly attributable to the significant dispersion for Zn<sup>2+</sup> migration shown in Figure 5.39a.

#### 5.4.3 Effect of Amount of Zeolite

The effect of amount of zeolite amendment on the migration of Cl<sup>-</sup> and K<sup>+</sup> through the unamended backfill (Test No. 1) and the backfills amended with 5 or 10 % chabazite-LB (Test Nos. 9 and 10, respectively) is illustrated in Figure 5.59. The superimposed breakthrough curves for Cl<sup>-</sup> in terms of elapsed time do not agree (Figure 5.59a), since the backfills amended with 5

or 10 % chabazite-LB were permeated at a significantly lower flow rate relative to that for the unamended backfill (see Table 5.3, section 5.2.3). However, when the effect of the flow rate is removed and the breakthrough curves for  $\text{Cl}^-$  are plotted in terms of dimensionless time ( $T$ ), excellent reproducibility of the test specimens is indicated (Figure 5.59b).

The  $R_d$  for  $\text{K}^+$  was 4.01 for the unamended backfill, 9.60 for the backfill amended with 5 % chabazite-LB, and 18.9 for the backfill amended with 10 % chabazite-LB, such that  $R_{d,\text{amended}}/R_{d,\text{unamended}}$  for  $\text{K}^+$  was 2.4 for the backfill amended with 5 % chabazite-LB and 4.7 for the backfill amended with 10 % chabazite-LB (Figures 5.60a,b; Table 5.8). These differences in  $R_d$  correlate reasonably well with the  $\text{CEC}$  of the backfills (Figure 5.60c), again supporting the previous conclusion that the primary mechanism for  $\text{K}^+$  sorption to the backfills was cation exchange (Chapter 3).

The  $P_L$  and  $D$  for  $\text{Cl}^-$  and  $\text{K}^+$  are shown in Figures 5.61a,c and 5.61b,d, respectively. In terms of  $\text{Cl}^-$ , the  $P_L$  and  $D$  for both zeolite-amended backfills are lower and higher, respectively than the values for the unamended backfills, whereas the opposite is true in the case of  $\text{K}^+$ . As previously mentioned, the differences in  $P_L$  and  $D$  for  $\text{Cl}^-$  may be due to the addition of the fine-grained zeolites. Nonetheless, the overall differences in  $P_L$  and  $D$  are less than a factor of 10. The  $D_{\text{Cl}^-}/D_{\text{K}^+}$  was 0.68 for the unamended backfill, 29 for the backfill amended with 5 % chabazite-LB, and 9.9 for the backfill amended with 10 % chabazite-LB. These differences can be attributed, again, to the more tortuous pore network and greater sorption capacity of the zeolite-amended backfills relative to the unamended backfill.

#### 5.4.4 Effect of Type of Metal

The migration of 35 mM KCl (Test No. 1) and 20 mM ZnCl<sub>2</sub> (Test No. 2) through the unamended backfill are illustrated in Figure 5.62. The closeness in the superimposed breakthrough curves for Cl<sup>-</sup> suggests excellent reproducibility of the test specimens (Figures 5.62a,b). In terms of migration, Zn<sup>2+</sup> was retarded to a greater extent than K<sup>+</sup> (Figures 5.62c,d). For Cl<sup>-</sup>,  $P_L$  for KCl was less than  $P_L$  for ZnCl<sub>2</sub>, such that  $D$  for KCl was greater than  $D$  for ZnCl<sub>2</sub> (Figures 5.63a,b). The  $R_d$  for migration of 35 mM KCl (Test No. 1) and 20 mM ZnCl<sub>2</sub> (Test No. 2) through the unamended backfill was 4.01 for K<sup>+</sup>, and 6.88 for Zn<sup>2+</sup>, which is 1.7 times that for K<sup>+</sup> (Figure 5.63c, Table 5.8). The differences in  $K_d$  based on the column test results somewhat correlate with the  $Q_L$  based on the BEAT results for each metal (Figure 5.63d). The  $P_L$  and  $D$  for K<sup>+</sup> and Zn<sup>2+</sup> are compared in Figures 5.63e and 5.63f, respectively. The value of  $D_{Cl^-}/D_{K^+}$  was 0.68 whereas  $D_{Cl^-}/D_{Zn^{2+}}$  was 1.2.

The migrations of 35 mM KCl (Test No. 3) and 20 mM ZnCl<sub>2</sub> (Test No. 4) through the backfills amended with 5 % chabazite-UB are illustrated in Figure 5.64. The closeness in the superimposed breakthrough curves for Cl<sup>-</sup> suggests excellent reproducibility of the test specimens (Figures 5.64a,b). In terms of migration, Zn<sup>2+</sup> was retarded to a greater extent than K<sup>+</sup> (Figures 5.64c,d), which is the same trend for the unamended backfill. For Cl<sup>-</sup>,  $P_L$  for KCl was greater than  $P_L$  for ZnCl<sub>2</sub>, such that  $D$  for KCl was greater than  $D$  for ZnCl<sub>2</sub> (Figures 5.65a,b), which is the opposite trend for the unamended backfill. The  $R_d$  for migration of 35 mM KCl (Test No. 3) and 20 mM ZnCl<sub>2</sub> (Test No. 4) through the backfills amended with 5 % chabazite-UB backfill was 13.0 for K<sup>+</sup>, and 15.0 for Zn<sup>2+</sup>, which is 1.2 times that for K<sup>+</sup> (Figures 5.65c, Table 5.8). The differences in  $K_d$  based on the column test results correlate with the  $Q_L$  based on the BEAT results for each metal (Figure 5.65d). The  $P_L$  and  $D$  for the backfill amended with 5 %

chabazite-UB for  $K^+$  and  $Zn^{2+}$  are compared in Figures 5.65e and 5.65f, respectively. The value of  $D_{Cl^-}/D_{K^+}$  was 2.9, whereas  $D_{Cl^-}/D_{Zn^{2+}}$  was 0.74.

The migrations of 35 mM KCl (Test No. 6) and 20 mM  $ZnCl_2$  (Test No. 7) through the backfills amended with 5 % clinoptilolite are illustrated in Figure 5.66. The closeness in the superimposed breakthrough curves for  $Cl^-$  suggests excellent reproducibility of the test specimens (Figures 5.66a,b). Unlike the unamended backfill and backfill amended with 5 % chabazite-UB, the migration of  $Zn^{2+}$  was retarded to a slightly lesser extent than  $K^+$  for the backfills amended with 5 % clinoptilolite (Figures 5.66c,d). For  $Cl^-$ ,  $P_L$  for KCl was less than  $P_L$  for  $ZnCl_2$ , such that  $D$  for KCl was greater than  $D$  for  $ZnCl_2$ , which is the same trend for the unamended backfill (Figures 5.67a,b). The  $R_d$  for migration of 35 mM KCl (Test No. 6) and 20 mM  $ZnCl_2$  (Test No. 7) through the backfill amended with 5 % clinoptilolite backfill was 9.77 for  $K^+$ , and 9.67 for  $Zn^{2+}$ , which is 0.99 times that for  $K^+$  (Figures 5.67c, Table 5.8). The differences in  $K_d$  based on the column test results again correlate with the  $Q_L$  based on the BEAT results for each metal (Figure 5.67d). The  $P_L$  and  $D$  for the backfills amended with 5 % clinoptilolite for  $K^+$  and  $Zn^{2+}$  are compared in Figures 5.67e and 5.67f, respectively. The  $D_{Cl^-}/D_{K^+}$  was 1.6, whereas  $D_{Cl^-}/D_{Zn^{2+}}$  was 2.5.

In summary, the dispersion of  $Cl^-$  associated with KCl migration was greater than that associated with  $ZnCl_2$  migration for the unamended backfill and the backfill amended with 5 % clinoptilolite, whereas the opposite trend occurred for the backfill amended with 5 % chabazite-UB. The  $R_d$  of  $Zn^{2+}$  relative to that for  $K^+$  ( $R_{d,Zn^{2+}}/R_{d,K^+}$ ) was 1.7 for the unamended backfill, 1.2 for the backfill amended with 5 % chabazite-UB, and 0.99 for the backfill amended with 5 % clinoptilolite. The differences in  $K_d$  correlated reasonably with the  $Q_L$  for each metal based on previously performed BEATs. The  $D_{Cl^-}/D_{K^+} < D_{Cl^-}/D_{Zn^{2+}}$  for the unamended backfill and

backfill amended with 5 % clinoptilolite, whereas  $D_{Cl^-}/D_{K^+} > D_{Cl^-}/D_{Zn^{2+}}$  for the backfill amended with 5 % chabazite-UB.

#### 5.4.5 Effect of Cation Competition

The effect of metals competition was evaluated for the backfills amended with 5 % chabazite-UB or 5 % clinoptilolite when permeated with the mixed salt solution (*i.e.*, 17.5 mM KCl plus 10 mM ZnCl<sub>2</sub>) by comparing the transport parameters for K<sup>+</sup> and Zn<sup>2+</sup> (Figures 5.68 – 5.69) with the previously discussed results for the same backfills permeated with the single salt solutions (*i.e.*, 35 mM KCl or 20 mM ZnCl<sub>2</sub>).

For the backfill amended with 5 % chabazite-UB and permeated with the mixed salt solution, the  $R_d$  was 14.1 for K<sup>+</sup>, and 13.6 for Zn<sup>2+</sup>. In contrast, the  $R_d$  based on permeation with the single salt solutions was 13.0 for K<sup>+</sup>, and 15.0 for Zn<sup>2+</sup>. Thus, the  $R_d$  for K<sup>+</sup> increased whereas the  $R_d$  for Zn<sup>2+</sup> decreased when permeated with the mixed salt solution compared to when permeated with the single salt solution. Also, the  $R_d$  for Zn<sup>2+</sup> relative to that for K<sup>+</sup>,  $R_{d,Zn^{2+}}/R_{d,K^+}$ , was 0.96 when permeated with the mixed salt solution and 1.2 when permeated with the single salt solution (Figures 5.64c,d, 5.65c, 5.68a). Thus, the competition between K<sup>+</sup> and Zn<sup>2+</sup> in the mixed salt solution apparently reflected the preferential adsorption of K<sup>+</sup> relative to Zn<sup>2+</sup> compared to when permeated with the single salt solution.

The  $R_d$  based on the *CMR* regression relative to the  $R_d$  based on the *BEATs* for the Langmuir and Freundlich model, or  $R_{d,CMR}/R_{d,BEAT}$ , for the backfill amended with 5 % chabazite-UB was 1.1 and 1.3, respectively, for K<sup>+</sup> (Test No. 3) and 1.8 and 1.9<sup>+</sup>, respectively, for Zn<sup>2+</sup> (Test No. 4) when permeated with the single salt solutions. These values of  $R_{d,CMR}/R_{d,BEAT} > 1$  support the assumption that the influence of competing soluble salts associated with the backfill

in the BEATs were flushed out in the column tests (Reynolds *et al.* 1982). Also,  $R_{d,CMR}/R_{d,BEAT}$  for  $Zn^{2+}$  greater than those for  $K^+$  suggests that removal of competing soluble salts (mainly  $Na^+$ ) associated with the backfill resulted in increased adsorption for  $Zn^{2+}$ , as indicated in Chapter 3.

The  $R_{d,CMR}/R_{d,BEAT}$  of the backfill amended with 5 % chabazite-UB when permeated with the mixed salt solution (Test No. 5) was 0.76 and 0.90 for  $K^+$ , and 1.2 and 1.5 for  $Zn^{2+}$ , such that the values of  $R_{d,CMR}/R_{d,BEAT}$  for  $K^+$  and  $Zn^{2+}$  when permeated with the mixed salt solution were lower than that when permeated with the single salt solution. As the removal of competing soluble salts associated with the backfill is equivalent for all column tests, this lower value of  $R_{d,CMR}/R_{d,BEAT}$  when permeated with the mixed salt solution compared to when permeated with the single salt solution indicate that competition existed between the added  $K^+$  and  $Zn^{2+}$  in the mixed salt solution.

The  $P_L$  for the backfill amended with 5 % chabazite-UB was 11.2 for  $K^+$  and 1.54 for  $Zn^{2+}$  when permeated with the single salt solution, whereas the  $P_L$  was 36.1 for  $K^+$  and 29.5 for  $Zn^{2+}$  when permeated with the mixed salt solution (Figure 5.68c, Table 5.8). Thus, the  $P_L$  for both  $K^+$  and  $Zn^{2+}$  increased when permeated with the mixed salt solution compared to when permeated with the single salt solution. Also, the  $P_L$  for  $Zn^{2+}$  relative to the  $P_L$  for  $K^+$ , or  $P_{L,K^+}/P_{L,Zn^{2+}}$ , was 7.3 for the single salt solution and 1.2 for the mixed salt solution, in that the difference between  $P_L$  for  $K^+$  versus that for  $Zn^{2+}$  was diminished when the mixed salt solution was used as the permeant liquid relative to use of the single salt solutions.

For the backfill amended with 5 % clinoptilolite and permeated with the mixed salt solution, the  $R_d$  was 10.3 for  $K^+$ , and 14.1 for  $Zn^{2+}$ . In contrast, the  $R_d$  based on permeation with the single salt solutions was 9.77 for  $K^+$ , and 9.67 for  $Zn^{2+}$ . Thus, the  $R_d$  for  $K^+$  and  $Zn^{2+}$  increased when permeated with the mixed salt solution compared to when permeated with the

single salt solution. The  $R_{d,Zn^{2+}}/R_{d,K^+}$  was 0.99 when permeated with the mixed salt solution and 1.4 when permeated with the single salt solution (Figures 5.66c,d, 5.67c, 5.68a). Thus, the competition between  $K^+$  and  $Zn^{2+}$  in the mixed salt solution apparently reflected the preferential adsorption of  $K^+$  relative to  $Zn^{2+}$  compared to when permeated with the single salt solution.

The  $R_{d,CMR}/R_{d,BEAT}$  for the backfill amended with 5 % clinoptilolite was 1.0 and 1.2 for  $K^+$  (Test No. 6) and 1.3 and 1.4 for  $Zn^{2+}$  (Test No. 7) when permeated with the single salt solution. The  $R_{d,CMR}/R_{d,BEAT}$  of the backfill amended with 5 % clinoptilolite when permeated with the mixed salt solution (Test No. 8) was 0.95 and 0.97 for  $K^+$ , and 1.5 and 2.0 for  $Zn^{2+}$ , such that the values of  $R_{d,CMR}/R_{d,BEAT}$  decreased for  $K^+$  but increased for  $Zn^{2+}$  when permeated with the mixed salt solution compared to when permeated with the single salt solution. Again, as the removal of competing soluble salts associated with the backfill is equivalent for all column tests, these values of  $R_{d,CMR}/R_{d,BEAT}$  when permeated with the mixed salt solution compared to when permeated with the single salt solution indicate that the competition between the added  $K^+$  and  $Zn^{2+}$  in the mixed salt solution resulted in reduced adsorption for  $K^+$  and increased adsorption for  $Zn^{2+}$ .

The  $P_L$  for the backfill amended with 5 % clinoptilolite was 4.28 for  $K^+$  and 10.9 for  $Zn^{2+}$  when permeated with the single salt solution, whereas the  $P_L$  was 13.1 for  $K^+$  and 22.7 for  $Zn^{2+}$  when permeated with the mixed salt solution (Figure 5.69c, Table 5.8). Thus, the  $P_L$  for both  $K^+$  and  $Zn^{2+}$  increased when permeated with the mixed salt solution compared to when permeated with the single salt solution. Also,  $P_{L,K^+}/P_{L,Zn^{2+}}$  was 0.39 for the single salt solution and 0.58 for the mixed salt solution, in that the difference between  $P_L$  for  $K^+$  versus that for  $Zn^{2+}$  reduced, or  $P_{L,K^+}/P_{L,Zn^{2+}}$  approached unity, when the mixed salt solution was used as the permeant liquid relative to use of the single salt solutions.

In summary, for the backfills amended with 5 % chabazite-UB or 5 % clinoptilolite, the  $R_{d,Zn^{2+}}/R_{d,K^+}$  when permeated with the mixed salt solution was lower than when permeated with the single salt solution, indicating that the competition between  $K^+$  and  $Zn^{2+}$  in the mixed salt solution apparently reflected the preferential adsorption of  $K^+$  relative to  $Zn^{2+}$  compared to when permeated with the single salt solution. For the backfill amended with 5 % chabazite-UB,  $R_{d,CMR}/R_{d,BEAT}$  for  $K^+$  and  $Zn^{2+}$  when permeated with the mixed salt solution were lower than that when permeated with the single salt solution, whereas for the backfill amended with 5 % clinoptilolite,  $R_{d,CMR}/R_{d,BEAT}$  decreased for  $K^+$  but increased for  $Zn^{2+}$  when permeated with the mixed salt solution compared to when permeated with the single salt solution. The  $P_{L,K^+}/P_{L,Zn^{2+}}$  approached unity for the mixed salt solution compared to when permeated with the single salt solution, indicating that the difference between  $P_L$  for  $K^+$  versus that for  $Zn^{2+}$  reduced when the mixed salt solution was used as the permeant liquid relative to use of the single salt solutions.

## 5.5 SUMMARY AND CONCLUSIONS

Long-term column tests were performed with specimens comprising unamended and zeolite-amended sand-bentonite (SB) backfills permeated with single salt solutions of either 35 mM KCl or 20 mM ZnCl<sub>2</sub> and a mixed salt solution of 17.5 mM KCl plus 10 mM ZnCl<sub>2</sub>. The pH of the 20 mM ZnCl<sub>2</sub> solution was adjusted with a small amount of HCl to 1.83 to remove visible precipitation in the form of zinc oxychloride and to simulate the pH of acid mine drainage. The backfills comprised fine mortar sand, 5.8 % (by dry weight) of a powdered sodium bentonite, and 0, 5, or 10 % (by dry weight) of one of three types of zeolite, viz., chabazite-LB, chabazite-UB, or clinoptilolite, with the backfill water content adjusted to achieve the target slump of 100 to 150 mm (3.9 to 5.9 in) for each backfill. The backfill column specimens were

prepared in flexible-wall permeameters and permeated with de-ionized water (DIW) prior to permeation with the single or mixed salt solutions using flow-pump systems that maintain a constant volumetric flow rate ( $q$ ). The test duration for the 10 column tests ranged from 1.05 to 3.75 yr. Each column test specimen was evaluated for both physical properties and  $k$ , and the effluent chemistry was monitored and analyzed for chemical transport parameters of chloride (Cl<sup>-</sup>), K, and Zn.

The final porosity ( $n_f$ ) of the specimens upon completion of the column tests was lower than that upon installation ( $n_i$ ), and the final shapes of the specimens were somewhat similar to that of an hourglass. The  $n_i < n_f$  resulted from consolidation of the specimen from an effective stress,  $\sigma'$ , of 34.5 kPa (5 psi) following back-pressure saturation to an  $\sigma'$  of 138 kPa (20 psi) prior to permeation. Therefore,  $n_f$  was considered to be more representative of the porosity of the specimens, such that analyses of the effluent concentrations were based on  $n_f$ .

The  $k$  based on permeation with a salt solution ( $k_{sol}$ ) was greater than that based on permeation with DIW ( $k_{DIW}$ ) for 70 % (7/10) of the column specimens. However, the increase in  $k_{sol}$  relative to  $k_{DIW}$  was relatively minor, *i.e.*,  $1.06 \leq k_{sol}/k_{DIW} \leq 1.94$ , and all resulting values of  $k_{sol}$  were  $< 1.0 \times 10^{-9}$  m/s. The small measure of incompatibility and low  $k_{sol}$  values were attributed to the dilute salt concentrations of the permeant liquids and the relatively high  $\sigma'$  of 138 kPa (20 psi) imposed on the specimens prior to permeation.

The elution/breakthrough of the primary chemical species in the effluent were in the general order  $\text{Na}^+ > \text{Cl}^- > \text{Ca}^{2+} \geq \text{K}^+ \text{ or } \text{Zn}^{2+}$ . The delayed breakthrough of  $\text{K}^+$  and  $\text{Zn}^{2+}$  was attributed primarily to preferential cation exchange of  $\text{K}^+$  and  $\text{Zn}^{2+}$  relative to exchangeable  $\text{Na}^+$  and/or  $\text{Ca}^{2+}$  initially bound to the exchange sites of the bentonite and zeolite components of the backfills. The charge balance was assessed by comparing the absolute value of the summation of

anion equivalents relative to the summation of cation equivalents (*i.e.*,  $|\sum \text{anions}| = \sum \text{cations}$ ) in the effluents from the column specimens. The resulting charge balances generally showed good agreement for all column tests. The final measured *EC* of the effluent approached the value for the permeant solution ( $EC_o$ ) except for the low pH (1.83), 20 mM ZnCl<sub>2</sub> solution, where the buffering capacity of the backfill specimens reduced the contribution of H<sup>+</sup> to the *EC* of the effluent resulting in a slight increase in the effluent pH ( $2.80 \leq \text{pH} \leq 3.74$ ). As a result, dissolution of the minerals comprising the backfill constituents was unlikely (pH > 2), but the pH was still sufficiently low to prevent precipitation in the form of zinc oxychlorides and minimize the formation of hydroxide complexes of Zn (*e.g.*, ZnOH<sup>+</sup>).

The transport parameters ( $R_d$ ,  $P_L$  and  $D$ ) for Cl<sup>-</sup>, K<sup>+</sup> and Zn<sup>2+</sup> were determined based on analysis of the measured effluent breakthrough curves in the form of either relative concentrations (*RCs*) or cumulative mass ratios (*CMRs*). The methods of analysis based on the *RC* approach included regressing the measured *RC* data using an analytical model based on the advection-dispersion-reaction equation (ADRE) governing one-dimensional solute transport through saturated porous media under steady-state flow conditions together with appropriate initial and boundary conditions (*i.e.*, *RC* regression) and the dimensionless time required to achieve  $RC = 0.5$  (*i.e.*,  $T_{0.5}$ ). The methods of analysis based on the *CMR* data included regressing the data using an analytical model based on the same ADRE and initial and boundary conditions as imposed for the *RC* analytical model (*i.e.*, *CMR* regression), and two alternative methods based on the *CMR* data referred to as the  $T_o$  and  $T - CMR$  methods of analysis. Overall, the results from the *CMR* regression were considered the most reliable for two reasons. First, the column tests were performed in accordance with the cumulative mass approach, such that the *CMR* data were more accurately represented relative to the *RC* data. Second, most of the  $R_d$  from

the  $T - CMR$  analysis generally provided essentially the same  $R_d$  as the  $CMR$  regression, thereby providing consistent results. Also, the  $T_o$  and  $T_{0.5}$  analyses were considered less reliable due to issues related to the inclusion of some transient transport data in the  $T_o$  analysis, which is based on the assumption of steady-state transport, and the inability to separate the effects of diffusion versus retardation in the  $T_{0.5}$  analysis. Therefore, the transport parameters ( $R_d$ ,  $P_L$  and  $D$ ) based on the  $CMR$  regression method of analysis were used for comparison of results.

The  $R_d$  for the zeolite-amended backfill relative to  $R_d$  for the unamended backfill, or  $R_{d,amended}/R_{d,unamended}$ , for  $K^+$  was 3.2 for the backfill amended with 5 % chabazite-UB and 2.4 for the backfill amended with 5 % clinoptilolite. For  $Zn^{2+}$ , the  $R_{d,amended}/R_{d,unamended}$  was 2.2 for the backfill amended with 5 % chabazite-UB and 1.4 for the backfill amended with 5 % clinoptilolite. In terms of amount of added zeolite, the  $R_{d,amended}/R_{d,unamended}$  for  $K^+$  was 2.4 for the backfill amended with 5 % chabazite-LB and 4.7 for the backfill amended with 10 % chabazite-LB. These differences in  $R_d$  correlated reasonably well with the  $CEC$  of the backfills, supporting the previous conclusion that the primary mechanism for  $K^+$  and  $Zn^{2+}$  sorption to the backfills was cation exchange, in that the zeolite amendment with higher  $CEC$  zeolite (chabazite > clinoptilolite) or increased amounts of high  $CEC$  zeolite (10 % > 5 %) resulted in higher  $R_d$  for the backfill. Thus, the zeolite-amended backfills evaluated in this study were effective in enhancing the retardation of the two metals, K and Zn, evaluated in this study.

In terms of different types of metal (K vs Zn), the  $R_d$  of  $Zn^{2+}$  relative to that for  $K^+$  ( $R_{d,Zn^{2+}}/R_{d,K^+}$ ) was 1.7 for the unamended backfill, 1.2 for the backfill amended with 5 % chabazite-UB, and 0.99 for the backfill amended with 5 % clinoptilolite. For the backfills amended with 5 % chabazite-UB or 5 % clinoptilolite permeated with the mixed salt solution, the  $R_{d,Zn^{2+}}/R_{d,K^+}$  was lower than when the backfills were permeated with the single salt solution,

indicating that the competition between  $K^+$  and  $Zn^{2+}$  in the mixed salt solution apparently reflected the preferential adsorption of  $K^+$  relative to  $Zn^{2+}$  compared to when permeated with the single salt solution. Also, for the backfill amended with 5 % chabazite-UB,  $R_{d,CMR}/R_{d,BEAT}$  for both  $K^+$  and  $Zn^{2+}$  for permeation with the mixed salt solution were lower than that for permeation with the single salt solution, whereas for the backfill amended with 5 % clinoptilolite,  $R_{d,CMR}/R_{d,BEAT}$  decreased for  $K^+$  but increased for  $Zn^{2+}$  for permeation with the mixed salt solution relative to permeation with the single salt solution. Thus, the relative adsorption of  $K^+$  and  $Zn^{2+}$  for permeation with either the single salt solution or the mixed salt solution differed for different types of zeolite amendment.

Table 5.1. Source chemical properties of the permeant liquids used for column testing.

Permeant Liquid	Source pH, $\text{pH}_o$	Source Electrical Conductivity, $EC_o$ (mS/m)	Source Ionic Strength, $I_o$ (mM) <sup>a</sup>
Deionized Water (DIW)	6.91	0.046	NA
35 mM KCl	5.92	496	35
20 mM ZnCl <sub>2</sub>	1.83	715	60
17.5 mM KCl + 10 mM ZnCl <sub>2</sub>	4.85	462	47.5

<sup>a</sup>  $I_o$  (mM) =  $\frac{1}{2} \sum C_i z_i^2$ , where  $C_i$  is the molar concentration of the  $i$ th ion, and  $z_i$  is the charge of the  $i$ th ion.

Table 5.2. Estimated electrical conductivity of typical groundwater.

Element	Charge, $z$	Concentration, $C$ (mM) <sup>a</sup>		$Cz^2$ (mM)		
		Min	Max	Min	Max	Solver <sup>b</sup>
Ca	+2	0.025	3.743	0.100	14.971	4.852
K	+1	0.026	0.256	0.026	0.256	0.026
Mg	+2	0.041	2.057	0.165	8.229	1.513
Na	+1	0.022	5.220	0.022	5.220	1.279
Fe	+2	0.000	0.179	0.001	–	–
	+3	0.000	0.179	–	1.612	–
Cl	–1	0.028	1.974	0.028	1.974	1.974
NO <sub>3</sub>	–1	0.003	0.323	0.003	0.323	0.323
SO <sub>4</sub>	–2	0.031	1.561	0.125	6.246	5.869
F	–1	0.005	0.263	0.005	0.263	-
Sr	+2	0.001	0.046	0.005	0.183	-
Ionic Strength, $I$ (mM) <sup>c</sup>				0.346	25.205	10.314
Electrical Conductivity, $EC$ (mS/m) <sup>d</sup>				5.09	200.82	83.57
Electroneutrality <sup>e</sup>				0.300	42.023	0.000

<sup>a</sup> Sparks (2003).

<sup>b</sup> For Na<sup>+</sup>, K<sup>+</sup>, Ca<sup>2+</sup>, Mg<sup>2+</sup>, Cl<sup>-</sup>, SO<sub>4</sub><sup>2-</sup>, NO<sub>3</sub><sup>-</sup>, used Excel solver to achieve electroneutrality of zero.

<sup>c</sup> Ionic Strength,  $I$  (mM) =  $\frac{1}{2} \sum C_i z_i^2$

<sup>d</sup> Griffin and Jurinak (1973):  $EC$  (mS/m) =  $[I$  (mM) + 0.3]/0.127

<sup>e</sup> Electroneutrality =  $\sum$  anion +  $\sum$  cation

Table 5.3. Test condition summary for column testing.

Test No.	Zeolite Amendment		Source Solution	Plunger (Piston) Displacement Rate, $r_p$ (mm/h)	Volumetric Flow Rate, $q$ (mL/d) <sup>a</sup>
	Type	Amount (%)			
1	NA <sup>b</sup>	0	35 mM KCl	1.04	7.86
2	NA <sup>b</sup>	0	20 mM ZnCl <sub>2</sub>	1.06	8.00
3	Chabazite-UB	5	35 mM KCl	1.06	8.00
4	Chabazite-UB	5	20 mM ZnCl <sub>2</sub>	1.05	7.91
5	Chabazite-UB	5	17.5 mM KCl + 10 mM ZnCl <sub>2</sub>	1.05	7.95
6	Clinoptilolite	5	35 mM KCl	1.07	8.05
7	Clinoptilolite	5	20 mM ZnCl <sub>2</sub>	1.06	8.01
8	Clinoptilolite	5	17.5 mM KCl + 10 mM ZnCl <sub>2</sub>	1.04	7.87
9	Chabazite-LB	5	35 mM KCl	0.27	2.06
10	Chabazite-LB	10	35 mM KCl	0.27	2.06

<sup>a</sup> 1 mL/d =  $1.16 \times 10^{-11}$  m<sup>3</sup>/s.

<sup>b</sup> NA = Not applicable (*i.e.*, unamended backfill).

Table 5.4. Physical properties of the column test specimens.

Test No.	Zeolite Amendment		Specific Gravity of Solids, $G_s$	Initial Column Specimen Properties			Final Column Specimen Properties					Test Duration, $t^a$ [d (yr)]
	Type	Amount (%)		Water Content, $w_i$ (%)	Porosity, $n_i$	Dry Density, $\rho_{d,i}$ (Mg/m <sup>3</sup> )	Water Content, $w_f$ (%)	Porosity, $n_f$	Dry Density, $\rho_{d,f}$ (Mg/m <sup>3</sup> )	Cross Section Area, $A_f$ ( $\times 10^{-3}$ m <sup>2</sup> )	Degree of Saturation, $S_f$ (%)	
1	NA <sup>b</sup>	0	2.69	40.7	0.540	1.24	29.6	0.437	1.51	3.26	102	385 (1.05)
2	NA <sup>b</sup>	0	2.69	40.8	0.530	1.26	28.9	0.424	1.55	3.22	105	500 (1.37)
3	Chabazite-UB	5	2.67	44.4	0.566	1.16	29.9	0.439	1.50	3.07	102	635 (2.74)
4	Chabazite-UB	5	2.67	42.3	0.530	1.26	30.3	0.447	1.48	3.33	100	750 (2.05)
5	Chabazite-UB	5	2.67	41.3	0.538	1.23	19.4 <sup>c</sup>	0.444	1.48	3.10	64.7 <sup>c</sup>	535 (1.47)
6	Clinoptilolite	5	2.67	38.3	0.525	1.27	27.3	0.420	1.55	3.23	101	635 (1.74)
7	Clinoptilolite	5	2.67	39.4	0.538	1.23	27.6	0.441	1.49	3.23	93.5	535 (1.47)
8	Clinoptilolite	5	2.67	39.4	0.525	1.27	27.8	0.437	1.50	3.19	95.7	545 (1.49)
9	Chabazite-LB <sup>d</sup>	5	2.67	39.3	0.533	1.25	27.1	0.433	1.52	3.31	95.0	1370 (3.75)
10	Chabazite-LB <sup>d</sup>	10	2.65	39.0	0.535	1.23	29.2	0.449	1.46	3.30	94.8	1370 (3.75)

<sup>a</sup> Total elapsed time from setup to breakdown of the specimen, including paused time due to minor experimental tasks.

<sup>b</sup> NA = Not applicable (*i.e.*, unamended backfill).

<sup>c</sup> Test was stopped due to leakage in the flow pump system, which resulted in lower  $w_f$  and  $S_f$ .

<sup>d</sup> Tested with a slower flow rate.

Table 5.5. Comparison of the chemical transport parameters corrected for the residual volume,  $V_{res}$ .

Test No.	Zeolite Amendment		Volumetric Flow Rate, $q$ (mL/d)	Replacement Time for the Residual Volume, $V_{res}$ (mL) <sup>a</sup>		Chemical Species	Retardation Factor, $R_d$						Péclet Number, $P_L$			
	Type	Amount (%)		d	$\Delta T$		$R_{d,uncorrected}$			$R_{d,corrected}$			$P_{L,uncorrected}$		$P_{L,corrected}$	
							RC	CMR	T-CMR	RC	CMR	T-CMR	RC	CMR	RC	CMR
1	NA <sup>b</sup>	0	7.86	1.348	0.0859	Cl <sup>-</sup>	1.03	0.993	1.00	0.962	0.963	1.00	10.1	15.4	8.09	7.18
						K <sup>+</sup>	3.96	4.04	4.05	3.88	3.95	3.96	5.75	5.02	5.45	4.77
9	Chabazite-LB <sup>c</sup>	5	2.06	5.170	0.0872	Cl <sup>-</sup>	0.961	1.03	1.03	0.979	1.02	1.00	2.06	1.11	1.20	0.757
						K <sup>+</sup>	9.90	9.68	9.61	9.82	9.60	9.54	18.9	22.2	18.6	21.8

<sup>a</sup>  $V_{res}/q$ , where  $V_{res} = V_{stone} (= 10.5 \text{ mL}) + V_{tube} (= 0.15 \text{ mL}) = 10.65 \text{ mL}$ .

<sup>b</sup> NA = Not applicable (*i.e.*, unamended backfill).

<sup>c</sup> Tested with a slower flow rate.

Table 5.6. Hydraulic properties of the column test specimens.

Test No.	Zeolite Amendment		Volumetric Flow Rate, $q$ (mL/d) <sup>a</sup>	Darcy Velocity, $v$ ( $\times 10^{-8}$ m/s) <sup>b</sup>	Permeant Liquid	Measured Values at Steady State			Duration		$EC_f$ (mS/m) <sup>e</sup>	$EC_f/EC_o$ <sup>f</sup>	$k_{sol,f}/k_{DIW,f}$ <sup>g</sup>
	Type	Amount (%)				Pressure Difference, $-\Delta u_{ss}$ (kPa, [psi])	Hydraulic Gradient, $i_{ss}$ <sup>c</sup>	Hydraulic Conductivity, $k$ ( $\times 10^{-10}$ m/s)	Time (d)	PVF <sup>d</sup>			
1	NA <sup>h</sup>	0	7.86	2.79	DIW	61 [8.8]	87	3.2	105	6.7	42.9	0.09	0.91
					35 mM KCl	66 [9.6]	95	2.9	385	17.5	501.0	1.01	
2	NA <sup>h</sup>	0	8.00	2.88	DIW	52 [7.6]	75	3.8	85	5.7	50.9	0.07	0.92
					20 mM ZnCl <sub>2</sub>	58 [8.4]	83	3.5	415	27.8	449.0	0.63	
3	Chabazite-UB	5	8.00	3.02	DIW	125 [18.1]	180	1.7	90	5.8	51.3	0.10	1.06
					35 mM KCl	117 [16.9]	167	1.8	545	35.3	523.0	1.05	
4	Chabazite-UB	5	7.91	2.75	DIW	114 [16.5]	163	1.9	105	6.6	85.7	0.12	1.47
					20 mM ZnCl <sub>2</sub>	70 [10.1]	100	2.8	645	40.2	441	0.62	
5	Chabazite-UB	5	7.95	2.97	DIW	58 [8.4]	83	3.6	85	5.4	133.84	0.29	1.94
					17.5 mM KCl + 10 mM ZnCl <sub>2</sub>	30 [4.3]	43	7.0	450	28.6	466.0	1.01	
6	Clinoptilolite	5	8.05	2.89	DIW	26 [3.7]	36	7.9	90	6.1	35.5	0.07	0.62
					35 mM KCl	41 [6.0]	59	4.9	545	37.1	526.0	1.06	
7	Clinoptilolite	5	8.01	2.87	DIW	66 [9.6]	95	3.0	50	3.1	105.8	0.15	1.47
					20 mM ZnCl <sub>2</sub>	46 [6.6]	65	4.4	500	32.2	442	0.62	
8	Clinoptilolite	5	7.87	2.85	DIW	79 [11.5]	114	2.5	85	5.4	77.1	0.17	1.44
					17.5 mM KCl + 10 mM ZnCl <sub>2</sub>	55 [8.0]	79	3.6	460	29.4	463.0	1.00	
9	Chabazite-LB	5	2.06	0.72	DIW	54 [7.8]	77	0.93	110	1.9	123.5	0.25	1.29
					35 mM KCl	41 [5.9]	59	1.2	1260	21.2	550.0	1.11	
10	Chabazite-LB	10	2.06	0.72	DIW	130 [18.8]	187	0.39	110	1.8	162.0	0.33	1.54
					35 mM KCl	83 [12.1]	120	0.62	1260	20.5	529.0	1.07	

<sup>a</sup> 1 mL/d =  $1.16 \times 10^{-11}$  m<sup>3</sup>/s; <sup>b</sup> Darcy velocity (liquid flux or specific discharge),  $v = q/A_f$  (Table 5.4); <sup>c</sup>  $i_{ss} = -\Delta u_{ss}/(L\rho_w g)$ , where  $L = 71$  mm = 0.071 m,  $\rho_w$  = density of water (1 Mg/m<sup>3</sup>), and  $g$  = acceleration due to gravity (9.81 m/s<sup>2</sup>); <sup>d</sup> PVF = pore volumes of flow; <sup>e</sup> Electrical conductivity,  $EC$ , at 25°C; <sup>f</sup>  $EC_o = EC$  of the salt solution (Table 5.1); <sup>g</sup> compatibility ratio,  $k_{sol}/k_{DIW}$ , where  $k_{sol}$  is the steady-state  $k$  when permeated with the salt solution (*i.e.*, 35 mM KCl, 20 mM ZnCl<sub>2</sub>, or 17.5 mM KCl + 10 mM ZnCl<sub>2</sub>); <sup>h</sup> NA = Not applicable (*i.e.*, unamended backfill).

Table 5.7. Evaluation of the measured pH of the column test effluents.

Test No.	Zeolite Amendment		Source Solution	pH <sup>a</sup>			
	Type	Amount (%)		pH <sub>DIW,f</sub>	pH <sub>DIW,f</sub> /pH <sub>DIW,o</sub>	pH <sub>sol,f</sub>	pH <sub>sol,f</sub> /pH <sub>sol,o</sub>
1	NA <sup>b</sup>	0	35 mM KCl	7.33	1.06	8.14	1.38
2	NA <sup>b</sup>	0	20 mM ZnCl <sub>2</sub>	7.89	1.14	2.80	1.53
3	Chabazite-UB	5	35 mM KCl	8.93	1.29	8.01	1.35
4	Chabazite-UB	5	20 mM ZnCl <sub>2</sub>	8.55	1.24	3.61	1.97
5	Chabazite-UB	5	17.5 mM KCl + 10 mM ZnCl <sub>2</sub>	9.17	1.33	6.31	1.30
6	Clinoptilolite	5	35 mM KCl	8.34	1.21	8.09	1.37
7	Clinoptilolite	5	20 mM ZnCl <sub>2</sub>	8.60	1.24	3.74	2.04
8	Clinoptilolite	5	17.5 mM KCl + 10 mM ZnCl <sub>2</sub>	8.73	1.26	6.55	1.35
9	Chabazite-LB	5	35 mM KCl	9.06	1.31	7.13	1.20
10	Chabazite-LB	10	35 mM KCl	9.24	1.34	7.05	1.19

<sup>a</sup> pH<sub>DIW,o</sub> is the pH of the DIW = 6.91; pH<sub>sol,o</sub> is the pH of the chemical solution (Table 5.1); pH<sub>DIW,f</sub> is the final measured pH for the DIW permeation stage; pH<sub>sol,i</sub> is the initial pH for the chemical solution permeation stage; pH<sub>sol,f</sub> is the final measured pH for the chemical solution permeation stage.

<sup>b</sup> NA = Not applicable (*i.e.*, unamended backfill)

Table 5.8. Chemical transport parameters of the column tested specimens of the unamended and zeolite-amended backfills.

Test No.	Zeolite Amendment		Seepage (Average Linear) Velocity, $v_s$ ( $\times 10^{-8}$ m/s) <sup>a</sup>	Source Solution	Chemical Species	Time to $C/C_o = 0.5$		Retardation Factor, $R_d$				Péclet Number, $P_L$		Dispersion Coefficient, $D$ ( $\times 10^{-10}$ m <sup>2</sup> /s) <sup>a</sup>	
	Type	Amount (%)				$T_{0.5}$	$t_{0.5}$ (d)	$RC$	$CMR$	$T_o$	$(T-CMR)_{ss}$	$RC$	$CMR$	$RC$	$CMR$
1	NA <sup>b</sup>	0	6.38	35 mM KCl	Cl <sup>-</sup>	0.905	14.2	1.01	1.01	0.954	1.00	6.54	6.56	6.93	6.91
					K <sup>+</sup>	3.25	51.0	3.93	4.01	3.96	4.02	5.23	4.47	8.66	10.1
2	NA <sup>b</sup>	0	6.78	20 mM ZnCl <sub>2</sub>	Cl <sup>-</sup>	0.979	14.7	1.13	1.15	1.18	1.15	9.46	8.33	5.09	5.78
					Zn <sup>2+</sup>	6.74	101	7.71	7.91	7.94	7.95	11.2	9.96	4.30	4.83
2 <sup>c</sup>	NA <sup>b,c</sup>	0	5.90	20 mM ZnCl <sub>2</sub>	Cl <sup>-</sup>	0.852	14.7	0.983	1.00	1.03	1.00	9.26	8.37	5.20	5.75
					Zn <sup>2+</sup>	5.87	101	6.71	6.88	6.92	6.91	11.2	9.93	4.30	4.85
3	Chabazite-UB	5	6.88	35 mM KCl	Cl <sup>-</sup>	0.836	13.2	1.02	1.01	0.924	1.00	4.14	3.92	11.8	12.5
					K <sup>+</sup>	11.8	183	12.9	13.0	13.0	13.0	12.6	11.2	3.88	4.36
4	Chabazite-UB	5	6.15	20 mM ZnCl <sub>2</sub>	Cl <sup>-</sup>	0.619	9.87	1.09	1.01	1.02	1.00	1.22	2.09	35.8	20.9
					Zn <sup>2+</sup>	11.2	178	14.4	15.0	12.8	12.8	1.84	1.54	23.7	28.4
5	Chabazite-UB	5	6.68	17.5 mM KCl + 10 mM ZnCl <sub>2</sub>	Cl <sup>-</sup>	0.580	9.17	0.753	0.965	0.658	1.00	4.35	0.726	10.9	65.3
					K <sup>+</sup>	13.4	211	14.1	14.1	14.1	14.1	38.9	36.1	1.22	1.31
					Zn <sup>2+</sup>	12.4	196	13.5	13.6	13.6	13.6	28.9	29.5	1.64	1.61
6	Clinoptilolite	5	6.88	35 mM KCl	Cl <sup>-</sup>	0.828	12.1	1.04	1.03	0.902	1.00	3.33	2.70	14.7	18.1
					K <sup>+</sup>	7.97	117	9.97	9.77	9.60	9.61	4.45	4.28	11.0	11.4
7	Clinoptilolite	5	6.52	20 mM ZnCl <sub>2</sub>	Cl <sup>-</sup>	0.773	13.3	0.932	1.00	0.900	1.00	8.47	4.29	5.47	10.8
					Zn <sup>2+</sup>	8.04	125	8.88	9.67	9.68	9.68	13.4	10.9	3.45	4.25
8	Clinoptilolite	5	6.53	17.5 mM KCl + 10 mM ZnCl <sub>2</sub>	Cl <sup>-</sup>	0.640	10.1	0.849	0.998	0.900	1.00	4.51	1.03	10.2	45.0
					K <sup>+</sup>	9.48	148	10.0	10.3	10.3	10.3	29.8	13.1	1.56	3.54
					Zn <sup>2+</sup>	12.8	201	13.8	14.1	14.0	14.0	22.1	22.7	2.10	2.04
9	Chabazite-LB <sup>d</sup>	5	1.66	35 mM KCl	Cl <sup>-</sup>	0.611	36.3	0.979	1.02	1.12	1.00	1.20	0.757	9.82	15.6
					K <sup>+</sup>	9.33	553	9.82	9.60	9.54	9.54	18.6	21.8	0.631	0.539
10	Chabazite-LB <sup>d</sup>	10	1.60	35 mM KCl	Cl <sup>-</sup>	0.488	30.0	0.947	1.01	1.22	1.00	2.05	1.21	5.54	9.39
					K <sup>+</sup>	18.5	1139	19.7	18.9	13.9	-	10.9	12.0	1.04	0.947

<sup>a</sup>  $D = v_s L / P_L$ , where  $L = 71$  mm.

<sup>b</sup> NA = Not applicable (*i.e.*, unamended backfill).

<sup>c</sup> Results based on adjusted values of  $T$  for revised final porosity,  $n_f$ , of 0.49.

<sup>d</sup> Tested with a slower flow rate.

Table 5.9. Comparison of the chemical transport parameters calculated from the batch equilibrium adsorption test (BEAT) with the chemical transport parameters of the column tested specimens of the unamended and zeolite-amended backfills.

Test No.	Zeolite Amendment		Chemical Species	$\rho_{d,f}/n_f$ (Mg/m <sup>3</sup> ) <sup>a</sup>	Adsorption Parameters from BEAT Results				Adsorption Parameters from Column Results							
	Type	Amount (%)			Distribution Coefficient, $K_d$ (L/kg) <sup>b</sup>		Retardation Factor, $R_d$ <sup>c</sup>		Retardation Factor, $R_d$ <sup>d</sup>				Distribution Coefficient, $K_d$ (L/kg) <sup>e</sup>			
					Langmuir	Freundlich	Langmuir	Freundlich	RC	CMR	$T_o$	T-CMR	RC	CMR	$T_o$	T-CMR
1	NA <sup>f</sup>	0	K <sup>+</sup>	3.43	0.48	0.48	2.65	2.65	3.93	4.01	3.96	4.02	0.85	0.88	0.86	0.88
2	NA <sup>f</sup>	0	Zn <sup>2+</sup>	3.52	1.63	1.80	6.74	7.34	7.71	7.91	7.94	7.95	1.91	1.96	1.97	1.97
2 <sup>g</sup>	NA <sup>f,g</sup>	0	Zn <sup>2+</sup>	3.18	1.63	1.80	6.18	6.72	6.71	6.88	6.92	6.91	1.80	1.85	1.86	1.86
3	Chabazite-UB	5	K <sup>+</sup>	3.41	3.22	2.70	12.0	10.2	12.9	13.0	13.0	13.0	3.49	3.52	3.52	3.52
4	Chabazite-UB	5	Zn <sup>2+</sup>	3.29	2.10	2.22	7.91	8.30	14.4	15.0	12.8	12.8	4.07	4.26	3.59	3.59
5	Chabazite-UB	5	K <sup>+</sup>	3.24	5.39	4.54	18.5	15.7	14.1	14.1	14.1	14.1	4.04	4.04	4.04	4.04
			Zn <sup>2+</sup>	3.24	2.42	3.23	8.85	11.5	13.5	13.6	13.6	13.6	3.85	3.88	3.88	3.88
6	Clinoptilolite	5	K <sup>+</sup>	3.69	2.28	2.02	9.41	8.45	9.97	9.77	9.60	9.61	2.43	2.38	2.33	2.33
7	Clinoptilolite	5	Zn <sup>2+</sup>	3.39	1.77	1.88	6.99	7.37	8.88	9.67	9.68	9.68	2.30	2.56	2.56	2.56
8	Clinoptilolite	5	K <sup>+</sup>	3.41	3.10	3.17	10.6	10.8	10.0	10.3	10.3	10.3	2.64	2.73	2.73	2.73
			Zn <sup>2+</sup>	3.41	2.02	2.75	6.89	9.38	13.8	14.1	14.0	14.0	3.75	3.84	3.81	3.81
9	Chabazite-LB <sup>h</sup>	5	K <sup>+</sup>	3.51	3.11	2.64	11.9	10.3	9.82	9.60	9.54	9.54	2.51	2.45	2.43	2.43
10	Chabazite-LB <sup>h</sup>	10	K <sup>+</sup>	3.25	5.20	4.15	17.9	14.5	19.7	18.9	13.9	-	5.75	5.51	3.97	-

<sup>a</sup>  $n_f$  is the final porosity, and  $\rho_{d,f}$  (Mg/m<sup>3</sup>) is the final dry density (Table 5.4).

<sup>b</sup> Based on secant formulation.

<sup>c</sup>  $R_d = 1 + (\rho_{d,f}/n_f)K_d$ .

<sup>d</sup> Based on regression analysis of column testing data, average of the  $R_d$  from RC, CMR, and (T-CMR).

<sup>e</sup>  $K_d = (R_d - 1)/(\rho_{d,f}/n_f)$ .

<sup>f</sup> NA = Not applicable (*i.e.*, unamended backfill).

<sup>g</sup> Results based on adjusted values of  $T$  for revised final porosity,  $n_f$ , of 0.488.

<sup>h</sup> Tested with a slower flow rate.

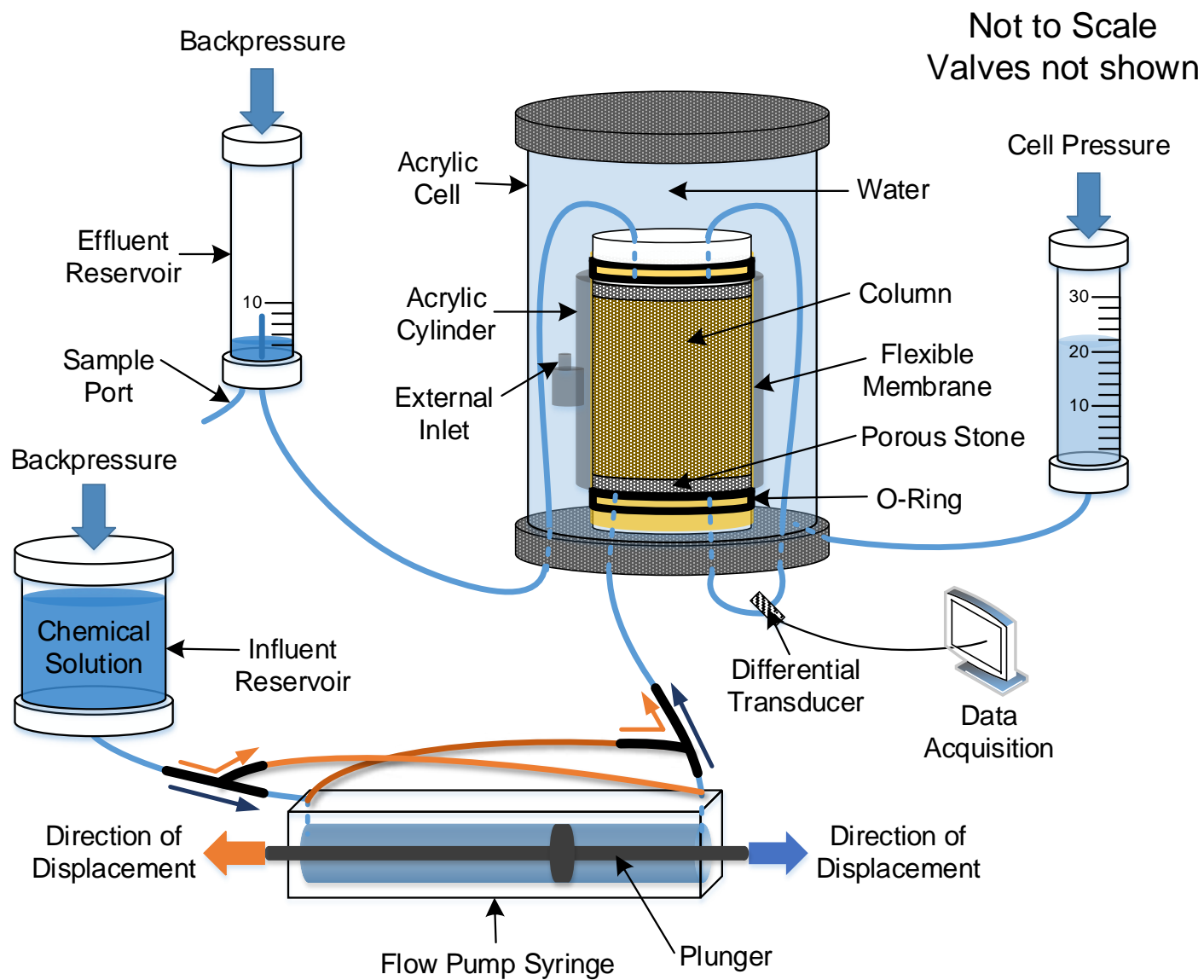


Figure 5.1. Schematic of testing apparatus.

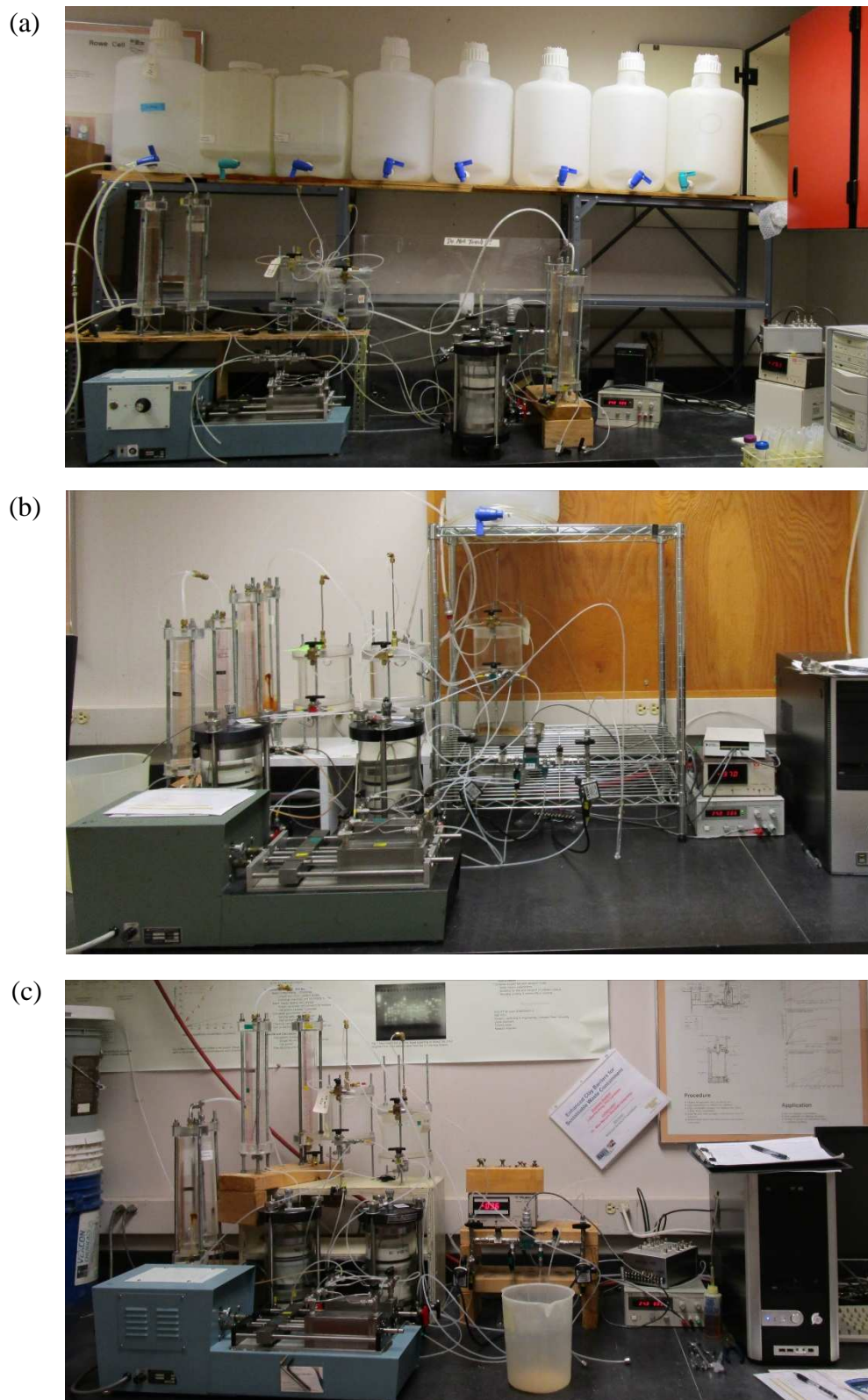


Figure 5.2. Pictorial views of (a) Apparatus No. 1 (Model 944); (b) Apparatus No. 2 (Model 940); (c) Apparatus No. 3 (Model 940).

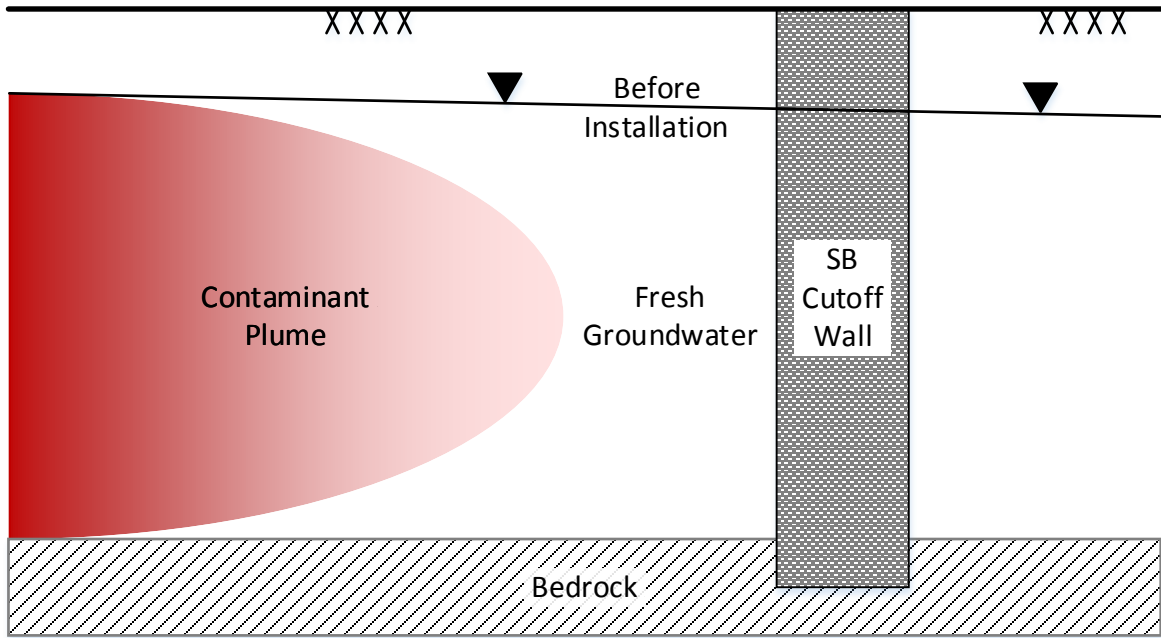


Figure 5.3. Schematic scenario for placement of soil-bentonite (SB) vertical cutoff wall down gradient from a migrating contaminant plume.

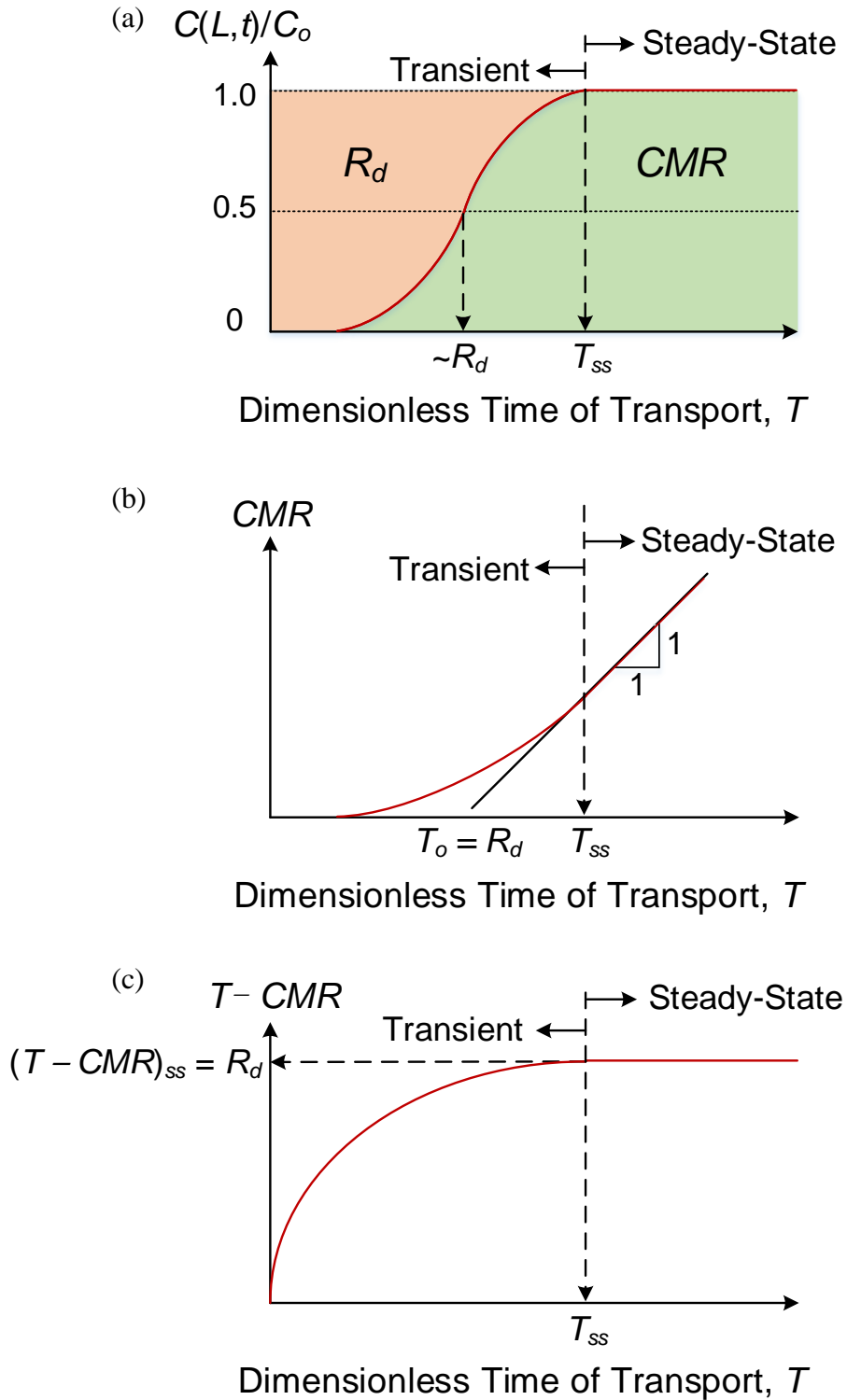


Figure 5.4. Comparison of the chemical analysis methods: (a) relative concentration ( $RC$ ); (b) cumulative mass ratio ( $CMR$ ) and the x-intercept from the  $CMR$ -to- $T$  plot; (c)  $T$ - $CMR$ .

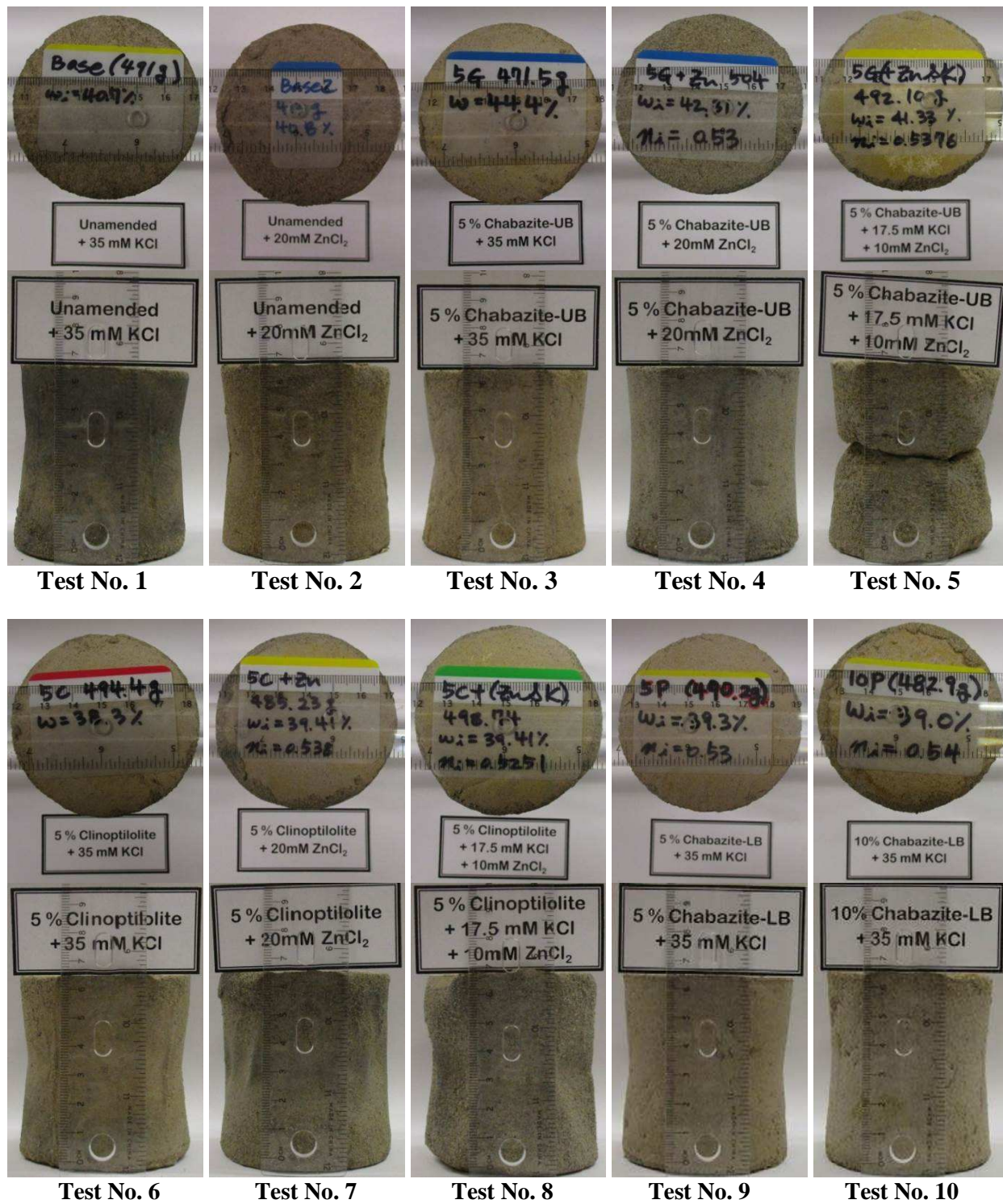


Figure 5.5. Pictorial view of the finished column test specimens.

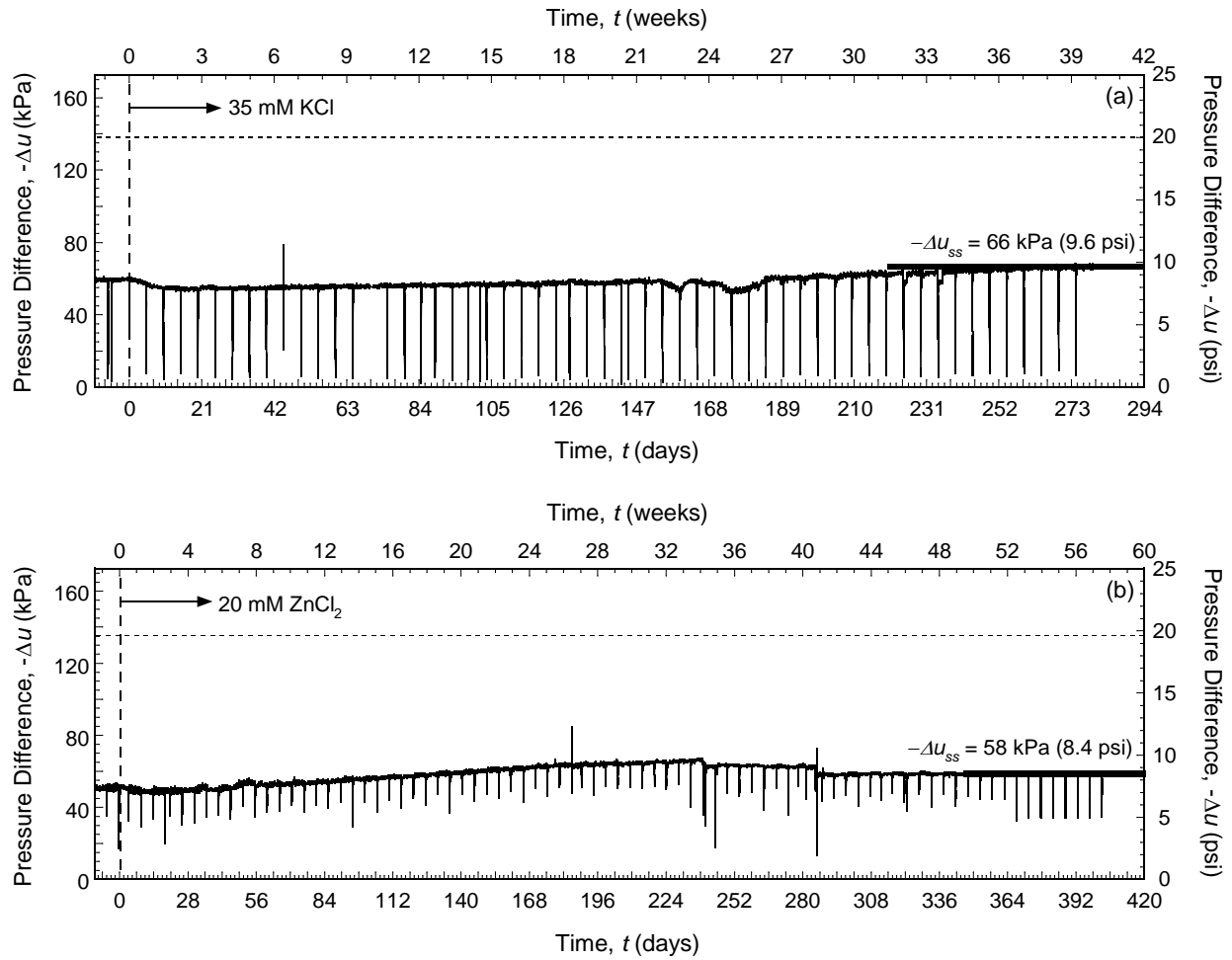


Figure 5.6. Temporal trends in pressure differences across columns of unamended backfills permeated with different salt solutions: (a) 35 mM KCl (Test No. 1); (b) 20 mM  $\text{ZnCl}_2$  (Test No. 2).

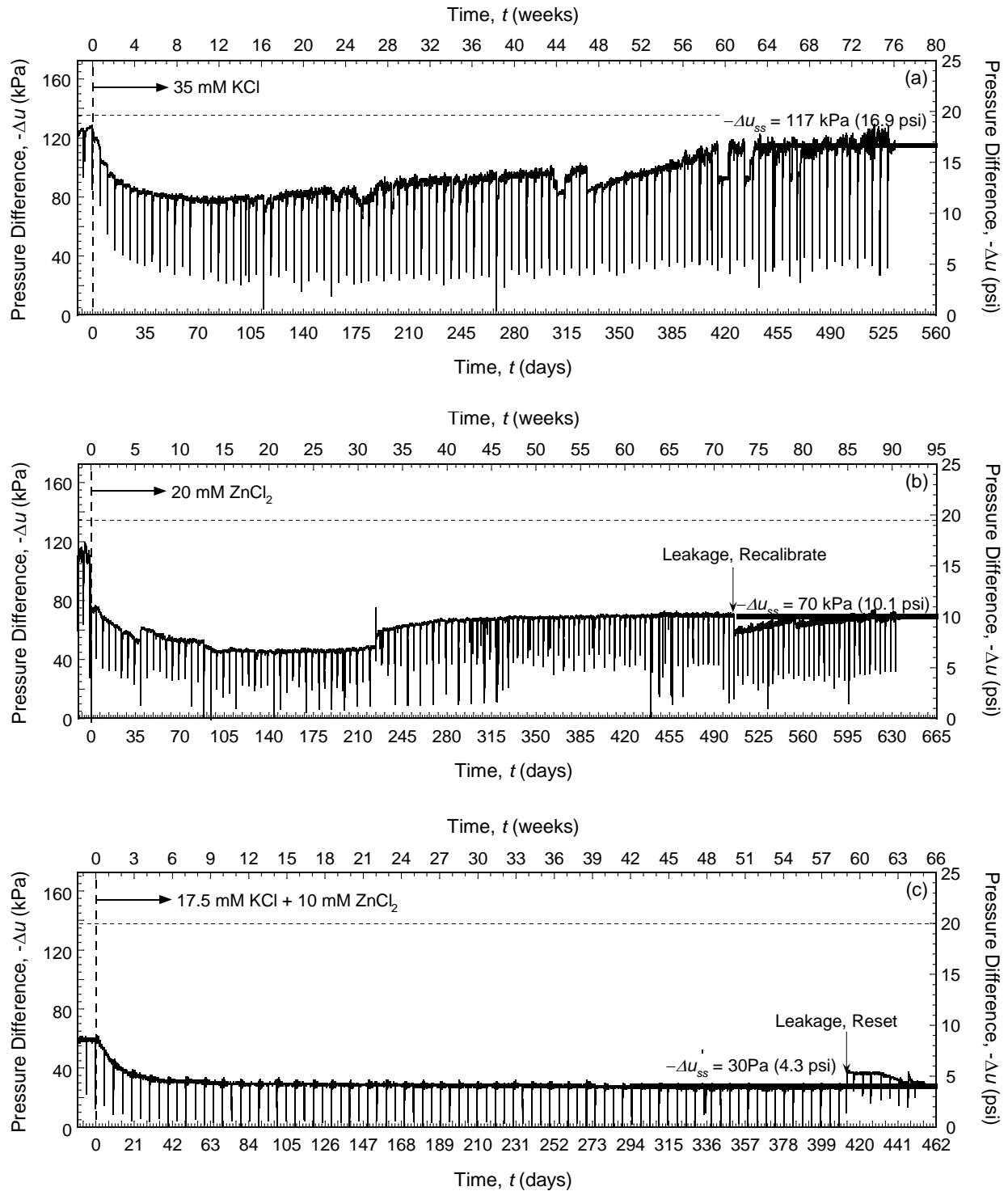


Figure 5.7. Temporal trends in pressure differences across columns of backfills amended with 5 % chabazite-UB and permeated with different salt solutions: (a) 35 mM KCl (Test No. 3); (b) 20 mM  $ZnCl_2$  (Test No. 4); (c) 17.5 mM KCl plus 10 mM  $ZnCl_2$  (Test No. 5).

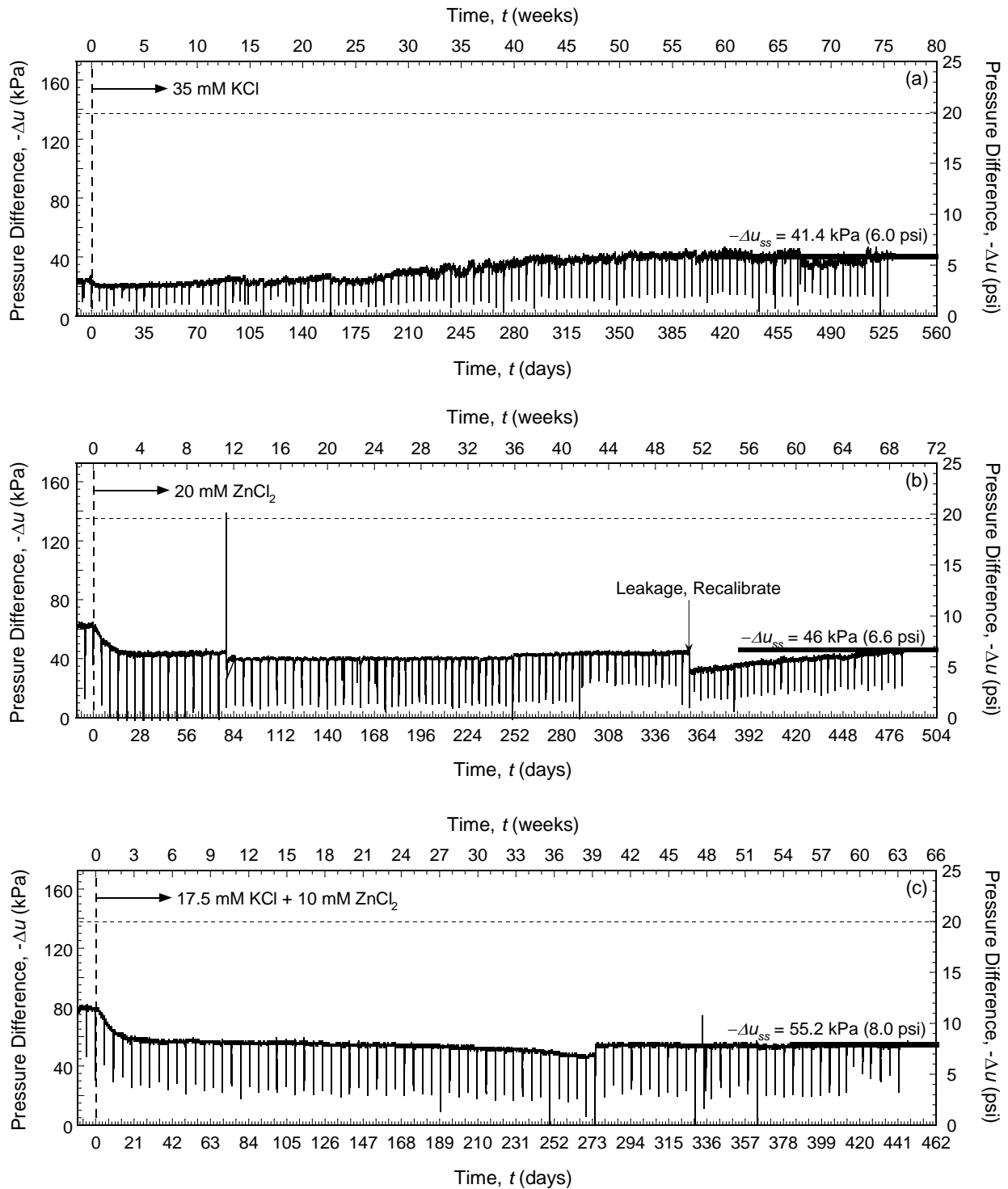


Figure 5.8. Temporal trends in pressure differences across columns of backfills amended with 5 % clinoptilolite and permeated with different salt solutions: (a) 35 mM KCl (Test No. 6); (b) 20 mM  $ZnCl_2$  (Test No. 7); (c) 17.5 mM KCl plus 10 mM  $ZnCl_2$  (Test No. 8).

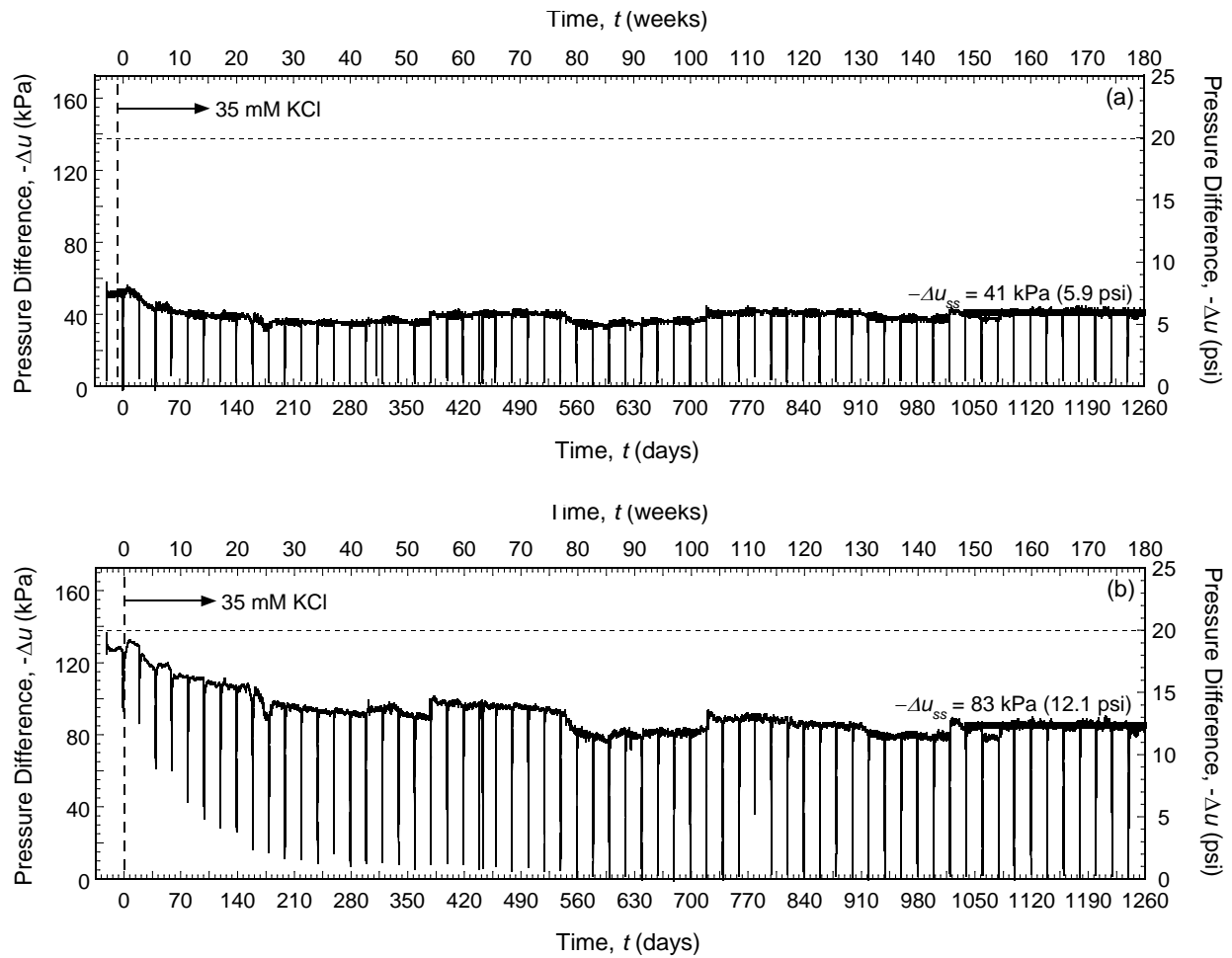


Figure 5.9. Temporal trends in pressure differences across columns of backfills amended with different amounts of chabazite-LB and permeated with a solution of 35 mM KCl: (a) 5 % chabazite-LB (Test No. 9); (b) 10 % chabazite-LB (Test No. 10).

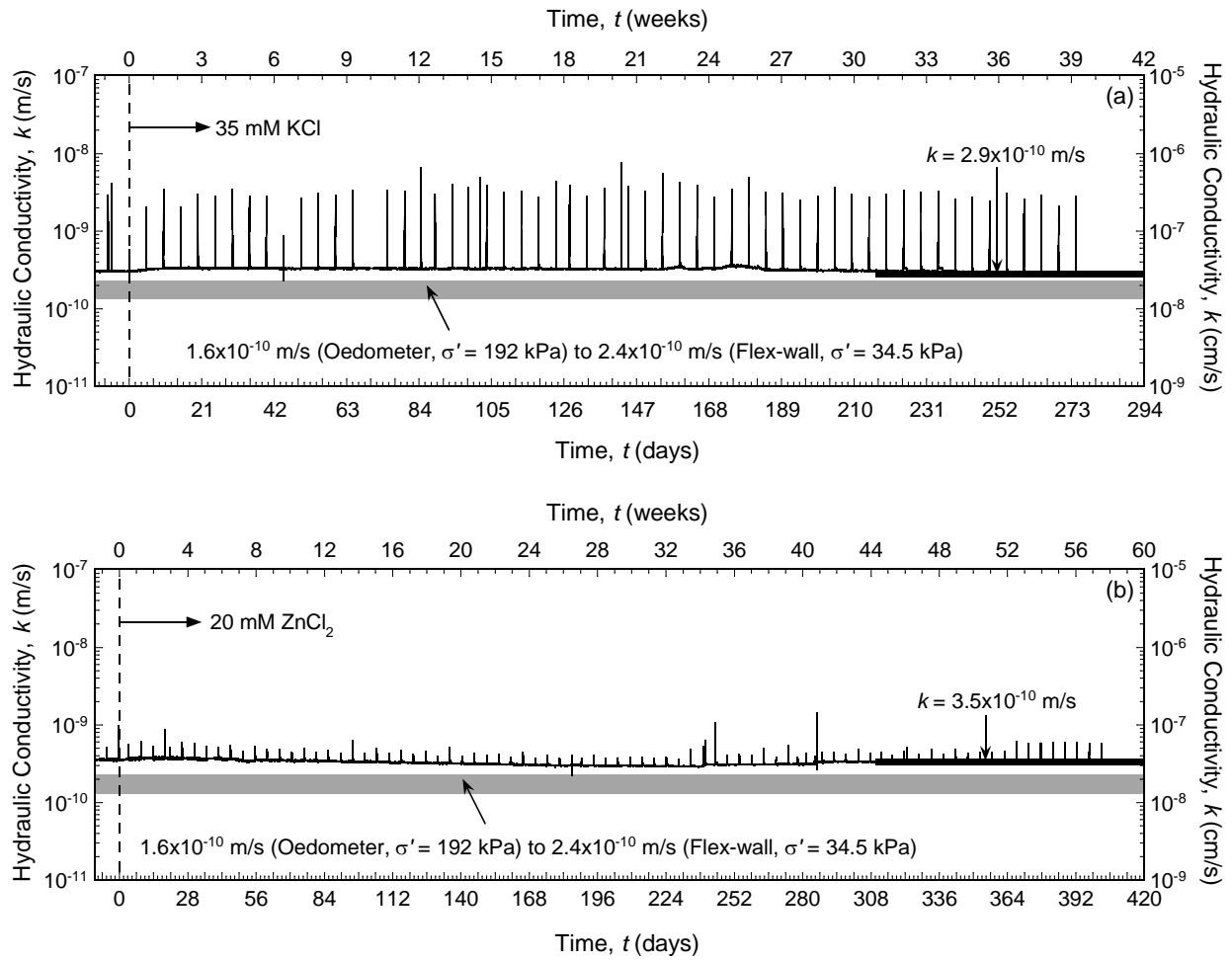


Figure 5.10. Temporal trends in hydraulic conductivity for columns of unamended backfills permeated with different salt solutions: (a) 35 mM KCl (Test No. 1); (b) 20 mM  $\text{ZnCl}_2$  (Test No. 2).

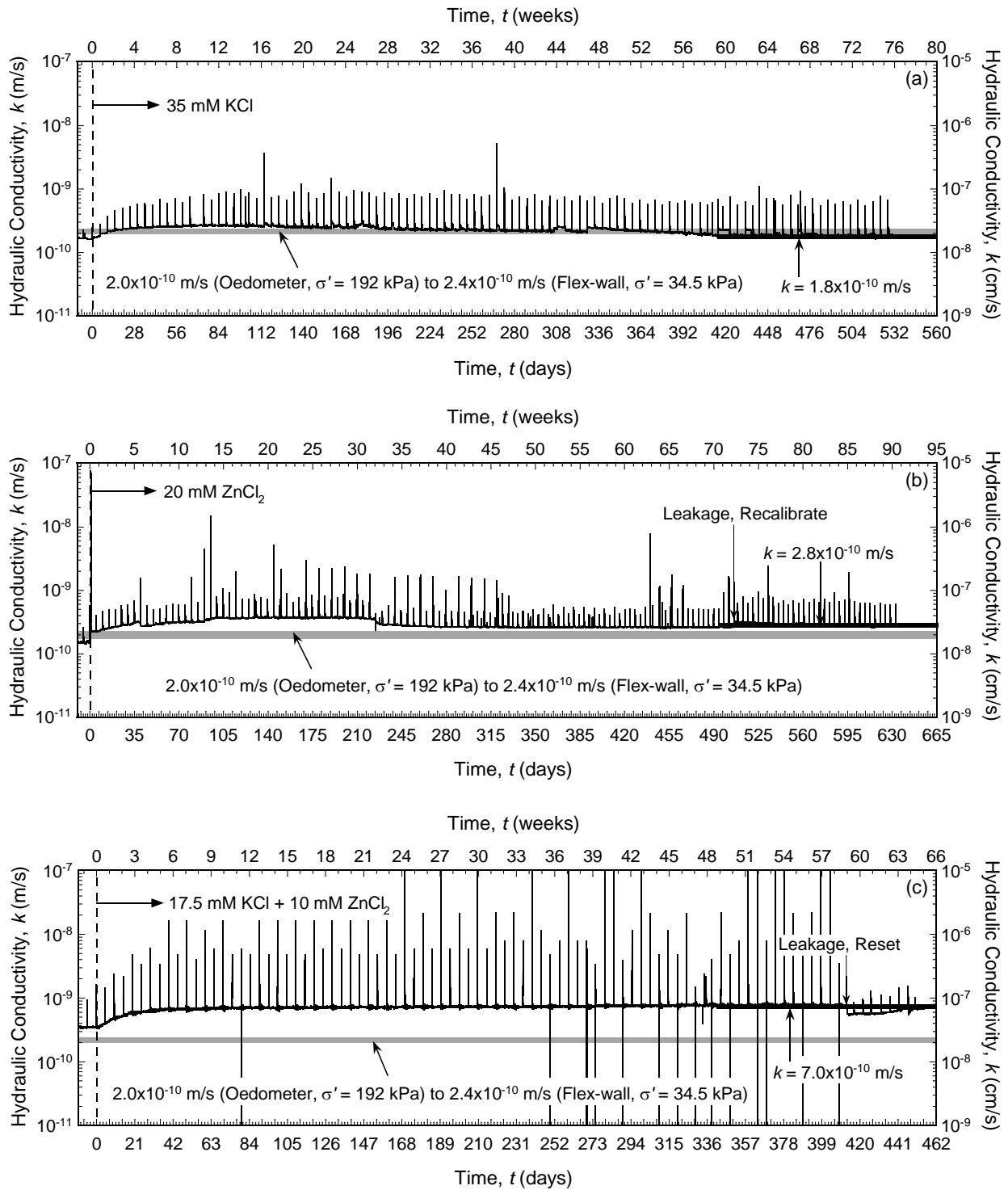


Figure 5.11. Temporal trends in hydraulic conductivity for columns of backfills amended with 5 % chabazite-UB and permeated with different salt solutions: (a) 35 mM KCl (Test No. 3); (b) 20 mM  $\text{ZnCl}_2$  (Test No. 4); (c) 17.5 mM KCl plus 10 mM  $\text{ZnCl}_2$  (Test No. 5).

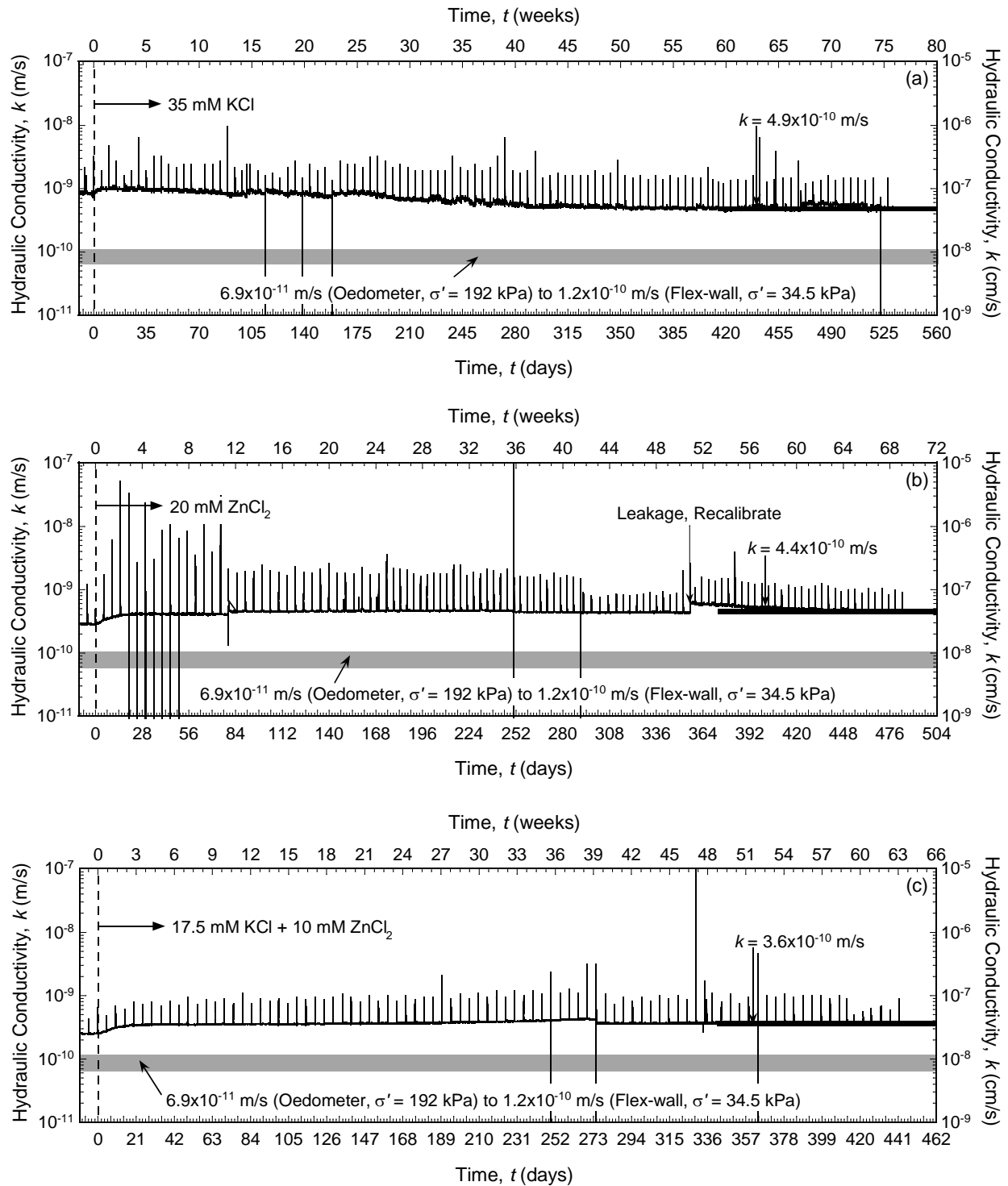


Figure 5.12. Temporal trends in hydraulic conductivity for columns of backfills amended with 5 % clinoptilolite and permeated with different salt solutions: (a) 35 mM KCl (Test No. 6); (b) 20 mM  $\text{ZnCl}_2$  (Test No. 7); (c) 17.5 mM KCl plus 10 mM  $\text{ZnCl}_2$  (Test No. 8).

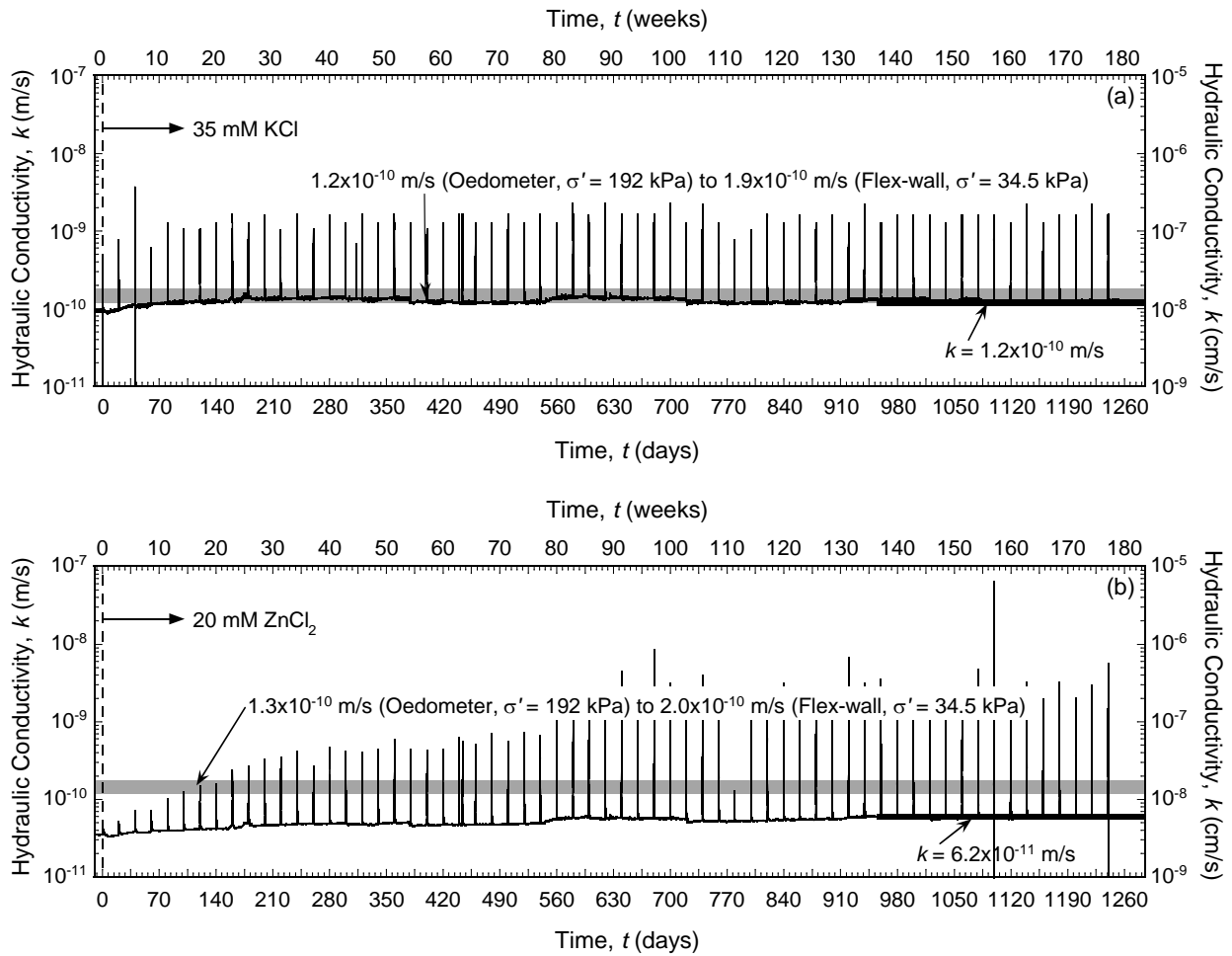


Figure 5.13. Temporal trends in hydraulic conductivity for columns of backfills amended with different amounts of chabazite-LB and permeated with a solution of 35 mM KCl: (a) 5 % chabazite-LB (Test No. 9); (b) 10 % chabazite-LB (Test No. 10).

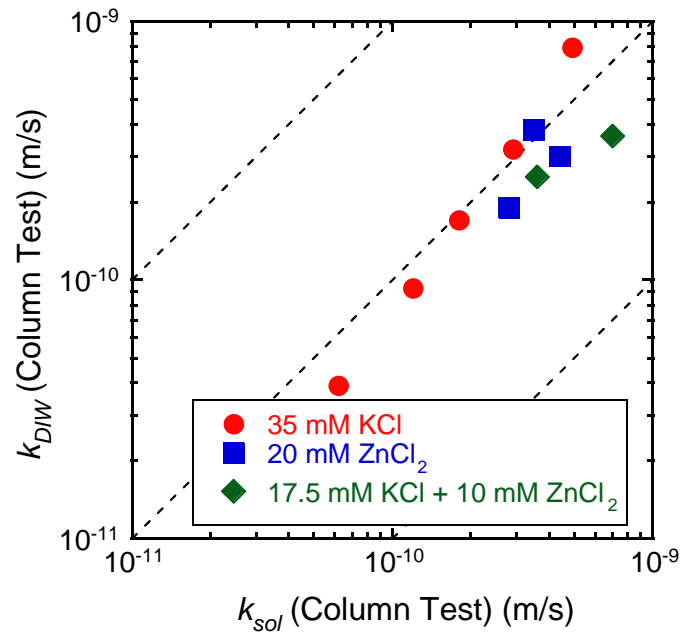


Figure 5.14. Comparison of the measured hydraulic conductivity based on column test,  $k_{DIW}$  versus  $k_{sol}$ .

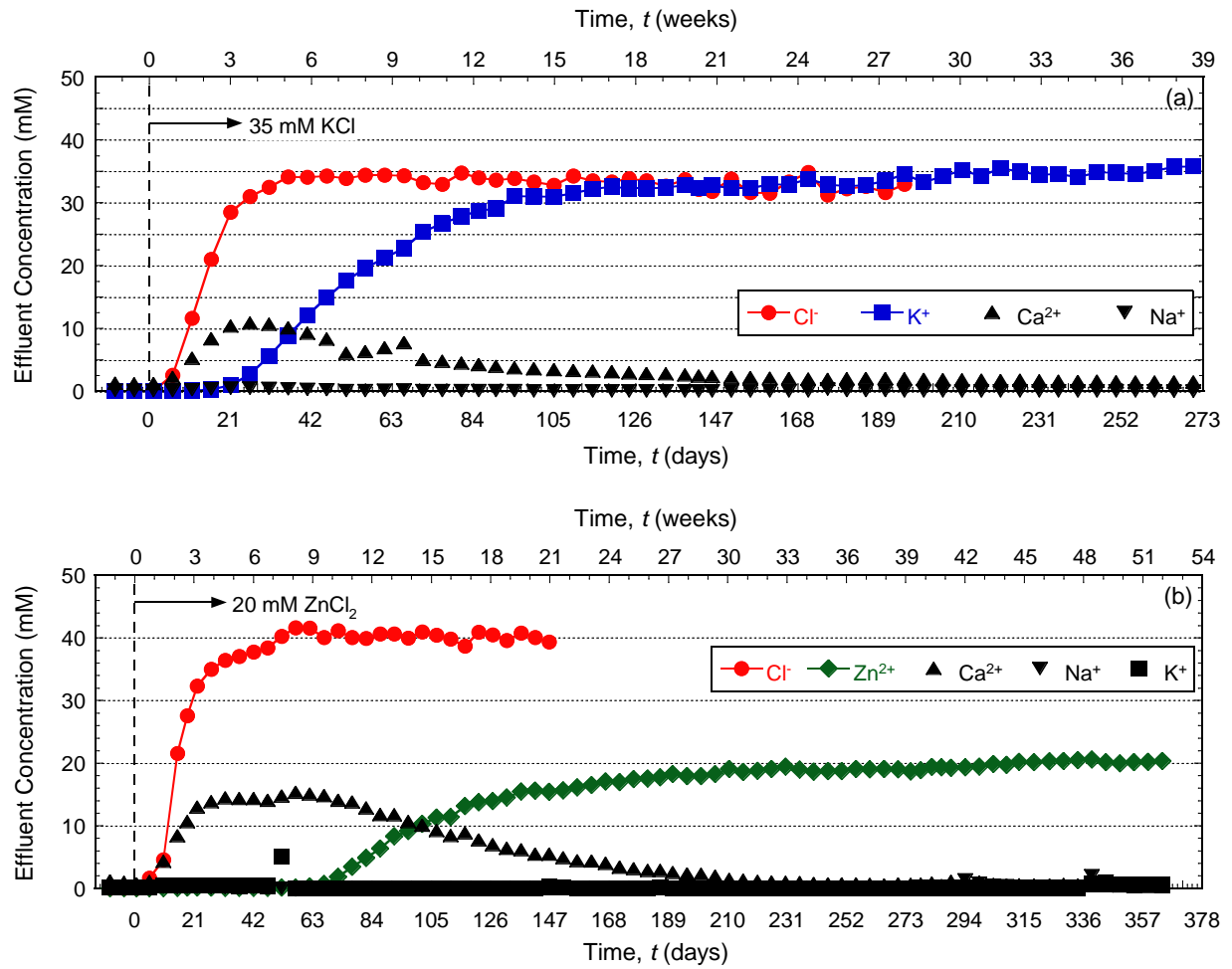


Figure 5.15. Temporal trends in effluent solute concentrations for columns of unamended backfills permeated with different salt solutions: (a) 35 mM KCl (Test No. 1); (b) 20 mM ZnCl<sub>2</sub> (Test No. 2).

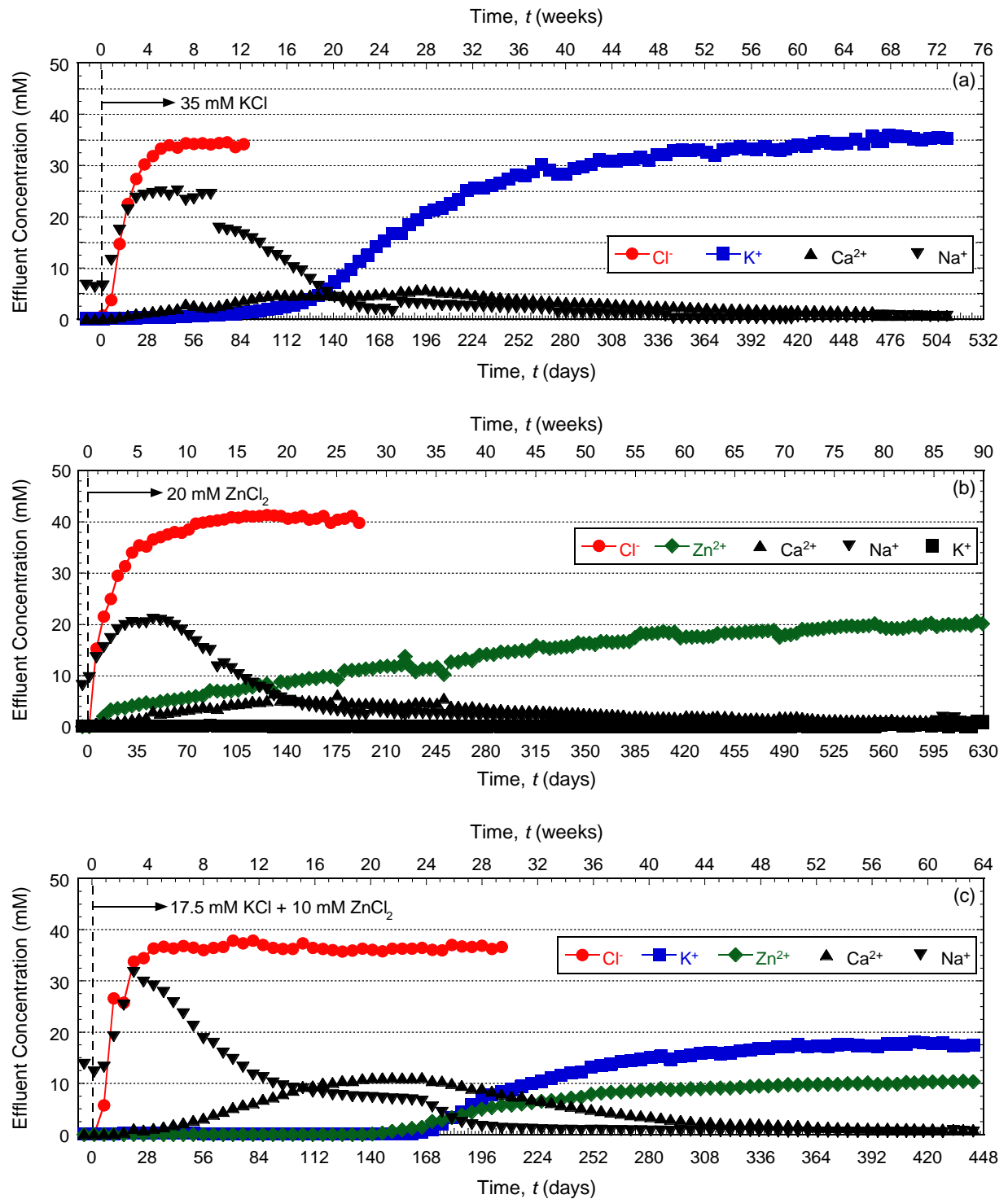


Figure 5.16. Temporal trends in effluent solute concentrations for columns of backfills amended with 5 % chabazite-UB and permeated with different salt solutions: (a) 35 mM KCl (Test No. 3); (b) 20 mM ZnCl<sub>2</sub> (Test No. 4); (c) 17.5 mM KCl plus 10 mM ZnCl<sub>2</sub> (Test No. 5).

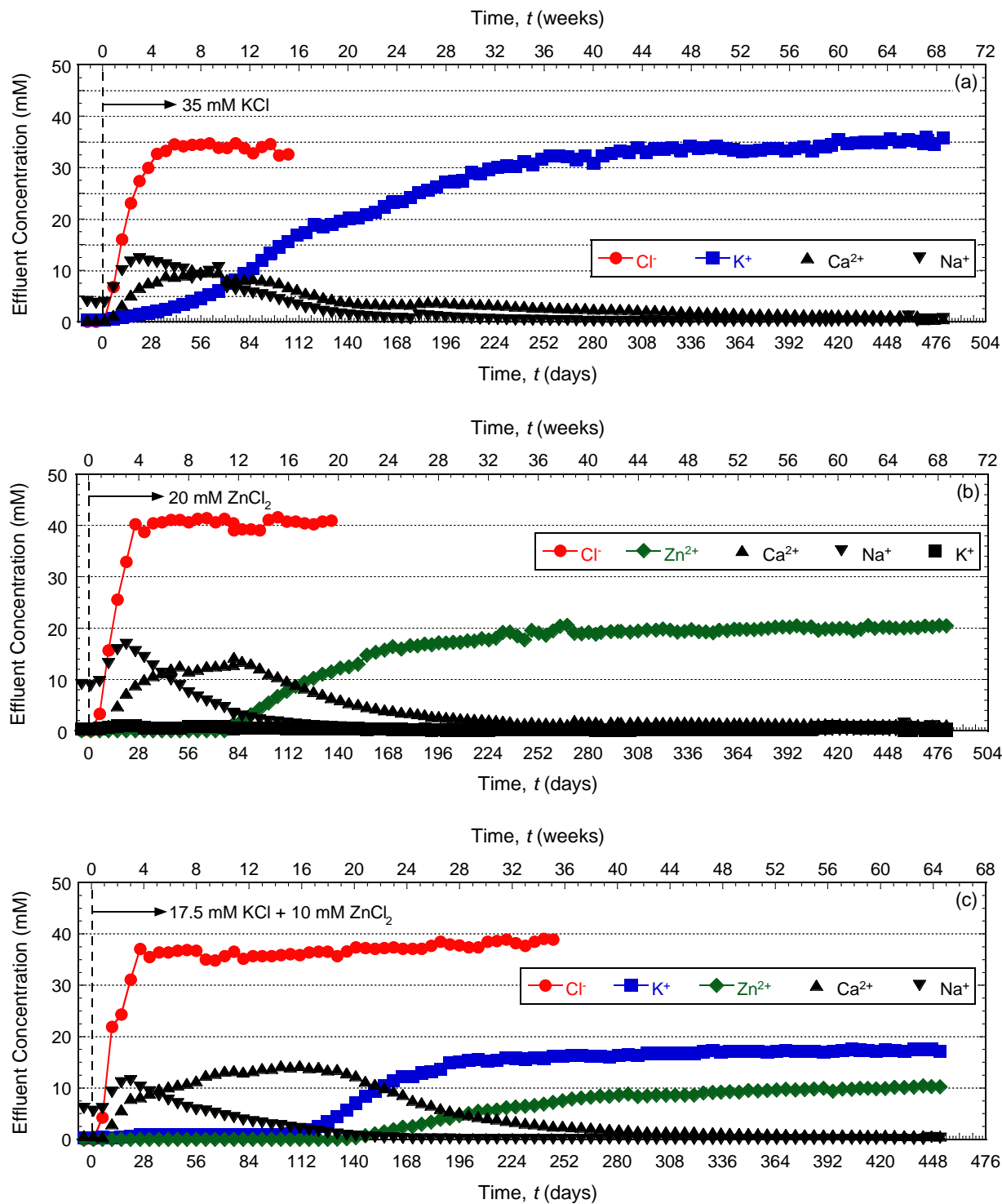


Figure 5.17. Temporal trends in effluent solute concentrations for columns of backfills amended with 5 % clinoptilolite and permeated with different salt solutions: (a) 35 mM KCl (Test No. 6); (b) 20 mM  $\text{ZnCl}_2$  (Test No. 7); (c) 17.5 mM KCl plus 10 mM  $\text{ZnCl}_2$  (Test No. 8).

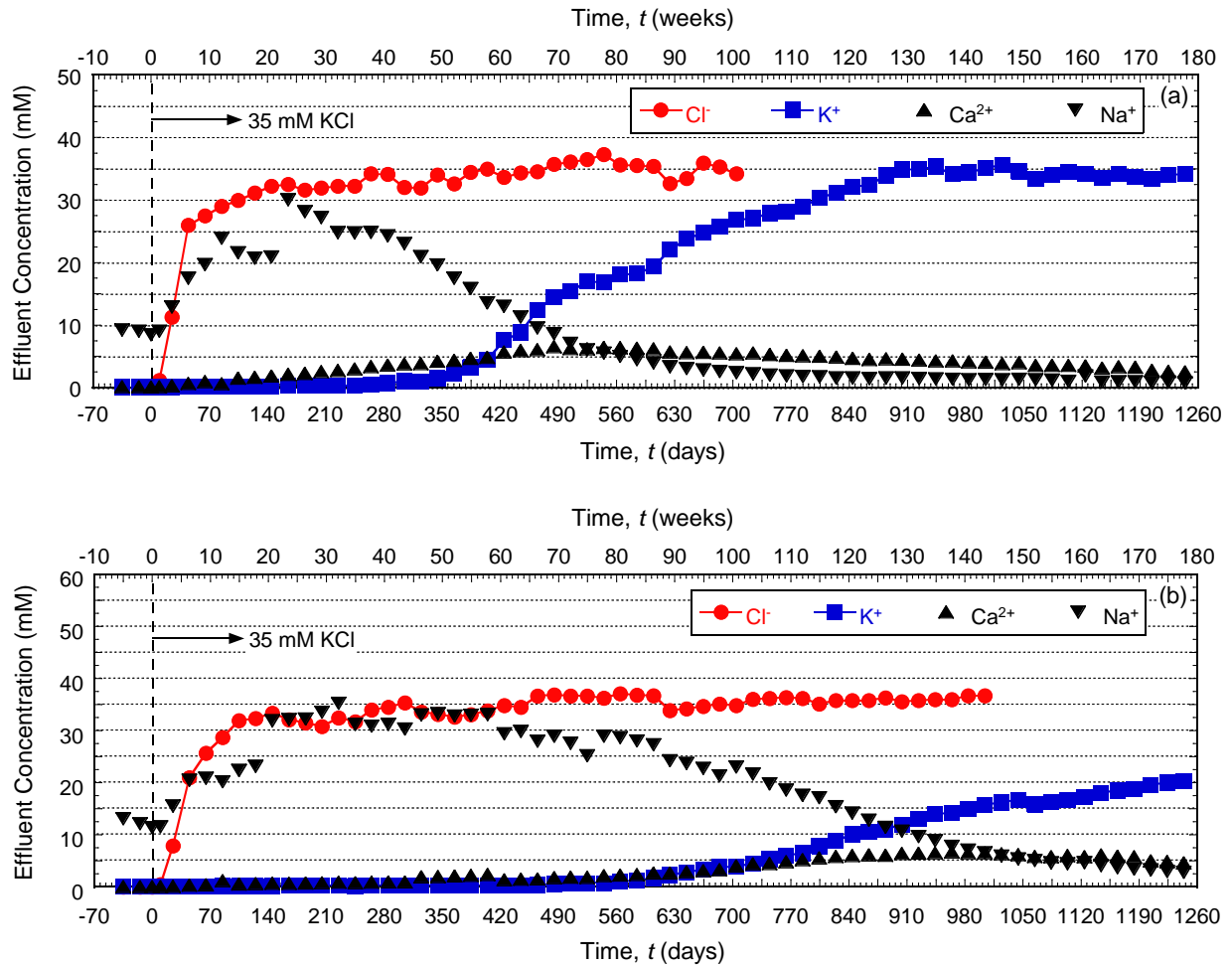


Figure 5.18. Temporal trends in effluent solute concentrations for columns of backfills amended with different amounts of chabazite-LB and permeated with a solution of 35 mM KCl: (a) 5 % chabazite-LB (Test No. 9); (b) 10 % chabazite-LB (Test No. 10).

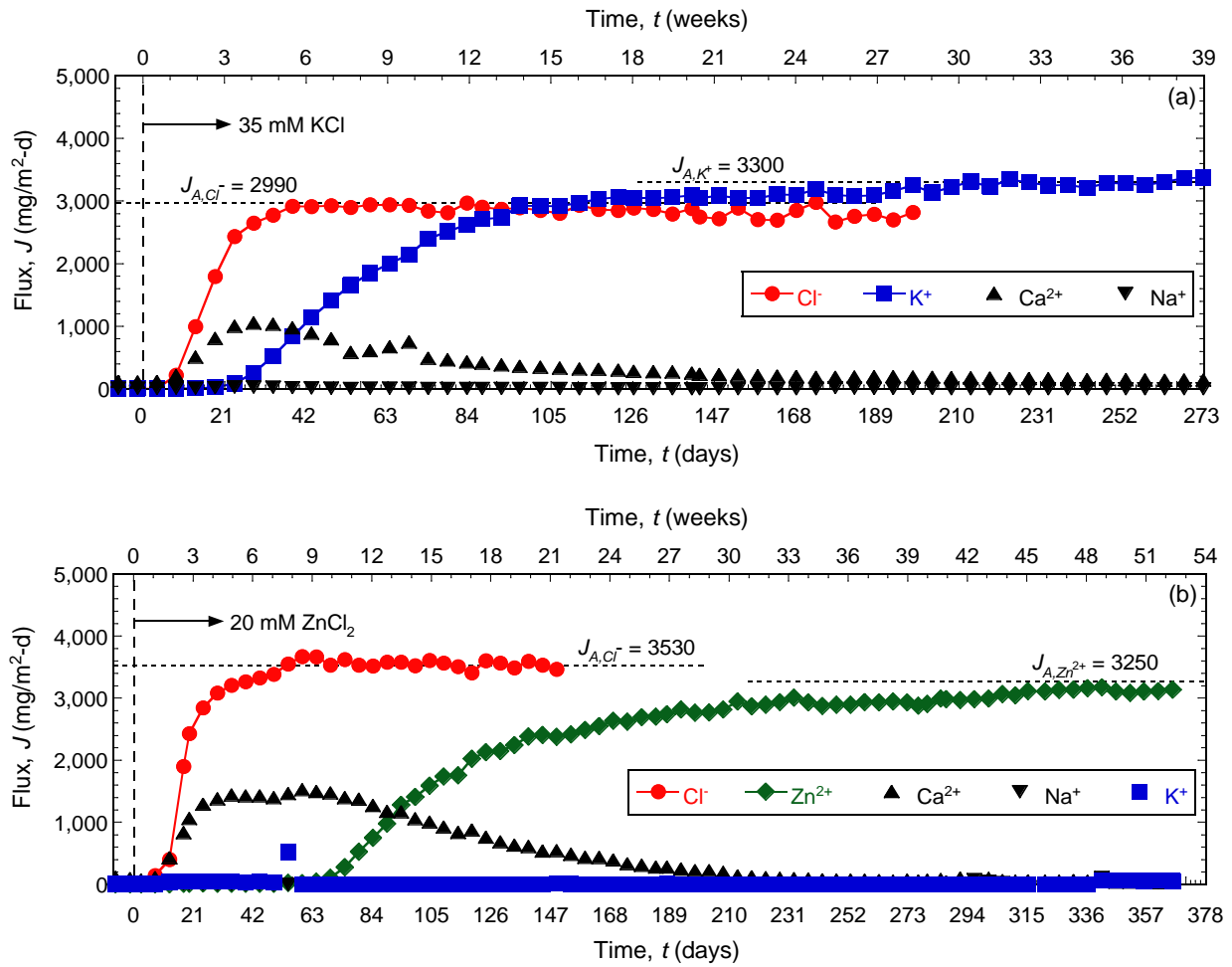


Figure 5.19. Temporal trends in effluent solute flux for columns of unamended backfills permeated with different salt solutions: (a) 35 mM KCl (Test No. 1); (b) 20 mM  $\text{ZnCl}_2$  (Test No. 2).

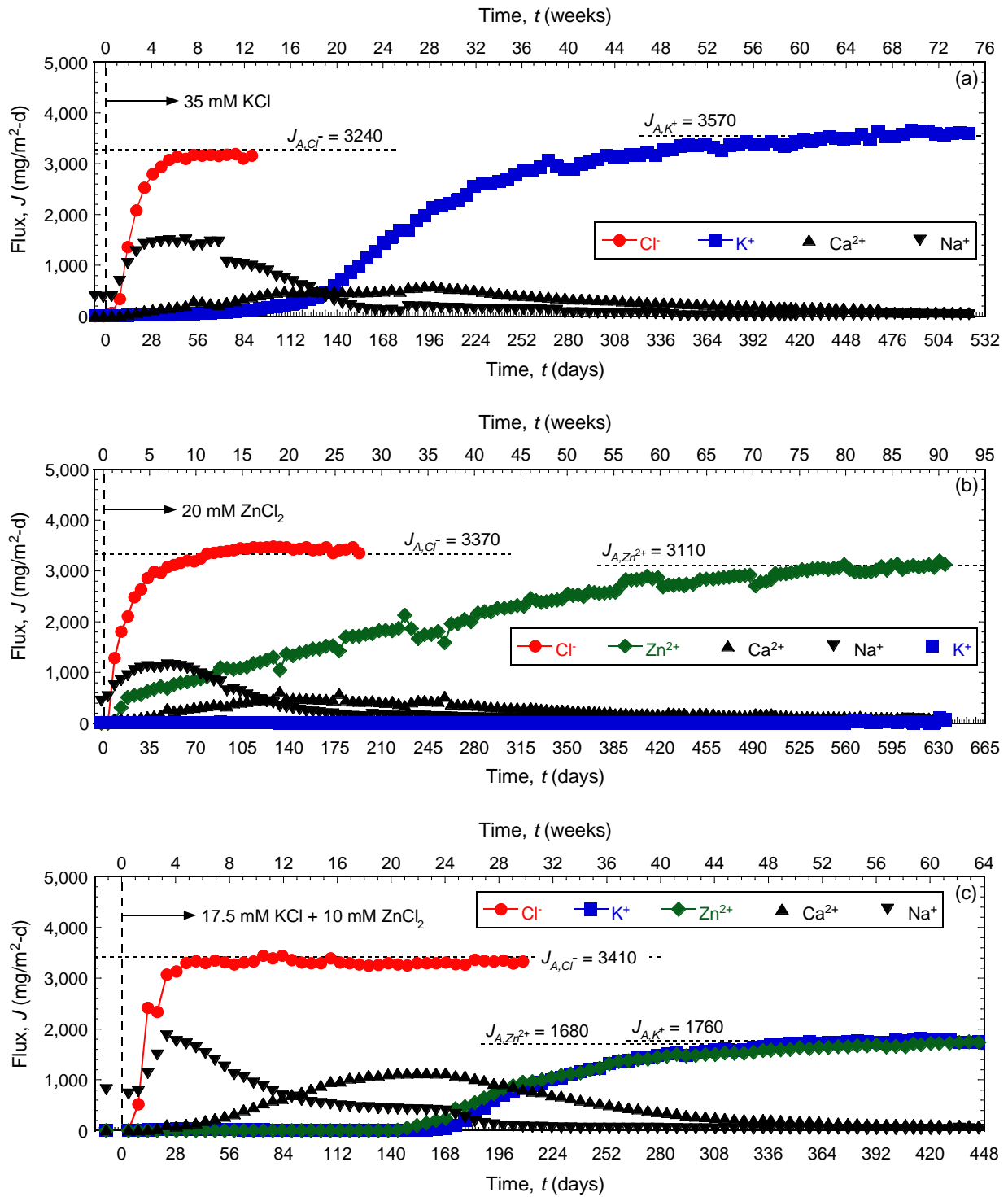


Figure 5.20. Temporal trends in effluent solute flux for columns of backfills amended with 5 % chabazite-UB and permeated with different salt solutions: (a) 35 mM KCl (Test No. 3); (b) 20 mM  $\text{ZnCl}_2$  (Test No. 4); (c) 17.5 mM KCl plus 10 mM  $\text{ZnCl}_2$  (Test No. 5).

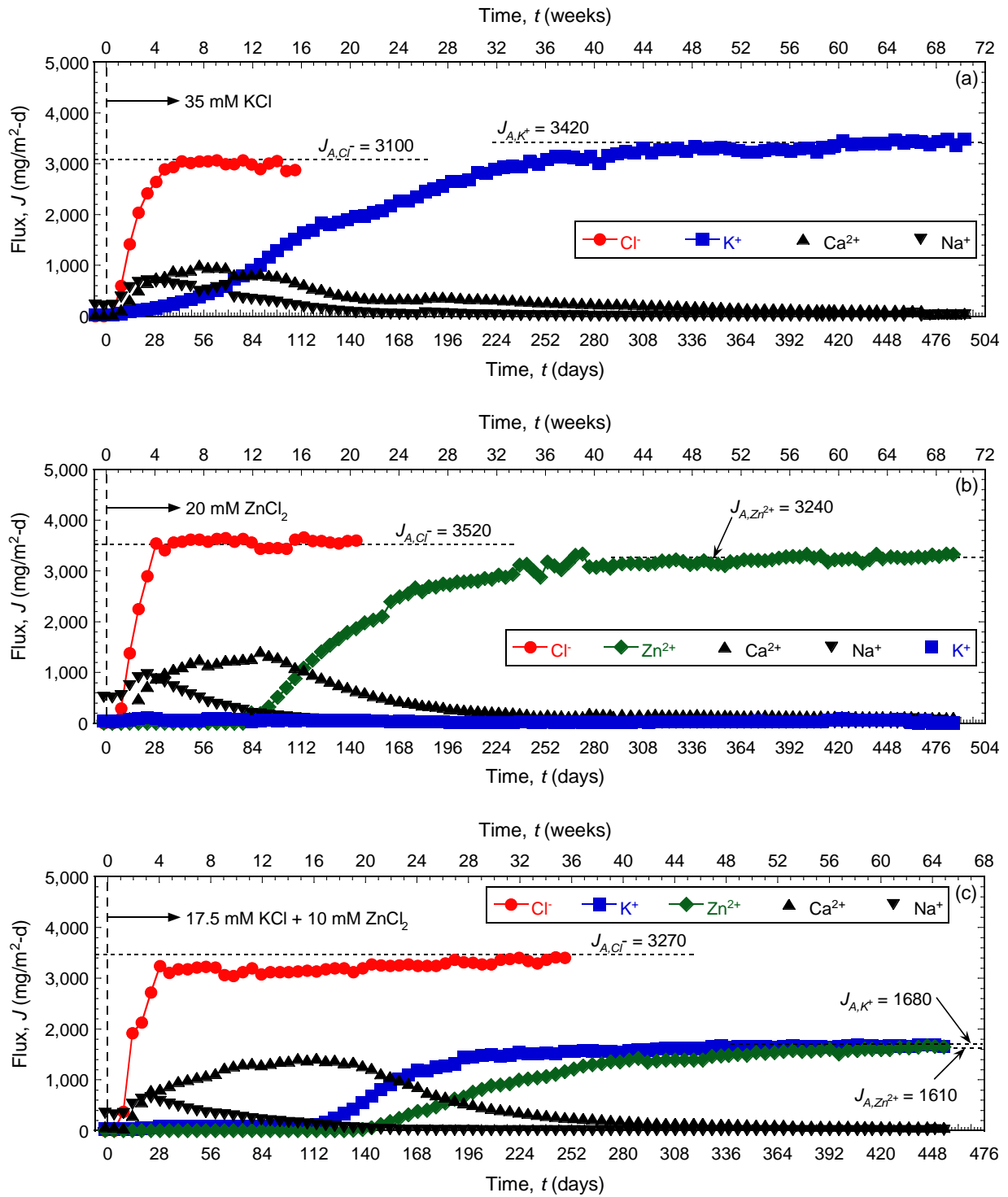


Figure 5.21. Temporal trends in effluent solute flux from for columns of backfills amended with 5 % clinoptilolite and permeated with different salt solutions: (a) 35 mM KCl (Test No. 6); (b) 20 mM  $\text{ZnCl}_2$  (Test No. 7); (c) 17.5 mM KCl plus 10 mM  $\text{ZnCl}_2$  (Test No. 8).

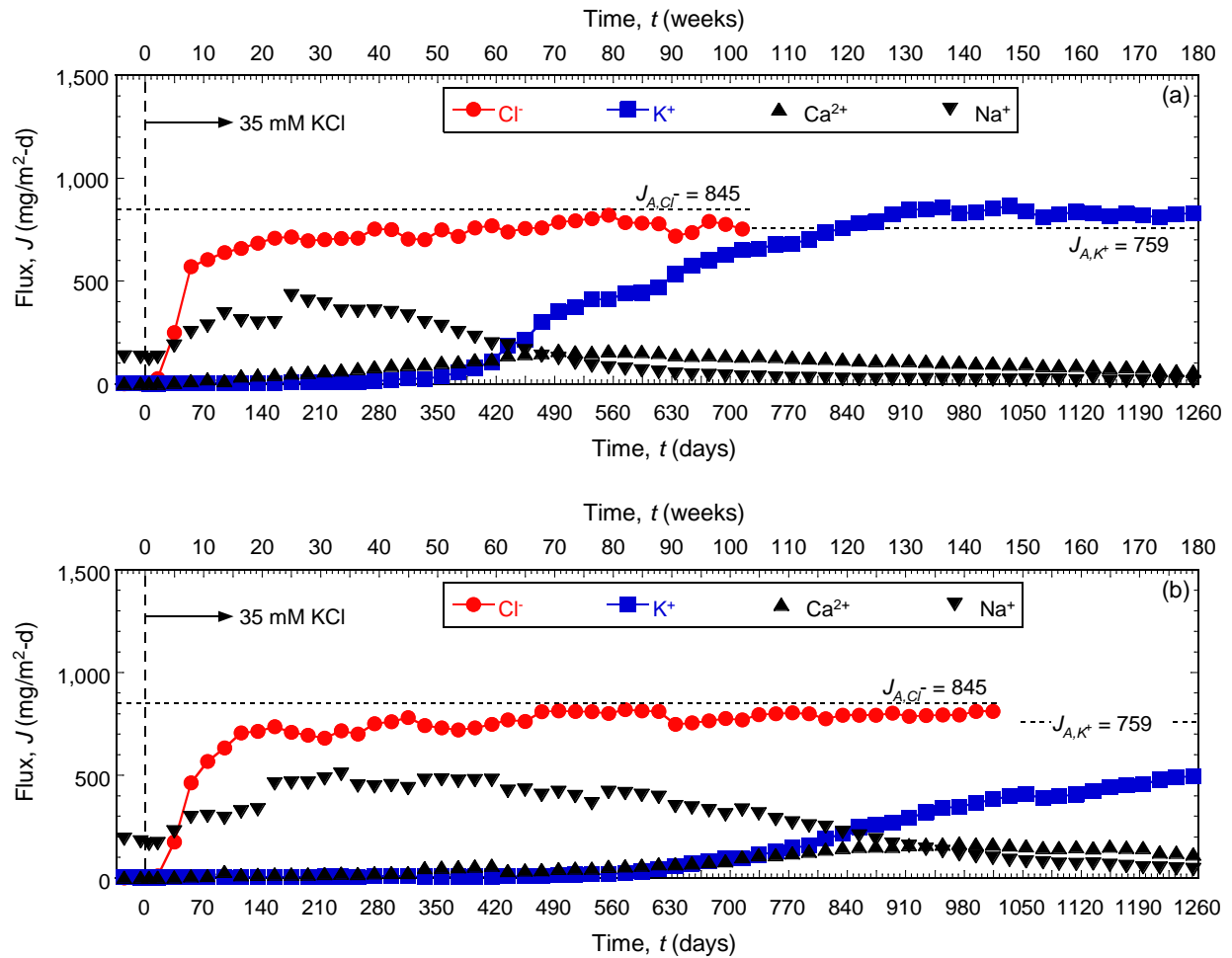


Figure 5.22. Temporal trends in effluent solute flux for columns of backfills amended with different amounts of chabazite-LB and permeated with a solution of 35 mM KCl: (a) 5 % chabazite-LB (Test No. 9); (b) 10 % chabazite-LB (Test No. 10).

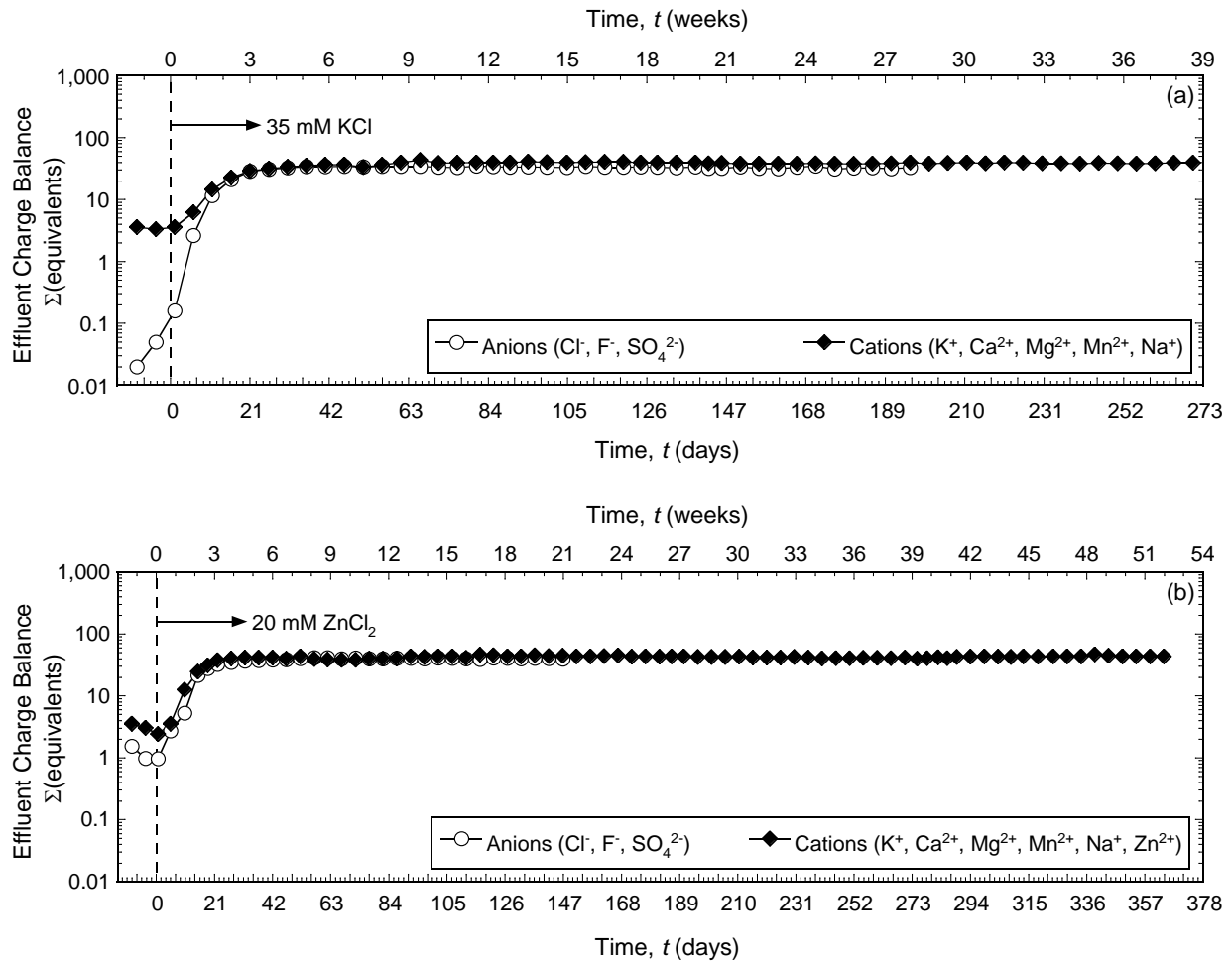


Figure 5.23. Temporal trends in effluent charge balance for columns of unamended backfills permeated with different salt solutions: (a) 35 mM KCl (Test No. 1); (b) 20 mM ZnCl<sub>2</sub> (Test No. 2). [Note: absolute values for the  $\Sigma$ anion equivalents are shown].

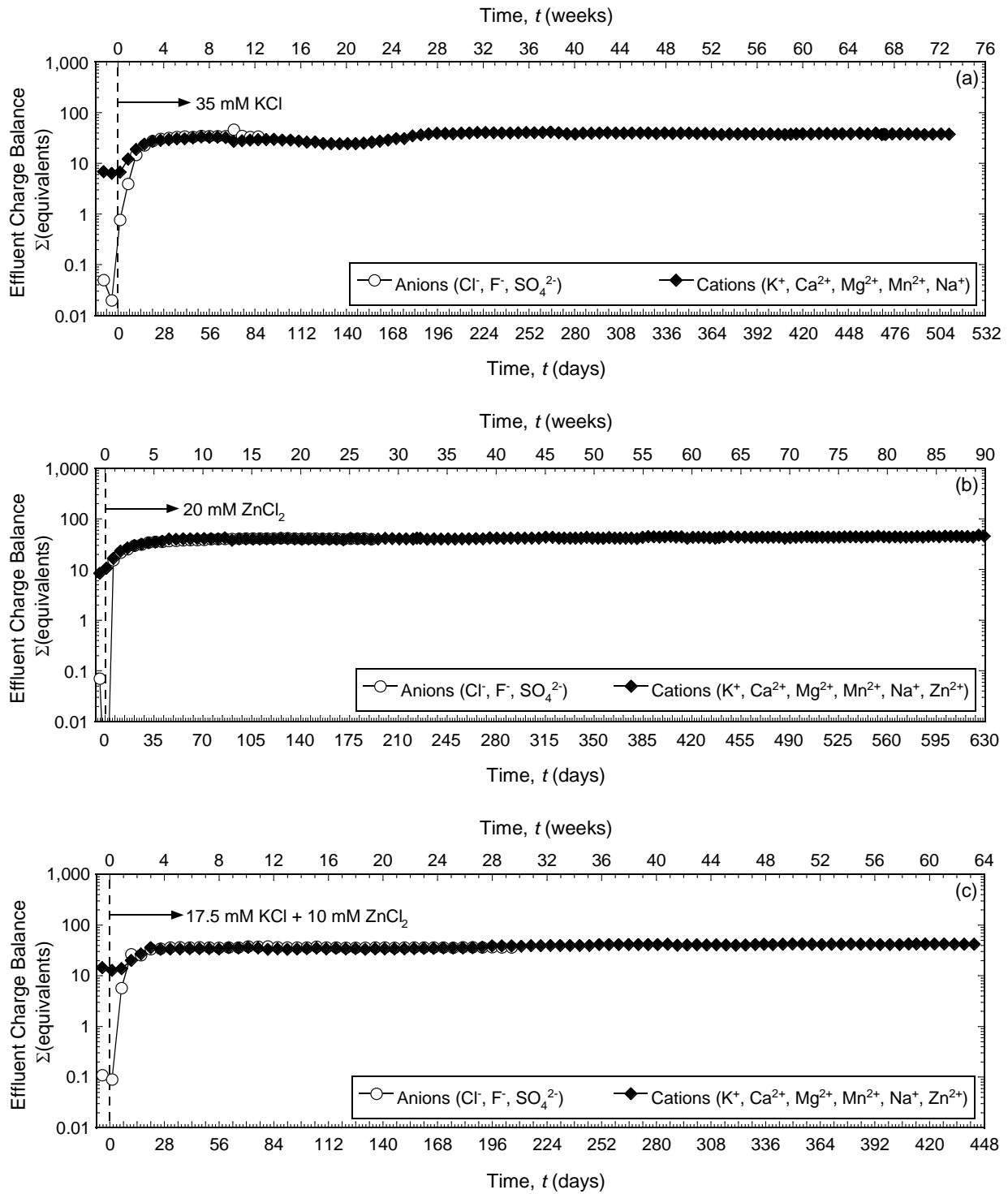


Figure 5.24. Temporal trends in effluent charge balance for columns of backfills amended with 5 % chabazite-UB and permeated with different salt solutions: (a) 35 mM KCl (Test No. 3); (b) 20 mM ZnCl<sub>2</sub> (Test No. 4); (c) 17.5 mM KCl plus 10 mM ZnCl<sub>2</sub> (Test No. 5). [Note: absolute values for the  $\Sigma$  anion equivalents are shown].

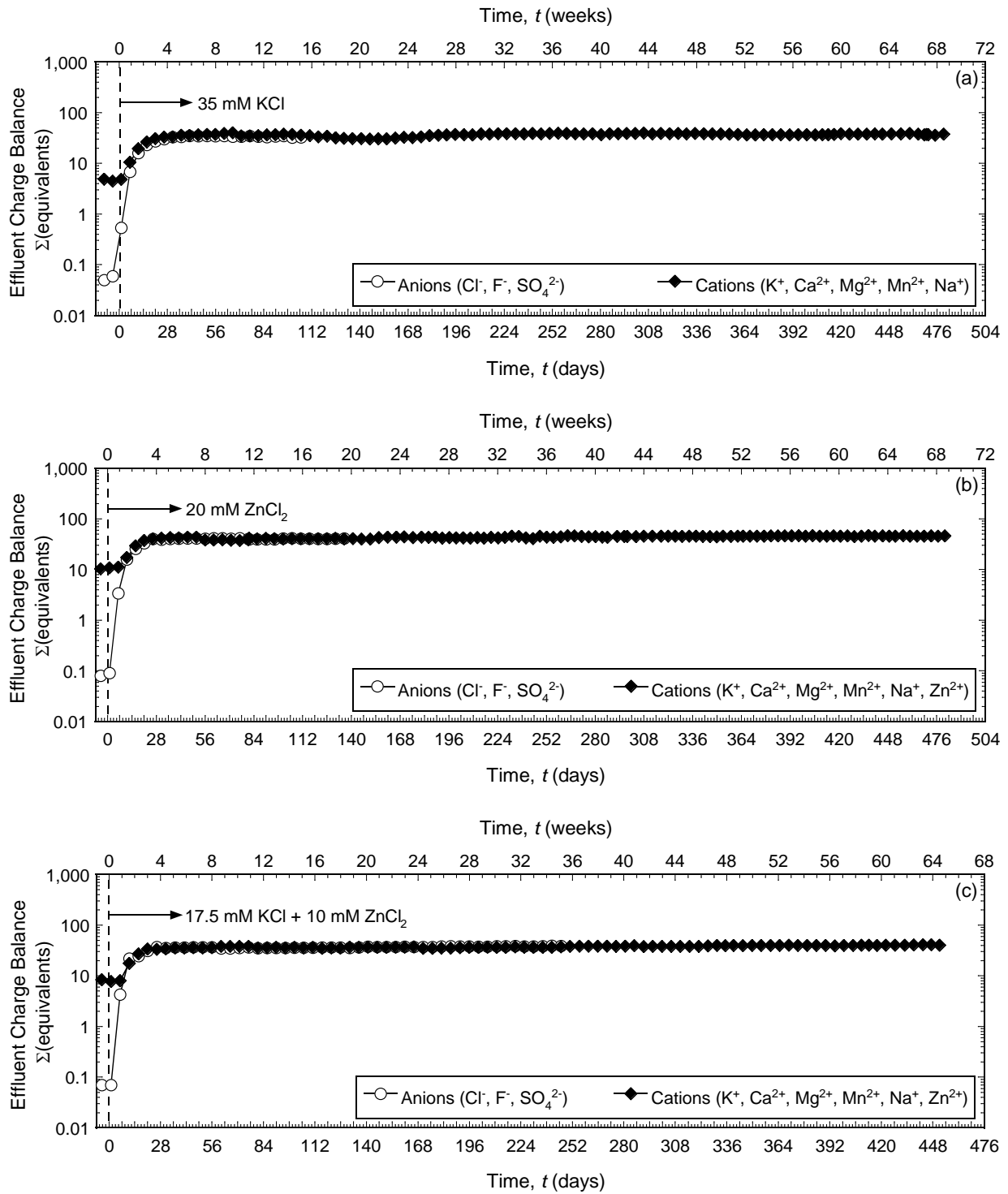


Figure 5.25. Temporal trends in effluent charge balance for columns of backfills amended with 5 % clinoptilolite and permeated with different salt solutions: (a) 35 mM KCl (Test No. 6); (b) 20 mM ZnCl<sub>2</sub> (Test No. 7); (c) 17.5 mM KCl plus 10 mM ZnCl<sub>2</sub> (Test No. 8). [Note: absolute values for the  $\Sigma$  anion equivalents are shown].

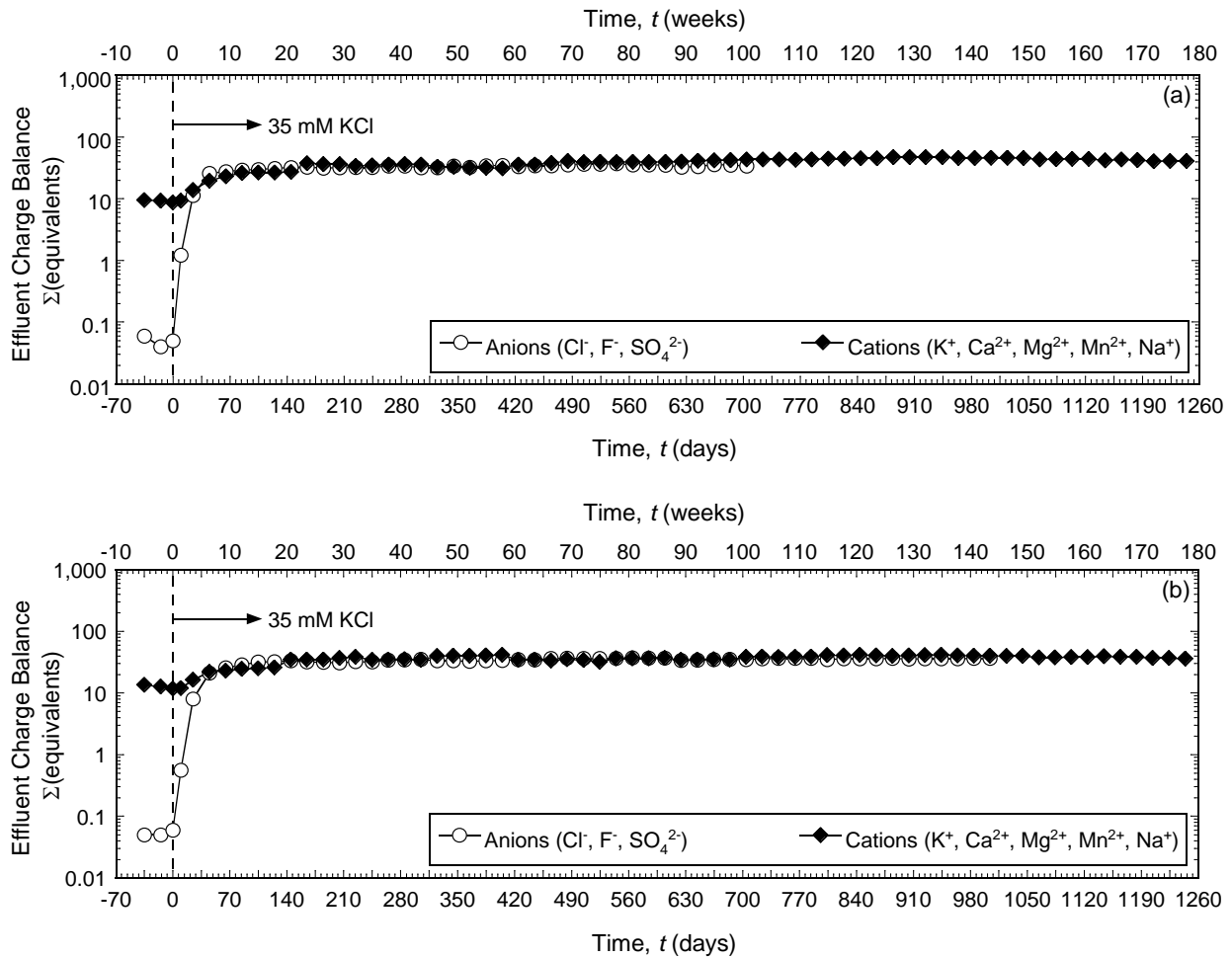


Figure 5.26. Temporal trends in effluent charge balance for columns of backfills amended with different amounts of chabazite-LB and permeated with a solution of 35 mM KCl (Test No. 9): (a) 5 % chabazite-LB; (b) 10 % chabazite-LB (Test No. 10). [Note: absolute values for the  $\Sigma$ anion equivalents are shown].

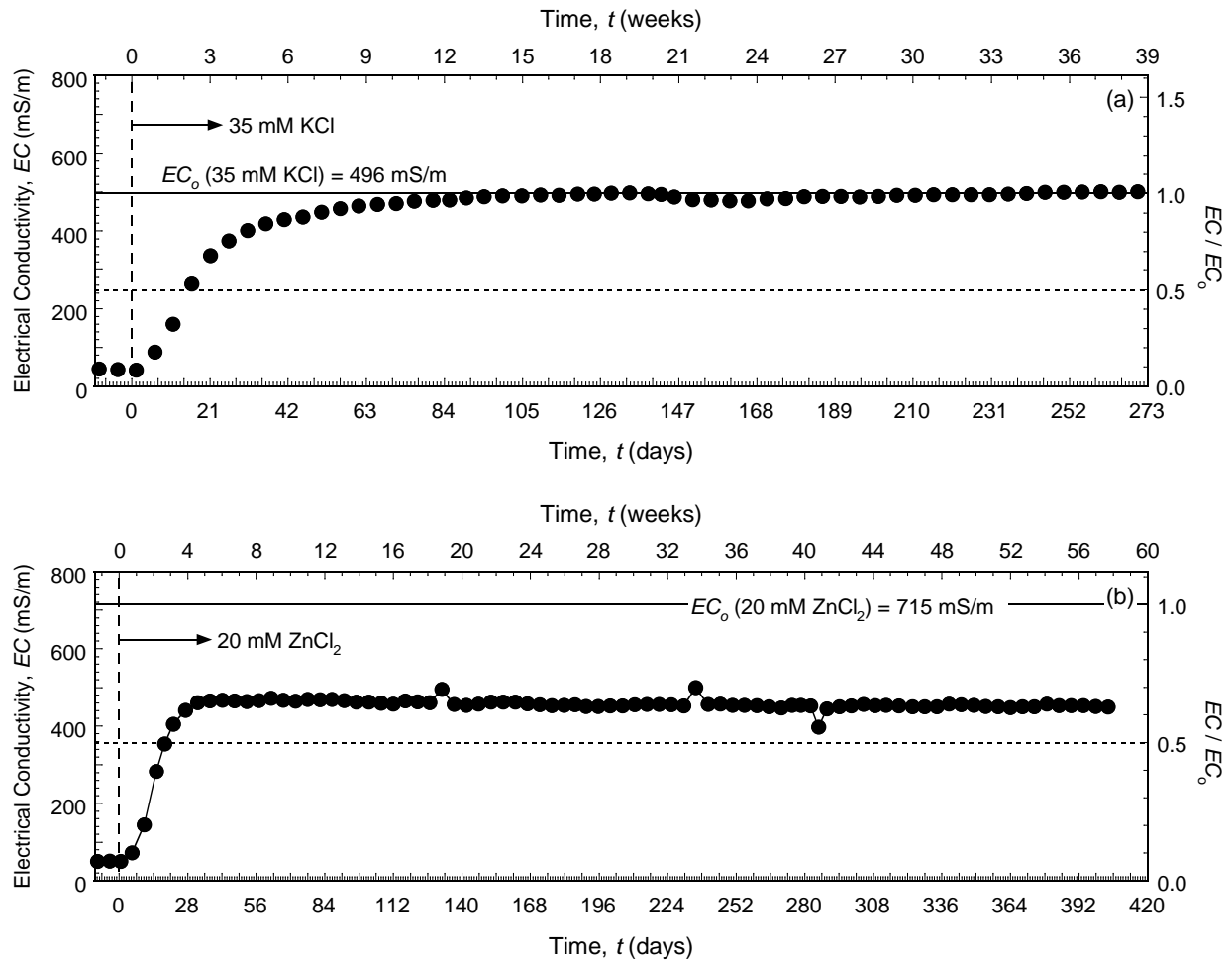


Figure 5.27. Temporal trends in the electrical conductivity of the effluent for columns with unamended backfills permeated with different salt solutions: (a) 35 mM KCl (Test No. 1); (b) 20 mM ZnCl<sub>2</sub> (Test No. 2).

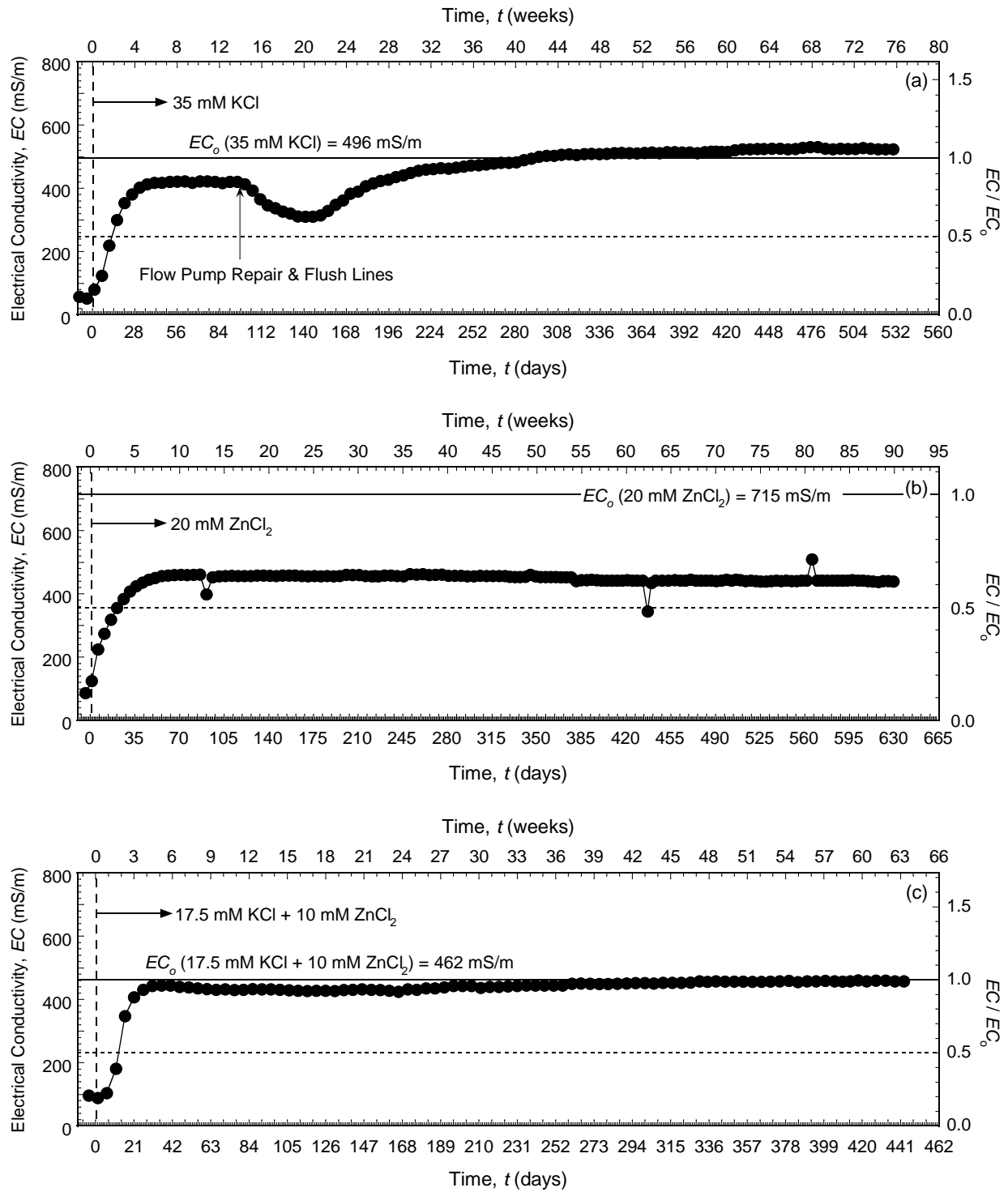


Figure 5.28. Temporal trends in the electrical conductivity of the effluent from columns of backfills amended with 5 % chabazite-UB permeated with different salt solutions: (a) 35 mM KCl (Test No. 3); (b) 20 mM ZnCl<sub>2</sub> (Test No. 4); (c) 17.5 mM KCl plus 10 mM ZnCl<sub>2</sub> (Test No. 5).

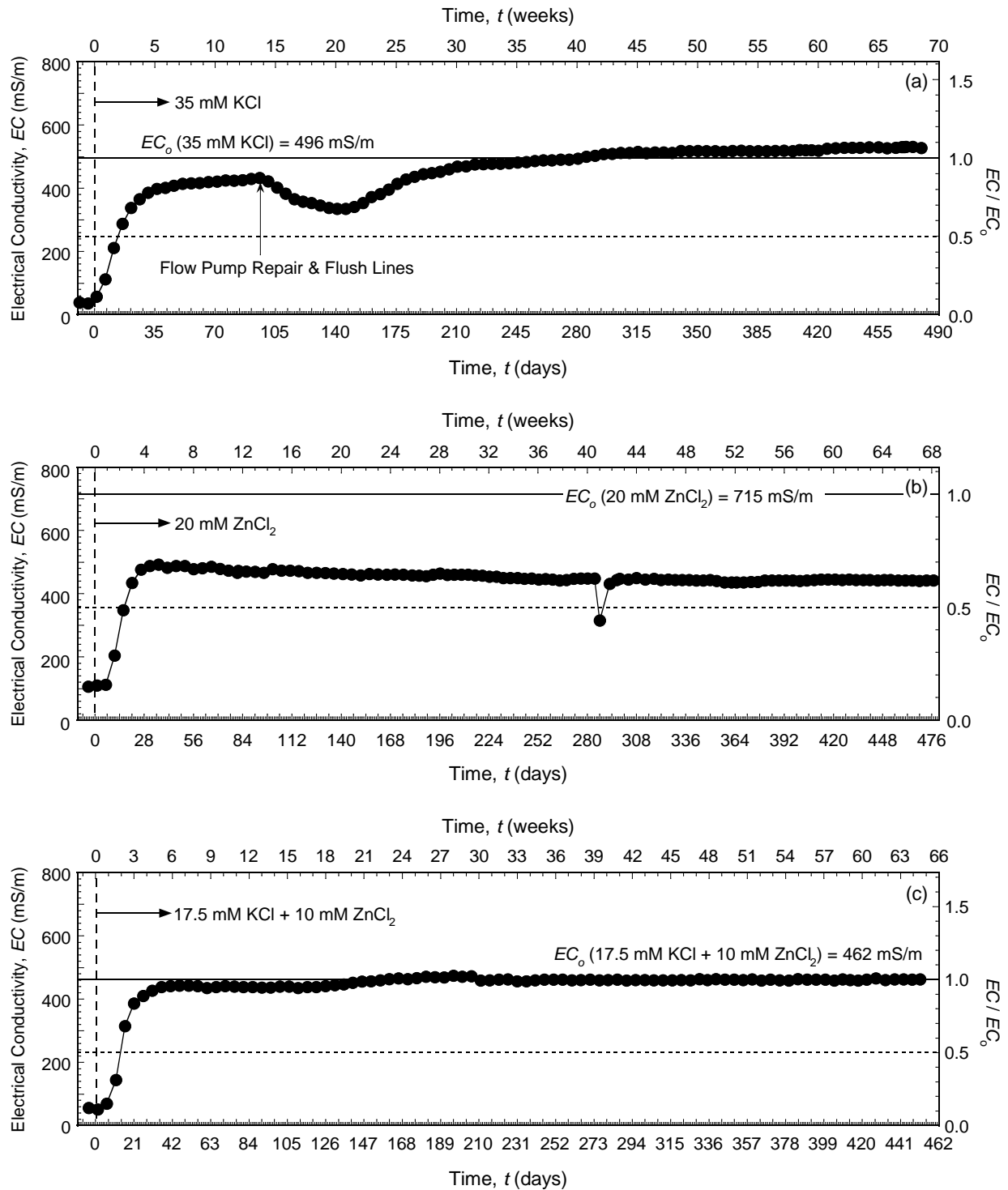


Figure 5.29. Temporal trends in the electrical conductivity of the effluent for columns of backfills amended with 5% clinoptilolite permeated with different salt solutions: (a) 35 mM KCl (Test No. 6); (b) 20 mM  $ZnCl_2$  (Test No. 7); (c) 17.5 mM KCl plus 10 mM  $ZnCl_2$  (Test No. 8).

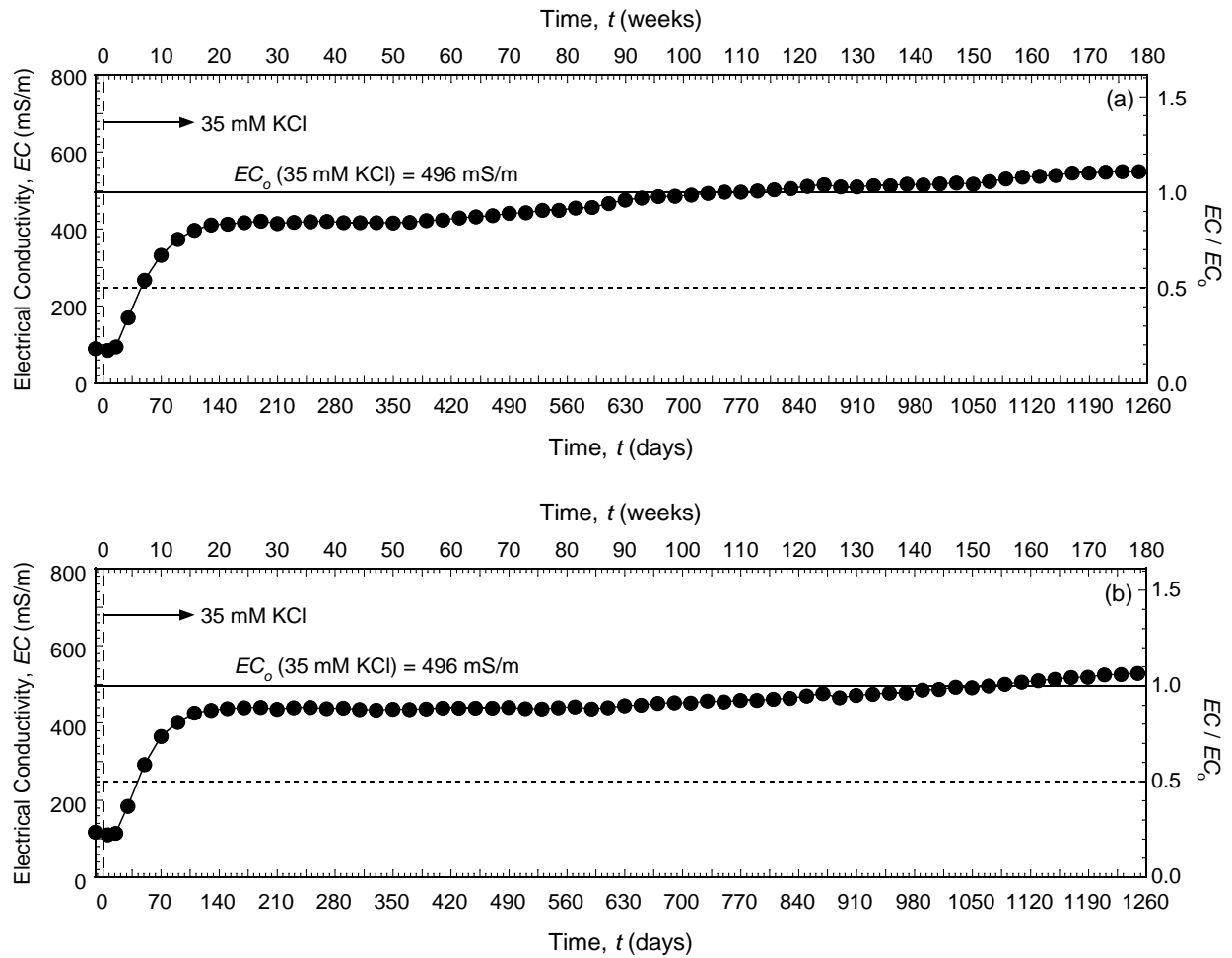


Figure 5.30. Temporal trends in the electrical conductivity of the effluent for columns of backfills amended with different amounts of chabazite-LB and permeated with a solution of 35 mM KCl: (a) 5 % chabazite-LB (Test No. 9); (b) 10 % chabazite-LB (Test No. 10).

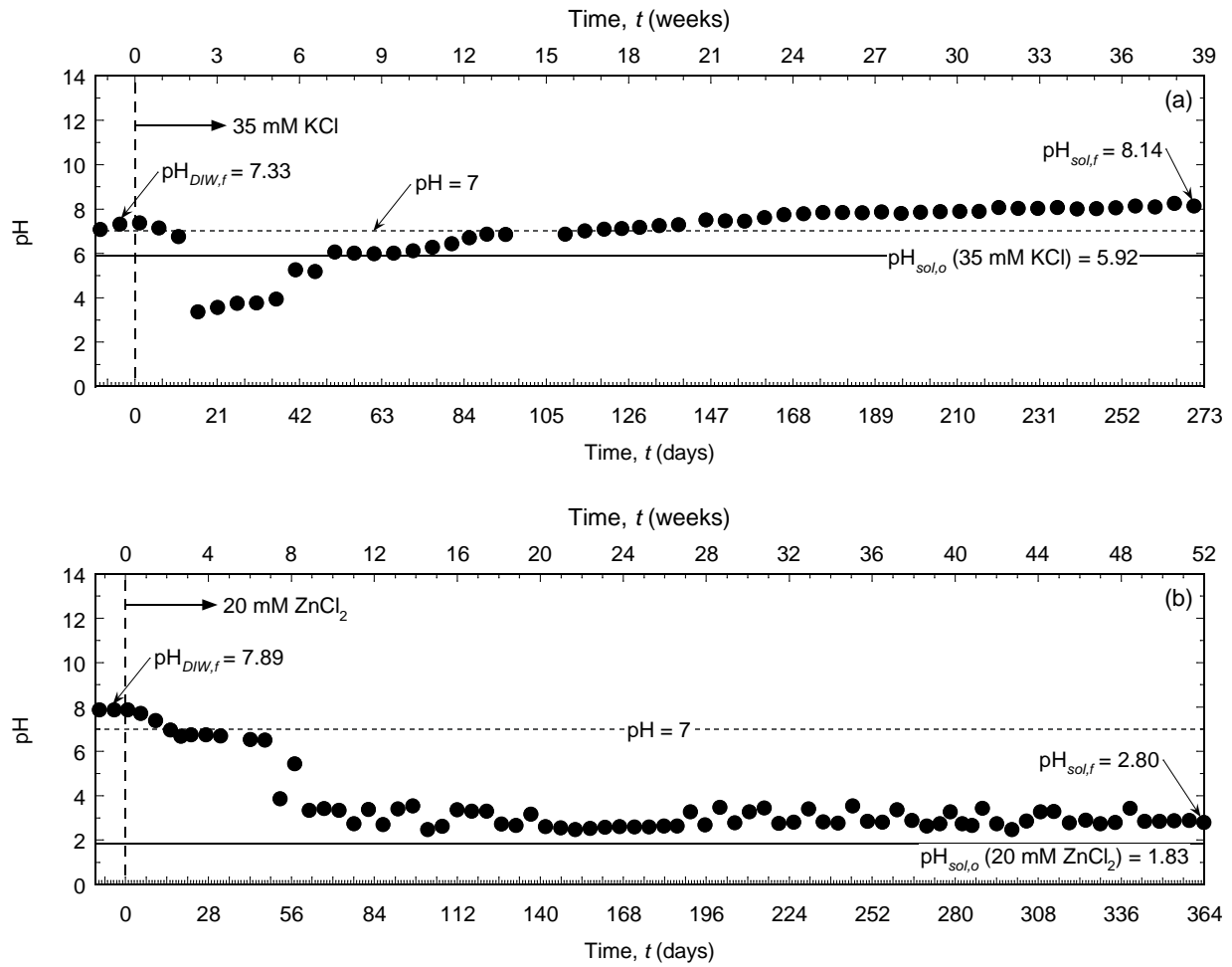


Figure 5.31. Temporal trends in the pH of the effluent for columns with unamended backfills permeated with different salt solutions: (a) 35 mM KCl (Test No. 1); (b) 20 mM  $\text{ZnCl}_2$  (Test No. 2).

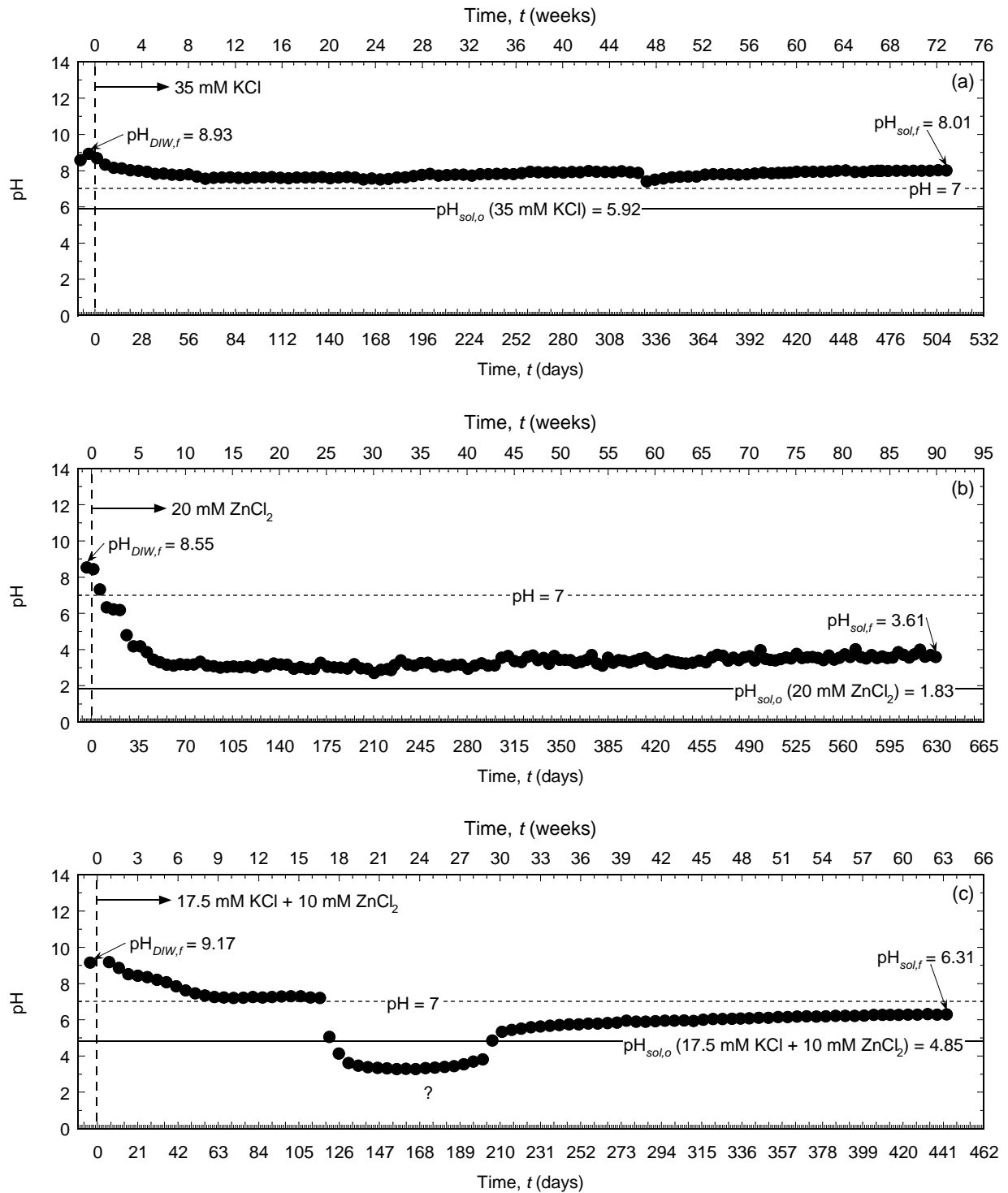


Figure 5.32. Temporal trends in the pH of the effluent from columns of backfills amended with 5 % chabazite-UB permeated with different salt solutions: (a) 35 mM KCl (Test No. 3); (b) 20 mM  $ZnCl_2$  (Test No. 4); (c) 17.5 mM KCl plus 10 mM  $ZnCl_2$  (Test No. 5).

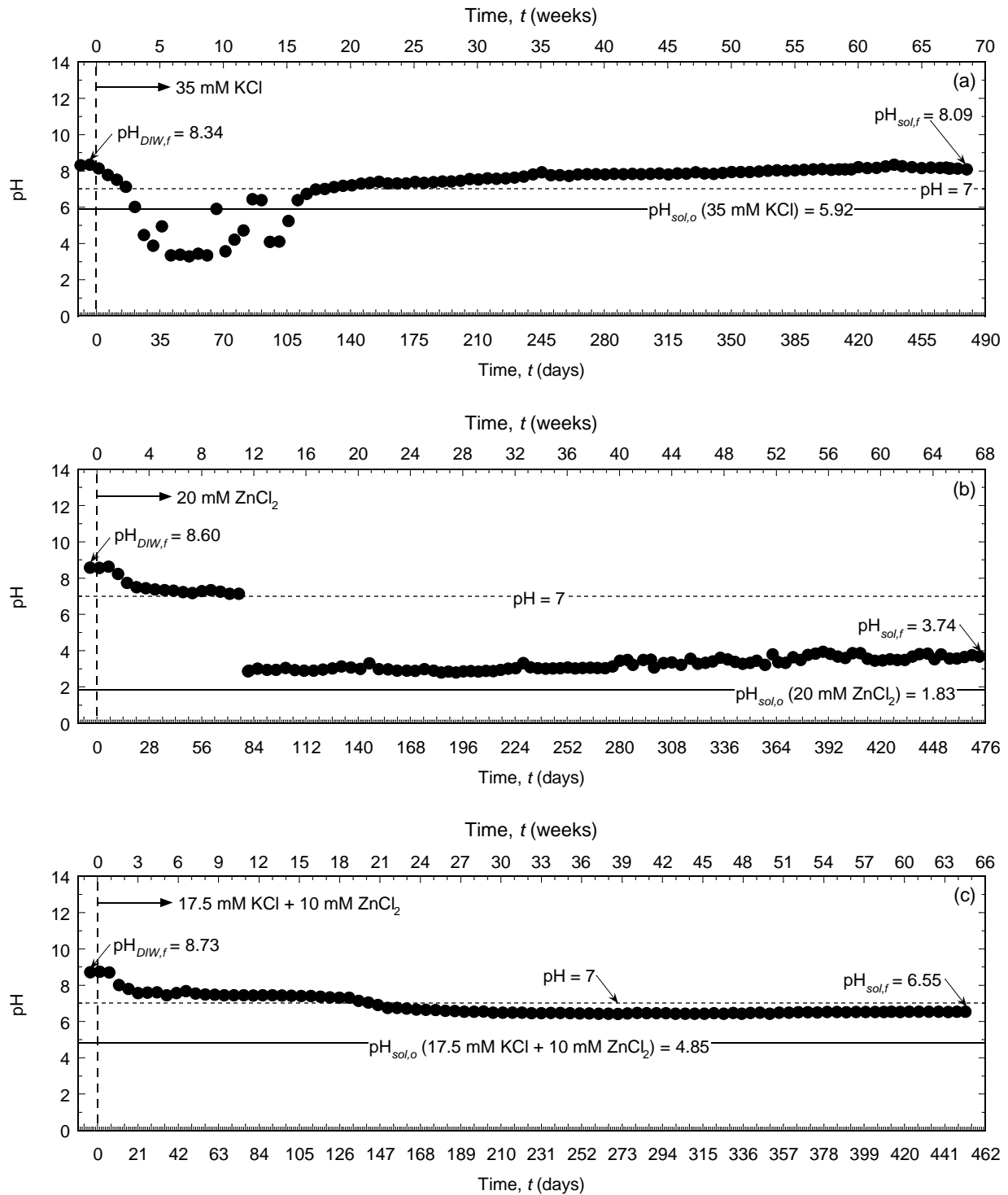


Figure 5.33. Temporal trends in the pH of the effluent for columns of backfills amended with 5 % clinoptilolite permeated with different salt solutions: (a) 35 mM KCl (Test No. 6); (b) 20 mM  $ZnCl_2$  (Test No. 7); (c) 17.5 mM KCl plus 10 mM  $ZnCl_2$  (Test No. 8).

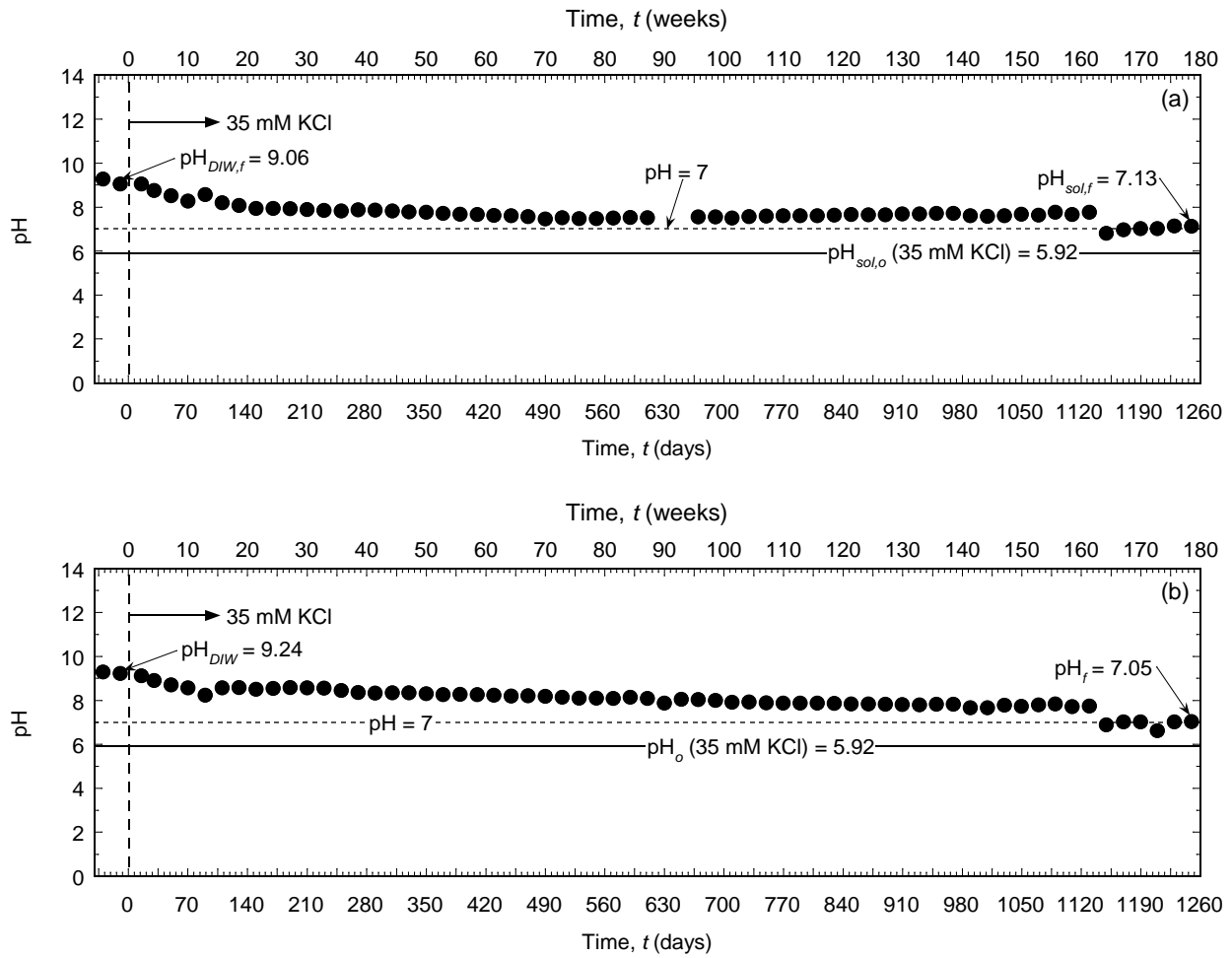


Figure 5.34. Temporal trends in the pH of the effluent for columns of backfills amended with different amounts of chabazite-LB and permeated with a solution of 35 mM KCl: (a) 5 % chabazite-LB (Test No. 9); (b) 10 % chabazite-LB (Test No. 10).

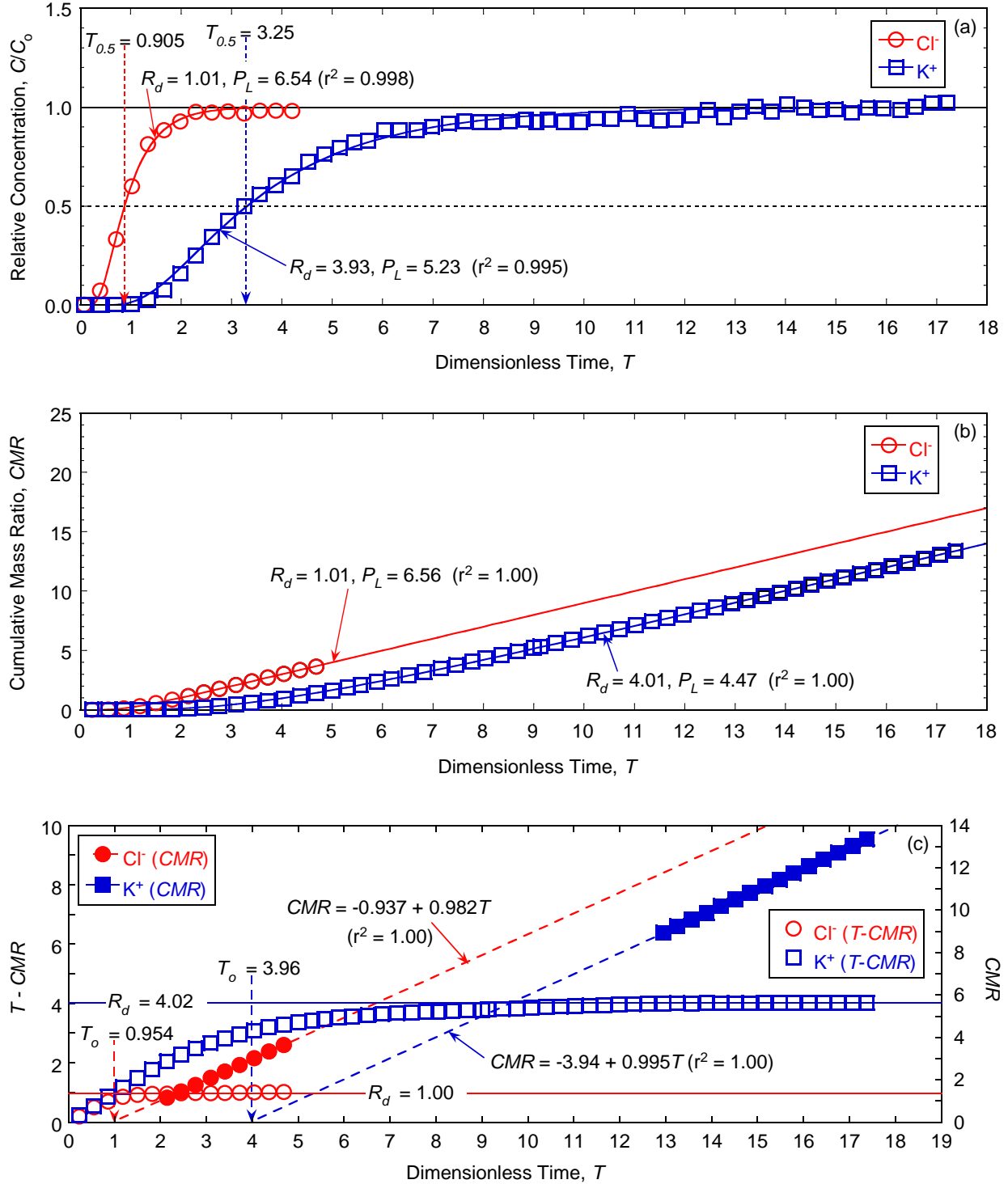


Figure 5.35. Chemical transport analyses for determination of column Péclet number ( $P_L$ ) and/or retardation factor ( $R_d$ ) for unamended backfill permeated with 35 mM KCl (Test No. 1): (a) regression of relative concentration (RC) data; (b) regression of cumulative mass ratio (CMR) data; (c)  $T_o (= R_d)$  and  $T - \text{CMR}$  analyses for  $R_d$ .

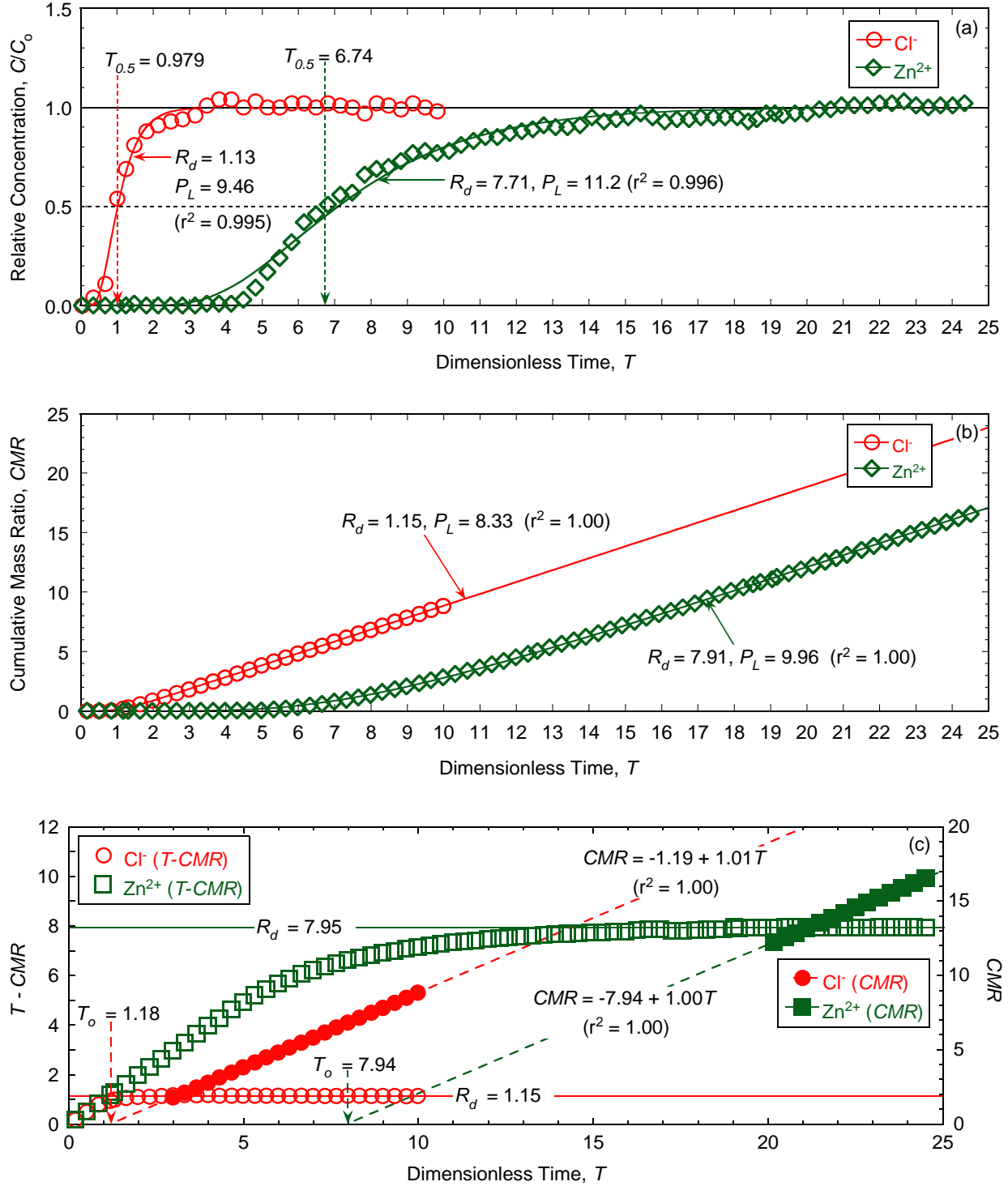


Figure 5.36. Chemical transport analyses for determination of column Péclet number ( $P_L$ ) and/or retardation factor ( $R_d$ ) for unamended backfill permeated with 20 mM  $\text{ZnCl}_2$  (Test No. 2): (a) regression of relative concentration ( $RC$ ) data; (b) regression of cumulative mass ratio ( $CMR$ ) data; (c)  $T_o$  ( $= R_d$ ) and  $T - \text{CMR}$  analyses for  $R_d$ .

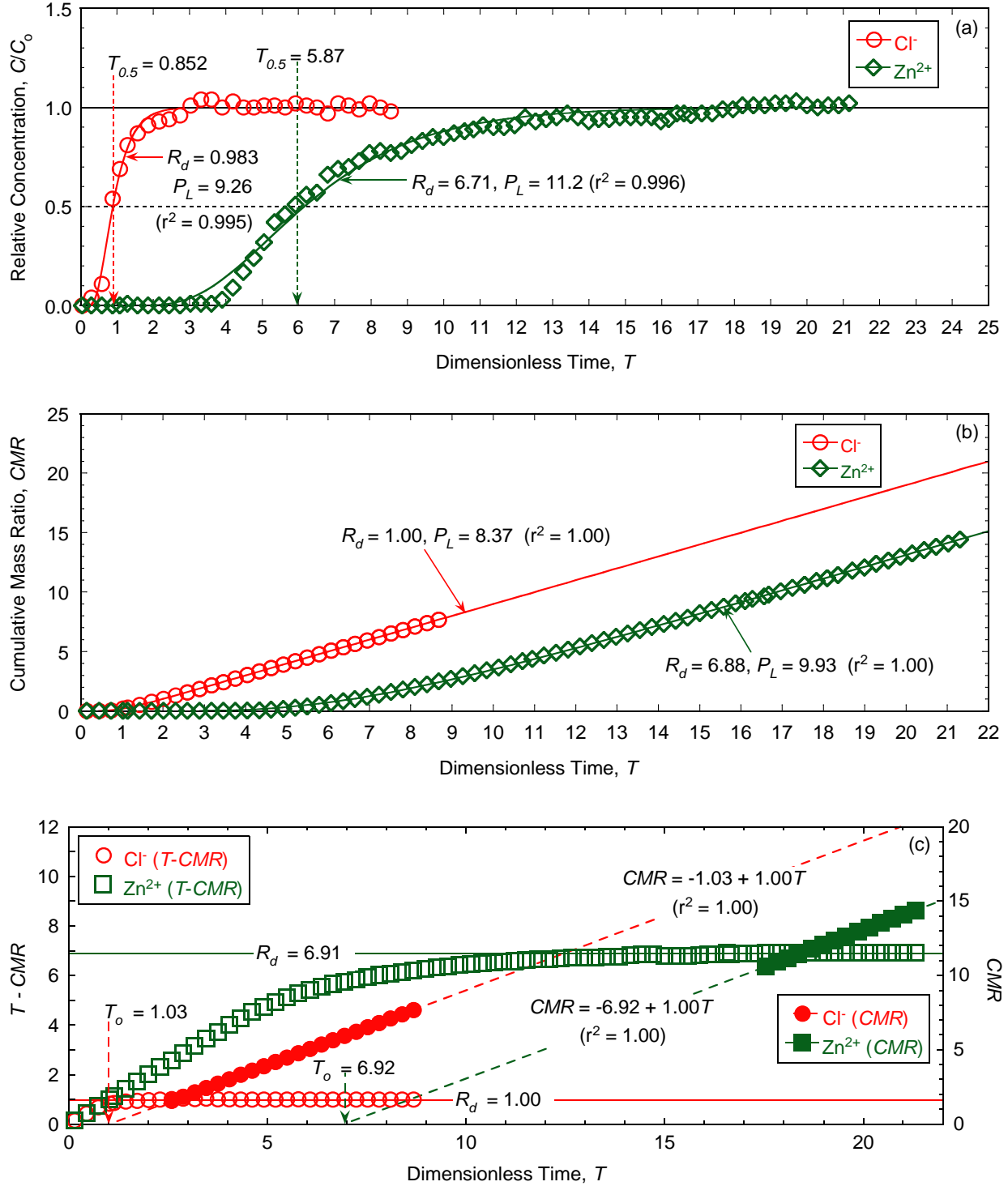


Figure 5.37. Chemical transport analyses for determination of column Péclet number ( $P_L$ ) and/or retardation factor ( $R_d$ ) for unamended backfill permeated with 20 mM ZnCl<sub>2</sub> (Test No. 2): (a) regression of relative concentration (RC) data; (b) regression of cumulative mass ratio (CMR) data; (c)  $T_o (= R_d)$  and  $T - \text{CMR}$  analyses for  $R_d$ .

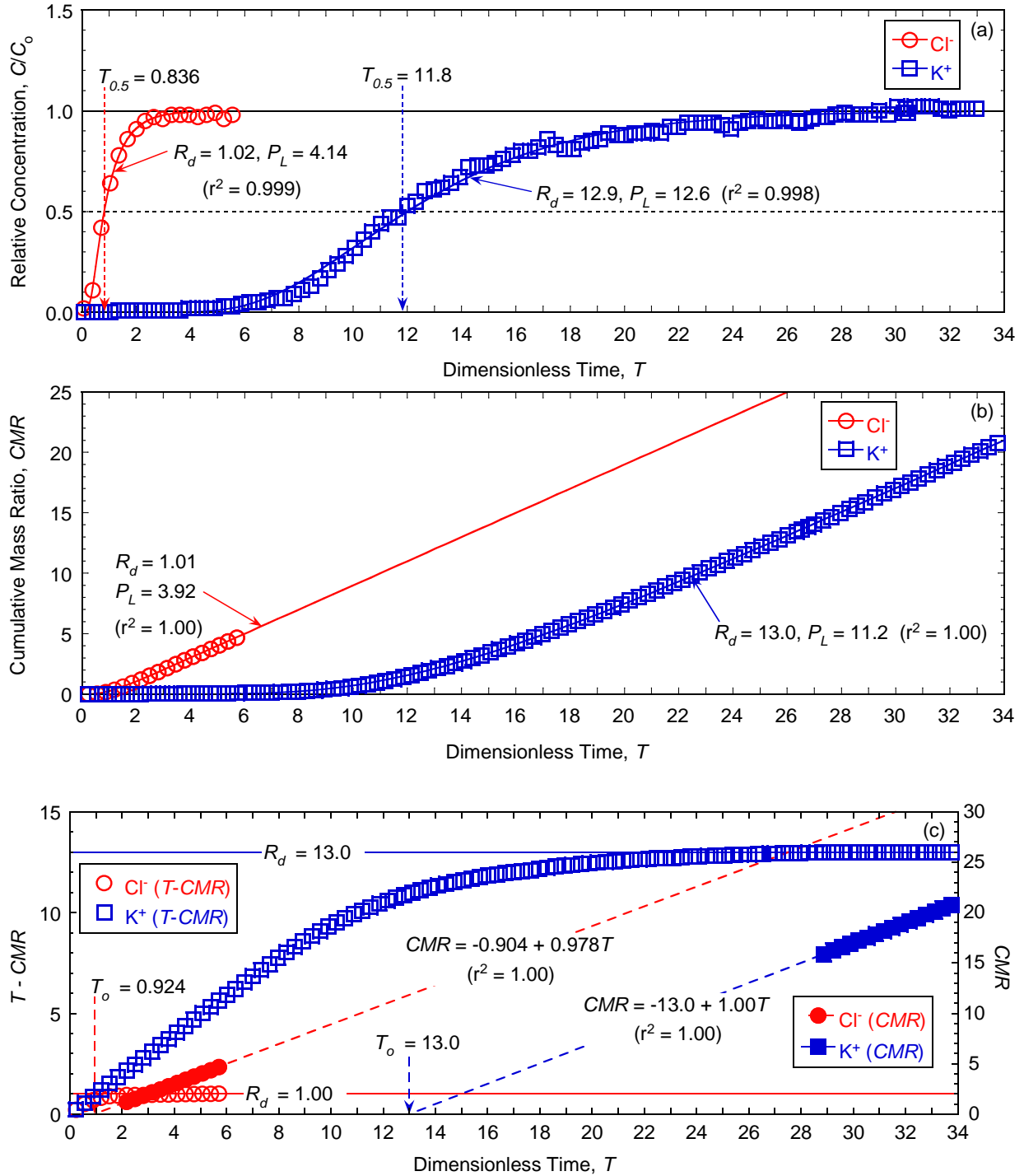


Figure 5.38. Chemical transport analyses for determination of column Péclet number ( $P_L$ ) and/or retardation factor ( $R_d$ ) for backfill amended with 5 % chabazite-UB and permeated with 35 mM KCl (Test No. 3): (a) regression of relative concentration ( $RC$ ) data; (b) regression of cumulative mass ratio ( $CMR$ ) data; (c)  $T_o$  ( $= R_d$ ) and  $T - \text{CMR}$  analyses for  $R_d$ .

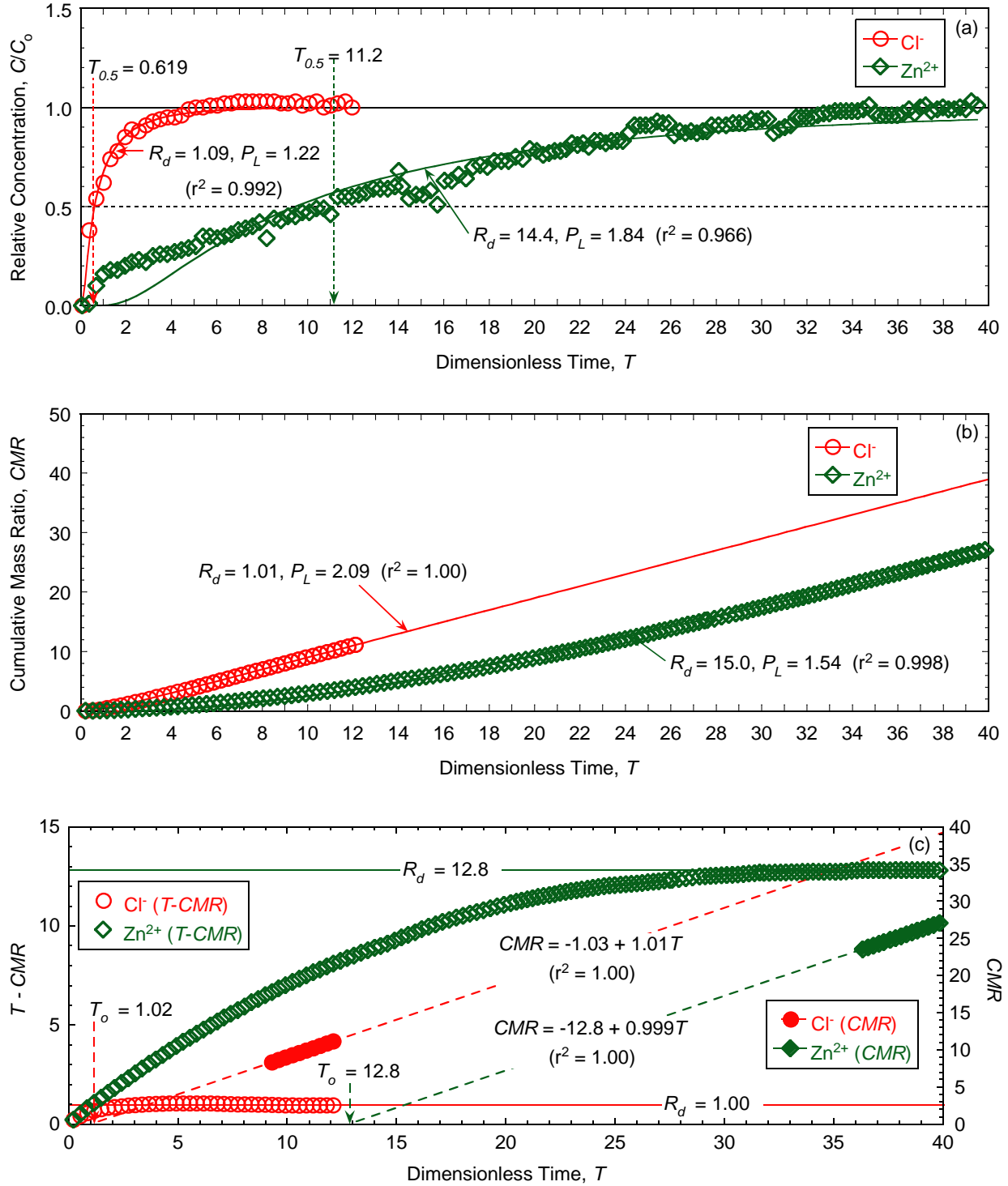


Figure 5.39. Chemical transport analyses for determination of column Péclet number ( $P_L$ ) and/or retardation factor ( $R_d$ ) for backfill amended with 5 % chabazite-UB and permeated with 20 mM ZnCl<sub>2</sub> (Test No. 4): (a) regression of relative concentration (RC) data; (b) regression of cumulative mass ratio (CMR) data; (c)  $T_o$  ( $= R_d$ ) and  $T - \text{CMR}$  analyses for  $R_d$ .

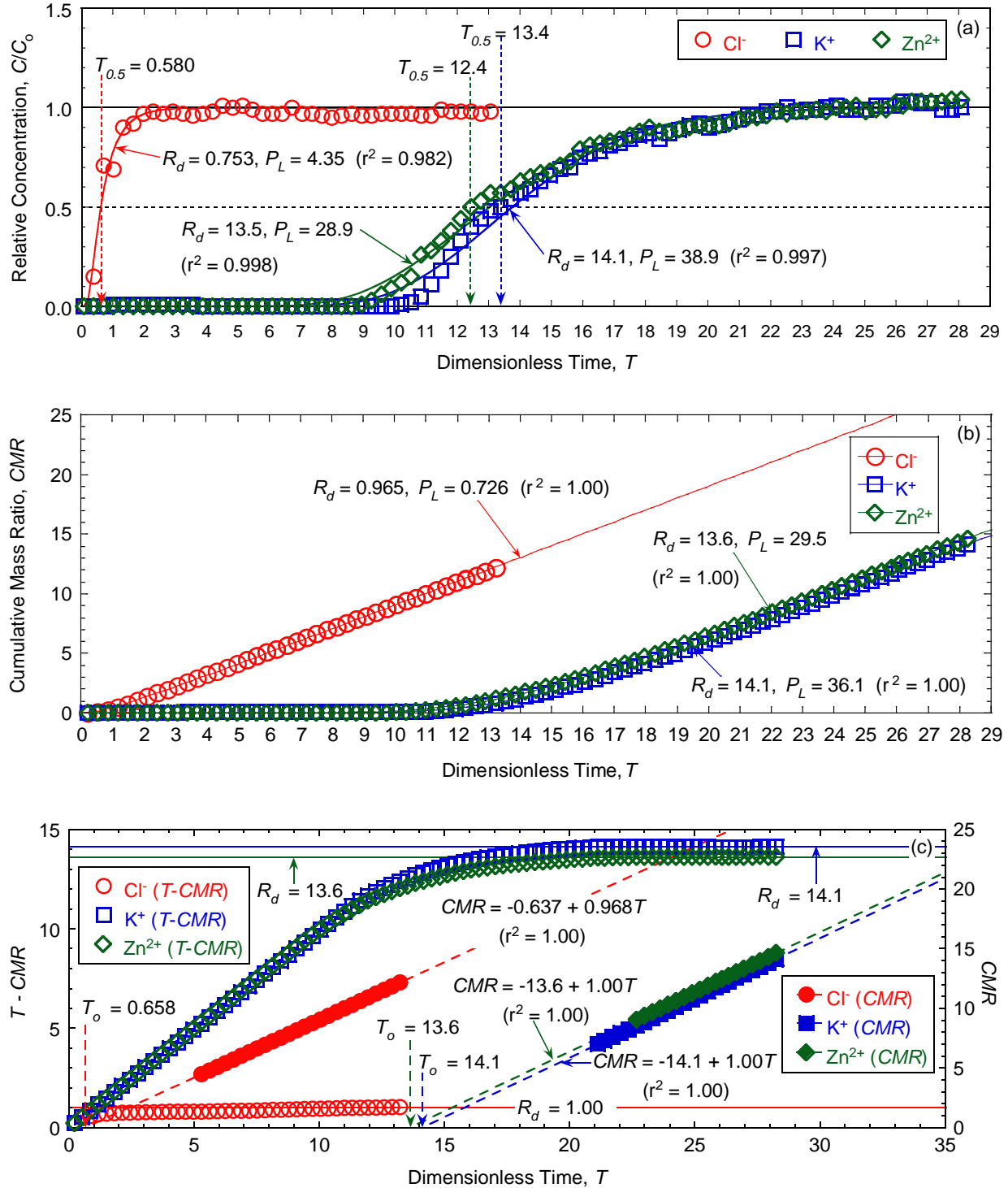


Figure 5.40. Chemical transport analyses for determination of column Péclet number ( $P_L$ ) and/or retardation factor ( $R_d$ ) for backfill amended with 5 % chabazite-UB and permeated with 17.5 mM KCl plus 10 mM  $\text{ZnCl}_2$  (Test No. 5): (a) regression of relative concentration ( $RC$ ) data; (b) regression of cumulative mass ratio ( $CMR$ ) data; (c)  $T_o$  ( $= R_d$ ) and  $T - \text{CMR}$  analyses for  $R_d$ .

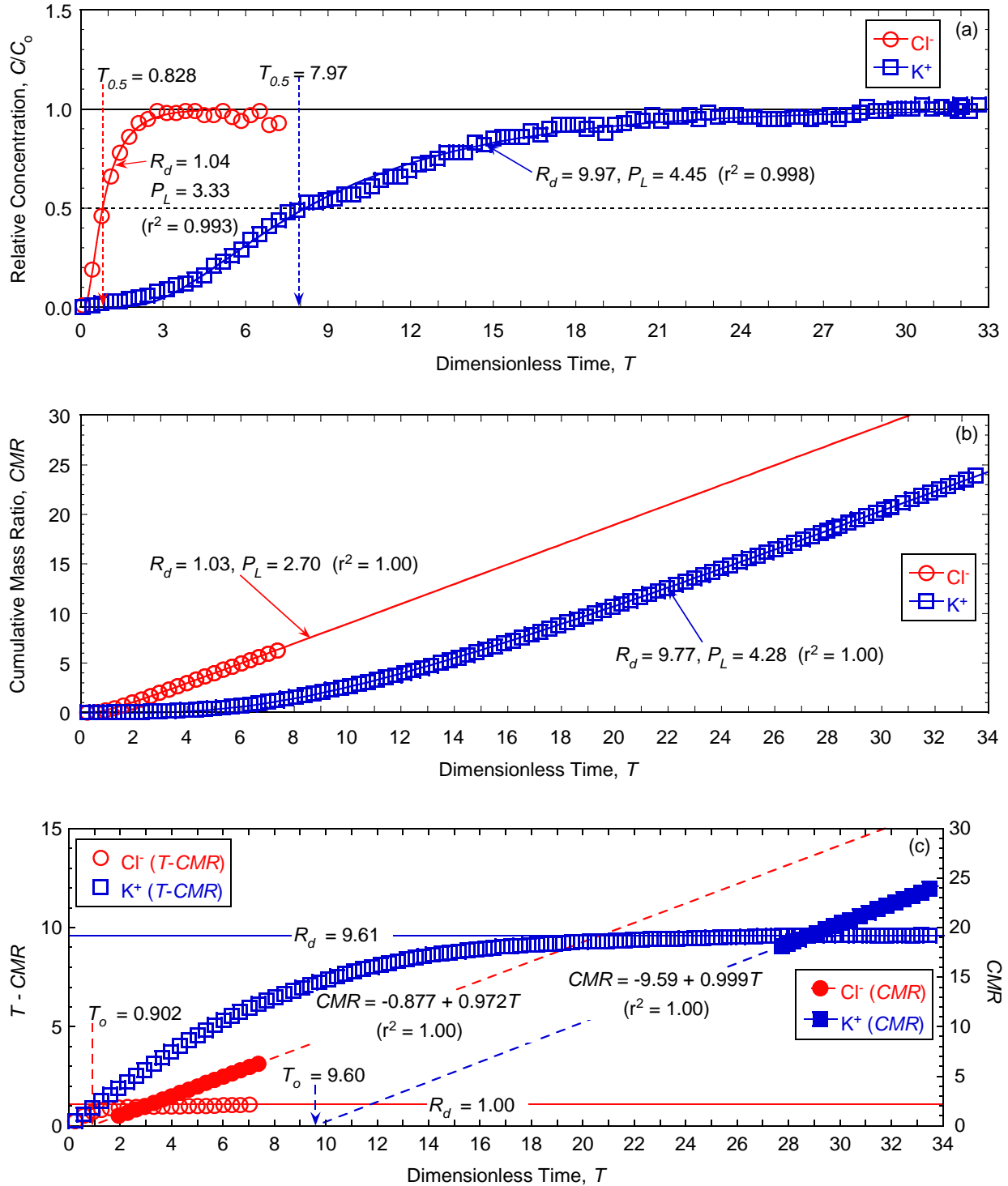


Figure 5.41. Chemical transport analyses for determination of column Péclet number ( $P_L$ ) and/or retardation factor ( $R_d$ ) for backfill amended with 5 % clinoptilolite and permeated with 35 mM KCl (Test No. 6): (a) regression of relative concentration ( $RC$ ) data; (b) regression of cumulative mass ratio ( $CMR$ ) data; (c)  $T_o$  ( $= R_d$ ) and  $T - \text{CMR}$  analyses for  $R_d$ .

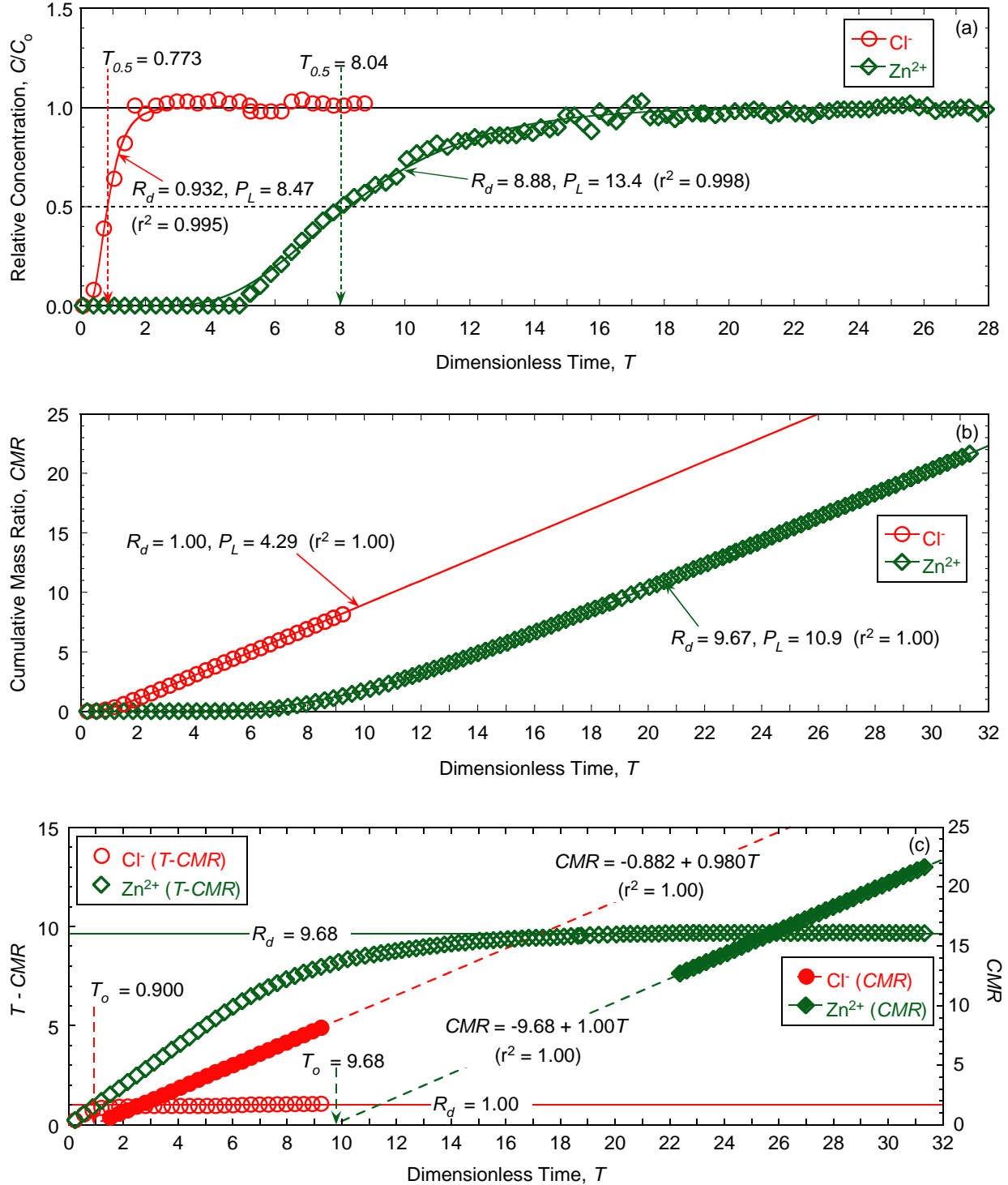


Figure 5.42. Chemical transport analyses for determination of column Péclet number ( $P_L$ ) and/or retardation factor ( $R_d$ ) for backfill amended with 5 % clinoptilolite and permeated with 20 mM  $\text{ZnCl}_2$  (Test No. 7): (a) regression of relative concentration (RC) data; (b) regression of cumulative mass ratio (CMR) data; (c)  $T_o$  ( $= R_d$ ) and  $T - \text{CMR}$  analyses for  $R_d$ .

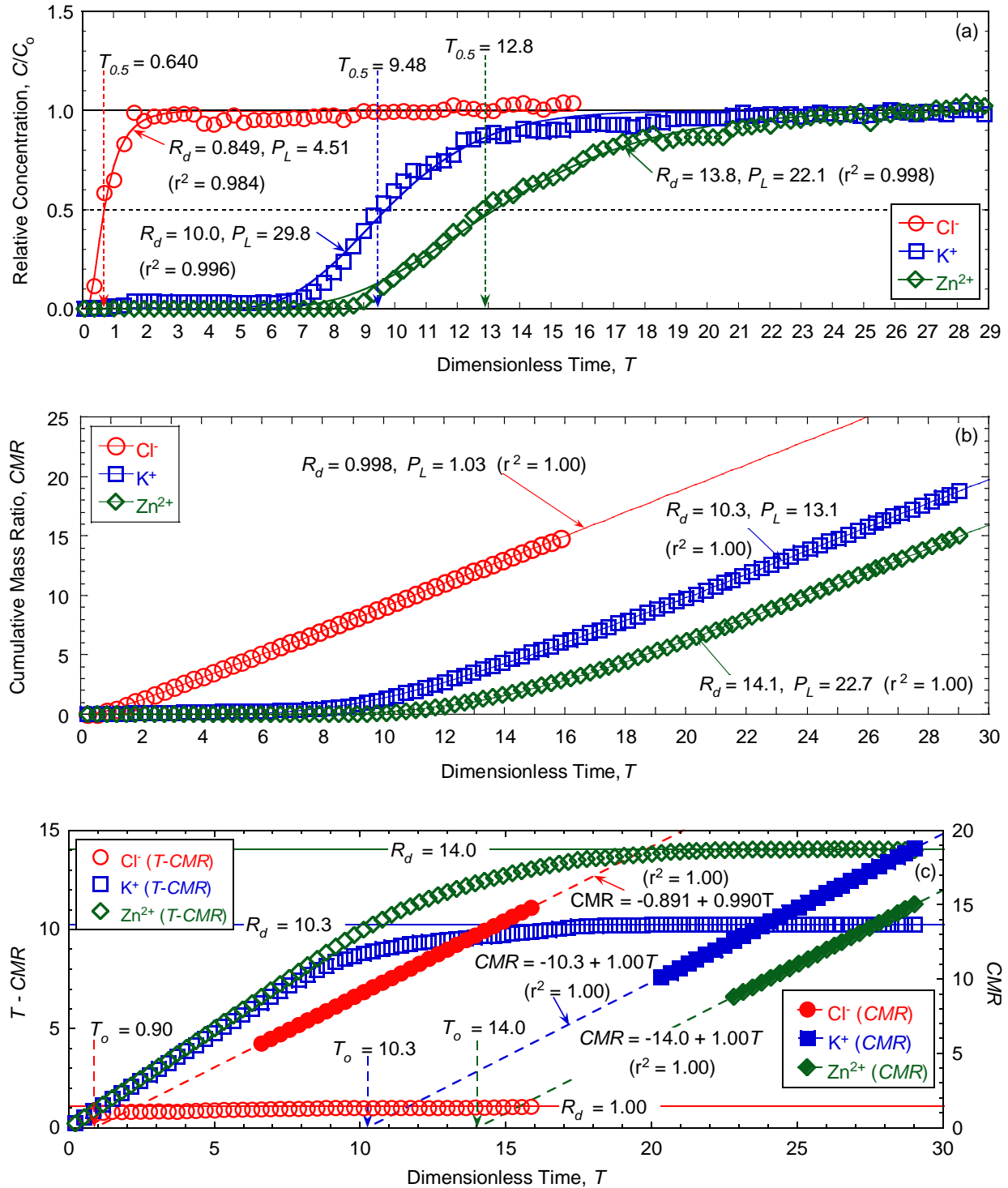


Figure 5.43. Chemical transport analyses for determination of column Péclet number ( $P_L$ ) and/or retardation factor ( $R_d$ ) for backfill amended with 5% clinoptilolite and permeated with 17.5 mM KCl plus 10 mM ZnCl<sub>2</sub> (Test No. 8): (a) regression of relative concentration ( $RC$ ) data; (b) regression of cumulative mass ratio ( $CMR$ ) data; (c)  $T_o$  ( $= R_d$ ) and  $T - CMR$  analyses for  $R_d$ .

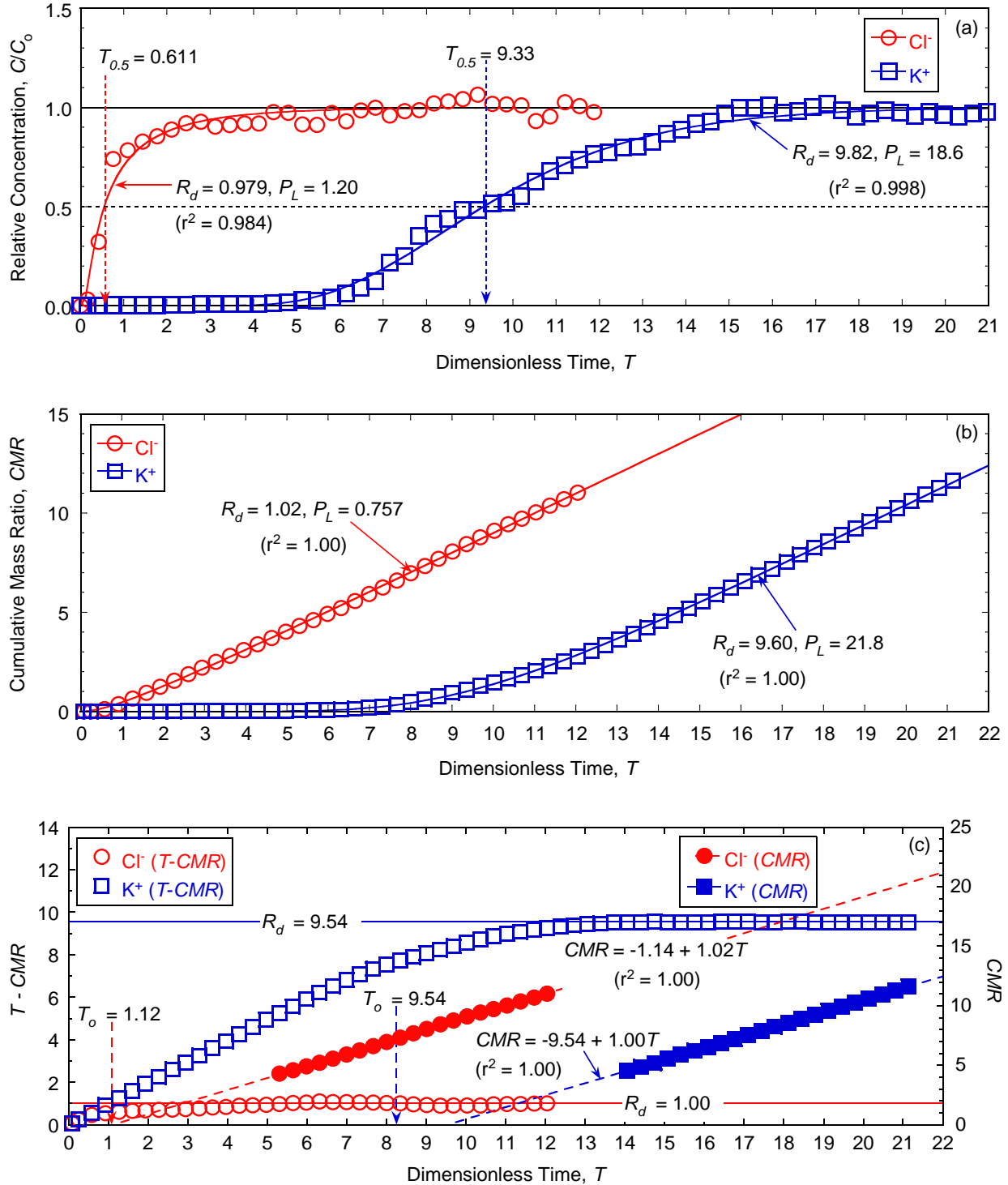


Figure 5.44. Chemical transport analyses for determination of column Péclet number ( $P_L$ ) and/or retardation factor ( $R_d$ ) for backfill amended with 5 % chabazite-LB and permeated with 35 mM KCl (Test No. 9): (a) regression of relative concentration (RC) data; (b) regression of cumulative mass ratio (CMR) data; (c)  $T_o (= R_d)$  and  $T - \text{CMR}$  analyses for  $R_d$ .

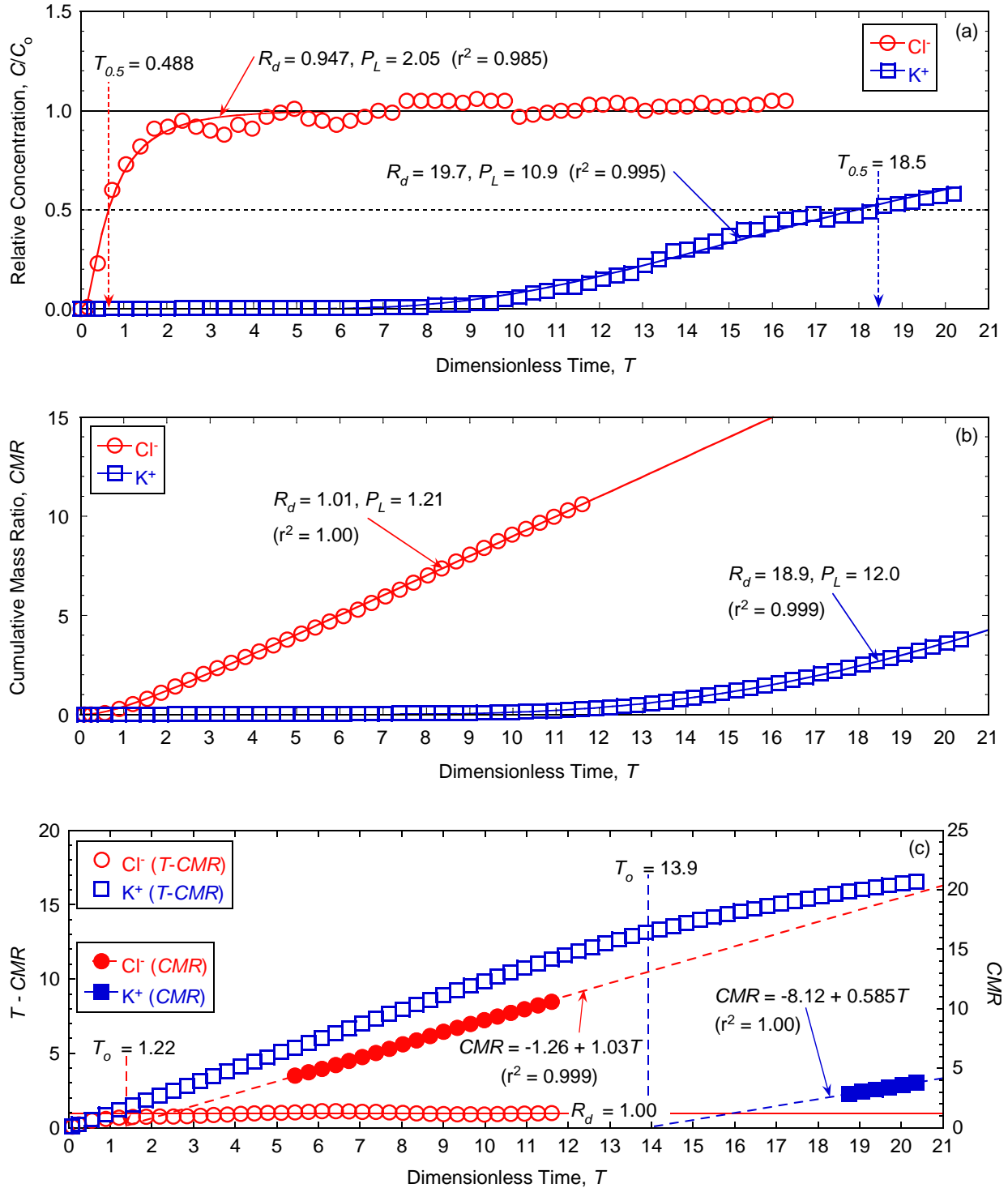


Figure 5.45. Chemical transport analyses for determination of column Péclet number ( $P_L$ ) and/or retardation factor ( $R_d$ ) for backfill amended with 10 % chabazite-LB and permeated with 35 mM KCl (Test No. 10): (a) regression of relative concentration (RC) data; (b) regression of cumulative mass ratio (CMR) data; (c)  $T_o (= R_d)$  and  $T - CMR$  analyses for  $R_d$ .

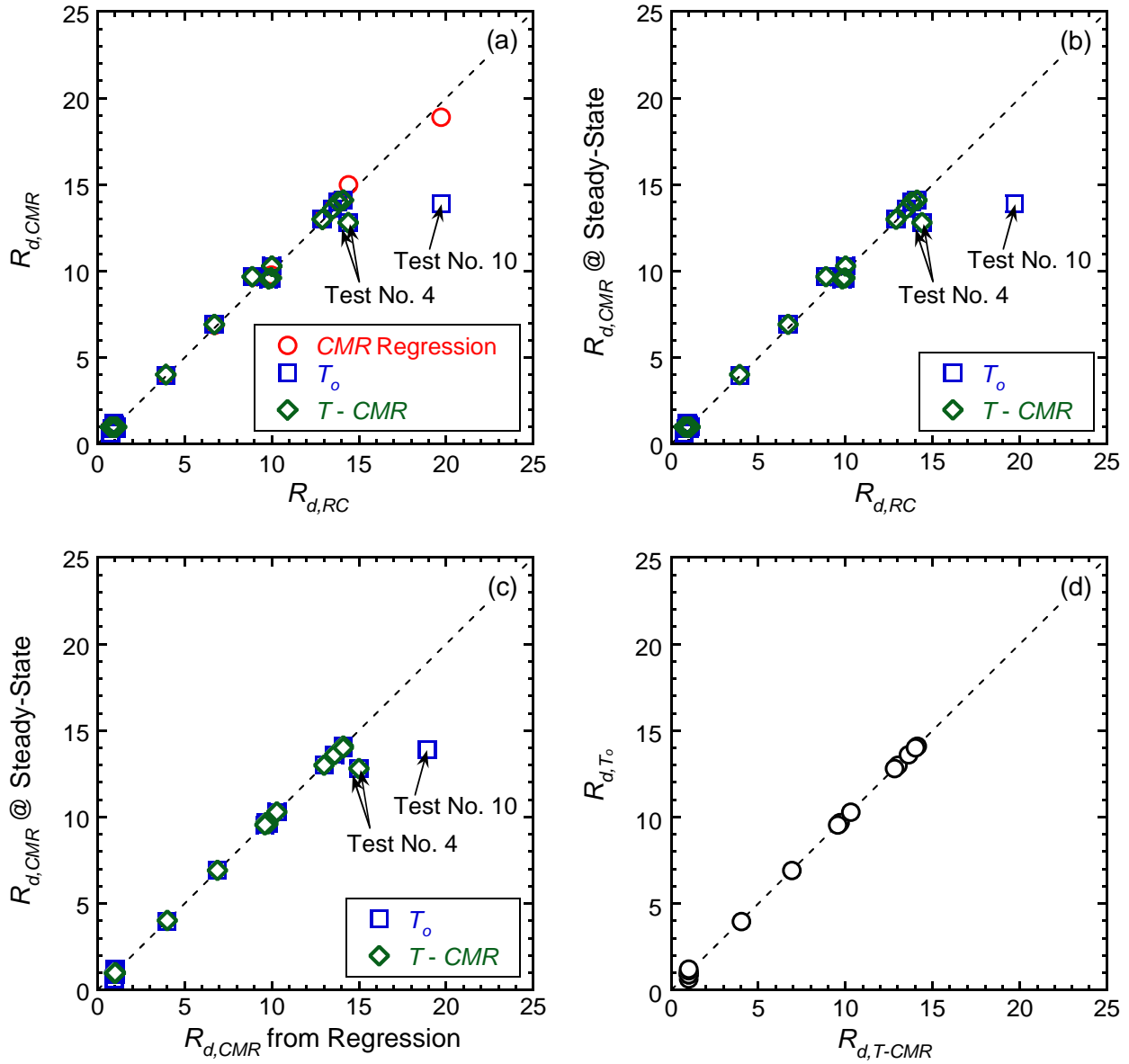


Figure 5.46. Comparison of the retardation factor ( $R_d$ ): (a)  $R_d$  from relative concentration (RC) versus  $R_d$  from cumulative mass ratio (CMR); (b)  $R_d$  from RC versus  $R_d$  from steady-state CMR; (c)  $R_d$  from CMR versus  $R_d$  from steady-state CMR; (d)  $R_d$  from ( $T-CMR$ ) versus  $T_o$ .

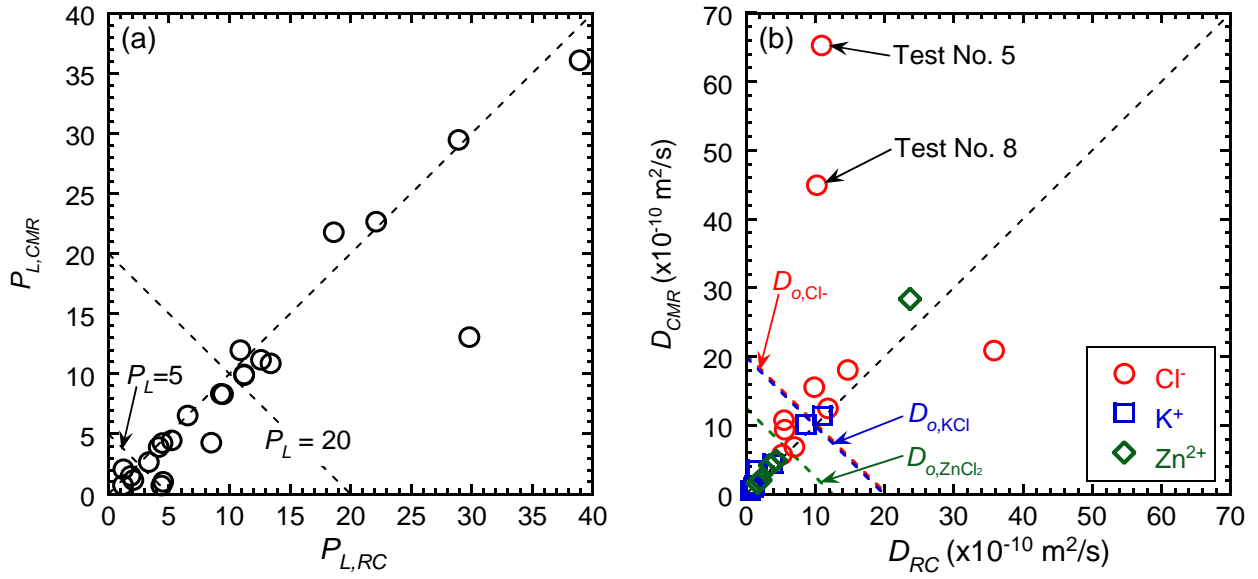


Figure 5.47. Comparison of the Péclet Number ( $P_L$ ), and dispersion coefficient ( $D$ ) from relative concentration ( $RC$ ) and cumulative mass ratio ( $CMR$ ): (a)  $P_L$  from  $RC$  versus  $CMR$ ; (b)  $R_d$  from  $RC$  versus steady-state  $CMR$ ; (b)  $D$  from  $RC$  versus  $CMR$ .

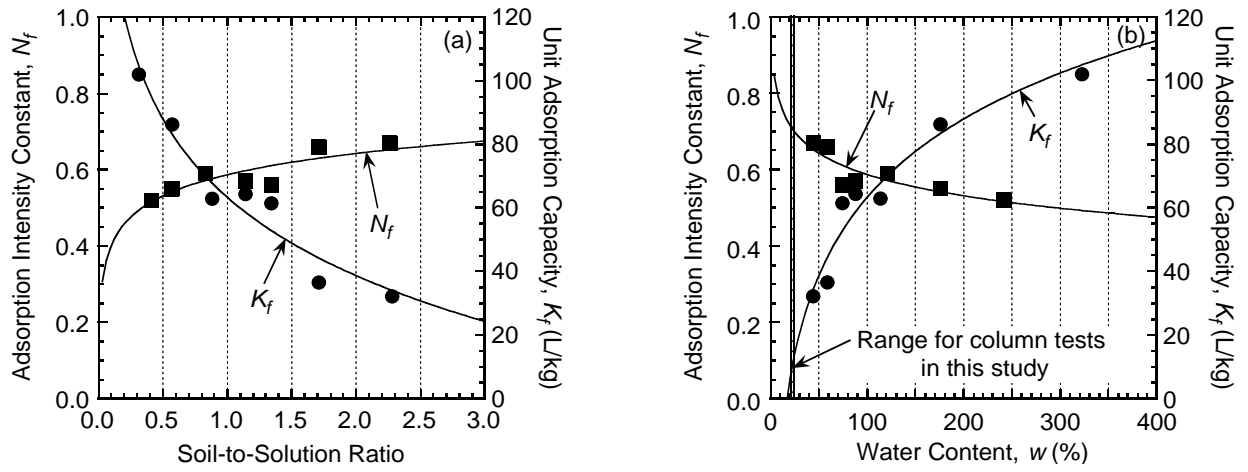


Figure 5.48. The Freundlich sorption parameters as a function of (a) soil-to-solution ratio and (b) the gravimetric water content (data from Manassero *et al.* 1998).

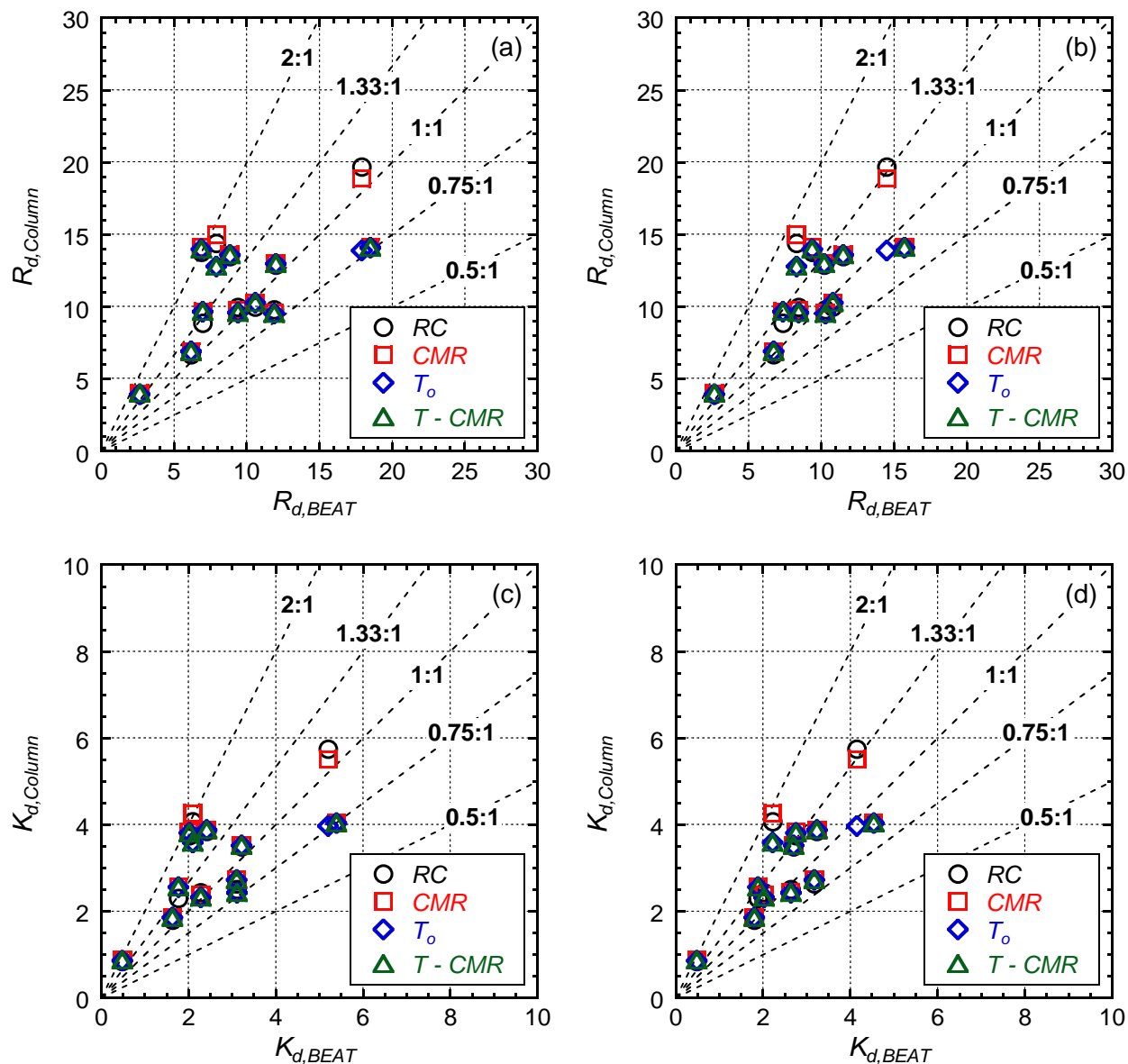


Figure 5.49. Comparison of the retardation factor ( $R_d$ ) and distribution coefficient ( $K_d$ ) based on the column test and batch equilibrium adsorption tests (BEATs): (a)  $R_{d,BEAT}$  (Langmuir model) versus  $R_{d,Column}$ ; (b)  $R_{d,BEAT}$  (Freundlich model) versus  $R_{d,Column}$ ; (c)  $K_{d,BEAT}$  (Langmuir model) versus  $K_{d,Column}$ ; (d)  $K_{d,BEAT}$  (Freundlich model) versus  $K_{d,Column}$ .

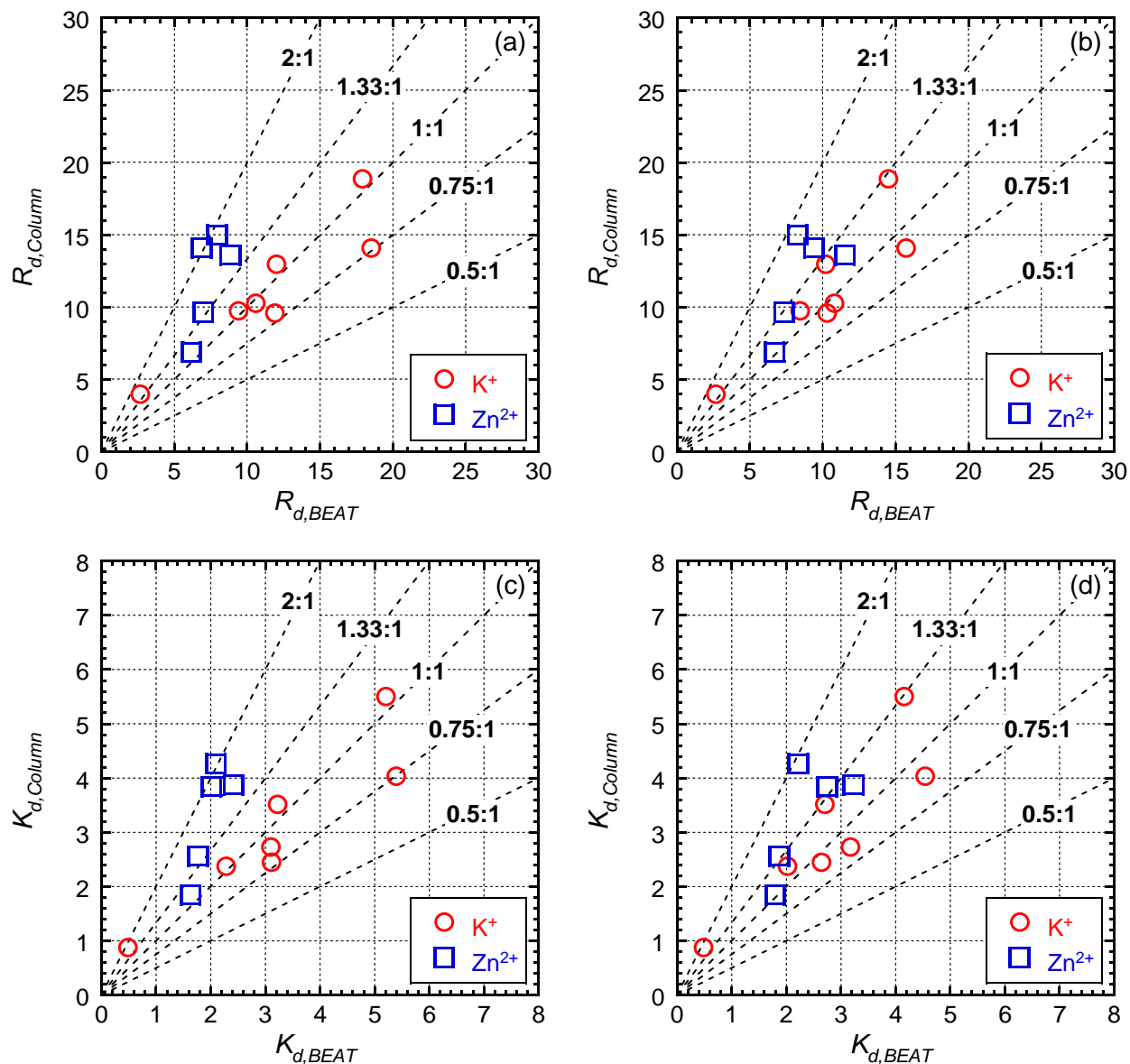


Figure 5.50. Comparison of the retardation factor ( $R_d$ ) and distribution coefficient ( $K_d$ ) based on the *CMR* regression to the column test and batch equilibrium adsorption tests (BEATs): (a)  $R_{d, BEAT}$  (Langmuir model) versus  $R_{d, Column}$ ; (b)  $R_{d, BEAT}$  (Freundlich model) versus  $R_{d, Column}$ ; (c)  $K_{d, BEAT}$  (Langmuir model) versus  $K_{d, Column}$ ; (d)  $K_{d, BEAT}$  (Freundlich model) versus  $K_{d, Column}$ .

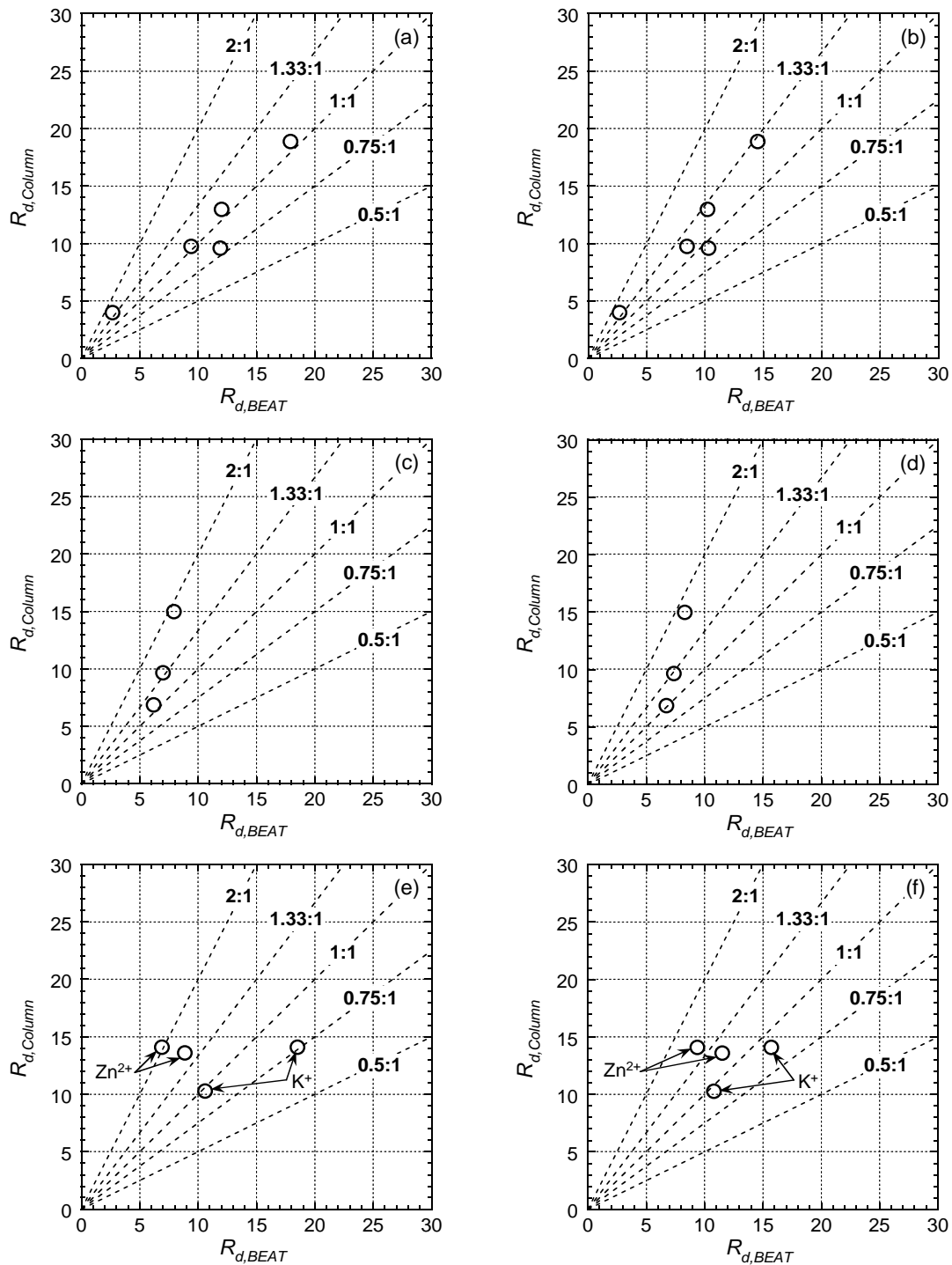


Figure 5.51. Comparison of the retardation factor ( $R_d$ ) based on the *CMR* regression to the column test and batch equilibrium adsorption test (BEAT): (a)  $R_{d,BEAT}$  (Langmuir model) versus  $R_{d,Column}$  for 35 mM KCl; (b)  $R_{d,BEAT}$  (Freundlich model) versus  $R_{d,Column}$  for 35 mM KCl; (c)  $R_{d,BEAT}$  (Langmuir model) versus  $R_{d,Column}$  for 20 mM  $ZnCl_2$ ; (d)  $R_{d,BEAT}$  (Freundlich model) versus  $R_{d,Column}$  for 20 mM  $ZnCl_2$ ; (e)  $R_{d,BEAT}$  (Langmuir model) versus  $R_{d,Column}$  for 17.5 mM KCl plus 10 mM  $ZnCl_2$ ; (f)  $R_{d,BEAT}$  (Freundlich model) versus  $R_{d,Column}$  for 17.5 mM KCl plus 10 mM  $ZnCl_2$ .

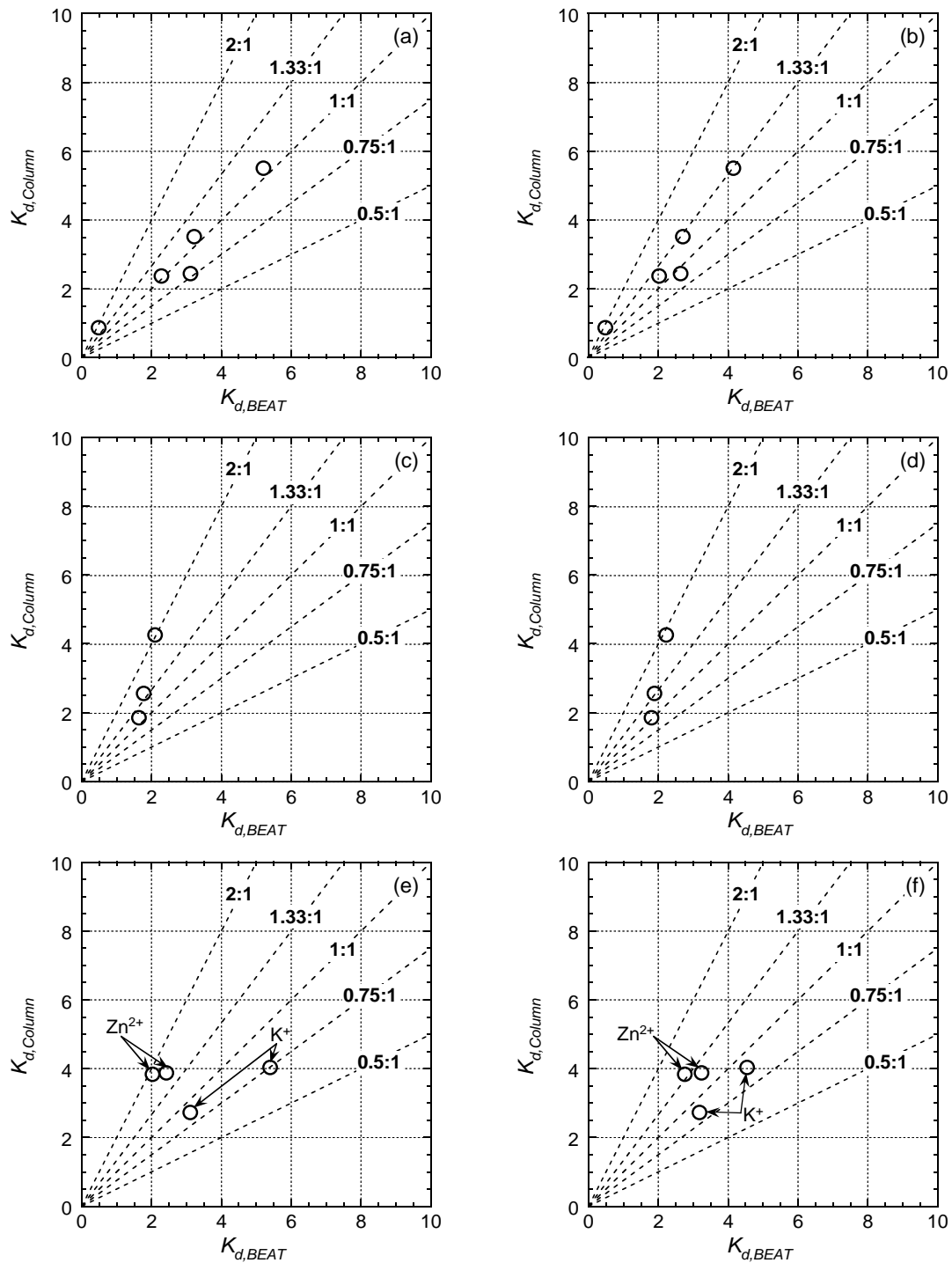


Figure 5.52. Comparison of the retardation factor ( $K_d$ ) based on the *CMR* regression to the column test and batch equilibrium adsorption test (BEAT): (a)  $K_{d, BEAT}$  (Langmuir model) versus  $K_{d, Column}$  for 35 mM KCl; (b)  $K_{d, BEAT}$  (Freundlich model) versus  $K_{d, Column}$  for 35 mM KCl; (c)  $K_{d, BEAT}$  (Langmuir model) versus  $K_{d, Column}$  for 20 mM  $ZnCl_2$ ; (d)  $K_{d, BEAT}$  (Freundlich model) versus  $K_{d, Column}$  for 20 mM  $ZnCl_2$ ; (e)  $K_{d, BEAT}$  (Langmuir model) versus  $K_{d, Column}$  for 17.5 mM KCl plus 10 mM  $ZnCl_2$ ; (f)  $K_{d, BEAT}$  (Freundlich model) versus  $K_{d, Column}$  for 17.5 mM KCl plus 10 mM  $ZnCl_2$ .

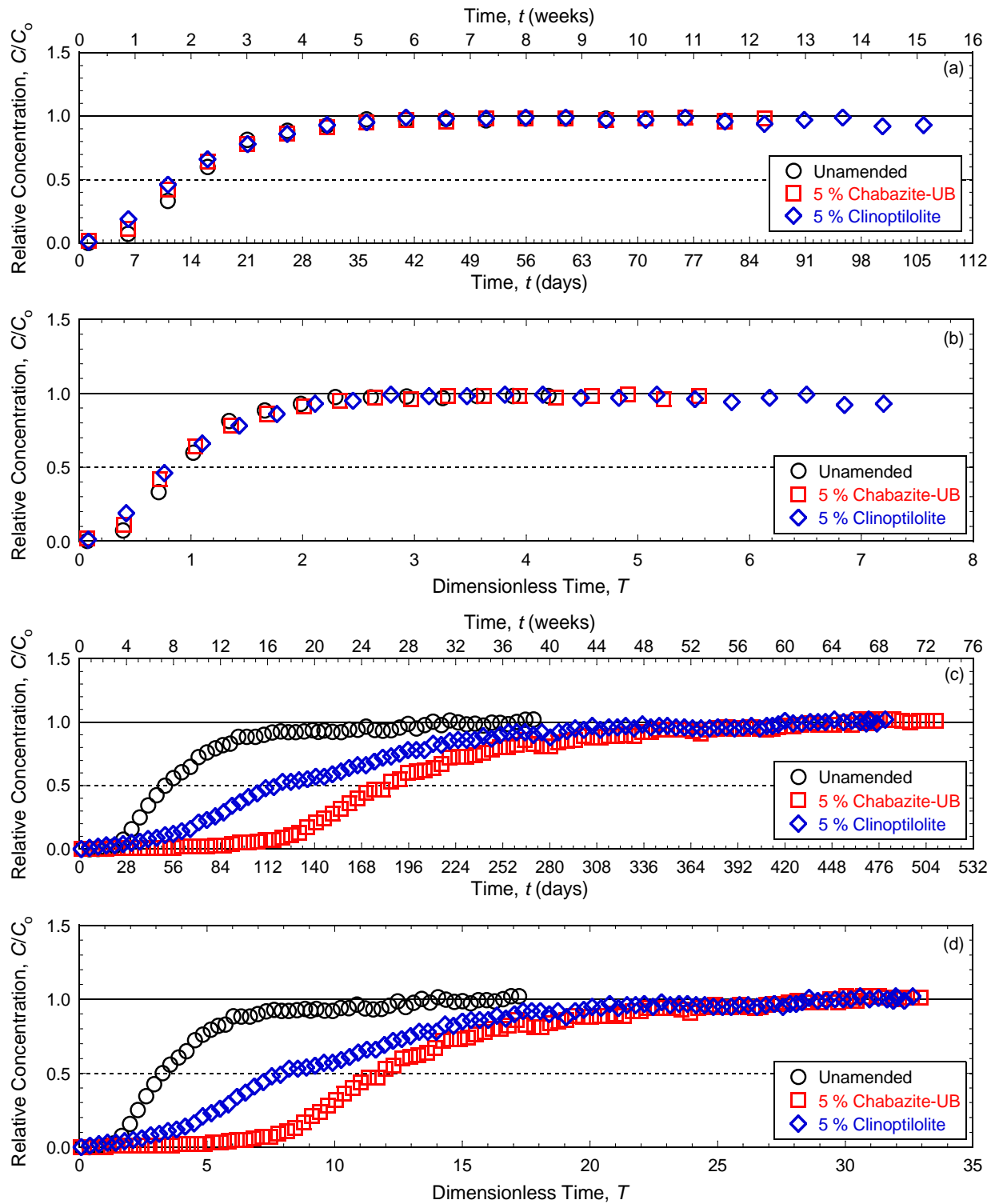


Figure 5.53. Breakthrough curves for unamended and zeolite-amended backfills permeated with 35 mM KCl: (a) chloride ( $\text{Cl}^-$ ) versus time ( $t$ ); (b)  $\text{Cl}^-$  versus dimensionless time ( $T$ ); (c) potassium ( $\text{K}^+$ ) versus  $t$ ; (d)  $\text{K}^+$  versus  $T$ .

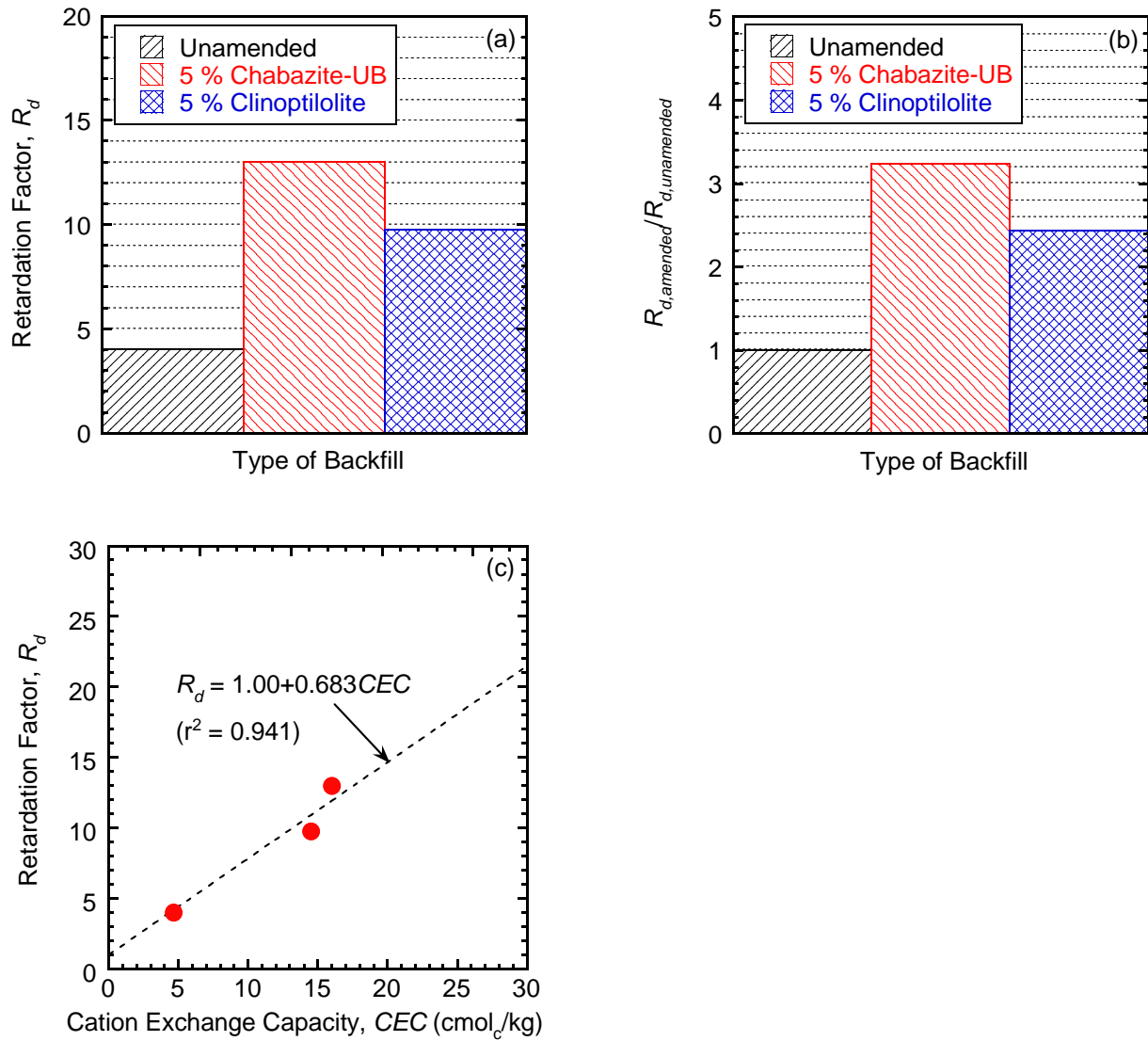


Figure 5.54. Effect of type of zeolite on retardation of potassium ( $K^+$ ) for columns of unamended and zeolite-amended backfills permeated with 35 mM KCl: (a) retardation factor ( $R_d$ ); (b) ratio of  $R_d$  for the zeolite-amended backfill relative to  $R_d$  for the unamended backfill ( $R_{d,amended}/R_{d,unamended}$ ); (c) cation exchange capacity (CEC) of backfill and  $R_d$  of  $K^+$ .

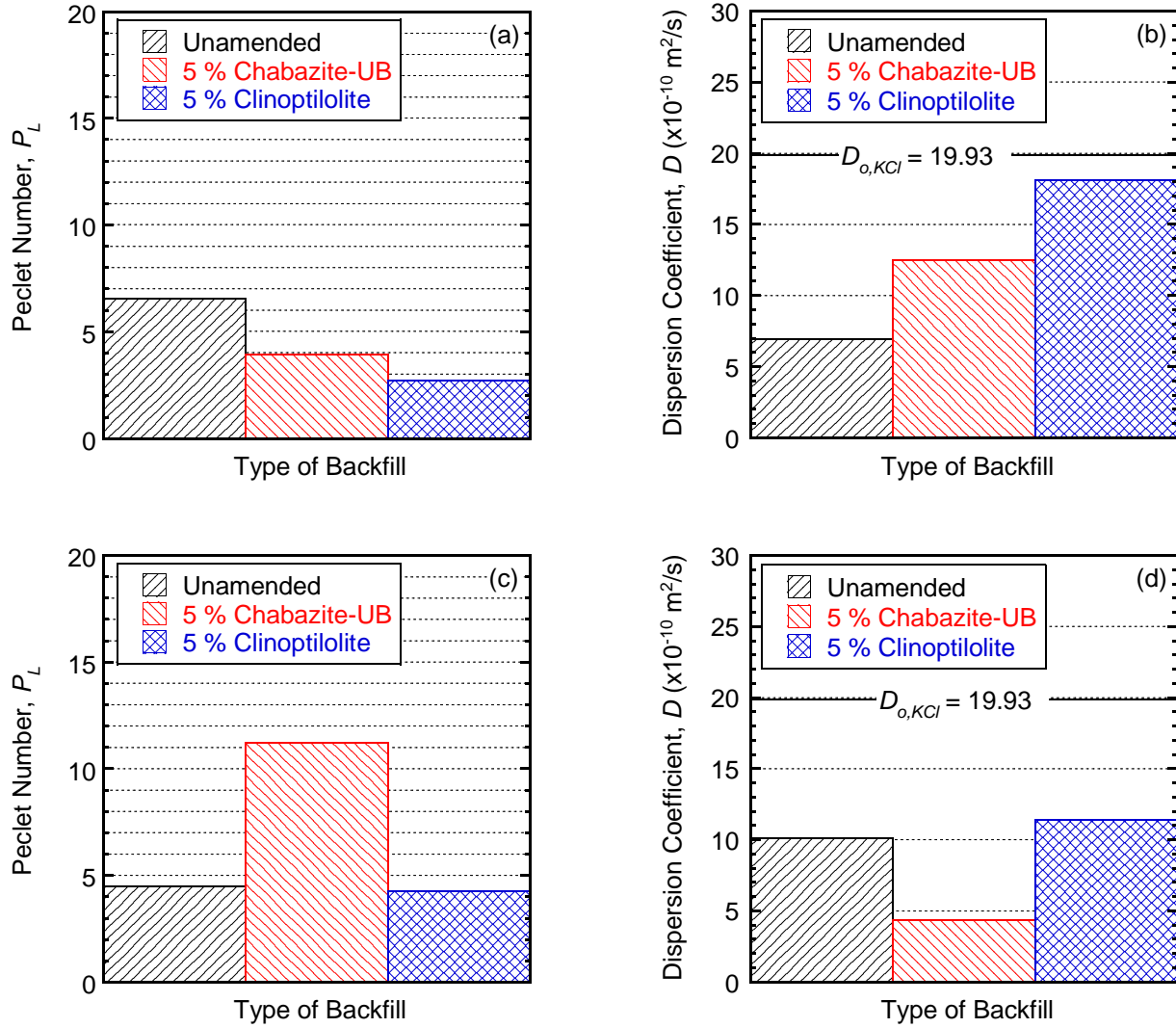


Figure 5.55. Effect of type of zeolite on transport parameters for columns of unamended and zeolite-amended backfills permeated with 35 mM KCl: (a) Péclet number ( $P_L$ ) for chloride ( $\text{Cl}^-$ ); (b) hydrodynamic dispersion coefficient ( $D$ ) for  $\text{Cl}^-$ ; (c)  $P_L$  for potassium ( $\text{K}^+$ ); (d)  $D$  for  $\text{K}^+$ .

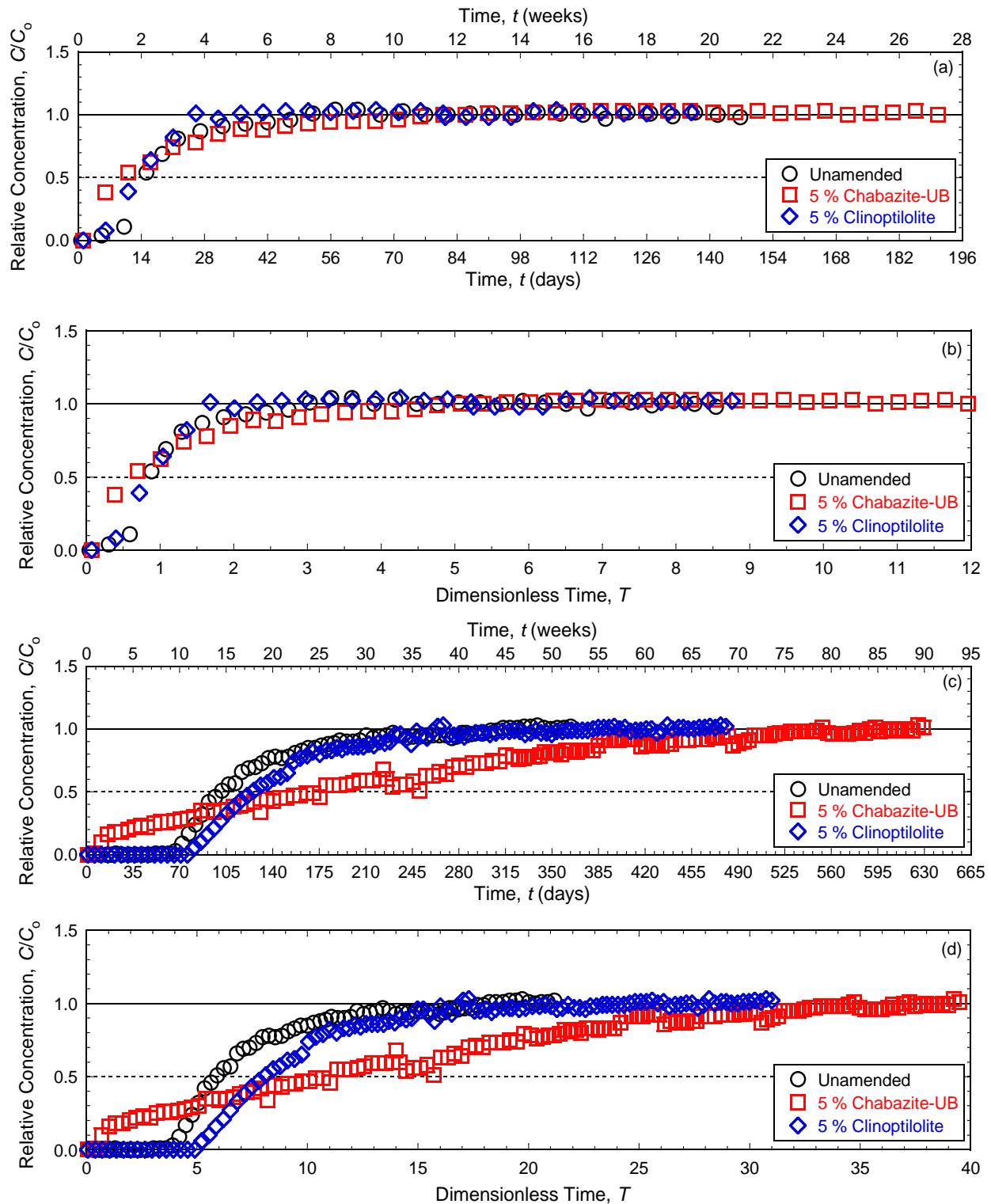


Figure 5.56. Breakthrough curves for unamended and zeolite-amended backfills permeated with 20 mM  $\text{ZnCl}_2$ : (a) chloride ( $\text{Cl}^-$ ) versus time ( $t$ ); (b)  $\text{Cl}^-$  versus dimensionless time ( $T$ ); (c) zinc ( $\text{Zn}^{2+}$ ) versus  $t$ ; (d)  $\text{Zn}^{2+}$  versus  $T$ .

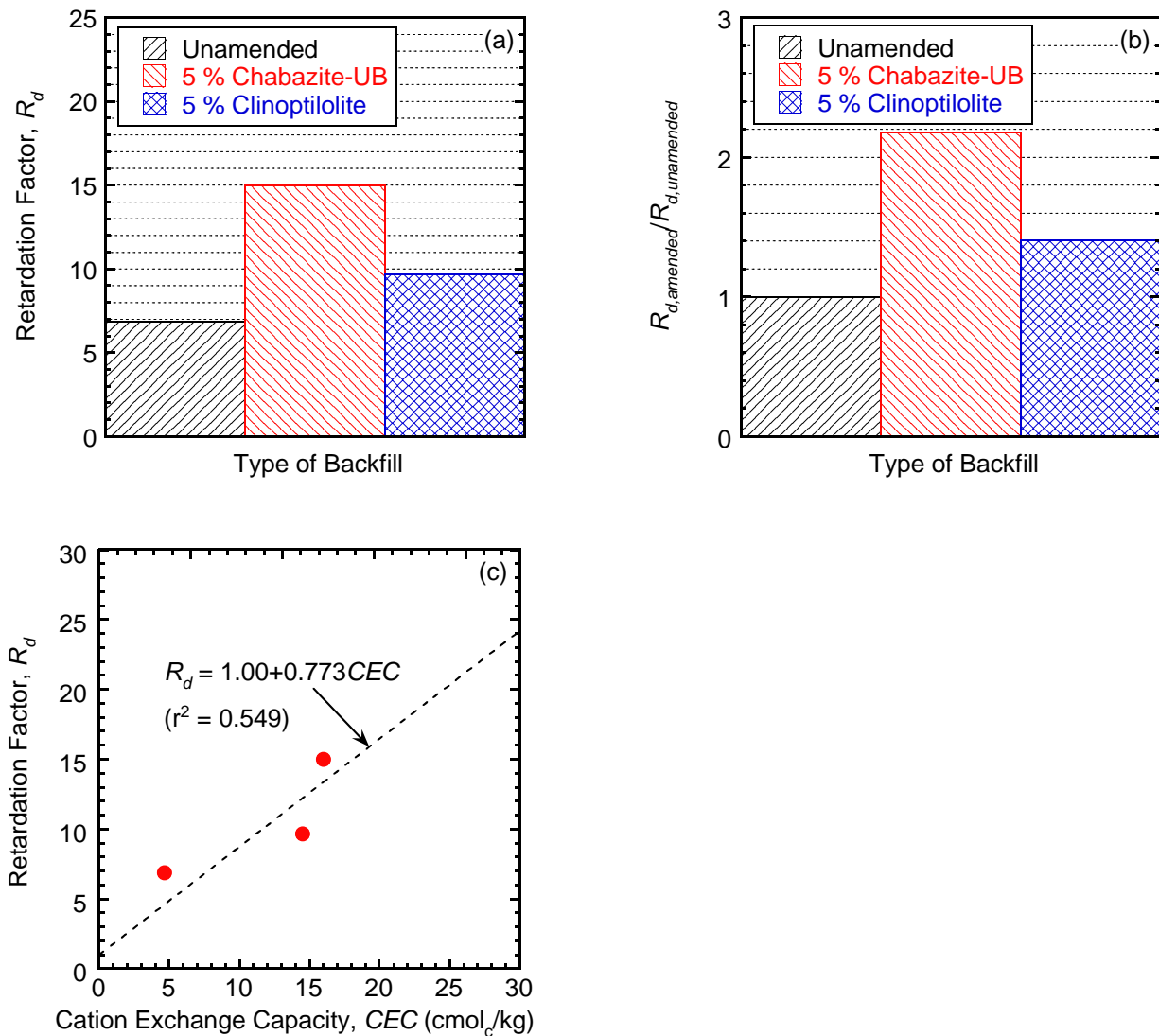


Figure 5.57. Effect of type of zeolite on retardation of zinc ( $Zn^{2+}$ ) for columns of unamended and zeolite-amended backfills permeated with 20 mM  $ZnCl_2$ : (a) retardation factor ( $R_d$ ); (b) ratio of  $R_d$  for the zeolite-amended backfill relative to  $R_d$  for the unamended backfill ( $R_{d,amended}/R_{d,unamended}$ ); (c) cation exchange capacity (CEC) of backfill and  $R_d$  of  $Zn^{2+}$ .

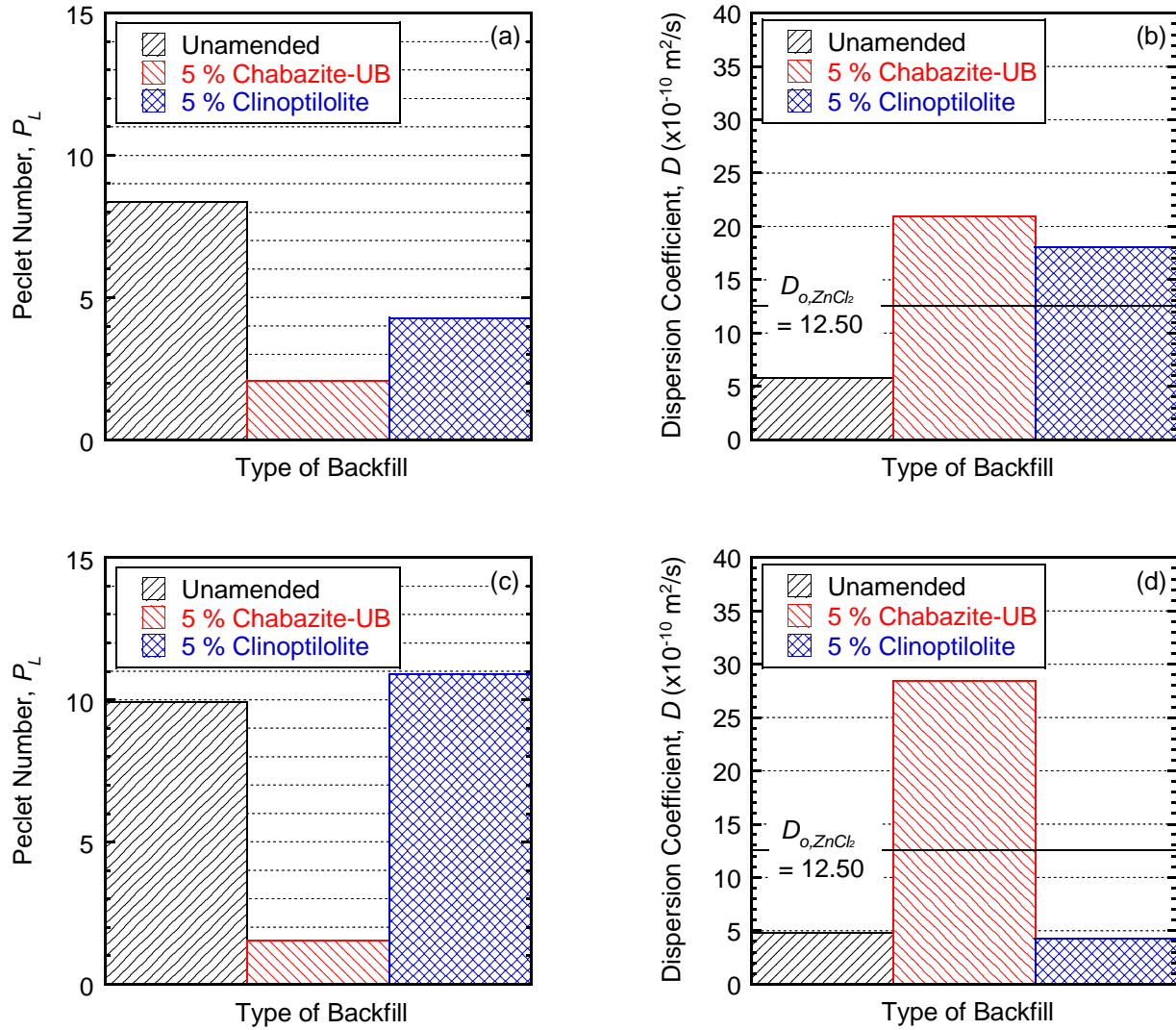


Figure 5.58. Effect of type of zeolite on transport parameters for columns of unamended and zeolite-amended backfills permeated with 20 mM ZnCl<sub>2</sub>: (a) Péclet number ( $P_L$ ) for chloride ( $\text{Cl}^-$ ); (b) hydrodynamic dispersion coefficient ( $D$ ) for  $\text{Cl}^-$ ; (c)  $P_L$  for zinc ( $\text{Zn}^{2+}$ ); (d)  $D$  for  $\text{Zn}^{2+}$ .

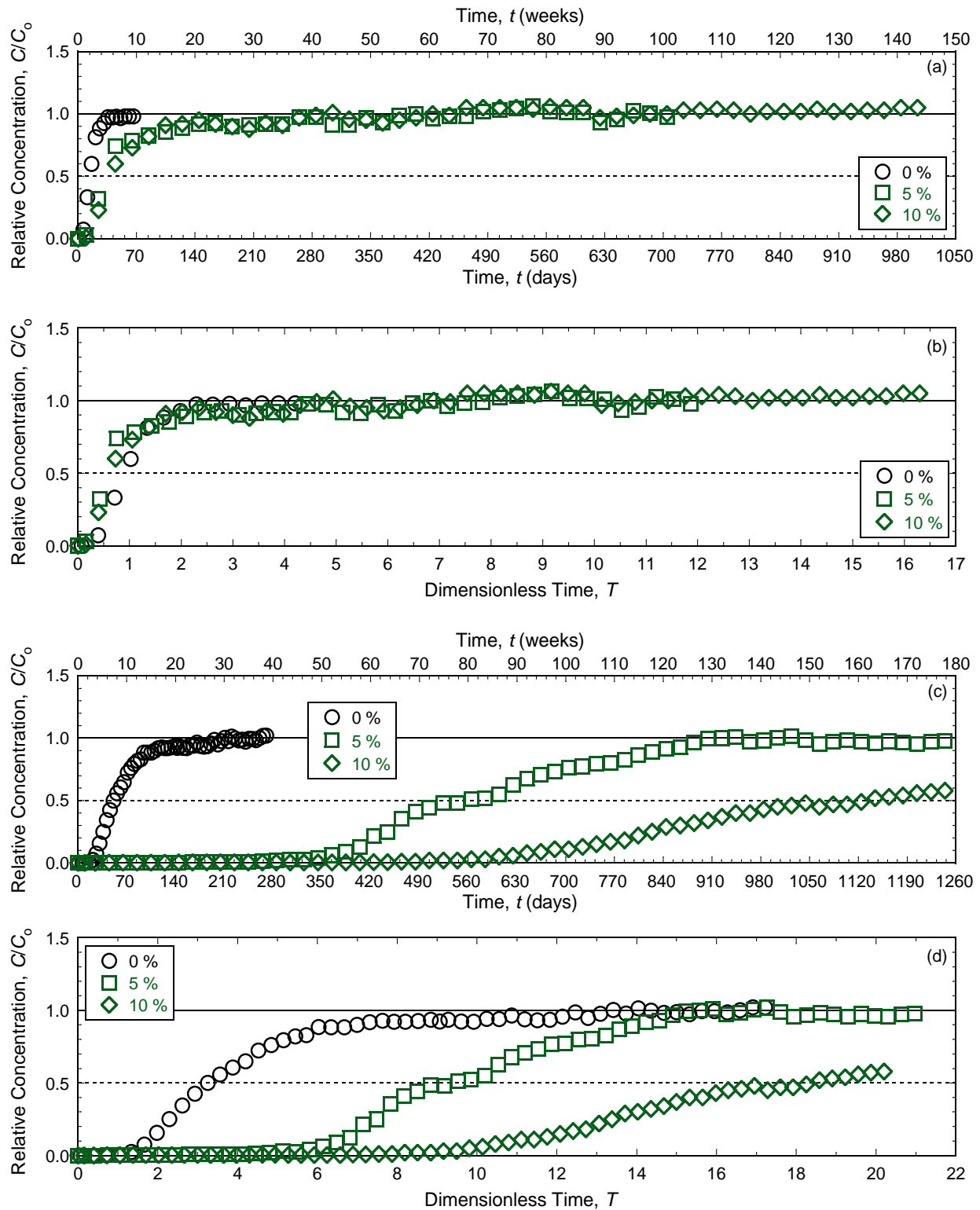


Figure 5.59. Breakthrough curves for backfills with 0 (unamended), 5 and 10 % chabazite-LB permeated with 35 mM KCl: (a) chloride ( $\text{Cl}^-$ ) versus time ( $t$ ); (b)  $\text{Cl}^-$  versus dimensionless time ( $T$ ); (c) potassium ( $\text{K}^+$ ) versus  $t$ ; (d)  $\text{K}^+$  versus  $T$ .

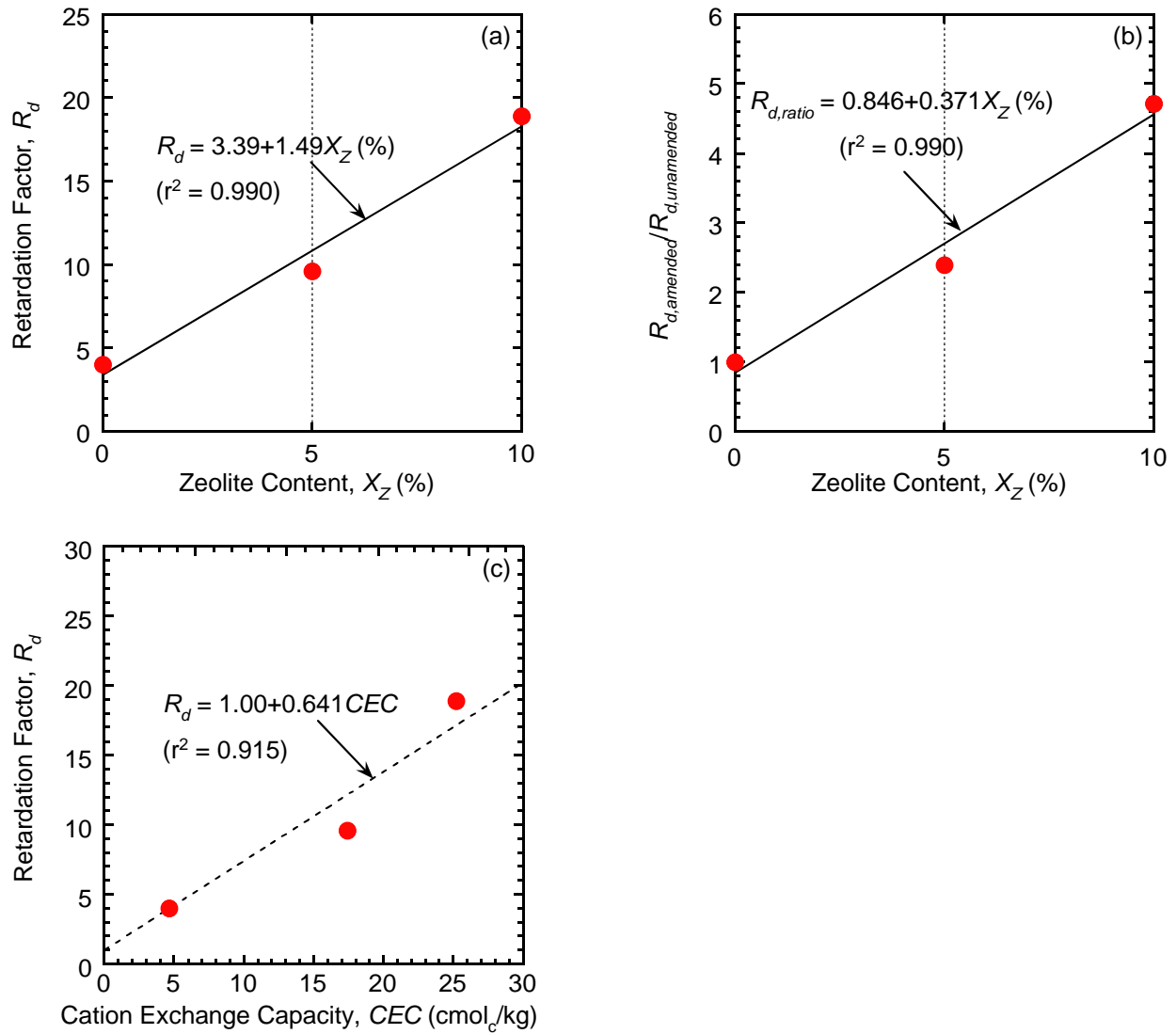


Figure 5.60. Effect of amount of zeolite on retardation of potassium ( $K^+$ ) for backfills with 0 (unamended), 5 and 10 % chabazite-LB permeated with 35 mM KCl: (a) retardation factor ( $R_d$ ); (b) ratio of  $R_d$  for the zeolite-amended backfill relative to  $R_d$  for the unamended backfill ( $R_{d,amended}/R_{d,unamended}$ ); (c) cation exchange capacity ( $CEC$ ) of backfill and  $R_d$  of  $K^+$ .

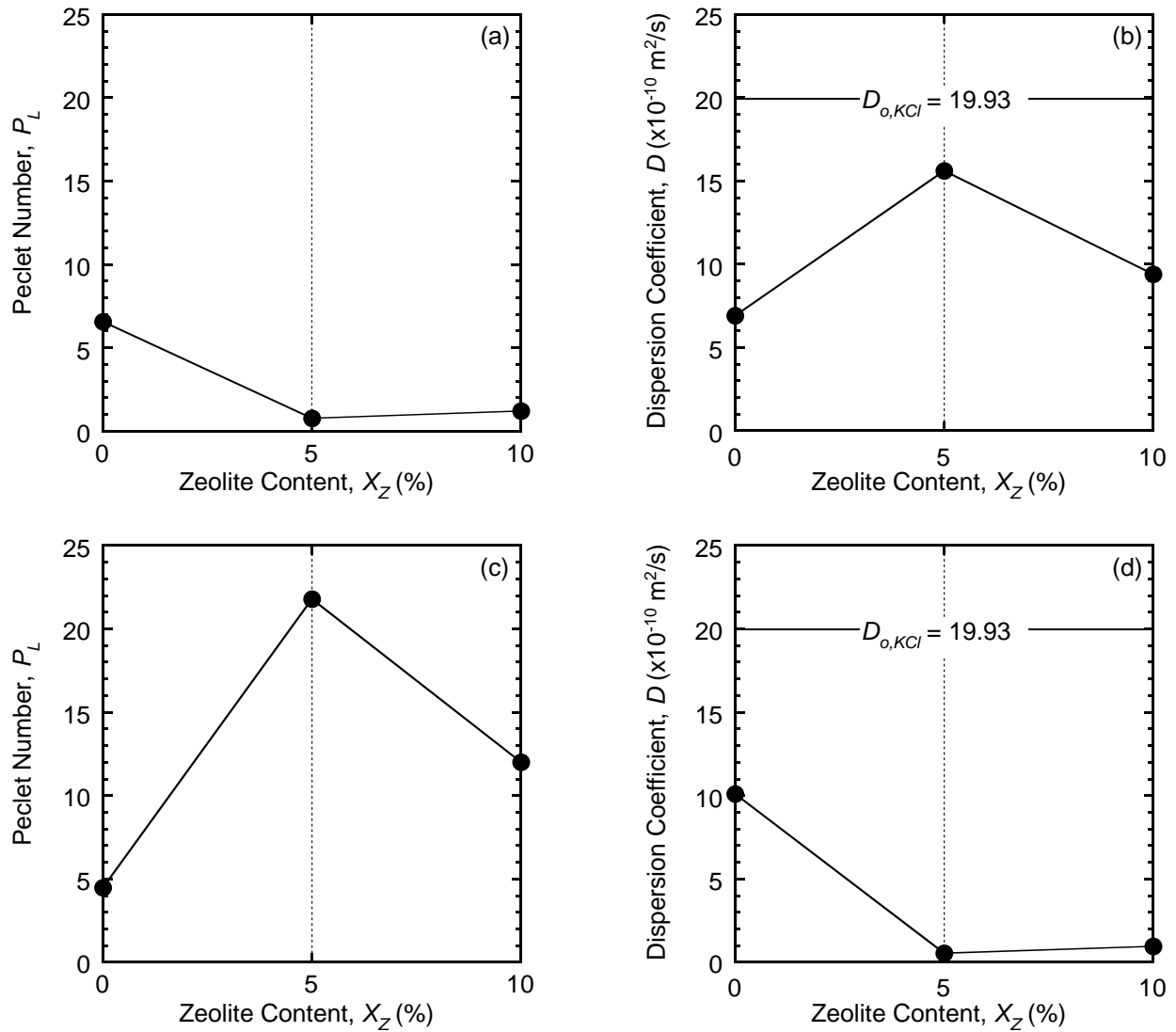


Figure 5.61. Effect of amount of zeolite on the Péclet number ( $P_L$ ) and hydrodynamic dispersion coefficient ( $D$ ) of chloride ( $\text{Cl}^-$ ) and potassium ( $\text{K}^+$ ) for backfills with 0 (unamended), 5 and 10 % chabazite-LB permeated with 35 mM KCl: (a)  $P_L$  for  $\text{Cl}^-$ ; (b)  $D$  for  $\text{Cl}^-$ ; (c)  $P_L$  for  $\text{K}^+$ ; (d)  $D$  for  $\text{K}^+$ .

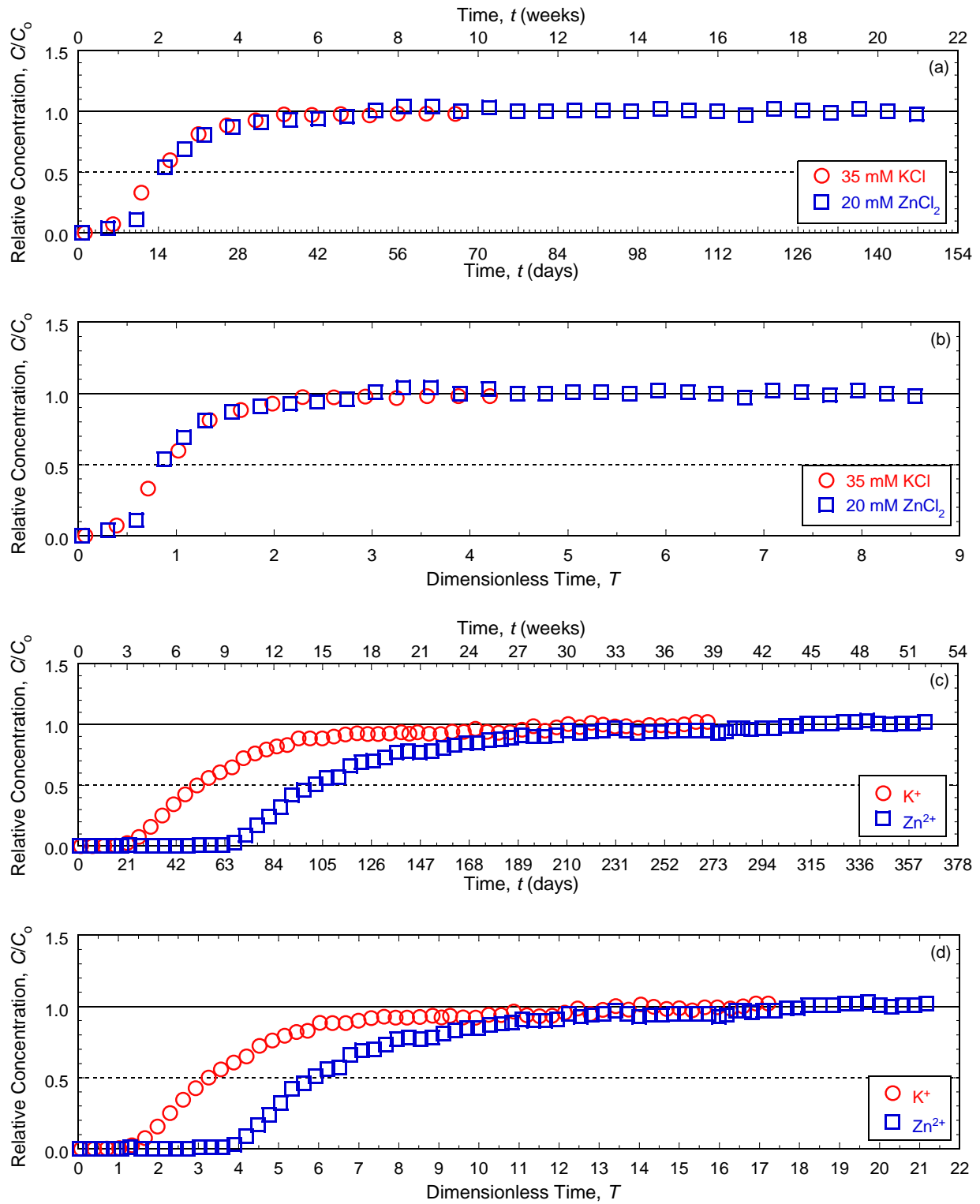


Figure 5.62. Breakthrough curves for unamended backfill permeated with 35 mM KCl or 20 mM  $\text{ZnCl}_2$ : (a) chloride ( $\text{Cl}^-$ ) versus time ( $t$ ); (b)  $\text{Cl}^-$  versus dimensionless time ( $T$ ); (c) potassium ( $\text{K}^+$ ) and zinc ( $\text{Zn}^{2+}$ ) versus  $t$ ; (d)  $\text{K}^+$  and  $\text{Zn}^{2+}$  versus  $T$ .

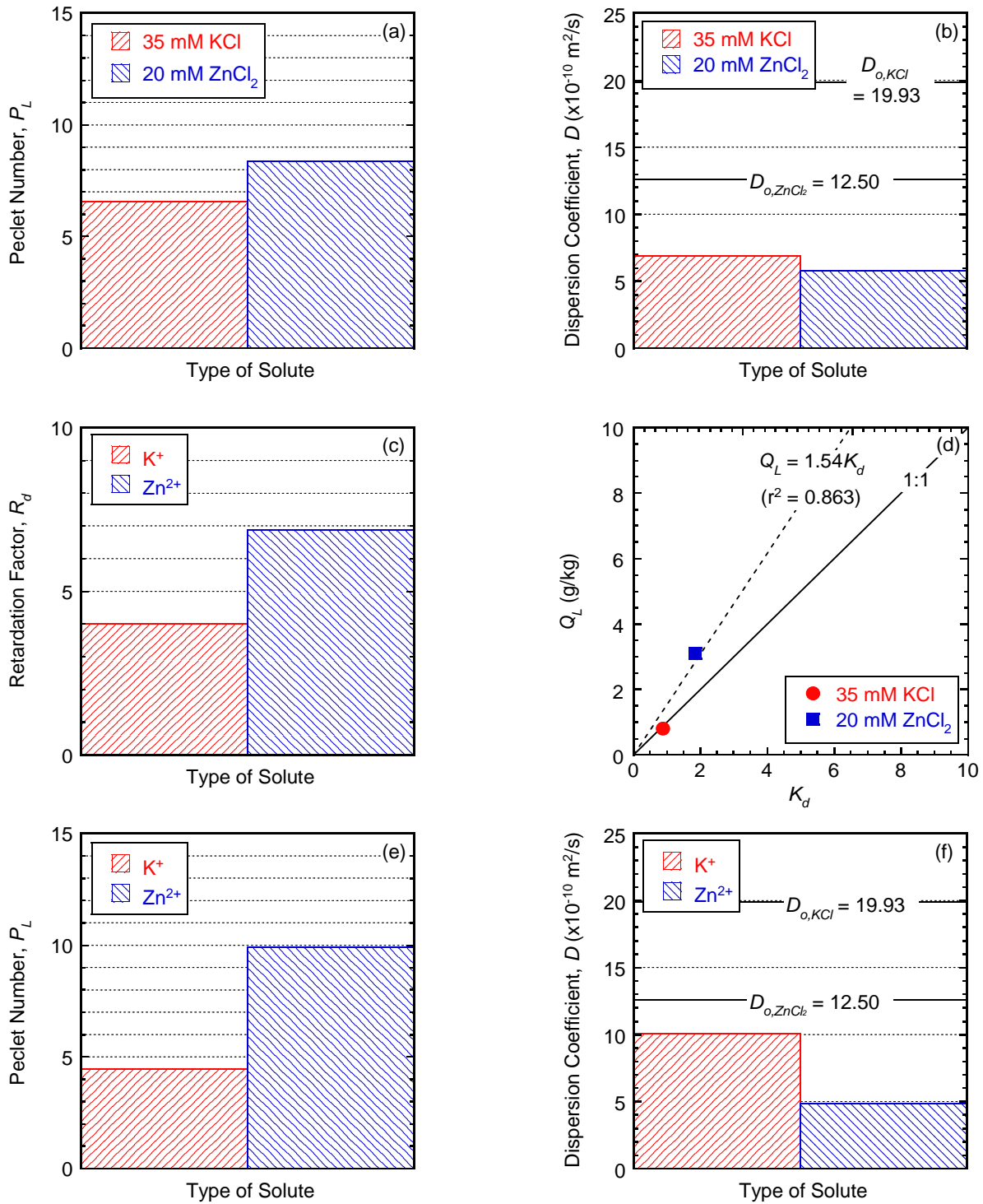


Figure 5.63. Effect of type of metal on transport parameters for columns of unamended backfill permeated with 35 mM KCl or 20 mM ZnCl<sub>2</sub>: (a) Péclet number ( $P_L$ ) for chloride (Cl<sup>-</sup>); (b) hydrodynamic dispersion coefficient ( $D$ ) for Cl<sup>-</sup>; (c) retardation factor ( $R_d$ ) for potassium (K<sup>+</sup>) and zinc (Zn<sup>2+</sup>); (d)  $Q_L$  versus  $K_d$ ; (e)  $P_L$  for K<sup>+</sup> and Zn<sup>2+</sup>; (f)  $D$  for K<sup>+</sup> and Zn<sup>2+</sup>.

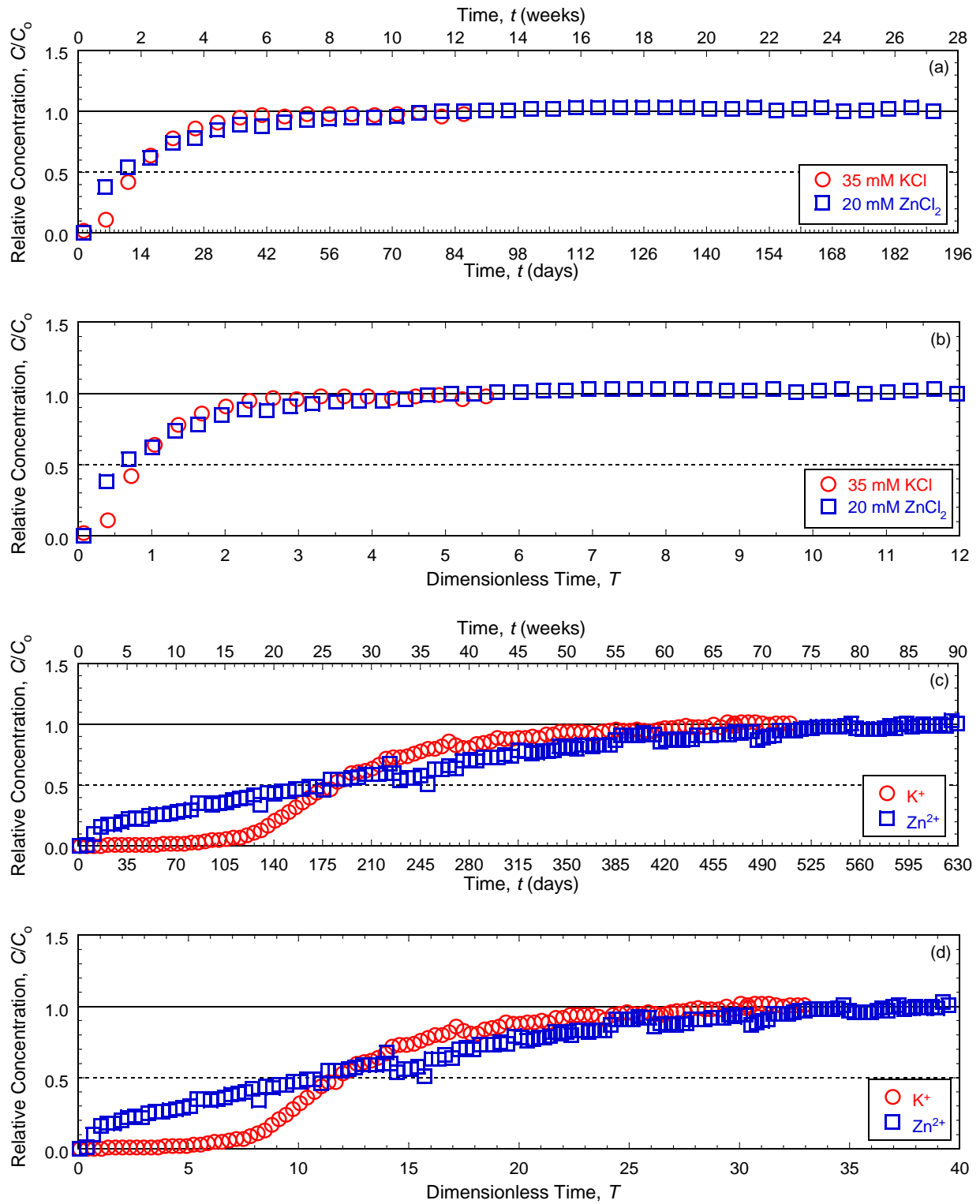


Figure 5.64. Breakthrough curves for backfill amended with 5 % chabazite-UB and permeated with 35 mM KCl or 20 mM  $ZnCl_2$ : (a) chloride ( $Cl^-$ ) versus time ( $t$ ); (b)  $Cl^-$  versus dimensionless time ( $T$ ); (c) potassium ( $K^+$ ) and zinc ( $Zn^{2+}$ ) versus  $t$ ; (d)  $K^+$  and  $Zn^{2+}$  versus  $T$ .

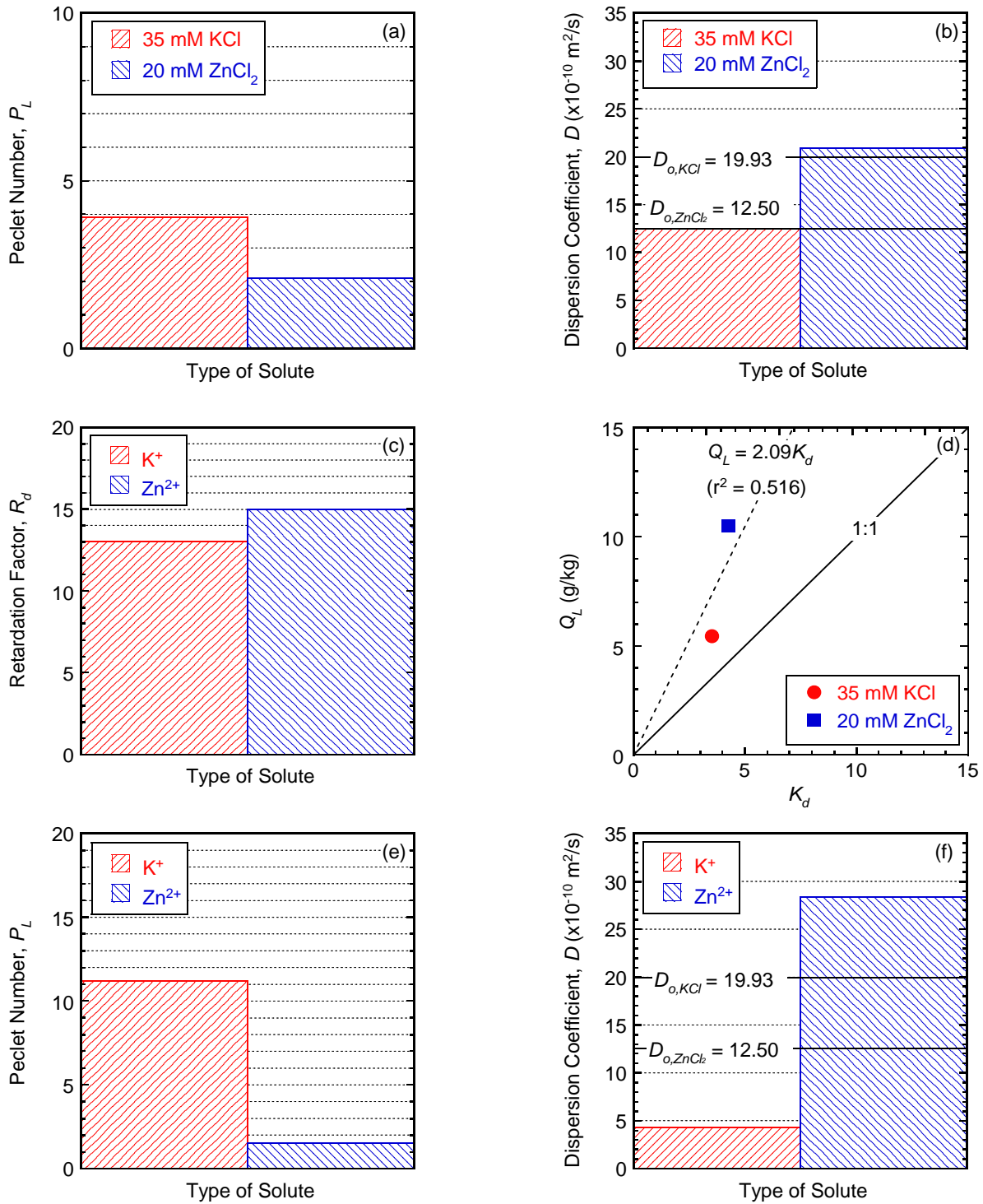


Figure 5.65. Effect of type of metal on transport parameters for columns of 5 % chabazite-UB-amended backfill permeated with 35 mM KCl or 20 mM  $ZnCl_2$ : (a) Péclet number ( $P_L$ ) for chloride (Cl); (b) hydrodynamic dispersion coefficient ( $D$ ) for Cl; (c) retardation factor ( $R_d$ ) for potassium ( $K^+$ ) and zinc ( $Zn^{2+}$ ); (d)  $Q_L$  versus  $K_d$ ; (e)  $P_L$  for  $K^+$  and  $Zn^{2+}$ ; (f)  $D$  for  $K^+$  and  $Zn^{2+}$ .

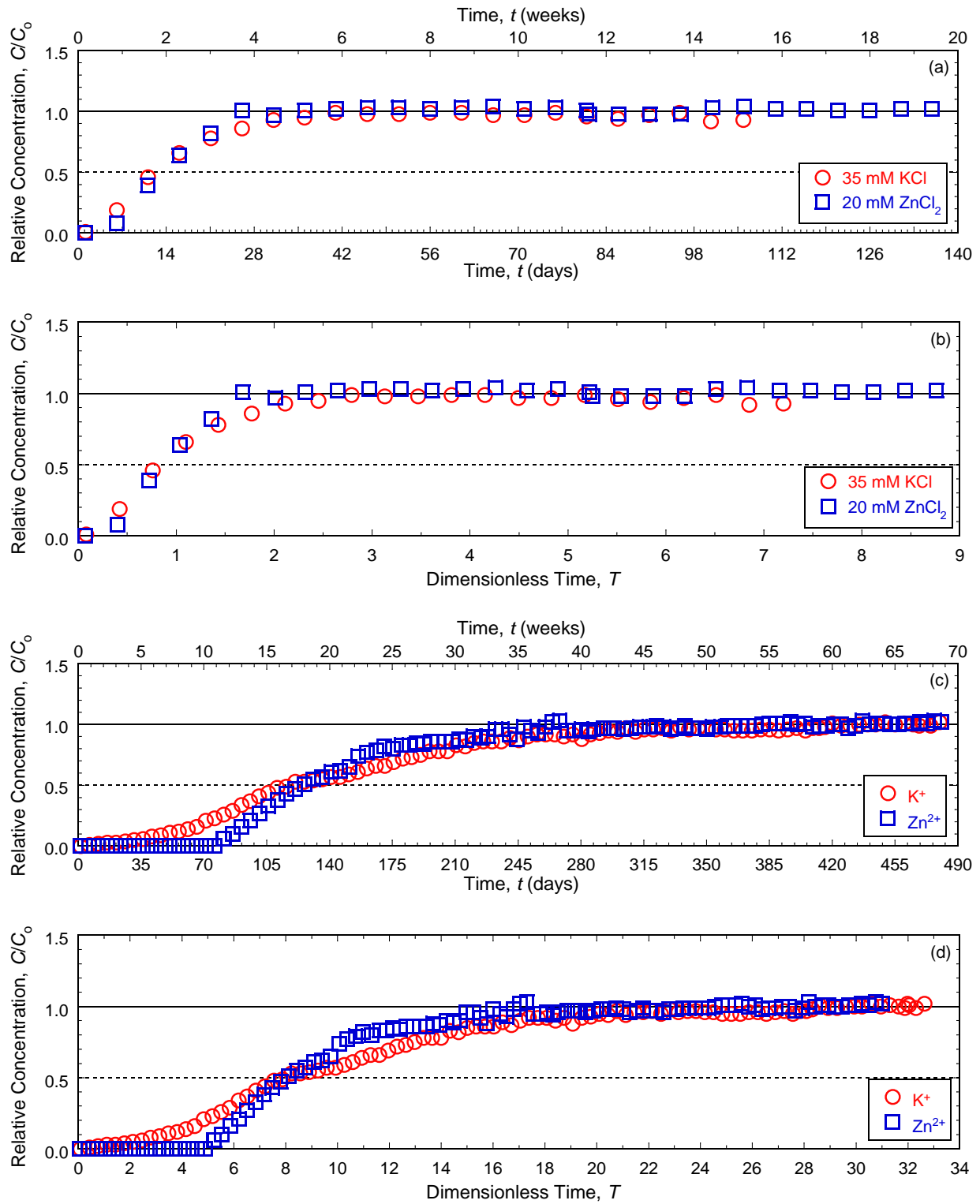


Figure 5.66. Breakthrough curves for backfill amended with 5 % clinoptilolite and permeated with 35 mM KCl or 20 mM  $ZnCl_2$ : (a) chloride ( $Cl^-$ ) versus time ( $t$ ); (b)  $Cl^-$  versus dimensionless time ( $T$ ); (c) potassium ( $K^+$ ) and zinc ( $Zn^{2+}$ ) versus  $t$ ; (d)  $K^+$  and  $Zn^{2+}$  versus  $T$ .

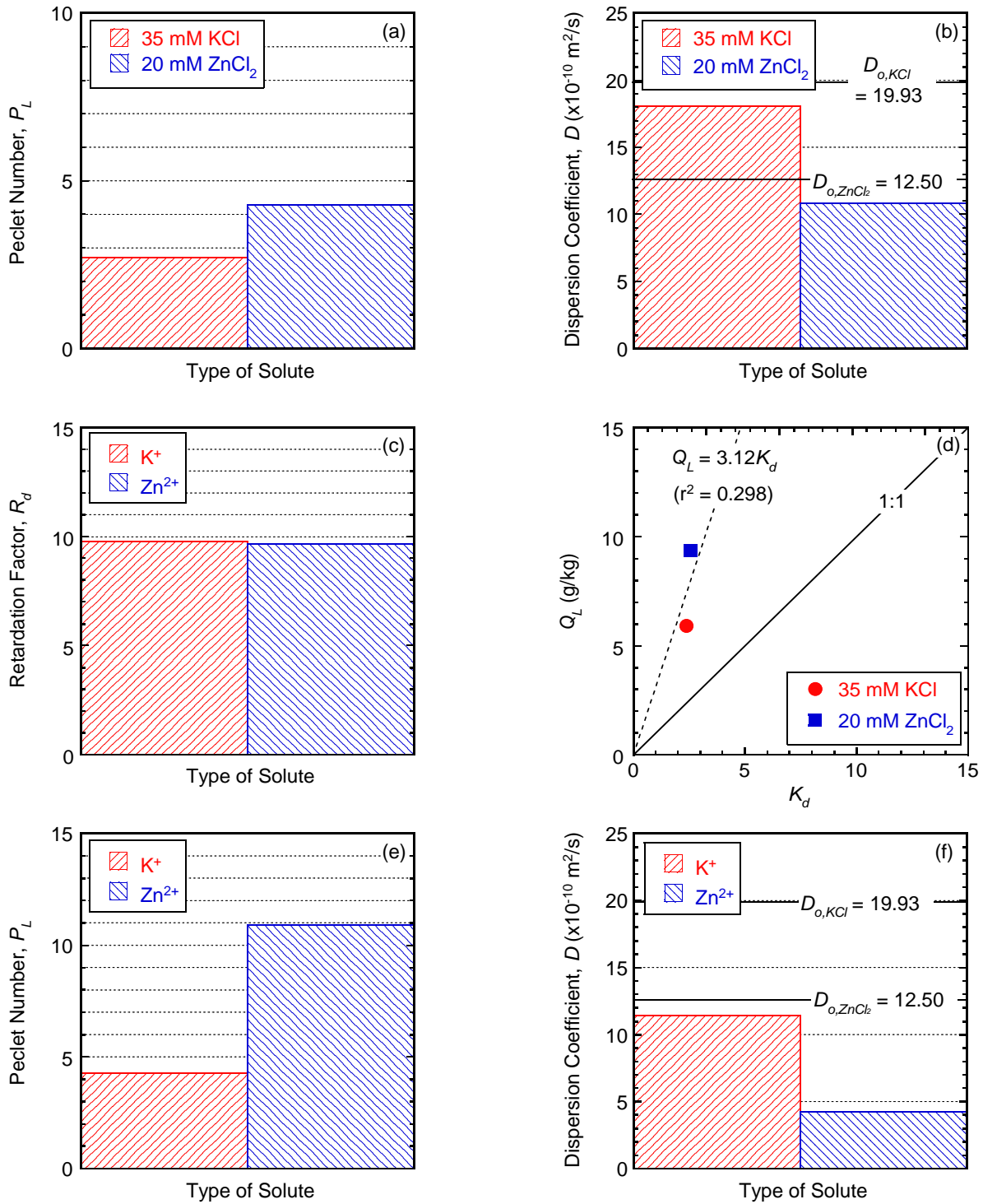


Figure 5.67. Effect of type of metal on transport parameters for backfill amended with 5 % clinoptilolite and permeated with 35 mM KCl or 20 mM ZnCl<sub>2</sub>: (a) Péclet number ( $P_L$ ) for chloride (Cl<sup>-</sup>); (b) hydrodynamic dispersion coefficient ( $D$ ) for Cl<sup>-</sup>; (c) retardation factor ( $R_d$ ) for potassium (K<sup>+</sup>) and zinc (Zn<sup>2+</sup>); (d)  $K_d$  versus  $R_d$ ; (e)  $P_L$  for K<sup>+</sup> and Zn<sup>2+</sup>; (f)  $D$  for K<sup>+</sup> and Zn<sup>2+</sup>.

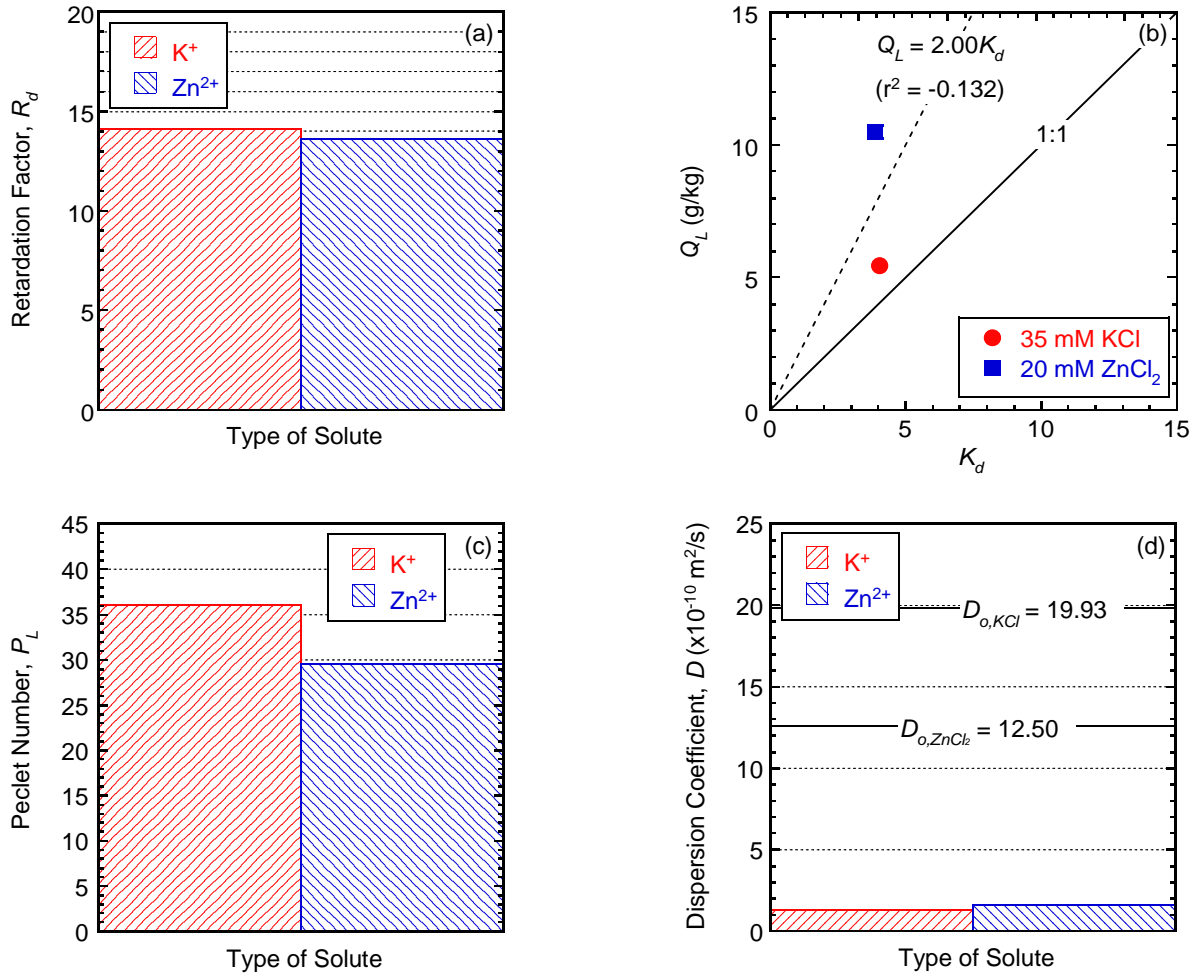


Figure 5.68. Effect of cation competition on transport parameters for backfill amended with 5 % chabazite-UB and permeated with 17.5 mM KCl plus 10 mM ZnCl<sub>2</sub> solution: (a) retardation factor ( $R_d$ ) for potassium (K<sup>+</sup>) and zinc (Zn<sup>2+</sup>); (b)  $Q_L$  versus  $K_d$ ; (c) Péclet number ( $P_L$ ) for K<sup>+</sup> and Zn<sup>2+</sup>; (d)  $D$  for K<sup>+</sup> and Zn<sup>2+</sup>.

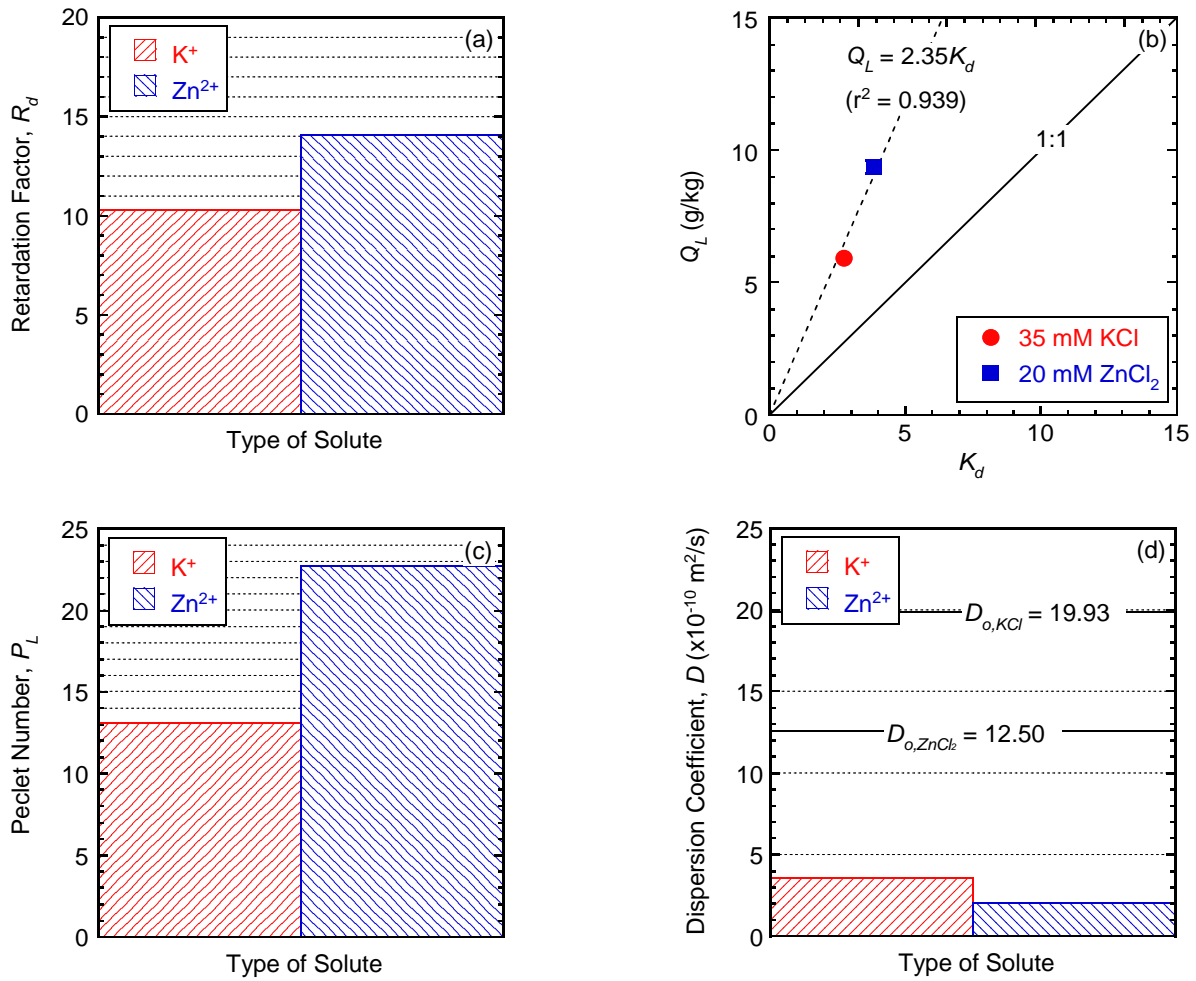


Figure 5.69. Effect of cation competition on transport parameters for backfill amended with 5 % clinoptilolite and permeated with 17.5 mM KCl plus 10 mM  $ZnCl_2$  solution: (a) retardation factor ( $R_d$ ) for potassium ( $K^+$ ) and zinc ( $Zn^{2+}$ ); (b)  $Q_L$  versus  $K_d$ ; (c) Péclet number ( $P_L$ ) for  $K^+$  and  $Zn^{2+}$ ; (d)  $D$  for  $K^+$  and  $Zn^{2+}$ .

## REFERENCES

- Allerton, D.K., Desborough, G.A., Olsen, H.W., and Chang, N.Y. (1996). "Waste containment barrier enhancement with zeolite." *Tailings and Mine Waste '96*, Balkema, Rotterdam, The Netherlands, 255-264.
- ASTM (2004). "Standard test methods for measurement of hydraulic conductivity of saturated porous materials using a flexible wall permeameter." *ASTM D5084-03*, ASTM International, West Conshohocken, PA.
- ASTM (2006). "Standard practice for classification of soils for engineering purposes (Unified Soil Classification System)." *ASTM D2487-06*, ASTM International, West Conshohocken, PA.
- ASTM (2010). "Standard test method for measuring the exchange complex and cation exchange capacity of inorganic fine-grained soils." *ASTM D7503-10*, ASTM International, West Conshohocken, PA.
- Bear, J. (1972). *Dynamics of Fluids in Porous Media*, Elsevier, New York.
- Bierck, B.R. and Chang, W.C. (1994). "Contaminant transport through soil-bentonite slurry walls: Attenuation by activated carbon." *Proceedings of the Specialty Conference on Innovative Solutions for Contaminated Site Management*, Water Environment Federation, Alexandria, VA, 461-472.
- Bish, D.L. (2006). "Parallels and distinctions between clay minerals and zeolites." Section 13.2, *Developments in Clay Science*, Elsevier, New York, 1097-1112.
- Bohnhoff, G., Shackelford, C.D., and Sample-Lord, K. (2014). "Calcium-resistant membrane behavior of polymerized bentonite." *Journal of Geotechnical and Geoenvironmental Engineering*, 140(3), 04013029.
- Bradl, H.B. (1997). "Vertical barriers with increased sorption capacities." *1997 International Containment Technology Conference*, St. Petersburg, FL, NTIS (National Technical Information Service), Springfield, VA, 645-651.
- Colella, C. (1996). "Ion exchange equilibria in zeolite minerals." *Mineralium Deposita*, 31(6), 554-562.
- Colombani, N., Mastrocicco, M., Di Giuseppe, D., Faccini, B., and Coltorti, M. (2015). "Batch and column experiments on nutrient leaching in soils amended with Italian natural zeolites." *CATENA*, 127(0), 64-71.
- Daniel, D.E. (1994). "State-of-the-art: Laboratory hydraulic conductivity tests for saturated soils." *Hydraulic Conductivity and Waste Contaminant Transport in Soil*, ASTM STP 1142, D.E. Daniel and S.J. Trautwein, Eds., ASTM, West Conshohocken, PA, 30-78.

- Daniel, D.E., Anderson, D.C., and Boynton, S.S. (1985). "Fixed-wall versus flexible-wall permeameters." *Hydraulic Barriers in Soil and Rock*. ASTM STP 874, Johnson, A.I., Frobels, R.K., Cavalli, N.J., Pettersson, C.B., Eds., ASTM, Philadelphia, PA, 107-126.
- Daniels, J.L., Inyang, H.I., and Chien, C.C. (2004). "Verification of contaminant sorption by soil bentonite barrier materials using scanning electron microscopy/energy dispersive X-ray spectrometry." *Journal of Environmental Engineering*, 130(8), 910-917.
- Evans, J.C. and Prince, M.J. (1997). "Additive effectiveness in mineral-enhanced slurry walls." *In Situ Remediation of the Geoenvironment*, J.C. Evans, Ed., ASCE, Reston, VA, 181-196.
- Evans, J.C., Costa, M.J., and Cooley, B. (1995). "The state-of-stress in soil-bentonite slurry trench cutoff walls." *Geoenvironment 2000*, Geotechnical Special Publication 46, Y.B. Acar and D.E. Daniel, Eds., ASCE, Reston, VA, 1173-1191.
- Evans, J.C., Sambasivan, Y., and Zarlinski, S. (1990). "Attenuating materials in composite liners." *Waste Containment Systems: Construction, Regulation, and Performance*, R. Bonaparte, Ed., ASCE, Reston, VA, 246-263.
- Evans, J.C., Adams, T.L., and Prince, M.J. (1997). "Metals attenuation in mineral-enhanced slurry walls." *1997 International Containment Technology Conference*, St. Petersburg, FL, NTIS (National Technical Information Service), Springfield, VA, 679-687.
- Fernandez, F. and Quigley, R.M. (1991). "Controlling the destructive effects of clay-organic liquid interactions by application of effective stresses." *Canadian Geotechnical Journal*, 28(3), 388-398.
- Filz, G.M. (1996). "Consolidation stresses in soil-bentonite backfilled trenches." *Proceedings, 2nd Int. Congress on Environmental Geotechnics*, Balkema, Rotterdam, The Netherlands, 497-502.
- Freeze, R.A. and Cherry, J.A. (1979). *Groundwater*, Prentice-Hall, Englewood Cliffs, NJ.
- Griffin, B. and Jurinak, J. (1973). "Estimation of activity coefficients from the electrical conductivity of natural aquatic systems and soil extracts." *Soil Science*, 116(1), 26-30.
- Hong, C.S., Shackelford, C.D., and Malusis, M.A. (2012). "Consolidation and hydraulic conductivity of zeolite-amended soil-bentonite backfills." *Journal of Geotechnical and Geoenvironmental Engineering*, 138(1), 15-25.
- Hong, C.S., Shackelford, C.D., and Malusis, M.A. (2016). "Adsorptive behavior of zeolite-amended backfills for enhanced metals containment." *Journal of Geotechnical and Geoenvironmental Engineering*, 142(7), 04016021.
- Kaya, A. and Durukan, S. (2004). "Utilization of bentonite-embedded zeolite as clay liner." *Applied Clay Science*, 25(1-2), 83-91.

- Kayabali, K. (1997). "Engineering aspects of a novel landfill liner material: Bentonite-amended natural zeolite." *Engineering Geology*, 46(2), 105-114.
- Kayabali, K. and Mollamahmutoğlu, M. (2000). "The influence of hazardous liquid waste on the permeability of earthen liners." *Environmental Geology*, 39(3-4), 201-210.
- Lee, J.M. and Shackelford, C.D. (2005). "Concentration dependency of the prehydration effect for a geosynthetic clay liner." *Soils and Foundations*, 45(4), 27-41.
- Li, Y.-C., Cleall, P.J., Wen, Y.-D., Chen, Y.-M., and Pan, Q. (2015). "Stresses in soil-bentonite slurry trench cut-off walls." *Geotechnique*, 65(10), 843-850.
- Lindstrom, F.T., Haque, R., Freed, V.H., and Boersma, L. (1967). "The movement of some herbicides in soils. Linear diffusion and convection of chemicals in soils." *Environmental Science and Technology*, 1(7), 561-565.
- Malusis, M.A., Barben, E.J., and Evans, J.C. (2009). "Hydraulic conductivity and compressibility of soil-bentonite backfill amended with activated carbon." *Journal of Geotechnical and Geoenvironmental Engineering*, 135(5), 664-672.
- Malusis, M.A., Maneval, J.E., Barben, E.J., Shackelford, C.D., and Daniels, E.R. (2010). "Influence of adsorption on phenol transport through soil-bentonite vertical barriers amended with activated carbon." *Journal of Contaminant Hydrology*, 116(1-4), 58-72.
- Manassero, M., Pasqualini, E., and Sani, D. (1998). "Potassium sorption isotherms of natural clayey-silt for pollutant containment." *3rd International Congress on Environmental Geotechnics*, P. Seco e Pinto, Ed., Lisboa, Portugal, Sept. 7-11, 1998, Balkema, Rotterdam, Vol. 1, 235-240.
- Mazzieri, F., Sante, M.d., and Fratolocchi, E. (2015). "Dilution effect of the apparatus on contaminant transport parameters assessed by column testing." *Journal of Geotechnical and Geoenvironmental Engineering*, 141(9), 06015006.
- Mott, H.V. and Weber, W.J. (1992). "Sorption of low molecular weight organic contaminants by fly ash: Considerations for the enhancement of cutoff barrier performance." *Environmental Science and Technology*, 26(6), 1234-1242.
- Mumpton, F.A. (1999). "La roca magica: Uses of natural zeolites in agriculture and industry." *Proceedings of the National Academy of Sciences of the United States of America*, 96(7), 3463-3470.
- Obiri-Nyarko, F., Grajales-Mesa, S.J., and Malina, G. (2014). "An overview of permeable reactive barriers for in situ sustainable groundwater remediation." *Chemosphere*, 111(0), 243-259.
- Ören, A.H., Kaya, A., and Kayalar, A.Ş. (2011). "Hydraulic conductivity of zeolite-bentonite mixtures in comparison with sand-bentonite mixtures." *Canadian Geotechnical Journal*, 48(9), 1343-1353.

- Park, J.K., Kim, J.Y., Madsen, C.D., and Edil, T.B. (1997). "Retardation of volatile organic compound movement by a soil-bentonite slurry cutoff wall amended with ground tires." *Water Environment Research*, 69(5), 1022-1031.
- Prince, M.J. and Evans, J.C. (1998). "Adsorptive additives to improve the performance of slurry trench cut-off walls." *Toxic and Hazardous Wastes: Proc.*, Thirtieth Mid-Atlantic Industrial Waste Conference, Technomic Publishing Co., Lancaster, PA, 712-721.
- Rabideau, A.J. and Khandelwal, A. (1998). "Boundary conditions for modeling transport in vertical barriers." *Journal of Environmental Engineering*, 124(11), 1135-1139.
- Rabideau, A., Shen, P., and Khandelwal, A. (1999). "Feasibility of amending slurry walls with zero-valent iron." *Journal of Geotechnical and Geoenvironmental Engineering*, 125(4), 330-333.
- Redmond, P.L. and Shackelford, C.D. (1994). "Design and evaluation of a flow pump system for column testing." *Geotechnical Testing Journal*, 17(3), 269-281.
- Reynolds, W.D., Gillham, R.W., and Cherry, J.A. (1982). "Evaluation of distribution coefficients for the prediction of strontium and cesium migration in a uniform sand." *Canadian Geotechnical Journal*, 19(1), 92-103.
- Roy, W.R., Krapac, I.G., Chou, S.F.J., and Griffin, R.A. (1992). "Batch-type procedures for estimating soil adsorption of chemicals." *EPA Technical Resource Document*, EPA/530-SW-87-006-F, U. S. Environmental Protection Agency, Washington, D.C.
- Shackelford, C.D. (1993). "Contaminant transport." *Geotechnical Practice for Waste Disposal*, D.E. Daniel, Ed., Chapman and Hall, London, 33-65.
- Shackelford, C.D. (1994a). "Critical concepts for column testing." *Journal of Geotechnical Engineering*, 120(10), 1804-1828.
- Shackelford, C.D. (1994b). "Waste-soil interactions that alter hydraulic conductivity. *Hydraulic Conductivity and Waste Contaminant Transport in Soil*, ASTM STP 1142, David E. Daniel and Stephen J. Trautwein, Eds., American Society for Testing and Materials, Philadelphia, 111-168.
- Shackelford, C.D. (1995a). "Analytical models for cumulative mass column testing." *Geoenvironment 2000*, Y.B. Acar and D.E. Daniel, Eds., ASCE Press, Reston, VA, 355-372.
- Shackelford, C.D. (1995b). "Cumulative mass approach for column testing." *Journal of Geotechnical Engineering*, 121(10), 696-703.
- Shackelford, C.D. (1997). "Modeling and analysis in environmental geotechnics: An overview of practical applications." *Second International Congress on Environmental Geotechnics, IS-Osaka '96*, M. Kamon, Ed., Osaka, Japan, Nov. 5-8, 1996, Balkema, Rotterdam, The Netherlands, Vol. 3, 1375-1404.

- Shackelford, C.D. and Jefferis, S.A. (2000). "Geoenvironmental engineering for in situ remediation." *Proceedings, International Conference on Geotechnical and Geoenvironmental Engineering (GeoEng2000)*, Melbourne, Australia, Nov. 19-24, Technomic, Lancaster, PA, Vol. 1, 121-185.
- Shackelford, C.D. and Redmond, P.L. (1995). "Solute breakthrough curves for processed kaolin at low flow rates." *Journal of Geotechnical Engineering*, 121(1), 17-32.
- Shackelford, C.D., Malusis, M.A., Majeski, M.J., and Stern, R.T. (1999). "Electrical conductivity breakthrough curves." *Journal of Geotechnical and Geoenvironmental Engineering*, 125(4), 260-270.
- Shackelford, C.D., Benson, C.H., Katsumi, T., Edil, T.B., and Lin, L. (2000). "Evaluating the hydraulic conductivity of GCLs permeated with non-standard liquids." *Geotextiles and Geomembranes*, 18(2-4), 133-161.
- Sparks, D.L. (2003). *Environmental Soil Chemistry*, Academic Press, London.
- Tuncan, A., Tuncan, M., Koyuncu, H., and Guney, Y. (2003). "Use of natural zeolites as a landfill liner." *Waste Management Research*, 21(1), 54-61.

## CHAPTER 6 SUMMARY AND CONCLUSIONS

### 6.1 SUMMARY

The results of an investigation into the applicability of zeolite as amendment to conventional soil-bentonite (SB) vertical cutoff walls for geoenvironmental containment were presented. The physical, chemical, and long-term performance of unamended and zeolite-amended SB backfills were compared in terms of batch equilibrium adsorption tests (BEATs), numerical simulations based on the BEAT results, and column tests with regard to monovalent ( $K^+$ ) or divalent ( $Zn^{2+}$ ) cations, and for different types and added amounts of zeolite.

### 6.2 CONCLUSIONS

- (1) Comparison of the measured physical properties of the unamended and zeolite-amended backfills indicated that adding a small amount of zeolite ( $\leq 10\%$  by dry weight) to the traditional soil-bentonite (SB) backfill had little effect on the slump, consolidation behavior and hydraulic conductivity ( $k$ ). For example, the compression index ( $C_c$ ) was 0.24 for the unamended, and  $0.19 \leq C_c \leq 0.23$  for the zeolite-amended backfills. Also,  $k$  measured in flexible-wall permeameters was  $2.4 \times 10^{-10}$  m/s for the unamended, and  $1.2 \times 10^{-10} \leq k \leq 3.9 \times 10^{-10}$  m/s for the zeolite-amended backfills, such that all backfills satisfied the required low  $k$  of  $\leq 1.0 \times 10^{-9}$  m/s typically required for SB vertical cutoff walls used for contaminant containment.
- (2) The batch equilibrium adsorption tests (BEAT) results indicated that the adsorptive behaviors of K and Zn to both the unamended and zeolite-amended backfill sorbents were nonlinear over the concentration ranges of interest (0.1 – 1,000 mM KCl or  $ZnCl_2$ ). Depending on the specific zeolite, the addition of only 5 % zeolite increased the

adsorption capacity relative to that for the unamended backfill sorbent by a factor ranging from 6.2 to 7.3 for K and from 2.8 to 3.4 for Zn, whereas 10 % zeolite amendment increased the adsorption capacity by a factor ranging from 7.5 to 13.5 for K and 3.1 to 3.7 for Zn. The lower increase in adsorption capacity for Zn relative to K was attributed to preferential selectivity of K relative to Zn and the competing soluble salts (cations) associated with the added zeolite. The adsorption behavior of both K and Zn was consistent with cation exchange as the dominant mechanism, provided chemical speciation (complexation) of Zn was taken into account.

- (3) The containment performance of a hypothetical 1-m-thick SB vertical cutoff wall comprising unamended or zeolite-amended SB backfills with respect to the migration of K and Zn was evaluated via numerical simulations using the BEAT results as input for the modeling. The improvement in the containment of a metal was reflected by an increase in the barrier flux breakthrough time,  $t_B$ . For K,  $t_B$  increased with decreasing  $C_o$  and increasing zeolite content. The results for Zn were similar to those for K except at lower values of  $C_o$  (*i.e.*, 100 and 1,000 mg/L), where anomalous adsorption behavior resulted in better performance with the unamended backfill relative to the zeolite-amended backfills. However, as the input for the numerical model was based on the BEAT results, the better performance of the unamended backfill relative to the zeolite-amended backfills for Zn was considered the reflection of BEAT results, where the adsorption of Zn was subjected to competition with the excess soluble and exchangeable cations associated with the added zeolite.
- (4) Long-term column tests (1.05 to 3.75 yr) were performed for the unamended and zeolite-amended backfills under conditions that were more representative of practical

applications relative to those imposed by the BEATs. The  $k$  increased when permeated with a salt solution (*i.e.*, 35 mM KCl, 20 mM ZnCl<sub>2</sub>, or 17.5 mM KCl plus 10 mM ZnCl<sub>2</sub>), indicating some incompatibility of the backfills. However, the  $k$  for all of the column specimens were  $\leq 1.0 \times 10^{-9}$  m/s such that all the specimens would be suitable as backfills for SB vertical cutoff walls used for contaminant containment. The improvement in attenuation capacity was reflected by an increase in the retardation factor ( $R_d$ ). The  $R_d$  for the 5 % zeolite-amended SB backfills relative to the  $R_d$  for the unamended backfill, or  $R_{d,amended}/R_{d,unamended}$ , was 2.4 to 3.2 for K and 1.4 to 2.2 for Zn. The lower increase in attenuation capacity for Zn relative to K is attributed to greater  $R_d$  for Zn of 6.88 with the unamended backfill relative to the  $R_d$  for K of only 4.01. The  $R_d$  also correlated with the measured *CEC* of the backfills, supporting the assertion that the adsorption mechanism for the backfills was cation exchange. Also, the  $R_d$  for Zn from the column tests were greater than those obtained from the BEAT results, which was attributed to removal of competing soluble salts (cations) associated with the added zeolite via permeation with deionized water prior to permeation with the salt solution in the column tests. Finally, for the salt solution mixture of 17.5 mM KCl plus 10 mM ZnCl<sub>2</sub>, K was retarded to a greater extent ( $R_d = 14.1$  for salt mixture vs.  $R_d = 13.0$  for single salt solution), but Zn was retarded to a lesser extent ( $R_d = 13.6$  for salt mixture vs.  $R_d = 15.0$  for single salt solution) for the SB backfill amended with 5 % chabazite-UB, whereas for the 5 % clinoptilolite-amended backfill K was retarded to a greater extent ( $R_d = 10.3$  for salt mixture vs.  $R_d = 9.77$  for single salt solution), and Zn was retarded to a greater extent ( $R_d = 14.1$  for salt mixture vs.  $R_d = 9.67$  for single salt solution). Therefore, competition between K and Zn within the salt mixture for the available sorption sites

affected the retardation of both K and Zn, but the effect on Zn retardation was different based on the type of zeolite used as the backfill amendment.

### **6.3 RELEVANCE OF RESEARCH**

The results of this study confirm the hypothesis that the use of zeolite amendment ( $\leq 10\%$  by dry weight) did not have significant effect on the engineering properties and resulted in more sustainable and chemical resistant attenuation capacity relative to the conventional, unamended soil-bentonite backfill commonly used in geoenvironmental containment applications.

### **6.4 RECOMMENDATIONS FOR FUTURE RESEARCH**

- (1) Batch equilibrium adsorption tests (BEATs) should be performed using sorbents (backfills) with bentonite and zeolites that have been subjected to dialysis to remove soluble salts to allow for a comparison with the results from Chapter 3 to confirm that the soluble cations associated with the zeolite-amended backfills interfere with the adsorption of Zn.
- (2) Additional BEAT results also should be performed to generate data that are sufficient to allow for regressions using the Langmuir and Freundlich adsorption models corresponding the concentrations ranging from zero to 100 mg/L and zero to 1,000 mg/L for the purpose of re-evaluating the anomalous adsorption behavior for Zn based on the regressions over the entire range of data (*i.e.*,  $\leq 10,000$  mg/L) as described in Chapter 4.
- (3) Additional field demonstration should be performed to address additional factors that may affect the performance of the zeolite-amended SB backfills as vertical cutoff walls for geoenvironmental containment.

APPENDIX A. SUPPLEMENTARY DATA FOR CHAPTER 2

Table A.1. Slump test data for the unamended and zeolite-amended soil-bentonite backfill-slurry mixtures.

Unamended		2 % Chabazite-LB		5 % Chabazite-LB		10 % Chabazite-LB		5 % Chabazite-UB		5 % Clinoptilolite	
$w_B$ (%) <sup>a</sup>	$-\Delta H$ (mm) <sup>b</sup>	$w_B$ (%) <sup>a</sup>	$-\Delta H$ (mm) <sup>b</sup>	$w_B$ (%) <sup>a</sup>	$-\Delta H$ (mm) <sup>b</sup>	$w_B$ (%) <sup>a</sup>	$-\Delta H$ (mm) <sup>b</sup>	$w_B$ (%) <sup>a</sup>	$-\Delta H$ (mm) <sup>b</sup>	$w_B$ (%) <sup>a</sup>	$-\Delta H$ (mm) <sup>b</sup>
33.06	4	36.50	85	35.50	40	35.70	10	37.80	44	29.20	7
33.13	9	36.60	92	35.60	40	35.20	17	37.80	45	29.80	14
36.30	45	36.80	92	36.00	52	35.10	22	38.20	45	30.10	17
36.30	50	38.00	105	38.60	75	38.80	60	37.50	46	31.90	18
39.54	95	37.90	107	37.80	90	38.80	60	37.20	50	31.20	20
39.54	100	38.10	108	39.20	110	38.80	80	38.20	50	31.70	25
40.07	100	39.30	117	40.90	130	41.70	110	38.60	53	34.80	54
41.92	139	39.60	120	40.70	150	41.00	115	39.00	54	34.70	63
42.15	134	39.50	128	41.00	155	41.00	120	38.10	70	34.30	68
42.38	139	40.00	130	42.30	160	43.40	165	40.70	75	36.80	85
45.97	214	40.30	132	42.10	177	43.90	168	41.30	115	37.10	100
46.20	220	39.80	135	42.50	180	43.90	170	41.00	130	37.10	105
		40.10	140	44.50	205	44.00	174	44.26	140	37.50	105
		39.50	145	45.10	210	43.50	180	43.98	145	36.50	108
		40.00	155	45.40	218	44.10	188	44.20	155	37.60	117
								50.10	194	37.90	123
								48.10	205	38.00	123
								48.30	210	38.30	135
										39.70	158
										39.60	165
										39.70	170

<sup>a</sup> Backfill water content,  $w_B$  (%)

<sup>b</sup> Slump,  $-\Delta H$  (mm)

Table A.2 Consolidation test data for SB backfill-slurry mixtures prepared at 125-mm slumps.

Effective stress, $\sigma'$ [kPa (psi)]	Void Ratio, $e$					
	Unamended	2 % Chabazite-LB	5 % Chabazite-LB	10 % Chabazite-LB	5 % Chabazite-UB	5 % Clinoptilolite
24 (3.5)	1.143	1.058	1.069	1.085	1.019	0.987
48 (7.0)	1.09	1	1	1.02	0.96	0.931
96 (14)	1	0.938	0.94	0.946	0.897	0.88
192 (28)	0.93	0.878	0.87	0.876	0.836	0.819
383 (56)	0.8565	0.82	0.804	0.807	0.78	0.76
766 (111)	0.794	0.758	0.738	0.737	0.7126	0.707
1532 (222)	0.72	0.699	0.672	0.668	0.652	0.651
383 (56)	0.73	0.7	0.679	0.673	0.6588	0.66
96 (14)	0.74	0.715	0.685	0.678	0.6655	0.67
24 (3.5)	0.743	0.719	0.689	0.68	0.67	0.674

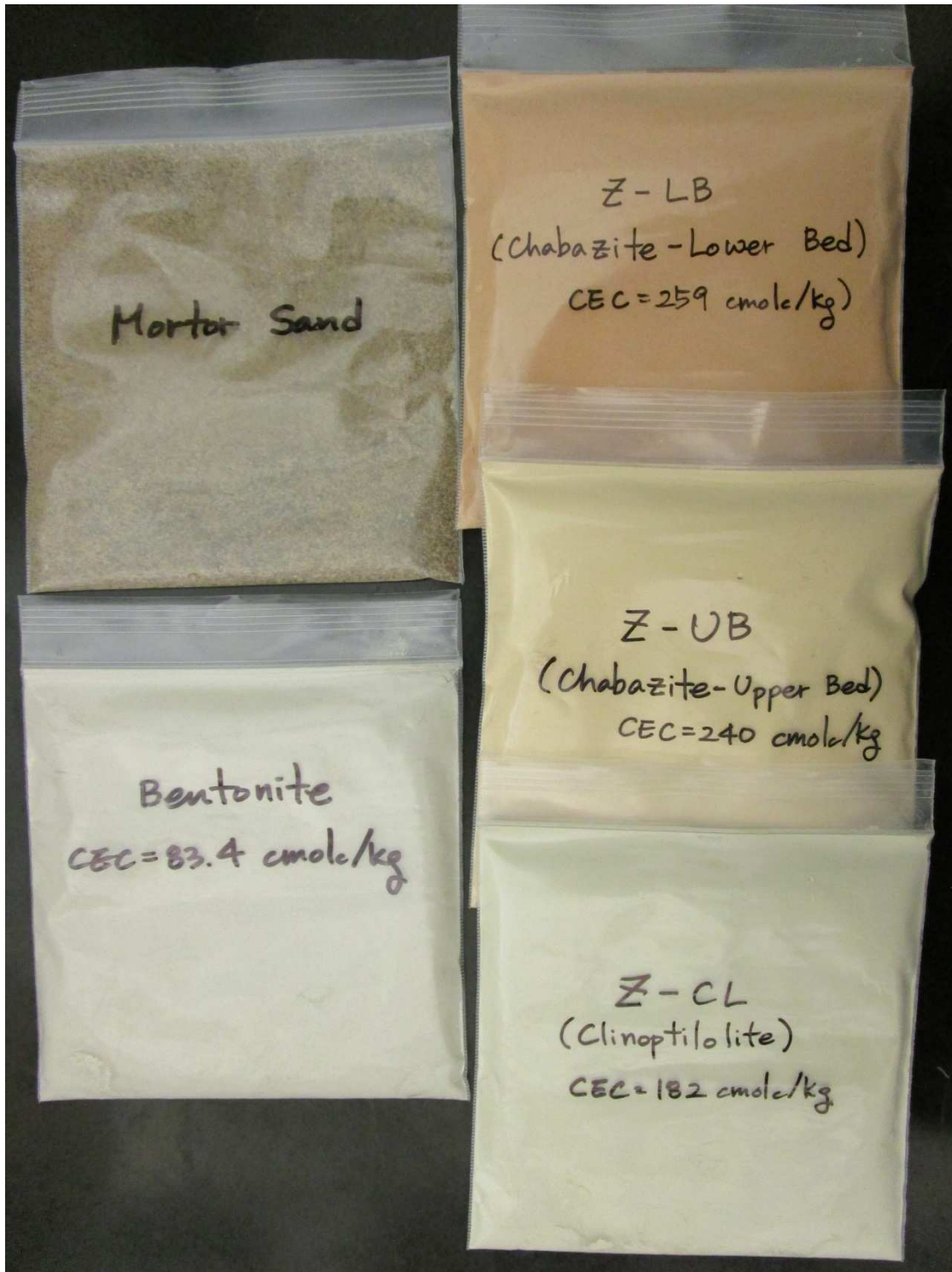


Figure A.1. Constituent materials used in this study.



Figure A.2. Pictorial view of the acrylic cylinder used for the flexible-wall setup.

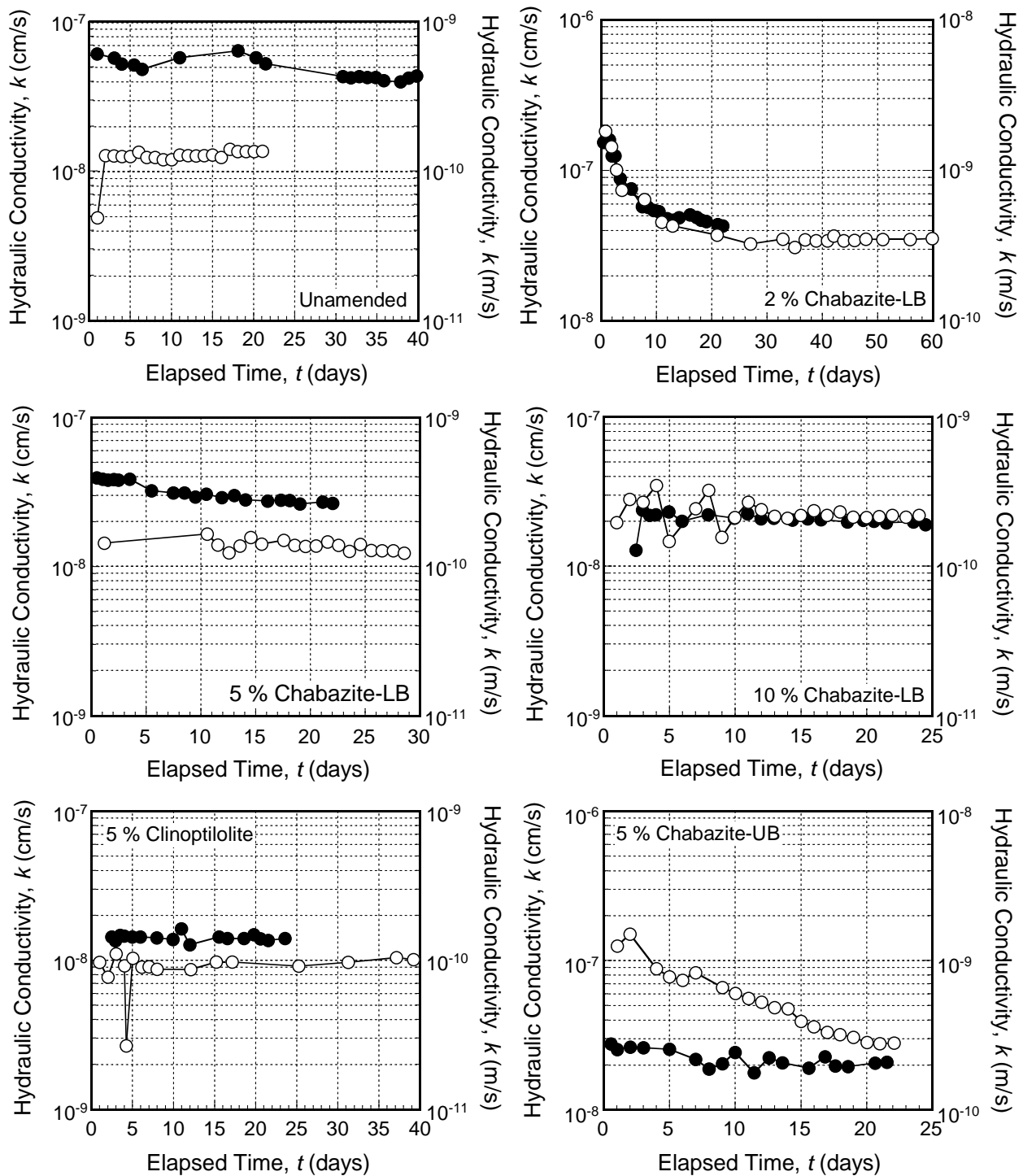


Figure A.3 Measured hydraulic conductivity for duplicate specimens in flexible-wall permeameters as a function of elapsed time for each unamended and zeolite-amended soil-bentonite backfills prepared at  $125 \pm 12.5$  mm slump.

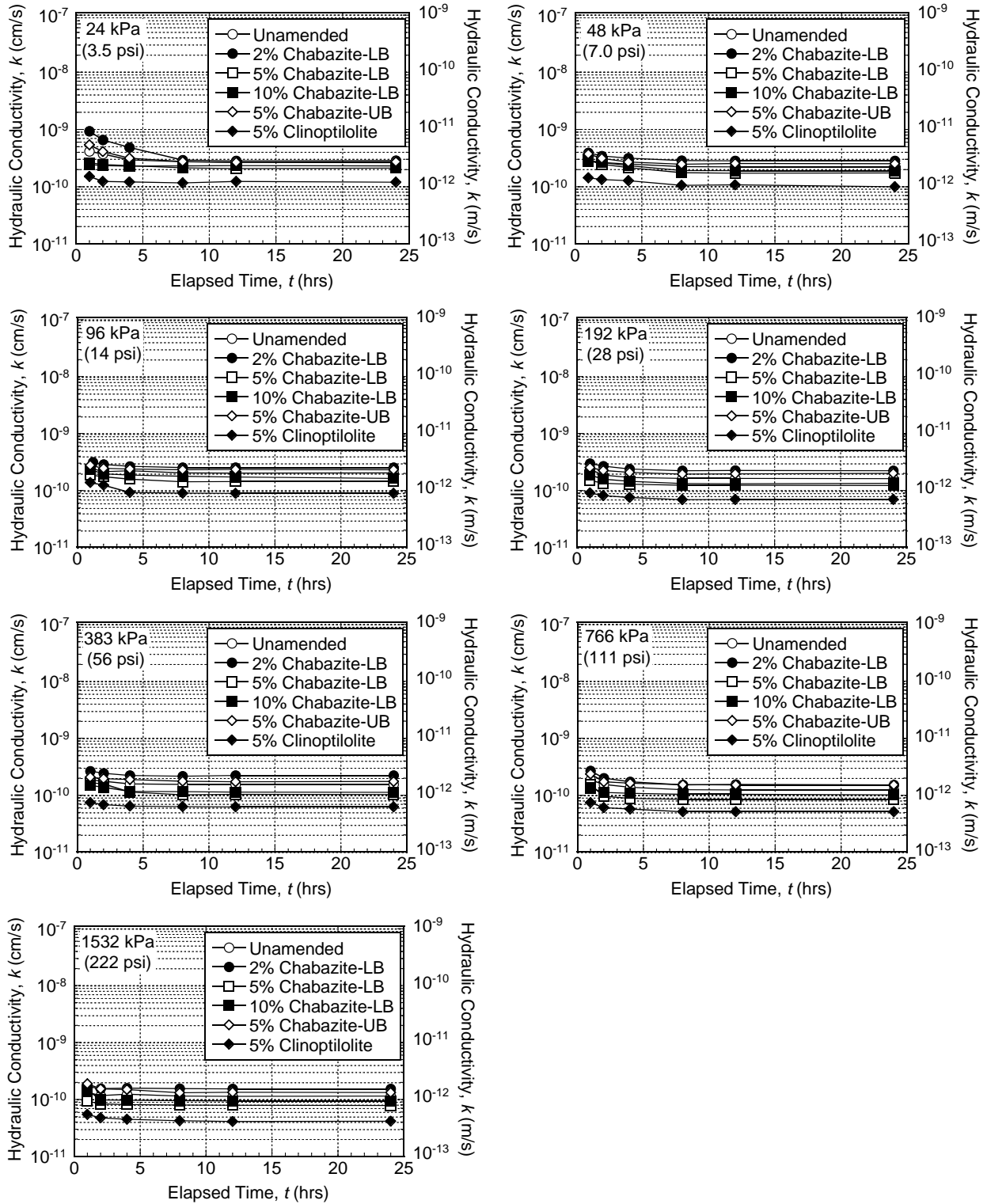


Figure A.4 Measured hydraulic conductivity in fixed-ring oedometer cells as a function of elapsed time for each unamended and zeolite-amended soil-bentonite backfills prepared at 125-mm slumps at different consolidation effective stress ( $\sigma'$ ).

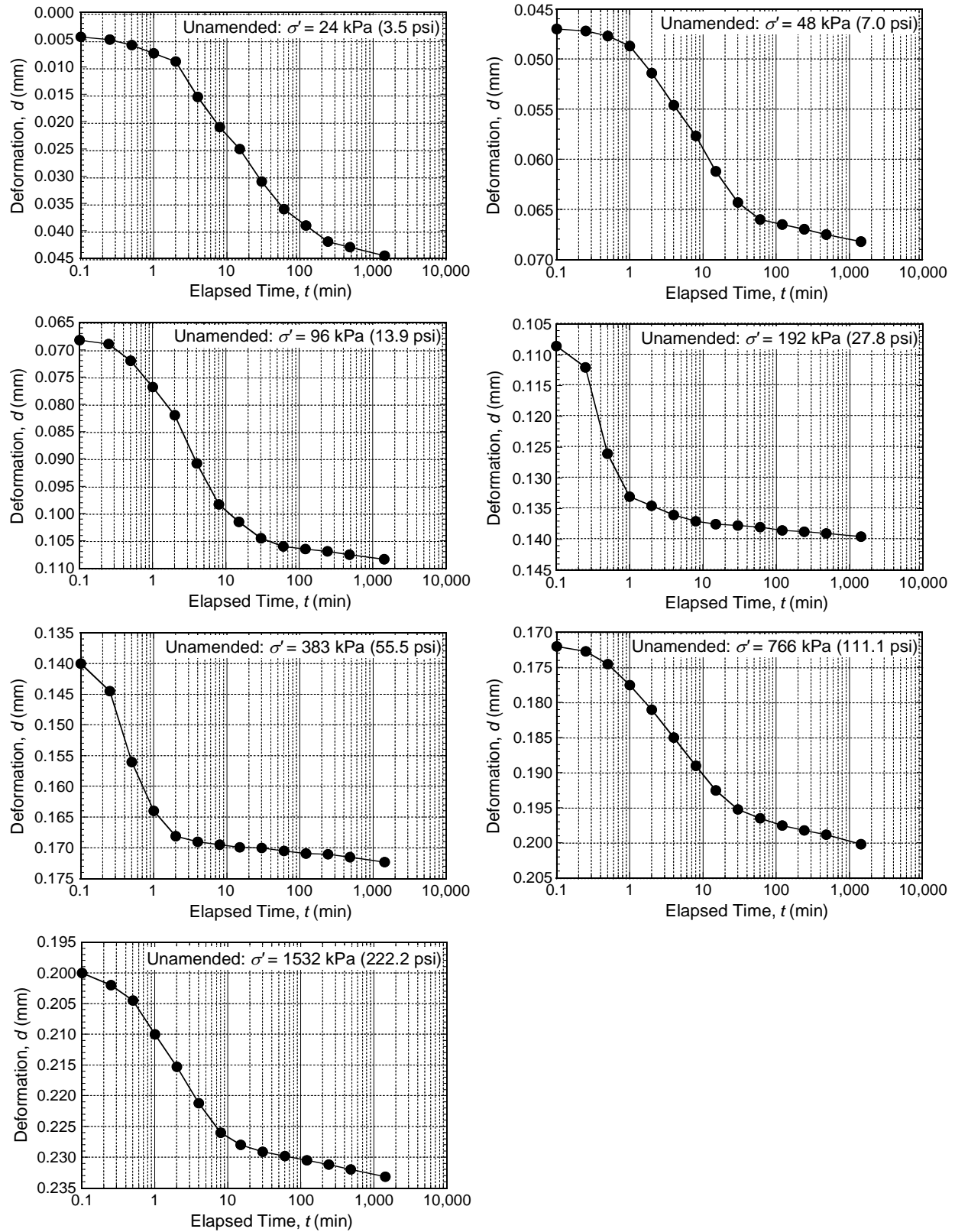


Figure A.5. Results of settlement as a function of log elapsed time for the unamended SB backfill.

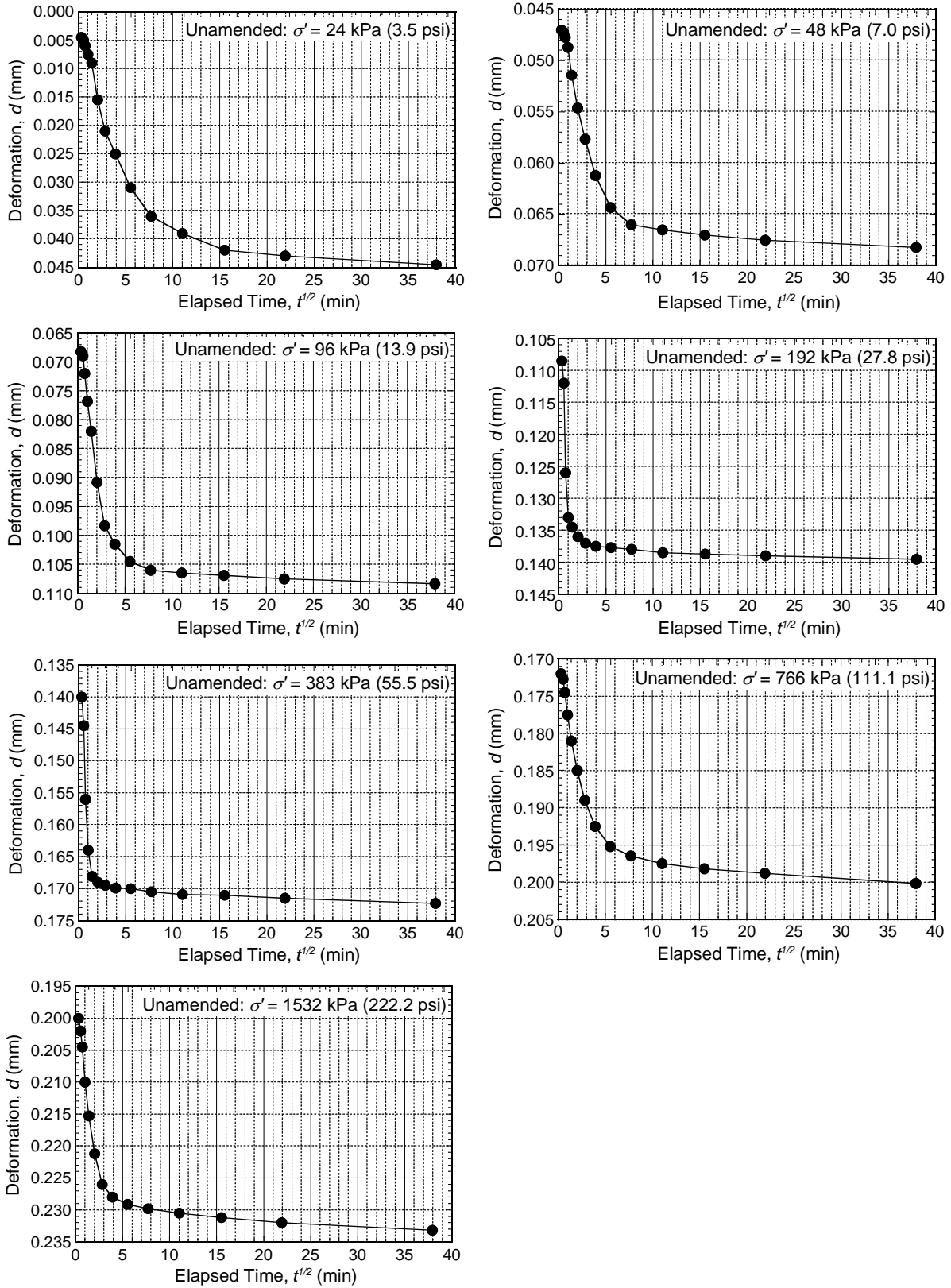


Figure A.6. Results of settlement as a function of square root elapsed time for the unamended SB backfill.

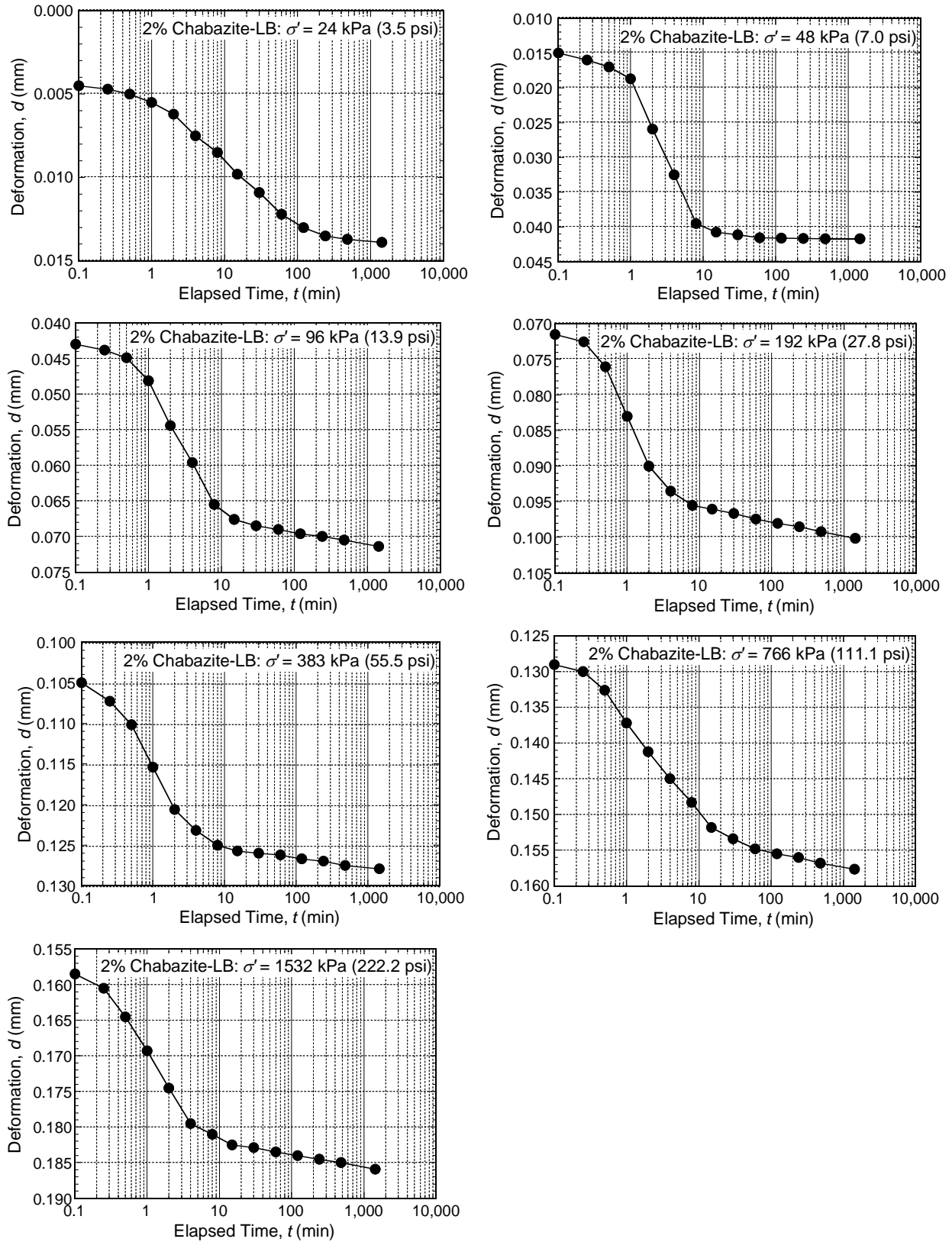


Figure A.7. Results of settlement as a function of log time for SB backfill amended with 2 % chabazite-LB.

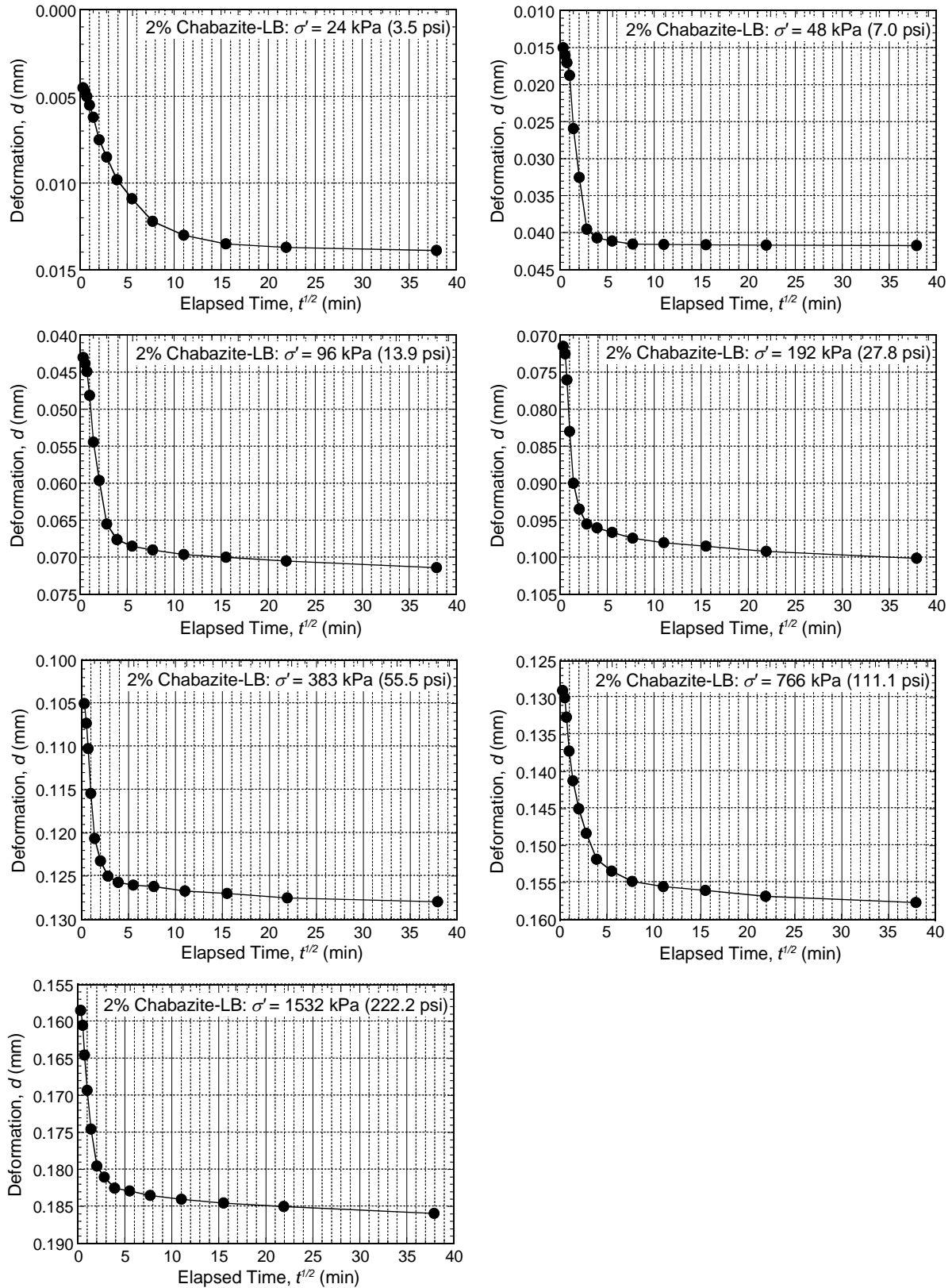


Figure A.8. Results of settlement as a function of square root time for SB backfill amended with 2 % chabazite-LB.

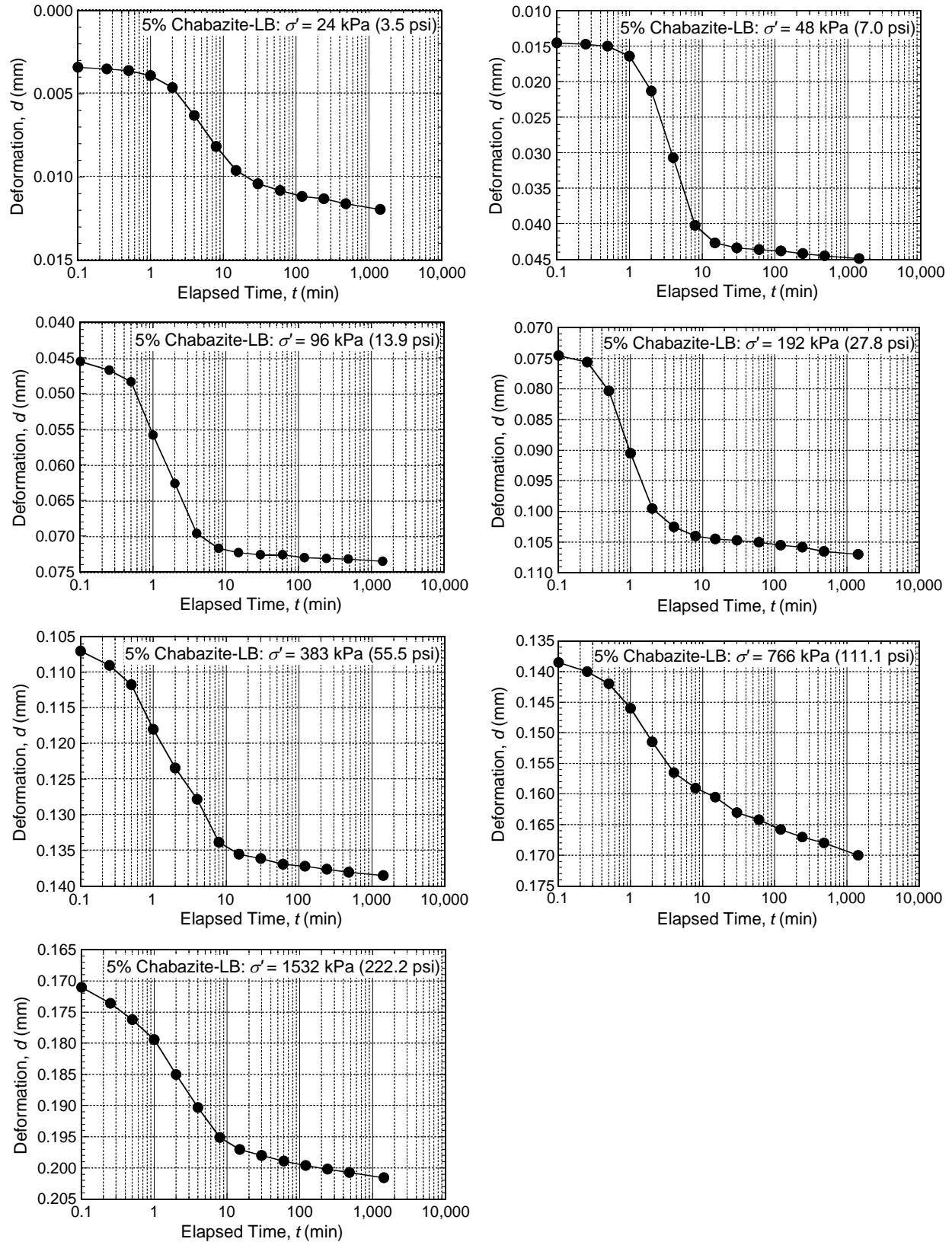


Figure A.9. Results of settlement as a function of log time for SB backfill amended with 5 % chabazite-LB.

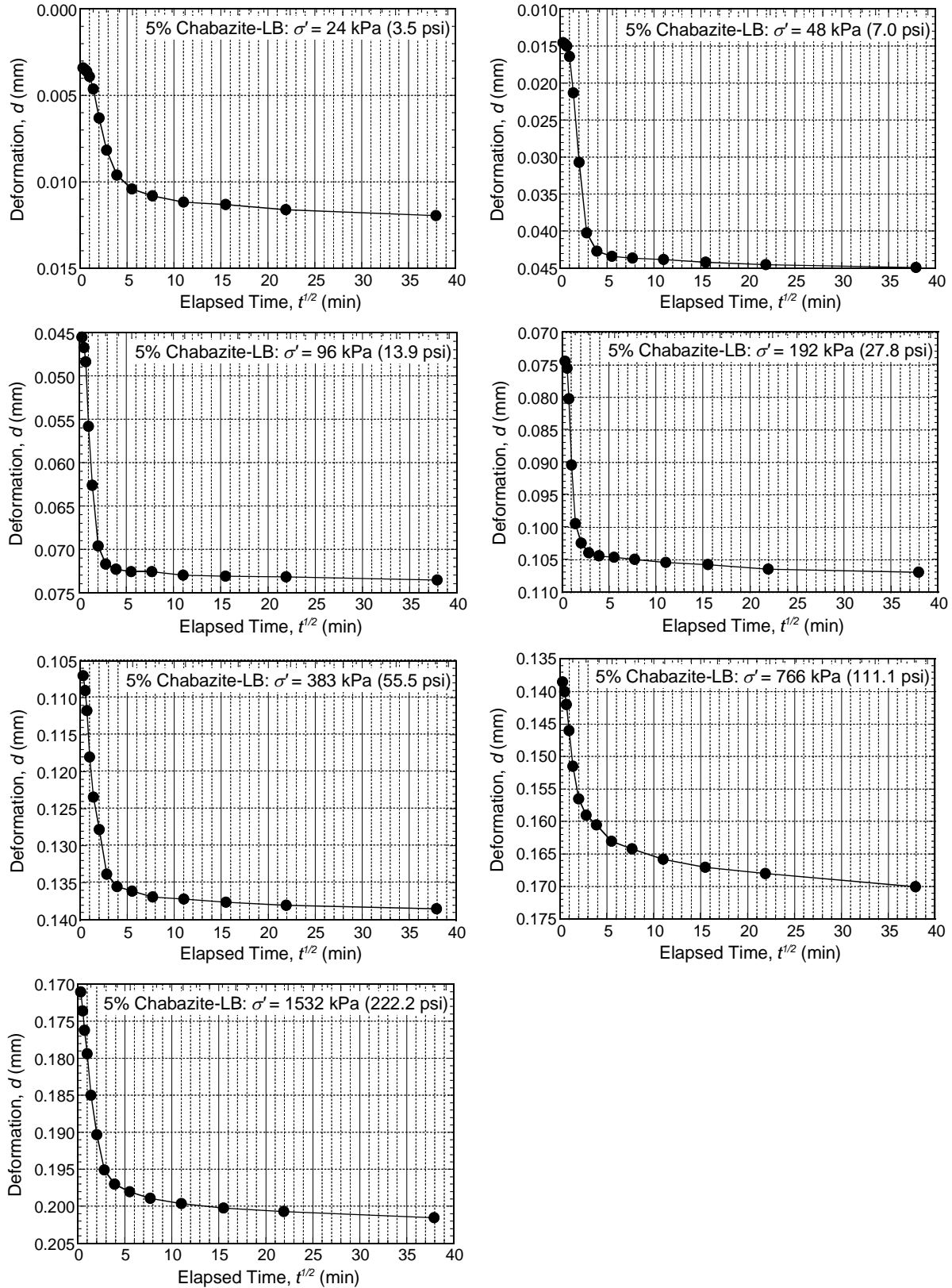


Figure A.10. Results of settlement as a function of square root time for SB backfill amended with 5 % chabazite-LB.

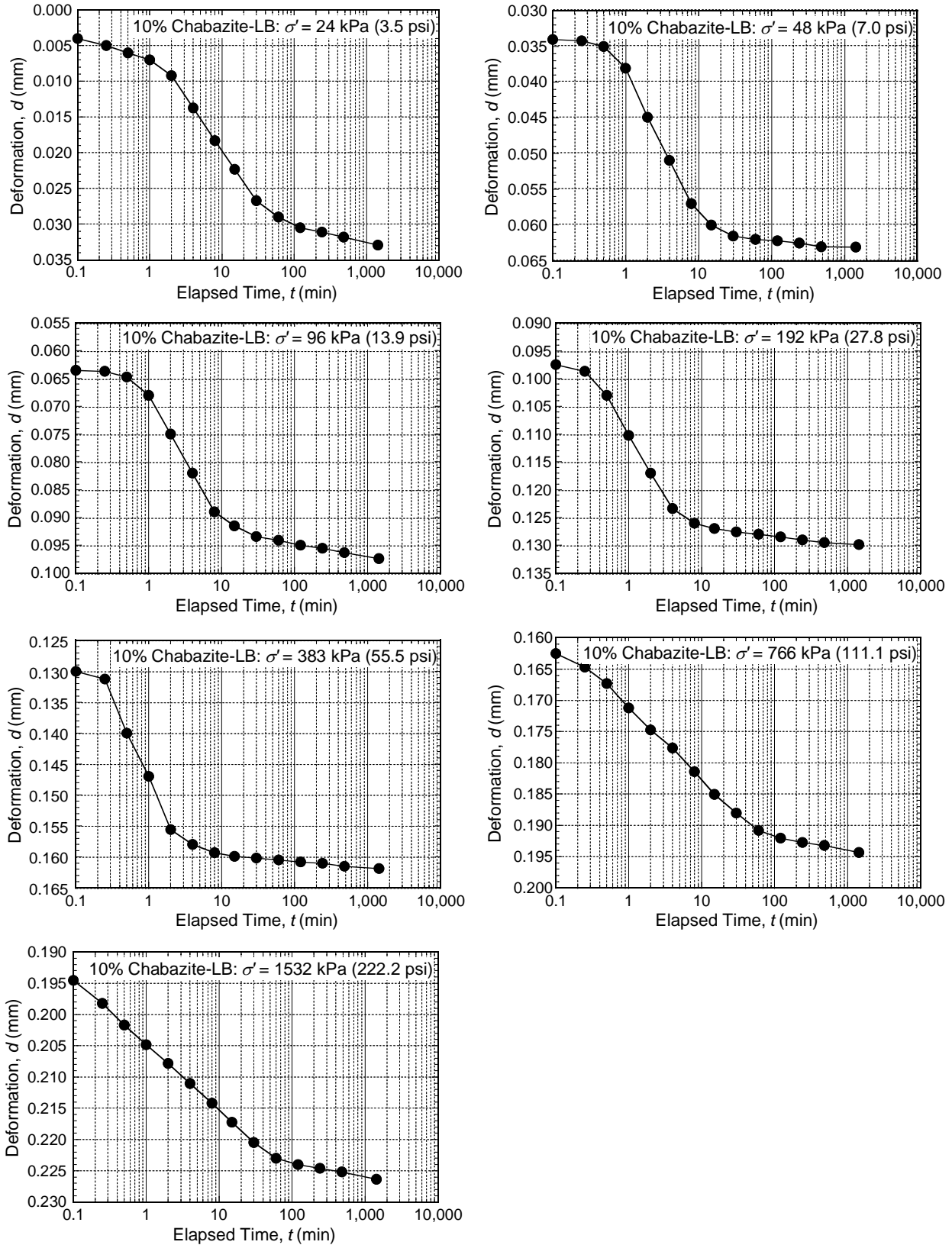


Figure A.11. Results of settlement as a function of log time for SB backfill amended with 10 % chabazite-LB.

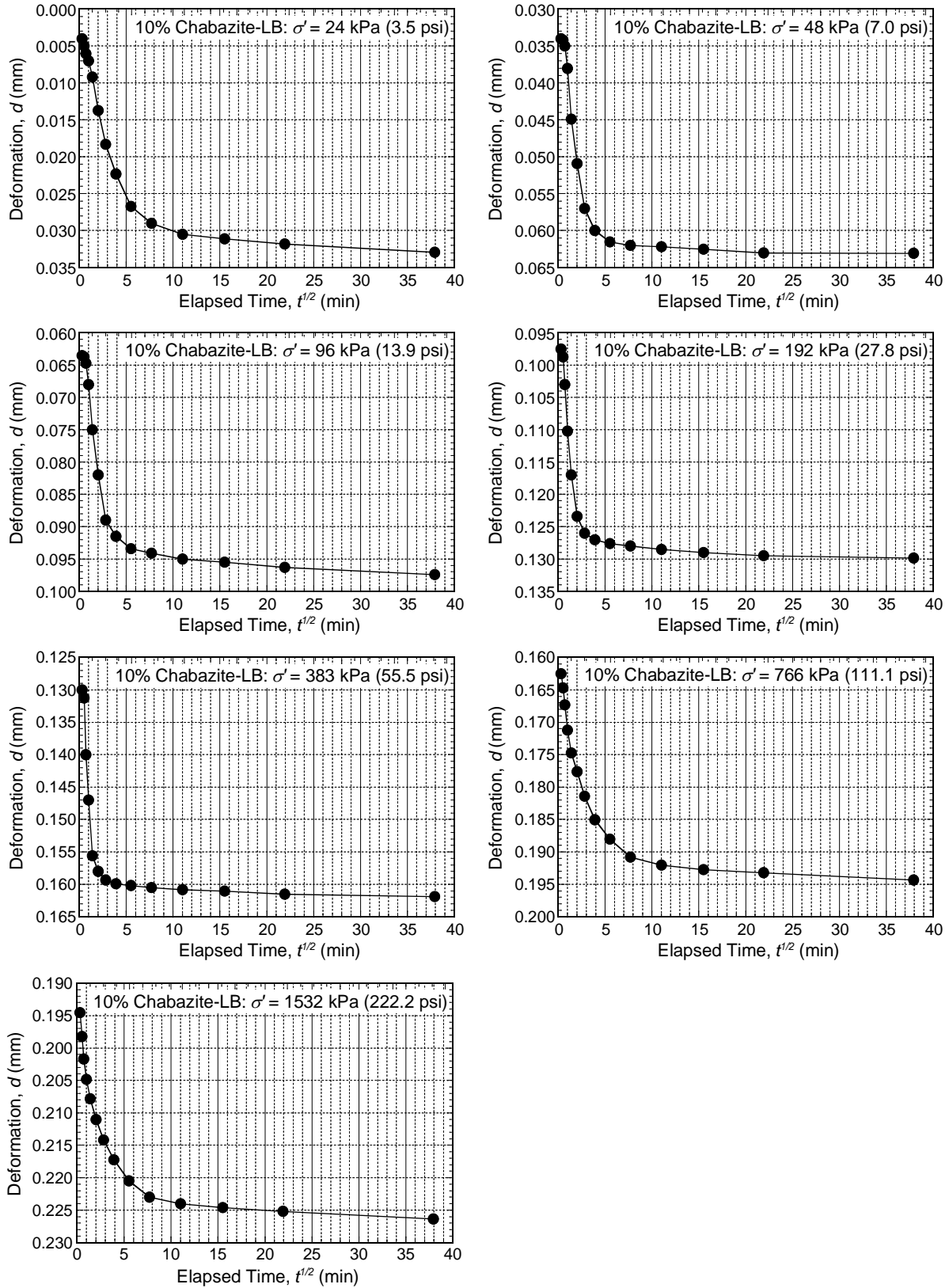


Figure A.12. Results of settlement as a function of square root time for SB backfill amended with 10 % chabazite-LB.

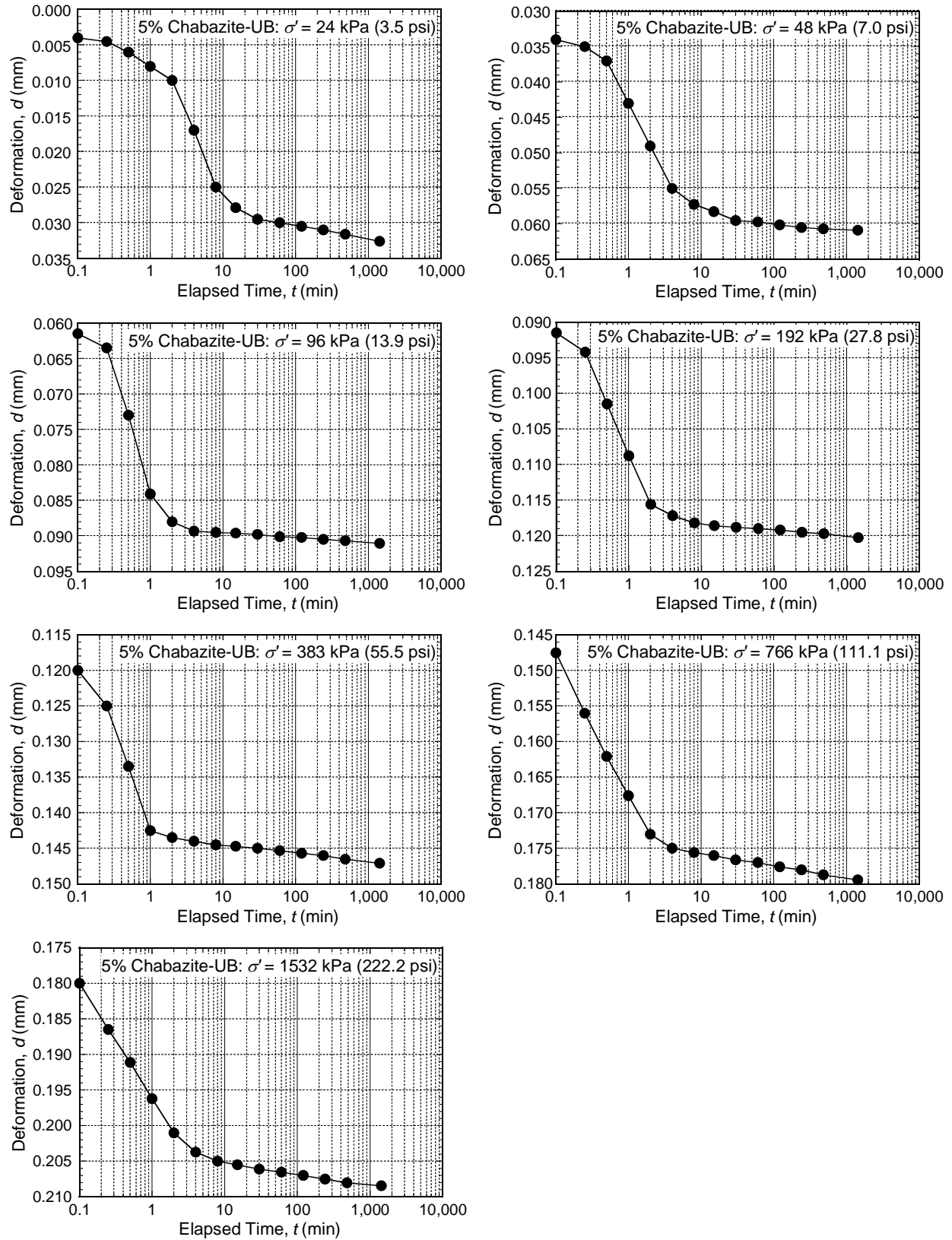


Figure A.13. Results of settlement as a function of log time for SB backfill amended with 5 % chabazite-UB.

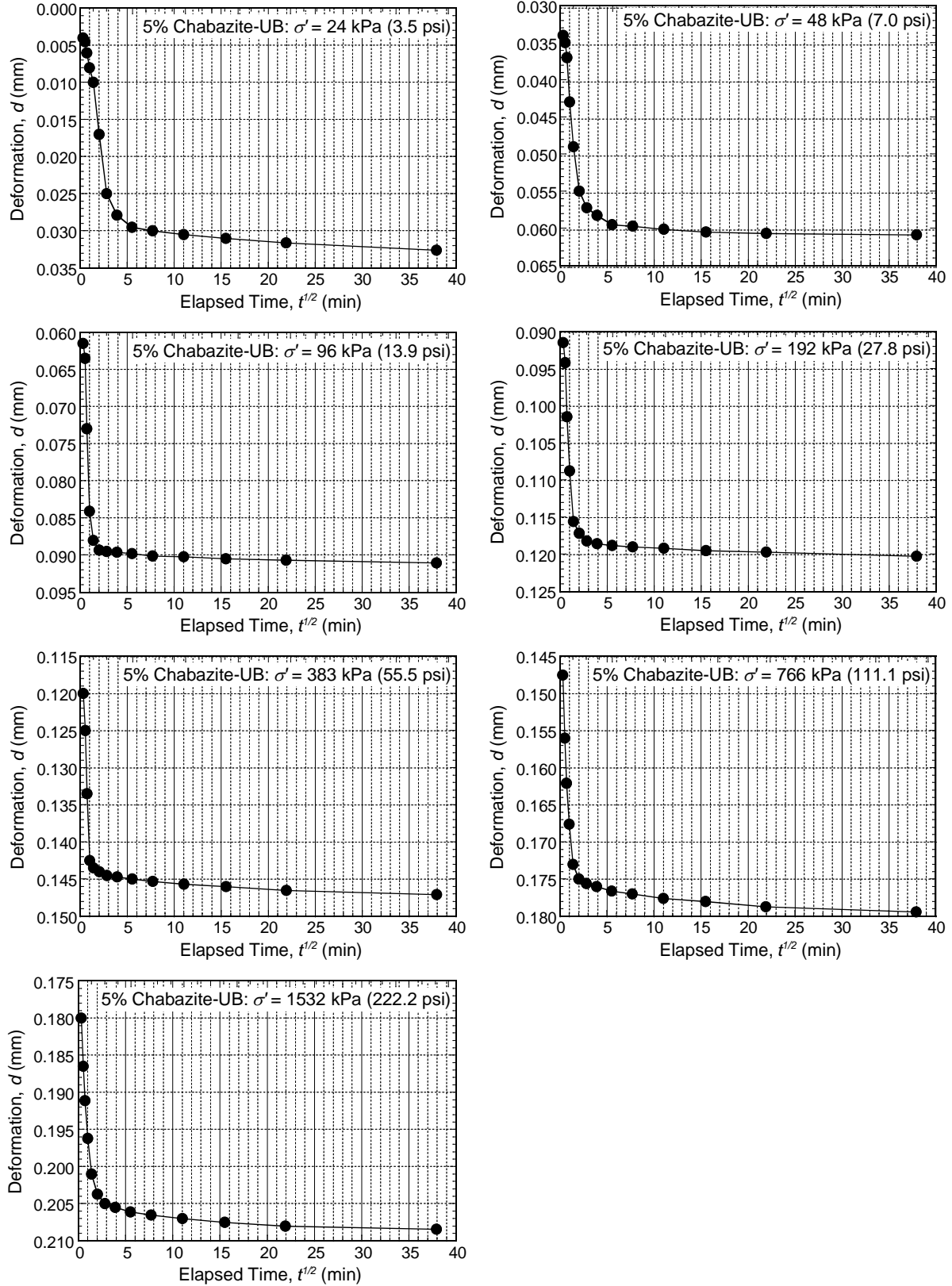


Figure A.14. Results of settlement as a function of square root time for SB backfill amended with 5 % chabazite-UB.

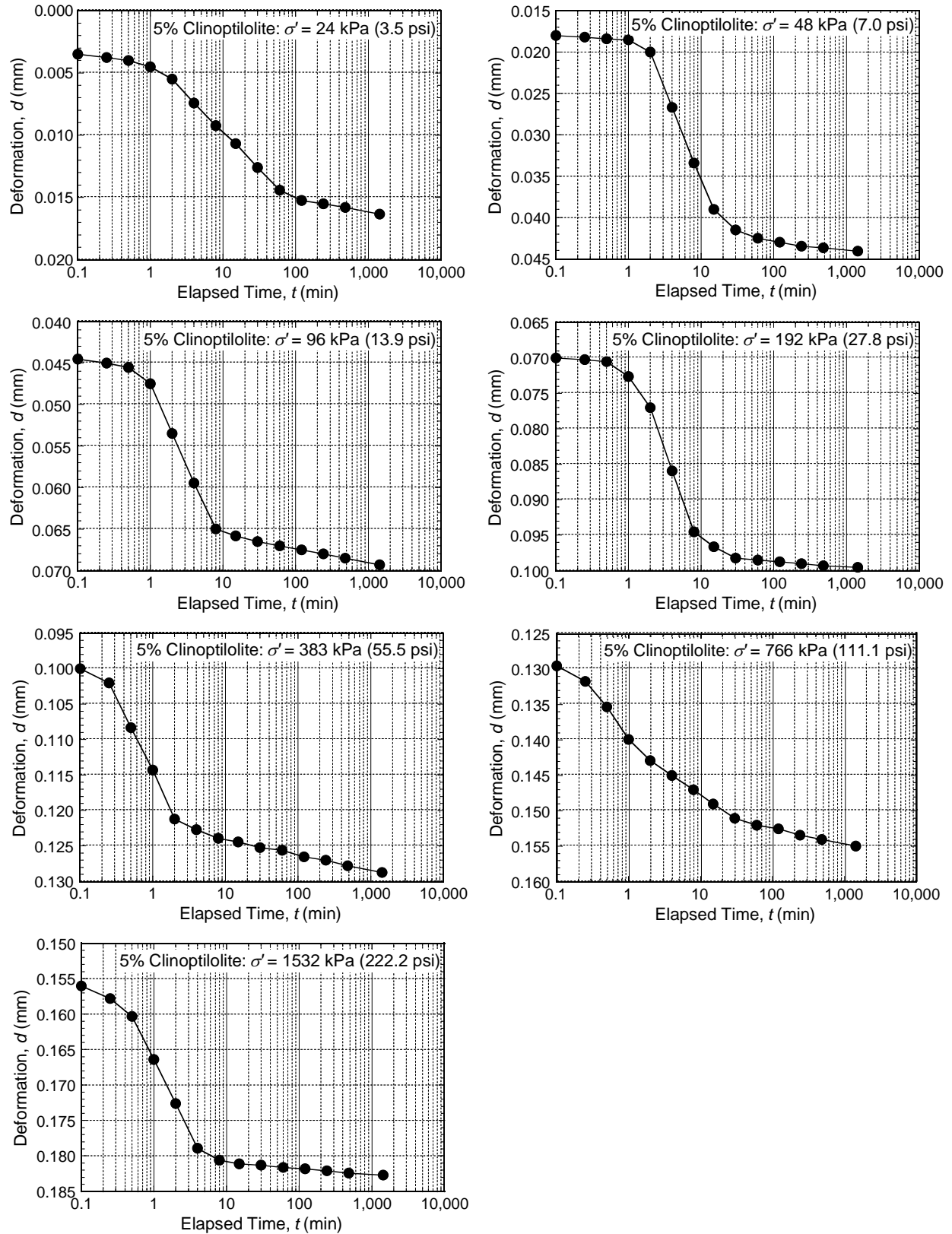


Figure A.15. Results of settlement as a function of log time for SB backfill amended with 5 % clinoptilolite.

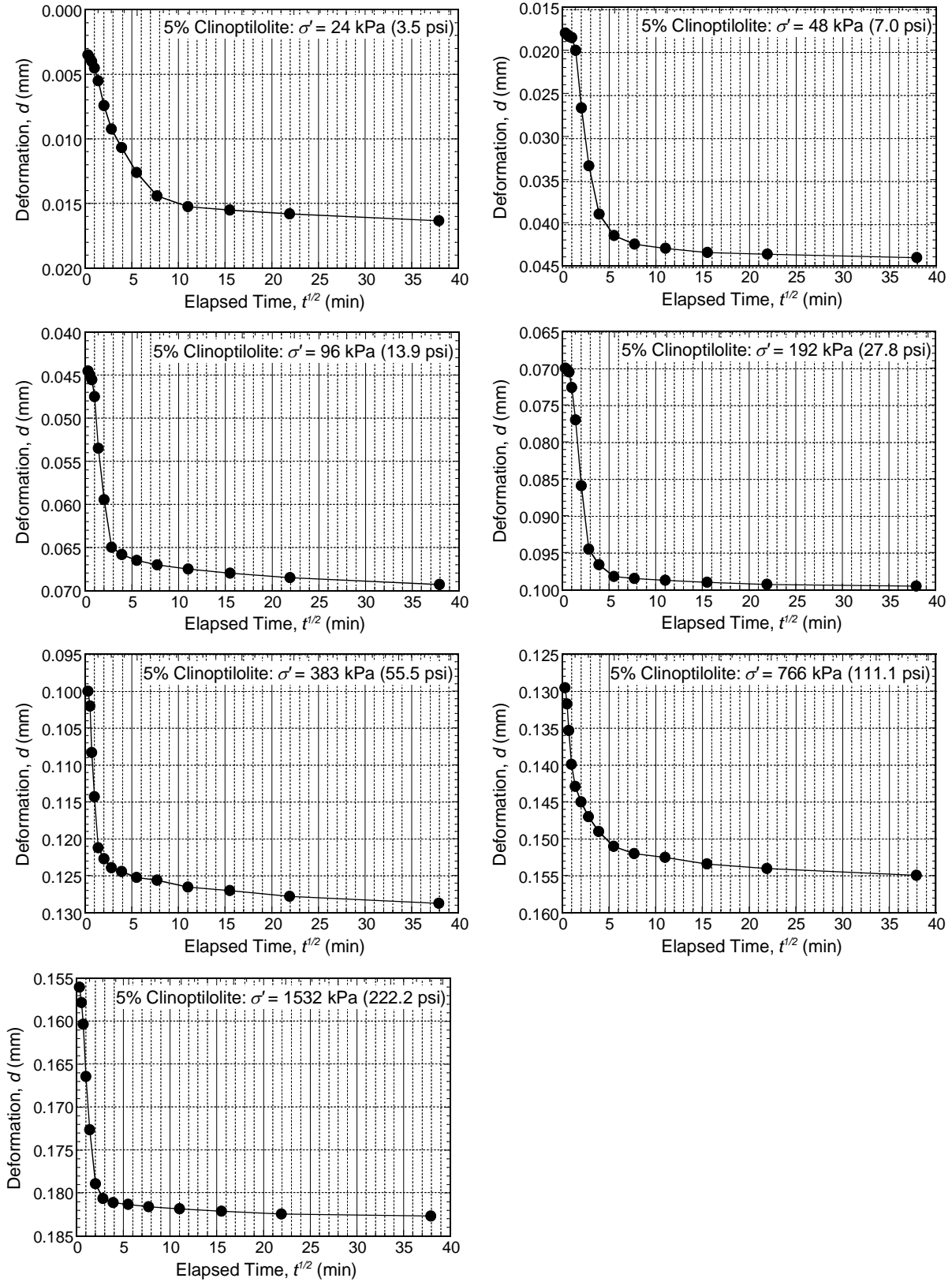


Figure A.16. Results of settlement as a function of square root time for SB backfill amended with 5 % clinoptilolite.

APPENDIX B. SUPPLEMENTARY DATA FOR CHAPTER 3

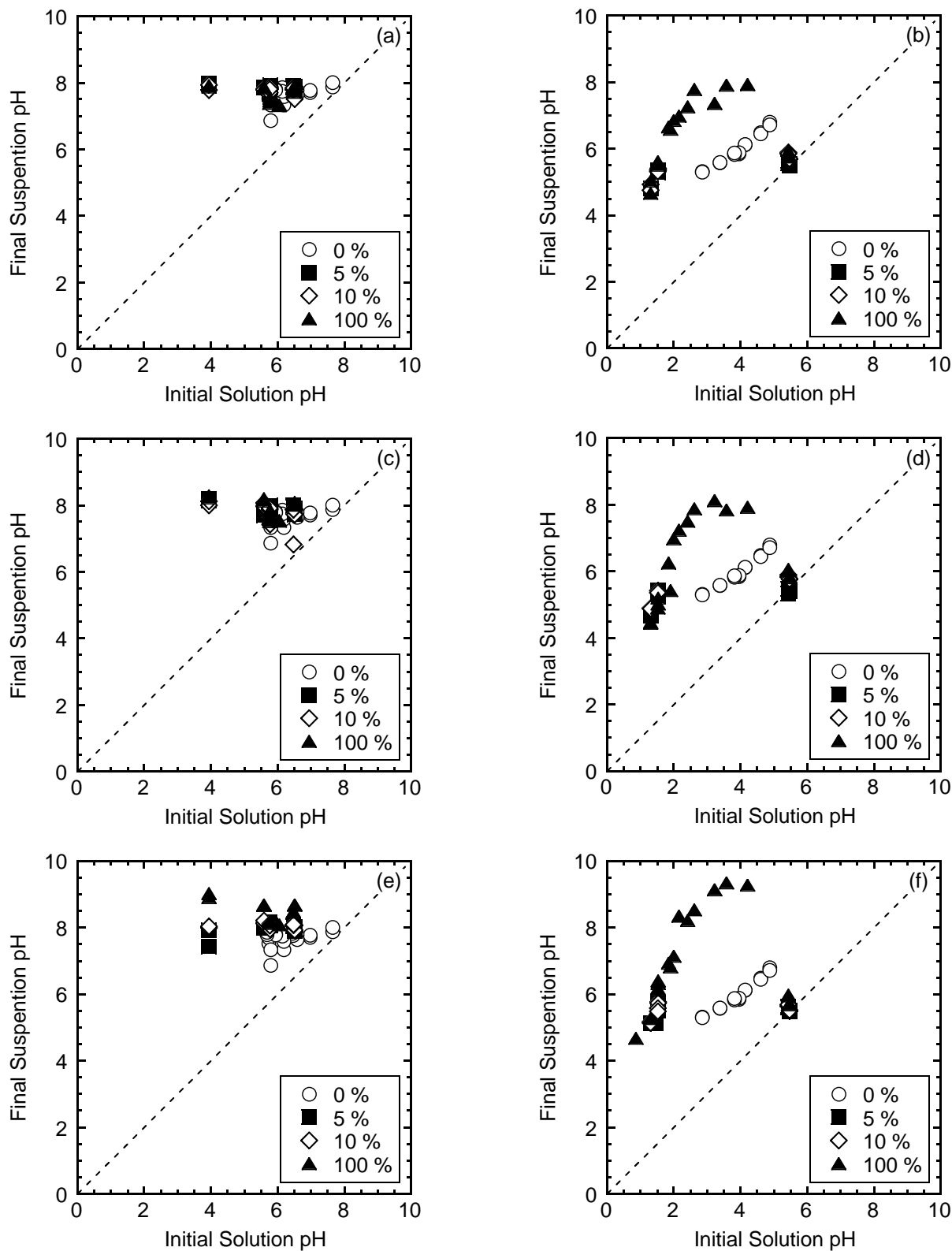


Figure B.1. Change in initial solution pH after the experiments for the unamended, zeolite-amended and 100 % zeolite: (a) chabazite-LB for  $K^+$ ; (b) chabazite-LB for  $Zn^{2+}$ ; (c) chabazite-UB for  $K^+$ ; (d) chabazite-UB for  $Zn^{2+}$ ; (e) clinoptilolite for  $K^+$ ; (f) clinoptilolite for  $Zn^{2+}$ .

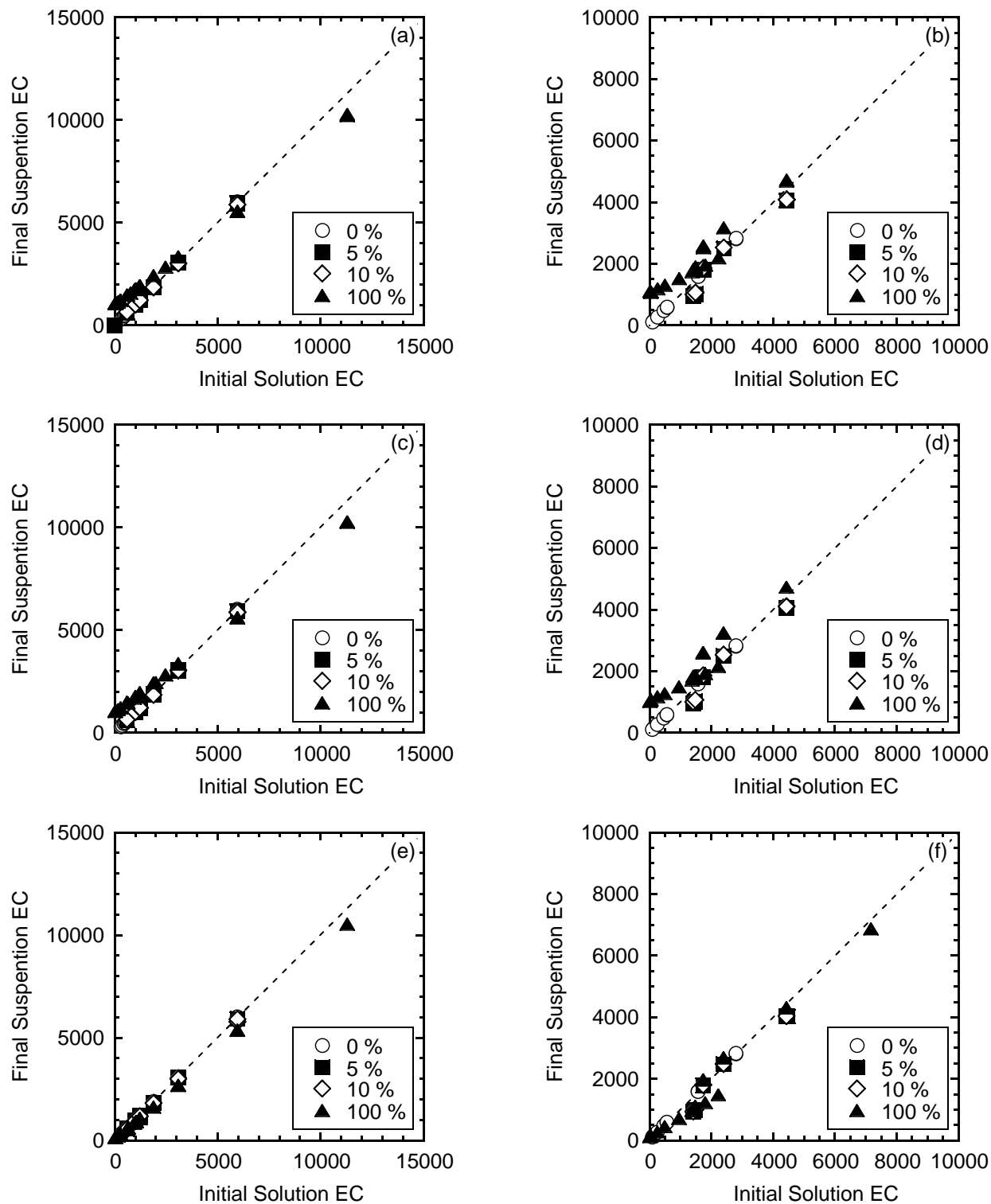


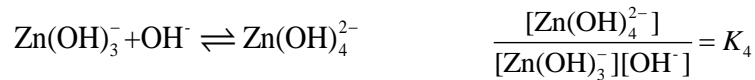
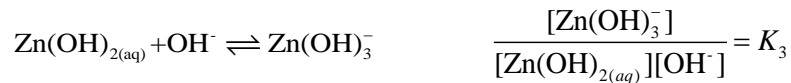
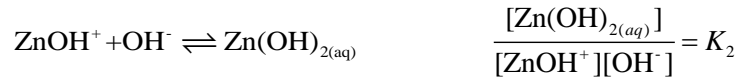
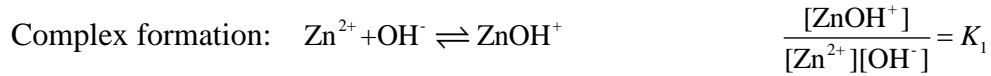
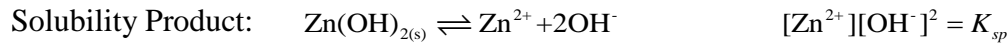
Figure B.2. Change in initial solution EC after the experiments for the unamended, zeolite-amended and 100 % zeolite: (a) chabazite-LB for K<sup>+</sup>; (b) chabazite-LB for Zn<sup>2+</sup>; (c) chabazite-UB for K<sup>+</sup>; (d) chabazite-UB for Zn<sup>2+</sup>; (e) clinoptilolite for K<sup>+</sup>; (f) clinoptilolite for Zn<sup>2+</sup>.

APPENDIX C. ZINC SPECIATION (CHAPTER 3)

The relative distribution of each hydroxyl-zinc species is derived based on the stability constant. As the sum of each species should equal to the total concentration,  $C_T$ , the concentration of each species for the correlating pH can be calculated. As the reported stability constants differ, the calculated zinc speciation differs. The pH range of interest for this study is marked as the shaded area in the figure.

1. Stability constants reported by Sillén and Martell (1964, 1971) in "Stability constants." Spec. Publs. 17, 1964, and 25, 1971, Chemical Society, London.

Total  $\text{Zn}(\text{OH})_2$  concentration:  $C_T$



$\rightarrow K_1 = 10^{4.15} = 1.4 \times 10^4$ ;  $K_2 = 1 \times 10^6$ ;  $K_3 = 10^{4.11} = 1.3 \times 10^4$ ;  $K_4 = 10^{1.26} = 1.8 \times 10^1$

Mass balance of zinc in solution:  $C_T = [\text{Zn}^{2+}] + [\text{ZnOH}^+] + [\text{Zn}(\text{OH})_{2(aq)}] + [\text{Zn}(\text{OH})_3^-] + [\text{Zn}(\text{OH})_4^{2-}]$

$$\frac{[\text{Zn}^{2+}]}{C_T} = \frac{1}{1 + \frac{K_1 K_w}{[\text{H}^+]} + \frac{K_1 K_2 K_w^2}{[\text{H}^+]^2} + \frac{K_1 K_2 K_3 K_w^3}{[\text{H}^+]^3} + \frac{K_1 K_2 K_3 K_4 K_w^4}{[\text{H}^+]^4}}$$

$$\frac{[\text{ZnOH}^+]}{C_T} = \frac{1}{\frac{[\text{H}^+]}{K_1 K_w} + 1 + \frac{K_2 K_w}{[\text{H}^+]} + \frac{K_2 K_3 K_w^2}{[\text{H}^+]^2} + \frac{K_2 K_3 K_4 K_w^3}{[\text{H}^+]^3}}$$

$$\frac{[\text{Zn(OH)}_{2(aq)}]}{C_T} = \frac{1}{\frac{[\text{H}^+]^2}{K_1 K_2 K_w^2} + \frac{[\text{H}^+]}{K_2 K_w} + 1 + \frac{K_3 K_w}{[\text{H}^+]} + \frac{K_3 K_4 K_w^2}{[\text{H}^+]^2}}$$

$$\frac{[\text{Zn(OH)}_3^-]}{C_T} = \frac{1}{\frac{[\text{H}^+]^3}{K_1 K_2 K_3 K_w^3} + \frac{[\text{H}^+]^2}{K_2 K_3 K_w^2} + \frac{[\text{H}^+]}{K_3 K_w} + 1 + \frac{K_4 K_w}{[\text{H}^+]}}$$

$$\frac{[\text{Zn(OH)}_4^{2-}]}{C_T} = \frac{1}{\frac{[\text{H}^+]^4}{K_1 K_2 K_3 K_4 K_w^4} + \frac{[\text{H}^+]^3}{K_2 K_3 K_4 K_w^3} + \frac{[\text{H}^+]^2}{K_3 K_4 K_w^2} + \frac{[\text{H}^+]}{K_4 K_w} + 1}$$

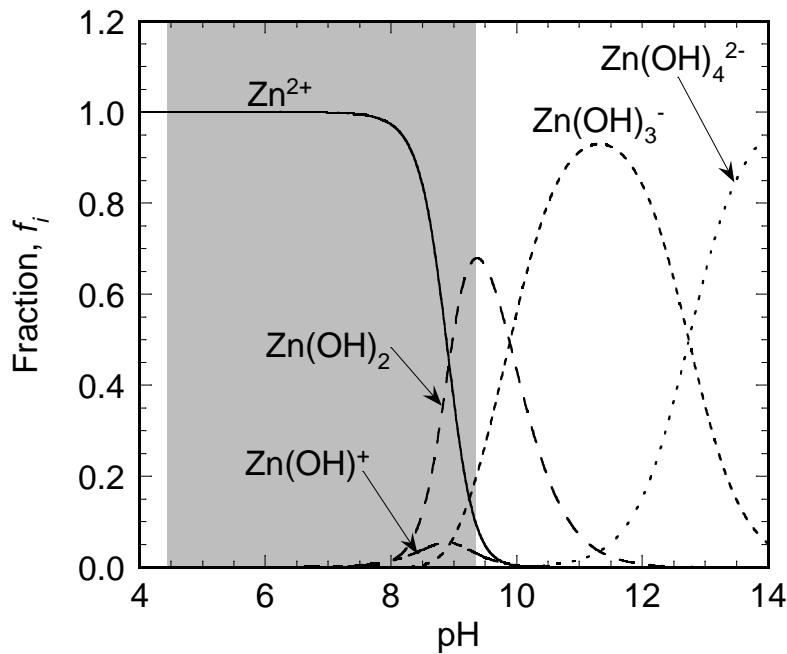
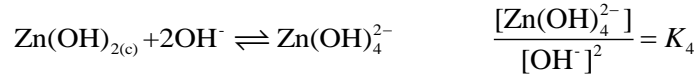
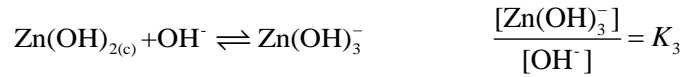
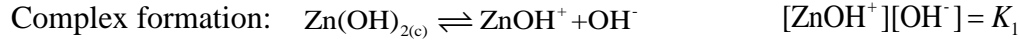
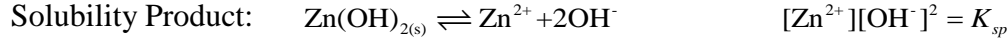


Figure C.1. The relative distribution of each hydroxyl-zinc species is based on the stability constants reported by Sillén and Martell (1964, 1971).

2. Stability constants reported by Reichle *et al.* (1975) in "Zinc Hydroxide: Solubility Product and Hydroxy-complex Stability Constants from 12.5–75 °C." *Canadian Journal of Chemistry*, 53(24), 3841-3845.

Total Zn(OH)<sub>2</sub> concentration:  $C_T$



→ @ 25.0 °C;  $K_{sp} = 1.74 \times 10^{17}$ ;  $K_1 = 2.54 \times 10^{11}$ ;  $K_2 = 2.62 \times 10^6$ ;  $K_3 = 1.32 \times 10^3$ ;  $K_4 = 6.47 \times 10^2$

Mass balance of zinc in solution:  $C_T = [\text{Zn}^{2+}] + [\text{ZnOH}^+] + [\text{Zn(OH)}_{2(aq)}] + [\text{Zn(OH)}_3^-] + [\text{Zn(OH)}_4^{2-}]$

$$\frac{[\text{Zn}^{2+}]}{C_T} = \frac{1}{1 + \frac{K_1 K_w}{K_{sp} [\text{H}^+]} + \frac{K_2 K_w^2}{K_{sp} [\text{H}^+]^2} + \frac{K_3 K_w^3}{K_{sp} [\text{H}^+]^3} + \frac{K_4 K_w^4}{K_{sp} [\text{H}^+]^4}}$$

$$\frac{[\text{ZnOH}^+]}{C_T} = \frac{1}{\frac{K_{sp} [\text{H}^+]}{K_1 K_w} + 1 + \frac{K_2 K_w}{K_1 [\text{H}^+]} + \frac{K_3 K_w^2}{K_1 [\text{H}^+]^2} + \frac{K_4 K_w^3}{K_1 [\text{H}^+]^3}}$$

$$\frac{[\text{Zn(OH)}_{2(aq)}]}{C_T} = \frac{1}{\frac{K_{sp} [\text{H}^+]^2}{K_2 K_w^2} + \frac{K_1 [\text{H}^+]}{K_2 K_w} + 1 + \frac{K_3 K_w}{K_2 [\text{H}^+]} + \frac{K_4 K_w^2}{K_2 [\text{H}^+]^2}}$$

$$\frac{[\text{Zn(OH)}_3^-]}{C_T} = \frac{1}{\frac{K_{sp} [\text{H}^+]^3}{K_3 K_w^3} + \frac{K_1 [\text{H}^+]^2}{K_3 K_w^2} + \frac{K_2 [\text{H}^+]}{K_3 K_w} + 1 + \frac{K_4 K_w}{K_3 [\text{H}^+]}}$$

$$\frac{[\text{Zn(OH)}_4^{2-}]}{C_T} = \frac{1}{\frac{K_{sp} [\text{H}^+]^4}{K_4 K_w^4} + \frac{K_1 [\text{H}^+]^3}{K_4 K_w^3} + \frac{K_2 [\text{H}^+]^2}{K_4 K_w^2} + \frac{K_3 [\text{H}^+]}{K_4 K_w} + 1}$$

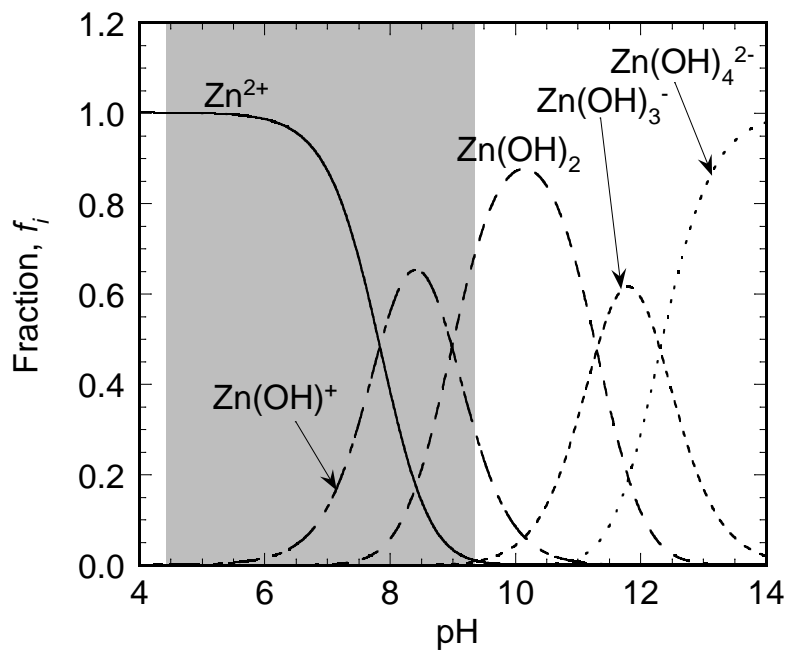
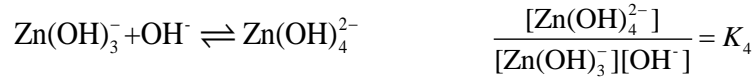
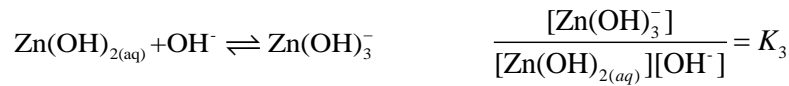
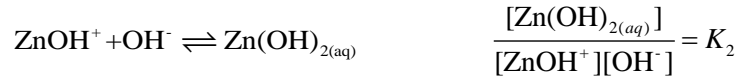
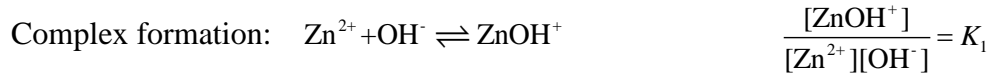
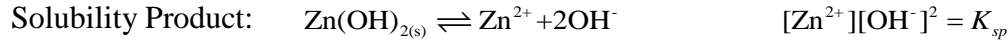


Figure C.2. The relative distribution of each hydroxyl-zinc species is based on the stability constants reported by Reichle *et al.* (1975).

3. Stability constants reported by Morel and Hering (1993) in *Principles and applications of aquatic chemistry*. Wiley-Interscience, New York

Total Zn(OH)<sub>2</sub> concentration:  $C_T$



$\rightarrow K_1 = 10^5$ ;  $K_2 = 10^{6.1} = 1.26 \times 10^6$ ;  $K_3 = 10^{2.5} = 3.16 \times 10^2$ ;  $K_4 = 10^{1.2} = 1.58 \times 10^1$

Mass balance of zinc in solution:  $C_T = [\text{Zn}^{2+}] + [\text{ZnOH}^+] + [\text{Zn(OH)}_{2(aq)}] + [\text{Zn(OH)}_3^-] + [\text{Zn(OH)}_4^{2-}]$

$$\frac{[\text{Zn}^{2+}]}{C_T} = \frac{1}{1 + \frac{K_1 K_w}{[\text{H}^+]} + \frac{K_1 K_2 K_w^2}{[\text{H}^+]^2} + \frac{K_1 K_2 K_3 K_w^3}{[\text{H}^+]^3} + \frac{K_1 K_2 K_3 K_4 K_w^4}{[\text{H}^+]^4}}$$

$$\frac{[\text{ZnOH}^+]}{C_T} = \frac{1}{\frac{[\text{H}^+]}{K_1 K_w} + 1 + \frac{K_2 K_w}{[\text{H}^+]} + \frac{K_2 K_3 K_w^2}{[\text{H}^+]^2} + \frac{K_2 K_3 K_4 K_w^3}{[\text{H}^+]^3}}$$

$$\frac{[\text{Zn(OH)}_{2(aq)}]}{C_T} = \frac{1}{\frac{[\text{H}^+]^2}{K_1 K_2 K_w^2} + \frac{[\text{H}^+]}{K_2 K_w} + 1 + \frac{K_3 K_w}{[\text{H}^+]} + \frac{K_3 K_4 K_w^2}{[\text{H}^+]^2}}$$

$$\frac{[\text{Zn(OH)}_3^-]}{C_T} = \frac{1}{\frac{[\text{H}^+]^3}{K_1 K_2 K_3 K_w^3} + \frac{[\text{H}^+]^2}{K_2 K_3 K_w^2} + \frac{[\text{H}^+]}{K_3 K_w} + 1 + \frac{K_4 K_w}{[\text{H}^+]}}$$

$$\frac{[\text{Zn(OH)}_4^{2-}]}{C_T} = \frac{1}{\frac{[\text{H}^+]^4}{K_1 K_2 K_3 K_4 K_w^4} + \frac{[\text{H}^+]^3}{K_2 K_3 K_4 K_w^3} + \frac{[\text{H}^+]^2}{K_3 K_4 K_w^2} + \frac{[\text{H}^+]}{K_4 K_w} + 1}$$

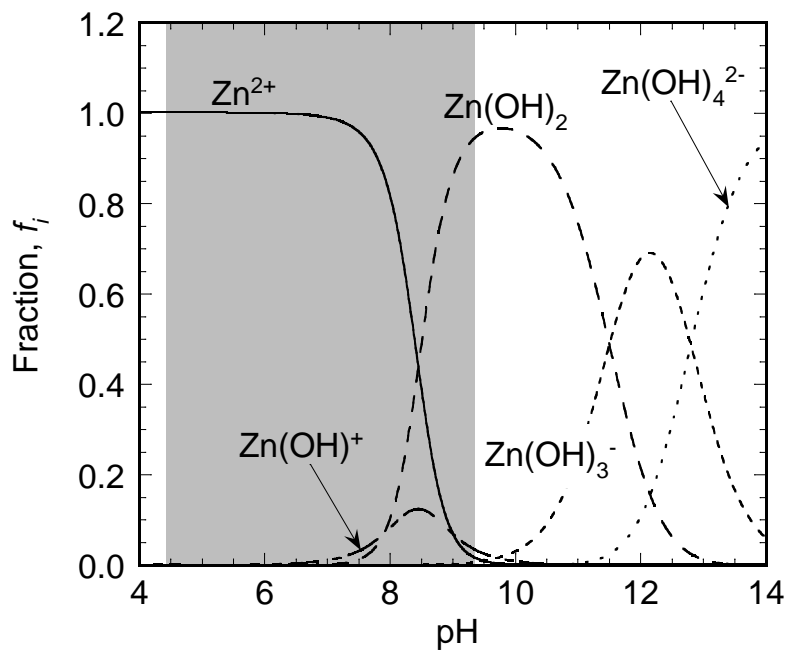
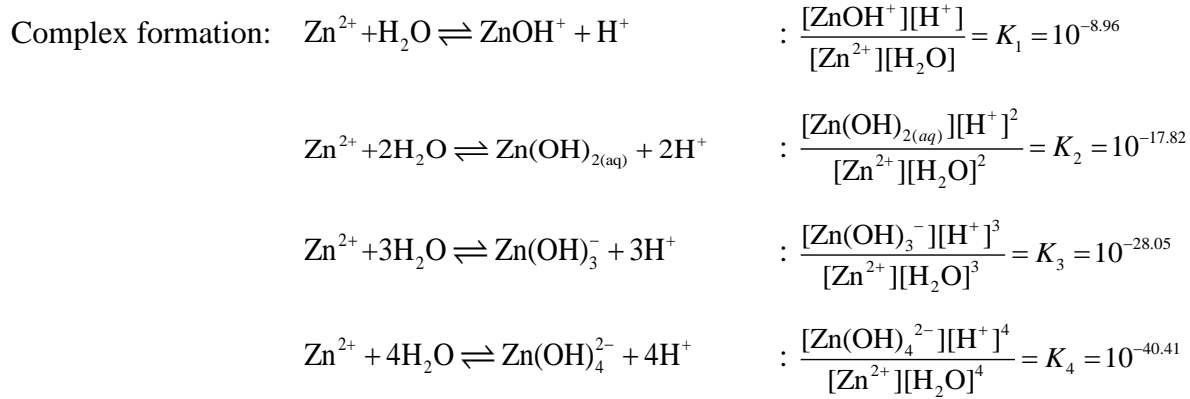


Figure C.3. The relative distribution of each hydroxyl-zinc species is based on the stability constants reported by Morel and Hering (1993).

4. Stability constants reported by Powell *et al.* (2013) in "Chemical speciation of environmentally significant metals with inorganic ligands. Part 5: The  $Zn^{2+} + OH^-$ ,  $Cl^-$ ,  $CO_3^{2-}$ ,  $SO_4^{2-}$ , and  $PO_4^{3-}$  systems (IUPAC Technical Report)." *Pure and Applied Chemistry Pure Appl. Chem.*, 85(12), 2249-2311.

Total Zn concentration:  $C_T$ :  $T = 298.15$  K,  $p = 100$  kPa,  $I_m = 0$  mol/kg



Etc:  $Zn_2OH^{3+}$ ,  $ZnO$ ,  $ZnCO_{3(aq)}$ ,  $ZnCO_{3(s)}$ ,  $Zn(CO_3)_2^{2-}$ ,  $ZnHCO_3^+$ ,  $\epsilon$ ,  $\beta_1$ ,  $\beta_2$ ,  $\gamma$ ,  $\delta$ - $Zn(OH)_{2(s)}$

$$C_T = [Zn^{2+}] + [ZnOH^+] + [Zn(OH)_{2(aq)}] + [Zn(OH)_3^-] + [Zn(OH)_4^{2-}]$$

$$\frac{[Zn^{2+}]}{C_T} = \frac{1}{1 + \frac{K_1}{[H^+]} + \frac{K_2}{[H^+]^2} + \frac{K_3}{[H^+]^3} + \frac{K_4}{[H^+]^4}}$$

$$\frac{[ZnOH^+]}{C_T} = \frac{1}{\frac{[H^+]}{K_1} + 1 + \frac{K_2}{K_1[H^+]} + \frac{K_3}{K_1[H^+]^2} + \frac{K_4}{K_1[H^+]^3}}$$

$$\frac{[Zn(OH)_2]}{C_T} = \frac{1}{\frac{[H^+]^2}{K_2} + \frac{K_1[H^+]}{K_2} + 1 + \frac{K_3}{K_2[H^+]} + \frac{K_4}{K_2[H^+]^2}}$$

$$\frac{[Zn(OH)_3^-]}{C_T} = \frac{1}{\frac{[H^+]^3}{K_3} + \frac{K_1[H^+]^2}{K_3} + \frac{K_2[H^+]}{K_3} + 1 + \frac{K_4}{K_3[H^+]}}$$

$$\frac{[Zn(OH)_4^{2-}]}{C_T} = \frac{1}{\frac{[H^+]^4}{K_4} + \frac{K_1[H^+]^3}{K_4} + \frac{K_2[H^+]^2}{K_4} + \frac{K_3[H^+]}{K_4} + 1}$$

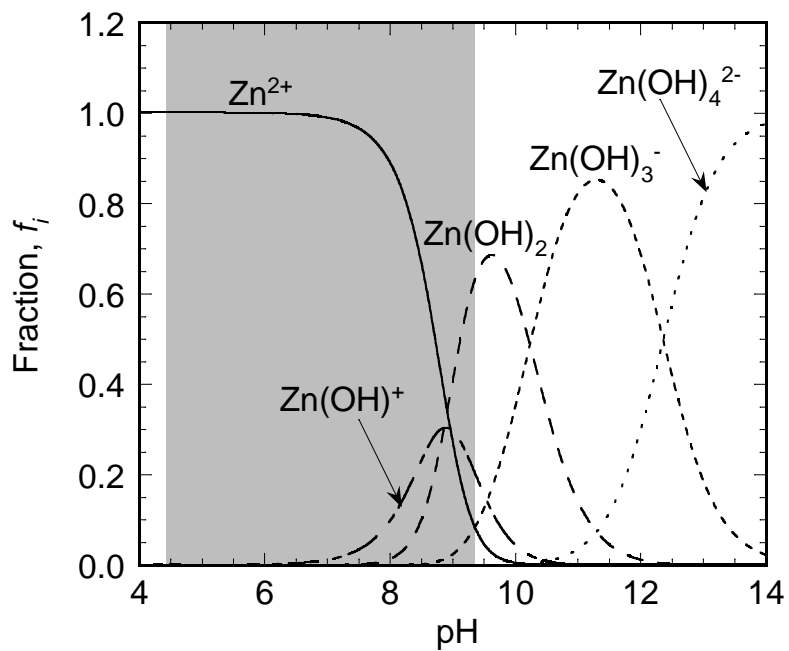


Figure C.4. The relative distribution of each hydroxyl-zinc species is based on the stability constants reported by Powell *et al.* (2013).

APPENDIX D. CONCAVE AND NONLINEAR ADSORPTION (CHAPTER 4)

The adsorption isotherm can be either linear or nonlinear, where the nonlinear isotherm can be either concave or convex. The concave isotherm is common for soil where the slope of the isotherm decreases as the concentration increases, whereas the convex isotherm represents infinite adsorption. When the solid-phase adsorbed concentration of the solute ( $C_s$ ) is expressed as a function of concentration, or,  $C_s = f(C)$ ,  $f''(C) < 0$  for the concave nonlinear isotherm. Since the retardation factor,  $R_d$ , is  $1 + \frac{\rho_d}{n} f'(C)$ , the  $R_d$  for the concave nonlinear isotherm decreases as the concentration increases (*i.e.*,  $f''(C) < 0$ ). Therefore, the  $R_d$  at low concentration is larger than the  $R_d$  at high concentration, meaning high concentration transports faster than low concentration. For a migrating plum of contaminants, the front and tail of the plum has lower concentration and travel slower due to the high  $R_d$ , whereas the as center of the plum travels faster due to the lower  $R_d$ . However, since the higher concentration center cannot travel past the lower concentration front, the concentration profile forms a steep front (or concentration step) with a strongly retarded tail, which is called the self-sharpening or front-sharpening effect (Melynk 1985; Shackelford 1999).

All the BEAT results show nonlinear concave isotherms (as  $N_f < 1$ ), however, the  $f''(C)$  for both Langmuir and Freundlich was calculated for verification. The first and second derivative of the Langmuir and Freundlich is as follows:

$$\text{Langmuir: } C_s = f(C) = \frac{K_L Q_L C}{1 + K_L C} \rightarrow f'(C) = \frac{K_L Q_L}{(1 + K_L C)^2} \rightarrow f''(C) = -\frac{2K_L^2 Q_L}{(1 + K_L C)^3} \quad (\text{D.1})$$

$$\text{Freundlich: } C_s = f(C) = K_f C^{N_f} \rightarrow f'(C) = K_f N_f C^{(N_f-1)} \rightarrow f''(C) = K_f N_f (N_f - 1) C^{(N_f-2)} \quad (\text{D.2})$$

The calculated  $f''(C)$  is summarized in Table 1 for  $C_o$ , showing that the fitted isotherm for Langmuir and Freundlich is nonlinear concave ( $f''(C) < 0$ ) for all cases. However, this approach is not sufficient to explain the difference in the shape of the generated flux breakthrough curves using the BEAT results. In order to quantify the nonlinearity of the BEAT results, the method suggested by Emancipator and Kroll (1993) was used. First, the linear function  $g(C)$  is assumed for the nonlinear function  $f(C)$  where  $0 \leq C \leq C_o$ , or  $0 \leq f(C) \leq C_s$ . In this case,  $g(C) = K_d C$ , where  $K_d$  is the secant distribution coefficient as follows:

$$\text{Langmuir: } K_d = \frac{C_s - 0}{C_o - 0} = \frac{K_L Q_L C_o}{1 + K_L C_o} \frac{1}{C_o} = \frac{K_L Q_L}{1 + K_L C_o} \quad (\text{D.3})$$

$$\text{Freundlich: } K_d = \frac{C_s - 0}{C_o - 0} = \frac{K_f C_o^{N_f}}{C_o} = K_f C_o^{(N_f - 1)} \quad (\text{D.4})$$

For the range of interest in this study ( $0 \leq C \leq C_o$ , or  $0 \leq f(C) \leq C_s$ ), the nonlinearity ( $L$ ) is defined as:

$$L = \sqrt{\frac{\int_0^{C_o} [f(C) - g(C)]^2 dC}{C_o - 0}} \quad (\text{D.5})$$

Since the calculation for the nonlinearity ( $L$ ) is complicated, the  $L^2$  is derived first as follows:

$$\begin{aligned} \text{Langmuir : } L^2 = & -\frac{2Q_L \ln(K_L C_o + 1)}{K_L C_o} \left\{ Q_L + \frac{K_d}{K_L} \right\} \\ & + Q_L^2 \left\{ 1 - \frac{1}{K_L C_o + K_L^2 C_o^2} + \frac{1}{K_L C_o} \right\} + K_d Q_L \left\{ \frac{2}{K_L} - C_o \right\} + \frac{K_d^2 C_o^2}{3} \end{aligned} \quad (\text{D.6})$$

$$\text{Freundlich : } L^2 = \frac{K_f^2 C_o^{2N_f}}{1 + 2N_f} + \frac{K_d^2 C_o^2}{3} - \frac{2K_d K_f C_o^{(N_f+1)}}{2 + N_f} \quad (\text{D.7})$$

For the range of interest ( $0 \leq C \leq C_o$ , or  $0 \leq f(C) \leq C_s$ ) in this study, the relative nonlinearity,  $\lambda$  ( $0 \leq \lambda \leq 0.5$ ) is defined as:

$$\lambda = \frac{L}{\Delta y} = \frac{L}{(C_s - 0)} = \sqrt{\frac{L^2}{C_s^2}} \quad (\text{D.8})$$

For the case where  $f(C)$  becomes linear (or  $f(C) = g(C)$ ), the relative nonlinearity  $\lambda = 0$ . The general form of  $\lambda$  can be obtained by substituting (D.1), (D.3), and (D.6) into (D.8) for Langmuir, and (D.2), (D.4), and (D.7) into (D.8) for Freundlich as follows;

Langmuir:

$$\text{Langmuir : } \lambda = \sqrt{\frac{L^2}{C_s^2}}$$

$$= \sqrt{\frac{\frac{2Q_L \ln(K_L C_o + 1)}{K_L C_o} \left\{ Q_L + \frac{K_L Q_L}{1 + K_L C_o} \right\} + Q_L^2 \left\{ 1 - \frac{1}{K_L C_o + K_L^2 C_o^2} + \frac{1}{K_L C_o} \right\} + \frac{K_L Q_L}{1 + K_L C_o} Q_L \left\{ \frac{2}{K_L} - C_o \right\} + \frac{K_L^2 Q_L^2 C_o^2}{(1 + K_L C_o)^2}}{\frac{K_L^2 Q_L^2 C_o^2}{(1 + K_L C_o)^2}}}$$

$$= \sqrt{\left[ -\frac{2(1 + K_L C_o) \ln(1 + K_L C_o)}{K_L^3 C_o^3} \left\{ (1 + K_L C_o) + 1 \right\} + \frac{(1 + K_L C_o)^2}{K_L^2 C_o^2} \left\{ 1 - \frac{1}{K_L C_o (1 + K_L C_o)} + \frac{1}{K_L C_o} \right\} + \frac{(1 + K_L C_o)}{K_L C_o^2} \left\{ \frac{2}{K_L} - C_o \right\} + \frac{1}{3} \right]}$$

(D.9)

$$\text{Freundlich : } \lambda = \sqrt{\frac{L^2}{C_s^2}} = \sqrt{\frac{\frac{K_f^2 C_o^{2N_f}}{1 + 2N_f} + \frac{K_f^2 C_o^{(2N_f - 2)} C_o^2}{3} - \frac{2K_f^2 C_o^{(2N_f)}}{2 + N_f}}{K_f^2 C^{2N_f}}} = \sqrt{\frac{1}{1 + 2N_f} + \frac{1}{3} - \frac{2}{2 + N_f}}$$

(D.10)

Table D.1. The second derivative of the fitted BEAT results with the Langmuir and Freundlich model as a function of source concentration ( $C_o = 100, 1,000, 10,000$  mg/L for K,  $C_o = 100, 500, 1,000, 5,000, 10,000$  mg/L for Zn) using data from Hong *et al.* (2016).

	Type of Adsorption Model	Source Concentration, $C_o$ (mg/L)	Second Derivative, $f''(C)$ <sup>a</sup>						
			Unamended	Chabazite-LB		Chabazite-UB		Clinoptilolite	
				5 %	10 %	5 %	10 %	5 %	10 %
K	Langmuir	100	-0.0066899	-0.0556518	-0.1129386	-0.0457078	-0.0516907	-0.0062005	-0.0332745
		1,000	-0.0002285	-0.0013279	-0.0019753	-0.0015292	-0.0032592	-0.0013154	-0.0018063
		10,000	-0.0000005	-0.0000025	-0.0000033	-0.0000033	-0.0000094	-0.0000103	-0.0000048
	Freundlich	100	-0.0051452	-0.0351435	-0.0553794	-0.0360500	-0.0603160	-0.0251984	-0.0373400
		1,000	-0.0000694	-0.0006107	-0.0009848	-0.0006411	-0.0012602	-0.0005641	-0.0007281
		10,000	-0.0000009	-0.0000106	-0.0000175	-0.0000114	-0.0000263	-0.0000126	-0.0000142
Zn	Langmuir	100	-0.0340703	-0.0033147	-0.0052047	-0.0014234	-0.0026561	-0.0010972	-0.0020864
		500	-0.0036823	-0.0020235	-0.0029200	-0.0010534	-0.0017731	-0.0008290	-0.0014736
		1,000	-0.0008129	-0.0012019	-0.0016118	-0.0007511	-0.0011432	-0.0006037	-0.0010030
		5,000	-0.0000113	-0.0001020	-0.0001113	-0.0001181	-0.0001254	-0.0001031	-0.0001326
		10,000	-0.0000015	-0.0000207	-0.0000212	-0.0000302	-0.0000278	-0.0000273	-0.0000316
	Freundlich	100	-0.0206399	-0.0322214	-0.0397397	-0.0221073	-0.0286501	-0.0190895	-0.0272894
		500	-0.0011576	-0.0022277	-0.0027475	-0.0018541	-0.0022530	-0.0015754	-0.0022162
		1,000	-0.0003347	-0.0007049	-0.0008694	-0.0006376	-0.0007536	-0.0005380	-0.0007516
		5,000	-0.0000188	-0.0000487	-0.0000601	-0.0000535	-0.0000593	-0.0000444	-0.0000610
		10,000	-0.0000054	-0.0000154	-0.0000190	-0.0000184	-0.0000198	-0.0000152	-0.0000207

$$^a f''(C) = -\frac{2K_L^2 Q_L}{(1+K_L C)^3} \text{ (for Langmuir); } f''(C) = K_f N_f (N_f - 1) C^{(N_f - 2)} \text{ (for Freundlich).}$$

APPENDIX E. SUPPLEMENTARY DATA FOR CHAPTER 4

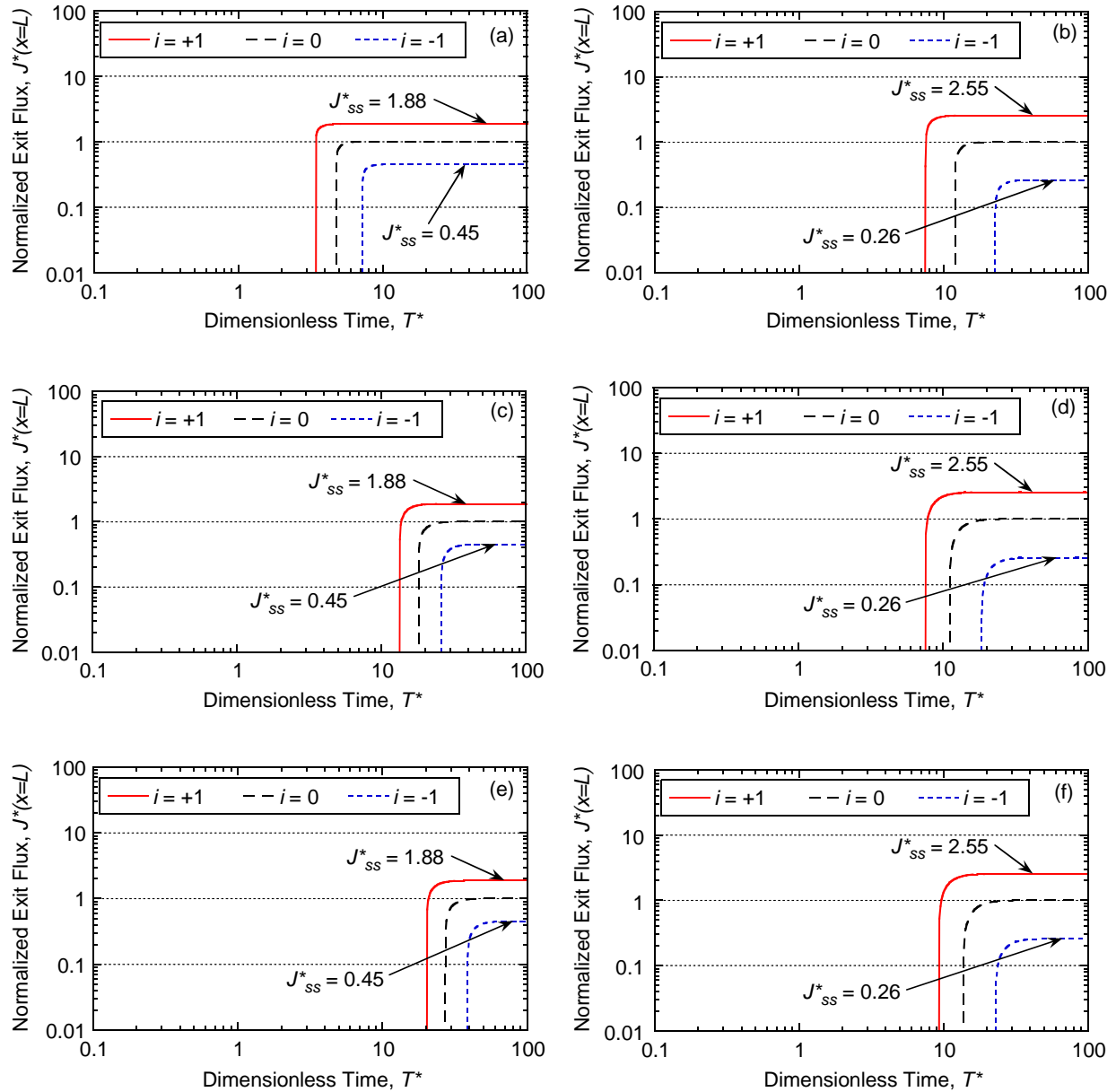


Figure E.1. Effect of Péclet number,  $P_L$ , on flux breakthrough curves with a constant source concentration,  $C_o = 100$  mg/L for: (a) unamended with potassium (K); (b) unamended with zinc (Zn); (c) amended with 5 % chabazite-LB with potassium (K); (d) amended with 5 % chabazite-LB with zinc (Zn); (e) amended with 10 % chabazite-LB with potassium (K); (f) amended with 10 % chabazite-LB with zinc (Zn), all based on the Freundlich adsorption model.

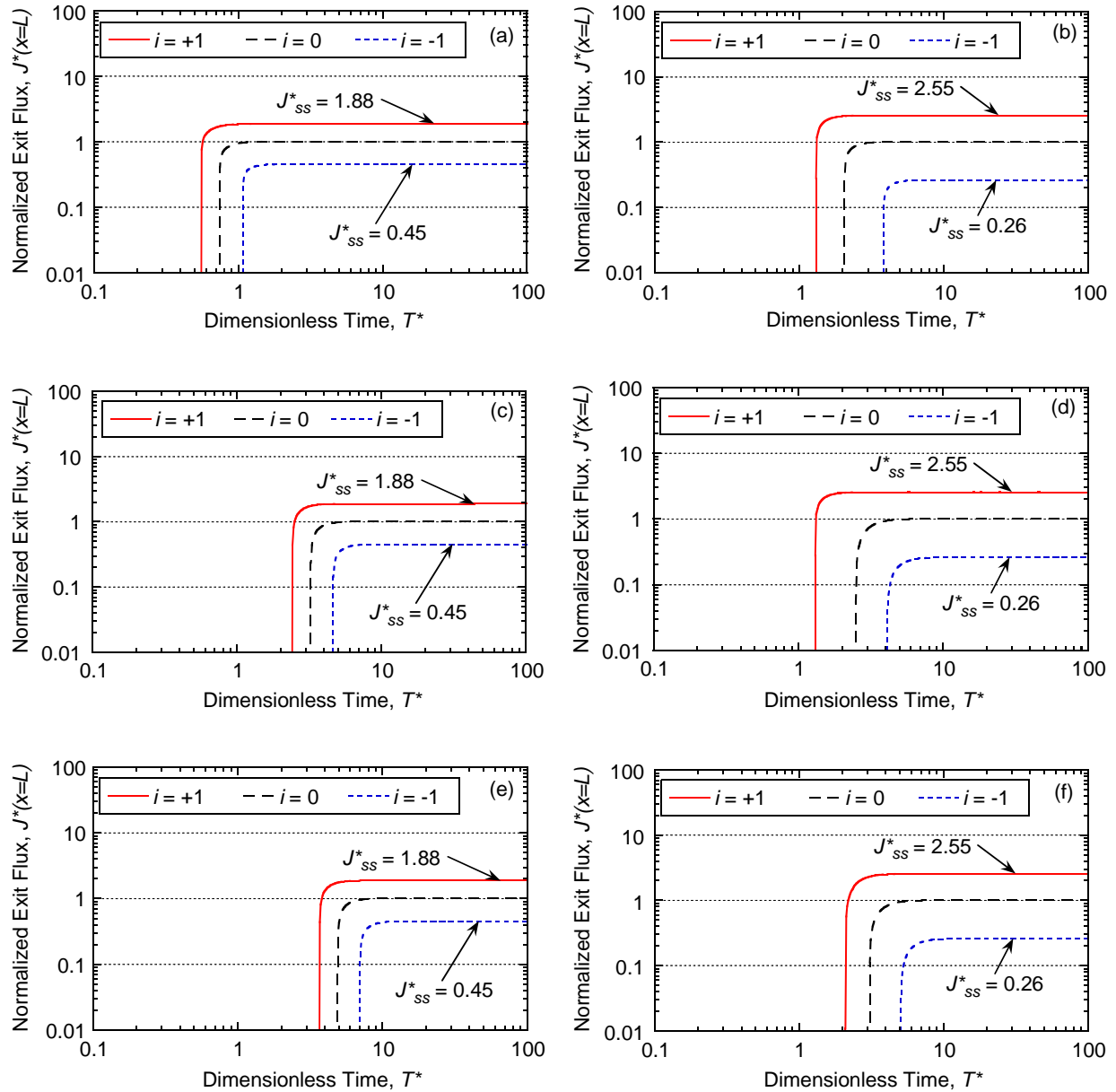


Figure E.2. Effect of Péclet number,  $P_L$ , on flux breakthrough curves with a constant source concentration,  $C_o = 1,000$  mg/L for: (a) unamended with potassium (K); (b) unamended with zinc (Zn); (c) amended with 5 % chabazite-LB with potassium (K); (d) amended with 5 % chabazite-LB with zinc (Zn); (e) amended with 10 % chabazite-LB with potassium (K); (f) amended with 10 % chabazite-LB with zinc (Zn), all based on the Freundlich adsorption model.

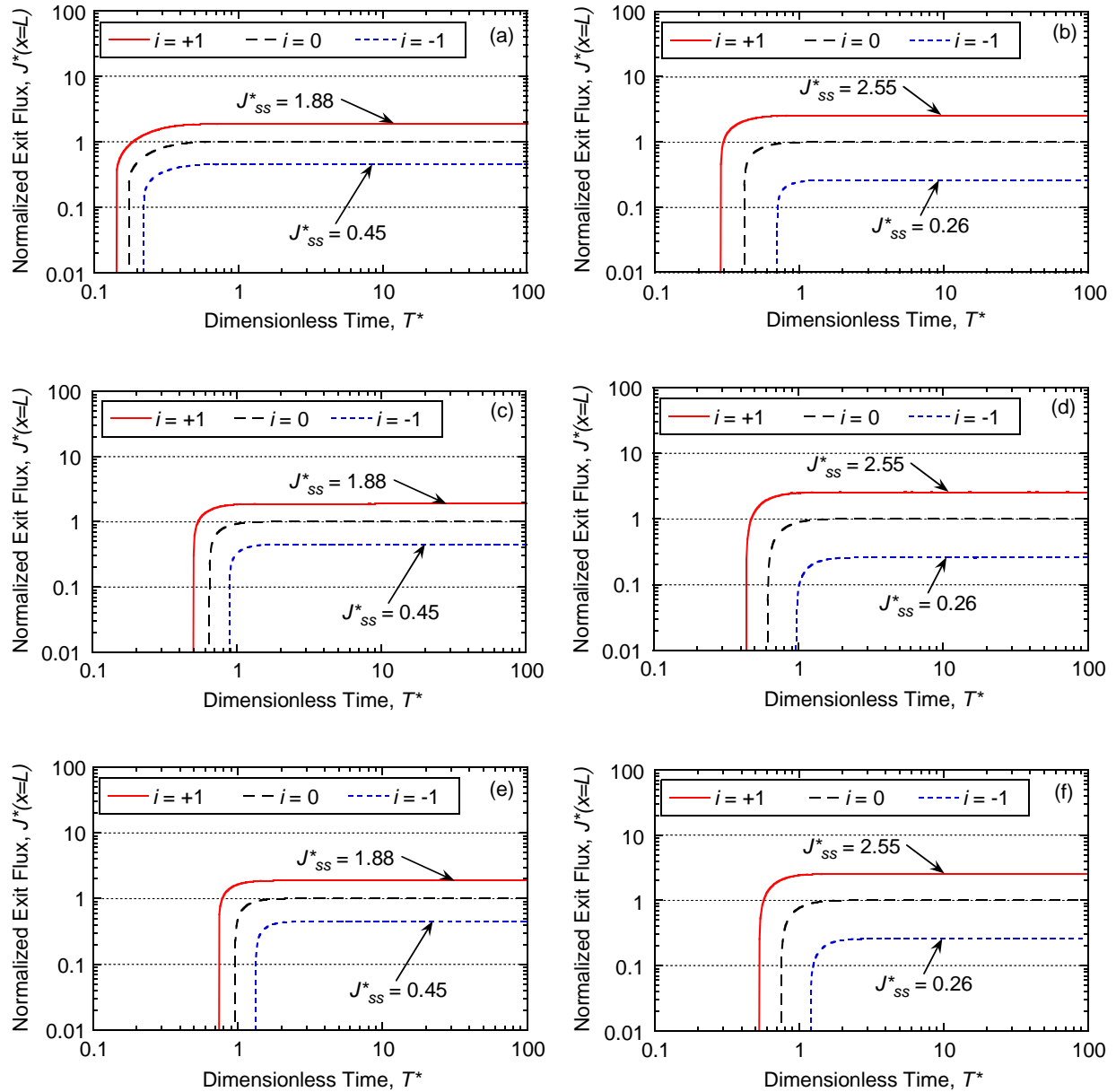


Figure E.3. Effect of Péclet number,  $P_L$ , on flux breakthrough curves with a constant source concentration,  $C_o = 10,000$  mg/L for: (a) unamended with potassium (K); (b) unamended with zinc (Zn); (c) amended with 5 % chabazite-LB with potassium (K); (d) amended with 5 % chabazite-LB with zinc (Zn); (e) amended with 10 % chabazite-LB with potassium (K); (f) amended with 10 % chabazite-LB with zinc (Zn), all based on the Freundlich adsorption model.

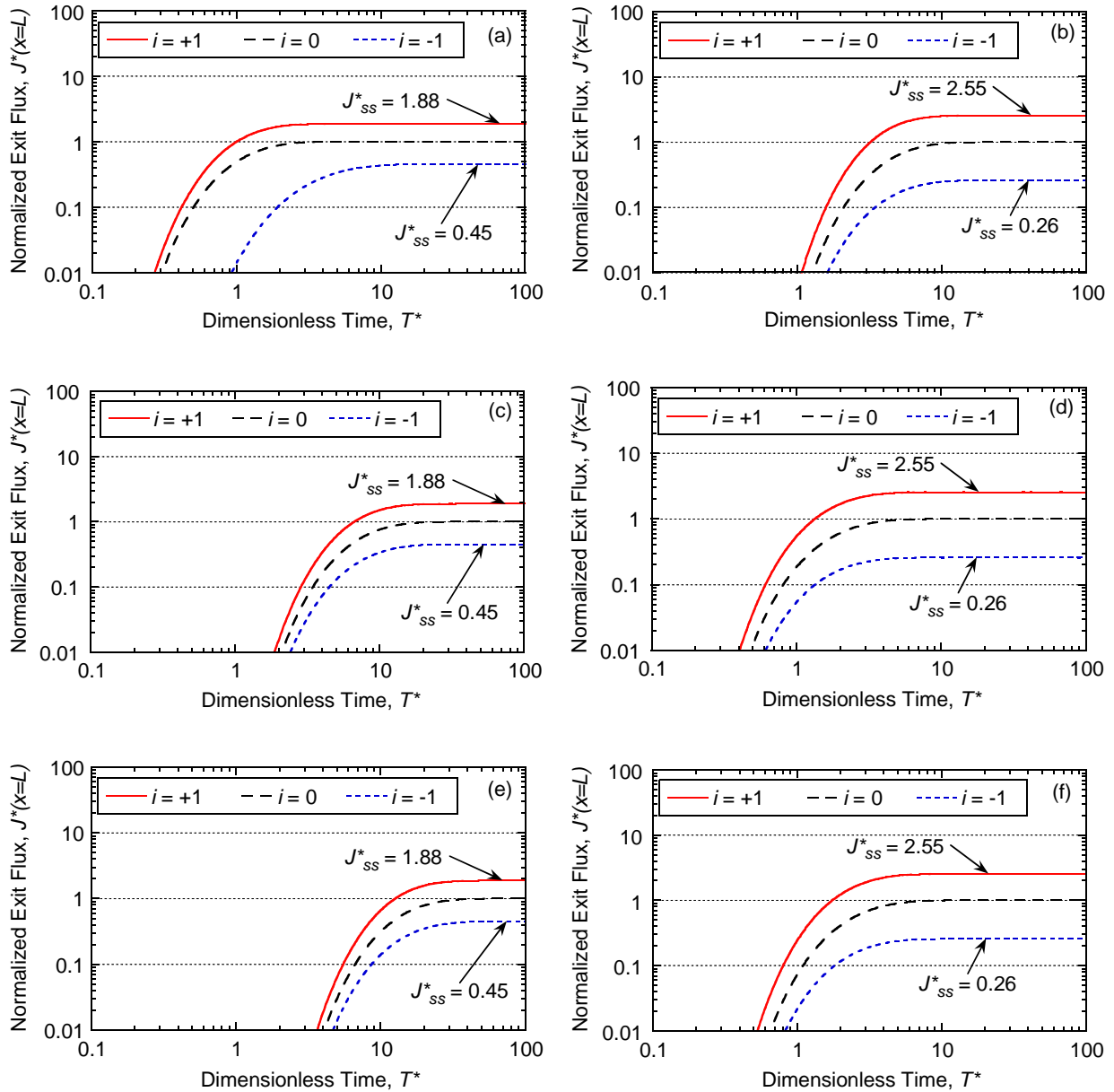


Figure E.4. Effect of Péclet number,  $P_L$ , on flux breakthrough curves with a constant source concentration,  $C_o = 100$  mg/L for: (a) unamended with potassium (K); (b) unamended with zinc (Zn); (c) amended with 5 % chabazite-LB with potassium (K); (d) amended with 5 % chabazite-LB with zinc (Zn); (e) amended with 10 % chabazite-LB with potassium (K); (f) amended with 10 % chabazite-LB with zinc (Zn), all based on the Langmuir adsorption model.

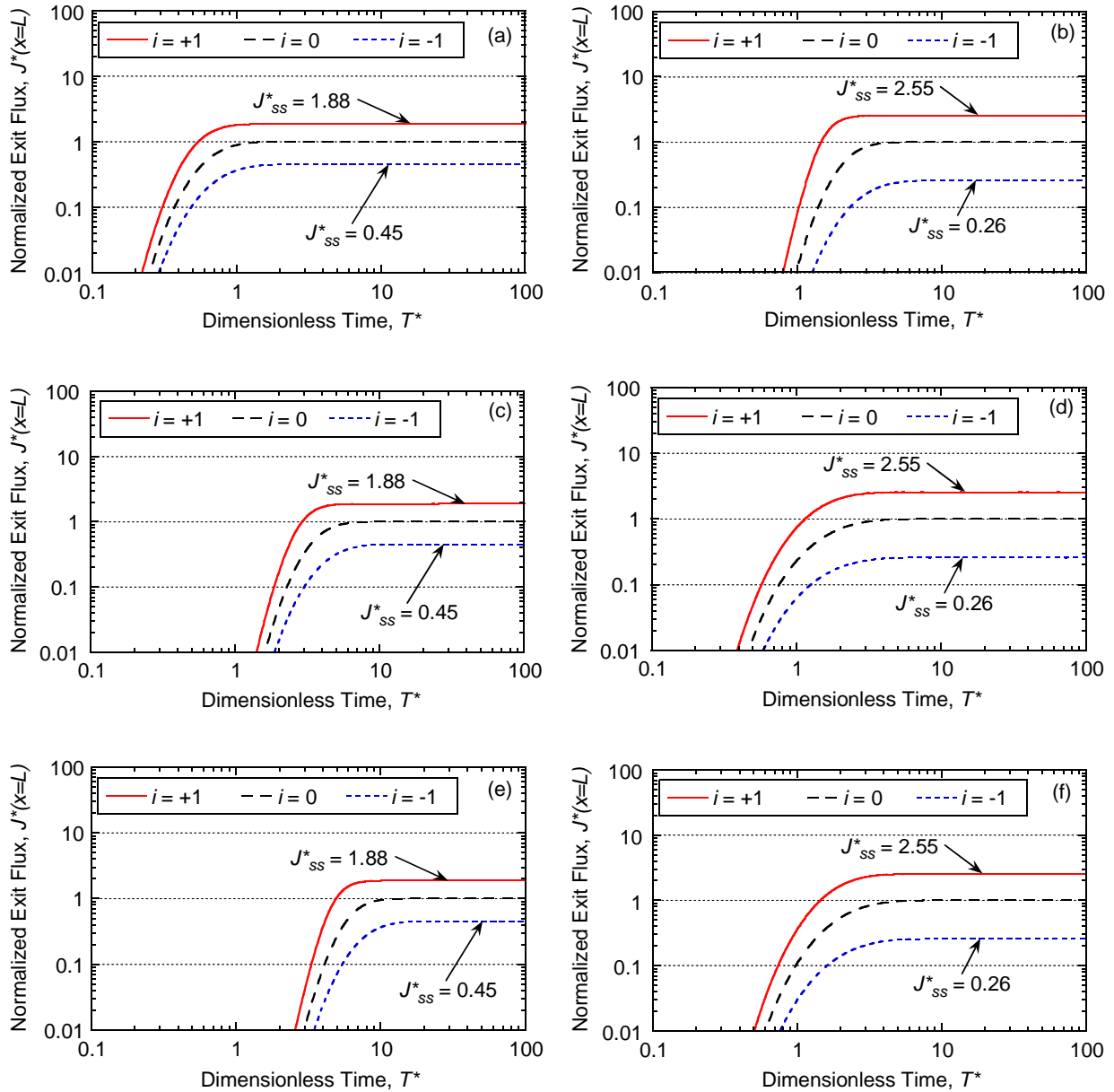


Figure E.5. Effect of Péclet number,  $P_L$ , on flux breakthrough curves with a constant source concentration,  $C_o = 1,000$  mg/L for: (a) unamended with potassium (K); (b) unamended with zinc (Zn); (c) amended with 5 % chabazite-LB with potassium (K); (d) amended with 5 % chabazite-LB with zinc (Zn); (e) amended with 10 % chabazite-LB with potassium (K); (f) amended with 10 % chabazite-LB with zinc (Zn), all based on the Langmuir adsorption model.

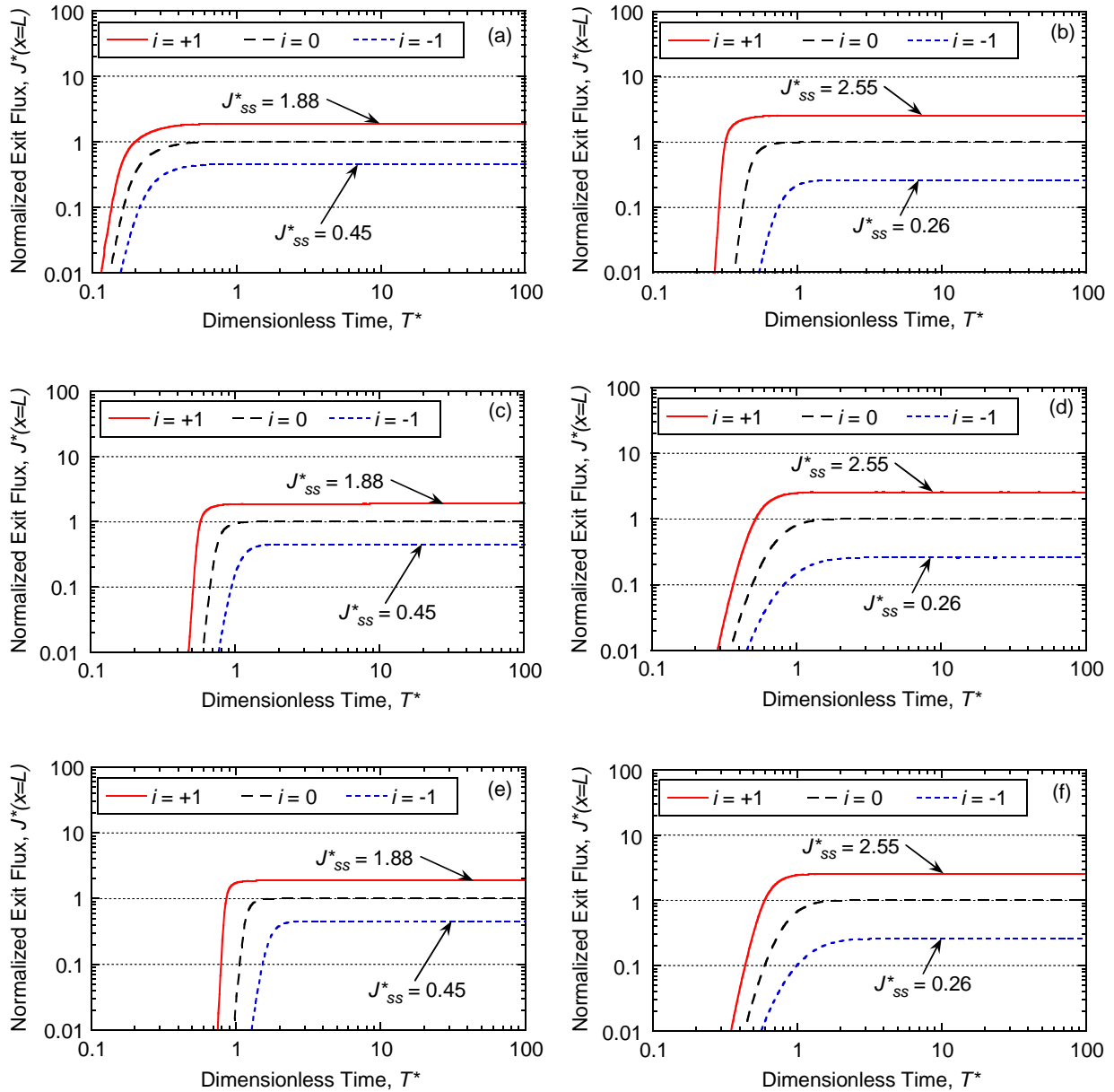


Figure E.6. Effect of Péclet number,  $P_L$ , on flux breakthrough curves with a constant source concentration,  $C_o = 10,000$  mg/L for: (a) unamended with potassium (K); (b) unamended with zinc (Zn); (c) amended with 5 % chabazite-LB with potassium (K); (d) amended with 5 % chabazite-LB with zinc (Zn); (e) amended with 10 % chabazite-LB with potassium (K); (f) amended with 10 % chabazite-LB with zinc (Zn), all based on the Langmuir adsorption model.

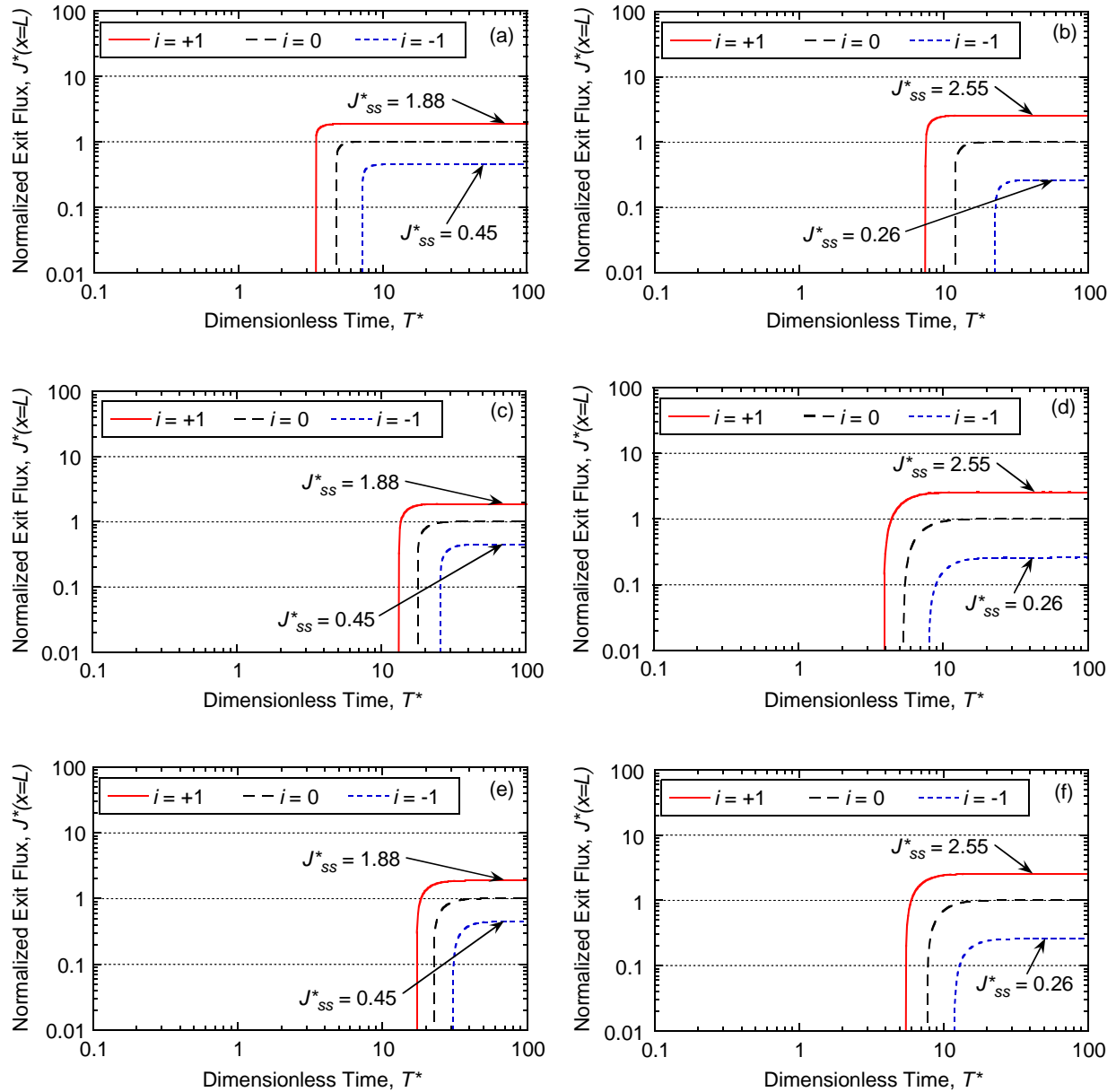


Figure E.7. Effect of Péclet number,  $P_L$ , on flux breakthrough curves with a constant source concentration,  $C_o = 100$  mg/L for: (a) unamended with potassium (K); (b) unamended with zinc (Zn); (c) amended with 5 % chabazite-UB with potassium (K); (d) amended with 5 % chabazite-UB with zinc (Zn); (e) amended with 10 % chabazite-UB with potassium (K); (f) amended with 10 % chabazite-UB with zinc (Zn), all based on the Freundlich adsorption model.

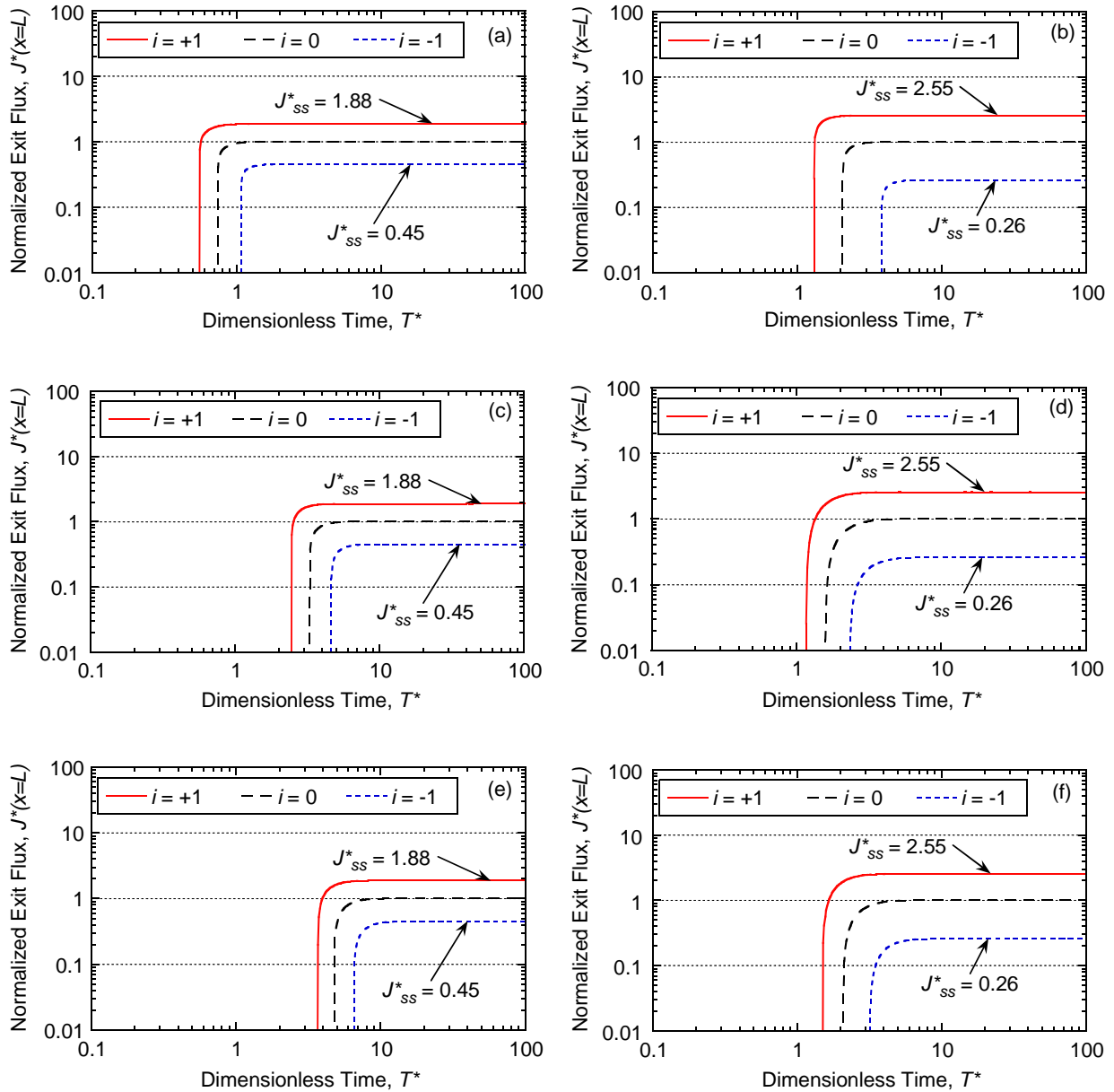


Figure E.8. Effect of Péclet number,  $P_L$ , on flux breakthrough curves with a constant source concentration,  $C_o = 1,000$  mg/L for: (a) unamended with potassium (K); (b) unamended with zinc (Zn); (c) amended with 5 % chabazite-UB with potassium (K); (d) amended with 5 % chabazite-UB with zinc (Zn); (e) amended with 10 % chabazite-UB with potassium (K); (f) amended with 10 % chabazite-UB with zinc (Zn), all based on the Freundlich adsorption model.

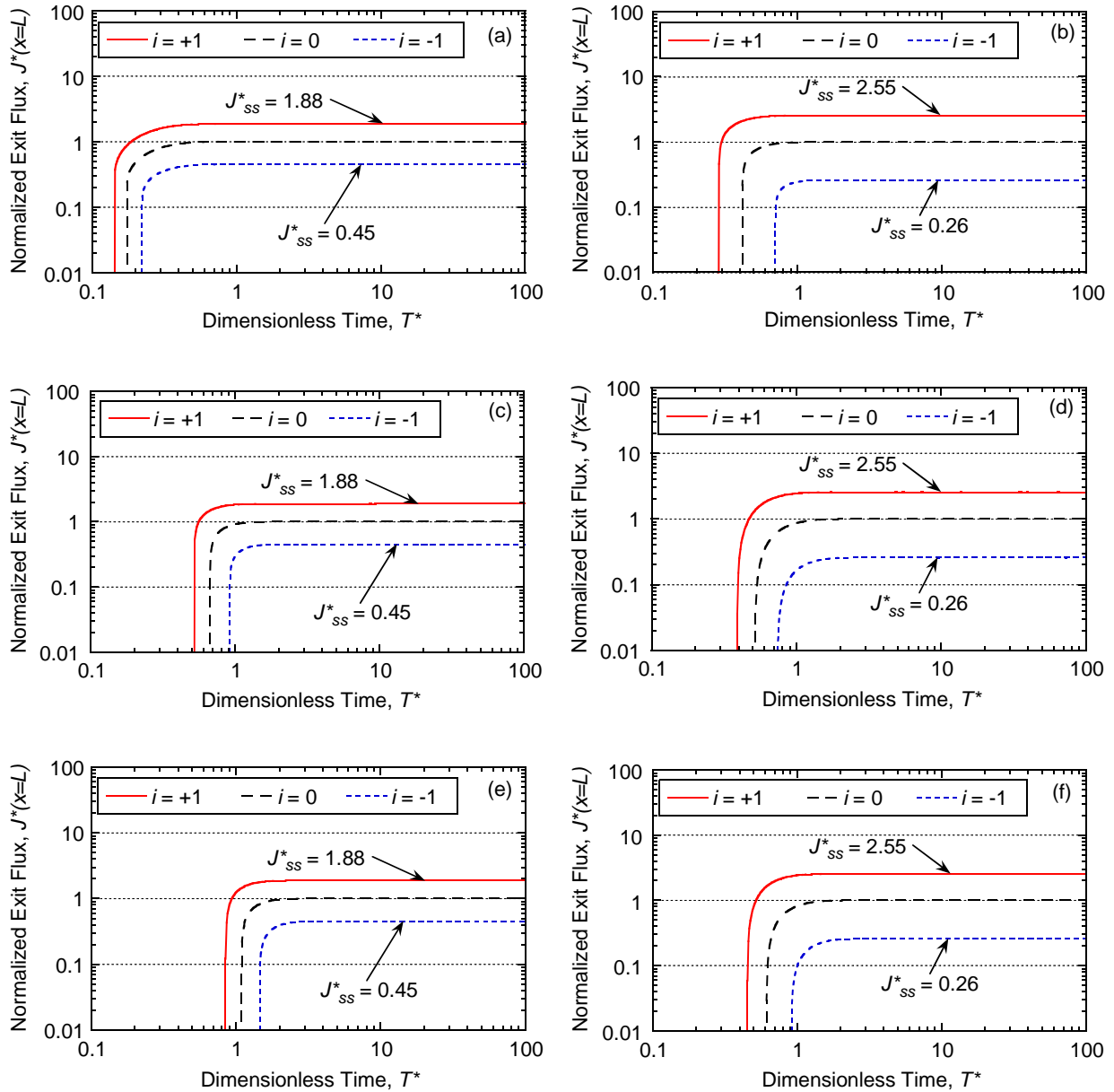


Figure E.9. Effect of Péclet number,  $P_L$ , on flux breakthrough curves with a constant source concentration,  $C_o = 10,000$  mg/L for: (a) unamended with potassium (K); (b) unamended with zinc (Zn); (c) amended with 5 % chabazite-UB with potassium (K); (d) amended with 5 % chabazite-UB with zinc (Zn); (e) amended with 10 % chabazite-UB with potassium (K); (f) amended with 10 % chabazite-UB with zinc (Zn), all based on the Freundlich adsorption model.

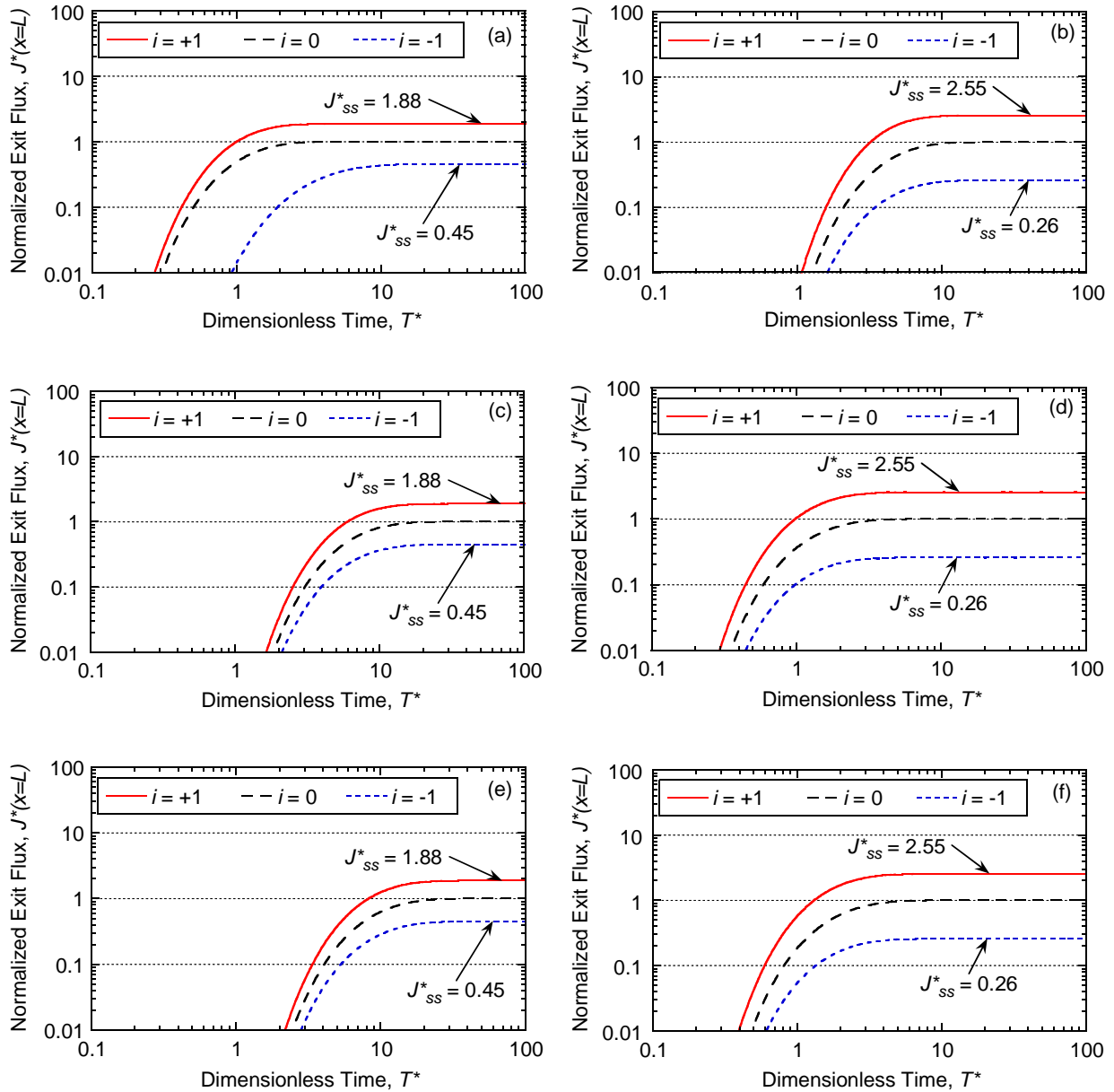


Figure E.10. Effect of Péclet number,  $P_L$ , on flux breakthrough curves with a constant source concentration,  $C_o = 100$  mg/L for: (a) unamended with potassium (K); (b) unamended with zinc (Zn); (c) amended with 5 % chabazite-UB with potassium (K); (d) amended with 5 % chabazite-UB with zinc (Zn); (e) amended with 10 % chabazite-UB with potassium (K); (f) amended with 10 % chabazite-UB with zinc (Zn), all based on the Langmuir adsorption model.

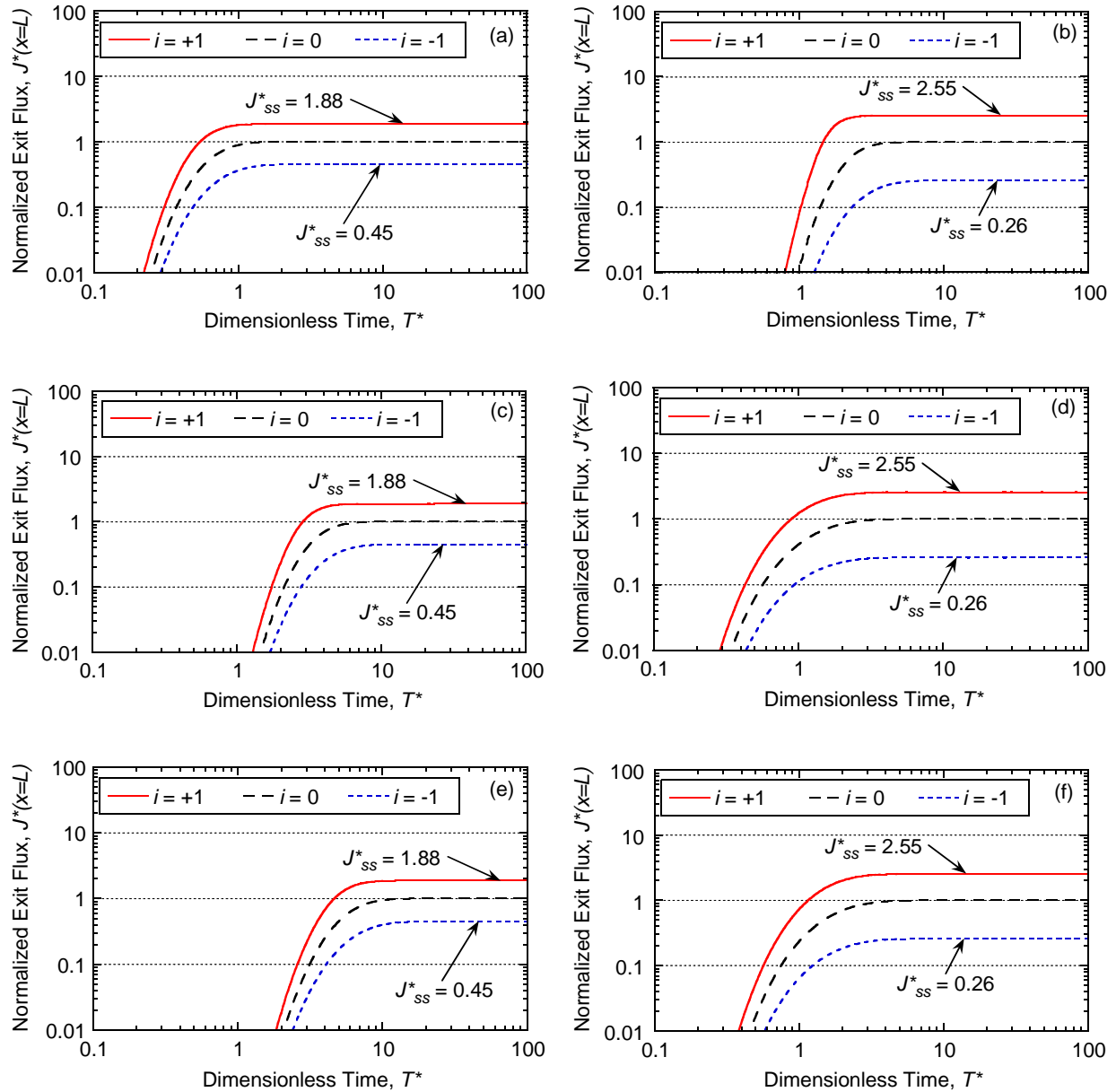


Figure E.11. Effect of Péclet number,  $P_L$ , on flux breakthrough curves with a constant source concentration,  $C_o = 1,000$  mg/L for: (a) unamended with potassium (K); (b) unamended with zinc (Zn); (c) amended with 5 % chabazite-UB with potassium (K); (d) amended with 5 % chabazite-UB with zinc (Zn); (e) amended with 10 % chabazite-UB with potassium (K); (f) amended with 10 % chabazite-UB with zinc (Zn), all based on the Langmuir adsorption model.

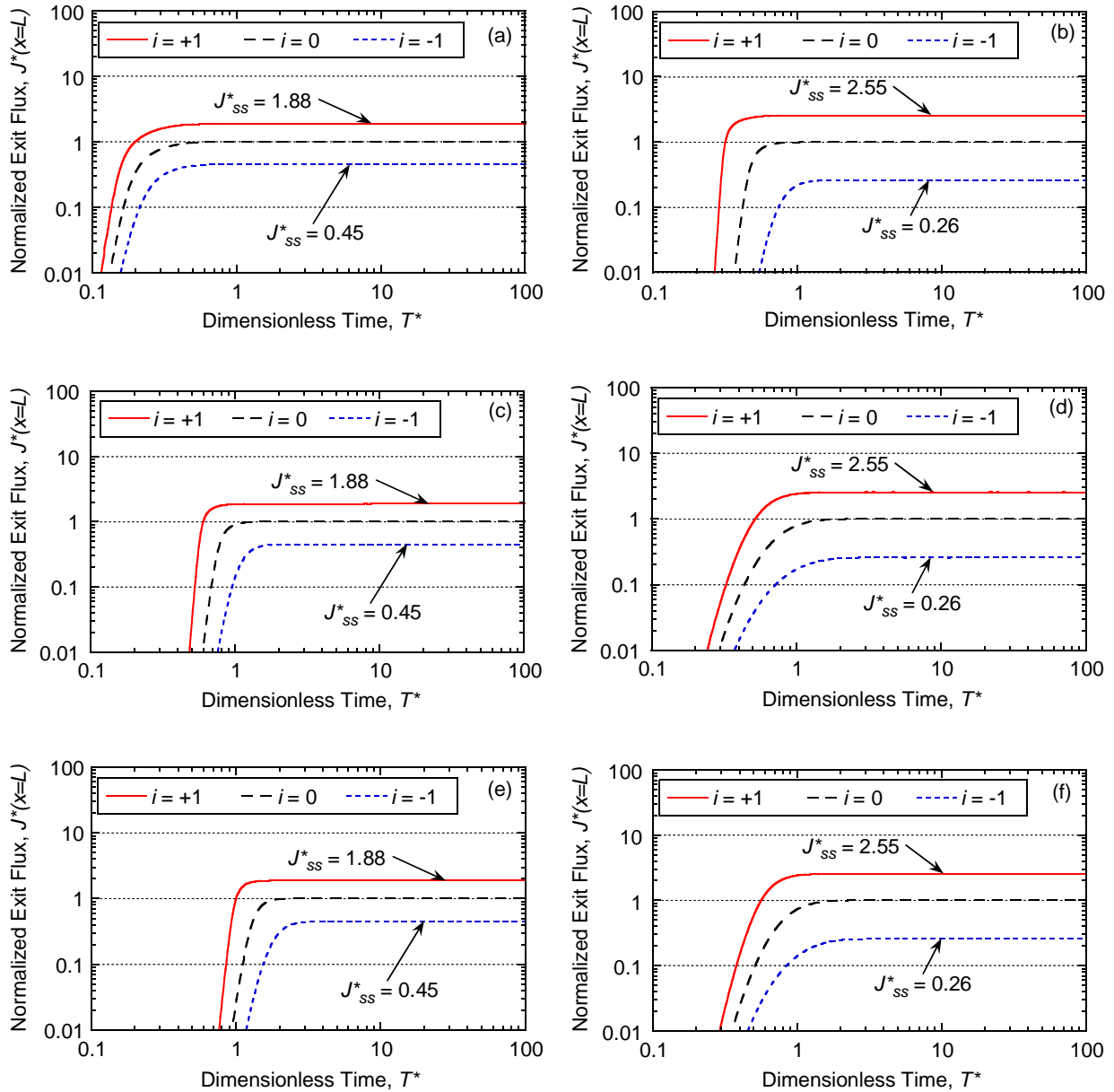


Figure E.12. Effect of Péclet number,  $P_L$ , on flux breakthrough curves with a constant source concentration,  $C_o = 10,000$  mg/L for: (a) unamended with potassium (K); (b) unamended with zinc (Zn); (c) amended with 5 % chabazite-UB with potassium (K); (d) amended with 5 % chabazite-UB with zinc (Zn); (e) amended with 10 % chabazite-UB with potassium (K); (f) amended with 10 % chabazite-UB with zinc (Zn), all based on the Langmuir adsorption model.

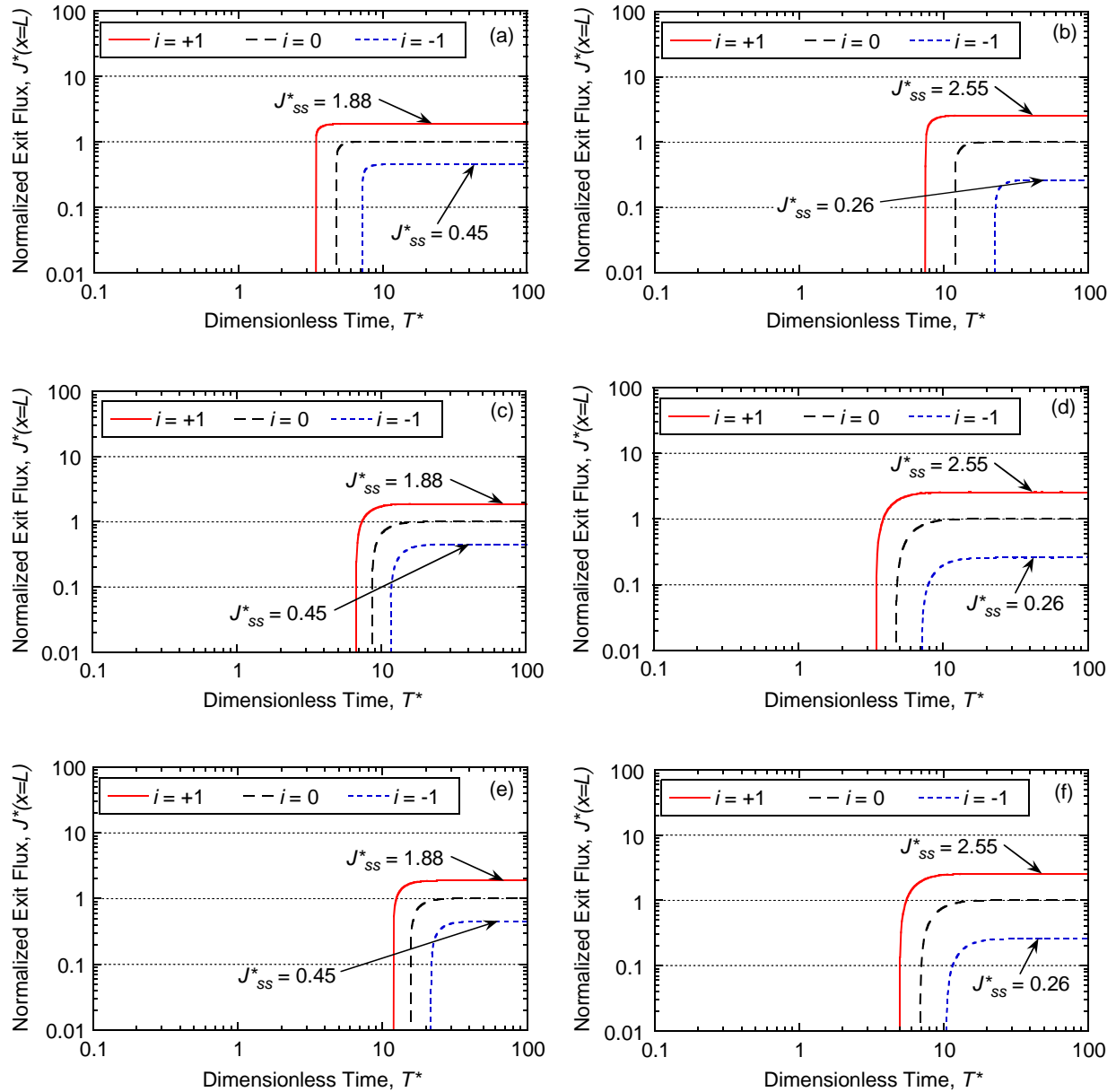


Figure E.13. Effect of Péclet number,  $P_L$ , on flux breakthrough curves with a constant source concentration,  $C_o = 100$  mg/L for: (a) unamended with potassium (K); (b) unamended with zinc (Zn); (c) amended with 5 % clinoptilolite with potassium (K); (d) amended with 5 % clinoptilolite with zinc (Zn); (e) amended with 10 % clinoptilolite with potassium (K); (f) amended with 10 % clinoptilolite with zinc (Zn), all based on the Freundlich adsorption model.

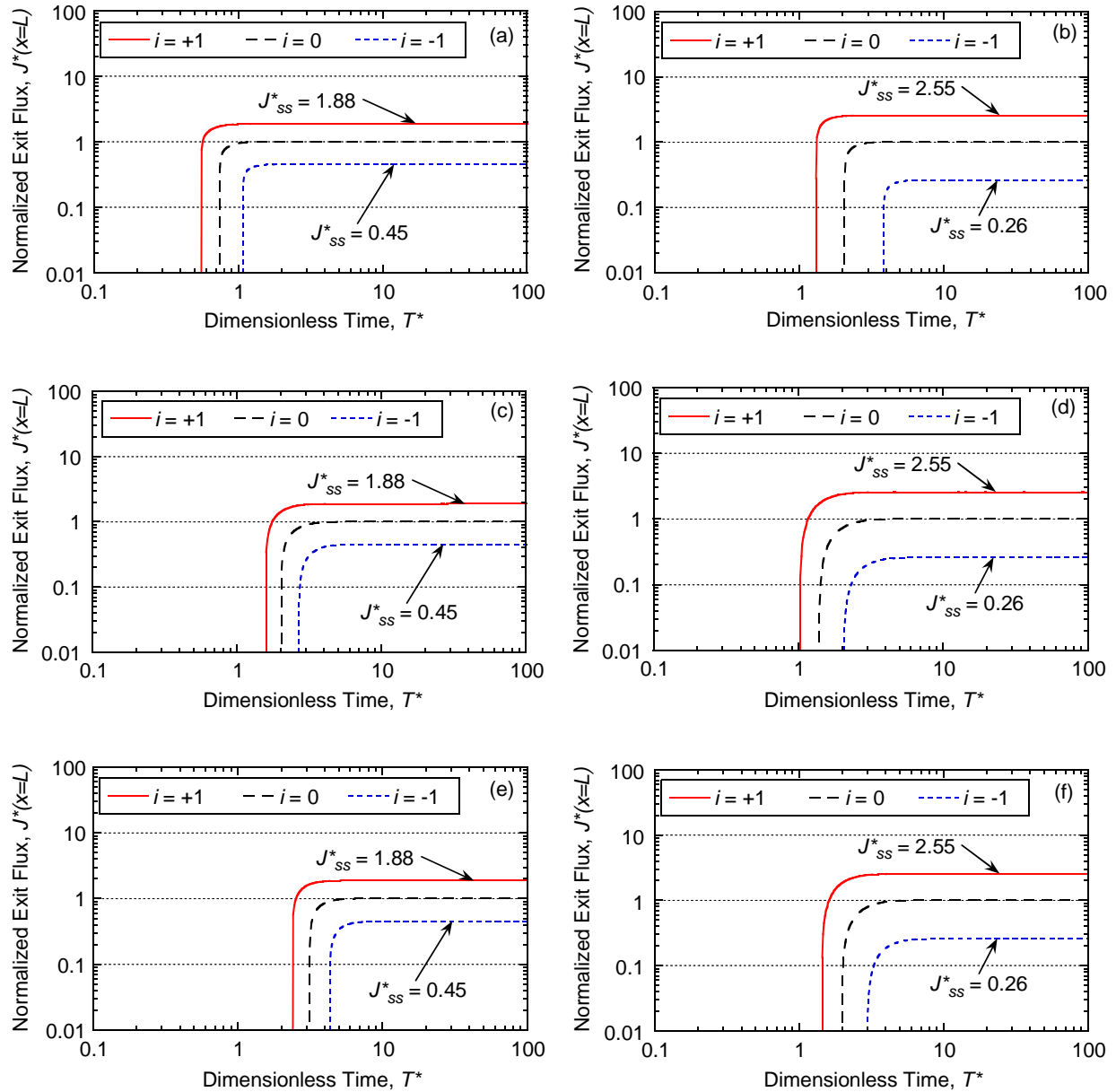


Figure E.14. Effect of Péclet number,  $P_L$ , on flux breakthrough curves with a constant source concentration,  $C_o = 1,000$  mg/L for: (a) unamended with potassium (K); (b) unamended with zinc (Zn); (c) amended with 5 % clinoptilolite with potassium (K); (d) amended with 5 % clinoptilolite with zinc (Zn); (e) amended with 10 % clinoptilolite with potassium (K); (f) amended with 10 % clinoptilolite with zinc (Zn), all based on the Freundlich adsorption model.

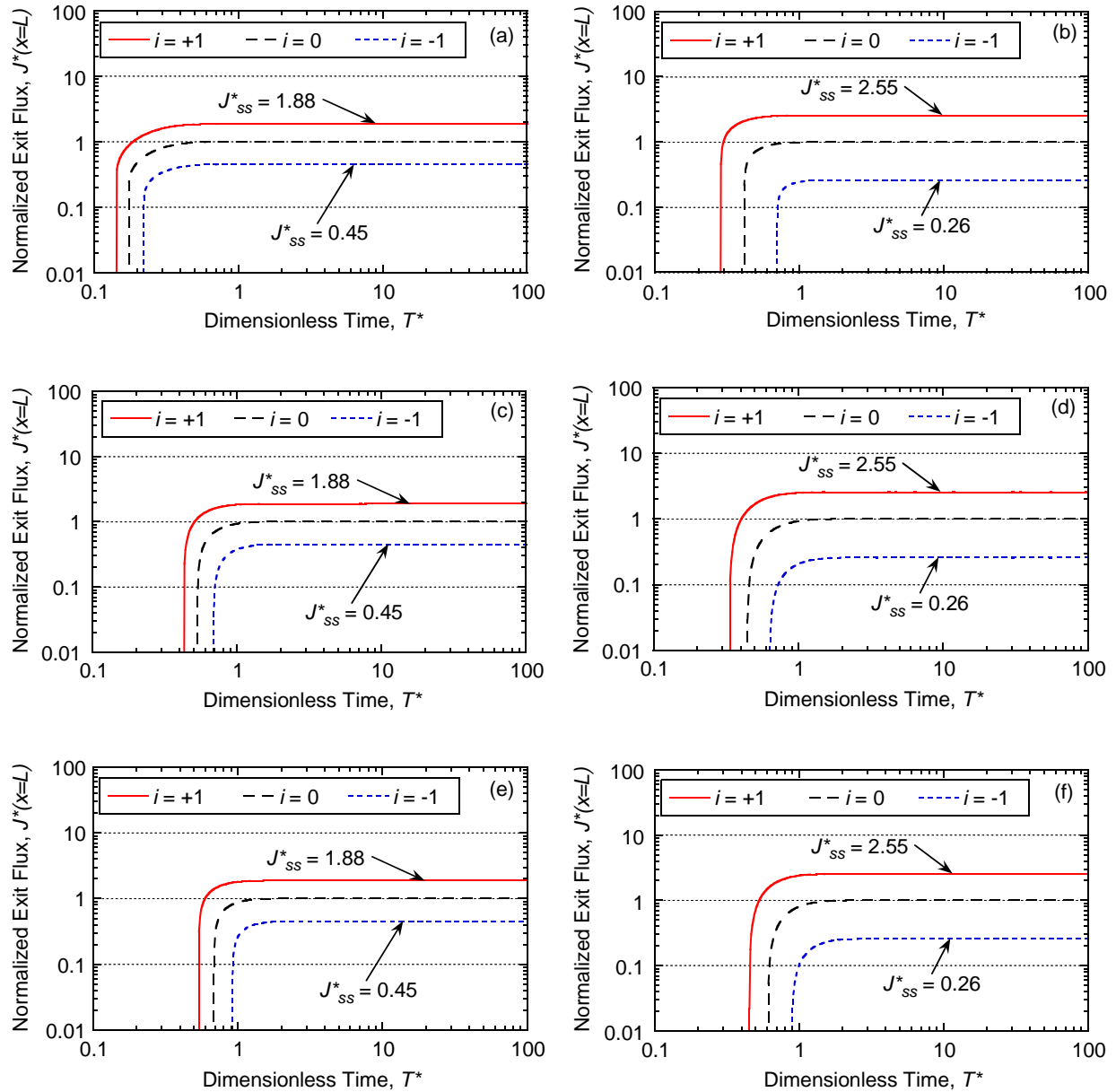


Figure E.15. Effect of Péclet number,  $P_L$ , on flux breakthrough curves with a constant source concentration,  $C_o = 10,000$  mg/L for: (a) unamended with potassium (K); (b) unamended with zinc (Zn); (c) amended with 5 % clinoptilolite with potassium (K); (d) amended with 5 % clinoptilolite with zinc (Zn); (e) amended with 10 % clinoptilolite with potassium (K); (f) amended with 10 % clinoptilolite with zinc (Zn), all based on the Freundlich adsorption model.

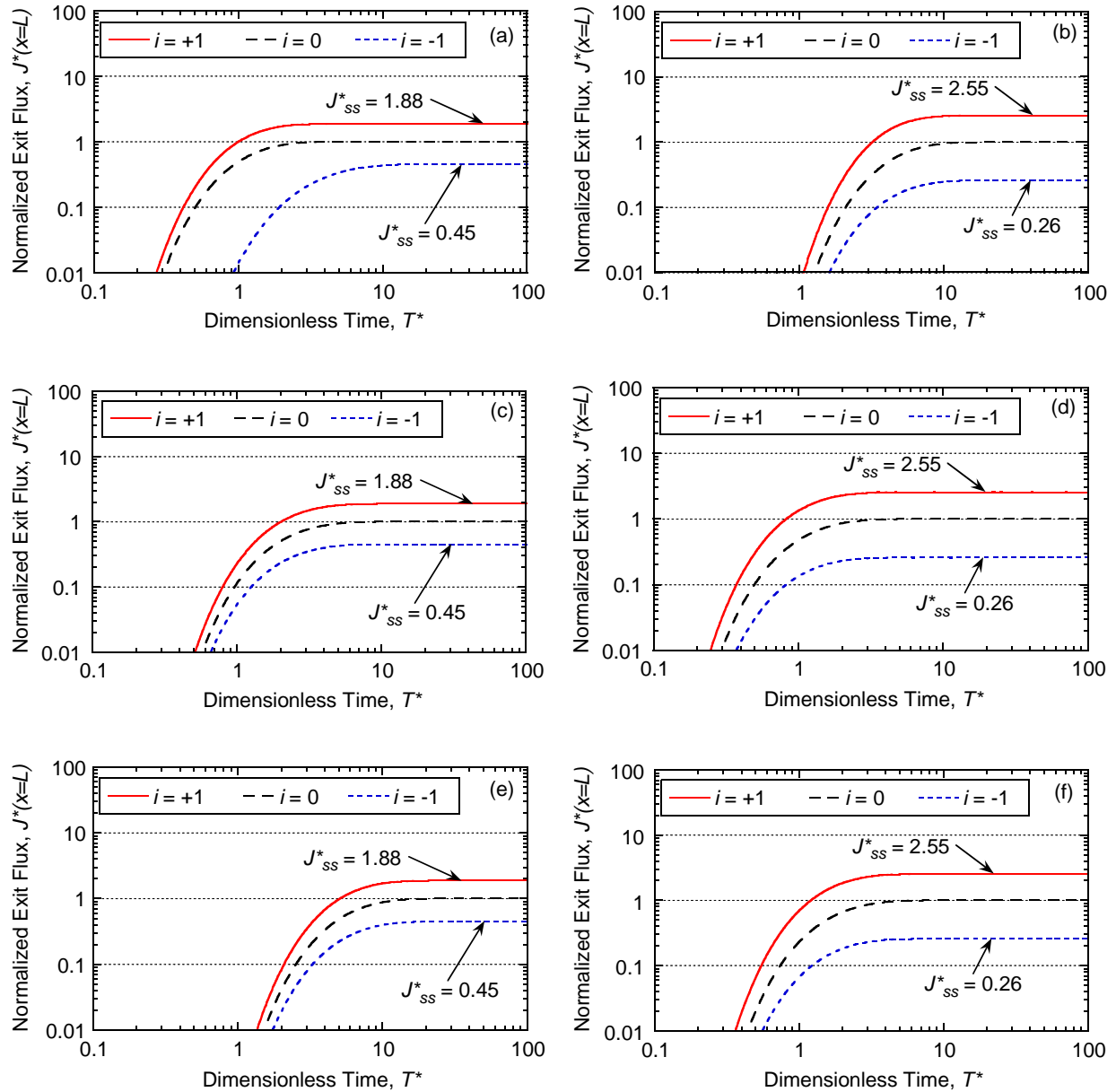


Figure E.16. Effect of Péclet number,  $P_L$ , on flux breakthrough curves with a constant source concentration,  $C_o = 100$  mg/L for: (a) unamended with potassium (K); (b) unamended with zinc (Zn); (c) amended with 5 % clinoptilolite with potassium (K); (d) amended with 5 % clinoptilolite with zinc (Zn); (e) amended with 10 % clinoptilolite with potassium (K); (f) amended with 10 % clinoptilolite with zinc (Zn), all based on the Langmuir adsorption model.

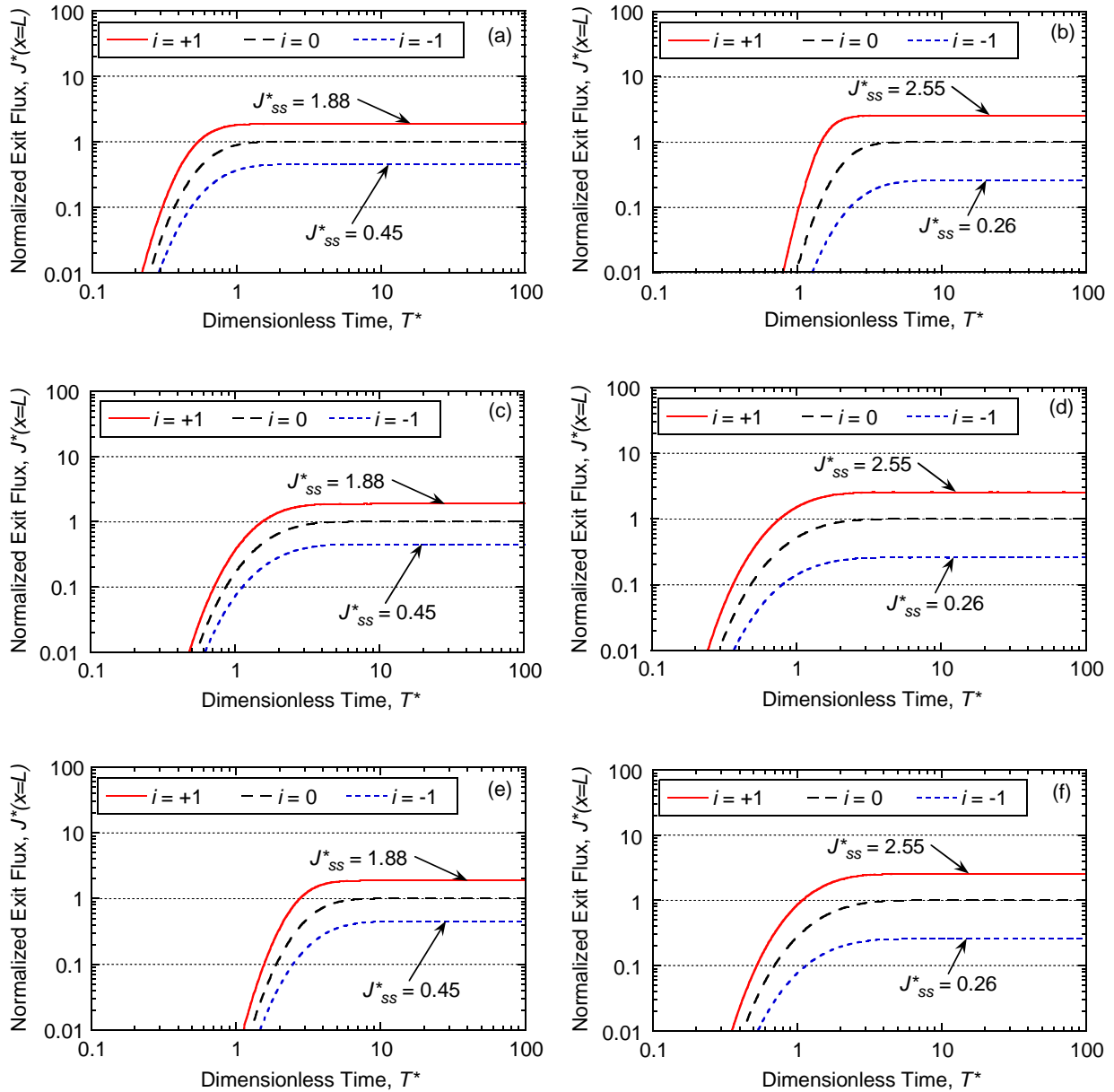


Figure E.17. Effect of Péclet number,  $P_L$ , on flux breakthrough curves with a constant source concentration,  $C_o = 1,000$  mg/L for: (a) unamended with potassium (K); (b) unamended with zinc (Zn); (c) amended with 5 % clinoptilolite with potassium (K); (d) amended with 5 % clinoptilolite with zinc (Zn); (e) amended with 10 % clinoptilolite with potassium (K); (f) amended with 10 % clinoptilolite with zinc (Zn), all based on the Langmuir adsorption model.

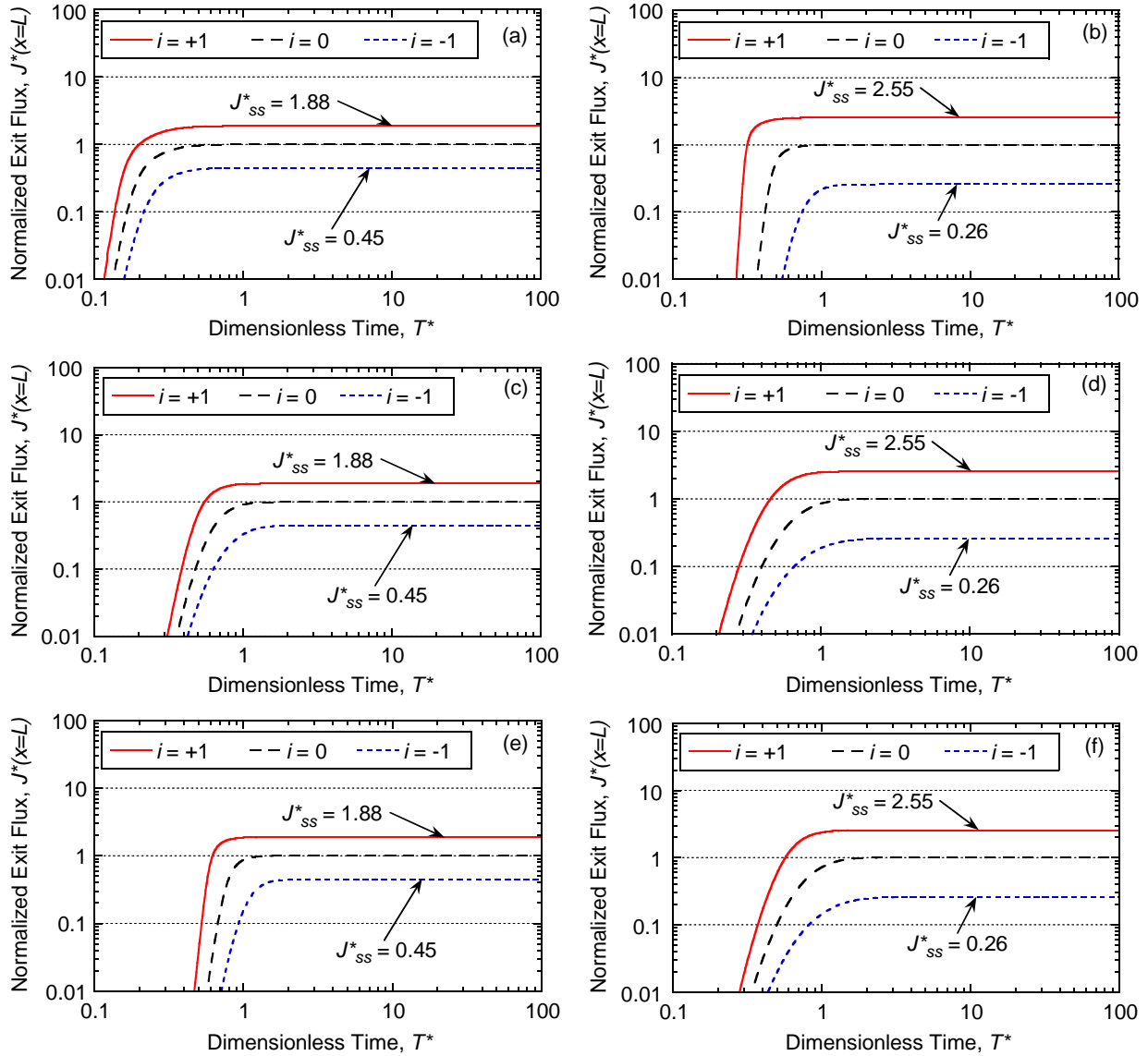


Figure E.18. Effect of Péclet number,  $P_L$ , on flux breakthrough curves with a constant source concentration,  $C_o = 10,000$  mg/L for: (a) unamended with potassium (K); (b) unamended with zinc (Zn); (c) amended with 5 % clinoptilolite with potassium (K); (d) amended with 5 % clinoptilolite with zinc (Zn); (e) amended with 10 % clinoptilolite with potassium (K); (f) amended with 10 % clinoptilolite with zinc (Zn), all based on the Langmuir adsorption model.

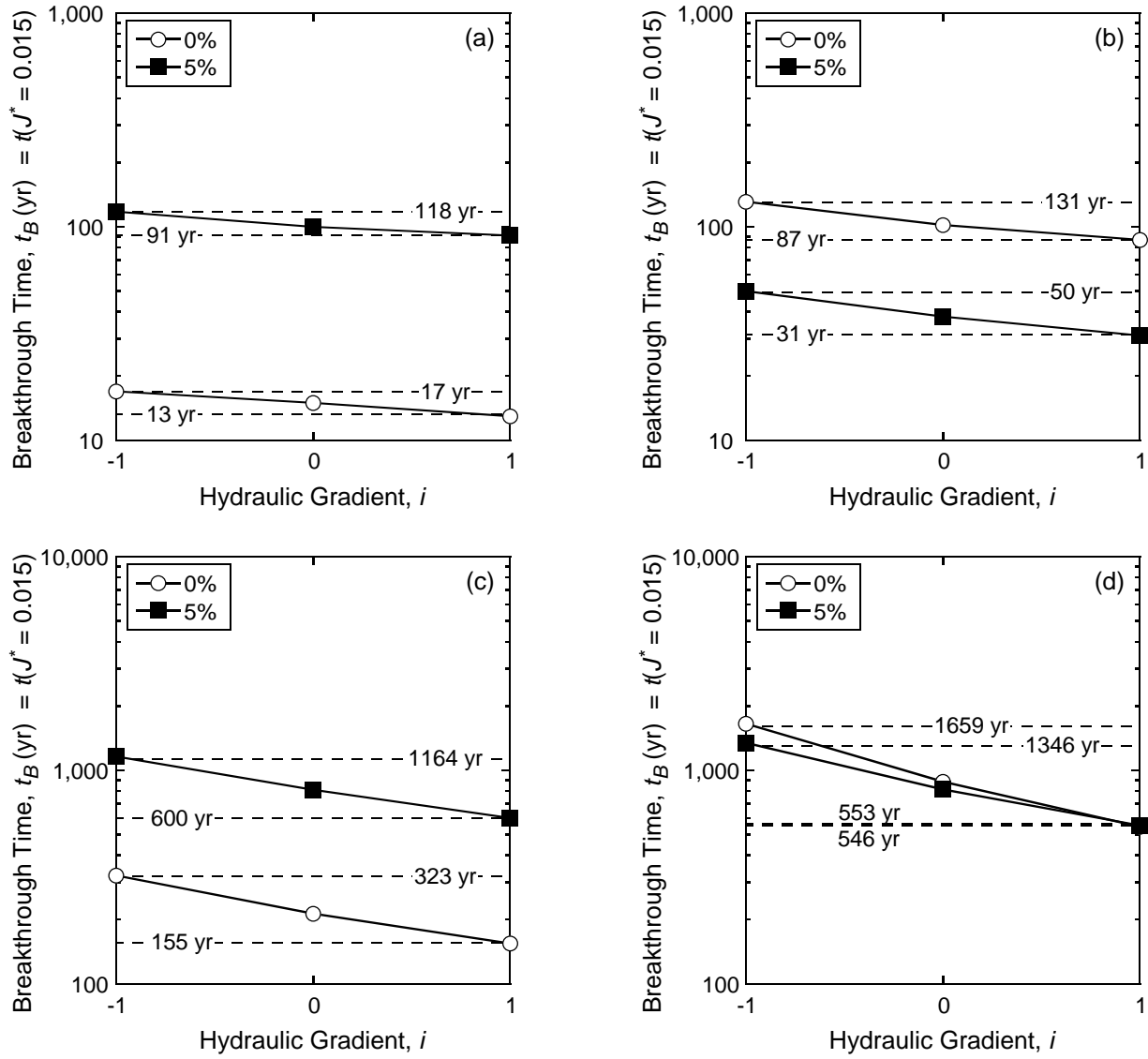


Figure E.19. Relationship between Péclet number,  $P_L$ , and predicted flux breakthrough times corresponding to  $J^*(x=L) = 0.015$  with a constant source concentration ( $C_o$ ) of 100 mg/L for the unamended and zeolite-amended cutoff wall with 5 % chabazite-LB: (a) potassium (K), Langmuir; (b) zinc (Zn), Langmuir; (c) potassium (K), Freundlich; (d) zinc (Zn), Freundlich.

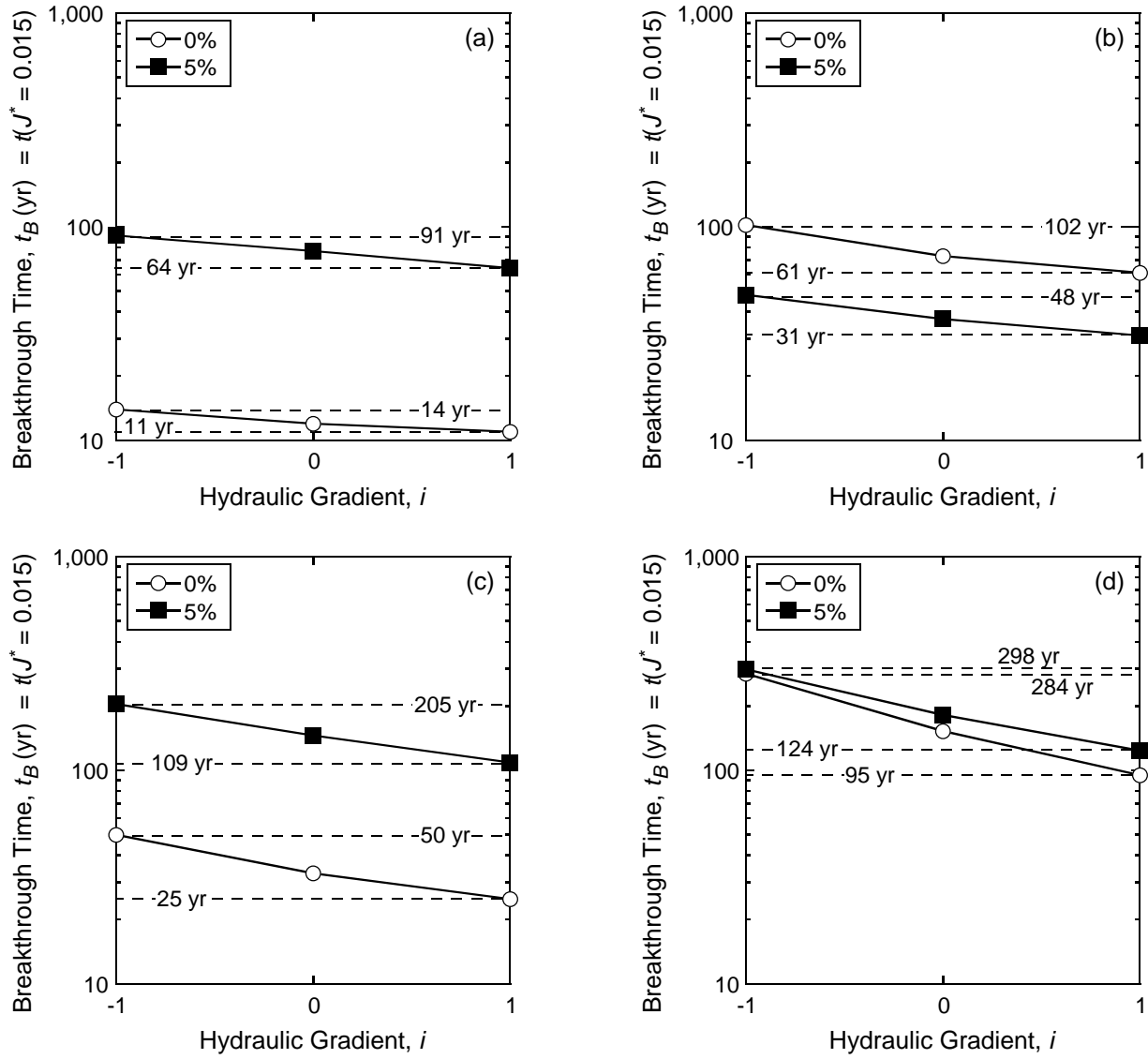


Figure E.20. Relationship between Péclet number,  $P_L$ , and predicted flux breakthrough times corresponding to  $J^*(x=L) = 0.015$  with a constant source concentration ( $C_o$ ) of 1,000 mg/L for the unamended and zeolite-amended cutoff wall with 5 % chabazite-LB: (a) potassium (K), Langmuir; (b) zinc (Zn), Langmuir; (c) potassium (K), Freundlich; (d) zinc (Zn), Freundlich.

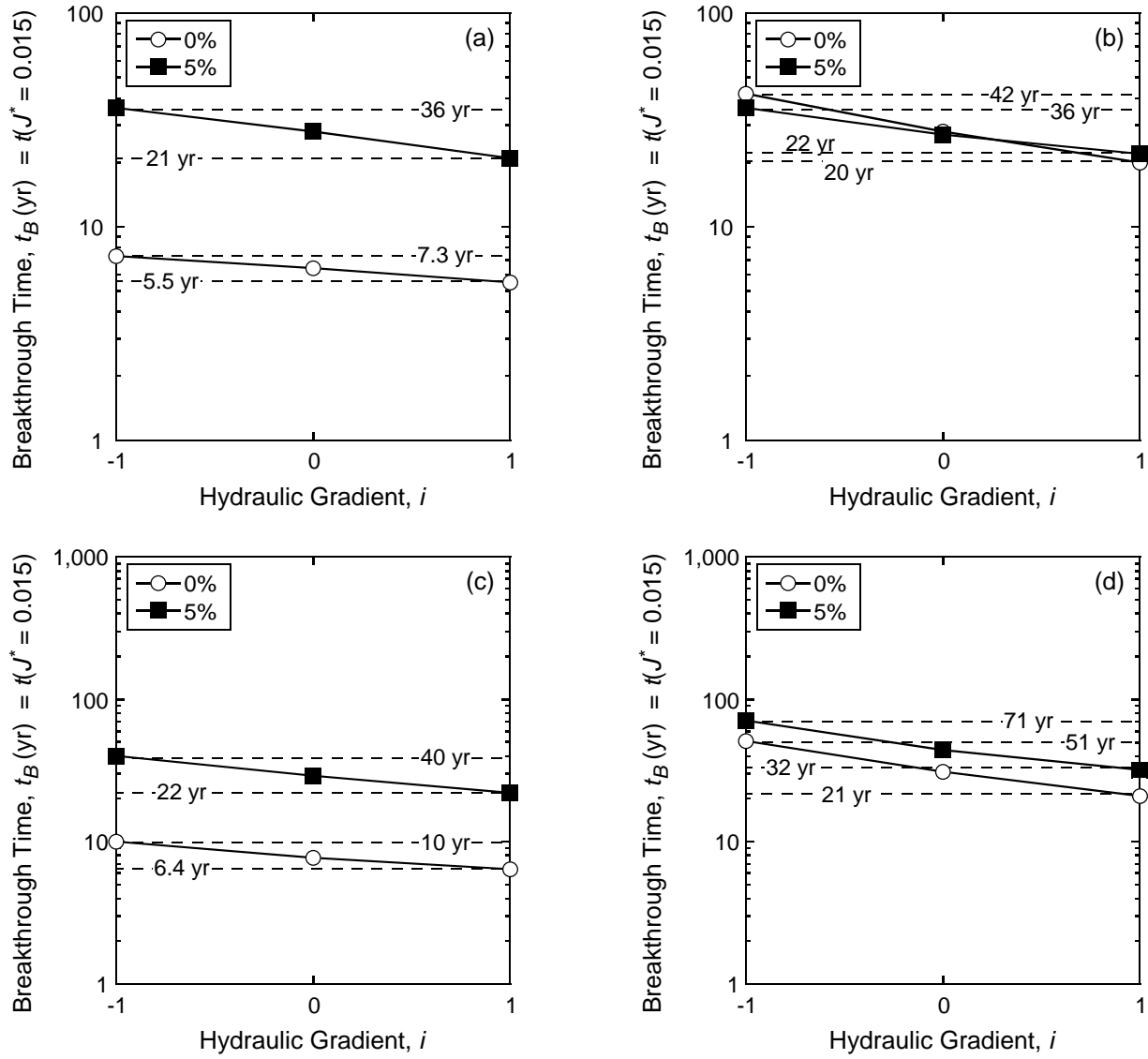


Figure E.21. Relationship between Péclet number,  $P_L$ , and predicted flux breakthrough times corresponding to  $J^*(x=L) = 0.015$  with a constant source concentration ( $C_o$ ) of 10,000 mg/L for the unamended and zeolite-amended cutoff wall with 5 % chabazite-LB: (a) potassium (K), Langmuir; (b) zinc (Zn), Langmuir; (c) potassium (K), Freundlich; (d) zinc (Zn), Freundlich.

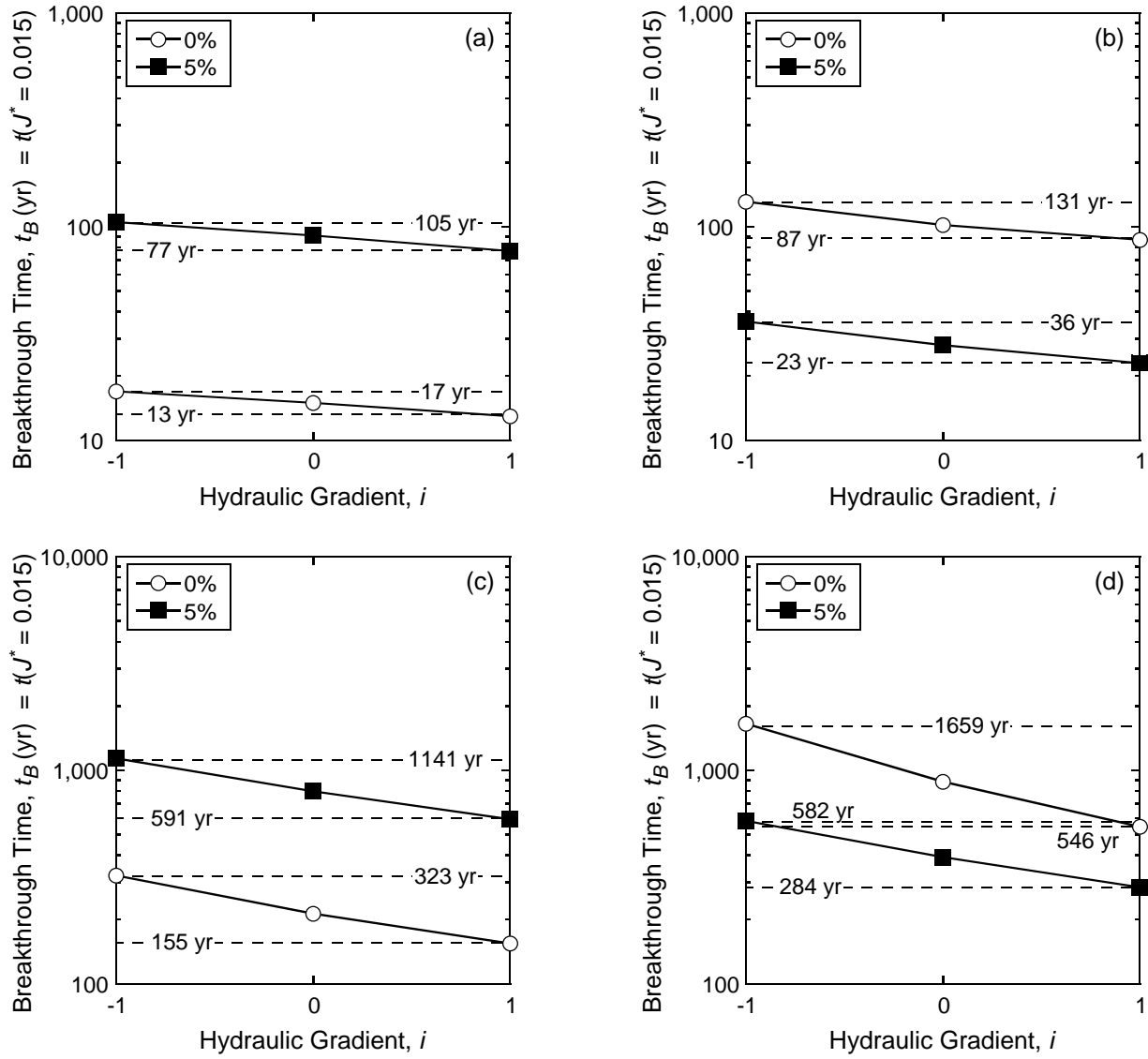


Figure E.22. Relationship between Péclet number,  $P_L$ , and predicted flux breakthrough times corresponding to  $J^*(x=L) = 0.015$  with a constant source concentration ( $C_o$ ) of 100 mg/L for the unamended and zeolite-amended cutoff wall with 5 % chabazite-UB: (a) potassium (K), Langmuir; (b) zinc (Zn), Langmuir; (c) potassium (K), Freundlich; (d) zinc (Zn), Freundlich.

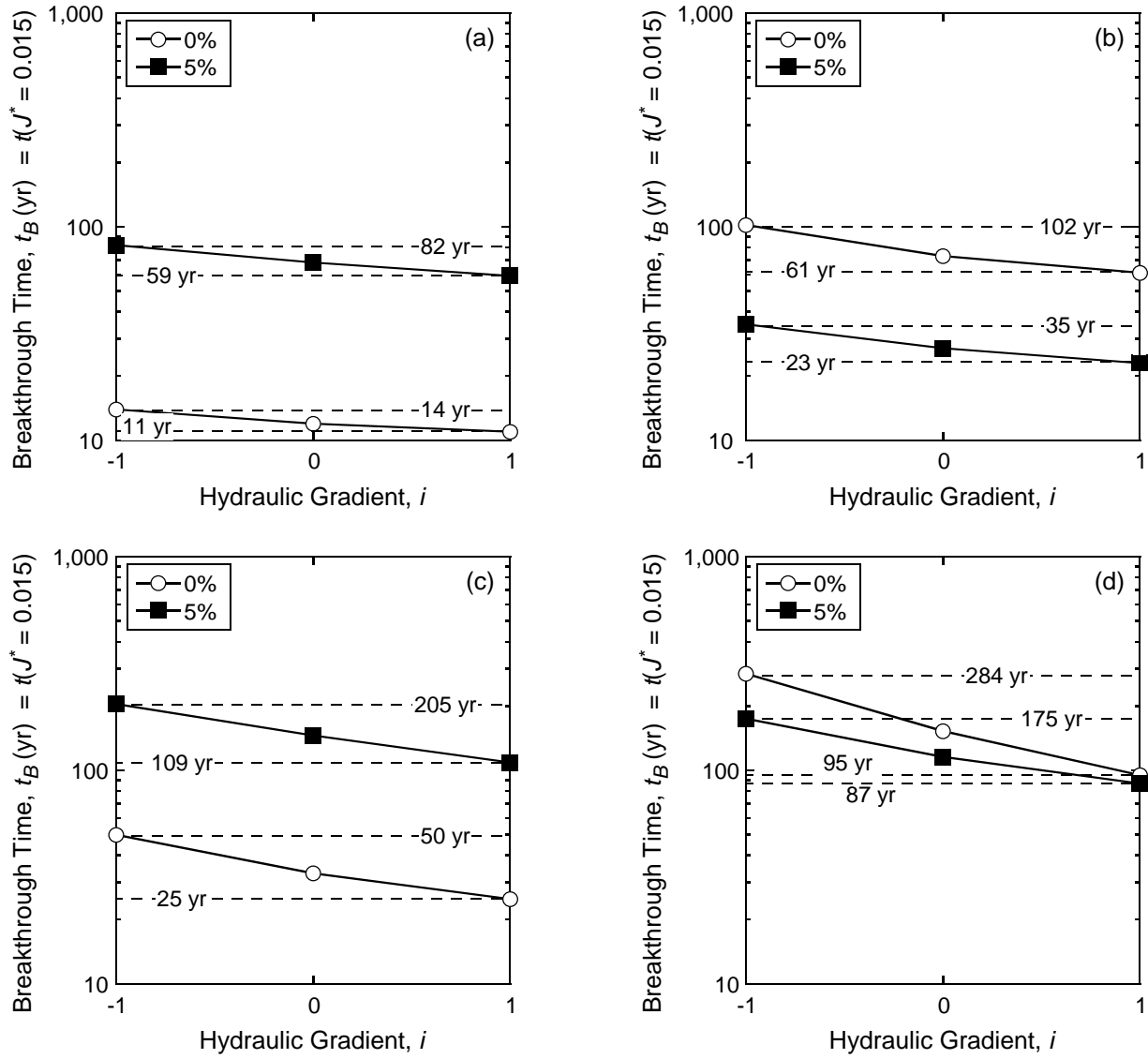


Figure E.23. Relationship between Péclet number,  $P_L$ , and predicted flux breakthrough times corresponding to  $J^*(x=L) = 0.015$  with a constant source concentration ( $C_o$ ) of 1,000 mg/L for the unamended and zeolite-amended cutoff wall with 5 % chabazite-UB: (a) potassium (K), Langmuir; (b) zinc (Zn), Langmuir; (c) potassium (K), Freundlich; (d) zinc (Zn), Freundlich.

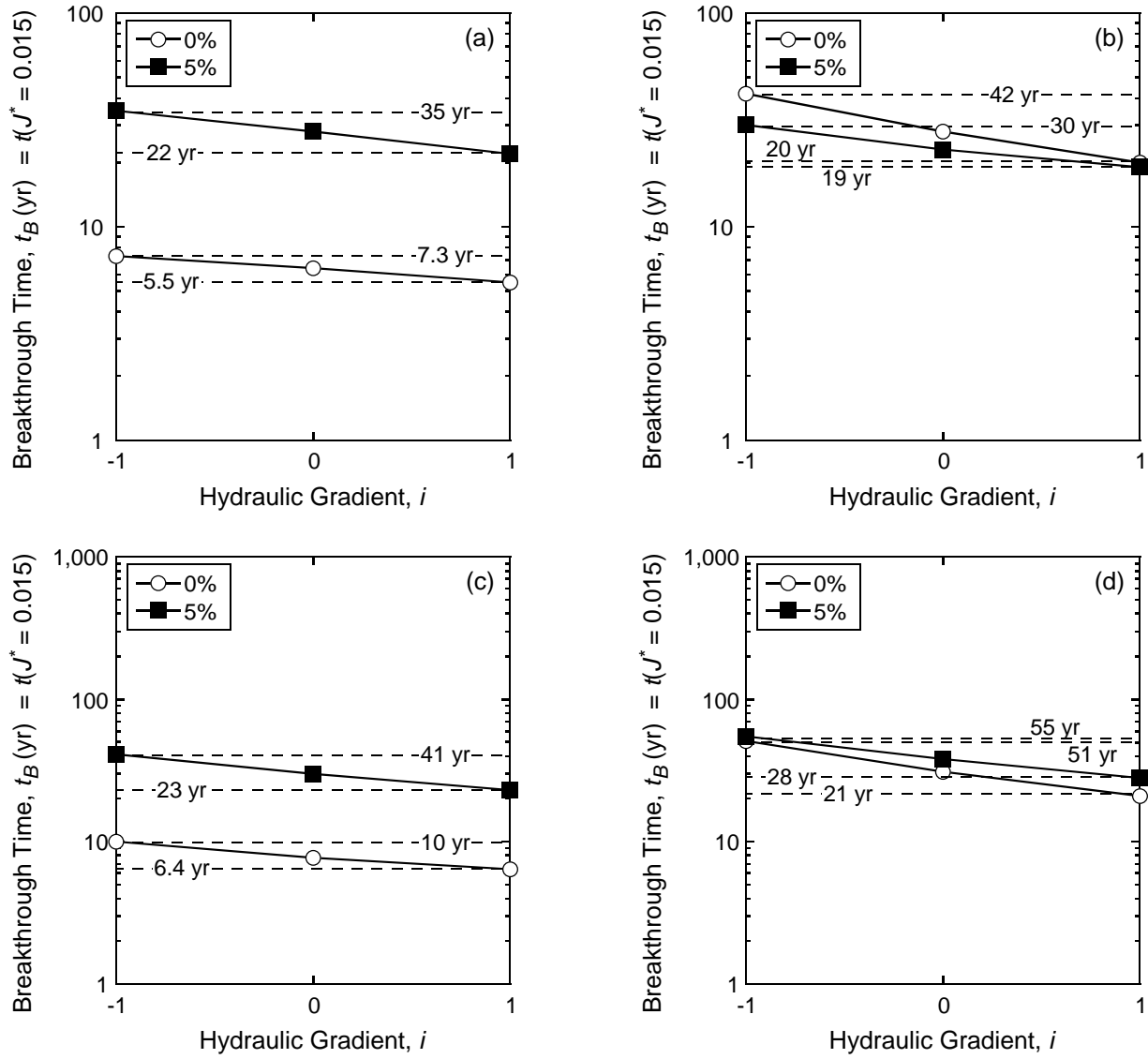


Figure E.24. Relationship between Péclet number,  $P_L$ , and predicted flux breakthrough times corresponding to  $J^*(x=L) = 0.015$  with a constant source concentration ( $C_o$ ) of 10,000 mg/L for the unamended and zeolite-amended cutoff wall with 5 % chabazite-UB: (a) potassium (K), Langmuir; (b) zinc (Zn), Langmuir; (c) potassium (K), Freundlich; (d) zinc (Zn), Freundlich.

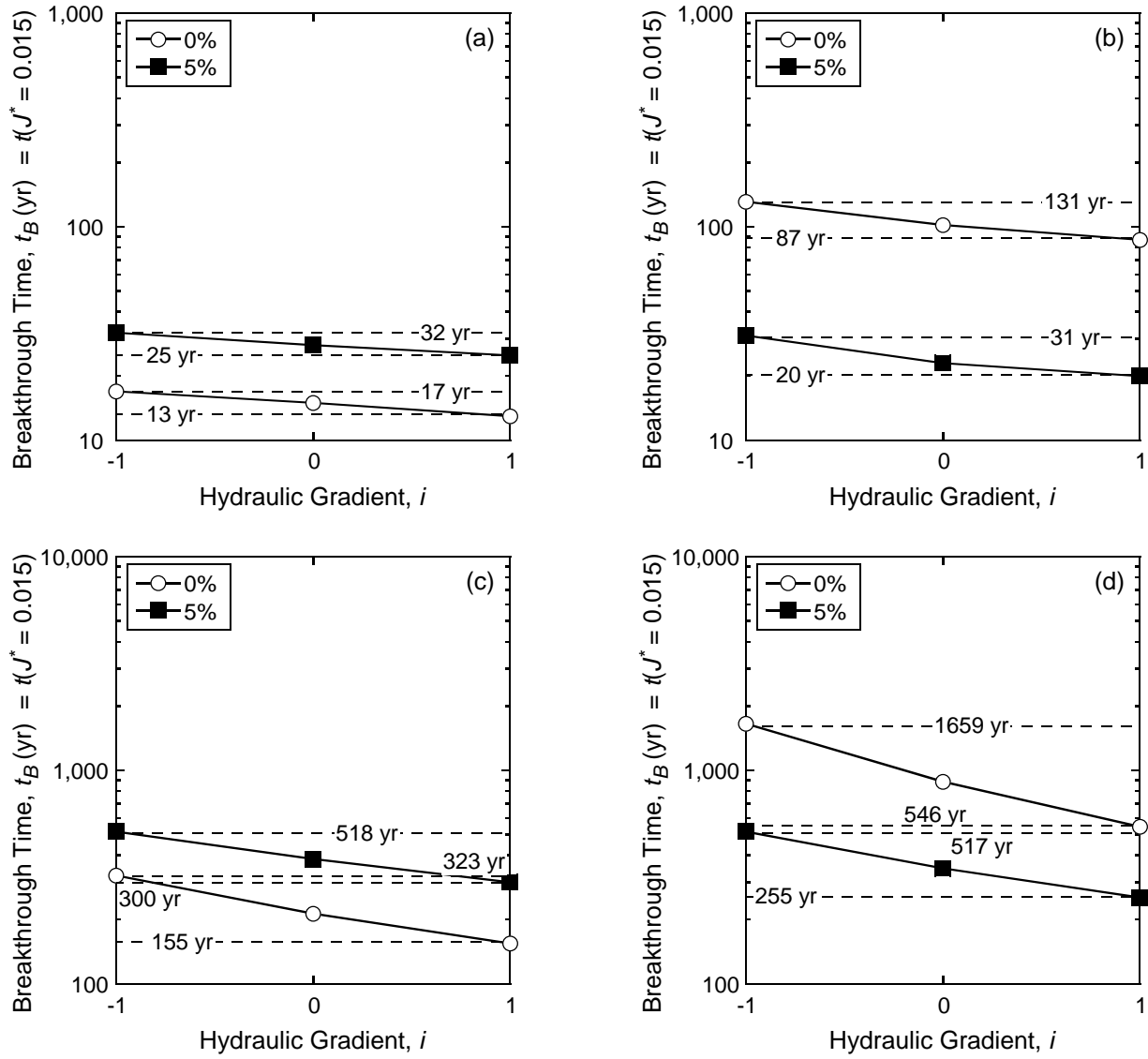


Figure E.25. Relationship between Péclet number,  $P_L$ , and predicted flux breakthrough times corresponding to  $J^*(x = L) = 0.015$  with a constant source concentration ( $C_o$ ) of 100 mg/L for the unamended and zeolite-amended cutoff wall with 5 % clinoptilolite: (a) potassium (K), Langmuir; (b) zinc (Zn), Langmuir; (c) potassium (K), Freundlich; (d) zinc (Zn), Freundlich.

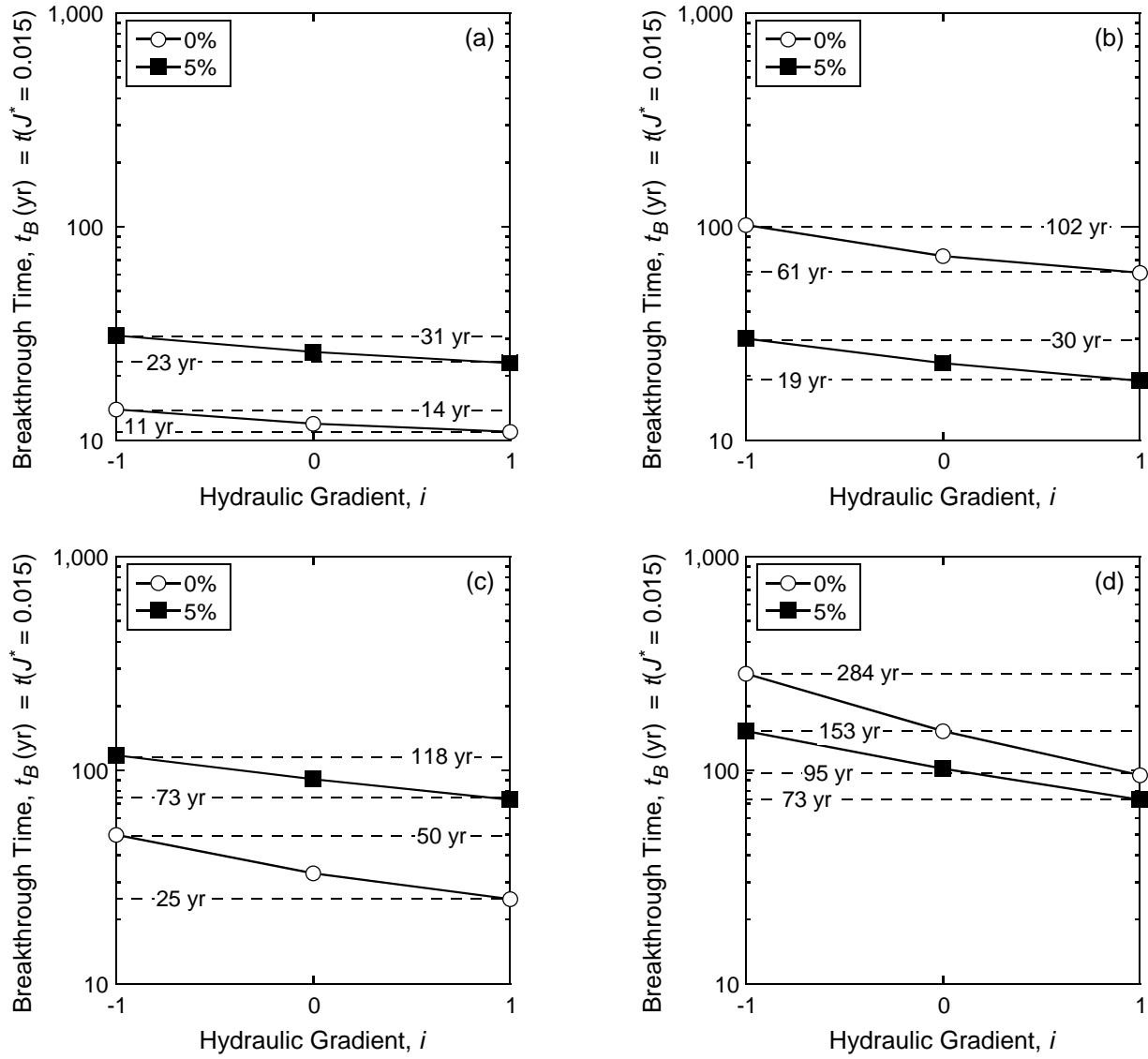


Figure E.26. Relationship between Péclet number,  $P_L$ , and predicted flux breakthrough times corresponding to  $J^*(x=L) = 0.015$  with a constant source concentration ( $C_o$ ) of 1,000 mg/L for the unamended and zeolite-amended cutoff wall with 5 % clinoptilolite: (a) potassium (K), Langmuir; (b) zinc (Zn), Langmuir; (c) potassium (K), Freundlich; (d) zinc (Zn), Freundlich.

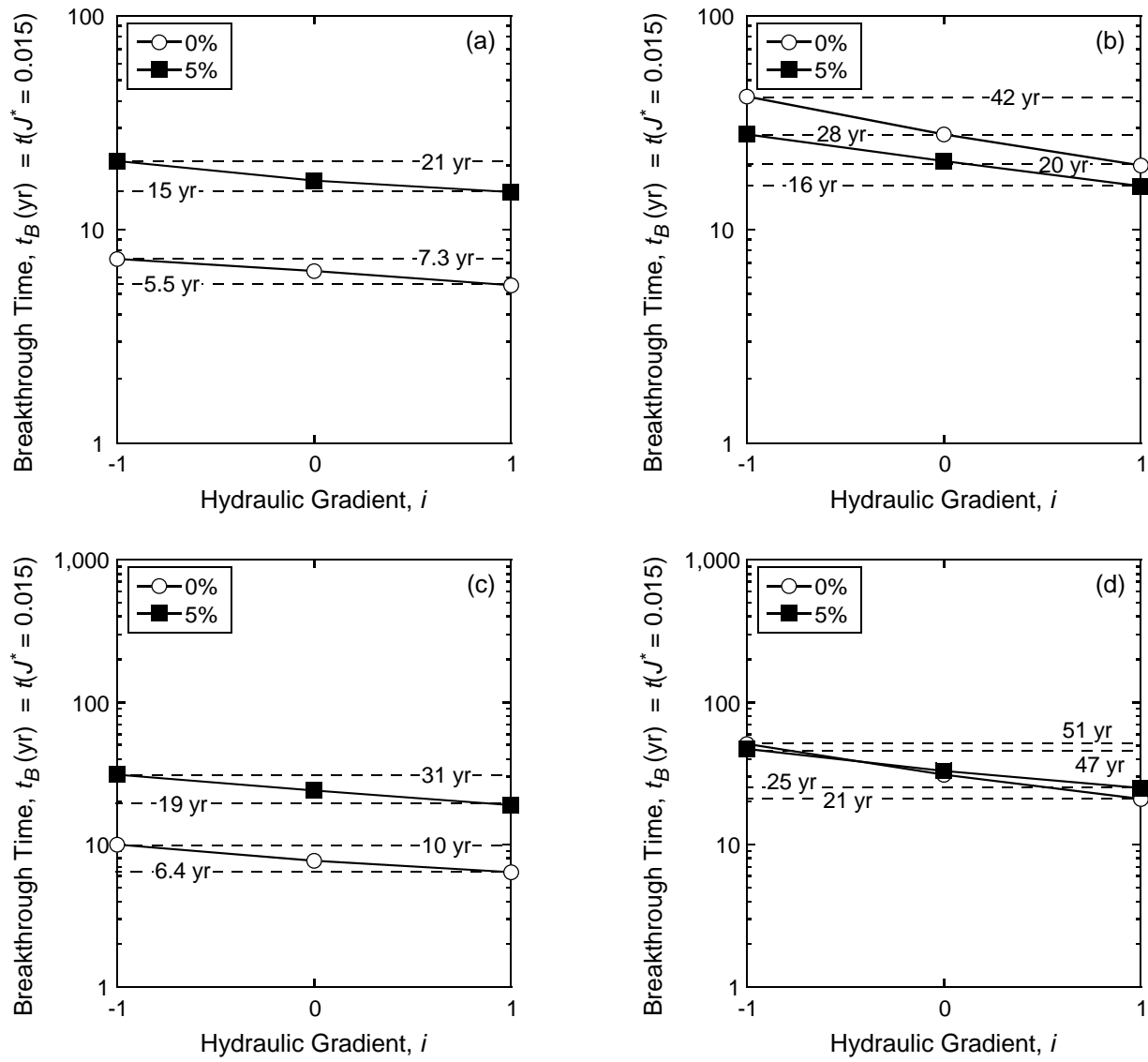


Figure E.27. Relationship between Péclet number,  $P_L$ , and predicted flux breakthrough times corresponding to  $J^*(x=L) = 0.015$  with a constant source concentration ( $C_o$ ) of 10,000 mg/L for the unamended and zeolite-amended cutoff wall with 5 % clinoptilolite: (a) potassium (K), Langmuir; (b) zinc (Zn), Langmuir; (c) potassium (K), Freundlich; (d) zinc (Zn), Freundlich.

APPENDIX F. SUPPLEMENTARY DATA FOR CHAPTER 5

Table F.1 Basis for defining the source concentration,  $C_o$ , and the according advective solute flux,  $J_A$ , for each backfill.

Test No.	Type of Zeolite	Amount of Zeolite (%)	Darcy Velocity, $v$ ( $\times 10^{-8}$ m/s) <sup>a</sup>	Permeant Liquid	Chemical Species	Source Concentration, $C_o$ (mM)				Advective Solute Flux at Steady-State, $J_A$ (mg/m <sup>2</sup> -d) <sup>b</sup>		
						Target	Measured			Target	Measured	
							Mean	Standard Deviation	Number of Data		Mean	Standard Deviation
1	NA <sup>c</sup>	0	2.79	35 mM KCl	Cl <sup>-</sup>	35	38.3	3.9	30	2990	3270	333
					K <sup>+</sup>	35	29.9	4.7	30	3300	2820	443
2	NA <sup>c</sup>	0	2.88	20 mM ZnCl <sub>2</sub>	Cl <sup>-</sup>	40	42.2	2.6	17	3530	3720	229
					Zn <sup>2+</sup>	20	17.6	0.8	24	3250	2680	130
3	Chabazite-UB	5	3.02	35 mM KCl	Cl <sup>-</sup>	35	38.3	3.9	30	3240	3540	361
					K <sup>+</sup>	35	29.9	4.7	30	3570	3050	479
4	Chabazite-UB	5	2.75	20 mM ZnCl <sub>2</sub>	Cl <sup>-</sup>	40	42.2	2.6	17	3370	3550	219
					Zn <sup>2+</sup>	20	17.6	0.8	24	3110	2730	124
5	Chabazite-UB	5	2.97	17.5 mM KCl + 10 mM ZnCl <sub>2</sub>	Cl <sup>-</sup>	37.5	38.4	1.9	13	3410	3490	173
					K <sup>+</sup>	17.5	17.0	1.5	17	1760	1710	150
					Zn <sup>2+</sup>	10	9.1	0.9	17	1680	1530	151
6	Clinoptilolite	5	2.89	35 mM KCl	Cl <sup>-</sup>	35	38.3	3.9	30	3100	3390	345
					K <sup>+</sup>	35	29.9	4.7	30	3420	2920	459
7	Clinoptilolite	5	2.87	20 mM ZnCl <sub>2</sub>	Cl <sup>-</sup>	40	42.2	2.6	17	3520	3710	229
					Zn <sup>2+</sup>	20	17.6	0.8	24	3240	2850	130
8	Clinoptilolite	5	2.85	17.5 mM KCl + 10 mM ZnCl <sub>2</sub>	Cl <sup>-</sup>	37.5	38.4	1.9	13	3270	3350	166
					K <sup>+</sup>	17.5	17.0	1.5	17	1680	1640	144
					Zn <sup>2+</sup>	10	9.1	0.9	17	1610	1470	145
9	Chabazite-LB	5	0.72	35 mM KCl	Cl <sup>-</sup>	35	38.3	3.9	30	772	845	86.0
					K <sup>+</sup>	35	31.2	5.8	32	851	759	141
10	Chabazite-LB	10	0.72	35 mM KCl	Cl <sup>-</sup>	35	38.3	3.9	30	772	845	86.0
					K <sup>+</sup>	35	31.2	5.8	32	851	759	141

<sup>a</sup> Darcy velocity (liquid flux or specific discharge),  $v = q/A_f$  (Table 5.4); <sup>b</sup> Advective solute flux at steady state,  $J_A (= vC_o = nv_s C_o)$ ; <sup>c</sup> NA = Not applicable (*i.e.*, unamended backfill).

Table F.2. Replacement time corrected for the residual volume,  $V_{res}$ .

Test No.	Type of Zeolite	Amount of Zeolite (%)	Volumetric Flow Rate, $q$ (mL/d) <sup>a</sup>	Replacement Time for the Residual Volume, $V_{res}$ (mL) <sup>b</sup>	
				$\Delta t$ (d)	$\Delta T$ <sup>c</sup>
1	NA <sup>d</sup>	0	7.86	1.348	0.0859
2	NA <sup>d</sup>	0	8.00	1.331	0.0891
3	Chabazite-UB	5	8.00	1.331	0.0861
4	Chabazite-UB	5	7.91	1.348	0.0841
5	Chabazite-UB	5	7.95	1.331	0.0845
6	Clinoptilolite	5	8.05	1.315	0.0895
7	Clinoptilolite	5	8.01	1.331	0.0858
8	Clinoptilolite	5	7.87	1.348	0.0861
9	Chabazite-LB	5	2.06	5.178	0.0873
10	Chabazite-LB	10	2.06	5.177	0.0841

<sup>a</sup> 1 mL/d =  $1.16 \times 10^{-11}$  m<sup>3</sup>/s; <sup>b</sup>  $V_{res}/q$ , where  $V_{res}$  = void volume of the 6.2 mm porous stone (10.5 mL) + 50 cm of tube (0.15 mL) = 10.65 mL; <sup>c</sup> corrected time in terms of pore volume of flow; <sup>d</sup> NA = Not applicable (*i.e.*, unamended backfill).

Table F.3 Basis for defining the volume of the column specimen.

Test No.	Type of Zeolite	Amount of Zeolite (%)	Specific Gravity, $G_s^a$	Diameter, $d$ ( $\times 10^{-2}$ m)		Cross Section Area, $A_f$ ( $\times 10^{-3}$ m <sup>2</sup> )	Height, $h$ ( $\times 10^{-2}$ m)		Total Volume, $V_T$ ( $\times 10^{-6}$ m <sup>3</sup> )
				Mean	Standard Deviation		Mean	Standard Deviation	
1	NA <sup>c</sup>	0	2.69	6.43	0.33	3.26	6.99	0.09	227.7
2	NA <sup>c</sup>	0	2.69	6.40	0.34	3.22	7.15	0.02	230.2
3	Chabazite-UB	5	2.67	6.25	0.41	3.07	7.06	0.02	216.5
4	Chabazite-UB	5	2.67	6.51	0.15	3.33	6.98	0.04	232.3
5	Chabazite-UB	5	2.67	6.28	0.39	3.10	7.23	0.05	224.1
6	Clinoptilolite	5	2.67	6.41	0.31	3.23	7.11	0.01	229.7
7	Clinoptilolite	5	2.67	6.41	0.26	3.23	7.12	0.07	230.0
8	Clinoptilolite	5	2.67	6.38	0.24	3.19	7.34	0.05	234.6
9	Chabazite-LB	5	2.67	6.50	0.25	3.31	7.01	0.01	232.3
10	Chabazite-LB	10	2.65	6.47	0.19	3.30	7.07	0.06	233.6

<sup>a</sup> Calculated based on the  $G_s$  and added amount of the constituent materials (*i.e.*, sand, bentonite, zeolite) for each backfill.

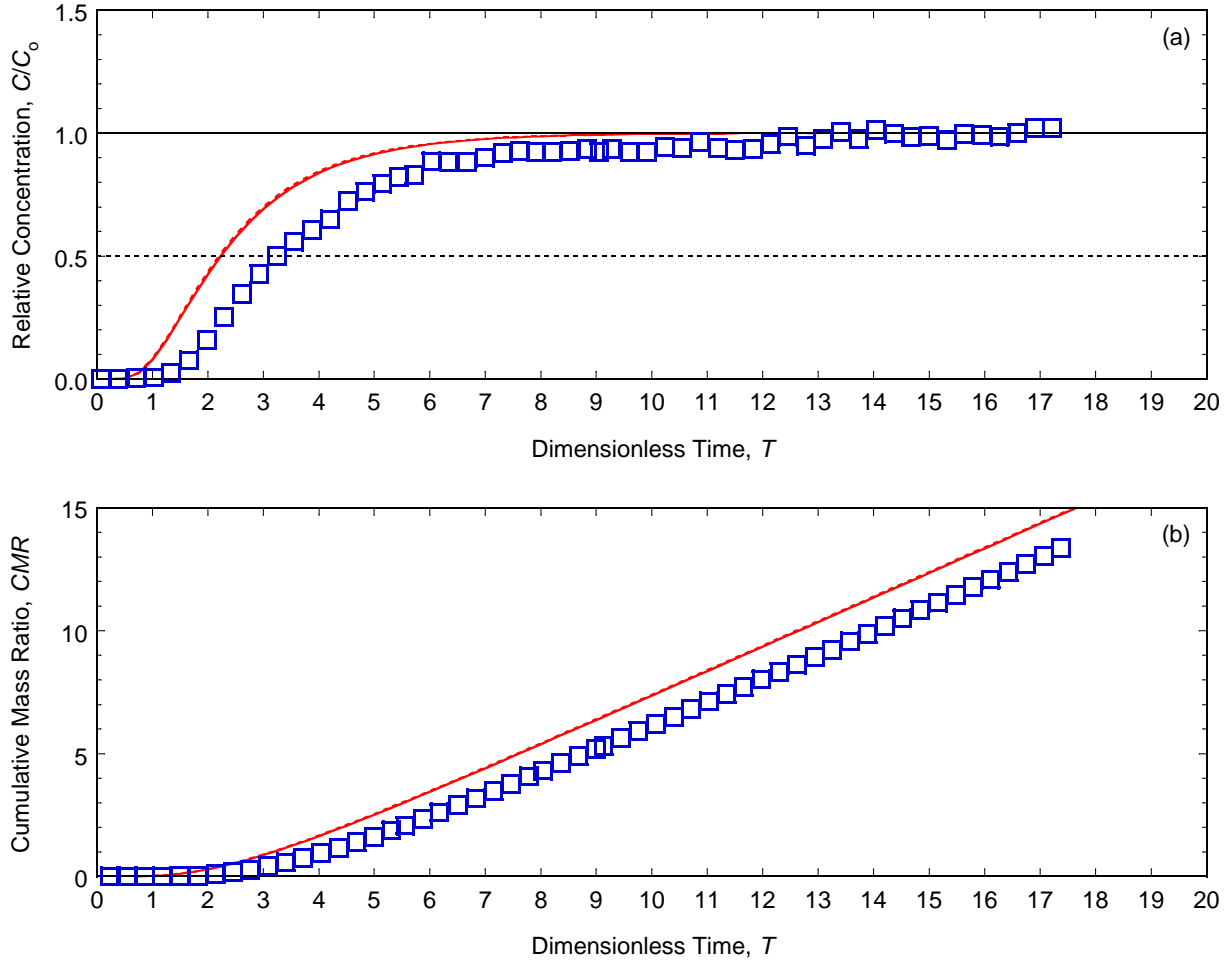


Figure F.1. Comparison of the measured column effluent data for potassium ( $K^+$ ) versus the model simulation using  $R_d$  based on the BEAT results and  $P_L$  from regression of the measured column effluent data for the unamended backfill permeated with 35 mM KCl (Test No. 1): (a) relative concentration ( $RC$ ) data; (b) cumulative mass ratio ( $CMR$ ) data. Note: dashed line =  $R_d$  based on Freundlich adsorption model; solid line =  $R_d$  based on Langmuir adsorption model.

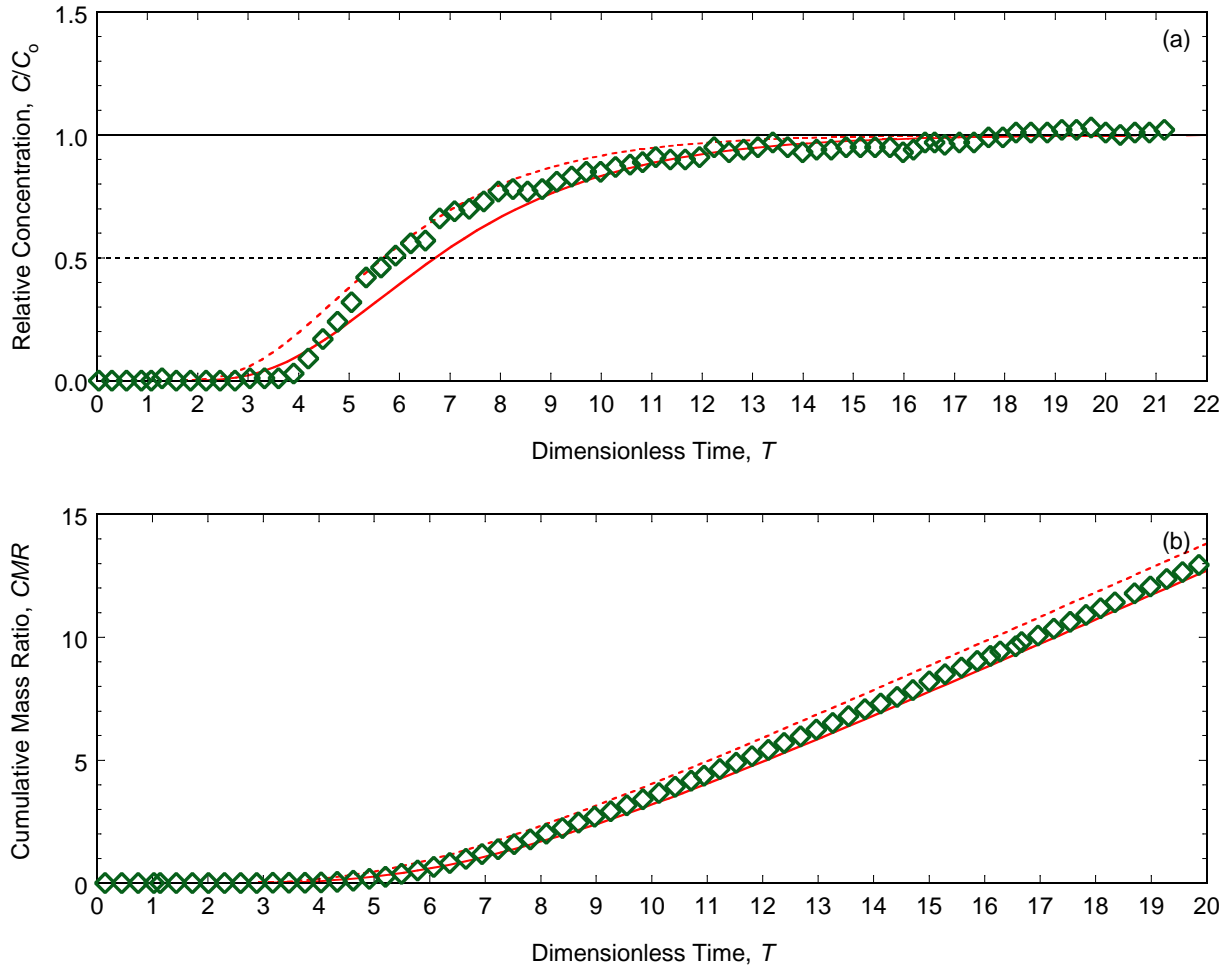


Figure F.2. Comparison of the measured column effluent data for zinc ( $Zn^{2+}$ ) versus the model simulation using  $R_d$  based on the BEAT results and  $P_L$  from regression of the measured column effluent data for the unamended backfill permeated with 20 mM  $ZnCl_2$  (Test No. 2): (a) relative concentration ( $RC$ ) data; (b) cumulative mass ratio ( $CMR$ ) data. Note: dashed line =  $R_d$  based on Freundlich adsorption model; solid line =  $R_d$  based on Langmuir adsorption model.

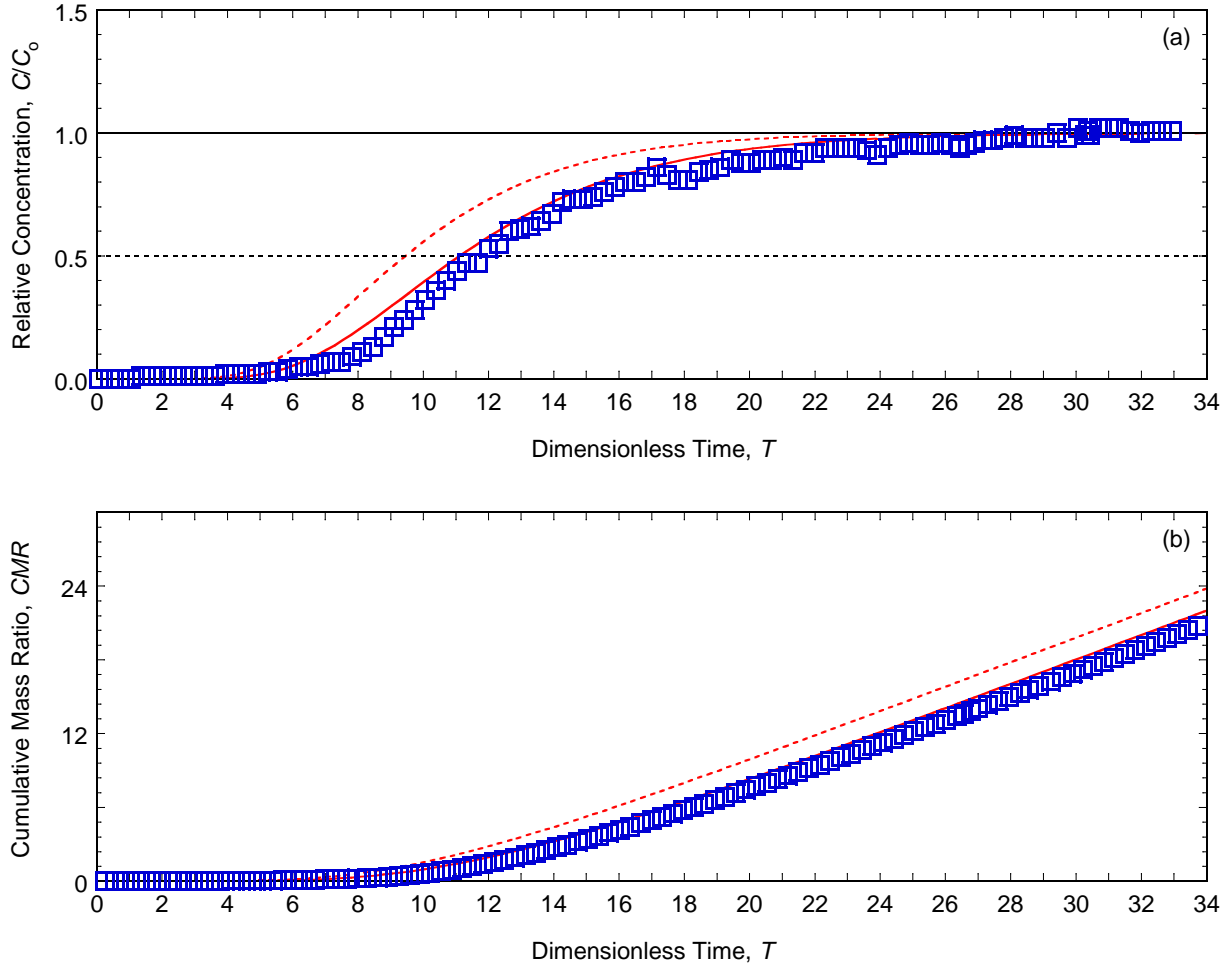


Figure F.3. Comparison of the measured column effluent data for potassium ( $K^+$ ) versus the model simulation using  $R_d$  based on the BEAT results and  $P_L$  from regression of the measured column effluent data for the backfill amended with 5 % chabazite-UB and permeated with 35 mM KCl (Test No. 3): (a) relative concentration ( $RC$ ) data; (b) cumulative mass ratio ( $CMR$ ) data. Note: dashed line =  $R_d$  based on Freundlich adsorption model; solid line =  $R_d$  based on Langmuir adsorption model.

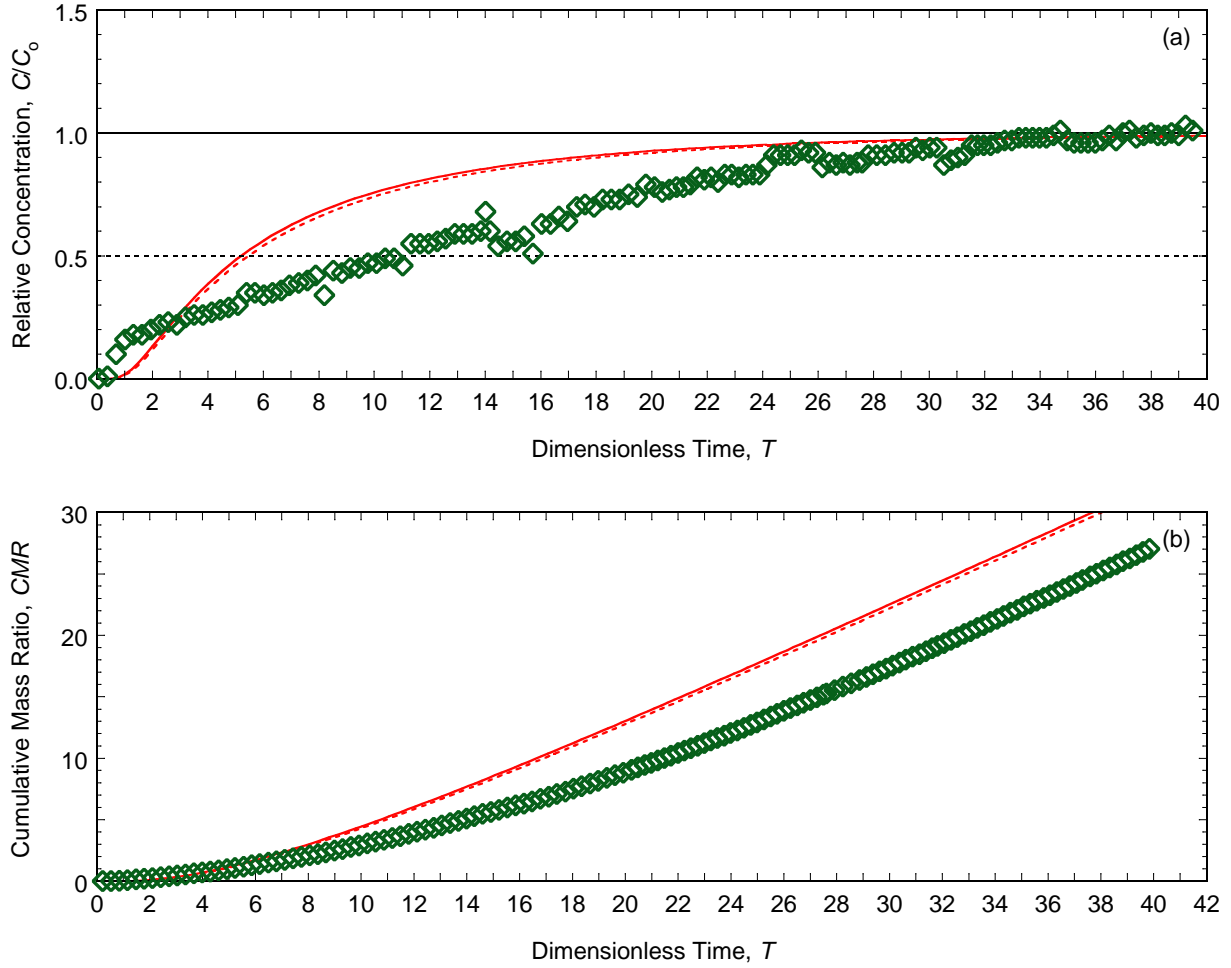


Figure F.4. Comparison of the measured column effluent data for zinc ( $Zn^{2+}$ ) versus the model simulation using  $R_d$  based on the BEAT results and  $P_L$  from regression of the measured column effluent data for the backfill amended with 5 % chabazite-UB and permeated with 20 mM  $ZnCl_2$  (Test No. 4): (a) relative concentration ( $RC$ ) data; (b) cumulative mass ratio ( $CMR$ ) data. Note: dashed line =  $R_d$  based on Freundlich adsorption model; solid line =  $R_d$  based on Langmuir adsorption model.

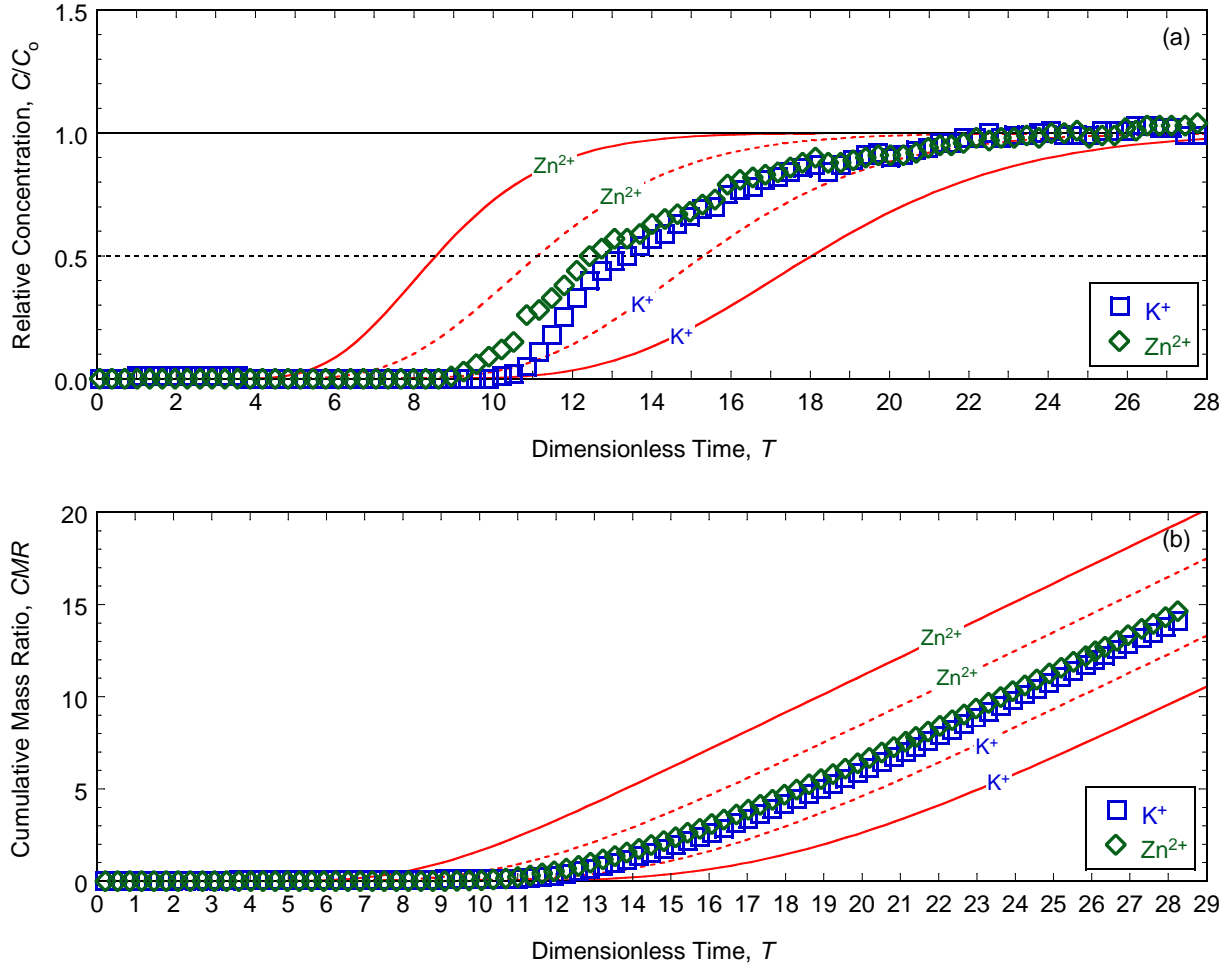


Figure F.5. Comparison of the measured column effluent data for potassium ( $K^+$ ) and zinc ( $Zn^{2+}$ ) versus the model simulation using  $R_d$  based on the BEAT results and  $P_L$  from regression of the measured column effluent data for the backfill amended with 5 % chabazite-UB and permeated with 17.5 mM KCl plus 10 mM  $ZnCl_2$  (Test No. 5): (a) relative concentration (RC) data; (b) cumulative mass ratio (CMR) data. Note: dashed line =  $R_d$  based on Freundlich adsorption model; solid line =  $R_d$  based on Langmuir adsorption model.

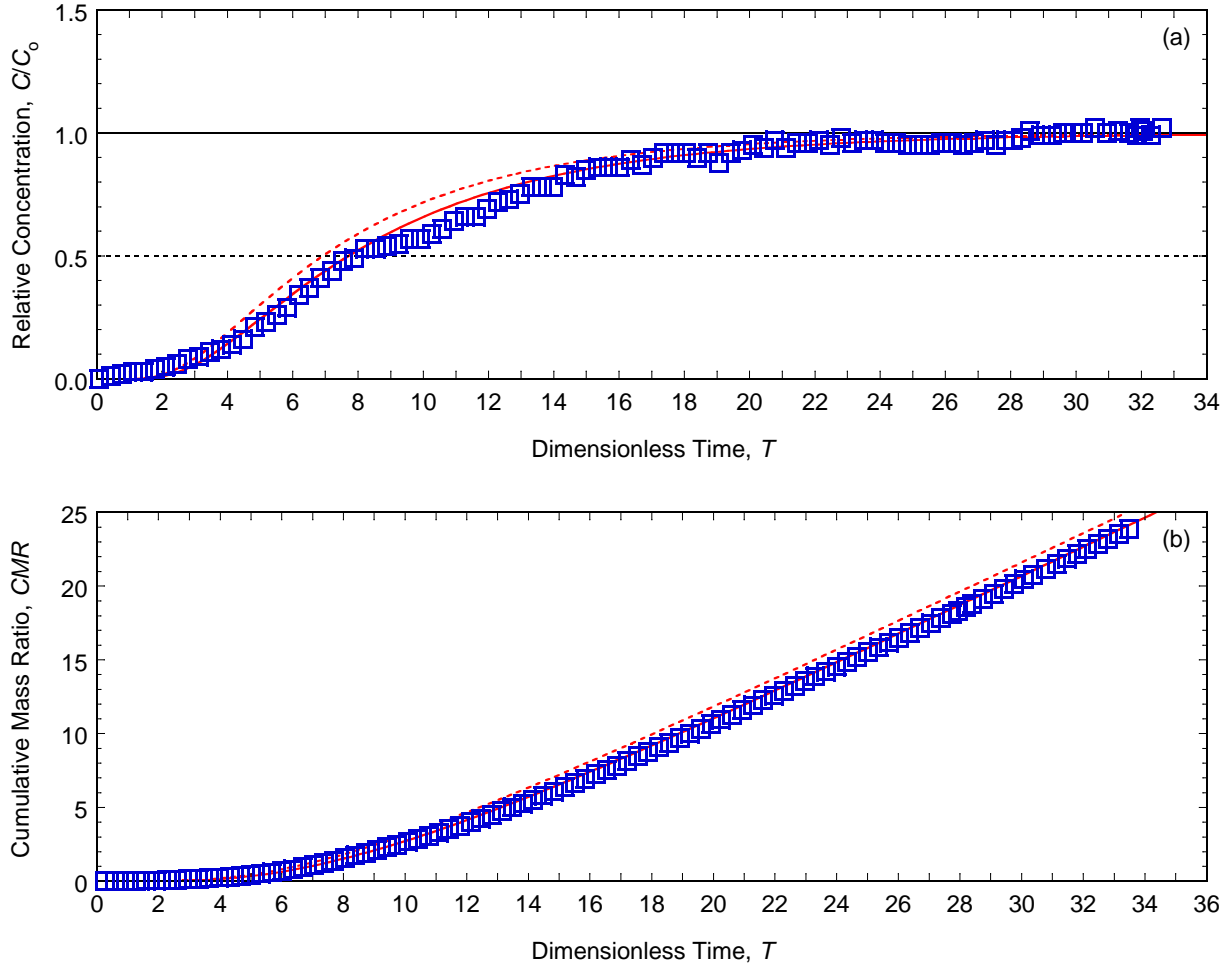


Figure F.6. Comparison of the measured column effluent data for potassium ( $K^+$ ) versus the model simulation using  $R_d$  based on the BEAT results and  $P_L$  from regression of the measured column effluent data for the backfill amended with 5 % clinoptilolite and permeated with 35 mM KCl (Test No. 6): (a) relative concentration ( $RC$ ) data; (b) cumulative mass ratio ( $CMR$ ) data. Note: dashed line =  $R_d$  based on Freundlich adsorption model; solid line =  $R_d$  based on Langmuir adsorption model.

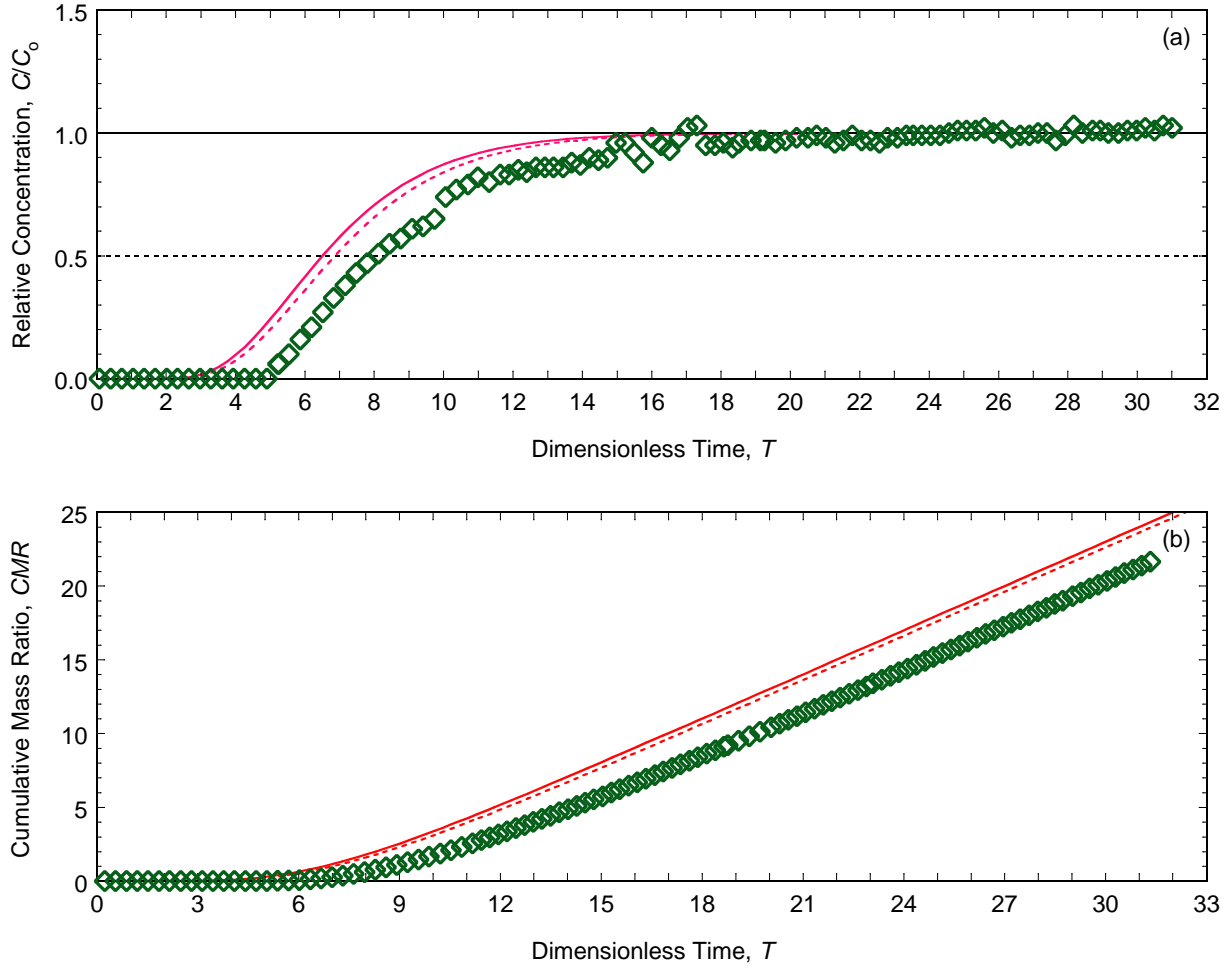


Figure F.7. Comparison of the measured column effluent data for zinc ( $Zn^{2+}$ ) versus the model simulation using  $R_d$  based on the BEAT results and  $P_L$  from regression of the measured column effluent data for the backfill amended with 5 % clinoptilolite and permeated with 20 mM  $ZnCl_2$  (Test No. 7): (a) relative concentration ( $RC$ ) data; (b) cumulative mass ratio ( $CMR$ ) data. Note: dashed line =  $R_d$  based on Freundlich adsorption model; solid line =  $R_d$  based on Langmuir adsorption model.

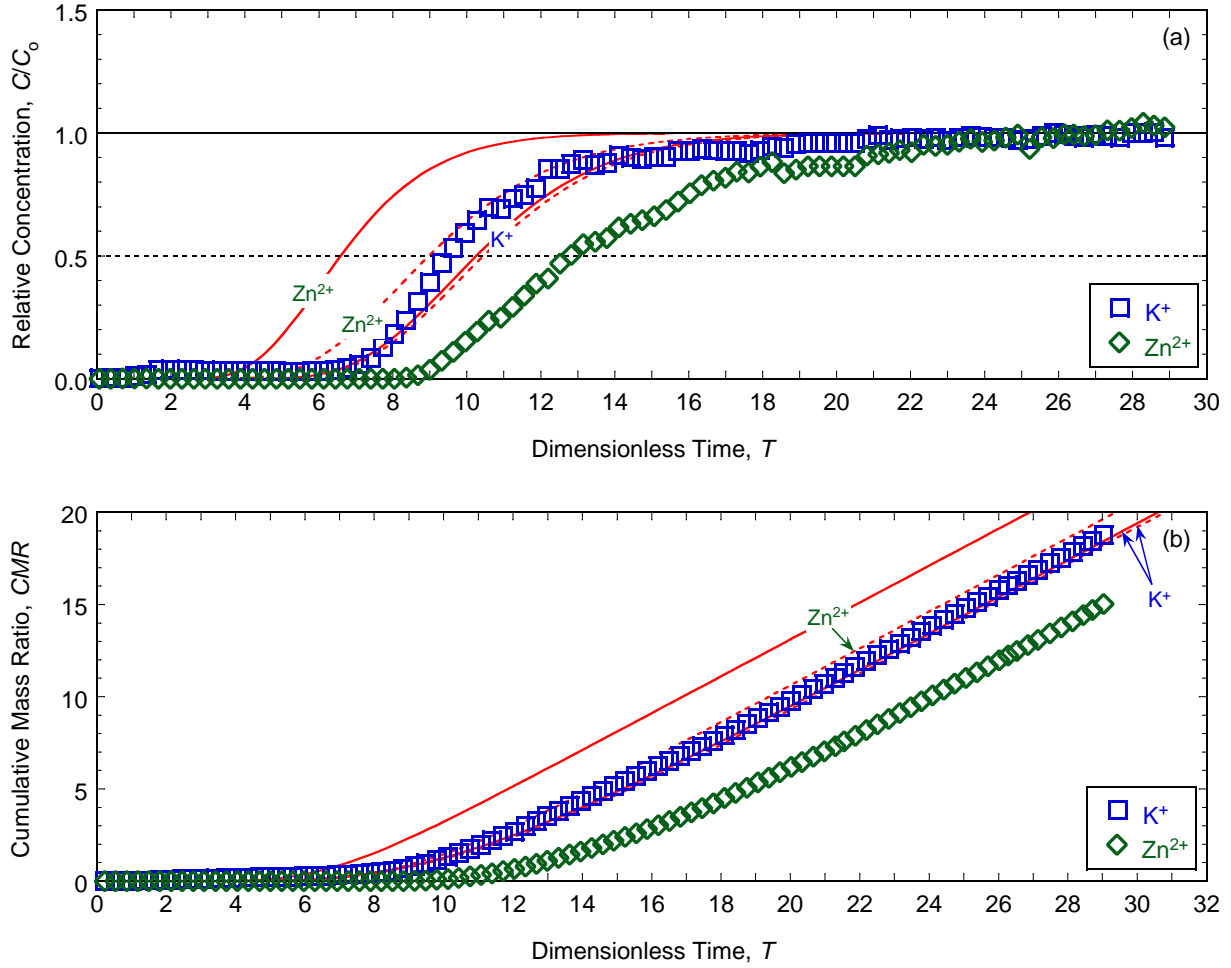


Figure F.8. Comparison of the measured column effluent data for potassium ( $K^+$ ) and zinc ( $Zn^{2+}$ ) versus the model simulation using  $R_d$  based on the BEAT results and  $P_L$  from regression of the measured column effluent data for the backfill amended with 5 % clinoptilolite and permeated with 17.5 mM KCl plus 10 mM  $ZnCl_2$  (Test No. 8): (a) relative concentration ( $RC$ ) data; (b) cumulative mass ratio ( $CMR$ ) data. Note: dashed line =  $R_d$  based on Freundlich adsorption model; solid line =  $R_d$  based on Langmuir adsorption model.

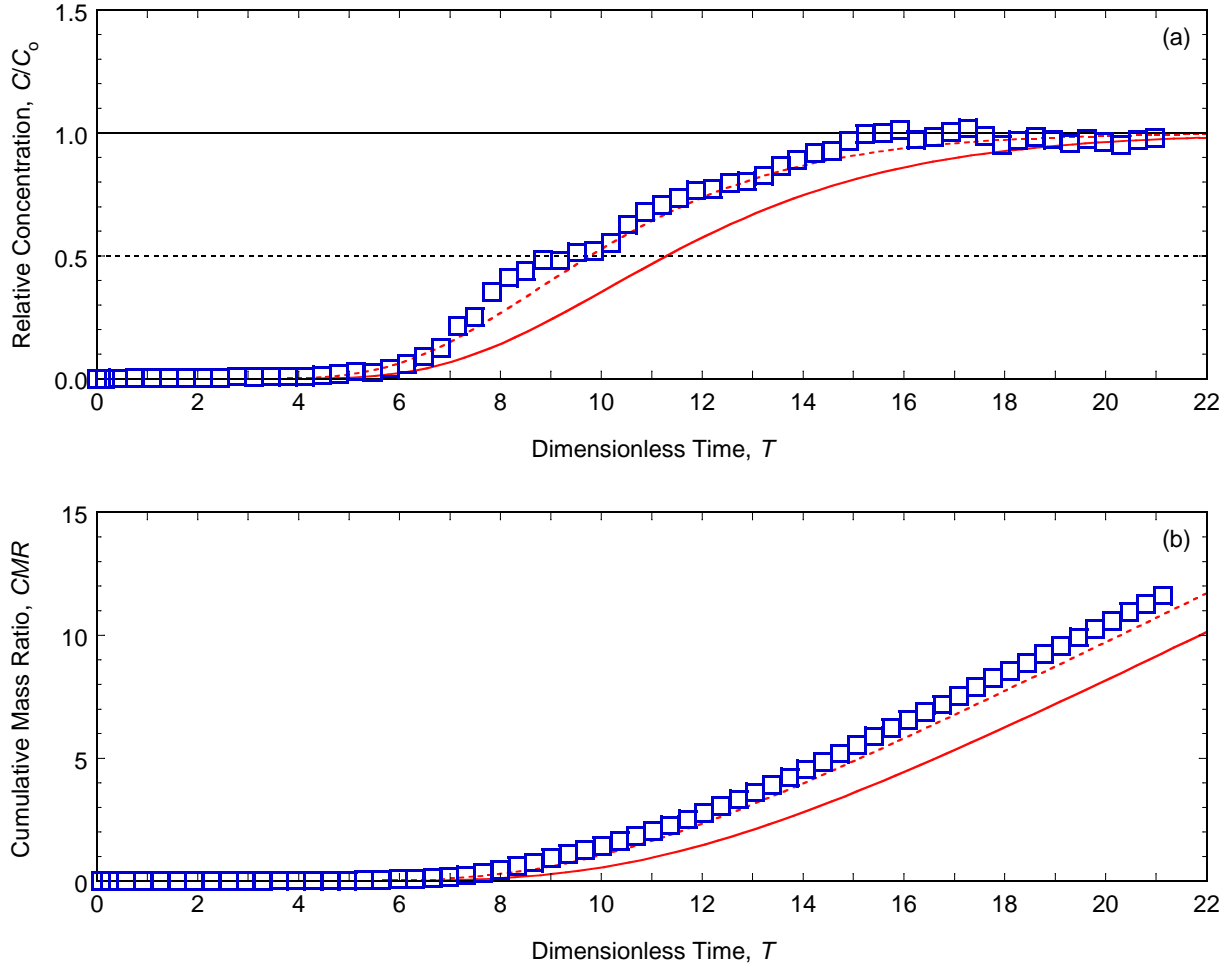


Figure F.9. Comparison of the measured column effluent data for potassium ( $K^+$ ) versus the model simulation using  $R_d$  based on the BEAT results and  $P_L$  from regression of the measured column effluent data for the backfill amended with 5 % chabazite-LB and permeated with 35 mM KCl (Test No. 9): (a) relative concentration ( $RC$ ) data; (b) cumulative mass ratio ( $CMR$ ) data. Note: dashed line =  $R_d$  based on Freundlich adsorption model; solid line =  $R_d$  based on Langmuir adsorption model.

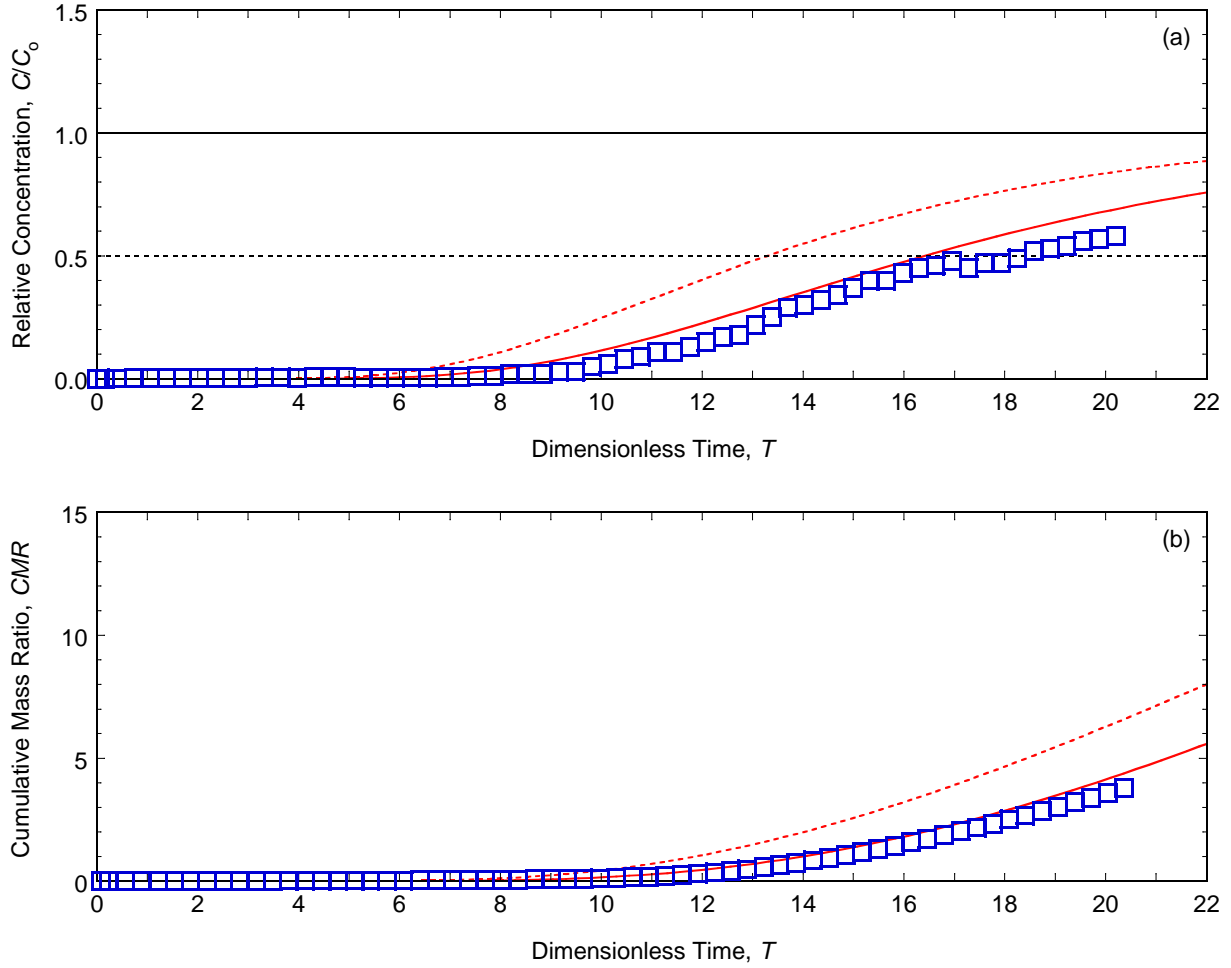


Figure F.10. Comparison of the measured column effluent data for potassium ( $K^+$ ) versus the model simulation using  $R_d$  based on the BEAT results and  $P_L$  from regression of the measured column effluent data for the backfill amended with 10 % chabazite-LB and permeated with 35 mM KCl (Test No. 10): (a) relative concentration ( $RC$ ) data; (b) cumulative mass ratio ( $CMR$ ) data. Note: dashed line =  $R_d$  based on Freundlich adsorption model; solid line =  $R_d$  based on Langmuir adsorption model.